Human pluripotent stem cells derived-cardiomyocytes (hPSC-CMs) to assess the impact of drug- and gene-induced changes on cell function



Submitted by

Nurul Ain Nasim Mohd Yusof, BSc MSc

School of Medicine

Department of Cancer & Stem Cells

The University of Nottingham

December 2019

Thesis submitted to The University of Nottingham for the degree of Doctor of Philosophy

Acknowledgements

Firstly, I would like to express my sincere gratitude for my supervisor, Professor Chris Denning, for all his time, patience, support and guidance throughout my PhD here at The University of Nottingham. His guidance and leadership helped me to survive the research and writing of this thesis.

Besides my supervisor, I would like to thank Dr Alexander Kondrashov who trained, supported, nurtured knowledge and inspired me when I have first joined the lab and know nothing. He is the backbone behind the gene function and β_2AR polymorphism studies. I am also grateful to all research collaborators from CRACK-IT consortium and β_2AR chapter for support, training and immerse fruitful inputs. I would like to acknowledge Dr. Minch Duc Hoang, Maria Barbadillo-Munoz, Jayson Bispham, Penny Howick, Dr Jamie Bhagwan, Dr Karl Firth, Puspita Katili and Nguyen Vo who trained me in cell culture/molecular works and provided technical supports. I thanks my fellow labmates in the stimulating discussion, journal club, cardiac updates and for all the tears and fun we had along the journeys.

To my PhD funders The University of Nottingham/Islamic Development Bank for the High Technology Merit Scholarships for the duration of 3 years. To my workplace, Institute for Medical Research Malaysia, Ministry of Health for granted my study leave and allow me to further my studies.

And most of all, I owe my most profound appreciation to my husband, Mr Muhammad Amiraizat, for his affection, encouragement, understanding and patience. Who supported and enabled me to complete my PhD thesis. To my son, Adi Suhayb, having him on the start of my PhD, certainly not easy but he made my life wonderful, and he is my inspiration to achieve greatness. To my parents (Mohd Yusof and Rashadah) and siblings, who 6500 miles away, thank you for being my champions, I hope that I have made you proud.

Declaration

I hereby declare that this thesis has been composed by myself and has not been submitted for any other degree previously. Acknowledgements of specific procedures not performed by myself are stated; otherwise, the work described is my own.

Nurul Ain Nasim Mohd Yusof _____

Date: 02 January 2020

Abstract

The majority of data available for drug predictive safety and disease/polymorphism modelling are based on results from genetic association studies or from models other than humans, which can lead to conflicting mechanistic explanations. This thesis considers whether human pluripotent stem cell-derived cardiomyocytes (hPSC-CMs) could complement existing assays to improve drug safety screening and disease/polymorphism modelling by assessing the impact of drug- and gene-induced changes on cell function.

To evaluate the suitability of hPSC-CMs for drug safety screening, changes in contractility and electrophysiology were quantitated. Protocols for the CellOPTIQ:hiPSC-CMs combination were established and unified via a drug 'training' set, allowing for the blinded evaluation of up to 27 drugs with known positive, negative or neutral inotropic effects. This demonstrated that the accuracy of CellOPTIQ:hiPSC-CMs configuration ranged from 50 to 60%, which was lower than might have been expected from a human cell-based system. Nevertheless, contraction and relaxation time appeared to be informative for positive inotropes, while contraction amplitude was informative for negative inotropes. Moreover, accuracy was further improved and increased to 75% (for CellOPTIQ) by refining the conditions that would reduce beat rate, increasing the signal to noise ration and enabling chronic long-term drug testing. The results show that hiPSC-CMs could be used to reduce socioeconomics cost and assist regulatory guidelines governing cardiac safety assessments.

To evaluate whether hPSC-CMs could be used to understand the gene-induced changes and influence of polymorphic variation in the genome on cell behaviour, the *ADRB2* locus (encodes Ƀeta$_2$-adrenergic receptor; Ƀ$_2$AR) was used as an exemplar. This is because the action of beta-blockers may be influenced by polymorphisms within the Ƀ$_2$AR, particularly at amino acid positions 16 and 27, and there is a potential association with cardiovascular disorders such as heart failure.

To study Ƀ$_2$AR polymorphism differences against a constant genetic background, CRISPR/Cas9 technology was used to genome-edit the HUES7 hESC line to

produce 4 isogenic β_2AR variants (single amino acid codes: GE, GQ, RE, RQ). The isogenic variants were able to retain their pluripotency and differentiation capabilities into hPSC-CMs whilst retaining responsiveness to β_2AR pharmacology.

For the functional assessment, an initial phenotypic analysis was carried out by luciferase-based real-time cAMP (cyclic adenosine monophosphates) assay to estimate the differential response during acute and chronic agonist exposure to individual β_2AR variants. It was found that RQ has the lower initial β_2AR density, GQ has the highest receptor desensitisation, Arg16 was resistant to desensitisation and GQ tended towards being the most downregulated.

Since β_2AR is regulated by multiple complex processes and their regulation has essential effects on signal transduction, it is expected that these isogenic models will help to understand the mechanisms that underlie 'disease' and drug- and gene-induced states. Moreover, the work shows how coupling hPSC-CMs with CRISPR/Cas9 technologies can be used to personalise diagnosis and identify new pathogenic variants for cardiovascular disease.

Thus, this thesis shows there is value in exploring the use of hPSC-CMs in assessing the impact of drug-induced changes on cell function, and provide a tool to gain mechanistic insights into how polymorphisms in the genome alter signalling cascades.

Table of Contents

Acknowledgements **2**

Declaration **3**

Abstract **4**

Table of Contents **6**

List of Figures **14**

List of Tables **22**

Abbreviations **24**

Chapter 1 Introduction **26**

1.1 Drug discovery and development. 26

1.1.1 Drug withdrawal 27

1.1.2 Drug monitoring, response and efficiency 28

1.1.3 Conventional drug discovery and new alternative methods 29

1.2 Cardiovascular disease 30

1.2.1 Disease Modelling 31

1.3 Clinical and preclinical cardiac safety screening in drug development . 32

1.3.1 Human primary cardiomyocytes 32

1.3.2 Animal models 32

1.4 Safety guidelines and initiatives 34

1.4.1 ICH S7B 34

1.4.2 ICH E14 34

1.4.3 Comprehensive *in-vitro* Proarrthymia Assay (CiPA) 35

1.4.4 Japanese iPS Cardiac Safety Assessment (JiCSA) 37

1.5 Cardiac electrophysiology and contractility 37

1.5.1 The cardiac action potential 37

1.5.2 Excitation-contraction (EC) coupling 40

1.6 Human pluripotent stem cells (hPSCs) as tools 41
1.6.1 Human embryonic stem cells (hESCs) 42
1.6.2 Human-induced pluripotent stem cells (hiPSCs) 43
1.7 Human pluripotent stem cell-derived cardiomyocytes (hPSC-CMs) 47
1.7.1 Differentiation approaches of hPSCs to hPSC-CMs 47
1.7.2 Stage-specific cardiac development 48
1.7.3 Differentiation protocols 50
1.7.4 Properties and pharmacological responses of hPSC-CMs 52
1.7.5 The hPSC-CMs vs primary cardiomyocytes 53
1.8 Methods for *in-vitro* hPSC-CMs functional analysis 56
1.8.1 Analysing electrophysiology 56
1.8.2 Analysing contractility 57
1.9 Cardiac maturation in hPSCs-CMs 61
1.10 The CRACK-IT InPulse Initiative 62
1.11 Genome-editing of hPSCs for disease modelling 63
1.12 ß-adrenergic function in heart 66
1.13 Thesis Aims 67
Chapter 2 Materials and Methods 68
2.1 Cell culture 68
2.1.1 General Cell Culture 68
2.1.2 Human pluripotent stem cells (hPSCs) culture condition 68
2.1.3 Growth curves 69
2.1.4 Karyotyping 69
2.1.5 Nottingham in-house cardiomyocytes differentiation 69
2.1.6 Cardiomyocytes dissociation 70
2.1.7 Cardiomyocytes cryopreservation 71
2.1.8 Nottingham thawing protocol 71

2.1.9 Dropwise thawing protocol 71
2.1.10 Cardiomyocytes transfection..... 72
2.2 Microscopy..... 73
2.2.1 General microscopy 73
2.2.2 Fluorescence and immunostained image analysis..... 73
2.3 Molecular biology..... 73
2.3.1 Genomic DNA extraction 73
2.3.2 Polymerase chain reaction (PCR) 73
2.3.3 Gel electrophoresis, extraction and purification 73
2.3.4 RNA extraction and cDNA synthesis 74
2.3.5 The qPCR analysis of gene expression 74
2.3.6 The hPSC and hPSC-CMs Immunostaining..... 74
2.4 CellOPTIQ platform analysis 77
2.4.1 In-house CMs culture conditions for CellOPTIQ..... 77
2.4.2 Commercial lines culture conditions for CellOPTIQ 77
2.4.3 Drug preparations 78
2.4.4 Contractility measurement 80
2.4.5 Voltage electrophysiology measurement 80
2.4.6 Pacing stimulation..... 80
2.4.7 Drug testing 81
2.5 RTCA CardioECR 81
2.6 GloSensor™ cAMP assay..... 82
2.6.1 GloSensor™ cAMP general principle 82
2.6.2 Downregulation chronic long-term assay..... 82
2.6.3 Acute short-term assay..... 83
2.7 Statistical analysis..... 84

Chapter 3 Establishment of CellOPTIQ drug screening system with 'training' set drugs and development of culture systems 85

3.1 Introduction 85

3.1.1 CRACK-IT InPulse initiative and its *in-vitro* platforms 85

3.1.2 Selection of hiPSC-CMs cell lines for assessment of cardiac toxicity 87

3.2 Training drugs (Tier 1) 88

3.3 Chapter aims and objectives 90

3.4 Results 92

3.4.1 Large scale production of in-house R-PAT-CMs 92

3.4.2 The hiPSC-CMs culture condition variations and quality control characteristics 96

3.4.3 The hiPSC-CMs culture conditions for CellOPTIQ..... 102

3.4.4 CellOPTIQ general principles 106

3.4.5 Drug assessment on R-PAT-CMs with seven 'training' (Tier1) drugs of known response. 113

3.5 Chapter Discussion 130

Chapter 4 Blinded compound testing in hiPSC-CMs.....133

4.1 Introduction 133

4.2 Tier 2 blinded test 133

4.2.1 Selection of drugs 135

4.2.2 Drug distribution and handling 136

4.2.3 CellOPTIQ blinded experimental layout 136

4.2.4 Evaluation and analysis parameters 136

4.2.5 The unblinding process 139

4.3 Chapter aims and objectives 140

4.4 Results 141

4.4.1 Blinded testing..... 147

4.4.2 Blinded test on top 10 priority drugs with iCell², Pluricyte and R-PAT-CMs 147

4.4.3 Blinded test with drugs rank 11 onwards on R-PAT-CMs 164

4.4.4 Blinded evaluation and assignment of Tier 2 drugs set across CRACK-IT partners 185

4.4.5 Predictivity scoring 191

4.4.6 The platform: cell-combination sensitivity 193

4.4.7 Informative parameter 196

4.5 Chapter discussion 197

4.5.1 The response and predictivity of different hiPSC-CMs lines 197

4.5.2 Predictivity evaluation of CellOPTIQ:hiPSC-CMs combination 197

4.5.3 Positive inotropy limitations 198

4.5.4 Negative inotropy limitations 199

4.5.5 Comparisons across other CRACK-IT platforms 200

4.5.6 Drugs integrated mechanism of action and *in-vitro* predictivity ... 201

4.5.7 Summary 201

Chapter 5 : Refinement to improve drug safety prediction 202

5.1 Introduction 202

5.1.1 Understanding the incorrect prediction of positive inotropes 202

5.1.2 Ivabradine as an agent to decrease spontaneous beating frequency 205

5.1.3 Short- term and long-term incubation of the drugs 207

5.1.4 RTCA CardioECR 207

5.2 Chapter aims and objectives 209

5.3 Results 210

5.3.1 Culture conditions refinement 210

5.3.2 Retesting under the refined conditions 216

5.3.3 Long-term exposure of the drugs to improve NE outcomes 227

5.3.4 RTCA CardioECR 228

5.4 Chapter discussion 235

Chapter 6 : Genome-edited hESC (hPSCs) as Tools to Study the Functionality of SSeta$_2$-adrenergic Receptor Polymorphisms 239

6.1 Introduction 239

6.2 SSeta-adrenergic receptors (ßARs) 240

6.2.1 ß-blockers 241

6.2.2 ß-agonists 241

6.2.3 Inconsistency in therapeutic response 242

6.3 SSeta$_2$-adrenergic receptor (ß$_2$AR) and their polymorphisms 243

6.3.1 ß$_2$AR polymorphisms in relation to cardiovascular diseases 245

6.3.2 SSeta$_2$-adrenergic receptor (ß$_2$AR) signal transduction 246

6.3.3 Desensitisation 249

6.4 Models to study positions 16 and 27 polymorphisms 251

6.5 ß$_2$AR Isogenic Lines 251

6.6 Human pluripotent stem cell-derived cardiomyocytes (hPSC-CMs) 252

6.7 Chapter rationale and objectives 253

6.8 Results 254

6.8.1 Generation of ß$_2$AR isogenic variants 254

6.8.2 Genotyping confirmation of genome-edited ß$_2$AR isogenic variants 259

6.8.3 Pluripotency characterisation of successful modified clones 261

6.8.4 Generation and cardiac differentiation efficiency of ß$_2$AR isogenic variants 263

6.8.5 Gene expression profiles of beta-adrenergic systems 265

6.8.6 Beta-adrenergic function by the cAMP accumulation 266

6.9 Functional assay to investigate the difference in the polymorphisms of ß$_2$AR isogenic hESC-CMs variants 271

6.9.1 GloSensor™ cAMP measurement assay 272

6.9.2 Optimisation of cultures condition for high-efficiency hESC-CMs transfection 275

6.9.3 Measurement of real-time intracellular cAMP production in response to Isoprenaline treatment by GloSensor™ cAMP Technology 277

6.9.4 β_2AR functional differences; desensitisation in acute and chronic phases 284

6.9.5 Acute short-term desensitisation 285

6.9.6 Chronic long-term desensitisation 299

6.10 Chapter discussion and conclusion 302

Chapter 7 General Discussion 306

7.1 Fulfilment of thesis objectives 308

7.1.1 Objective 1: Establish the CellOPTIQ drug screening system by sequentially analysing contractility and voltage output by validating 'training' sets of drug compounds and developing the culture systems.. 308

7.1.2 Objective 2: Blinded compound testing in hiPSC-CMs 308

7.1.3 Objective 3: To refine and improve the CellOPTIQ and culture system after 'unblinding', if needed. 309

7.1.4 Objective 4: To investigate the β_2-adrenergic receptor polymorphism via gene-induced changes to cell function by utilising genome-editing hPSC-CMs 309

7.2 Limitation of the study 311

7.2.1 Drug-induced changes chapters 311

7.2.2 Gene-induced changes chapters 312

7.3 Implications of this investigation 313

7.3.1 3Rs (Replacement, reduction and refinement) 313

7.3.2 In-vitro clinical trials 313

7.3.3 Commercialisation 313

7.4 Final remarks and future work 314

7.4.1 Drug-induced changes chapters 314

7.4.2 Gene-induced changes chapter 315

References 316

List of Figures

Figure 1.1: Conventional pharmaceutical compares to iPSC-based drug discovery. 30

Figure 1.2: Small and large animal cardiac differences relative to humans. .. 33

Figure 1.3: Overview of CiPA elements. Taken from Gintant et al. (2016) 36

Figure 1.4: Action potential overview. 39

Figure 1.5:Structure involved in excitation-contraction (EC) coupling. 41

Figure 1.6: Illustration of human embryonic stem cells (hESCs) and human induced pluripotent stem cell (hiPSCs) derivation. 45

Figure 1.7: The reprogramming delivery methods and reprogramming factors for making induced pluripotent stem cells. 46

Figure 1.8: Schematic illustration for differentiation methods for hPSC-CMs. 48

Figure 1.9: Schematic representation of differentiation stages, signalling pathway and cellular markers for cardiac lineage commitment. 49

Figure 1.10: Illustration of a cell showing the rationale of different measurable properties of cardiomyocytes along with methods used to analyse. 59

Figure 1.11: Generation, engineering and utility of hPSC-CMs. 65

Figure 1.12: Schematic representation of βAR function in cardiomyocytes ... 66

Figure 3.1: Schematic illustration for the drug-targeted mechanism of actions and pathways influencing the cardiomyocytes contraction. 91

Figure 3.2: Large-scale R-PAT differentiation and cardiomyocytes purity. 93

Figure 3.3: Recovery of R-PAT-CMs after cryopreservation. 95

Figure 3.4: Cardiac ventricular and atrial subtype in hiPSC-CMs (R-PAT, iCell^2 and Pluricyte) by immunostaining analysis of MLC-2a and MLC-2v. 98

Figure 3.5: Example of good and bad sarcomeric organisation in CMs based on MLC-2v expression. 99

Figure 3.6: Connexin-43 (Cx43) in hiPSC-CMs (R-PAT, iCell^2 and Pluricyte) by immunostaining analysis of α-actinin and Cx43. 101

Figure 3.7: Optimum culture conditions for cryopreserved R-PAT-CMs..... 104

Figure 3.8: Schematic description and proposed parameters for contraction and voltage measurement to quantify drug effects in hiPSC-CMs..... 107

Figure 3.9: CellOPTIQ electronic pacing 108

Figure 3.10: Contractility baseline characterisation under electrical pacing for R-PAT-CMs, iCell^2 and Pluricyte. 110

Figure 3.11: Voltage electrophysiology baseline characterisation under electrical pacing for R-PAT-CMs, iCell^2 and Pluricyte 112

Figure 3.12: The mode of action for listed Tier 1 drugs and cardiac signalling pathways. 114

Figure 3.13: Contractility and voltage electrophysiological analysis of R-PAT-CMs treated with isoprenaline. 116

Figure 3.14: Contractility and voltage electrophysiological analysis of R-PAT-CMs treated with digoxin. 118

Figure 3.15: Contractility and voltage electrophysiological analysis of R-PAT-CMs treated with Bay K 8644. 120

Figure 3.16: Contractility and voltage electrophysiological analysis of R-PAT-CMs treated with EMD 50377. 122

Figure 3.17: Contractility and voltage electrophysiological analysis of R-PAT-CMs treated with nifedipine. 124

Figure 3.18: Contractility and voltage electrophysiological analysis of R-PAT-CMs treated with ryanodine. 126

Figure 3.19: Contractility and voltage electrophysiological analysis of R-PAT-CMs treated with thapsigargin. 128

Figure 3.20: Schematic description of the parameters to be used to quantify drug effects in hiPSC-CMs. 132

Figure 4.1: Tier 2 blinded test flow chart as part of the CRACK-IT consortium 135

Figure 4.2: Schematic description for parameters used to quantify the drug effects and terminology used to evaluate the response in hiPSC-CMs. 138

Figure 4.3 Contractility and voltage electrophysiological analysis of iCell^2, Pluricyte and R-PAT-CMs treated with epinephrine. 150

Figure 4.4: Contractility and voltage electrophysiological analysis of iCell^2, Pluricyte and R-PAT-CMs treated with forskolin. 151

Figure 4.5: Contractility and voltage electrophysiological analysis of iCell^2, Pluricyte and R-PAT-CMs, treated with levosimendan 152

Figure 4.6: Contractility and voltage electrophysiological analysis of iCell^2, Pluricyte and R-PAT-CMs treated with pimobendan 153

Figure 4.7: Contractility and voltage electrophysiological analysis of iCell^2, Pluricyte and R-PAT-CMs treated with acetylsalicylic acid. 155

Figure 4.8: Contractility and voltage electrophysiological analysis of iCell^2, Pluricyte and R-PAT-CMs treated with atenolol 156

Figure 4.9: Contractility and voltage electrophysiological analysis of iCell^2, Pluricyte and R-PAT-CMs treated with verapamil 159

Figure 4.10: Contractility and voltage electrophysiological analysis of iCell^2, Pluricyte and R-PAT-CMs treated with doxorubicin 160

Figure 4.11: Contractility and voltage electrophysiological analysis of iCell^2, Pluricyte and R-PAT-CMs treated with sunitinib 162

Figure 4.12: Contractility and voltage electrophysiological analysis of iCell^2, Pluricytes and R-PAT-CMs treated with captopril. 163

Figure 4.13: Contractility and voltage electrophysiological analysis of and R-PAT-CMs treated with dobutamine. 168

Figure 4.14: Contractility and voltage electrophysiological analysis of and R-PAT-CMs treated with glibenclamide. 169

Figure 4.15: Contractility and voltage electrophysiological analysis of and R-PAT-CMs treated with milrinone. 170

Figure 4.16: Contractility and voltage electrophysiological analysis of and R-PAT-CMs treated with omecamtiv mecarbil. 171

Figure 4.17: Contractility and voltage electrophysiological analysis of and R-PAT-CMs treated with enalaprilat. 172

Figure 4.18: Contractility and voltage electrophysiological analysis of and R-PAT-CMs treated with citalopram..... 173

Figure 4.19: Contractility and voltage electrophysiological analysis of and R-PAT-CMs treated with clonidine..... 174

Figure 4.20: Contractility and voltage electrophysiological analysis of and R-PAT-CMs treated with itraconazole..... 175

Figure 4.21: Contractility and voltage electrophysiological analysis of and R-PAT-CMs treated with sorafenib. 176

Figure 4.22: Contractility and voltage electrophysiological analysis of and R-PAT-CMs treated with ivabradine. 177

Figure 4.23: Contractility and voltage electrophysiological analysis of and R-PAT-CMs treated with terbutaline. 178

Figure 4.24: Contractility and voltage electrophysiological analysis of and R-PAT-CMs treated with flecainide..... 179

Figure 4.25: Contractility and voltage electrophysiological analysis of and R-PAT-CMs treated with paracetamol. 180

Figure 4.26: Contractility and electrophysiological voltage analysis of and R-PAT-CMs treated with phentolamine. 181

Figure 4.27: Contractility and voltage electrophysiological analysis of and R-PAT-CMs treated with tolbutamide. 182

Figure 4.28: Contractility and voltage electrophysiological analysis of and R-PAT-CMs treated with pravastatin. 183

Figure 4.29: Contractility and voltage electrophysiological analysis of R-PAT-CMs treated with sildenafil. 184

Figure 4.30: Most informative contractility marker for inotropes prediction. 196

Figure 5.1: High variance between data masks drug effect and causes poor sensitivity of prediction. 203

Figure 5.2: Cardiomyocytes paced at a different cycle length (333 ms lowest, highest 2000 ms) and their potency information generated from positive inotropes. 204

Figure 5.3: Mechanism of action for ivabradine 205

Figure 5.4: Ivabradine decreased the spontaneous beating frequency. 206

Figure 5.5: The components of xCELLigence Real-Time Cell Analysis (RTCA) CardioECR System. 208

Figure 5.6: No difference in spontaneous beating rates between fresh and cryo R-PAT-CMs. 210

Figure 5.7: The ivabradine decrease spontaneous beating rates without changing contraction parameters..... 212

Figure 5.8: The protein-free medium (SFM) increases spontaneous beating rates and data distribution. 214

Figure 5.9: Epinephrine retesting in R-PAT-CMs under refined conditions. ... 217

Figure 5.10: Forskolin retesting in R-PAT-CMs under refined conditions. 218

Figure 5.11: Levosimendan retesting in R-PAT-CMs under refined conditions. 219

Figure 5.12: Pimobendan retesting in R-PAT-CMs under refined conditions. . 220

Figure 5.13: Dobutamine retesting in R-PAT-CMs under refined conditions. . 221

Figure 5.14: Milrinone retesting in R-PAT-CMs under refined conditions..... 222

Figure 5.15: Omecamtiv mecarbil retesting in R-PAT-CMs under refined conditions. 223

Figure 5.16: Terbutaline retesting in R-PAT-CMs under refined conditions... 224

Figure 5.17: Prolonged exposure detects NIs in CellOPTIQ-R-PAT-CMs culture. 227

Figure 5.18: Contractility analysis of R-PAT-CMs treated with long-term exposure of the highest doxorubicin concentration (100 µM) in the RTCA CardioECR platform. 229

Figure 5.19: Contractility analysis of R-PAT-CMs treated with long-term exposure of highest doxorubicin concentration (100 µM) in RTCA CardioECR platform. 231

Figure 5.20: Contractility analysis of R-PAT-CMs treated with long-term exposure of highest levosimendan concentration (1 µM) in RTCA CardioECR platform. 232

Figure 5.21: Contractility analysis of R-PAT-CMs treated with long-term exposure of highest acetylsalicylic acid concentration (1000 μM) on the RTCA CardioECR platform. 233

Figure 6.1: Schematic diagram of GPCR pharmacogenomics. 240

Figure 6.2: The $ß_2$AR gene (OMIM=109690) with polymorphism at codon position 16 and 27..... 244

Figure 6.3: Schematic diagram ß-adrenergic receptor (ßAR) via adenylyl cyclase signalling cascade..... 247

Figure 6.4: ßeta2-adrenergic signalling regulation..... 248

Figure 6.5: $ß_2$AR desensitisation pathways. 250

Figure 6.6: Overview of the works. 254

Figure 6.7: The general CRISPR/Cas9-*PiggyBac* editing strategy for SNPs position 16 and 27 of HUES7 hESCs *ADRB2* locus. 256

Figure 6.8: The targeting strategy introduced changes at nucleotide position 46 and 79 (nonsynonymous in peptide) and 124 and 126 (synonymous in peptide) as indicated. 258

Figure 6.9: Genotyping confirmation of engineered $ß_2$AR isogenic variants derived from a conventional two-step Footprint free and Shortcut approach. 260

Figure 6.10: Cell culture, karyotyping and phenotype assessment of $ß_2$AR isogenic variants (GE, GQ, RE and RQ) 262

Figure 6.11: Generation and cardiac differentiation efficiency of $ß_2$AR isogenic variants..... 264

Figure 6.12: ßeta-adrenergic gene expression profile of $ß_2$AR isogenic hESC-CMs. 266

Figure 6.13: Accumulation of cAMP as measured through the incorporation of tritiated adenine..... 270

Figure 6.14: Description of GloSensor™ cAMP Technology. The cAMP assay based on luminescence intensity..... 273

Figure 6.15: Representation of GloSensor™ cAMP reporter assay to quantify βARs activity 274

Figure 6.16: Efficiency of Lipofectamine 3000 mediated transfection of GE hESC-CMs 276

Figure 6.17: An overview of the GloSensor™-20F cAMP Assay. 279

Figure 6.18: Kinetic response of the GloSensor™-20F cAMP Assay. 280

Figure 6.19: GloSensor™-20F cAMP assay to determine β_1AR and β_2AR kinetics profile in β_2AR isogenic hESC-CMs. 281

Figure 6.20: Real-time cAMP Glosensor™ luminescence kinetic profile for β_2AR isogenic hESC-CMs treated with the antagonist and stimulated with β-agonist (ISO) 283

Figure 6.21: Acute and chronic phases of desensitisation. 284

Figure 6.22: Layout for acute short-term desensitisation (2 hours and 30 minutes ISO pretreatment) followed by ISO acute rechallenge and FSK induction. 286

Figure 6.23: The effects of short-term ISO exposure ISO (30 minutes and 2 hours) over β_2AR isogenic hESC-CMs variants; 288

Figure 6.24: Measured metrics to quantitate the difference in β_2AR response between isogenic hESC-CMs over acute short-term desensitisation. 289

Figure 6.25: cAMP response on ISO induced acute short term desensitisation after being untreated, 30 minutes and 2 hours of 1 μM ISO pretreatment. ... 291

Figure 6.26: Percentage of cAMP change relative to No ISO pretreatment with 30 minutes and 2 hours of 1 μM ISO pretreatment. 293

Figure 6.27: Percentage of β_2AR desensitisation (uncoupling) relative to No ISO pretreatment in 30 minutes and 2 hours of 1 μM ISO pretreatment. 294

Figure 6.28: Rate of receptor activation based on linear regression of cAMP up. 296

Figure 6.29: Rate of receptor uncoupling based on linear regression of cAMP down. 298

Figure 6.30: Layout for chronic long-term desensitisation (24 hours 10 μM ISO pretreatment) followed by ISO acute rechallenge and FSK induction. 299

Figure 6.31: The effects of long-term ISO exposure ISO (24 hours 10 μM ISO) over β2AR isogenic hESC-CMs variants..... 300

Figure 6.32: Percentage of cAMP change relative to No ISO pretreatment in 24 hours of 10 μM ISO pretreatment. 301

List of Tables

Table 1.1: : Example of hPSC-CMs monolayer cardiac differentiation protocols and Nottingham cardiac differentiation protocol in the red box. The other cell types that may present other than cardiomyocytes (CMs) are include endothelial cells, smooth muscle cells and fibroblasts. 51

Table 1.2: The difference between fetal cardiomyocytes, hPSC-CM and adult cardiomyocyte. The table is taken from Jiang et al., (2018)..... 55

Table 1.3: Overview of the main characteristics of electrophysiology and contractility methods currently used for hPSC-CMs functionality analysis. Table adapted from (Laurila et al., 2016..... 60

Table 2.1: Lipofectamine 3000 transfection reagents and complexes mixture. 72

Table 2.2: Antibodies used for pluripotent hPSCs immunostaining..... 75

Table 2.3: Antibodies used for hPSC-CMs immunostaining..... 76

Table 2.4: Table of drugs used for training. 78

Table 2.5: Table of drugs used for blinded drug assessment. 79

Table 3.1: The details of Tier 1 'training set' drugs with known positive (PI) or negative inotropic (NI) effects, and the outcomes. 129

Table 4.1: Established working Standard Operating Procedures (SOPs) for CellOPTIQ (CO) platforms. 134

Table 4.2: The rank, drugs coding number of blinded test drugs and drugs name with their assignation after unblinding by GSK. 141

Table 4.3: Detailed information about Tier 2 blinded drugs within the CRACK-IT study. 142

Table 4.4: Effects of compounds on cardiomyocyte contractility *in vitro*. ... 185

Table 4.5: Predictivity scoring for hiPSC-CMs in CellOPTIQ (CO) platform based on correct PI, NE and NI. 191

Table 4.6: Predictivity scoring of data from all platform-cell combinations. 192

Table 4.7: Sensitivity of platform-cell combinations for predicting PIs. 194

Table 4.8: Sensitivity of platform-cell combinations for predicting NIs. 195

Table 5.1: Refined contractility Standard Operating Procedures (SOPs) for R-PAT-CMs testing in CellOPTIQ. 215

Table 5.2: The details R-PAT-CMs retesting of Tier 2 positive inotrope (PI) drugs: the outcomes under refined conditions. 226

Table 5.3: The long-term exposure to drugs on the RTCA CardioECR platform and their respective outcomes. 234

Table 6.1: Summary of *ADRB2* polymorphisms at position 16 and 27. G(allele)=GGA(codon)/Gly/Glycine(amino acid); R = AGA/Arg/Arginine; Q=CAA/Gln/Glutamine; E= GAA/Glu/Glutamic Acid 245

Table 6.2: The *ADRB2* gene polymorphisms characteristics and their functional implications to ischemic heart failure. 250

Table 6.3: Summary of *ADRB2* gene editing. 256

Table 6.4: The EC_{50} and E_{max} values of ISO concentration curves 269

Table 6.5: The average percentage of maximum cAMP response 287

Abbreviations

Abbreviation	Description
%	Percentage
ANOVA	Analysis of variance
cDNA	Complementary DNA
CM	Cardiomyocyte
CRISPR	Clustered Regularly Interspaced Short Palindromic Repeats
DAPI	Di-amino phenyl-indole
DMEM	Dulbecco's (Modified Eagle's) minimal essential medium
DMSO	Dimethyl sulfoxide
DNA	Deoxyribonucleic acid
dNTP	Deoxyribonucleotide triphosphate
DPBS	Dulbecco's Phosphate Buffered Saline
DSB	Double-strand break
E8	Essential 8 medium
gDNA	Genomic DNA
HDR	Homology-directed repair
hESC	Human embryonic stem cell
hESC-CM	Human embryonic stem cell derived cardiomyocyte
hiPSC	Human induced pluripotent stem cell
hiPSC-CM	Human induced pluripotent stem cell derived cardiomyocyte
hPSC	Human pluripotent stem cell
hPSC-CM	Human pluripotent stem cell derived cardiomyocyte
NEAA	Non-essential amino acids
NHEJ	Non-homologous end joining
PBS	Phosphate buffered saline
PCR	Polymerase chain reaction
RLU	Relative luminescence units
RNA	Ribonucleic acid
ROCKi	Rho-associated kinase inhibitor
RT-PCR	Reverse transcriptase PCR
SEM	Standard error of the mean
SERCA	Sarcoplasmic reticulum Ca^{2+}-ATPase
sgRNA	Single guide RNA

SNP	Single nucleotide polymorphism
SR	Sarcoplasmic reticulum
TALEN	Transcription activator-like effector nuclease
hERG	human ether-a-go-go gene
ADRB2	Adrenoreceptor beta 2
ADRB1	Adrenoreceptor beta 1
CO	CellOPTIQ
EHTs	Engineered heart tissues
TTM	Triple transient measurement
APD	Action potential duration
CA	Contraction Amplitude
CT	Contraction Time
RT	Relaxation Time
βARs	βeta-adrenergic receptors
β_2AR	β_2 adrenergic receptor
B_1AR	B_1 adrenergic receptor
GPCRs	G-protein coupled receptors
GE	Gly16Glu27
GQ	Gly16Gln27
RE	Arg16Glu27
RQ	Arg16Gln27
^{0}C	Degree Celsius
7TMRs	Seven-transmembrane

Chapter 1 Introduction

In the past decade, drug discovery and disease modelling have been and continue to be a challenge. Numerous drugs are associated with various cardiovascular side effects, such as lethal arrhythmias, reduced ventricular ejection fraction and heart failure (Sharma et al., 2018). In that respect, 8.5% of phase II drugs in development have failed (Arrowsmith and Miller, 2013) and 28% of drugs have been withdrawn from the USA market due to unexpected cardiotoxicity (Gwathmey et al., 2009). On the other hand, numerous genetic mutations or polymorphisms have been implicated in cardiovascular diseases. Correspondingly, variations in genetics, epigenetics and non-genetic environmental factors have contributed to different responses in drug toxicity and gene function.

For this reason, cardiotoxicities and efficacy may only be revealed during the later phase of drug development or after its release to the market. Two major factors contribute to this situation: 1) Inaccurate models or platforms to detect human cardiac response and 2) Genetic polymorphisms or interindividual variations across populations, which make detection difficult in a small cohort of patients (Magdy et al., 2018). Therefore, to overcome the limitations, a sensitive system must be developed to detect toxicity in the cardiac context together with patient-specific variation to improve treatment, which can ultimately lead to improvement in drug screening and disease modelling.

1.1 Drug discovery and development.

The pharmaceutical industry is currently experiencing a worrying trend, where the number of new chemical entities (NCEs) approved by regulatory agencies is gradually decreasing. For example, the number of NCEs approved by United States Food and Drug Administration (FDA) declined from 35 in 1997 to 16 in 2010 (Killeen, 2012). This indirectly increases the cost of developing a new drug as such new drug development can take between 5 to 10 years from preclinical to FDA approval, costing an estimated $1395 million per compound approval (DiMasi et al., 2003, DiMasi et al., 2016).

Indeed, very few molecules reach development and are ultimately approved as drugs; for example, out of 10000 compounds that passed initial screening assay, fewer than ten made it into the clinical trial, and only two were eventually approved (Golan and Tashjian, 2012). Whether unapproved drugs cause harm to patients remains uncertain. During phase II (shorter follow-up) and phase III (longer follow up) of clinical trials, safety failure rates are 22% and 35% respectively (Arrowsmith and Miller, 2013). This increase in failure from phase II to III occurs mainly because many drug toxicities progress chronically over time (longer trials) and only becomes apparent in larger numbers of patients in broader populations (Arrowsmith and Miller, 2013). Accordingly, this reflects that current methodologies for premarket screening can only detect toxicities that are common and develop within a shorter time, indirectly overlooking potential adverse cardiac events (Magdy et al., 2018).

1.1.1 Drug withdrawal

Between January 1990 to August 2009, after post-marketing, 41 pharmaceutical products were withdrawn from the market due to serious adverse events (Killeen, 2012). The highest recalls, accounting for 14% of all recalls, were associated with a cardiovascular system (Killeen, 2012). Such withdrawals not only exacerbate the negative image of a specific drug in the public eye but also influences the sale of drugs that have a similar mechanism of action, which consequently causes an economic burden. For example, the closing share price of Rofecoxib (Vioxx) fell dramatically from $45.09 in September 2004 to $26.8 in November 2004 and voluntarily withdrawn from worldwide market after a study found patients taking the drug for long-term basis faced double the risk of heart attack relative to placebo (Killeen, 2012, Sibbald, 2004). Interestingly Rofecoxib had been available on the market for five years (1999-2004), with the first drug-induced cardiotoxicity reported in 2002 (Onakpoya et al., 2016). The drugs withdrawal happened because existing drug screening for candidate molecules was insufficient to identify adverse effects during compound development.

1.1.2 Functional and structural toxicity

Drug toxicity remains as the primary component of drug withdrawal, while cardiotoxicity accounted for one-third of drug discontinuation (MacDonald and Robertson, 2009). Among the causes of drug-induced toxicity can be functional and/or structural toxicity in nature. In the context of cardiotoxicity, functional toxicity contributes to the change in cardiac electrophysiology or cardiac beating by changes in cardiac ion channels (for example hERG) and changes in QT interval (Doherty et al., 2015). Subsequently, this cause alteration to the mechanical function of myocardium (Pointon et al., 2013). While structural toxicity cause changes and damage to the structural integrity of cardiac tissue such as direct cardiomyocytes damage and mitochondrial injury. This lead to morphological damage or loss of viability which further contributes to heart diseases such as heart failure, cardiomyopathy, myocardial infarction and necrosis (Doherty et al., 2015).

The sequence of functional or structural toxicity manifestation is compound-specific, as such one compound could cause structural toxicity while the functional toxicity only appeared months after structural defects. As the consequences, most toxicity only manifested at the post-approval stage of drug development.

1.1.3 Drug monitoring, response and efficiency

After drug development comes drug monitoring, which aims not only to reduce toxicity but also to enhance efficacy. Most patients will gain the desired drug effects, but some may suffer detrimentally or gain no benefit (Stingl et al., 2015). A classic example was drugs based on digitalis, which used to treat congestive heart failure; while many patients monitored with congestive heart failure were efficiently treated, toxicity was also recorded (Dasgupta, 2012). Therapeutic drug monitoring is hard as it must take into account the influence of many factors, including genetic polymorphism and considerable interindividual variation, making individualised drug dosage exceedingly challenging (Ghiculescu, 2008).

1.1.4 Conventional drug discovery and new alternative methods

Conventional drug discovery involves less than ideal non-human (animal) models after a large laboratory and preclinical test **(Figure 1.1).** The current approach by the pharmaceutical industry involves *in-vitro* cell lines such as overexpression and transformed cell lines. These *in-vitro* models do not recapitulate complex biology in human. This cause drugs failed to be developed or marketed due to imprecise prediction of their safety and efficacy by using conventional approaches. Therefore there is a need to use alternative functional human models such as hiPSC-CMs, disease on-chip, organ on-chip or body on-chip for comprehensive toxicity study and as an addition to the conventional drug screening process. In more advance model, the incorporation of multiple 'organ' on-chip does not only accurately test the toxicity of inhaled/administered parent compounds, but also their liver-based metabolite (liver is the primary organ for compound metabolisation). This may alter the toxicity profile of the administered compound (Bovard et al., 2018).

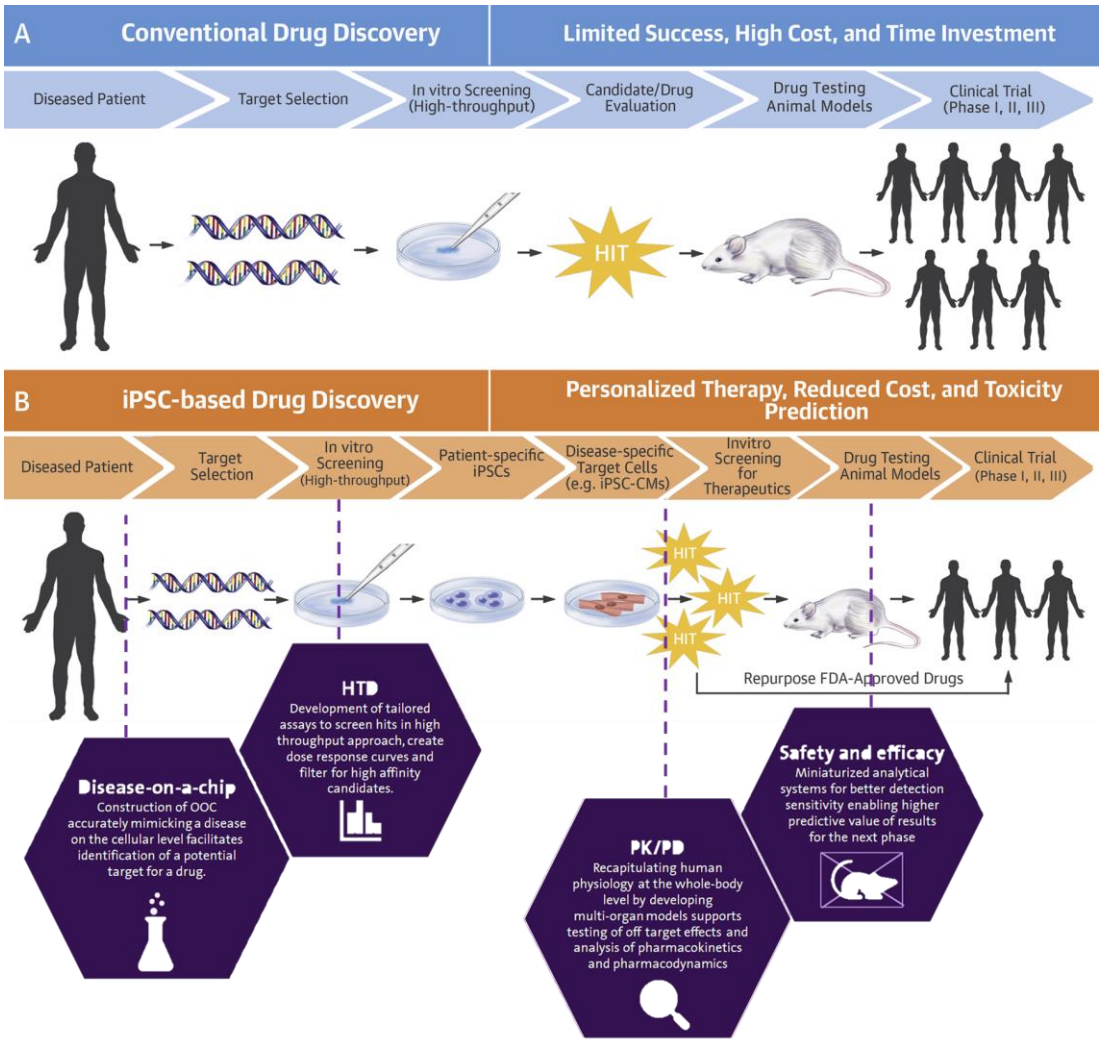


Figure 1.1: Conventional pharmaceutical compares to iPSC-based drug discovery.

(A) The conventional pharmaceutical drug discovery process is inefficient with high attrition rate due to the dependence of animal/non-animal models that do not recapitulate human pathophysiology. **(B)** Alternative technologies may add value and provide improved prediction tools that allow the decision to be made earlier during drug development. Modified from (Sayed et al., 2016a).

1.2 Cardiovascular disease

Cardiovascular disease (CVD) remains the number one cause of mortality. Often the problems related to CVD are adverse effects of drugs to patients and the variation of the effectiveness of these drugs treatments according to various groups of people in the population. This is because most medical interventions are based on averagely healthy patients using a 'one size fits all' approach which ignores interindividual genetic and epigenetic variation. Consequently, while

some drugs treatments are successful, others may be ineffective or worse, detrimental, for some patients. As already identified, interindividual variation, environment factor and or genetic polymorphism contribute to this. Polymorphism variations that affect cardiovascular response include CYP2D6, CYP2C9, CYP3A4, β_1-adrenergic receptor (*Ser4Gly, Arg389Gly*) and β_2-adrenergic receptor (*Arg16Gly, Gln27Glu*) (Ma and Lu, 2011, Humma and Terra, 2002, Stingl et al., 2015).

1.2.1 Disease Modelling

Before patient-specific and genome editing of *in-vitro* models existed, knowledge about disease models was gained by understanding healthy and diseased animals and transformed cell lines. Despite the proven success and relevance of *in-vivo* animal testing for cardiac adverse events, some liabilities have only been detected in patients with different susceptibilities (i.e. age, gender, genetic, etc.)(Guth et al., 2019a). Meanwhile, immortalised transformed cell lines such as human embryonic kidney (HEK) and Chinese hamster ovary (CHO), are engineered to overexpress ion-channels that are not precisely functioning during normal and pathological conditions (Rajamohan et al., 2013). Furthermore, those cells have tendencies to accumulate mutation and are immune to newly developed drug-induced toxicity (Liang et al., 2013).

For this purpose, the advancement of studies at the genomic and functional level has brought the gap closer with regards to understand human cardiovascular diseases at the individual level, primarily in the area of precise prediction, prevention and therapy. Studies looking at the improvement of the correlation between the patient's genotype-phenotype have revealed how genetic differences among individuals can determine their response to therapies. To make sure that predictions are as accurate as possible, there is a need for a model that recapitulates particular individual disease or polymorphism variation, together with high-quality cardiac differentiation and an excellent platform to quantify both characterisation and functional assay.

1.3 Clinical and preclinical cardiac safety screening in drug development

During drug discovery and development, the preclinical cardiac safety and efficacy investigations are done with the use of a relatively small number of experimental systems such as isolated cardiac tissue, isolated heart and *in-vivo* animals models to predict clinical events (Killeen, 2012).

1.3.1 Human primary cardiomyocytes

Ideally, the most acceptable system is human primary cardiomyocytes (CMs). However, the availability of healthy primary human CMs is extremely limited, and the harvesting is time-consuming and labour-intensive. Even within hours after isolation under the physiological temperature of 37ºC, the important expression, activity, density, localisation of T-tubules, ion channels and contractile machinery can be altered (Louch et al., 2011). Therefore, critical attention needs to be given to obtaining physiologically relevant data from this of primary CMs. In addition, these cells are mitotically inactive; they have a limited life span, which means that they do not last long in culture and therefore, have low throughput for cardiotoxic or response measurement (Killeen, 2012). The human primary cardiomyocytes are also challenging to work for functionality tests as their adhesiveness to common cell culture is low and coculture is impossible as they do not bind to other cultured cells (Bird et al., 2003). They are also unsuitable for disease models, as they are limited in quantities in specific pathological phenotype phases and are limited in terms of genetic variety that reflects the healthy and diseased phenomenon (Casini et al., 2017, Ribeiro et al., 2019).

1.3.2 Animal models

One of the earliest methods used in the preclinical evaluation of cardiotoxicity is based on animal models. However, the cardiac physiology of animals is relatively different from humans due to species-specific factors, and there is no ideal animal model available for cardiac research (Mercola et al., 2013, Milani-Nejad and Janssen, 2014).

1.3.2.1 Small animal models

Although small animal models and the human heart share some similar properties, for example, the ionic current between mouse and the human heart is nearly identical (Nerbonne et al., 2001), there is a striking difference between the mouse and the human heart. The resting heart rate of a mouse ranges between ~500 to 700 beats per minutes, which is approximately ten times the human resting heart rate. The difference in cardiac contractile kinetics is highlighted in **Figure 1.2A** (Janssen et al., 2016).

1.3.2.2 Large animal models

Larger animals such as rabbits, canines, swine and sheep which appear to have more similar electrophysiology, cardiac contractile and kinetics relative to humans, nonetheless exhibit variations **Figure 1.2B** (Dixon and Spinale, 2009, Schmitto et al., 2010, Milani-Nejad and Janssen, 2014). Besides, the use of a large animal model for high throughput screening is not feasible due to ethical reasons and the high cost of animal maintenance (Avior et al., 2016).

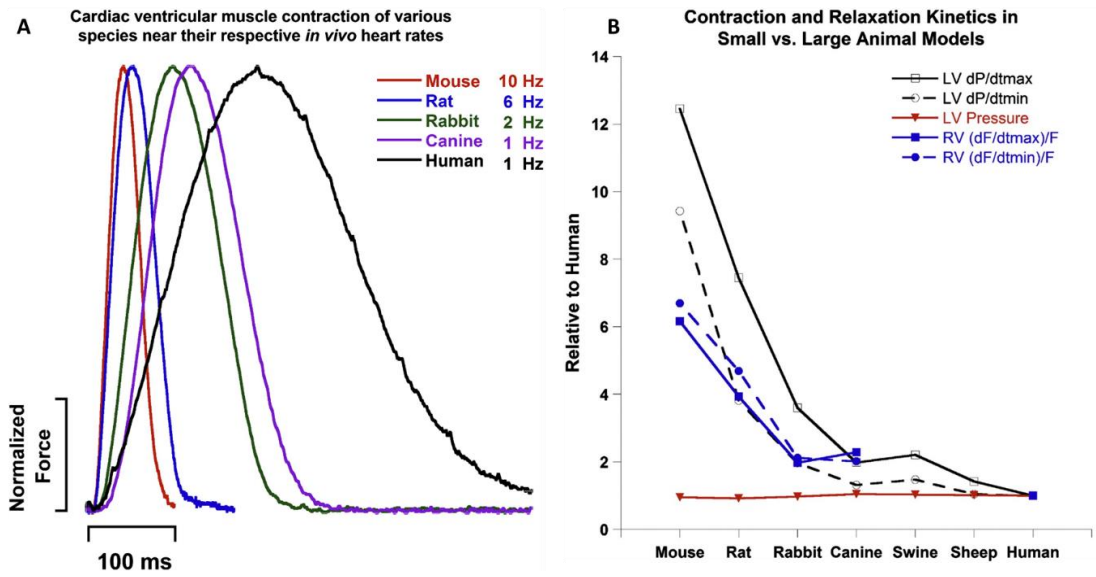


Figure 1.2: Small and large animal cardiac differences relative to humans.

A) Tracing of resting heart rates. B) Contractile and relaxation parameters normalised to human value. The larger the animal, the more it is similar to humans. LV dP/dtmax; left ventricular maximal rate of pressure rise, LV dP/dtmin; left ventricular maximal rate of pressure decline, RV (dF/dtmax)/F; maximal velocity of contraction divided by developed force in right ventricular trabeculae, RV (dF/dtmin)/F; maximal velocity of relaxation divided by developed force in right ventricular trabeculae. Picture taken from Milani-Nejad and Janssen (2014)

1.4 Safety guidelines and initiatives

1.4.1 ICH S7B

Preclinical cardiac safety experiments are viewed as important as information obtained from these can help to guide the clinical development of drugs. In 2005, the regulatory bodies of The International Council for Harmonisation of Technical Requirements for Pharmaceutical for Human Use (ICH) issued a guideline for preclinical and nonclinical safety assessments (Turner, 2019). The guideline ICH S7B aimed to integrate the assessment of hERG channel-related proarrhythmic risk of pharmaceutical into two primary assays (Friedrichs et al., 2005, ICH, 2005). The first assay focuses on the *in-vitro* measurement of the human ether-a-go-go gene (hERG) channel potassium current I_{Kr} using cell lines that express heterologous hERG. The second, an *in-vivo* QT assay, involves the use of animal models to test the effect of drugs on electrocardiographic (ECG) QT intervals.

However, testing hERG current in a non-cardiac cell that heterologously expresses hERG may not accurately reflect the electrophysiology of the human heart (Magdy et al., 2018). This is because they lack CM-specific structural components, such as sarcomeres (Sharma et al., 2018). Also, the inhibition of hERG alone is not predictive of cardiotoxicity as hERG is not the only ion channel that regulates ventricular repolarisation (Kramer et al., 2013). As evidence, for hERG assay, sensitivity is 64-82% while the specificity is 75-88% (Gintant, 2011, Wallis, 2010). This suggests that many non-cardiotoxic drugs can lead to false-positives and would be discarded at this stage, while tested drugs that can cause detrimental adverse cardiac events could pass the screening stage (Magdy et al., 2018).

1.4.2 ICH E14

Once a drug candidate has passed the *in-vitro* and *in-vivo* preclinical safety screening, the clinical evaluation guideline of ICH E14 suggests QT interval prolongation and potential proarrhythmic studies in humans (ICHE14, 2005). However, the QT interval prolongation alone is not an ideal predictive marker for cardiac arrhythmia risk (van Opstal et al., 2001). Furthermore, the combination of QT prolongation with hERG blockage is still debatable. For

example, in marketed drugs such as amiodarone and ranolazine which both tested positive in hERG blockage and QT prolongation in the human subject, their pro-arrhythmic effect in clinics is unusually low (Antzelevitch et al., 2004). Nonetheless, the success of the safety paradigm underpinning these guidelines is undeniable as such terfenadine, which was removed from the market worldwide due to QT interval prolongation, and since then no hERG channel association has been reported regarding any marketed drug (Kratz et al., 2017, Roy et al., 1996). In conclusion, while both guidelines have been useful to exclude some compounds from market release, there are concerns about low specificity and oversensitivity of these assays in detecting pro-arrhythmic potential (Sager et al., 2014).

1.4.3 Comprehensive *in-vitro* Proarrthymia Assay (CiPA)

To rectify this situation, in 2013, the FDA proposed The Comprehensive *in-vitro* Proarrthymia Assay (CiPA) initiative, supported by various international governments and commercial bodies (Fermini et al., 2016). The CiPA was a pioneering initiative that uses hiPSC-CMs in drug evaluation for proarrhythmia. Its aimed was to establish a new paradigm for assessing cardiac safety as opposed to those causing QT prolongation and beyond hERG block (Sharma et al., 2018). CiPA approaches were based on new technologies that identify cardiotoxic drugs: a) by evaluation of multiple cardiac ion channels as a tool to profile risk rather than hERG alone, b) by the use of *in-silico* computer modelling, c) by applying integrated biological systems of human induced pluripotent stem cell-derived cardiomyocytes (hiPSC-CMs) and d) through use of the human ECG which helps to estimate whether a drug is proarrhythmic or not, as illustrated in **Figure 1.3** (Colatsky et al., 2016, Blinova et al., 2018).

The CiPA study revealed high variability between test sites for individual drugs (Blinova et al., 2018). This is potentially associated with variability in the analysis platform, inter-operator, inter-lab and variation in culture conditions (Korte, 2019).

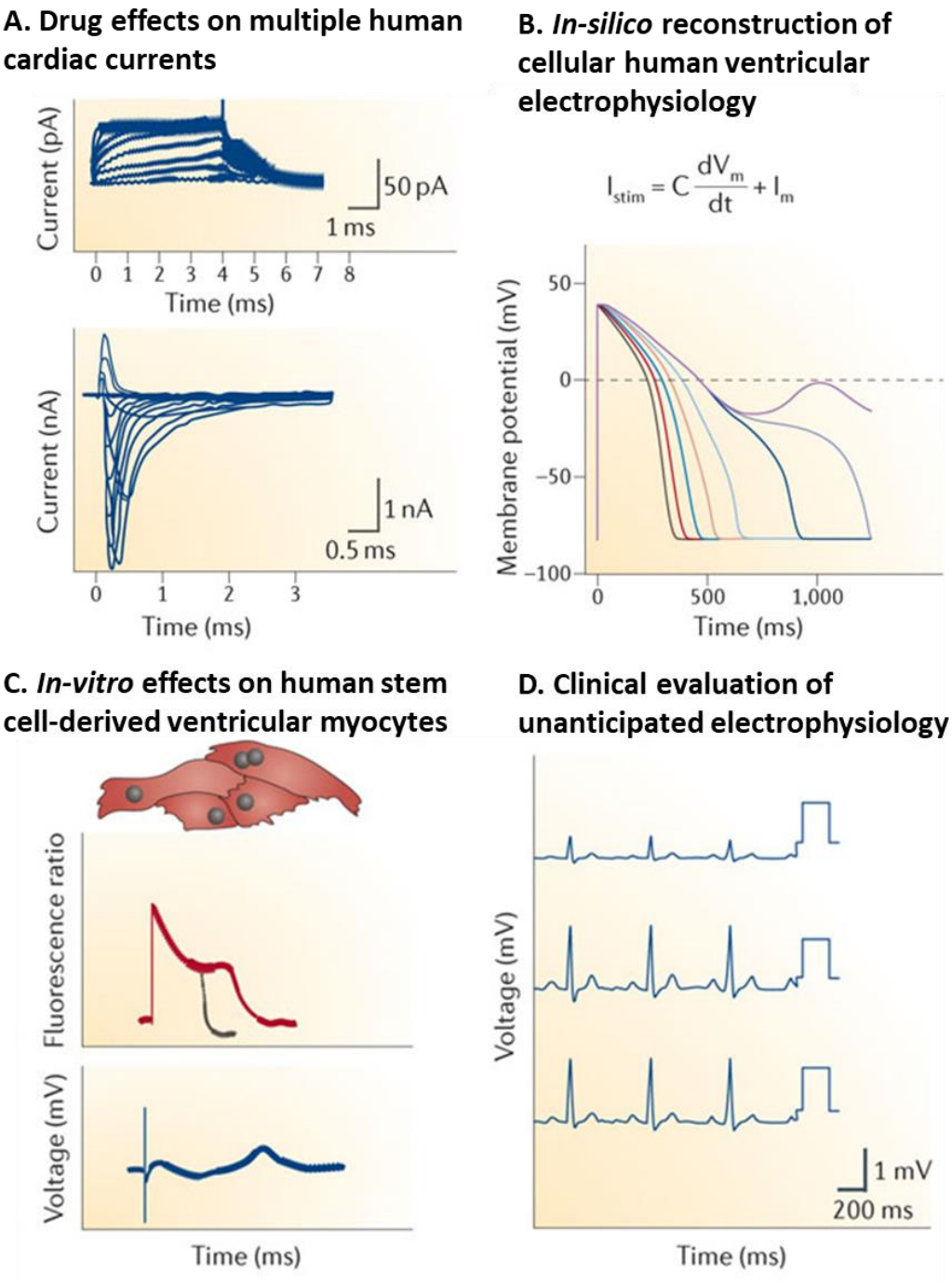


Figure 1.3: Overview of CiPA elements. Taken from Gintant et al. (2016)

1.4.4 Japanese iPS Cardiac Safety Assessment (JiCSA)

In the JiCSA initiative which established in 2014 to develop a new paradigm for assessing drug-induced pro arrhythmia risk, the only platform used to assess the torsadogenic potential of the compound towards hiPSC-CMs was based on the multi-electrode array (MEA)(Kanda et al., 2018). The initiative has demonstrated for the first time that hiPSC-CMs are likely to share similar electrophysiological properties with the human heart, and therefore as promising in terms of predicting arrhythmogenic potential (Yamamoto et al., 2016). The study also showed high reproducibility and reliability among laboratories as compared to CiPA. The site to site variability and inter-operator variability were improved as a result of collective training of users across the study and standardised MEA protocol were established across sites together with standardising cell type (Kanda et al., 2018).

1.5 Cardiac electrophysiology and contractility

Although the regulatory expectation of preclinical guidelines is not based on the assessment of drug-induced inotropic (contractility) effects, it has been recognised that the evaluation of potential inotropic effects *in-vivo* is the critical safety endpoint in drug development (Guth et al., 2015b). Guth (2019) suggests that since inotropic effects potentially affect drug development, the detection of drug-induced effects on *in-vivo* myocardial contractility should be detected as early as possible (Guth et al., 2019a), preferably before *in-vivo* testing, which is during the *in-vitro* pharmacological safety test of all new drugs. The changes in cardiac electrophysiology can also be observed from ion channels that generate the action potential.

1.5.1 The cardiac action potential

Cardiac contractility requires the rapid activation of CMs that are electrically excitable. The electrical conduction system is initiated by cardiac action potential, which relies on ion channels, ligand or receptor-bound gated channels (Grant Augustus, 2009). The initiation of action potential results in depolarisation while their recovery to baseline resting membrane potential results in repolarisation (Lester et al., 2019). There are five phases of action potential (0-4) which begin and end with phase 4: upstroke/depolarisation (0),

early repolarisation (1), plateau phase (2), final repolarisation (3) and final resting (4), illustrated in **Figure 1.4**.

During phase 0, the membrane potential moves towards the positive voltage range, which causes a sharp upstroke/depolarisation due to the opening of the Na^+ channel. This stage is central to the rapid propagation of cardiac impulse with conduction velocity = 1 m/s (Grant Augustus, 2009). During phase 1, the upstroke action potential is terminated and early repolarisation is initiated by the inactivation of the Na^+ channel and activation of the transient outward movement of K^+ through the K^+channel (Lester et al., 2019). In phase 2, the action potential plateau results from a balance between an influx of Ca^{2+} through the opening of the L-type Ca^{2+} channel and efflux of the repolarising K^+ currents. The sustained downward slope in phase 3 is due to repolarisation by the inward K^+ current through the K channel. The final phase 4 is the resting potential maintained by an open K_1 channel, where healthy working myocardial cells are stable at ~-90 mV (Grant Augustus, 2009). In some hPSC-CMs, there was a lack of Na^+ channel (I_{NA}), but the cells still beat due to the Ca^{2+} being used in Phase 0. These intrinsic electrical activities and measurement of activities can be used to determine the ability of a drug to prolong repolarisation (Killeen, 2012).

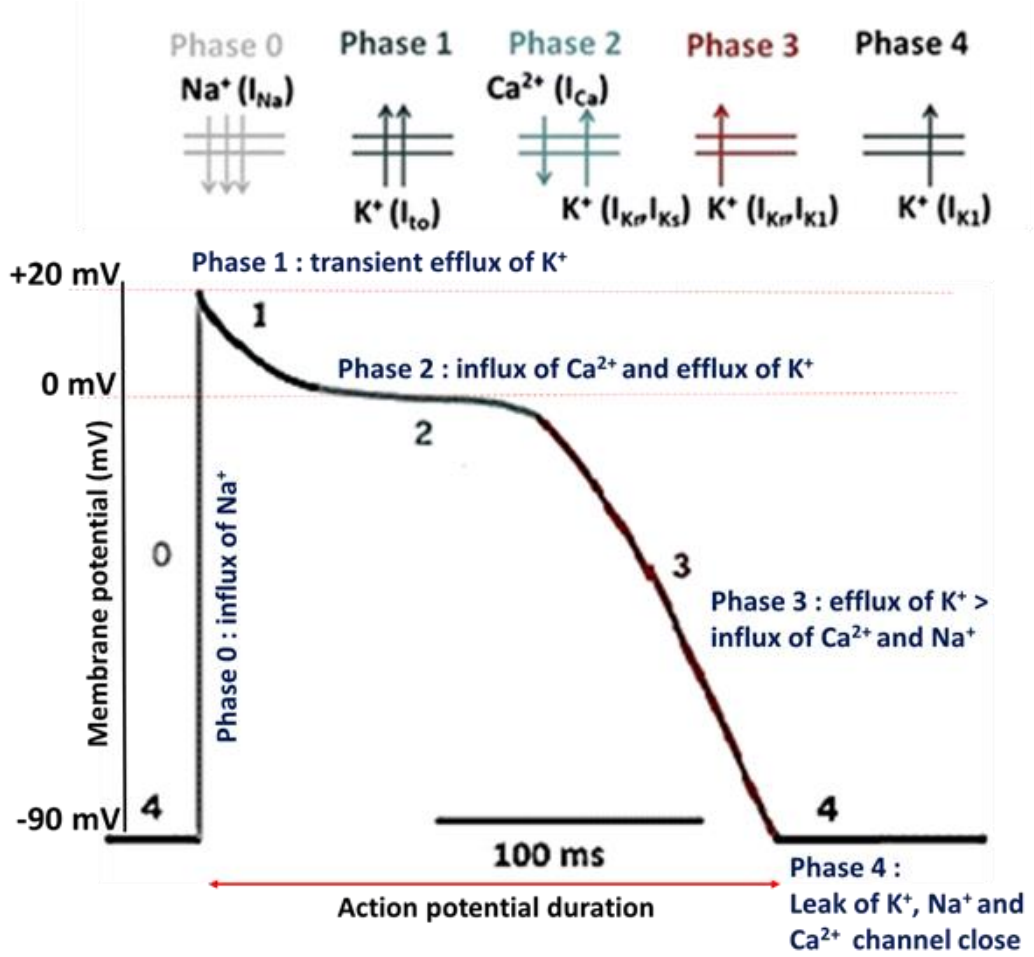


Figure 1.4: Action potential overview.

The action potential of cardiac muscle (ventricular) and the different phases involved. (modified from Li et al., 2016).

1.5.2 Excitation-contraction (EC) coupling

Contractility is connected to electrophysiology via the process of excitation-contraction coupling (Eisner et al., 2017). The essential role of this process is controlled by changes in intracellular calcium (Ca^{2+}) and depends on the combination of calcium channels, transporters and organelles at their precise locations. During the action potential plateau phase (phase 2; **Figure 1.4**), calcium ion flows down in a steep concentration gradient and enters the cardiac myocytes via L-type calcium channels (LTCC) which are situated in the surface membrane and T-tubule (**Figure 1.5**). The calcium influx stimulates further calcium release from the sarcoplasmic reticulum (SR) (calcium-induced calcium release; CICR) via the opening of the ryanodine receptor (Pinnell et al., 2007).

The free intracellular calcium binds to C subunit of troponin, which leads to a troponin/tropomyosin configuration change. This, in turn, activates myofilaments and causes cardiomyocytes shortening, hence resulting in cardiac contraction. During repolarisation, the intracellular calcium is removed from the cytoplasm by sarcoplasmic reticulum Ca^{2+} ATPase (SERCA) near phospholamban, through sodium/calcium: Na^{+}/Ca^{2+} exchange (NCX) by utilising mitochondrial uniport. The calcium dissociates from the troponin, hence resulting in cardiac relaxation (Pinnell et al., 2007). The adaptation of CMs to metabolic demands and autonomic stimulation has causes changes in contractility. Therefore, it can be used as one of the clinical biomarkers for safety prediction.

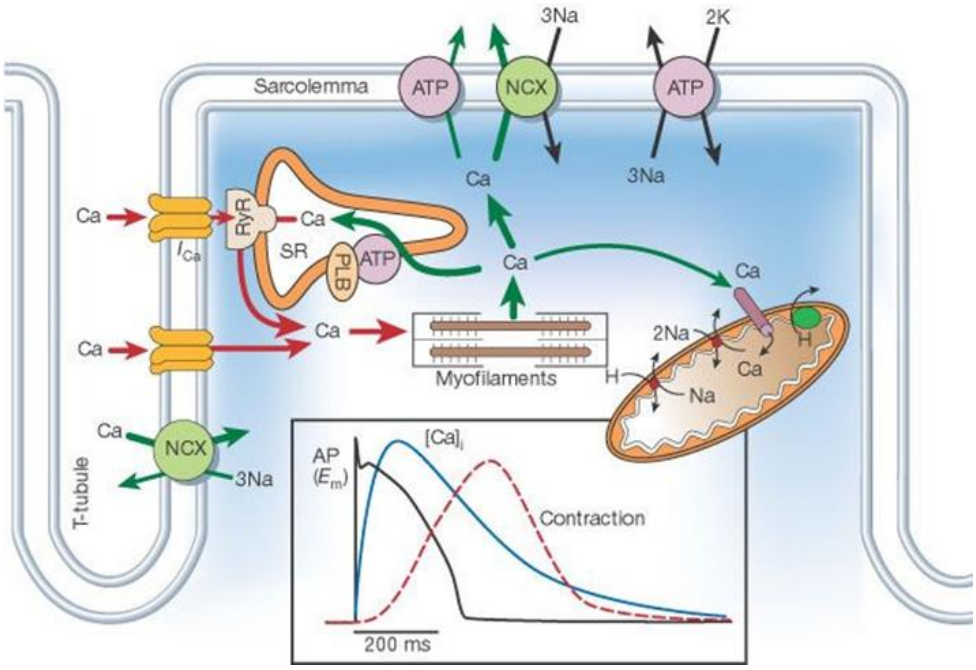


Figure 1.5:Structure involved in excitation-contraction (EC) coupling.

Schematic diagram of the surface membrane, transverse tubule (t-tubule), sarcoplasmic reticulum (SR), mitochondria, channels and transporters. RyR, ryanodine receptor; NCX, Na^+/Ca^{2+} exchange; ATP, ATPase; PLB, phospholamban. Picture taken from (Bers, 2002)

1.6 Human pluripotent stem cells (hPSCs) as tools

Since the ultimate goal is to address human cardiac safety and efficacy, experimental verification should be done on actual human tissue. It is hoped that the humanised screening platform will improve efficacy and toxicity prediction in patients, based on integrated preclinical data. This notion together would facilitate a 'fail early, fail cheap' approach to avoid late-stage failure and drug withdrawal (Korte, 2019). As has been discussed, human primary cardiomyocytes are not the best option, due to lack of availability. The next best sources are human pluripotent stem cells **(Figure 1.6)**. The ability to culture hPSCs for the long term and induce their differentiation to a variety of cells, especially cardiomyocytes, is favourable for understanding drug screening and disease modelling. Human pluripotent stem cells come from two different sources: embryonic and induced pluripotent stem cells.

1.6.1 Human embryonic stem cells (hESCs)

1.6.1.1 Derivations of hESCs

Pioneering work with embryonic stem cells (ESCs) involved isolation from early blastocyst of developing mouse embryo and the ability to differentiate in the form of embryoid bodies in *in-vitro* cultures dishes and developed *in-vivo* teratomas in mice (Evans and Kaufman, 1981, Martin, 1981). Following the success, Martin cultured mouse embryonic stem cells on fibroblast feeder cells supplemented with growth factors from an embryonic carcinoma conditioned medium (Martin, 1981). Accordingly, in 1995, the first non-human primate ESC line was derived from rhesus monkey blastocyst, which remained undifferentiated over one year of continuous passaging (Thomson et al., 1995). Subsequently, human embryonic stem cells (hESCs) were first derived from the inner cell mass of blastocyst in 1998 by Thomson et al. (1998) (**Figure 1.6a)** (Thomson et al., 1998). The cell lines derived qualified as human pluripotent as they maintained a prolonged undifferentiated state (4 to 5 months in culture), exhibited pluripotency markers and were able to generate all three embryonic germ layers (endoderm, ectoderm and mesoderm) when injected into immunodeficient mice (Thomson et al., 1998).

1.6.1.2 hESCs development

The suboptimal culture conditions were shown to lead to the spontaneous somatic differentiation of neurons and muscle cells from blastocyst-derived hESCs for the first time in 2000 (Reubinoff et al., 2000). Subsequently, Schuldiner and colleagues revealed that hESCs *in-vitro* differentiation could be controlled by using several factors (such as Activin A, BMP-4, bFGF and HGF) to direct into specific embryonic lineages (Schuldiner et al., 2000). This work provided the basis for a number of differentiations such as neurons (Cohen et al., 2007), hepatocytes (Sasaki et al., 2009), osteocytes (Sottile et al., 2003) and cardiomyocytes (Kehat et al., 2001).

1.6.1.3 hESCs limitation

Blastocysts are usually derived from the surplus of *in-vitro* fertilisation (IVF) embryos; however, due to technical and ethical challenges, they are not entirely favourable (Zhao et al., 2017a). As such it not feasible to produce a large

number of such lines or derive them from patients with diseases which limit their use to studies normal cellular function (Bassett, 2017).

1.6.2 Human-induced pluripotent stem cells (hiPSCs)

The mechanisms underlying the pluripotency control of hESCs have brought additional discoveries into the field, such as the technology of reprogramming somatic cells into human-induced pluripotent stem cells (hiPSCs), **Figure 1.6b**.

1.6.2.1 Derivations of hiPSCs

The hiPSC was first derived by Yamanaka, from reprogrammed adult somatic cells using a combination of four genetic factors: Oct3/4, Sox2, c-Myc, and Klf4 (Takahashi and Yamanaka, 2006, Takahashi et al., 2007). The early works of reprogramming, although efficient and reliable, involved transcription factors delivery by integrated retroviral and lentiviral vectors (Yu et al., 2007, Takahashi et al., 2007) **(Figure 1.6)**. The integrating viral vectors resulted in random integration in the genome that may increase tumorigenic, mutagenesis risks and heterogeneity among cell lines (González et al., 2011). To address the problem, excisable methods such as cre/loxP lentiviral (Soldner et al., 2009) and piggyback transposon system (Woltjen et al., 2009) were employed in addition to the various non-integration delivery methods such as episomal DNA plasmid (Yu et al., 2009, Burridge et al., 2011), Sendai virus (Churko et al., 2013), adenovirus (Stadtfeld et al., 2008), RNA (Warren et al., 2010), protein (Zhou et al., 2009) and small molecule-based reprogramming for hiPSCs generation (Huangfu et al., 2008) **(Figure 1.6b and Figure 1.7)**. The Sendai, mRNA and episomal are more preferable and are employed routinely, while protein and small molecules are not desirable due to their poor efficiency. As time has progressed, different combinations of fewer or different factors have been successfully used for reprogramming, making it safer and more efficient (Rowntree and McNeish, 2010, Nakagawa et al., 2008, Maehr et al., 2009). Fundamentally, the association between lethal tumour formation and c-Myc as potent oncogenes has been gradually reduced (Takahashi and Yamanaka, 2016).

1.6.2.2 hiPSCs features

The hiPSCs are similar to hESCs in terms of morphology, proliferation, cell surface markers and gene expression profiles (Murata et al., 2010). Their pluripotency is also similar to hESCs (Yokoo et al., 2009b, Zhang et al., 2009). The technology overcomes both ethical and translational obstacles in hESCs; ethically, no embryo destruction is involved and the starting materials such as from skin, plucked hair, urine and blood are easily accessible for reprogramming (Aasen and Izpisua Belmonte, 2010, Okita et al., 2013, Zhou et al., 2012).

In contrast to hESCs, the generation of hiPSCs is possible in any period of a patient or healthy individual's life, whether young or old and is directly linked to the genetic phenotype with a robust medical history (Eguizabal et al., 2019). Together with cell culture advancement, the researcher potentially differentiates an unlimited supply of human CMs at different stages of the disease for patient-specific cell-based therapy and as a tool for disease modelling (Kim, 2015)

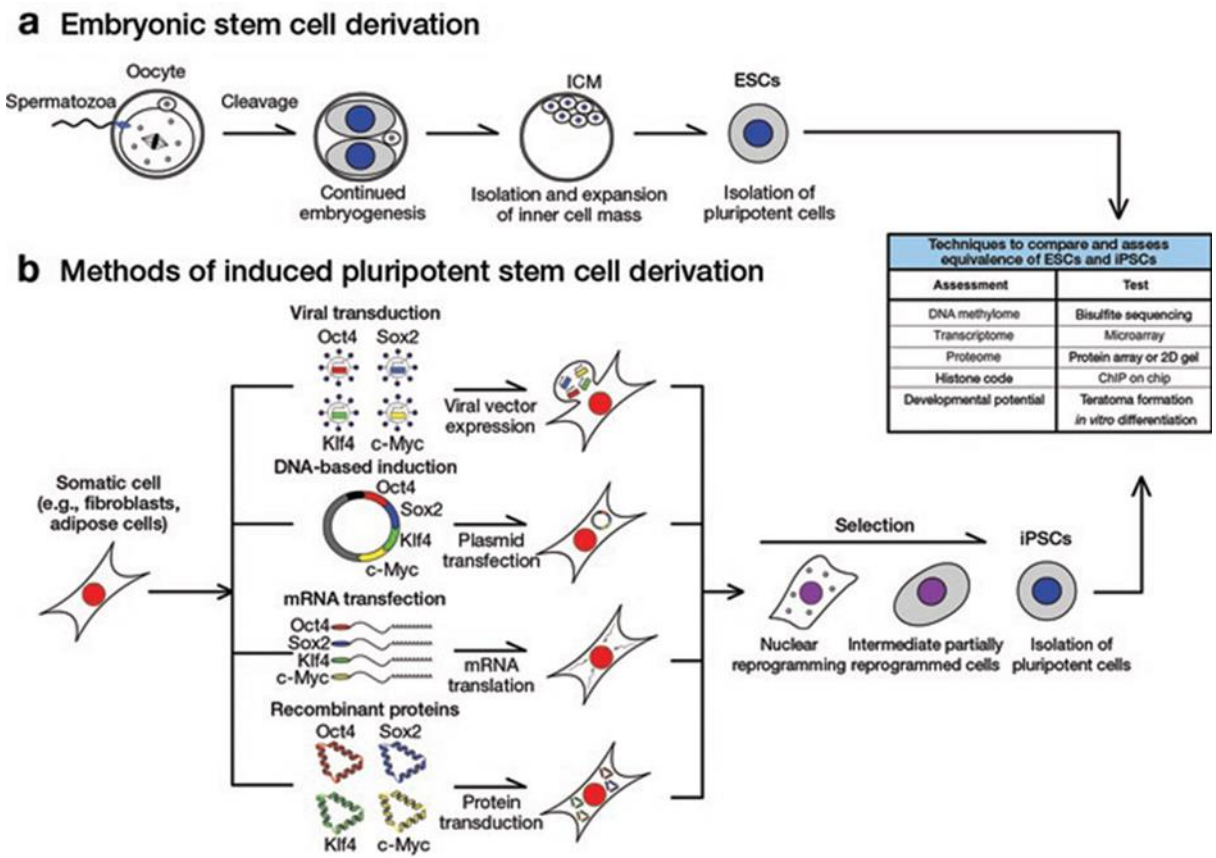


Figure 1.6: Illustration of human embryonic stem cells (hESCs) and human induced pluripotent stem cell (hiPSCs) derivation. **a)** The human embryonic stem cells (hESCs) derived from inner cell mass of the blastocyst, **b)** human-induced pluripotent stem cell (hiPSCs) derived from reprogrammed somatic cells, such as skin, plucked hair, urine and blood. This human pluripotent stem cell (hPSCs) have a similar characteristic, including long-term proliferation and expansion capabilities, the potential to differentiate into any other cells, including cardiomyocytes (hPSC-CMs). Picture taken from **(Narsinh et al., 2011)**

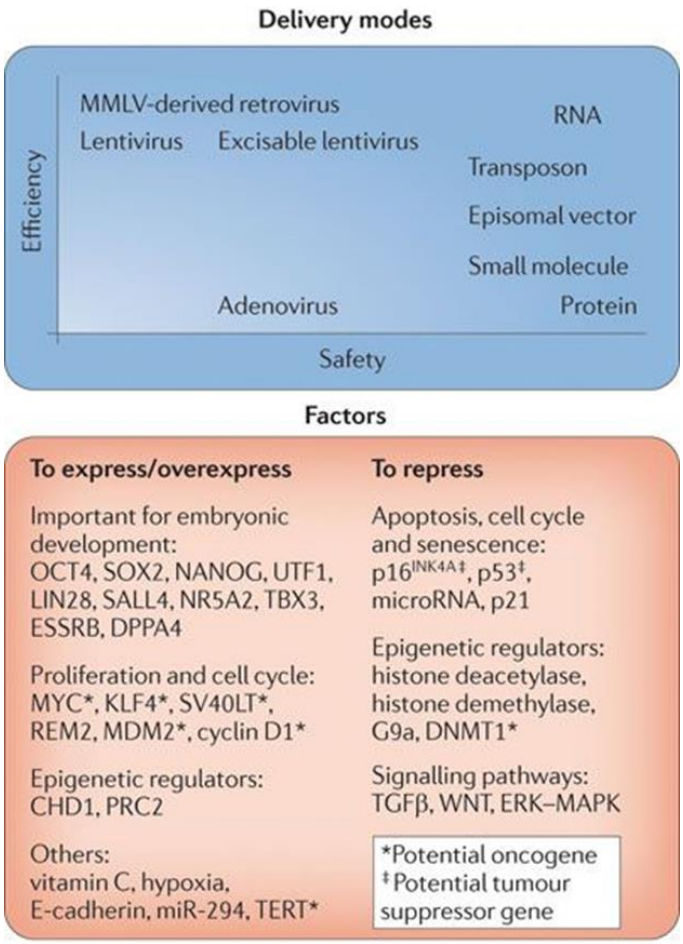


Figure 1.7: The reprogramming delivery methods and reprogramming factors for making induced pluripotent stem cells.

CHD1, chromodomain-helicase-DNA-binding protein 1; DNMT1, DNA methyltransferase 1; DPPA4,developmental pluripotency associated 4; E-cadherin, epithelial cadherin; ERK, extracellular signal-regulated kinase; MAPK, mitogen-activated protein kinase; MMLV, Moloney murine leukaemia virus; PRC2, Polycomb repressive complex 2; SV40LT, SV40 large T antigen; TERT, telomerase reverse transcriptase; TGFß, transforming growth factor-ß. Adapted from (Gonzalez et al., 2011):

1.7 Human pluripotent stem cell-derived cardiomyocytes (hPSC-CMs)

1.7.1 Differentiation approaches of hPSCs to hPSC-CMs

The hPSCs can undergo in-vitro differentiation into the three primary germ layers which potentially generate all types of cells in the human body (Mummery et al., 2012). The embryoid body (EB) and monolayer in-vitro culture protocols are regularly used to initiate cardiac differentiation (Fujita et al., 2019) **(Figure 1.8)**. The EBs formation involves growing hPSCs in the combination of physical and chemical cues into small spherical aggregates. The established embryoid body methods, however, yield low purity CMs which restrain their downstream application. Besides, complex diffusional barriers may restrict the growth factors and other molecule penetration (Mummery et al., 2003). Meanwhile, monolayer-based methods are preferable as they have improved efficacy, consistency and scalability of cardiomyocytes differentiation (Batalov and Feinberg, 2015). For example, monolayer differentiation by Burridge 2014 could produce beating cardiomyocytes with more than 85% purity without any purification after seven days of differentiation initiation (Burridge et al., 2014). Earlier studies also involved inductive co-culture with visceral endoderm-like (END2) cells from mice **(Figure 1.8)**, which mimic *in-vivo* cell environment to enhance cardiac differentiation. However the efficiency of the protocol is relatively low and exposed to the risk of xenogenic contamination; therefore it is not commonly used (Leitolis et al., 2019, Mummery et al., 2003).

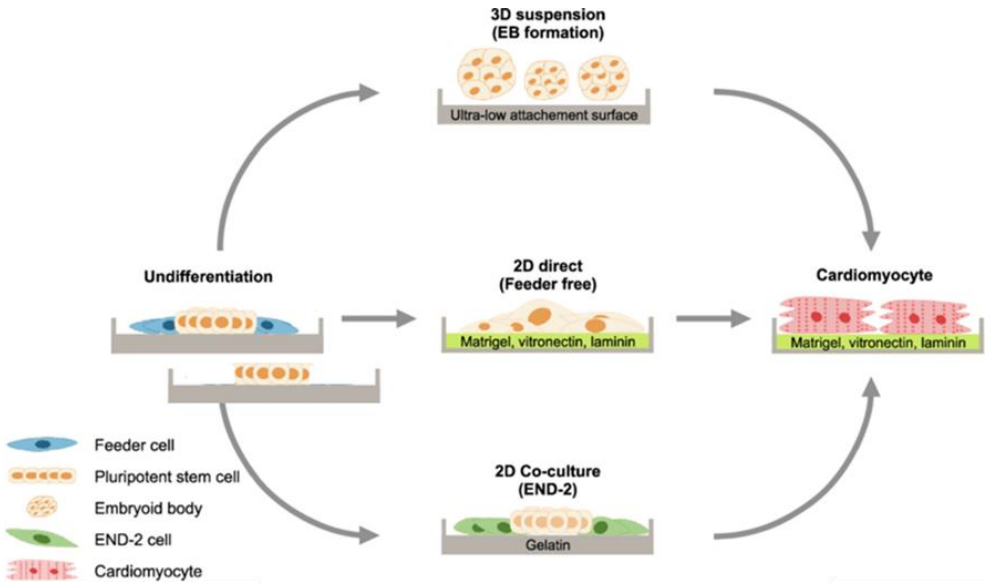


Figure 1.8: Schematic illustration for differentiation methods for hPSC-CMs.

Three commonly use differentiation methods 1) via embryoid bodies (EBs) formation, 2) 2D monolayer differentiation and 3) cocultured system. END-2 = mouse visceral endodermal-like cells. Adapted from (Moon et al., 2017)

1.7.2 Stage-specific cardiac development

Stem cell pluripotency and self-renewal is controlled by pluripotency factors such as OCT4, SOX2 and NANOG. The downregulation of the pluripotency factor is essential in order to start hPSCs differentiation into specific lineages (Batalov and Feinberg, 2015). Throughout normal embryonic heart development, the differentiation into cardiac lineage is under the specific regulation of internal and external stimuli. Differentiation protocols are ideally needed to recapitulate stepwise stages of embryological development as the mechanism of *in-vitro* differentiation.

The embryonic cardiac commitment is complex, and consists of various signalling pathway which play a role in determining its fate. During heart development, Wingless WNT/beta-catenin, Activin/Nodal, fibroblast growth factor (FGF) and bone morphogenetic protein (BMP) signalling are capable of inducing SCs into the mesoderm and thus are useful for the mesoderm modulation in hPSCs ((Egashira et al., 2011). Once the mesoderm has established, followed by cardiac mesoderm, the mesodermal precursor cell mediates the fate to either become the first or second heart field (FHF and SHF)

(Sun and Kontaridis, 2018, Leitolis et al., 2019). The signalling pathway that determined cell differentiation stages and expressed cell markers are illustrated in **Figure 1.9**. These pathways have become guidance for *in-vitro* cardiac lineage specification.

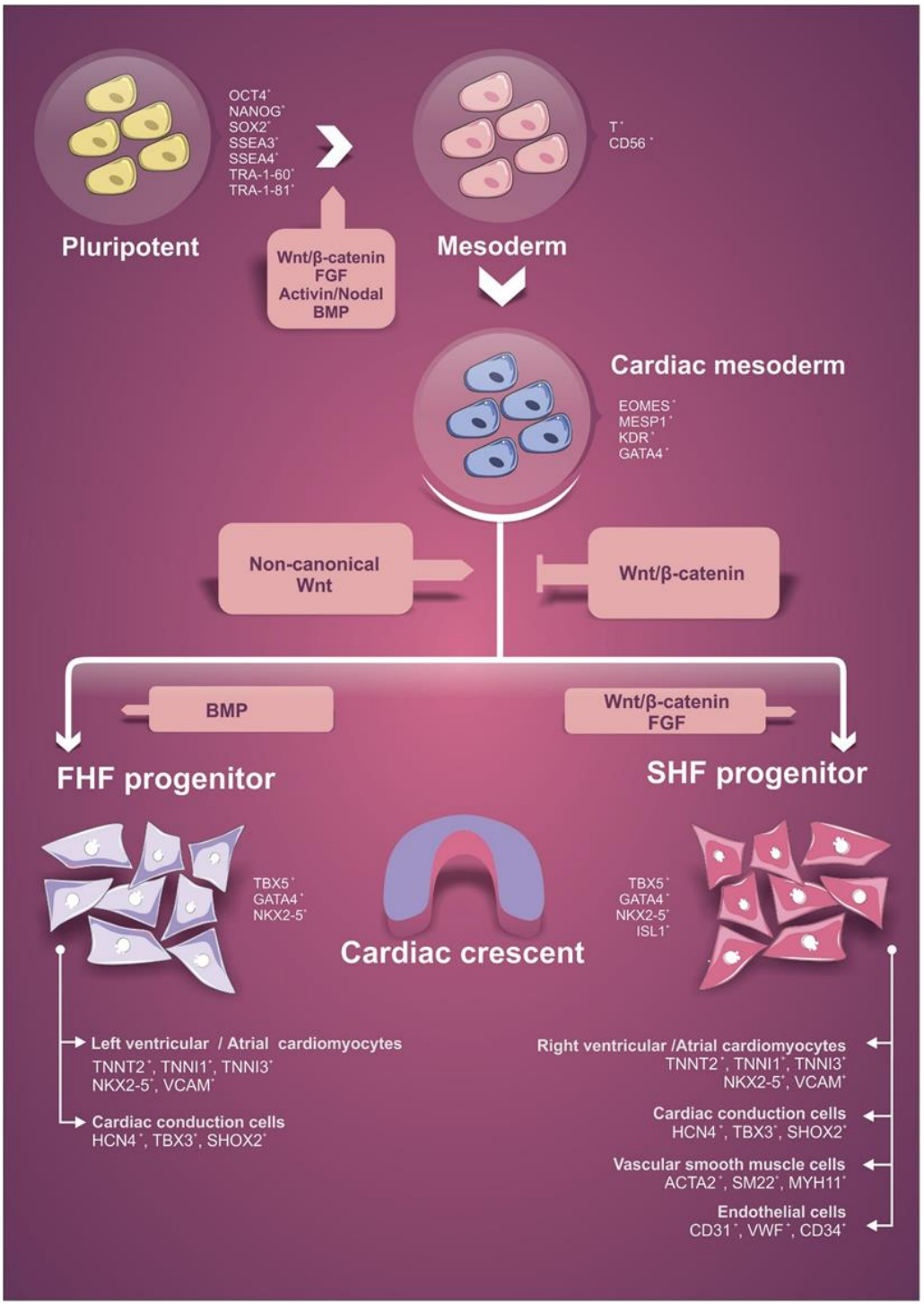


Figure 1.9: Schematic representation of differentiation stages, signalling pathway and cellular markers for cardiac lineage commitment.

Picture taken from Leitolis et al., (2019)

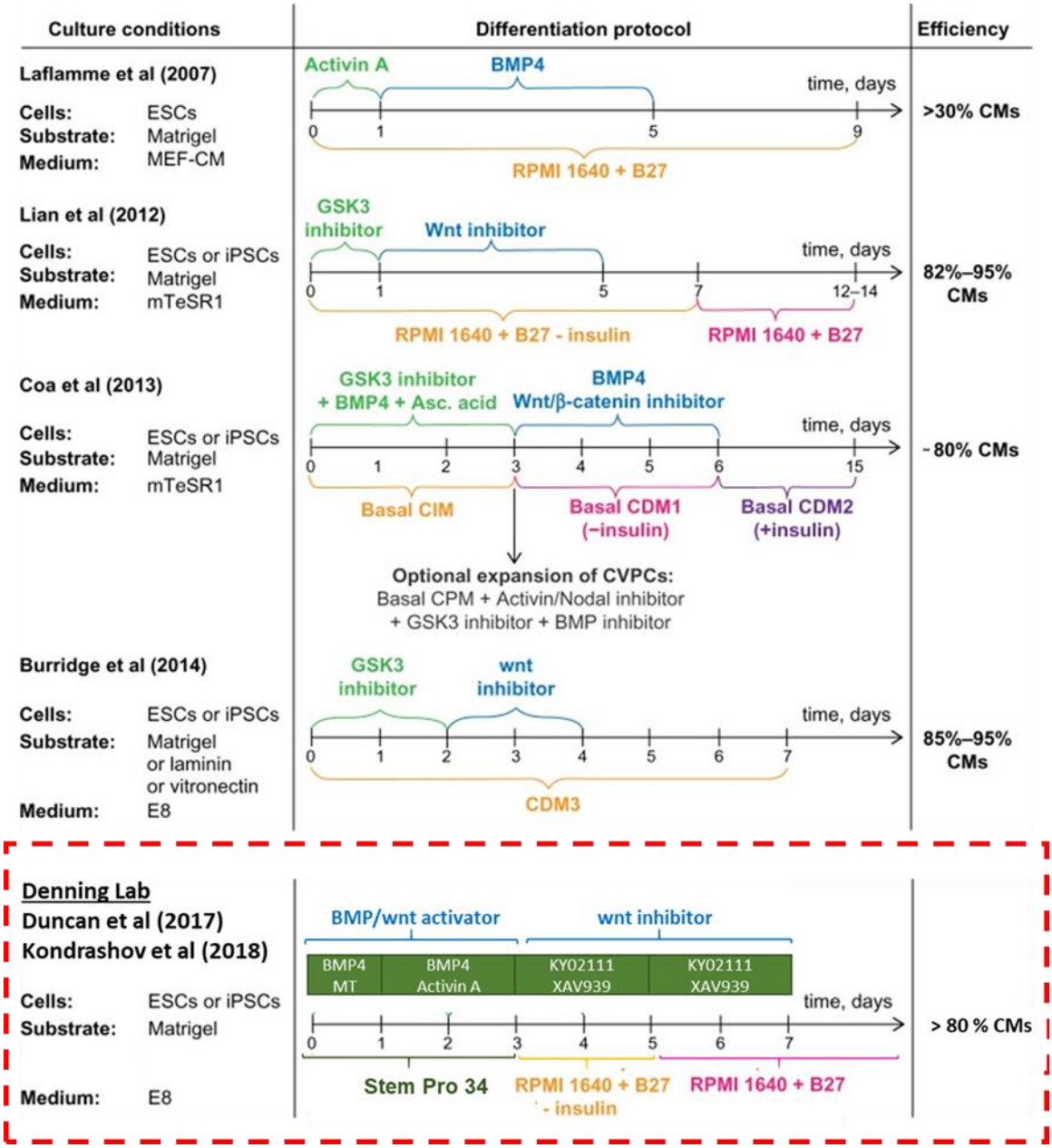
1.7.3 Differentiation protocols

Various attempts to induce *in-vitro* cardiac differentiation have been made with small molecules that alter signalling and DNA methylation. An early study by Paige et al. (2010) demonstrated that Activin A and BMP4 stimulate the WNT/ß-catenin signalling to regulate cardiac mesoderm specification. WNT/ß-catenin signalling stimulation is vital during the early stage of differentiation, while its inhibition after mesoderm formation is crucial for cardiomyocytes (Batalov and Feinberg, 2015). Conversely, suppressing WNT/ß-catenin at an early stage or stimulation after mesoderm formation will lead to a reduction in cardiomyocytes yield.

In 2012, Lian et al. (2012) showed that the addition of the GSK3-inhibitor compound, CHIR 99021at the beginning of differentiation does stimulate WNT/ß-catenin signalling and their elimination after mesoderm formation is sufficient to generate cardiomyocytes (Lian et al., 2012). They also demonstrated that insulin, which is one of the components in B27 media supplement, does interrupt cell differentiation during the first five days of differentiation initiation. Therefore, once the insulin was removed from differentiation media by utilising B27 without insulin, differentiation gradually increased. Examples of monolayer differentiation culture conditions are demonstrated in **Table 1.1** (Laflamme and Murry, 2011, Lian et al., 2012, Cao et al., 2013, Burridge et al., 2014). Nottingham laboratory (Denning lab) has also successfully developed an in-house cardiac differentiation protocol which is capable of generating more than 80% pure cardiomyocytes (Duncan et al., 2017, Kondrashov et al., 2018). **(Table 1.1 (red box))**

Table 1.1: Example of hPSC-CMs monolayer cardiac differentiation protocols and Nottingham cardiac differentiation protocol in the red box.

The other cell types that may present other than cardiomyocytes (CMs) are included endothelial cells, smooth muscle cells and fibroblasts. BMP4; Bone morphogenetic protein 4, CDM1 and CDM2; Cardiomyocyte differentiation medium 1 and 2, CDM3; 3-component chemically defined medium. Adapted from (Batalov and Feinberg, 2015)



1.7.4 Properties and pharmacological responses of hPSC-CMs

When adequately differentiated, both hESC-CMs and hiPSC-CMs give rise to spontaneously beating cells (Bedut et al., 2016). Studies have shown that the hiPSC-CMs express all major cardiac ion channels at a similar level to hESC-CMs (Liang et al., 2013). The hPSC-CMs have become a useful platform for evaluating the impact of drugs and on various cellular parameters that relate to cardio physiology (Meseguer-Ripolles et al., 2017).

Studies have revealed that CMs from hiPSC more accurately modelled cardiotoxicities when comparing head to head with commercial hERG cell lines (HEK293) (Liang et al., 2013). Fundamentally, Yokoo et al. (2009) have demonstrated that functional embryoid bodies cardiomyocytes derived from both hiPSCs and hESCs are equally responsive in a predictable pharmacologically manner. Their beating frequency and contractility when tested with cardioactive drugs (such as adrenaline, isoproterenol, procainamide and verapamil), were compatible with empirical results obtained in the clinical setting (Yokoo et al., 2009b). These results suggest there is no significant difference in fundamental characteristics between both hPSC-CMs and highlight their potentials for drug screening.

In terms of drug-induced toxicity in the disease model, a group of researchers have demonstrated that patient-specific hiPSC-CMs could recapitulate the prediction to doxorubicin-induced toxicity in individuals with breast cancer at the cellular level (Burridge et al., 2016), hence providing some insight into cardiac safety and theoretically, able to guide the policy of using doxorubicin in cancer treatment.

In terms of cardiac diseases, many hiPSC-CMs disease models have been successfully generated, for example Long QT1, Long QT2, LQT3/ Brugada syndrome, LQT8/ Timothy syndrome, Catecholaminergic polymorphic ventricular tachycardia CPVT, Arrhythmogenic right ventricular dysplasia ARVD, Familial hypertrophic cardiomyopathy HCM, Familial dilated cardiomyopathy DCM and others. In this regard, Moretti and colleagues derived hiPSCs from two patients with long QT-syndrome type 1 and two healthy individuals: the patient’s hiPSCs demonstrated susceptibility to catecholamine-induced

tachyarrhythmia and their electrophysiological ensemble to the syndrome (Moretti et al., 2010), hence successfully showing that hiPSC-CMs models can recapitulate the aspects of genetic disease. These models could be used to reflect the molecular and cellular phenotype of cardiovascular disease and to predict patient response/toxicity to known or newly developed drugs.

1.7.5 The hPSC-CMs vs primary cardiomyocytes

With technological advancement, both hPSC-CMs can be grown at high purity, in large numbers and cryopreserved to facilitate ease of use. To be relevant, hPSC-CMs should express structural and functional characteristics that are comparable to *in-vivo* cardiomyocytes (Guth et al., 2019a). Features include the presence of L-type calcium channel, ryanodine, SERCA, cytoskeletal complexes like actin and myosin, as well as ATP producing mitochondria. Both hPSC-CMs express all dominant cardiac ion currents, and channel genes that are found in adult left ventricular cardiac tissue, which includes the sodium channel (*SCN5A*), L-type calcium channels (*CACNA1C and CACNA1D*) and potassium channels (*KCNH2 and KCNQ1*). The hPSC-CMs also express genes that are important for calcium cycling such as inositol triphosphate receptor (IPTR3), ryanodine receptor 2 (RYR2), sarcoplasmic reticulum Ca2+ ATPase (SERCA), calsequestrin2 (CASQ2), calreticulin (CALR), junctophilin 2(JPH2)), phospholamban (PLN), sodium calcium exchanger (NCX1) and triadin (TDX)(Karakikes et al., 2015). These characteristics may mediate electrophysiological activity in a similar manner to human cardiac myocytes, which provides a great deal of physiologically relevant information (Ma et al., 2011).

At the same time, hPSC-CMs exhibit poorly developed SR and the absence of T-tubules. Due to this fundamental functional characteristic, both hPSC-CMs cells are considered immature and exhibit more fetal rather than adult cardiomyocytes (Sayed et al., 2016b). Although their fetal-like properties limit clinical predictivity, their functionality test outweighs the primary cardiomyocytes. They also have the potential to produce results with higher reproducibility and robustness than primary tissue (Mannhardt et al., 2017a). This characteristic makes them suitable to be used in the screening of drug-induced changes based on cardiac cellular contractility and electrophysiology (Sharma et al., 2018). However, considerable attention is needed to evaluate

the use of drugs on these cells to ensure physiologically relevant results when translated to patients. The comparison between fetal cardiomyocyte, hPSC-CM and adult cardiomyocyte is summarised in **Table 1.2**

Table 1.2: The difference between fetal cardiomyocytes, hPSC-CM and adult cardiomyocyte. The table is taken from Jiang et al., (2018)

	Parameters	Fetal CM	hPSC–CM	Adult CM
Morphology	Cell shape	Circular	Circular	Rod-shaped
	Nucleation	Mononucleated	Mononucleated	25–30% Binucleated
Mitochondria	Structure	Small and round	Slender and long, smaller than adult	Ovular shape, 35% total volume
	Distribution	Close to nucleus and at periphery	Close to nucleus and at periphery	In the direction of the sarcomere
Metabolic substrate		Glucose	Glucose	Fatty acid
Sarcomere	Length	≈1.6 μm	?	≈2.2 μm
Myofibrillar isoform switch	*Titin*	N2BA	N2BA	N2B
	MYH	$\beta > \alpha$	$\beta \approx \alpha$	$\beta \gg \alpha$
T-tubules	Presence	No	No	Yes
Gap junction	Distribution	Circumferential	?	Intercalated disc
Conduction velocity	Velocity	?	10–20 cm/s	60cm/s
Electrophysiology properties	Upstroke velocity	≈50 V/s	≈50 V/s	≈250 V/s
	Synchronous contraction	No	No	Yes
	RMP	≈-60 mv	≈-60 mv	≈-90 mv

1.8 Methods for *in-vitro* hPSC-CMs functional analysis

Functional *in-vitro* analysis of hPSC-CMs is crucial for conducting preclinical safety together with efficacy studies in order to understand the mechanisms of cardiac disease. The ideal *in-vitro* model needs to be fast, sensitive, reliable and permit high throughput analysis. Variable approaches have been developed to analyse hPSC-CMs by measuring the output of electrophysiology, contractile machinery, morphology and metabolic changes (Mannhardt et al., 2016, Ribeiro et al., 2017, Li et al., 2018, Brandão et al., 2017). This thesis focuses on analysing electrophysiology and contractility. The methods are tabulated in **Table 1.3,** and the rationale behind the analysis methods are explained in **Figure 1.10**. To obtain a full mechanistic understanding of drug effects, the combination of voltage electrophysiology and contraction recording would be preferable. In addition, the listed *in-vitro* technologies below are not applicable for adult primary cardiomyocytes or isolated cardiac tissue due to their culture challenges, and therefore, although hPSC-CMs are immature, they do have potential offer to improve the prediction of clinical drug effects.

1.8.1 Analysing electrophysiology

The **patch-clamp** method is the gold standard to study the impact of a compound with regards to cardiac electrophysiology due to its sensitivity and ability to detect current directly from single cells (Bedut et al., 2016, Mansor and Ahmad, 2015). However, it is invasive as the strong seal can easily break the cells and therefore, long term chronic or time course measurements are not even possible. Additionally, this technique is highly technical, time-consuming and not feasible for high throughput experiments or screening.

Multi-electrode arrays (MEA) requires cells to be seeded on a dish covered with electrodes in the bottom and can be scaled up for high throughput (Pradhapan et al., 2013). The method offers an alternative to patch-clamp, as it is non-invasive and non-terminal. As opposed to single-cell measurement in patch-clamp, MEA is only able to record data from cluster or monolayers cells. Nonetheless, the field potential duration (FPD) in MEA is partially comparable to patch-clamp action potential (Laurila et al., 2016).

Fluorescent imaging relies on either calcium indicators or voltage-sensitive dyes and provides a non-invasive method for obtaining intracellular ion fluctuations and voltage changes (Laurila et al., 2016). However, the chemical indicators such as Fura2 and Fluo4 often have pharmacological and phototoxic effects on cells. While conventional voltage-sensitive dyes such as di-4-ANEPPS and di-8-ANEPPS are faster, they are low in sensitivity and non-negligible phototoxicity. High sensitivity dye is usually slower and unsuitable for rapid action potential in cardiac cells. The voltage-sensitive dye, FluoVolt allows fast imaging with moderate toxicity (Bedut et al., 2016). Meanwhile, a genetically encoded calcium indicator is less toxic and therefore suitable for chronic imaging over days and weeks (Herron Todd et al., 2012). The ideal dyes for fluorescent imaging need to be high in sensitivity, fast, and low on unwanted interaction or toxicity with the tested cells.

1.8.2 Analysing contractility

Cardiac contractility involves mechanical beating behaviours such as contractile force and beating motion. Ribeiro et al. (2019) suggest platforms for assessing *in-vitro* contractility should provide contractile parameters that reflect cardiac function such as force, tension, kinetics of contraction and relaxation, contraction times, synchronicity of movement or any other related parameters. The force produced from cardiomyocytes during contraction can be quantified with the non-invasive method of **traction force microscopy** (Laurila et al., 2016). The adherent cells attach to the substrate ECM surfaces and, as the cell contracts, it deforms the substrates proportional to the mechanical forces. The substrate deformation can be detected by capturing the lateral mechanical displacement of markers, in the form of fluorescent beads that become embedded in the substrate (Plotnikov et al., 2014). The displacement/ contraction is quantified by comparing images of fluorescent beads in the contracted and relaxed substrate. In 2012, Hazeltine and colleagues successfully quantified hPSC-CMs using this method (Hazeltine et al., 2012).

Mechanical cardiac force changes can also be monitored using **atomic force microscopy (AFM).** It is a three-dimensional high-resolution topographic technique that quantifies the bending of a small cantilever probe with high precision and has been developed to characterise the inotropy and chronotropy

of self-beating cardiomyocytes (Chang et al., 2013). However, the method is not popular due to major disadvantages, namely, relatively slow scan time which can lead to thermal drift on the sample and therefore, low throughput.

As technology has evolved, **impedance assay** offers a non-invasive and label-free analysis method, which has a high potential for high throughput. The multi-well plate contains electrodes at the bottom, and the cells are seeded on top of the electrode (Lamore et al., 2013). As the cells move or beat on top of the electrode, the impedance signal changes correspondingly. The advantage of this system is that it allows the continuous short and long term monitoring of cell viability and contractility which is, therefore, useful in both acute and chronic cardiotoxicity assessment (Koci et al., 2017). The output parameters are variable such as amplitude, beating frequency, raising time, falling time and cell index. The Nanion CardioExcyte 96 and ACEA Biosciences xCelligence RTCA cardio multiwell sensor are among the systems that have adopted this technology (Xi et al., 2011, Koci et al., 2017). The technology has also been widely tested using hiPSC-CMs (Scott et al., 2014).

The rhythmic characteristic of contracting cardiomyocytes can also be quantified by **video microscopy and video optical imaging**. The video microscopy records the cells' beating area and processes using a combination of computational motion algorithms analysis. Among the systems that have adopted this technology is contractility assay by CellOPTIQ and Musclemotion algorithms (Lemme et al., 2018, van Meer et al., 2019, Sala et al., 2018). Video optical imaging is capable of analysing the hPSC-CMs in a 3D structure like engineered heart tissues (EHTs). The camera records the movement of EHT for a given time and determines the distance between the end of EHT muscle strip based on the deflection of PDMS post (Hansen et al., 2010, Mannhardt et al., 2017a). The output of video microscopy and optical imaging includes force, frequency, contraction time and relaxation time, which is based on predefined algorithms. However, each system has its unique predefined algorithms for generating and quantified motions and therefore, the performance might be relative. The advantage of these systems are non-invasive, non-toxic and have potential; for automation which permits the medium to high throughput.

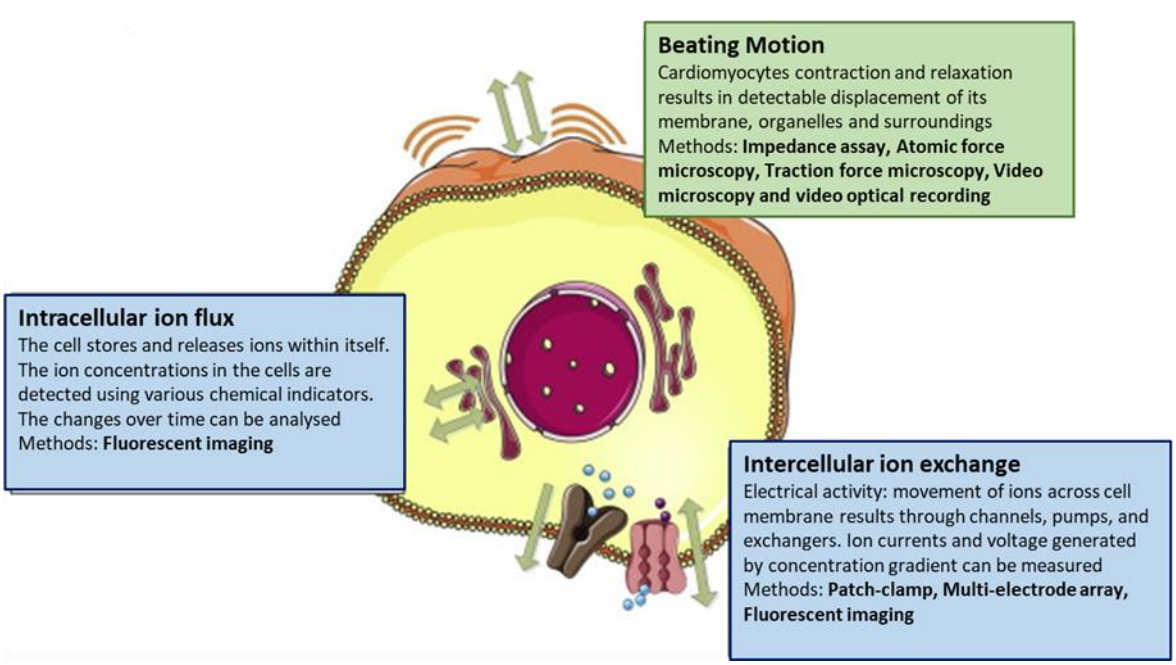


Figure 1.10: Illustration of a cell showing the rationale of different measurable properties of cardiomyocytes along with methods used to analyse.

Adapted from (Laurila et al., 2016)

Table 1.3: Overview of the main characteristics of electrophysiology and contractility methods currently used for hPSC-CMs functionality analysis. Table adapted from (Laurila et al., 2016

Analysis	Method	Main Target	Main Characteristic
Electrophysiology	**(1) Patch-clamp**	Single cells	Precise data on action potentials, requires advance skills and equipment, invasive and terminally ended
	(2) Multi-electrode array (MEA)	Clusters, sheets	A non-invasive method for obtaining electrophysiological data (field potentials), non-terminal, does not record single cells
	(3) Fluorescent imaging	Single cells, clusters, sheets	Specific fluorescent dye-based measurement of local membrane voltage or ion concentrations, toxic and potentially terminal
Contractility	**(4) Traction force microscopy**	Single cells, small clusters	Measures movement of fluorescent beads and determines the beating forces indirectly, is non-invasive and non-terminal
	(5) Atomic force microscopy (AFM)	Single cells, clusters, sheets	Measures beating force directly from the cell, not invasive but contacts with cell, requires advance equipment
	(6) Impedance assay	Cell sheets	Non-invasive, non-terminal, based on measuring electric impednce of an electrode with a cell on it
	(7) Video microscopy and optical recording	Single cells, clusters, sheets	Non-invasive, non-toxic, non-terminal, potential for automation

1.9 Cardiac maturation in hPSCs-CMs

To address the immaturity of hPSC-CMs several strategies have been implemented to improve cardiomyocytes maturation, which includes prolonged culture, electrical stimulation, adjustment of medium composition and supplement or culture in a 3D environment. One of the most studied systems in the cardiovascular system includes engineered heart tissue (EHT). The model was developed by Eschenhagen et al. (1997) and is being developed further by several groups. Disassociated hPSC-CMs are remodelled into hydrogel and form beating syncytium. Mannhardt et al. (2017) have used hiPSC-CMs engineered heart tissue (EHT) in comparison to human atrial trabeculae as standard to evaluate responses to inotropic drugs (Mannhardt et al., 2017a). By comparing the contractile effects of drug response to milrinone rolipram, citalopram, nifedipine, lidocaine, formoterol, tacrolimus, digoxin, acetylsalicylic acid and ryanodine, the EHTs perform better with regards to robustness and reliability (Mannhardt et al., 2017a). The only drawback of the system is that it requires 1 million cells per EHT and two weeks of incubation time after casting (Mannhardt et al., 2016).

Li et al. (2018) used an engineered human ventricular cardiac organoid chamber that consists of coculture of hiPSC-CMs with dermal fibroblast as a 3D organoid, known as 'human-heart-in-a-jar'(Li et al., 2018). They are the first to provide *in-vitro* systems that directly measure cardiac performance as a pump in clinical relevance to *in-vivo* measurement such as pressure, stroke volume, ejection fraction and cardiac output. Furthermore, the organoid can be electrically paced. The platform also demonstrates a comparable contractile response to a previously reported Langerndorff experiment, once exposed to various concentrations of isoproterenol, digoxin, verapamil, nifedipine and disopyramide.

Ronaldson- Bouchard et al. (2019) evaluated the response of hiPSC-CMs incorporated with fibroblast generating 3D bioengineered cardiac tissue to drugs, after being summited to different types of electromechanical stimulation at increasing intensity for 21 days (Ronaldson-Bouchard et al., 2019). The results of conditioning such cells/tissue in the early stage of differentiation led to the

recapitulation of both the force-frequency and force-length relationship of the heart. The tissue also led to different responses to nifedipine, verapamil, caffeine, thapsigargin and isoproterenol. Without such proposed conditioning, the response to such drugs did not correspond to the clinical effects.

As cardiomyocytes alignment is one of the contributing factors to immaturity, a group of researchers tried to use topographic cues to induce physiological cellular organisation, hoping that it would influence some cardiac response. Nanotopographic substrates were integrated with self-assembling peptide and the cardiomyocytes that grew on it were structurally developed according to nanotopographical organisation (Carson et al., 2016). Rao(2013) adopted a similar method that seeded hiPSC-CMs onto fibronectin-coated PDMS. The microgroove PDMS help to improve the hiPSC-CMs sarcomere structure organisation. While treated with caffeine, calcium cycling improved with organised calcium release, suggesting mature cellular properties and representation of adult myocardium (Rao et al., 2013).

1.10 The CRACK-IT InPulse Initiative

The CRACK-IT InPulse Challenge is an international public-private consortium that consists of academia, pharmaceutical and biotech companies (University of Nottingham, Leiden University Medical Center, University Medical Center Hamburg Eppendorf, University of Glasgow, National Centre for the Replacement, Refinement & Reduction of Animals in Research (NC3Rs), GlaxoSmithKline (GSK), Clyde Biosciences and Ncardia (Korte,2019). It aimed to generate physiologically relevant contractility platforms with hiPSC-CMs that are phenotypically mature, pose functional contractile machinery and move calcium between intracellular and extracellular spaces.

The initiative aimed to develop suitable platforms that require small quantities of tested compound and cells, with medium throughput abilities to measure contractility of hPSC-CM relevant to early safety screening in drug development. A parallel or simultaneous measure of calcium handling and/or voltage with or without physiological loading, if possible, was included as supplementary information to decide integrated decision-making.

1.11 Genome-editing of hPSCs for disease modelling

Because of the complexity of human cardiovascular pathology, it is crucial to develop disease models that recapitulate key aspects of cardiovascular disease in humans (Chun et al., 2018), especially when generating hiPSCs is unfeasible and lacking in finding appropriate controls with matching genetic backgrounds when studying low-signal to noise phenotypes (Zhu et al., 2011). Furthermore, it is difficult to obtain genetically different human tissues of disease or polymorphism variation for statistically significant studies, so genome-editing-based disease modelling is more favourable (Kim, 2015). Disease models could be enhanced by utilising a site-specific nucleases (SSNs) approach from genome editing technologies. The SSNs generate a double-strand break at distinct genomic sites which can be healed by either a non-homologous end joining (NHEJ)-DNA pathway or by homology-directed repair (HDR) machinery (Hockemeyer and Jaenisch, 2016).

Earlier tools of SSNs comprised zinc-finger nucleases (ZFNs) and transcription activator-like nucleases (TALENs). The ZFNs proteins consist of a zinc finger DNA domain that is fused to restriction endonuclease enzyme known as FokI, which when coming together as a dimer will subsequently cleave DNA to generate a double-strand break (DSB)(Chen and Knoepfler, 2016). Following the break, the endogenous DNA repair mechanism plays a role, resulting in genome modification near the cleavage site. Urnov et al (2005) have demonstrated that ZFNs can induce modification to correct X-linked severe combined immune deficiency (SCID) disease mutations in patient-specific cells in more than 18% (Urnov et al., 2005). Similar to ZFNs, TALENs contain FokI. The incorporation of FokI into TALENs tandem repeats which is accountable for nucleotide-binding specificity for targeted DSB, thus reducing the off-target binding effects (Chen and Knoepfler, 2016, Musunuru, 2013). TALENs are shown to have lower toxicity and are easier to design than ZFNs. Both ZFNs and TALENs are, however, limited to the high cost, labour intensive and reduced specificity which has caused their rather slow implementation as research tools (Eguizabal et al., 2019, Hockemeyer and Jaenisch, 2016).

Additionally, with advances in technology, the clustered regularly interspaced short palindromic repeat-associated nuclease-Cas9 (CRISPR/Cas9) is increasingly preferred because of its efficiency, ease of use and versatility (Christidi et al., 2018). The Cas9 enzyme is directed by single guide RNA (gRNA), which can be designed and engineered for precise editing (Mali et al., 2013). Thus in general, CRISPR/Cas9 can be easily adapted to target genomic sequence by modifying the gRNA. The CRISPR/Cas9 generates double-strand breaks, and in combination with single-stranded oligo DNA nucleotide (ssODN) template, the repair process occurs via HR and the introduction of specific mutations can be readily achieved (Richardson et al., 2016).

As such, the technologies enable researchers to edit, introduce a mutation or polymorphism into a gene to unravel many mechanistic or differences in response (Christidi et al., 2018, Chun et al., 2018). This meant to elucidate the contribution of a single mutation, double mutation, polymorphisms or variants to understand different effects or severity of the disease. Genome-editing is appealing for pharmacogenomics applications as it can be tested in the very early stages via cell culture. This system could generate novel isogenic lines that enable genetic modification but maintain the same background as the most suitable control to study genetic variants that affect drug response, gene function or cause diseases **(Figure 1.11)** (Bruyneel et al., 2018).

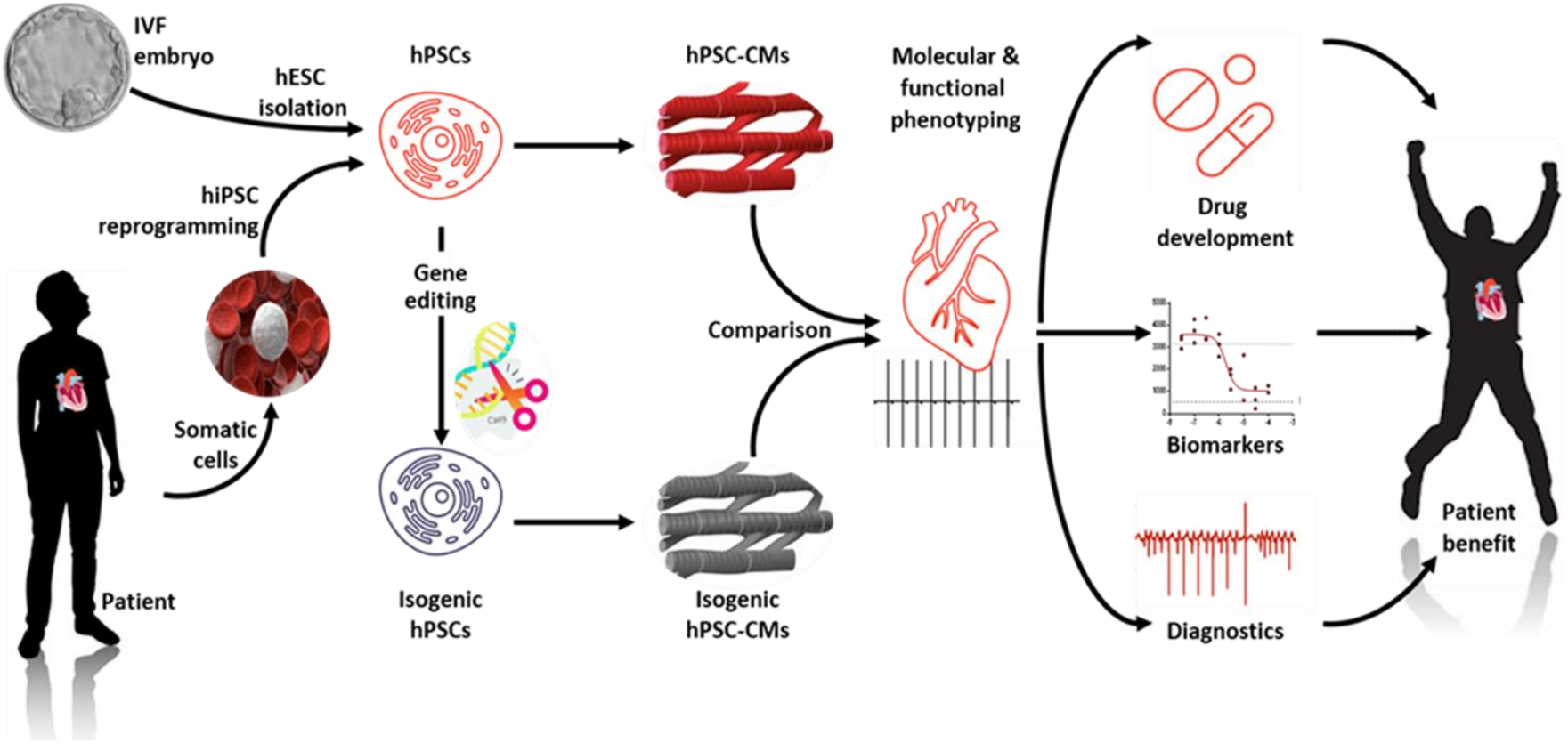


Figure 1.11: Generation, engineering and utility of hPSC-CMs.

The hPSCs can be genome-edited by, for example, CRISPR/Cas9 to produce isogenic hPSCs that have an exact background and only differ in specific engineered differences. By utilising this technology, there is the potential to advance the development of drugs, efficacy and diagnostics for end patient benefits. Schematic photo taken from Korte (2019).

1.12 ß-adrenergic function in heart

Heart contractility contributes to cardiac output that is essential for the maintenance of blood circulation throughout the body (Guth et al., 2019). As part of haemostasis, during stress, the ß-adrenergic receptors (ßARs) mediate the interference between the sympathetic and cardiovascular system to stimulate the heart **(Figure 1.11)**. The catecholamines (Epi/Norepi) activate ßARs to produce cyclic adenosine monophosphate (cAMP) and enhance the activity of protein kinase A (PKA). This leads to the phosphorylation of calcium channels and enhanced intracellular calcium level. The phosphorylation of myosin also occurs, increasing the rate of cross-bridge cycling, and thus further contraction. Increase in contractility, however, can lead to impaired cardiac function and increased proarrhythmic risk, while a decrease in contractility can lead to hemodynamic effects that cause a drop in blood pressure and loss of blood supply to vital organs (Xiang and Kobilka, 2003). To complicate matters further, the genetic polymorphisms of the $ß_1$-adrenergic receptor such as *Ser4Gly, Arg389Gly* and $ß_2$-adrenergic receptor such as *Arg16Gly, Gln27Glu,* might yield different cardiac side effects or functionality effects upon catecholamine/drug administration (Bruck et al., 2003). For this reason, *in-vitro* modelling of cardiac disease or polymorphisms is needed for identification and validation of different pharmacological response.

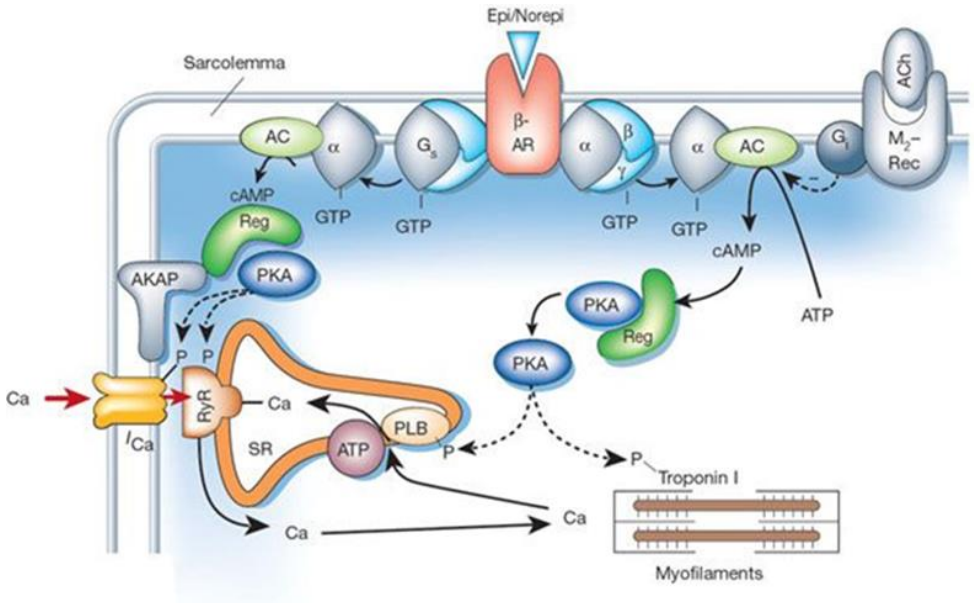


Figure 1.12: Schematic representation of ßAR function in cardiomyocytes
AC, adenylyl cyclase; ACh, acetylcholine; AKAP, A-kinase anchoring protein; ß-AR, ß-adrenergic receptor; PLB, phospholamban; Reg, PKA regulatory subunit; SR, sarcoplasmic reticulum (Bers, 2002).

1.13 Thesis Aims

The cardiac safety paradigm is costly and time-consuming, yet many compounds fail at the *in-vivo* stage in big animals like dogs or in the early clinical phase. This is a risk to pharmaceutical companies and the treatment of patients. Evolving technologies in hPSC-CMs, diversity of *in-vitro* platforms and improvement in cardiac maturity are providing opportunity for the development of a relevant human system approach for cardiac safety assessment and drug efficacy screening.

Current initiatives for cardiotoxicity rely mostly on electrophysiology and structural changes of drug-induced adverse events in hPSC-CMs. Nonetheless, cardiac contractility, which is crucial for cardiomyocytes function, does also play an essential role in predicting cardiotoxicity. Additionally, voltage quantification would strengthen decision-making and the evaluation of the reliability of the results.

In addition to drug safety and efficacy, some gene/receptor polymorphisms, particularly β_2-adrenergic receptors, play a role in influencing patient response towards the treatment. However, many studies are redundant as the effects of β_2-adrenergic receptor polymorphisms are influenced by many factors including genetic and environmental factors. A genome-edited disease model from hPSC-CMs would be ideal for investigating the impact of gene-induced changes on cell function based on β_2-adrenergic receptor polymorphisms and studying genotype-phenotype associations for predicting the cardiovascular risks of individual patients and their responses to therapies. Therefore the aims of this thesis were:

1) To establish the CellOPTIQ drug screening system by sequentially analysing contractility and voltage output by validating 'training' sets of drug compounds and developing culture systems.
2) To test the cellOPTIQ system with up to 27 blinded compounds provided by GSK with three different sets of hiPSC-CMs.
3) To refine and improve the CellOPTIQ and culture system after 'unblinding', if needed.
4) To investigate the β_2-adrenergic receptor polymorphisms via gene-induced changes to cell function by utilising genome-editing hPSC-CMs

Chapter 2 Materials and Methods

2.1 Cell culture

2.1.1 General Cell Culture

All cell culture procedures were conducted in antibiotic-free conditions using type II Biological Safety Cabinet (BSC). Cells were maintained at 37°C in a humidified atmosphere with 5% CO_2 (Heraeus HERAcell 150). All growth factors were kept in -20ºC and -80ºC (according to manufacturer instruction) during storage and thawed to room temperature before being added fresh into media for cell culture usage.

2.1.2 Human pluripotent stem cells (hPSCs) culture condition

The hPSCs cryovial was thawed in a water bath for 1 minute until the icy solution was half dissolved, followed by resuspending in 9ml of Essential8 (E8) medium (LifeTech: A1517001). Cells were then centrifuged down at 160g for 4 minutes, and the cell pellet was dissolved in E8 supplemented with 10 μM Y-27632 ROCK inhibitor (ROCKI) (Tocris: 1254) and re-seeded into previously prepared 25 cm^2 (T25) culture-treated flask coated with matrigel (Corning: 354234) 1:100 in DMEM medium. The culture medium was completely refreshed every day until the cells reached their 70% confluency.

Once ready, the confluence cultures were washed once with Dulbecco's Phosphate Buffered Saline (DPBS) (ThermoFisher: 14190250) before dissociated using 1ml of TrypLE Select (ThermoFisher: 12563029) at 37C for 3 minutes. The enzyme was aspirated out, and cells were resuspended with E8-ROCKI and centrifuged for 4 minutes at 160g. Cells were manually counted using a hemacytometer. The cells were then reseeded into a new matrigel coated T25 flask at the required density, usually with 800,000 cells/per T25. The medium was changed after 24 hours with just E8 and refreshed daily until subsequent dissociation (usually after 72 hours in culture). The hPSCs were passaged every 3-4 days to ensure they did not enter senescence and for a maximum of ten times and terminated to prevent the accumulation of abnormal karyotypes due to serial passages.

2.1.3 Growth curves

To assess the growth kinetics of genome-edited lines, the growth curves were carried out with culture conditions (described in 2.1.2). The hPSCs involved normal passaging and were seeded at a fixed number of cells into newly made culture vessels. The number of cells seeded were kept similar for all (more than 5) passages. Cumulative population doublings and population doubling time were calculated according to the formula below:

Cumulative population doublings = Σ (Log_{10} number of cells doublings / Log_{10} (2))

Population doubling time (hour) = Total time in culture (hour)/ Cumulative population doublings

2.1.4 Karyotyping

To prepare samples for karyotype evaluation, the hPSC in growing phases were treated with 100 ng/ml of KaryoMAX Colcemid (ThermoFisher: 15212-012) for 30 minutes in order to arrest cells in their metaphase stage. Cells were later harvested and centrifuged at 160g, for 4 minutes. The pellets were resuspended drop by drop on a vortex with hypotonic solution (0.6% sodium citrate; ThermoFisher: S/3320/53) and incubated at room temperature for 10 minutes, followed by centrifugation at 300g for 5 minutes. The supernatants were aspirated and pellets were fixed with 10 ml of fix solution (5:1 ratio of Methanol: Glacial acetic acid; Methanol, ThermoFisher: M/4000/17; Glacial acetic acid, ThermoFisher: A/0400/PB17) dropwise on vortex. The fixation steps were repeated three times and centrifuged for 300g, 5 minutes, then resuspended in 1ml fixation solution and stored at -20ºC. The karyogram analysis was carried out by Nigel Smith group at Nottingham City Hospital.

2.1.5 Nottingham in-house cardiomyocytes differentiation

The hPSCs cardiac differentiation was carried out using an in-house monolayer differentiation method (Duncan et al., 2017; Kondrashov et al., 2018). The hPSCs were passaged as described above and seeded in density between 30,000 – 50,000 cells/cm^2 according to hPSC cell lines. Once the cells reached the

confluency of 70-80%, they were preconditioned using a matrigel overlay method which consists of diluted matrigel (1:100 dilution) in StemPro-34 medium (ThermoFisher: 10639011) containing 1% v/v L-glutamine (ThermoFisher: 25030081), supplemented with 1 ng/ml recombinant human bone morphogenetic protein 4 (BMP4) (R&D: 314-BP-050) for overnight incubation (12 to 16 hours) and known as day -1 of differentiation. Around 12 to 16 hours later (day 0 of differentiation), the medium was changed to StemPro-34, supplemented with a combination of 10 ng/ml BMP4 and 8 ng/ml recombinant human Activin A (ThermoFisher: PHC9564) (BMP4+Activin A) and incubated for two days. Roughly 48 hours later (day 2 of differentiation), the culture medium was replaced with RPMI 1640 basal medium (ThermoFisher: 21875034) with B27 minus insulin (ThermoFisher: A1895601) (RPMI-B27-No Insulin), supplemented with small molecules 100 µM KY02111 (R&D: 4731) and 100 µM XAV 939 (R&D: 3748). On day 4 of differentiation, the medium was replaced with RPMI 1640 with B27 (ThermoFisher: 17504-044) (RPMI-B27), supplemented with both KY02111 and XAV 939 at 100 µM for another 48 hours. The culture medium was refreshed with RPMI-B27 every two days (48 hours) starting on day 6 onwards, until the day of assay. The beating cardiomyocytes were usually observed from day 7 onwards, and a monolayer synchronous beating sheet was formed around day 10 onwards, ready to be dissociated.

2.1.6 Cardiomyocytes dissociation

Throughout the study, the hPSC-CMs were routinely dissociated on day 11 of differentiation for R-PAT and day 13 of differentiation for β_2 isogenic lines when the beating sheet was observed. The dissociation was performed for downstream applications such as CellOPTIQ assay, immunostaining, GloSensor™ assay and to prevent cells from peeling off from the culture vessel for the long-term study of day 30 cardiomyocytes. The hPSC-CMs were washed two times with warmed 37ºC calcium and magnesium-free Hank's Balanced Salt Solution (HBSS) (ThermoFisher: 14170112). The CMs were later incubated with 200 units/ml collagenase II (Worthington: LS004176), containing 10 µM ROCKI, 1 mM HEPES (Sigma-Aldrich: H4034) and 30 nM N-Benzyl-p-toluenesulphonamide (BTS) (TCI chemicals: B3082) for 3 hours in a humidified incubator at 37°C, 5% CO_2. The flask was tapped gently to dislodge CMs, which were harvested with basal RPMI containing 24 µg/ml DNaseII (Sigma-Aldrich: D8764). The medium was

centrifuged at 100x g for 15 minutes, and the cell pellet was resuspended with RPMI-B27 and passed through a 100 µm cell mesh (VWR: 89508-840) to remove clumps. The single cells were then counted using a haemocytometer and subsequently replated onto culture vessels with appropriate stated culture density in media containing RPMI-B27 with ROCKI.

2.1.7 Cardiomyocytes cryopreservation

Subsequently, after CMs dissociation, for cryopreservation purpose, the CMs were resuspended in cryo medium containing 90% Fetal Bovine Serum (ThermoFisher: 26140079) with 10% DMSO (Sigma-Aldrich: D2650) at 3.2 million cells at a final 1 ml volume per vial. The vials were stored in Mr Frosty at -80ºC overnight and later transferred to liquid nitrogen for long-term storage.

2.1.8 Nottingham thawing protocol

The hPSC-CMs cryovial was thawed in the water bath for 1 minute until the icy solution was half dissolved, followed by resuspending in warmed 37ºC 9ml of thawing medium containing RPMI-B27, 10% FBS and 10 µM ROCKI. The CMs were centrifuged down at 250 g for 4 minutes, and the cell pellet was dissolved in RPMI-B27 plus FBS and ROCKI and re-seeded into culture vessels with stated density and appropriate coating.

2.1.9 Dropwise thawing protocol

The frozen hPSC-CMs cryovial was placed in a 37ºC incubator for precisely 6 minutes for the thaw. The content was gently transferred into a 50 ml falcon tube using a p1000 pipette; pipetting up and down was avoided. The empty vial was rinsed with 1 ml thawing medium and added to cells dropwise by one drop every 5 seconds, using a p1000 pipette and gently swirled after each drop. This process was repeated three times. Next, 4.7 ml thawing medium was added dropwise into the tube with one drop every 2 seconds using a 5ml pipette. The CMs were centrifuged down at 250 g for 3 minutes, counted and seeded accordingly.

2.1.10 Cardiomyocytes transfection

The cardiomyocytes transfection was achieved using Lipofectamine 3000 (ThermoFisher: L3000015). Cells were plated on 96-well plate, 100 µl/well at the density of 40,000 cells per well. The media were changed with 50 µl RPMI-B27, at least 30 to 60 minutes prior to transfection. The transfection reagents and complexes were prepared according to the below protocol (Table 2.1). The mixture was combined, vortex and incubated for 10 to 15 m minutes to allow the formation of complexes. After 4-6 hours of transfection, the culture was topped up with 50 µl of RPMI-B27+10% FBS and incubated with the cells for 24 h at 37 °C in a humidified incubator supplying 5% CO_2. After 24 hours of incubation, the cells were replaced with 100 µl RPMI-B27. All transfection assays were carried out with GFP control and no reagent group as controls. Imaging of transfected cells was performed 48 hours after transfection.

Table 2.1: Lipofectamine 3000 transfection reagents and complexes mixture.

Step	Tube	Complexation components	Amount per well (96-well)
1	Tube 1	Lipofectamine 3000 reagent	0.15 µl
		Opti-MEM I medium (ThermoFisher: 31985062)	4.85 µl
2	Tube 2a	P3000 reagent	0.2 µl
		Opti-MEM	4.6 µl
		DNA amount (DNA concentration = 0.496 µg/µL GloSensor™ 20F stock)	0.2 µl
	Tube 2b (GFP control)	P3000 reagent	0.02 µl
		Opti-MEM	4.7 µl
		DNA amount (DNA concentration= 1.0 ug/ul GFP stock)	0.1 µl
3	Spin down both tubes (1) and (2a and 2b)		
4	Add tube 2 solution to tube 1 and mix well to form lipid- DNA complex		
5	Incubate mixture from step 3 at room temperature for 10–15 min		
6	Add solution dropwise to the well (10 µl of lipid-DNA complex into each well); gently swirl plate to ensure homogeneous distribution of complex to the entire well		

2.2 Microscopy

2.2.1 General microscopy

For simple general microscopy, images in this study were taken as bright field images using a Nikon ECLIPSE RE2000-S inverted microscope.

2.2.2 Fluorescence and immunostained image analysis

For fluorescence live-imaging and immunostained samples, microscopy was conducted on an Operetta™ high content image analysis system (PerkinElmer). Data were analysed using Columbus™ software (PerkinElmer).

2.3 Molecular biology

2.3.1 Genomic DNA extraction

The genomic DNA was harvested using a DNeasy Blood and Tissue kit (Qiagen: 69506) following manufacturer instructions. The DNA was eluted in 30 µl molecular grade water. DNA concentration together with purity was measured using a NanoDrop DN100 spectrophotometer. The genomic DNA was stored in -20 ºC until the day of the assay.

2.3.2 Polymerase chain reaction (PCR)

For the PCR, 2.5 µl of 10 µM of each forward and reverse primers were utilised with DNA concentration (below 250 ng in total) into the PCR master mix (dNTP,5x buffer, water and phusion polymerase). The PCR reaction was conducted in a thermal cycler with:1) initial denaturation 98ºC for 5 minutes (for Phusion polymerase), 2) 25 to 33 repeated cycles of denaturation at 98ºC for 30 seconds, 3) annealing at 64ºC for 30 seconds, 4) extension at 72ºC for 30 seconds and 5) final extension step at 72^{o}C for 10 minutes.

2.3.3 Gel electrophoresis, extraction and purification

Gel electrophoresis was done in 1% agarose gel (Sigma-Aldrich: A7431), in TAE buffer (Tris Acetate with EDTA) and ethidium bromide (EtBr) with 100 mV. The gels were captured in LAS-4000 (Fujifilm) image analyser. The DNA amplicon generated by PCR was purified using the QIAquick Gel Extraction kit (Qiagen:

28704) following manufacturer instruction. DNA was eluted in 30 µl molecular grade water and quantitated using NanoDrop DN100. The PCR products were also sent for sequencing using the external Sanger sequencing service (Source Bioscience).

2.3.4 RNA extraction and cDNA synthesis

The RNA was extracted using the RNeasy Mini Kit (Qiagen: 74104) according to manufacturer protocol and eluted in 30 µl molecular grade water and the DNA concentration together with purity was measured using the NanoDrop DN100 spectrophotometer. A 260/280 ratio between 1.8 and 2.2 is generally accepted as pure for RNA. The extracted RNA was stored in -80 ºC until the day of the assay. The cDNA synthesis was accomplished using SuperScript™ IV Reverse Transcriptase (ThermoFisher: 18090050) following the manufacturer's instructions to convert RNA into cDNA for quantitative PCR (qPCR).

2.3.5 The qPCR analysis of gene expression

The qPCR reaction mixture contains 10 µl of TaqMan® Fast Advanced Master Mix (2X) (ThermoFisher: 4444557), 1 µl Taqman Assay (20X), 7 µl Nuclease-free water, and 2 µl of cDNA template. The real-time PCR reaction was performed using the 7500 Fast Real-time PCR template. Expression values were normalised to the average expression of *GAPDH*. Taqman assay IDs for *ADRB1* and *ADRB2* are Hs02330048_s1 and Hs00240532_s, respectively. The experiments were performed by Nguyen Vo.

2.3.6 The hPSC and hPSC-CMs Immunostaining

The immunostaining was performed in hPSCs to assess the nuclear pluripotent associated transcription factors **(Table 2.2)**. The hPSCs were cultured at a density of 10,000 cells in 96- well plate and once the confluency reached 60%, the cultures were fixed accordingly. To characterise cardiac markers cells hPSC-CMs were plated into 96 well, fixed and stained according to **Table 2.3**. Cells were maintained up to at least day 20 (day of the assay) for the 'drug-induced chapter' and day 30 for the 'gene-induced chapter' and washed with DPBS to remove debris and medium residue.

Cells were then fixed with 4% paraformaldehyde (PFA) solution (Sigma-Aldrich: P6148) at room temperature for 15 minutes. Cells were rewashed twice with DPBS and stored in DPBS with 20% FBS at 4°C for up to 2 months until staining. On the day of immunostaining, the cells were permeabilised with 0.1% Triton-X (Sigma-Aldrich: T8532) 100 µl/well diluted in DPBS at room temperature for 15 minutes. After being permeabilised, cells were rewashed with DPBS three times for 1 minute each and incubated with blocking solution (10% human serum in DPBS) for at least 30 minutes. The primary antibodies (e.g. α-actinin, OCT4) were diluted in 1% human serum (see **Table 2.2 and Table 2.3),** and incubated with cells 50 µl/well for at least 2 hours or overnight at 4°C. Subsequently, the following day the wells were washed with 0.1% Tween (Fisher Scientific: BP337-100) diluted in DPBS (Tween-DPBS) three times. Secondary antibodies were prepared accordingly (see **Table 2.2 and Table 2.3),** and staining was done by incubating the diluted secondary antibodies (50 µl/well) at room temperature for 1 hour. Cells were then again washed with Tween-DPBS three times to remove the unspecific binding. Stained cells were then co-stained with nuclear stain DAPI (Sigma-Aldrich: D9542) at dilution 1:500 in DPBS at room temperature for 20 minutes. Cells were then finally washed once with DPBS and proceeded for imaging using Operetta™ High Content Imaging System by PerkinElmer or stored at 4ºC.

Table 2.2: Antibodies used for pluripotent hPSCs immunostaining

Expression	OCT4	SOX2	NANOG
Primary antibody	Mouse anti-OCT3/4 (Santa Cruz: SC-5279)	Goat anti-SOX2 (R&D Systems; AF2018)	Goat anti-NANOG (R&D Systems: AF1997)
Dilution for primary antibody	1:200	1:200	1:200
Secondary antibody	Goat Anti-mouse AlexaFluor 488 (Thermofisher: A11001)	Rabbit anti-goat FITC (Jackson LAB: 305-095-003)	
Dilution for secondary antibody	1:400		

Table 2.3: Antibodies used for hPSC-CMs immunostaining

Expression	Cardiac α-Actinin	MLC2A	MLC2V	CX43
Primary antibody	Mouse anti-alpha actinin (Sigma-Aldrich: A7811)	Mouse anti-myosin light chain 7 antibody (Abcam: ab68086)	Rabbit anti-myosin light chain 2 antibody (Abcam: ab79935)	Rabbit anti-connexin-43 (Sigma-Aldrich: C6219)
Dilution for primary antibody	1:800	1:1000	1:800	1:400
Secondary antibody	Goat anti-mouse AlexaFluor 488 (Thermofisher: A11001)		Goat anti-rabbit AlexaFluor 647 (ThermoFisher: A21244)	
Dilution for secondary antibody	1:400		1:400	

2.4 CellOPTIQ platform analysis

CellOPTIQ platform by Clyde Biosciences Ltd was used as a main platform in assessing contractility and the voltage electrophysiology properties of hPSC-CMs. For experimental plates that involved voltage studies, the CMs were cultured in a serum-free medium (SFM) one day prior to the assay. The SFM consists of Dulbecco's Modified Eagle Medium (DMEM) (Gibco, 21969035), 10mM galactose (Sigma-Aldrich: G0750) and 1 mM sodium pyruvate (Sigma-Aldrich: P2256). The SFM can be stored up to one week.

2.4.1 In-house CMs culture conditions for CellOPTIQ

The culture condition for frozen cryopreserved in-house CMs involved a dropwise thawing method with 40,000 cells seeding density into 96-well plates, maintained in RPMI-B27. Meanwhile, for fresh in-house CMs, the cells were cultured with 30,000 cells per 96-well plate. For CellOPTIQ assessment (contractility and electrophysiology analysis), experiments were carried out at around day 20-21 post differentiation and changed to SFM 24 hours before the CellOPTIQ assay.

2.4.2 Commercial lines culture conditions for CellOPTIQ

2.4.2.1 iCell^2-CMs

The iCell^2-CMs (Cellular Dynamics: C1016) from the vials were seeded at the density of 25,000 cells per well into 96-well plates (Nunclon™ Delta Surface; Thermo, 167008) using iCell cardiomyocytes plating medium (Cellular Dynamics: M1001) and were maintained in iCell cardiomyocytes maintenance medium (Cellular Dynamics: M1003) for 10 days post-thawed for use in the drug-induced changes evaluation study. Similar to R-PAT-CMs, the media were changed 24 hours before CellOPTIQ assay with SFM.

2.4.2.2 Pluricyte-CMs

The Pluricyte-CMs (Ncardia: PCK-1.5) were seeded at a density of 35,000 cells into 96-well plates (Greiner Bio-One-655087) following manufacturing recommendations and then maintained in the Pluricyte medium. The assay windows were between day 8-9 post-thawed. The Pluricyte medium was

changed into 50% SFM + 50% Pluricyte cardiomyocytes medium (serum-free) 24-hours before CellOPTIQ assay and during the day were changed into 100% SFM.

2.4.3 Drug preparations

2.4.3.1 Training drugs

The training drugs were all dissolved in DMSO (except isoprenaline which was diluted in hydrochloric acid and sterile water) with the maximum final DMSO concentration being added to the cells was at 0.1%. For drug treatment, 50% of the well volume was replaced with 50% of the drug solution prepared in RPMI-B27 media at a defined concentration. Parallel vehicle controls were made using DMSO only diluted in RPMI-B27. The list of drugs used in this study with the respective supplier is tabulated in **Table 2.4**.

Table 2.4: Table of drugs used for training.

Drug	**Supplier: Cat no.**
Isoprenaline	Sigma-Aldrich: I5627
Digoxin	Sigma-Aldrich: 20830-75-5
Bay K 8644	Sigma-Aldrich: 71145-03-4
EMD 57033	Sigma-Aldrich: 530657
Nifedipine	Sigma-Aldrich: 21829-25-4
Ryanodine	Tocris: 1329
Thapsigargin	Sigma-Aldrich: T9033

2.4.3.2 Blinded drugs

For drug assessment studies, the drugs were purchased, weighted and formulated by GSK. The working stock solution of drugs was made at the indicated concentrations, using formula sheets provided by GSK. The final vehicle concentration (DMSO) was at a maximum of 0.1% DMSO for all concentrations. The following drugs were used for blinded studies, some of the catalogue numbers being provided by GSK after the unblinded meeting (**Table 2.5)**.

Table 2.5: Table of drugs used for blinded drug assessment.

Drug	Supplier: Cat no.
Epinephrine	-
Forskolin	-
Levosimendan	-
Pimobendan	Cambridge Biosciences : P3456
Acetylsalicylic acid	Sigma-Aldrich: A5376
Atenolol	-
Verapamil	Sigma-Aldrich: V4629
Doxorubicin	Sigma-Aldrich: D1515
Sunitinib	Sigma-Aldrich: PZ0012
Captopril	Sigma-Aldrich: C4042
Dobutamine	-
Glibenclamide	-
Milrinone	-
Omecamtiv mecarbil	-
Enalaprilat	Sigma-Aldrich: E6888
Citalopram	Sigma-Aldrich: C7861
Clonidine	-
Itraconazole	Sigma-Aldrich: I6657
Sorafenib	Cambridge Biosciences : SM95-500
Ivabradine	Sigma-Aldrich: SML0281
Terbutaline	-
Flecainide	Sigma-Aldrich: F6777
Paracetamol	-
Phentolamine	Sigma-Aldrich: P7547
Tolbutamide	Sigma-Aldrich: T0891
Pravastatin	Sigma-Aldrich: P4498
Sildenafil	Sigma-Aldrich: PZ0003

2.4.4 Contractility measurement

The beating CMs were recorded at 40x objective for 100 frames per second and analysed offline using ImageJ_Man plug-in and Contractility Tool software developed and copyrighted by Clyde Biosciences Ltd. The software analysis is based on the sum of absolute differences (SAD) algorithms between images. The absolute difference between pixels in original frames and corresponding frames based on changes on pixel intensities were calculated to determine the contraction amplitude, contraction time and relaxation time. The statistical analysis was conducted using GraphPad Prism (GraphPad Software, Inc) by one-way ANOVA, followed by the Dunnett test.

2.4.5 Voltage electrophysiology measurement

In order to assess the voltage electrophysiology, the CMs were stained with voltage-sensitive dye (VSD) that penetrated inside the cell membrane. A FluoVolt membrane potential kit (ThermoFisher: F10488) with the fluorescence of 490nm excitation has been utilised throughout this study. The CMs were loaded in 50 µl/well SFM containing FluoVolt (1:200 powerload concentrate and 1:2000 FluoVolt dye) for 20 minutes at 37°C and 5% CO_2. After incubation, the medium was replaced with 200 µl/well and incubated for at least 15 minutes before recording started. The voltage recording was made for each well for 10 seconds. The voltage analysis was done using CellOPTIQ proprietary software and normalised to the maximum amplitude of 1 and a minimum of 0 to standardise the height for comparison of traces. The voltage traces were developed using OriginPro (OriginLab version 7.5). The statistical analysis was conducted using GraphPad Prism (GraphPad Software, Inc) by a one-way ANOVA followed by Dunnett test.

2.4.6 Pacing stimulation

The electrical stimulation used a custom made stim strip consisting of 8 pairs of electrode (Clyde Biosciences Ltd). The stim strip was placed in a row of 96-well plate and was connected externally to the power modulator (DC power supply: Lavota). The hPSC-CMs were paced at the frequency of 0.7 to 1.7 Hz with an amplitude of 8 Volts and a pulse width of 2 milliseconds. Each pacing was stimulated for 10 seconds.

2.4.7 Drug testing

The baseline reading (without treatment) was recorded before treatment and the location of the cells was saved. Drugs incubation were added directly after the baseline measurement by removing 100 µl medium and adding 100 µl drug/vehicle solution (30 min at 37 °C), prepared according to formulation instructions. After 30 minutes incubation with drugs or DMSO vehicle, the same CMs location with the same pacing stimulus was recorded. Data were plotted as the percentage of change relative to the baseline recording.

2.5 RTCA CardioECR

The long term studies for contractility and impedance were done using the xCELLigence RTCA CardioECR instrument (ACEA Biosciences). The platform is a non-invasive, label-free platform that integrates impedance and field potential recording for the simultaneous measurement of contractility and electrical activity, respectively. The hPSC-CMs were seeded in the electronic 48-well microtiter plate; E-Plate CardioECR 48 (ACEA Biosciences: 300600940) coated with fibronectin (Roche: 11051407001). The cells were cultured according to general culture conditions but alternatively were fed with a final volume of 180 µl medium. The recordings were performed from day 4 post-plating. The media were replaced 4 to 24 hours before recording by removing 90 µl medium and gently replaced with 90 µl medium to the side of the well, using a multichannel pipettor to avoid disturbing the CMs monolayer. The activities of the CMs were monitored to ensure regular beating. The drugs were prepared in the respective culture medium at 10x final concentration in a regular 96-well culture plate and equilibrated in a cell culture incubator at 37°C, 5% CO_2. The 10 µl/well of 10x drugs were quickly added from a 48 well cell culture plate into the E-plate and gently pipetted 3 to 5 times. As the beat rate and amplitude are temperature dependent, the E-Plate was not kept outside the incubator for more than 5 minutes while the drugs were added. The data were acquired and analysed using the RTCA software (ACEA Biosciences). The recording results acquired for after drug treatments were compared to untreated wells.

2.6 GloSensor™ cAMP assay

2.6.1 GloSensor™ cAMP general principle

The $ß_2$AR CMs (GE, GQ, RE and RQ), isogenic lines at the density of 30,000 cells/well, were transiently transfected with pGloSensor™-20F cAMP plasmid (Promega: E1171) 0.1µg plasmid DNA per well of 96-well plate using Lipofectamine 3000. 24 hours after transfection, cells were changed into standard RPMI-27 media and allowed for 48 hours.

Since pGloSensor™-20F plasmid is sensitive to temperature, the plates were allowed to equilibrate for at least 10 minutes for a stable temperature of 37°C before reading the basal luminescence. All medium and drugs were prewarmed at 37°C while dispensing were performed using integrated Envision injectors with pumps, to prevent the signal's fluctuation (without taking the plate in and out) to deliver compounds to cells. Reading in an envision luminometer required 0.5s integration time between wells.

To observe the ßARs cAMP effect, the systems were tested by using an administered compound by both Envision injector pumps. One pump contained isoprenaline (ISO)(R&D Systems: 1747) to induce cAMP signal for 60 minutes, while the second pump contained Forskolin (FSK) (R&D System: 1099), a direct activator of adenylyl cyclase as a positive control to stimulate maximum cAMP for 30 minutes into the same well, respectively. Ideally, a negative control is needed, meaning a vehicle only (without ISO and FSK) throughout the experiments. However, due to the machine limitation, only two injectors could be used, and only the plate with dispensed compound (from injectors) could be read.

2.6.2 Downregulation chronic long-term assay

24 hours prior to the assay, cells were treated with 10 µM ISO to stimulate downregulation. Cells were incubated at 37ºC for 2 hours in RPMI-B27 media, supplemented with 25 mM HEPES (Sigma-Aldrich: H4034), 10% FBS and 2% GloSensor™ cAMP reagent (Promega: E1291) stock solution with $ß_1$ blocker 200 nM CGP-20712A methanesulfonate (CGP) (Sigma-Aldrich: C231-10MG) and with/without ISO 10 µM. Each condition was performed in triplicates. Washout

was performed by removing GloSensor™ cAMP reagent mix/ incubation medium, by twice washed with fresh wash medium (RPMI-27) without ISO for a total duration of 10 minutes. The cultures were replaced with GloSensor™ cAMP mix medium with CGP but without ISO. Control wells received the same number of washes in the same volume of wash media without ISO. Luminescence was read on an EnVision Multilabel Plate Reader (Perkin Elmer) in a temperature-controlled chamber at 37ºC. Basal/baseline signals were measured for 20 minutes. ISO was added to wells at 1 µM final concentration to 'rechallenge' the system and luminescence was read for 60 minutes. Later, 10 µM FSK was added to the wells to stimulate total cAMP and luminescence was read for another 30 minutes. Signals were measured by normalised to maximum FSK and subtracted the baseline. Three separate experiments, each conducted in triplicates, were quantitated and analysed using Microsoft Excel and GraphPad Prism.

2.6.3 Acute short-term assay

Cells were incubated at 37ºC for 2 hours in RPMI-B27 media, supplemented with 25 mM HEPES, 10% FBS and 2% GloSensor™ cAMP Reagent stock solution with β1 blocker 200 nM CGP. At the start of pre-incubation, a final concentration of 1 µM ISO was added at 2 hours and 30 minutes time points. Each condition was performed in at least duplicate. Washout was performed by removing GloSensor™ cAMP reagent mix/ incubation medium, washing twice with fresh wash medium (RPMI-27) without ISO for a total duration of 10 minutes, and then adding the replacement GloSensor™ cAMP mix medium with CGP but without ISO. Control wells received the same number of washes in the same volume of wash media without ISO. Luminescence was read on EnVision Multilabel Plate Reader in a temperature-controlled chamber at 37ºC. The basal/baseline signal was measured for 10 minutes. ISO was added to the wells at 1 µM final concentration to 'rechallenge' the system and luminescence was read for 30 minutes. Later, 10 µM FSK was added to the wells to stimulate total cAMP and luminescence was read for another 15 minutes.

2.7 Statistical analysis

All data are presented as mean with standard error of mean (SEM) unless otherwise stated. Statistical analysis of multiple data sets was performed using GraphPad software. For multiple comparisons between data sets, a one-way ANOVA with Tukey's multiple comparison test was chosen. For comparing multiple data sets to a single control column, one-way ANOVA with Dunnett's multiple comparison test was chosen. Significance tests were based on p-values as follows: * $p < 0.05$; ** $p < 0.01$; *** $p < 0.001$; **** $p < 0.0001$.

Chapter 3 Establishment of CellOPTIQ drug screening system with 'training' set drugs and development of culture systems

3.1 Introduction

As discussed in Chapter 1, there is a growing demand for humanised screening platforms to facilitate the investigation on *in-vitro* contractility drug screening effects in hPSC-CMs that will boost patient-specific predictions as to the effectiveness and/or toxicity of drugs. In addition, the electrophysiological effects of either intracellular Ca^{2+} or voltage measurement are highly beneficial. Ideally, the platform for hPSC-CMs drug screening must be at least capable of medium-throughput.

This chapter describes the establishment of the screening platform (CellOPTIQ) by utilising hiPSC-CMs for the use in drug assessment, as part of the CRACK-IT consortium initiative. During the establishment, the large in-house hiPSC-CMs production and optimal culture conditions for various hiPSC-CMs were evaluated. The CellOPTIQ establishment was based on seven training drugs. This chapter outlines the key cardiac parameters for contractility and voltage calculation, which were subsequently used to evaluate the blinded Tier 2 in the next chapter.

3.1.1 CRACK-IT InPulse initiative and its *in-vitro* platforms

As described in Chapter 1.10, **the CRACK-IT InPulse Initiative** consists of a multinational consortium by a public-private partnership, consisting of four academic research teams in the United Kingdom, Germany and the Netherlands, together with two biotech companies (Clyde Biosciences and Ncardia), a pharmaceutical company (GSK) and a UK funding agency (NC3Rs). The initiative aimed at developing at least medium-throughput technology platforms to evaluate its utility for preclinical safety evaluation. Within CRACK-IT, three different platforms were used, which subdivided into 3D and 2D configurations to achieve the goals.

3.1.1.1 3D configuration

3.1.1.1.1 Engineered heart tissues (EHTs)

The EHTs utilise 3D construct of hiPSC-CMs, casting within fibrin hydrogel into 24-well systems (Mannhardt et al., 2017a). The EHT is held by two parallel polydimethylsiloxanes (PDMS) posts; their deflection over each beat can then be quantitated by video-optical recording into the absolute force of contraction, allowing the monitoring of contractility. Meanwhile, the transgenic incorporation of encoded calcium indicator (GECI-GCAMP6f) into EHT allows the assessment of Ca^{2+} handling (2017). The hiPSC-CMs in EHTs exhibit more mature phenotypes than those grown in a 2D configuration (Greenberg et al., 2018) due to mechanical loading by elastic PDMS posts and contraction under auxotonic state conditions (Mannhardt et al., 2016).

3.1.1.2 2D Configuration

Most of the test systems that use hiPSC-CMs as 2D configuration rely on the stiff plastic surface of cell-culture vessels which do not allow the cells to execute auxotonic physiology but exhibit isometric contraction instead (Mannhardt et al., 2016). As a result, the contractile function can only be analysed in a restricted manner, for example, by using platforms described below.

3.1.1.2.2 Triple transient measurement (TTM)

The TTM is a system that is capable of generating interlaced 1000 frames per second movie to measure contractility, voltage action potential and cytosolic Ca^{2+} handling, in 2D monolayers seeded in 96 well plates using fluorescent sensors simultaneously (van Meer et al., 2019). Simultaneous fluorescent imaging is enabled by using high-speed switching between wavelengths, coupled with the selection of dyes that have no or minimal overlapping excitation wavelength: cell membrane label-CellMASK Deep Red (656nm), voltage-sensitive dye- ANNINE-6plus (470 nm) and calcium-sensitive dye- Rhod 3 (560nm) (van Meer et al., 2019). The measurements are then automatically processed, quantified and analysed by a hypothesis-based statistical algorithm, which was developed as part of the system.

3.1.1.2.3 CellOPTIQ (CO)

The CellOPTIQ platform developed by Clyde Biosciences is capable of delivering readouts on an integrated platform. It is a multiwell (6 wells up to 96-wells) proprietary system platform, with a multiparametric medium-throughput assay platform to screen for the inotropic and electrophysiological response of 2D monolayer hiPSC-CMs. The platform records the contractility using a high-speed camera and measures contractility (based on bright-field imaging) by using the sum of absolute differences (SAD) algorithms that evaluate the difference in pixel intensity between continuous photo frames (video). Whereas to measure electrophysiology response, voltage via fluorescence measurement of membrane voltage-sensitive dyes (di-4-ANEPPS or FluoVolt) and intracellular Ca^{2+} measurement (Fura2 or Fura4) can be quantitated using acquisition and analysis packages that come together with the system (McGlynn et al., 2018, Hortigon-Vinagre et al., 2018).

The voltage electrophysiology represents the first signal, followed by Ca^{2+} signal and contraction signal. The measurement of voltage and Ca^{2+} involve sensitive dyes that could cause toxicity in cells if they were co-stained with both. Therefore this study focuses only on voltage action potential and contraction, which represents the first and last event of EC coupling.

3.1.2 Selection of hiPSC-CMs cell lines for assessment of cardiac toxicity

As part of the CRACK-IT project, it was recommended to include at least two hiPSC-CMs lines for pharmacological and cardiotoxicity testing in CellOPTIQ. Due to the cost of commercial lines and the amount of work required to carry out the drug screening, it was agreed that the 'training' drugs in this chapter would be conducted in R-PAT hiPSC-CMs only. The R-PAT is a human-induced pluripotent stem cell line (hiPSC) that was reprogrammed by Denning Lab, The University of Nottingham from skin fibroblast using non-integrating Sendai virus (Duncan et al., 2017). In this study, the R-PAT-CMs were generated using the Nottingham in-house cardiac differentiation protocol as described in Chapter 2.1.5 (Nottingham in-house cardiomyocytes differentation)(Smith et al., 2018, Mosqueira et al., 2018, Kondrashov et al., 2018).

Two commercial hiPSC lines (Pluricyte and iCell^2) were selected to be used in subsequent blinded (Tier 2) testing (Chapter 4). Pluricyte are fully functional hiPSC-derived ventricular CMs which were purchased from Pluriomics/Ncardia. While iCell^2 hiPSC-CMs were purchased from Cellular Dynamic International, and represent the 2nd generation of original iCell with accelerated maturation process (Taylor et al., 2016).

Their suitability for the project was assessed based on their functional characteristics, and baseline characteristics (for contractility and voltage measurement).

3.2 Training drugs (Tier 1)

In order to establish the working parameters and refine the standard operating protocols for CellOPTIQ-2D hiPSC-CMs platform, a selection of seven unblinded drugs with known modes of action were chosen as a 'training set'. Since cardiac contractility is vital in excitation-contraction coupling and in predicting cardiotoxicity, the selection-defined priority included drugs that increase contraction (positive inotropy; PI) and decrease contraction (negative inotropy; NI).

Undeniably, inotropic support is essential and commonly used for patients with impaired contractile function; however, the focus of this thesis remains to investigate the unwanted drug-induced changes in term of cardiac toxicity and their associated risks. As such, at the physiological level, increases in cardiac contractility can result in myocardial hypertrophy (if chronic), impaired myocardial energy and increased proarrhythmic potential. The reduction in cardiac contractility can be clinically equally problematic, which leads to hemodynamic effects such as a decrease in systemic blood pressure (hypotension) and loss of blood flow to vital organs (Guth et al., 2019a).

The mechanisms underlying an increase in contraction depends on; 1) increase in cytoplasmic Ca^{2+} concentration by, for example, activation of L-type Ca^{2+} channels which induce the opening of ryanodine receptors (RyRs) by i) Ca^{2+} Na^{2+} agonists (Kuo and Ehrlich, 2015), ii) cardiac glycosides (Aldred et al., 2009) and iii) hERG channel blockers (Roden, 2008, Cockerill and Mitcheson, 2006).

Subsequently, the increase of intracellular free Ca^{2+} induces the release of internal calcium stores from SR via calcium-induced calcium release (CICR), which leads to the release of inhibitory tropomyosin complexes which actin and myosin myofilament move along the axis to cause shortening of cells (contraction) (Guth et al., 2019a). Hence, contraction is also stimulated through 2) myofilament activation via for example i) myosin activators and ii) Ca^{2+} binding sensitizers (Davis and Tikunova, 2007); or 3) by an increase in cyclic AMP (cAMP) via ß-adrenergic agonists (catecholamines) stimulation or PDE inhibitors (Mika et al., 2013, Maack et al., 2018) (**Figure 3.1**).

The mechanisms underlying a reduction in contraction are opposite to the above and depend on for example; 1) reduction in intracellular Ca^{2+} by i) Ca^{2+} channel blockers, ii) reuptake of intracellular calcium into SR by SERCA or decrease SR Ca^{2+} release by ryanodine and iii) pump out Ca^{2+} of the cell by Na^{+}–Ca^{2+} exchange (NCX) (Eisner, 2014); 2) myofilaments inhibition via myosin inhibitors; 3) reduction in cAMP concentration via ß-blockers; and 4) general toxicity which includes mitochondrial dysfunction, apoptosis and necrosis (van Meer et al., 2019) (**Figure 3.1**). The seven selected training drugs consist of four PI (Isoprenaline, digoxin, BayK8644, and EMD-57033) and three NI (nifedipine, ryanodine and thapsigargin)(**Figure 3.1**).

3.3 Chapter aims and objectives

The aims of this chapter are to outline the objectives of this phase. The working parameters and drug-induced changes frameworks for CellOPTIQ-hiPSC-CMs establishment were done by sequentially measuring contractility and voltage output based on the seven training drugs. The primary source of hiPSC (R-PAT) thus had to be largely differentiated into working cardiomyocytes with the ability to successfully thaw after cryopreservation. It was also important to investigate the suitability of two other commercial hiPSC-CMs (Pluricyte and iCell^2) in the CellOPTIQ before continuing to blinded testing. The following objectives had to be met to fulfil this aim:

1) Validate the quality control of the large scale of differentiation for the primary source of hiPSC-CMs; the R-PAT CMs
2) Compare the characteristics of all three hiPSC-CMs
3) Compare the baseline (contractility and voltage) response of all three hiPSC-CMs in CellOPTIQ platform
4) Utilise the selected seven training drugs of known response to define and unify standard operating procedures and data analysis for contractility and voltage measurement of CellOPTIQ-hiPSC-CMs system.

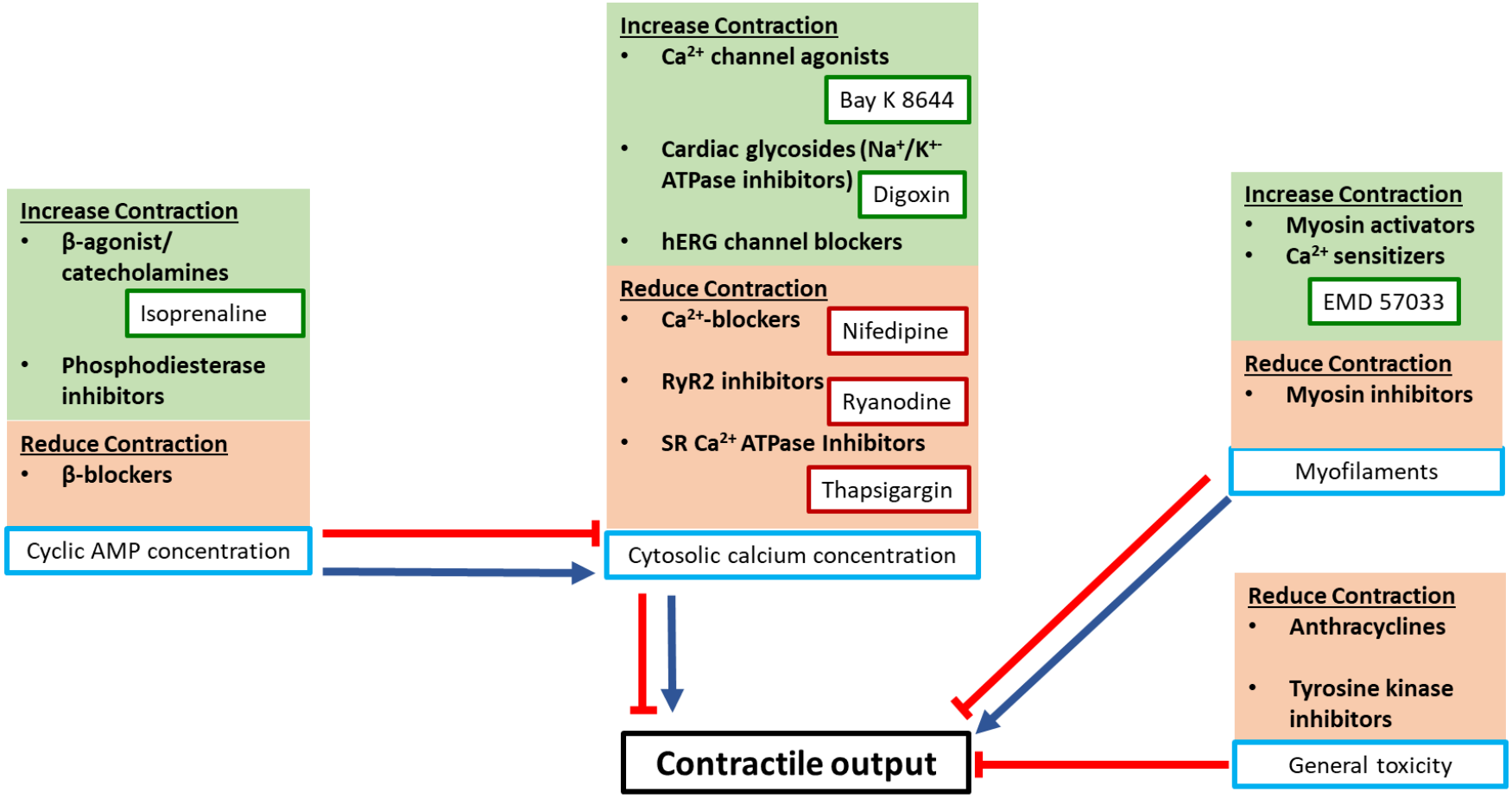


Figure 3.1: Schematic illustration for the drug-targeted mechanism of actions and pathways influencing the cardiomyocytes contraction.
The blue line with the arrow indicates stimulation, while the red line with death end indicates inhibition. Adapted from (van Meer et al., 2019)

3.4 Results

3.4.1 Large scale production of in-house R-PAT-CMs

Since the main aim was to test the suitability of CellOPTIQ platform in combination with hiPSC-CMs in predicting drug-induced changes in relative to cell function and toxicity, it was essential to generate hiPSC-CMs on a large scale to ensure enough repeats throughout the experiments. It was also aimed to standardise cell production and ensure enough supply to the CRACK-IT partners. Throughout the study, 34 different drug testing needed to be conducted, not including the repeats. Each drugs on each plate configuration required 40 wells = 5 wells for vehicle control, 5 wells for nifedipine control, 5 wells to digoxin control, 5 wells for concentration 1, 5 wells for concentration 2, 5 wells for concentration 3, 5 wells for concentration 4, 5 wells for concentration 5 with 40,000 cells each well = 1.6 million cells/plate. By taking into factor of 50% survival percentage; 3.2 million cells needed for per drug/plate. The total number of drugs tested across all sites on R-PAT-CMs = 102. Therefore, for total drugs of 102 x 3.2 million CMs = 326.4 million CMs required.

Another reason for in-house differentiation is the cost of commercial hiPSC-CMs. One vial of 2.5 million viable commercial hiPSC-CMs (iCell^2) cost $1000 at the time of this study, not including media for maintenance (https://fujifilmcdi.com/products-services/icell-products/icell-cardiomyocytes2/.

3.4.1.1 R-PAT-CMs differentiation efficiency

The R-PAT line was put forward as this cell line is regularly used within Denning laboratory, and the associated stem cell culture and in-house cardiac differentiation protocols had been optimised for use as described in method Chapter 2. The CMs produced from R-PAT beats on day seven onwards and dissociations were routinely performed on day 11. All quality control for fresh cells was carried out on day 14-15 post differentiation.

In order to investigate batch to batch variation between several batches of large scale in-house R-PAT-CMs and their differentiation efficiency, quality controls were conducted. The immunostaining analysis for α-actinin positive cells was

performed to evaluate the purity of cardiomyocytes. The α-actinin is a major component of Z-disks in sarcomeres (a basic contractile unit within cardiomyocytes) as an indicator for early CM markers (Wilsbacher and Coughlin, 2015).

Throughout the study, at least 14 independent batches of R-PAT-CMs differentiation were achieved using our in-house cardiac differentiation protocol **(subchapter 2.1.5)**. The majority (13/14) were found to be at least 80% pure cardiomyocytes **(Figure 3.2)**. The one batch below 80% cardiomyocyte purity was excluded from any further assay. The differentiations indicated that small variations existed between batches but all exhibited high cardiomyocytes purity.

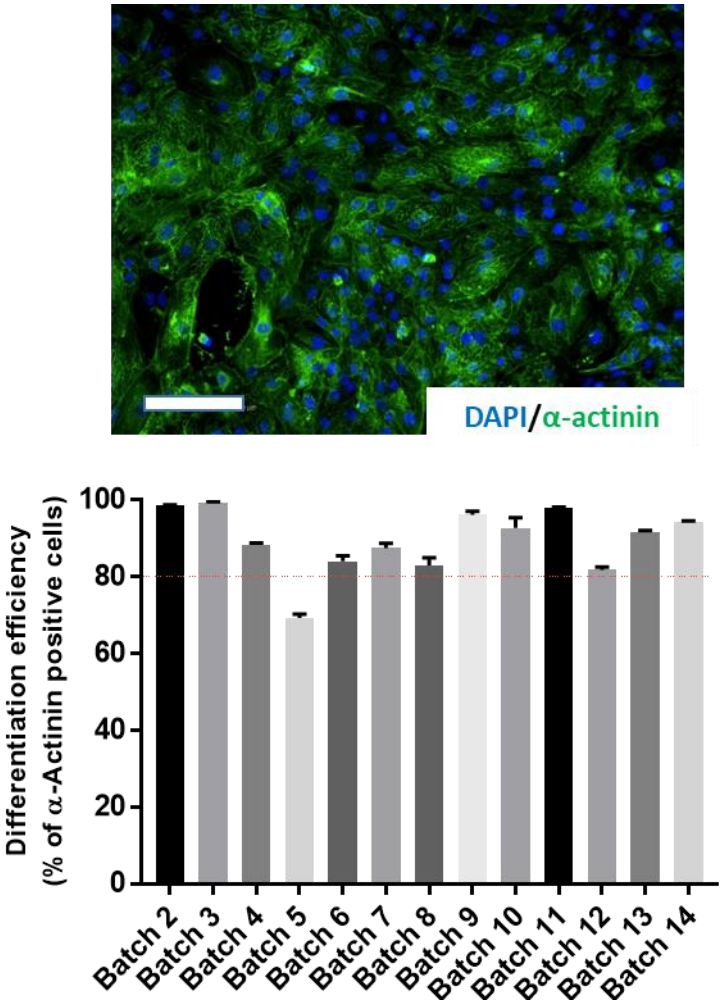


Figure 3.2: Large-scale R-PAT differentiation and cardiomyocytes purity. **A)** Representative image of R-PAT-CMs stained with DAPI and α-actinin. Scale bar = 100μm. **B)** Percentage of α-actinin cells measured by immunostaining of day 14-15 post-cardiac differentiation for different R-PAT CMs batches. All R-PAT were cultured in E8 medium for at least three passages before starting cardiac induction. n= 4 independent technical replicates. Error bar= SEM.

3.4.1.2 R-PAT-CMs viability and recovery after thawing

Throughout the study, all assays for R-PAT-CMs needed to be conducted on day 20~21 post differentiation in Nottingham and across CRACK-IT partners. Therefore for ease of use and transportation convenience, cryopreserved hiPSC-CMs were utilised. The thawed R-PAT-CMs were then fixed for immunostaining on day 15 post differentiation (4 days after thawing) to ensure functional recovery after thawing. In addition, different densities for R-PAT-CMs thawing were tested, as a continuous, synchronous monolayer of hiPSC-CMs is important for the CellOPTIQ assay. Both fresh and cryopreserved cells were seeded at different densities (20,000, 40,000, 60,000 and 80,000 cells per 96-well plates) (**Figure 3.3 A & B**).The cryopreserved cells should retain their cardiomyocytes purity with good viability after thawing to ensure valid data for future assays.

As observed in **Figure 3.3 A &** B, comparably as expected, the cryopreserved cells were attached and recovered less well than fresh cells. The best monolayer density for fresh cells was 20,000 cells. Meanwhile, the best densities for cryopreserved cells were at 40,000 and 60,000 cells **(Figure 3.3 B)**. Overcrowding of cells should be avoided as the attachment to culture vessels is reduced and encourages cells to peel off. Furthermore, overcrowding prevents good contractility recording.

Although the percentage of cardiomyocytes purity of cryopreserved cells was less than fresh cells after thawing, it was still above the acceptable level of 80% CM purity **(Figure 3.3 C)**. Quantitatively as expected, the cells' viability/ recovery after thawing was at least 50% less than that of fresh cells **(Figure 3.3D)**. Therefore, the double amount of cryopreserved cells is needed for thawing. Albeit again the best density for fresh R-PAT-CMs is of 20,000 cells while preferable for cryopreserved cells is of 40,000 and 60,000 cells per 96-well plate.

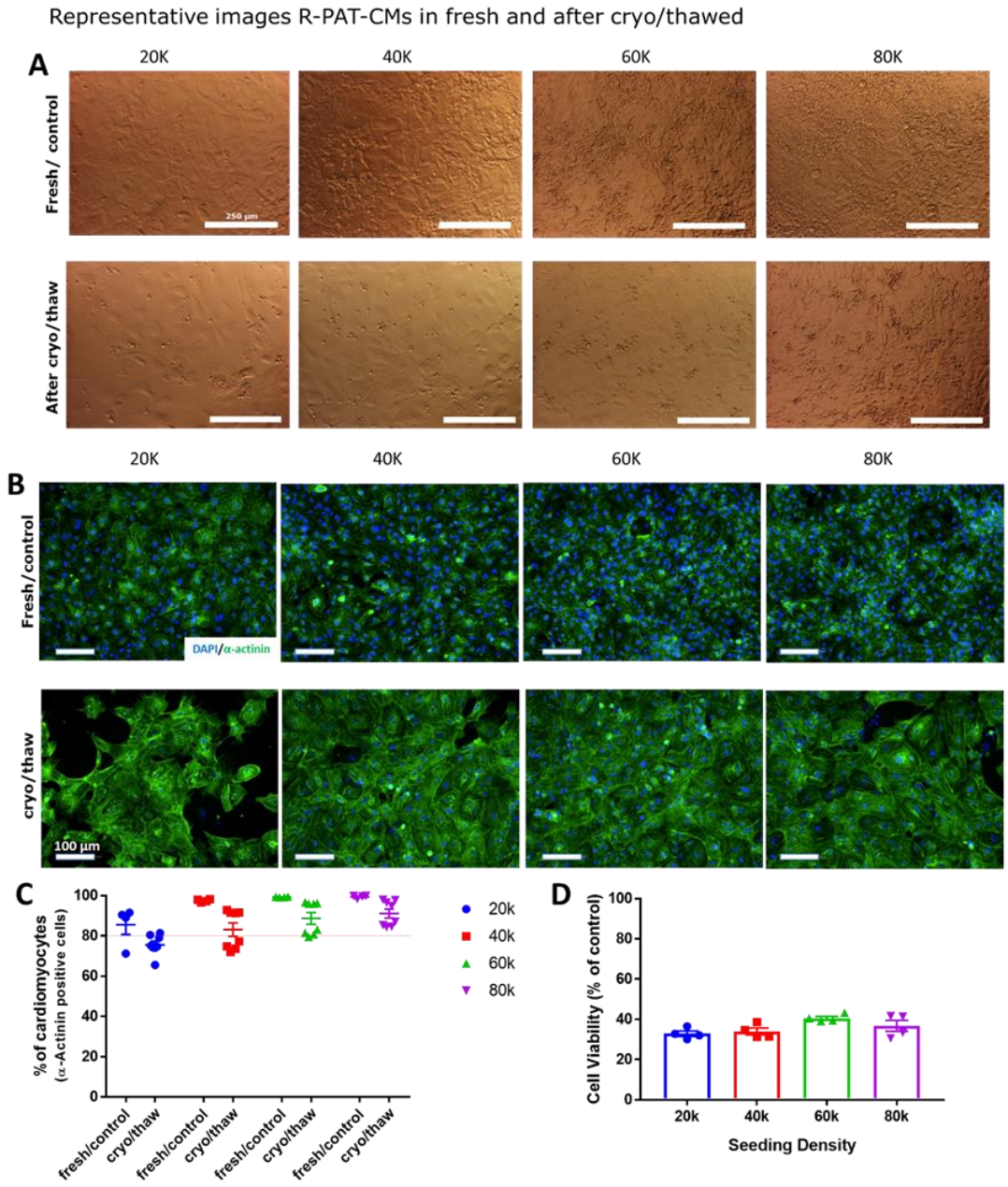


Figure 3.3: Recovery of R-PAT-CMs after cryopreservation.
(A) Brightfield images representation of fresh R-PAT-CMs on day 15 of differentiation and cryopreserved R-PAT-CMs on day 15 differentiation (day 4 post thawed) at densities of 20,000, 40,000, 60,000 and 80,000 cells per 96-well plates. Scale bar = 250 µm. **(B)** Immunostaining images of R-PAT-CMs stained with α-actinin and captured using Operetta confocal microscope. Scale bar = 100 µm. **(C)** Percentage of CMs quantification before and after thawing at different densities. **(D)** R-PAT-CMs viability after thawing at different densities. Data are mean ± SEM, n=4-8; technical replicates.

3.4.2 The hiPSC-CMs culture condition variations and quality control characteristics

One of the limitations of using hiPSC-CMs for drug testing is the fact that various sources of hiPSC-CMs are available from different vendors and derived from various cardiac differentiation protocols (Denning et al., 2016). The various differentiation protocols and variable medium compositions can yield CMs with different chamber-specific characteristic or level of maturity (Ribeiro et al., 2019) which then potentially cause different physiological phenotypes and responses to drugs.

As the main objective is to utilise hiPSC-CMs as an *in-vitro* model for drug-induced changes screening, it is crucial to evaluate the differences between cell lines in order to understand how these differences impact future experimental outcomes.

This section reports the investigation into the specific chamber characteristics for all three hiPSC-CMs, notably because high levels of variability are often reported between cell lines (Carcamo-Orive et al., 2017, Kallur et al., 2017).

3.4.2.1 MLC-2a vs MLC-2v

The mediation of different cardiac fields by cardiac gene expression is important for different physiological properties. For instance, the two main chamber-specific for functional cardiomyocytes include atrial and ventricular subtypes, which requires the expression of two distinct isoforms of myosin light chain genes that are essential for heart development: the *MLC-2a* and *MLC-2v*, respectively. The two genes are highly homologous with 56% identity and 86% similarity in amino acid sequence between MLC-2a and MLC-2v (Gulick et al., 1997). During embryogenesis, MLC-2a is expressed earlier than MLC-2v and uniformly expressed throughout the heart tube while MLC-2v is expressed in adult ventricular and slow-twitch skeletal muscles (Chen et al., 1998).

The two genes contribute to different contractile properties of heart chambers according to the experiment conducted on mice by replacing MLC-2v with MLC-2a, leading to a defect in sarcomere assembly and reduced contractility of the

heart (Chen et al., 1998). The expression patterns of MLC-2a and MLC-2v are considered as specific markers for mature atrial and ventricular cardiomyocytes.

3.4.2.1.4 Analysis for ventricular and atrial subtype in hiPSC-CMs

All three hiPSC-CMs (R-PAT, iCell^2 and Pluricyte) were fixed on day 8 (near assay day) post thawing for immunostaining, using MLC-2a/MYL7 (ab68086) to stain the atrial, and MLC-2v/MYL2 (ab79935) to stain ventricular isoform for subtype-specific markers **(Figure 3.4A).**

The results indicated in R-PAT-CMs show that approximately 56% of CM populations expressed atrial subtype (MLC-2a), 26.6% expressed ventricular subtype (MLC-2v) and 17% expressed both atrial and ventricular subtypes (MLC-2a+MLX-2v) **(Figure 3.4B)**. Meanwhile, in iCell^2-CMs, different patterns were observed where they exhibited no ventricular only, but with dominantly 64% MLC-2a and secondly, dual expression of 36% MLC-2a+MLC-2v **(Figure 3.4B)**. Strikingly, in the Pluricyte-CMs, the expression of both atrial and ventricular (MLC-2a+MLC-2v) was dominant with 97%, together with 1% MLC-2a and approximately 2% of MLC-2v **(Figure 3.4B)**.

In summary, these data showed that the R-PAT-CMs and iCell^2 are predominant atrial subtypes, while Pluricyte CMs dominantly combine both atrial and ventricular subtypes. However in human, although MCL-2v are maybe majorly distributed in ventricles, their expression in nodal tissue of the conductance system cannot be omitted as described by Chuva et al. 2006 (Chuva de Sousa Lopes et al., 2006, Kane and Terracciano, 2017). Potentially there are sinoatrial-node (SAN) cells in these population. To further exclude ventricle-like cells, MLC-2v in combination with a marker that would eliminate nodal cells is beneficial.

The explanation of why Pluricyte is more dominant in ventricular subtypes compared to R-PAT is beyond this thesis. The differentiation protocol, culture media components and differentiation age for both Pluricyte and iCell^2 are proprietary to the respective company and therefore could not be entirely compared to the R-PAT.

In addition to these subchapter findings, it was confirmed that without MLC-2v expression, there is a defect in the sarcomere assembly and organisation **(Figure 3.5).** The alignment of myofilaments in CMs was not organised in CMs with poor MLC-2v expression (in the dotted box).

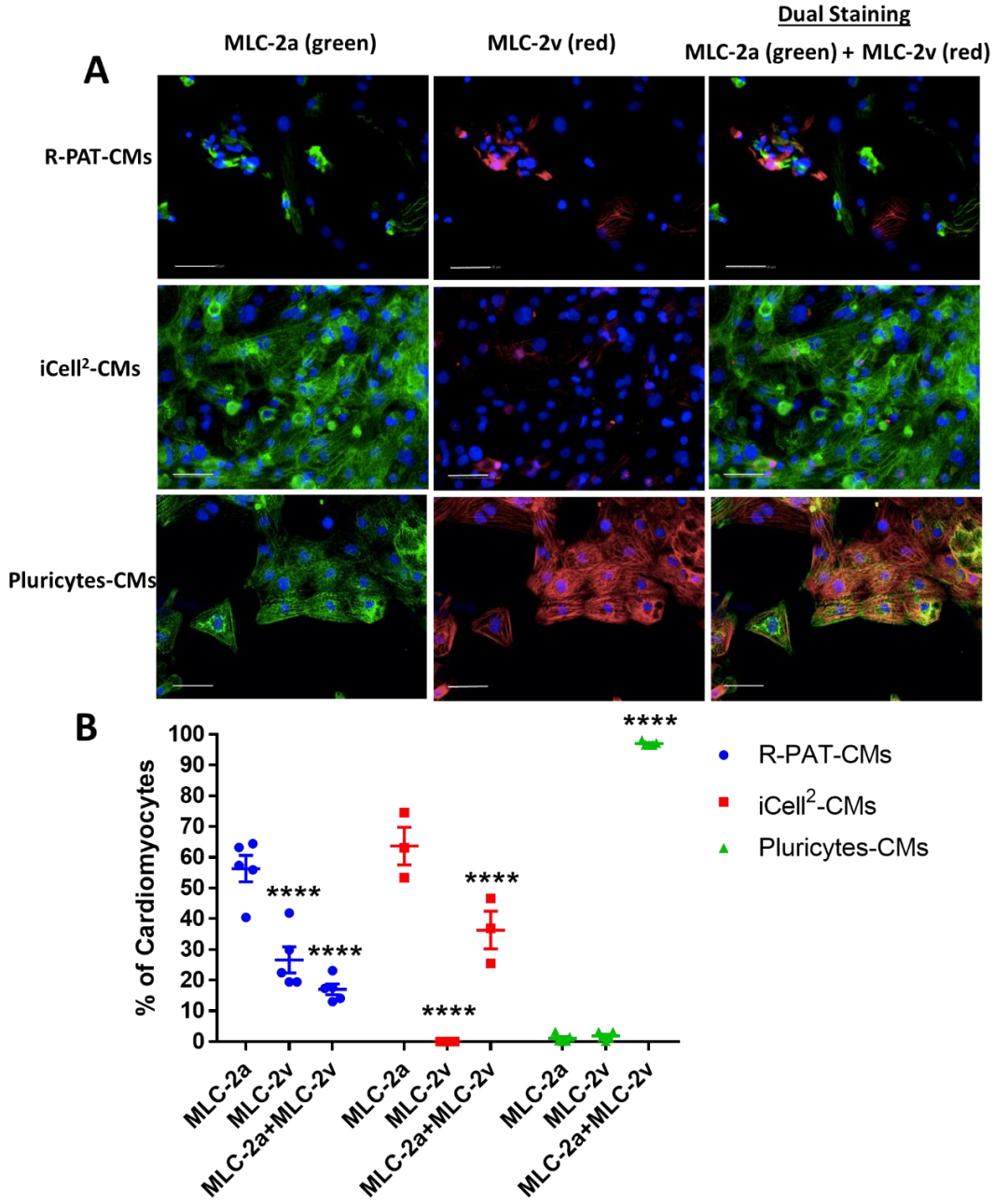


Figure 3.4: Cardiac ventricular and atrial subtype in hiPSC-CMs (R-PAT, iCell² and Pluricyte) by immunostaining analysis of MLC-2a and MLC-2v.

(A) Representative images of dual staining. Sample collected on day 8 post thawing. Scale bar = 50 µm. **(B)** The quantification of MLC-2a, MLC-2v and MLC-2a+MLC-2v. All data are mean ± SEM, n=3-5. Statistical analysis was done using two-way ANOVA with Tukey's multiple comparison test compared to MLC-2a. Significance tests were based on p-values as follows: * $p < 0.05$; ** $p < 0.01$; *** $p < 0.001$; **** $p < 0.0001$.

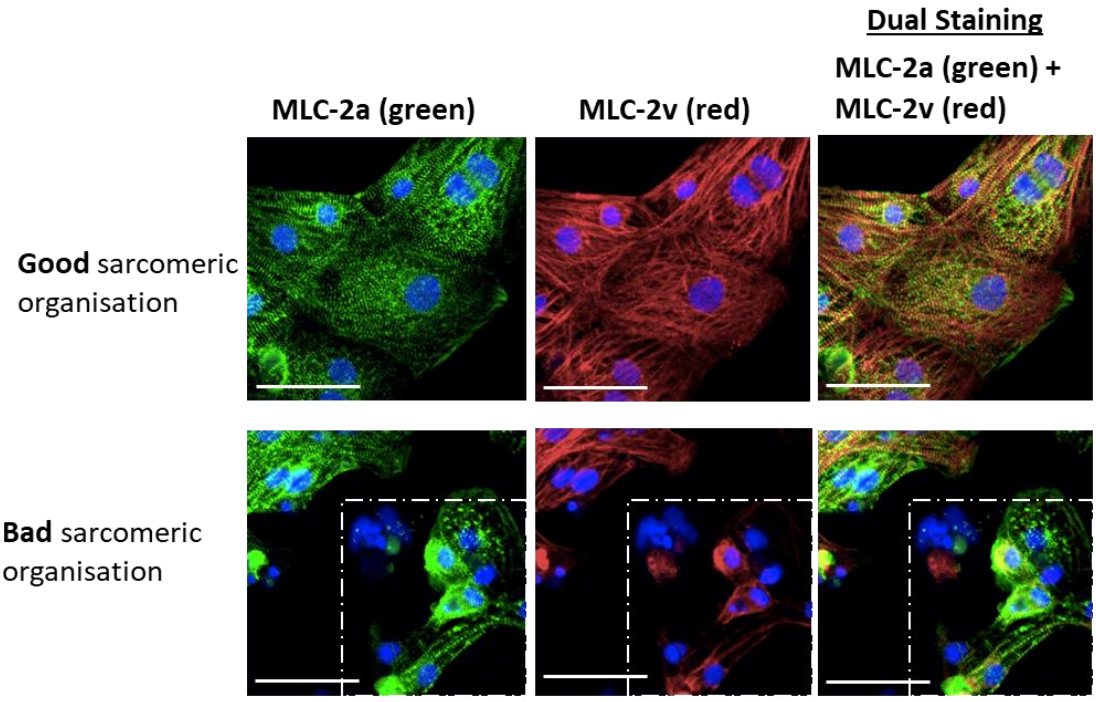


Figure 3.5: Example of good and bad sarcomeric organisation in CMs based on MLC-2v expression.

Based in double immunostained, by considering MLC-2v/a incorporation into sarcomeres, the immunostained revealed improved striated muscle formation in cells with induced MLC-2v formation (upper figure). The bottom dotted box exhibits poor sarcomeric organisation as the expression of MLC-2v low. More organised sarcomere in MLC-2v population but only a few clear MLC-2a sarcomeric organisation probably due to the presence of distinct ranges on maturation in cultures.

3.4.2.2 Connexin-43

The gap junction is important for the heart as cell-cell interaction via gap junctions has been shown to be necessary to ensure coordinated contraction and pumping activity (Ribeiro-Rodrigues et al., 2017). The Connexin-43 (Cx43) is a major ventricular gap junction and is essential in maintaining a well-regulated intercellular communication between cells (Martins-Marques et al., 2015, van Kempen et al., 1995), the distribution allowing the heart to work as a functional syncytium by intercellular exchange of ions, nucleotides and small molecules between adjacent cells (Smyth and Shaw, 2012).

3.4.2.2.5 Analysis for Connexin-43 in α-actinin positive hiPSC-CMs

All three hiPSC-CMs (R-PAT, iCell^2 and Pluricyte) were fixed on day 8 (near assay day) post thawing for immunostaining by using α-actinin (green) to stain for sarcomeric protein and connexin-43 (red) to stain gap junction protein **(Figure 3.6A)**. The cells were counterstained using DAPI (blue) to allow the visualisation of the nuclei.

The α-actinin is a protein which localises at the Z-band of sarcomeres. It implicates in actin anchoring which is essential for intracellular structure. The localisation of α-actinin stain can indicate the maturity of cardiomyocytes (Grosberg et al., 2011). It is diffuse in the cytoplasm of the differentiating cells, appears as a fibrous structure in immature myocyte while localising into the regular lattice of Z-disks in mature myocytes (Pasqualini et al., 2015). The expression of α-actinin appeared to be homogenously throughout the cell as longitudinal fibrous strands **(Figure 3.6).**

The results indicated both R-PAT and iCell^2-CMs as being approximately 6% and 7.6% of Cx43 percentage in CM populations **(Figure 3.6B)**. Meanwhile, Pluricyte exhibited the highest content of Cx43: 35% in CMs **(Figure 3.6B).** In summary, these data show that the Pluricyte-CMs are equipped with a high percentage of major ventricular gap junctions and therefore, are more mature than R-PAT and iCell^2.

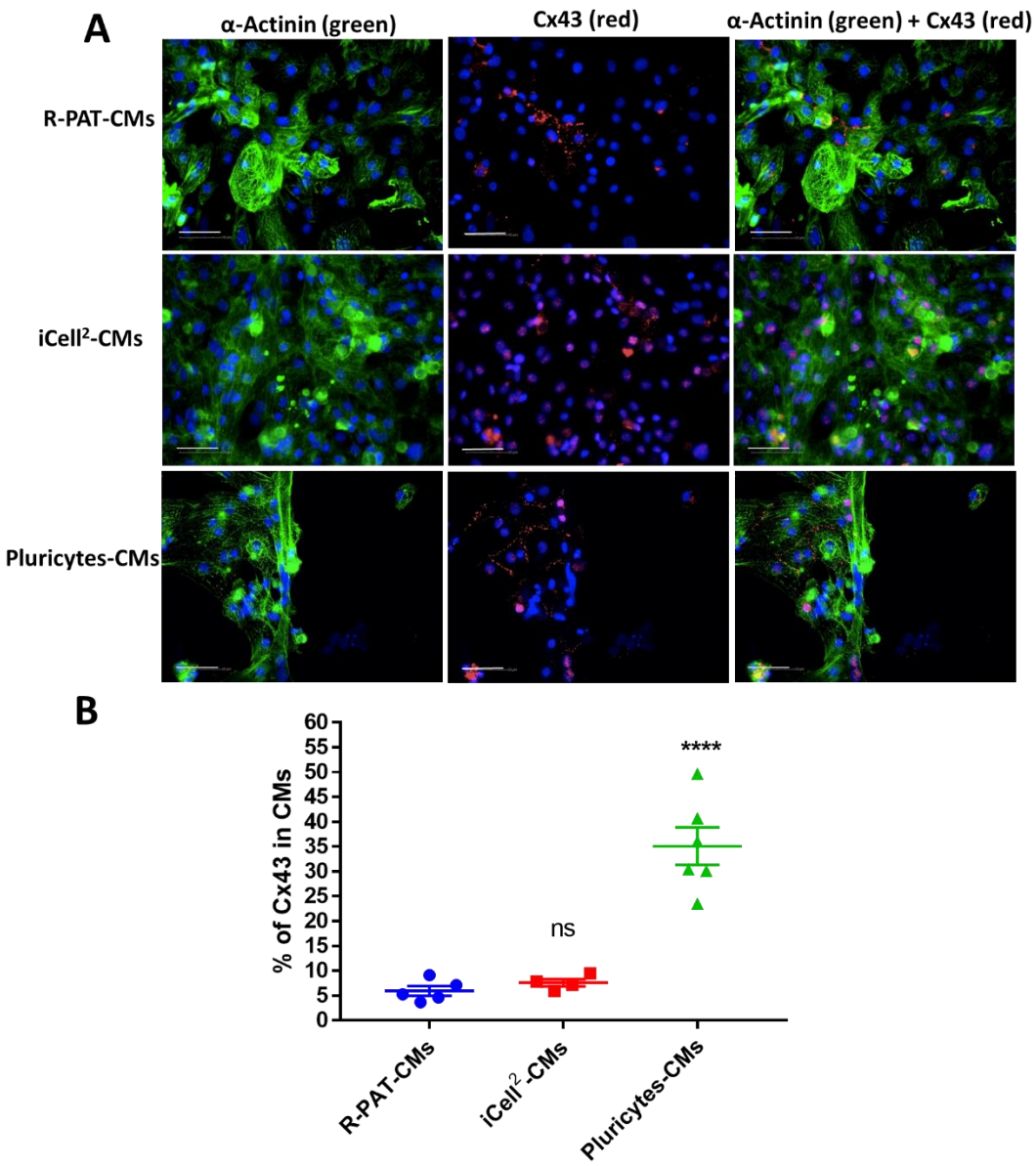


Figure 3.6: Connexin-43 (Cx43) in hiPSC-CMs (R-PAT, iCell² and Pluricyte) by immunostaining analysis of α-actinin and Cx43.

(A) Representative images of dual staining. Sample collected on day 8 post thawing. Scale bar = 50 µm. **(B)** The quantification of Cx43 in α-actinin positive cells. All data are mean ± SEM, n=4-6. Statistic analysis was done using one-way ANOVA with Dunnett's multiple comparison test comparing to R-PAT-CMs. Significance tests were based on p-values as follows: * $p < 0.05$; ** $p < 0.01$; *** $p < 0.001$; **** $p < 0.0001$.

3.4.3 The hiPSC-CMs culture conditions for CellOPTIQ

3.4.3.1 Optimisation for R-PAT-CMs culture condition for CellOPTIQ

As previously mentioned, low frequency is necessary to unmask the drug effects on repolarisation (Lemoine et al., 2018). As such, some antiarrhythmic drugs, for example, sotalol, lengthen the action potential at normal heart rates, but as the heart rate increases, the magnitude of prolongation declines (Hondeghem and Snyders, 1990). Therefore, it is crucial to slow down and establish protocols for low beat rates R-PAT-CMs in cultures for drug assessment. As suggested in the previous subchapter, the best seeding density for cryo R-PAT-CMs was 40,000 and 60,000 cells per 96-well plate. The seeding density was further evaluated by monitoring their baseline beat rate in the culture using CellOPTIQ in order to recapitulate the actual drug assessment scenario. On the day of the assay, it is crucial to conduct experiments in serum-free media (SFM; Dulbecco's Modified Eagle Medium (DMEM) + 10mM galactose + 1 mM sodium pyruvate) as any presence of serum could interfere with the voltage-sensitive dye signal.

Different culture conditions were tested in order to establish the optimum beat rate for R-PAT-CMs **(Figure 3.7A)**. The representative traces for each culture conditions are illustrated in **Figure 3.7B.** The first condition (condition 1), involving the standard Nottingham thawing method, maintained in RPMI-27 (medium changed every three days) and switch to SFM on assay day. It was observed that in this condition, the beat rate of 60,000 cells density was higher (~1.5 Hz) than 40,000 cells (~1.1 Hz) **(Figure 3.7C)**. As advised by CRACK-IT partners, the Hamburg dropwise thawing protocol as described in Material and Methods subchapter 2.1.9 was adopted. The dropwise thawing method (condition 2) further successfully lowered the beat rate down to 0.9 Hz and ~1.3-1.4 Hz, respectively for 40,000 and 60,000 cells **(Figure 3.7C)**.

However, it was also observed that the cells tended to peel off drastically on the day of assay due to the effect of the immediate medium change to SFM and small toxicity by voltage-sensitive dyes. Therefore, to avoid sudden media change, the medium was changed into SFM 24 hours before the CellOPTIQ assay, which was adopted in condition 3 and 4 in combination with standard and dropwise thawing protocols. The beat rate in condition 3 did slow down;

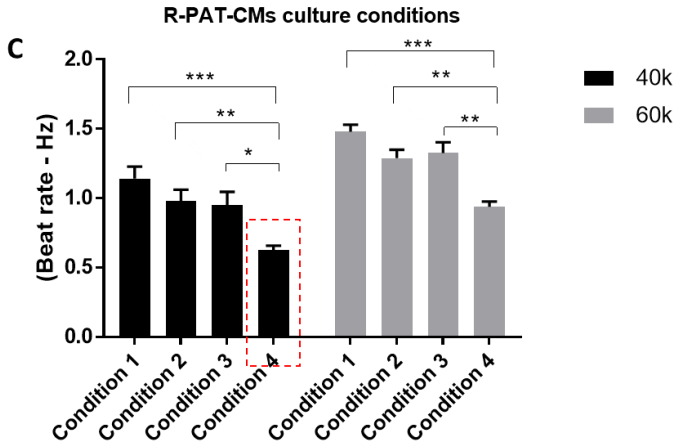
however, statistically, it was comparably similar to condition 2 of both 40,000 cells(0.9 Hz) and 60,000 cells (1.3 Hz) **(Figure 3.7C)**. The best culture condition was condition 4 with the dropwise thawing method and a 24-hour medium change before the assay, as it successfully lowered the beat rate to 0.6 Hz and 0.9 Hz.

In summary, the best culture condition for R-PAT-CMs **(Figure 3.7C dotted in red)** for CellOPTIQ involved the dropwise thawing method with 40,000 cells seeding density into 96-well plates, maintained in RPMI-B27 with the medium changed every three days. Consequently, the drug safety assessment (contractility and electrophysiology analysis) was carried out on around day 20-21 post differentiation and changed to SFM 24-hours before the CellOPTIQ assay **(Figure 3.7C)**.

In addition to the culture condition, the cells population could be validated by measuring the beat rate within different patches of culture. The cells population arise from different cell density and culture condition could also be verified by running PCR to established whether nodal cells involve or not, that may contribute to high beating. An appropriate comparator also should be used, such as commercial human cardiac cells.

A

Culture conditions	Day 10	Day 14	Day 17	Day 19	Day 20 (Assay day)
Condition 1	RPMI-B27	RPMI-B27	RPMI-B27	-	SFM
Condition 2	RPMI-B27 (dropwise)	RPMI-B27	RPMI-B27	-	SFM
Condition 3	RPMI-B27	RPMI-B27	RPMI-B27	SFM	SFM
Condition 4	RPMI-B27 (dropwise)	RPMI-B27	RPMI-B27	SFM	SFM



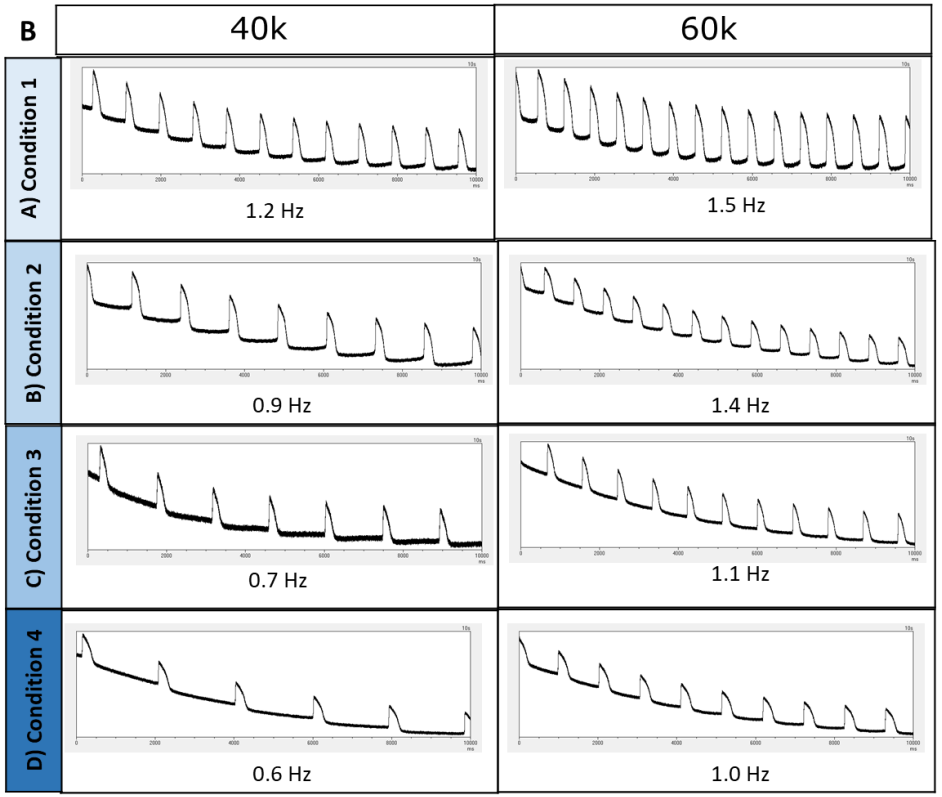


Figure 3.7: Optimum culture conditions for cryopreserved R-PAT-CMs.

(A) Different culture condition for cells with a seeding density of 40,000 and 60,000 cells. The difference between each condition is highlighted in RED. **(B)** Representative voltage traces for each culture conditions. **(C)** Beat rate quantification for each culture conditions. Data are mean ± SEM, n=4-5; technical replicate significance tests were based on p-values as follows: * $p < 0.05$; ** $p < 0.01$; *** $p < 0.001$; **** $p < 0.0001$.

3.4.3.2 Commercial iCell^2-CMs and Pluricyte-CMs culture conditions

Each of the commercial CMs was maintained in each of their unique culture media, which may/may not contain serum/protein. The iCell^2 from the vial were seeded at the density of 25,000 cells per well into 96-well plates and were maintained for 10 days post-thaw for use in the drug assessment study. Similarly to R-PAT-CMs, the medium for iCell^2 were changed into SFM 24h before the CellOPTIQ assay. Meanwhile, Pluricyte-CMs were seeded at 35 000 cells into 96-well plates following the manufacturer's recommendation and maintained in a Pluricyte medium. The assay window for Pluricyte-CMs was suggested to be between day 8-9 after thawing. The Pluricyte medium was changed into 50% SFM + 50% Pluricyte maintenance medium (serum-free) 24-hour before the CellOPTIQ assay and during the day were changed into 100% SFM-medium.

Each of the different hiPSC-CM sources differs in cell size and/or spread. This was not a surprise as each of the lines have a different cryopreserved method and cryo medium, hence recovery after thawing was also slightly different. The iCell^2 was relatively large and/or spread well compared with Pluricyte or R-PAT CMs; therefore iCell^2 was seeded at 25,000 cells according to the commercial supplier's recommendation. Meanwhile, Pluricyte were seeded at 35,000 cells as at 25,000 cells, they do not form a reliable interconnected monolayer. As discussed previously, overcrowding should be avoided as hiPSC-CMs tend to peel off from the growth substrate before or during the assay period, especially in an SFM medium.

3.4.4 CellOPTIQ general principles

On the CellOPTIQ platform, the monolayer cells are supplemented with SFM medium in tissue culture plate and placed within a built-in chamber at 37ºC temperature and 5% $C0_2$. Monolayer cells are preferred, as the sparse and single cells have been shown to have a high level of heterogeneity that potentially reduces the discrimination power (personal observation).

3.4.4.1 Contractility

Contractility is defined as the ability of the cardiomyocytes fibre to shorten and elongate (Guth et al., 2019a). The proposed contraction parameter includes the inotropic state, which refers to the definition for the level of contractility amplitude (CA), contraction time (CT) and relaxation time (RT), referred to as the ability for the cardiac muscle to relax following contraction **(Figure 3.8 A)**. Contractility on the CellOPTIQ platform was recorded using a high frame rate camera (Hamamatsu Photonics) coupled to the machine. Contractility assessments were measured based on CM beats and recorded at 100 frames per second (fps) for 10 seconds, which resulted in a stack of 1000 images per recording. The resulting images were analysed using contractility tools software copyrighted by Clyde Biosciences based on the principle of the sum of absolute difference (SAD) algorithm which analysed the pixel displacement between frames.

3.4.4.2 Voltage

Voltage measurement in CellOPTIQ involved the preloaded confluent monolayer hiPSC-CMs with a voltage-sensitive dye. This study utilised FluoVolt, which is capable of detecting submillisecond changes in membrane potential (Bedut et al., 2016). The electrical voltage activity was translated from FluoVolt using the optical recording principle by measuring FluoVolt fluorescence signal using a 40x objective. The voltage recordings were then analysed by using CellOPTIQ software, developed by Clyde Biosciences. To determine whether the electrophysiology was altered, the action potential duration at 20%, 50% and 90% of the repolarisation time (APD20, APD 50 and APD90) were extracted and measured from voltage waveforms **(Figure 3.8 B)**.

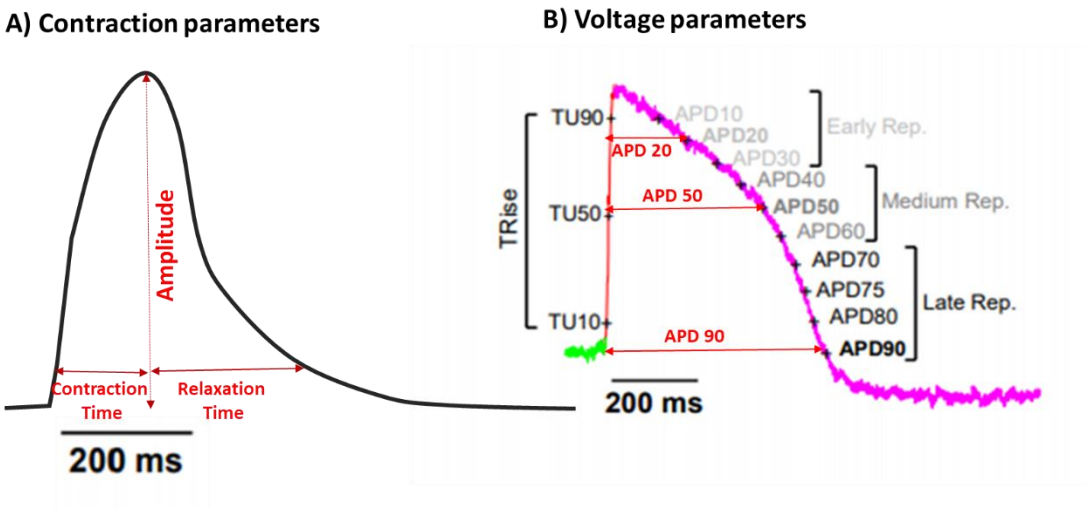


Figure 3.8: Schematic description and proposed parameters for contraction and voltage measurement to quantify drug effects in hiPSC-CMs.

(A) Contraction parameters include contraction amplitude, contraction time and relaxation time. **(B)** Voltage parameters include action potential duration at 20%, 50% and 90% of the repolarisation. Data calculated using Clyde proprietary software.

3.4.4.3 Electronic Pacing

One of the upcoming challenges working with hiPSC-CMs is their variable spontaneous activity before and during the assay, which can influence the underlying action potential duration. Therefore, all experiments were conducted under pacing conditions with an adapted frequency based on the baseline of each well. Hence, the beat rate was expected to be the same before and after drug treatment, unless the drug caused the beat rate that either exceeded the pacing rate or drugs that lower the beat rate.

The pacing was done by using an electrode strip (stim strip) containing 8 pairs of graphite rod that fit into 8 wells of 96-well plate format (**Figure 3.9A**). The pacing was done manually well by well by connecting the appropriate external line to the power modulator that provides electrical stimulation to prevent overheating the medium and to avoid adverse reaction to cells (**Figure 3.9A**), a process is that is undeniably labour intensive.

The spontaneous R-PAT-CMs were able to follow the pace accordingly from spontaneous 1 Hz **(Figure 3.9B)** to 1.2 Hz **(Figure 3.9C)** and 1.5 Hz **(Figure 3.9D)**. Hence their suitability for drug assessment.

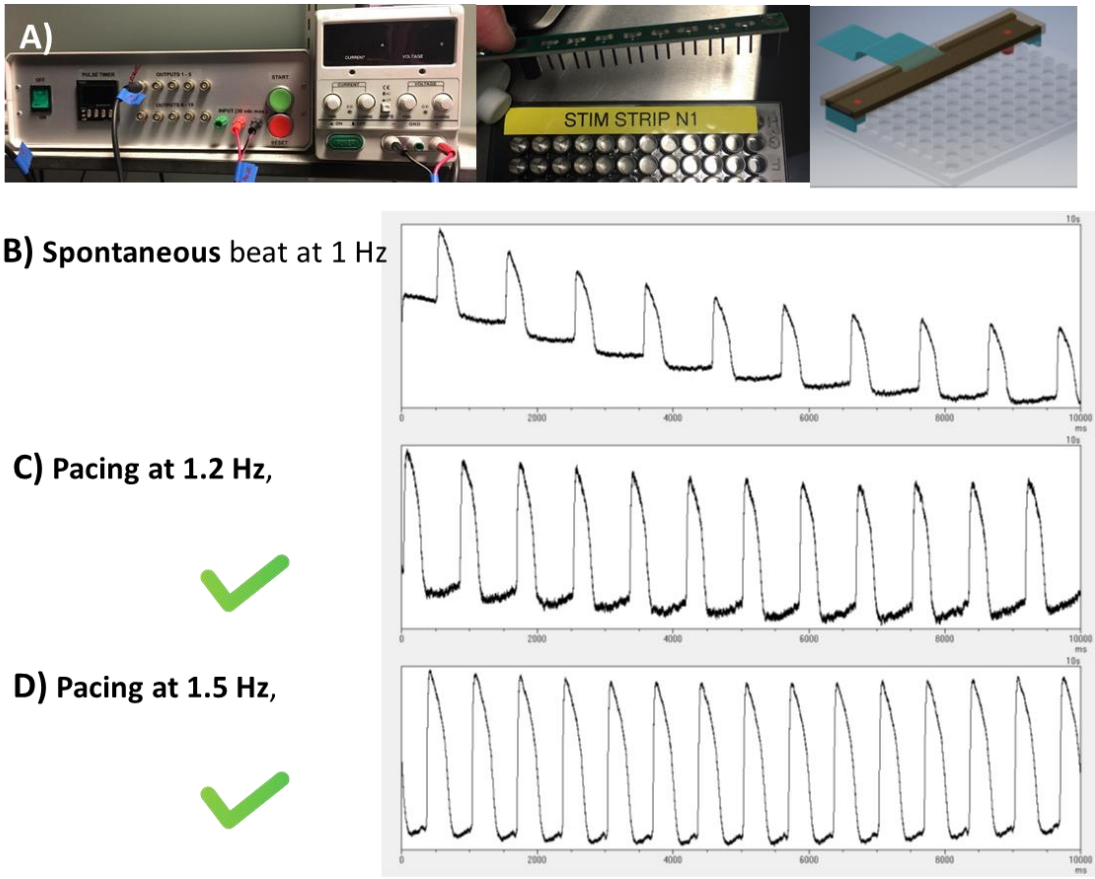


Figure 3.9: CellOPTIQ electronic pacing

(A) The power supply, modulator, stim strip with 8 pairs of graphite electrodes, and graphic illustration to show the position of the stim strip for the assay. Representative traces obtained from **(B)** spontaneous 1Hz beat **(C)** pacing at 1.2 Hz and **(D)** pacing at 1.5 Hz. The R-PAT-CMs can follow the pace.

3.4.4.4 Establishment and baseline characterisation (contractility and voltage) for hiPSC-CMs; R-PAT CMs, iCell^2 and Pluricyte

The initial experiments were to set up a system to measure contractility and voltage readouts from all three hiPSC-CMs; R-PAT-CMs, iCell^2 and Pluricyte. The CMs were cultured accordingly to each unique hiPSC-CMs culture conditions with assigned density. The voltage-sensitive dye, FluoVolt with 1:2000 concentration (The manufacturer does not specify the concentration of FluoVolt); 50 ul per well (2.5 µl of FluoVolt + 25 µl of PowerLoad in 5000 µl of SFM) was added for 20 minutes on the day of the assay for voltage measurement, with a window duration of 12 hours. The hiPSC-CMs baseline (without any treatment) characterisation under electrical pacing condition for contractility and voltage were generated using CellOPTIQ system. The assays were done between 0.8 Hz to 1.2 Hz pacing using Clyde Biosciences graphite electrode for 96-well plates. Subsequent analysis was carried out offline using Clyde software.

3.4.4.4.6 Contractility baseline

The hiPSC-CMs baseline (without any treatment) for contractility was obtained for CA, CT and RT. The overlaid recording traces for the contractility of all three hiPSC-CMs revealed that iCell^2 CMs have the lowest amplitude compare to the R-PAT-CMs and Pluricyte **(Figure 3.10A)**. Quantitatively, the results showed the low iCell^2 amplitude as 926 ± 194, followed by R-PAT-CMs with 1881 ± 51, while Pluricyte showed the highest amplitude among all as 2740 ± 390 **(Figure 3.10B)**. The differences between Plurictyes and iCell^2 were statistically significant **(Figure 3.10B)**. The CT was similar between R-PAT-CMs (137 ± 9.9 ms) and iCell^2 (128 ± 14 ms) **(Figure 3.10C)**. The Pluricyte also exhibited a significantly higher CT with (238.9 ± 42 ms) **(Figure 3.10C)**. Also, the RT for R-PAT-CMs (271.6 ± 9.6 ms) and iCell^2 (276.2 ± 12 ms) were significantly lower than Pluricyte (418.4 ± 53 ms) **(Figure 3.10D)**.

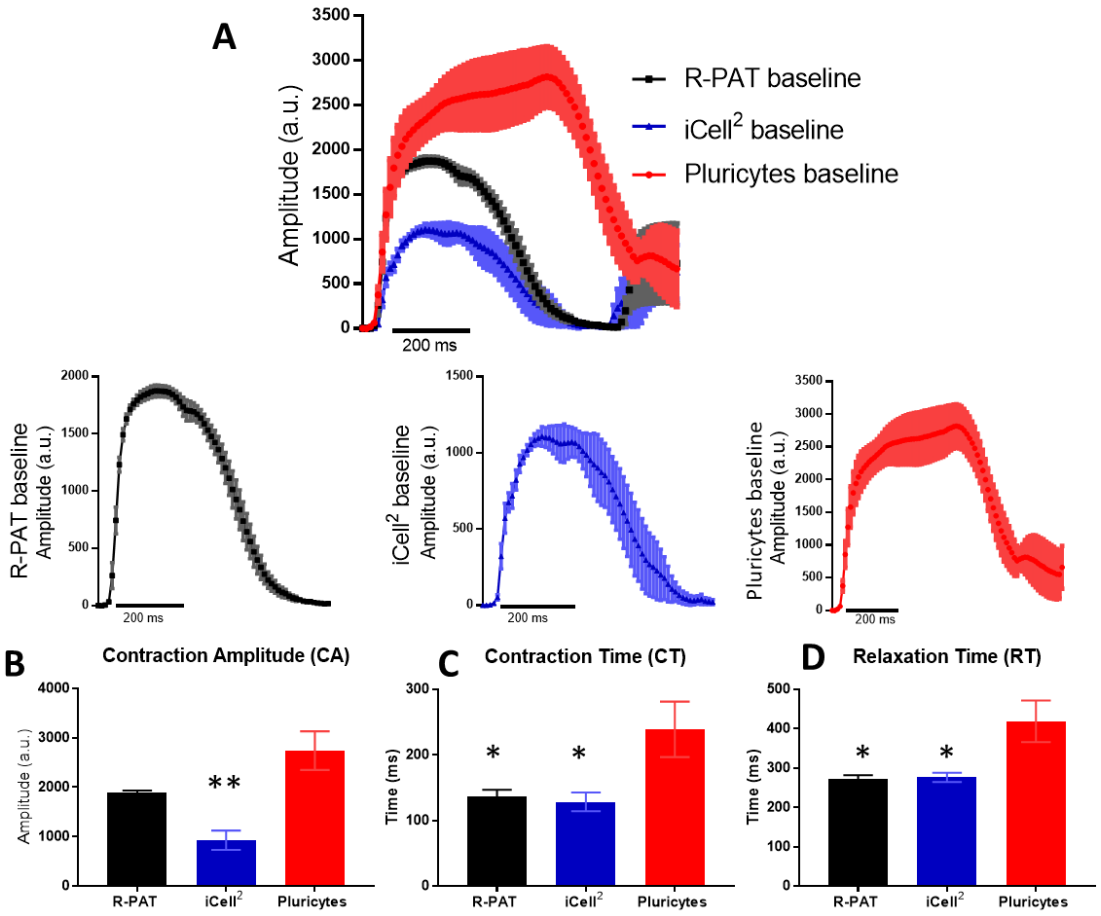


Figure 3.10: Contractility baseline characterisation under electrical pacing for R-PAT-CMs, iCell² and Pluricyte.

The CMs were recorded for 10 seconds using a high-speed camera (100 frames per second). The analysis was subsequently carried out using ImageJ contractility tools plugin algorithms, developed by Clyde Biosciences, by detecting frame changes in terms of pixel displacement. **(A)** Representation of contractility traces for R-PAT-CMs, iCell² and Pluricyte. **(B)** Contraction amplitude. (C) Contraction time and **(D)** Relaxation time. Data are mean ± SEM, n=5. Statistical analysis was carried out using one-way ANOVA with Dunnett's multiple comparison test compared to Pluricyte. Significance tests were based on p-values as follows: * $p < 0.05$; ** $p < 0.01$; *** $p < 0.001$; **** $p < 0.0001$

3.4.4.4.7 Voltage baseline

The hiPSC-CMs baseline (without any treatment) for voltage was obtained for action potential duration at 20% (APD20), 50% (ADP50) and 90% (APD90) of the repolarisation. The overlaid recording traces for the voltage of all three hiPSC-CMs revealed that R-PAT-CMs has similar APD shortening to iCell^2, while Pluricyte have prolonged repolarisation **(Figure 3.11A)**. Quantitatively, the results showed significantly shorter APD repolarisation at all durations for both R-PAT-CMs and iCell^2 compared to Pluricyte ($p<0.0001$). The APD20 were 143 ± 9 ms, 129 ± 8.8 ms and 300.5 ± 9.2 ms, respectively, for R-PAT-CMs, iCell^2 and Pluricyte **(Figure 3.11B)**. The APD50 was 218.6 ± 11 ms, 227.8 ± 8.9 ms and 520.4 ± 6.6 ms, respectively for R-PAT-CMs, iCell^2 and Pluricyte **(Figure 3.11C)**. The APD90 was 270 ± 13 ms, 292 ± 7 ms and 589.9 ± 6 ms, respectively for R-PAT-CMs, iCell^2 and Pluricyte **(Figure 3.11D)**. However, when further analysed, based on the RO index, all hiPSC-CMs had RO index above >1.5; R-PAT-CMs (1.59 ± 0.09), iCell^2 (1.77 ± 0.02) and Pluricyte (5.3 ± 0.45) demonstrating the presence of ventricular CMs **(Figure 3.11E)**.

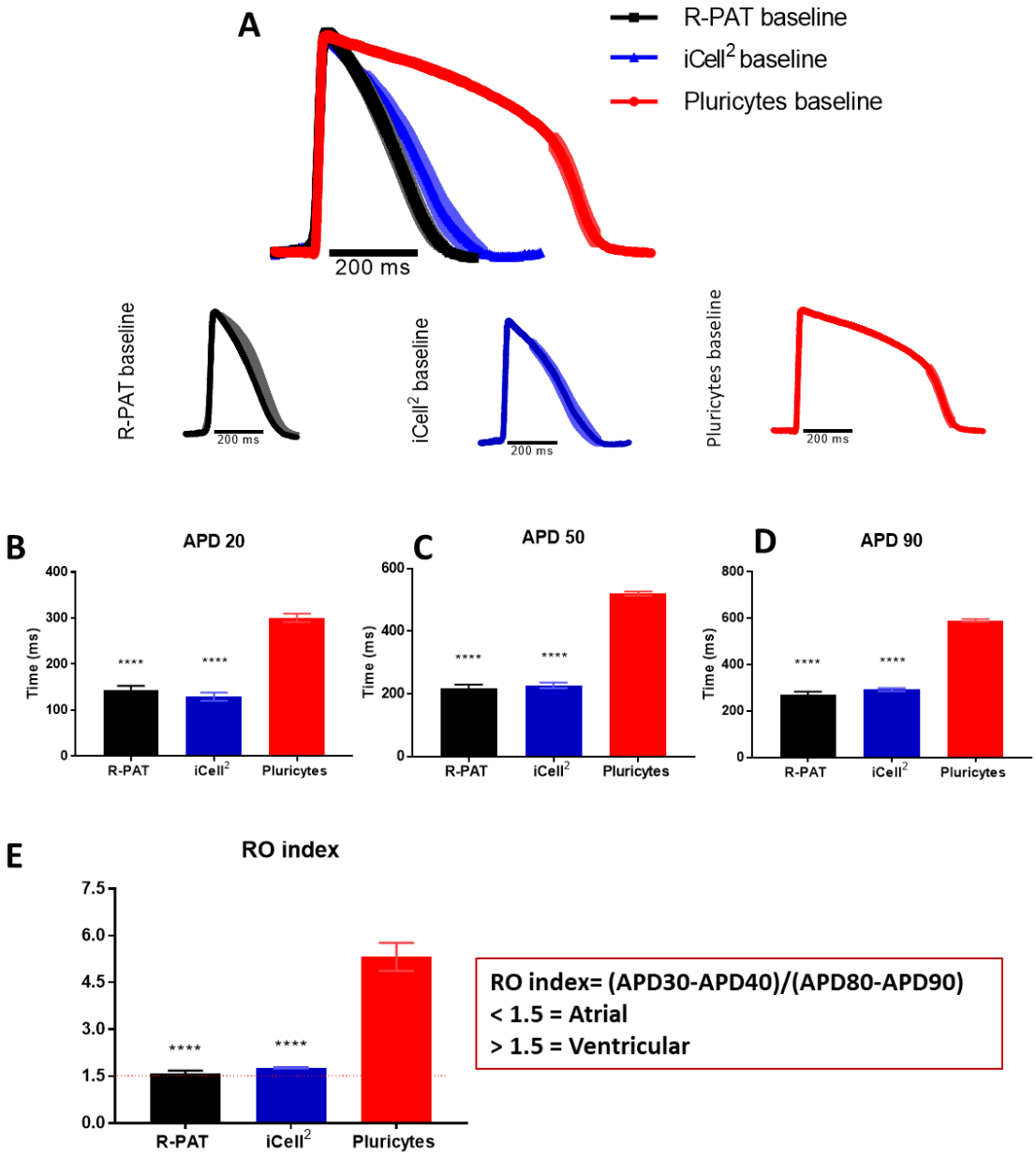


Figure 3.11: Voltage electrophysiology baseline characterisation under electrical pacing for R-PAT-CMs, iCell² and Pluricyte

The CMs were preloaded with voltage-sensitive dye, FluoVolt for 20 minutes and replaced with SFM for the voltage assay. The fluctuation signals from the dye were recorded. **(A)** Representation of voltage traces for R-PAT-CMs, iCell² and Pluricyte. **(B)** APD20, **(C)** APD50, (D) APD90 and (E) RO index. Data are mean ± SEM, n=5. Statistical analysis was carried out using one-way ANOVA with Dunnett's multiple comparison test compared to Pluricyte. Significance tests were based on p-values as follows: * $p < 0.05$; ** $p < 0.01$; *** $p < 0.001$; **** $p < 0.0001$

3.4.5 Drug assessment on R-PAT-CMs with seven 'training' (Tier1) drugs of known response.

As the hiPSC-CMs culture conditions for CellOPTIQ had been established for assessing contractility and voltage, the drug assessment was further assessed. To validate the system, the R-PAT-CMs were tested with the addition of seven 'training' (Tier 1) drugs with known effects in altering the contraction either by increasing (positive inotropy) or reducing contraction (negative inotropy). The seven selected training drugs consist of four PI (isoprenaline, digoxin, Bay K 8644, and EMD 57033) and three NI (nifedipine, ryanodine and thapsigargin). The mechanisms of action for the listed drugs are illustrated in **Figure 3.12.**

Experiments were performed at a density of 40,000 cells per well. The drug stocks were made fresh on the day using four different concentrations per training drug together with 0.1% DMSO as vehicle control. For voltage, R-PAT-CMs were loaded with FluoVolt (1:2000); 50 ul per well (2.5 µl of FluoVolt + 25 µl of PowerLoad in 5000 µl of SFM). The concentration of FluoVolt is not specified by the manufacturer. Cells were electrically paced at the rate of 1-1.2 Hz. The baseline for contractility and voltage electrophysiology were recorded for each well of each condition. The R-PAT-CMs were then incubated with the drug/vehicle for 30 minutes before the treatment measurements were recorded. One data point per well was recorded for each baseline and treatment.

All analysis was carried out using CellOPTIQ software and calculated as a percentage of change from their baseline (before treatment) recording.Formula= (drug/drug baseline) or (vehicle/vehicle baseline)*100-100 Data for contractility includes: contraction amplitude (CA), contraction time (CT) and relaxation time (RT). Data for voltage readout included action potential duration (APD) and recordings were taken from 20, 50 and 90% repolarisation time.

Readouts, in response to Tier1 drug treatments, were plotted as the percentage of change relative to the baseline with mean ± SEM and compared to the vehicle. The resulting traces recorded for the baseline (before drug treatment) are in black while during drug treatment are in red. The results were as follows:

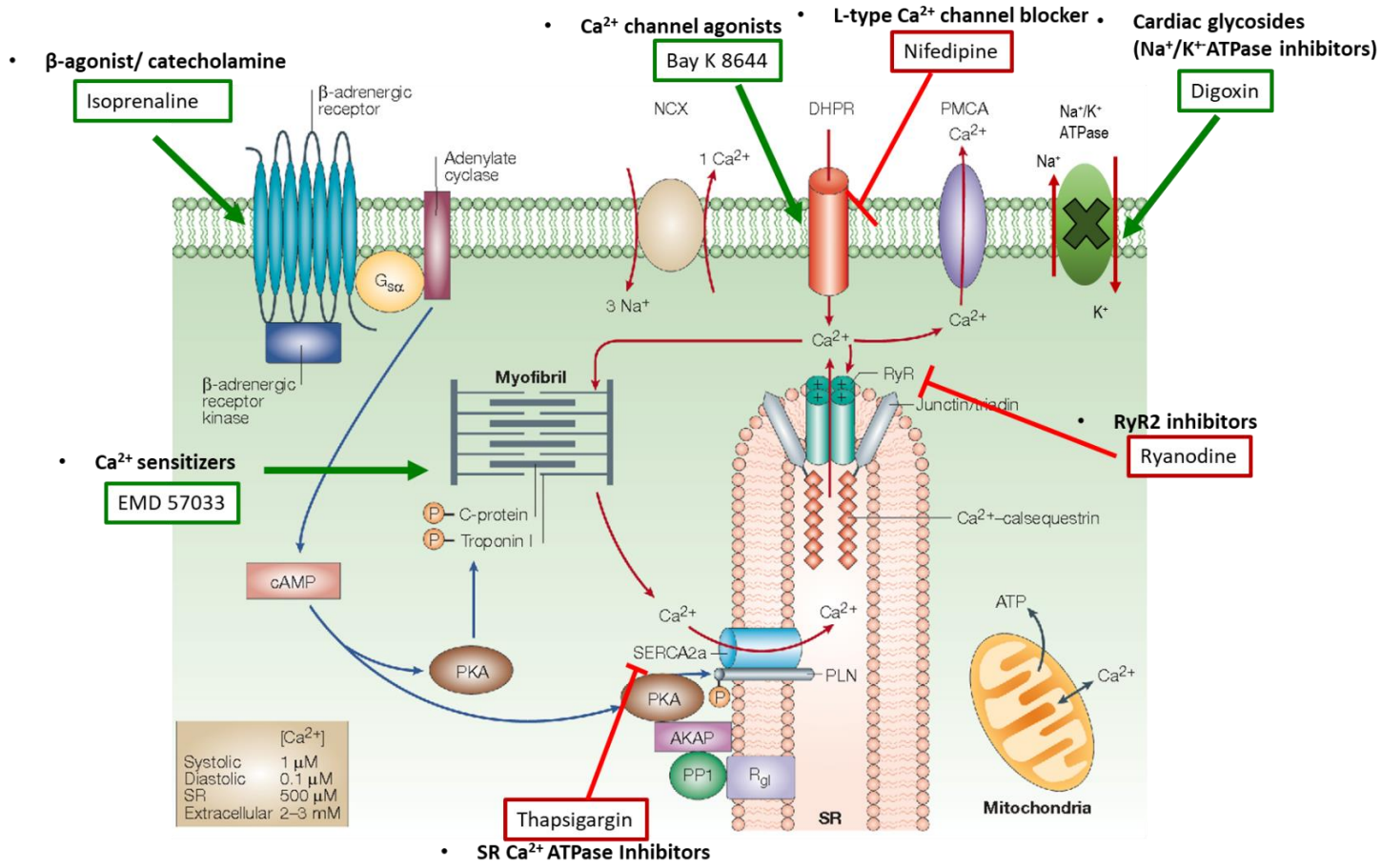


Figure 3.12: The mode of action for listed Tier 1 drugs and cardiac signalling pathways.

The green arrow indicates positive inotrope drugs, the red blunt end indicates negative inotrope drugs. RyR; ryanodine, SERCA2a; Sarcoplasmic reticulum Ca^{2+} ATPase, PKA; Protein Kinase A, DHPR (dihydropyridine receptors);L-type Ca^{2+} channel. Schematic adapted from (MacLennan and Kranias, 2003)

Positive Inotrophy

3.4.5.1 Isoprenaline treatment

Isoprenaline is the synthetic β_1 and β_2-adrenergic receptor agonist that is used extensively to treat life-threatening cardiac and pulmonary conditions (Gordon and Kittleson, 2008). Isoprenaline plays a role towards an increase in cyclic AMP concentration that influences the Ca^{2+} influx, SR Ca^{2+} uptake and SR load (Reyes et al., 1993). The known effects in human adult CMs include increasing forces, shortening time peak (contraction time) and shortening relaxation time.

The overlaid traces between baseline and highest isoprenaline concentration (0.03μM) reflect an increase in amplitude **(Figure 3.13A)**. The isoprenaline at higher doses than expected (0.03 μM) although not significant, was required to induce an increase in contraction amplitude (CA) (+35.4 ± 17.7%), and dose-dependent (0.003 μM to 0.03 μM) trends in reduction (faster) contraction time (CT) **(Figure 3.13A)**. Reduction in relaxation time (RT) was not detected, but instead, a trend increased in RT with an increase in isoprenaline concentrations was detected **(Figure 3.13A)**.

The effects on contraction function were supported by a significant reduction (shortening) at 0.03 μM for all voltage action potential duration (APD) at APD 20 (-30.3 ± 6.8%), APD 50 (-30 ± 4.2%) and APD 90 (-22.7 ±3.2%)**(Figure 3.13B)**. The shortening of APD repolarisation is illustrated in the traces between the baseline and isoprenaline 0.03μM **(Figure 3.13B)**.

In summary, both predictions for contractility and voltage data for isoprenaline were correct and as expected.

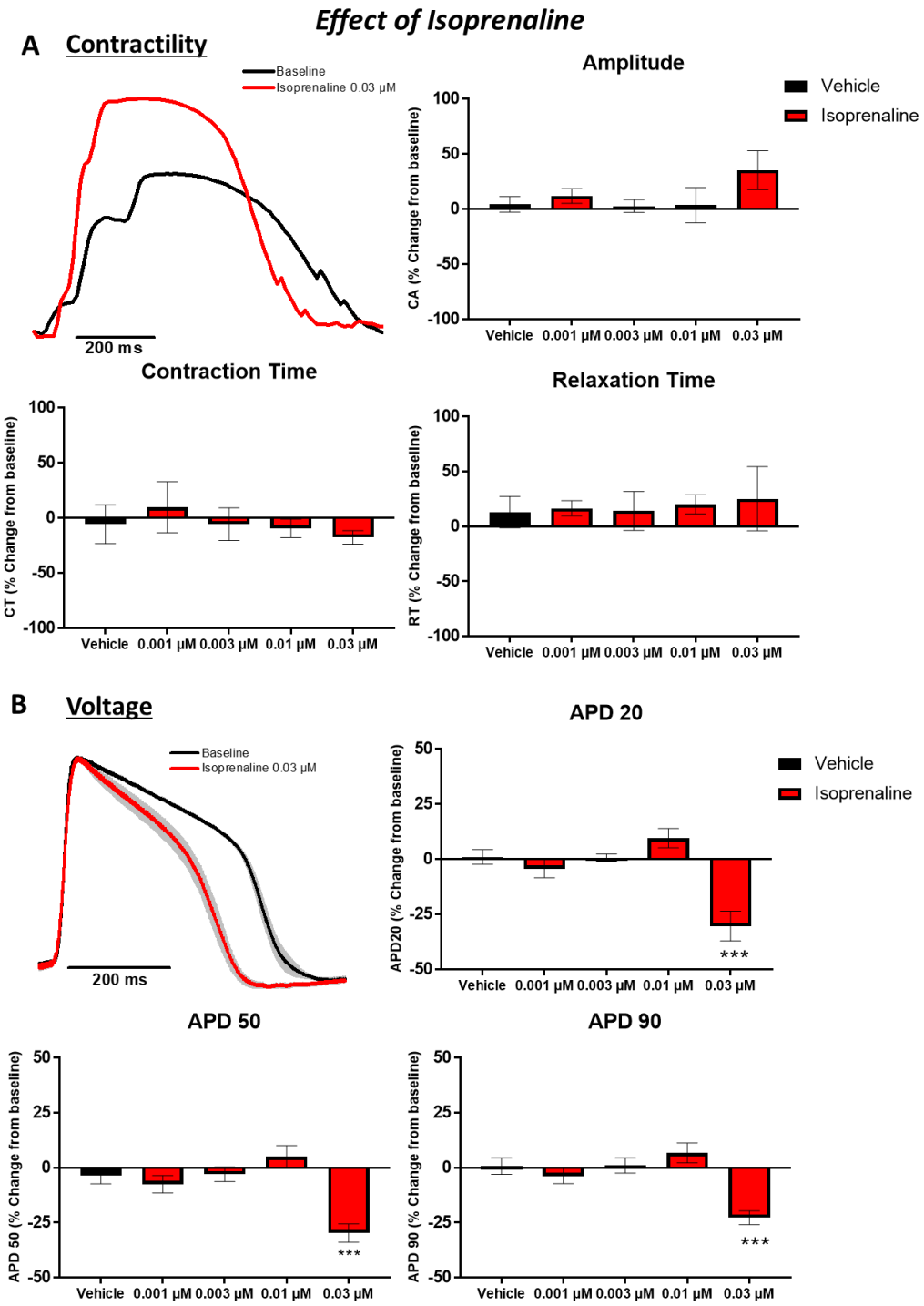


Figure 3.13: Contractility and voltage electrophysiological analysis of R-PAT-CMs treated with isoprenaline.

Increase in contraction and APD shortening **(A)** Increase in trend for CA at the highest isoprenaline concentration of 0.03µM, no changes in CT and trend increased in RT as concentration-dependence were observed. **(B)** A decrease in APD for CMs treated with isoprenaline relative to the vehicle is shown. Shortened repolarisation was observed in all APDs at the highest isoprenaline concentration of 0.03 µM. All data are mean ± SEM, n=6 Statistical analysis was carried out using one-way ANOVA with Dunnett's multiple comparison test compared to the vehicle. Significance tests were based on p-values as follows: * $p < 0.05$; ** $p < 0.01$; *** $p < 0.001$; **** $p < 0.0001$

3.4.5.2 Digoxin treatment

Digoxin is a cardiac glycoside that plays a role as a sodium-potassium pump (Na^+/K^+ ATPase) inhibitor (Levi et al., 1994). As the sodium-potassium is inhibited, it reverses the action of the sodium-calcium exchanger (NCX) thereby increasing the cytosolic calcium concentration. By increasing the SR Ca^{2+} release, digoxin generates Ca^{2+} transient, which results in an increased force contraction in the cardiac muscle (Levi et al., 1994).

The digoxin (0.3 μM, 1μM to 3 μM) led to an increase in CA (+28.5 ± 10%, +71.6 ± 17.6%, to +56.7 ±13.2%)**(Figure 3.14A)**. The increase in amplitude is demonstrated by contractility traces between the baseline and digoxin 3 μM **(Figure 3.14A)**. The CT significantly increased (slower) for 0.1 μM (+4.9 ± 8.7%), 0.3 μM (+28.5 ± 10.4%), 1 μM (+71.6 ± 17.6%) and 3 μM (+56 ± 13.2%)**(Figure 3.14A)**. Meanwhile no significant changes were detected on RT.

The positive effect of contraction was further validated by dose-dependent APD remodelling by shortening of all APDs from concentration 1 μM to 3 μM; with the maximum changed at 3 μM for APD 20 (-90 ± 6%), APD 50 (-87 ± 4.8%) and APD 90 (-80 ± 7.5%) and arrhythmias were observed in the illustrated voltage traces at the highest concentration of 3 μM **(Figure 3.14B)**.

In summary, the findings of R-PAT-CMs treated with digoxin were parallel with previous early studies by Lullmann (Lullmann and Ravens, 1973); wherein cardiac glycoside action, an increase of contraction (amplitude) is accompanied by a marked shortening of action potential duration. Thus, the predictions in terms of digoxin treatment were correct and as expected.

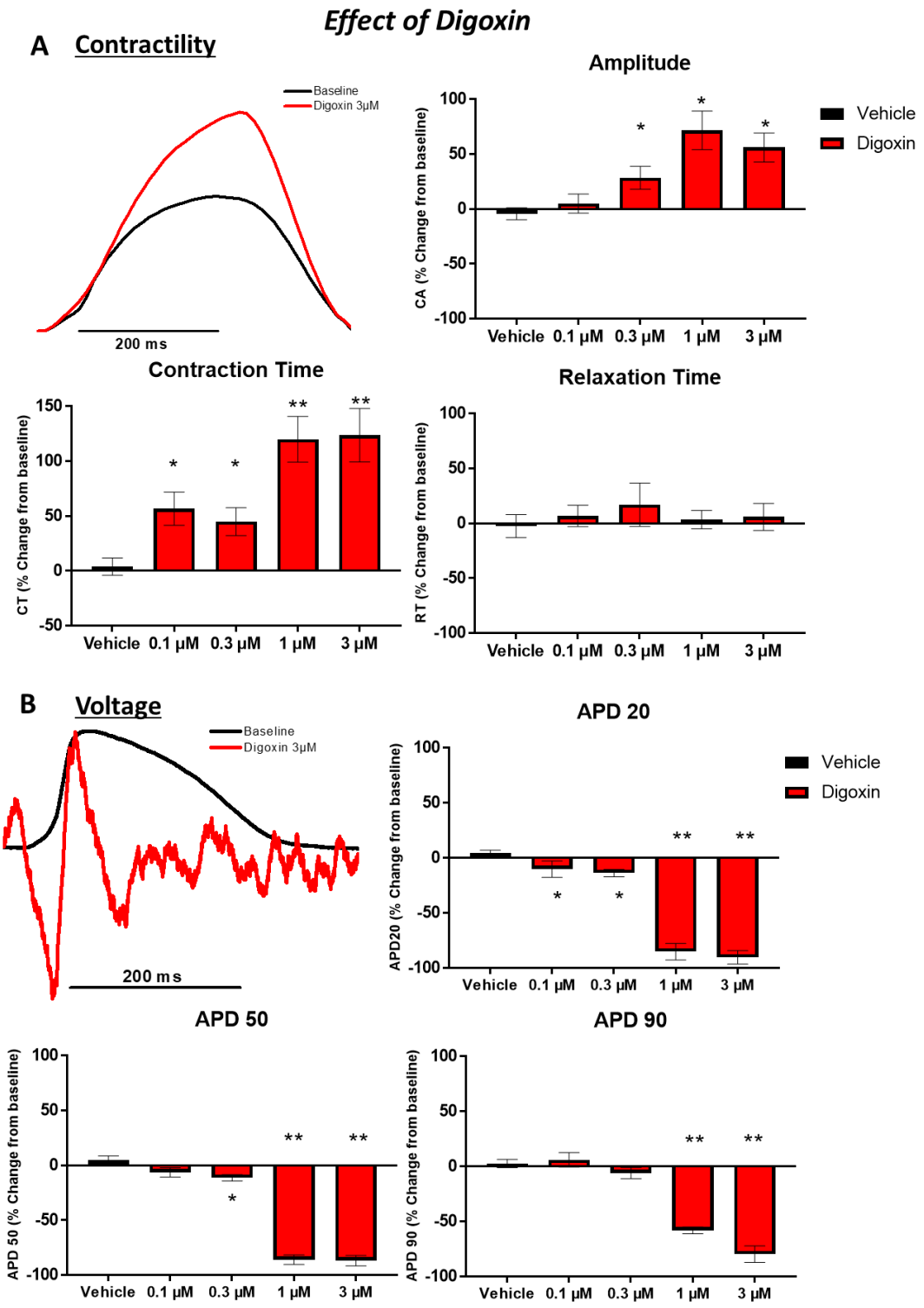


Figure 3.14: Contractility and voltage electrophysiological analysis of R-PAT-CMs treated with digoxin.

Digoxin induces contraction and shortens APD in R-PAT-CMs. **(A)** An increase in CA and CT **(B)** Decrease in APD. Traces for CMs treated with the highest concentration of digoxin relative to the baseline are shown. Data are mean ± SEM, n=6. Statistical analysis was carried out using one-way ANOVA with Dunnett's multiple comparison test compared to vehicle. Significance tests were based on p-values as follows: * $p < 0.05$; ** $p < 0.01$; *** $p < 0.001$; **** $p < 0.0001$

3.4.5.3 Bay K 8644 treatment

Bay K 8644 is a calcium channel agonist that interacts with an L-type calcium channel (LTCC) (Kwang Seo and Van Breemen, 1985, Schramm et al., 1983). The interaction alters its gating kinetics that increases the calcium influx. The increase in cytosolic calcium concentration causes positive inotropic effects in native human CMs while in nodal cells, it accelerates AP depolarisation, causing an increase in beat rate. Enhanced calcium influx has also been found to cause delayed AP in native ventricular myocytes (Frotscher et al., 2015).

This set of experiments for Bay K 8644 was carried out in 2 independent plates for contraction and voltage assessment. In terms of contractility effects by Bay K 8644 on R-PAT-CMs, at the lower dose no significant increase in CA was observed (0.03 µM; +5.7 ± 6.2%)**(Figure 3.15A)** while at higher concentrations of 0.1 and 0.3 µM no statistically significant changes in CA were observed, -15.9 ± 8.0% and -18.1 ± 6.6% respectively **(Figure 3.15A)**. Interestingly, with the same higher concentrations (0.1 and 0.3 µM), cells were observed to be in a state of fibrillation **(Figure 3.15A).** At the highest 1 µM, significant increases in CA were observed. No changes in CT were observed across concentrations while for RT, positive significant changes were observed for the lowest concentration of 0.03 µM (+78.3 ± 27%) and the highest 1 µM (+75.2 ± 21.6%) **(Figure 3.15A)**. However, overlaid traces of each of the baselines across various concentrations (0.03, 0.3 and 1µM) seems to be the biphasic effects of Bay K 8644 for CM contraction **(Figure 3.15A)**.

Meanwhile, for voltage significantly increased in all APD, at all concentrations (0.03, 0.1, 0.3 and 1 µM) **(Figure 3.15B).** APD20 were +45.9 ± 3.6%, +41.8 ± 3.4%, +52.2 ± 3.6% and +48.2 ± 2.7% respectively for 0.03, 0.1, 0.3 and 1 µM **(Figure 3.15B).** While APD90 were +56.7 ± 2.6%, +60.3 ± 4.0%, +57.2 ± 3.7% and +52.5 ± 0.7% respectively for 0.03, 0.1, 0.3 and 1 µM **(Figure 3.15B)**. The repolarisation increased and is reflected in the voltage traces.

In summary, the predictions for both contraction and voltage data for Bay K 8644 were incorrect and not as expected (supposed to be PI).

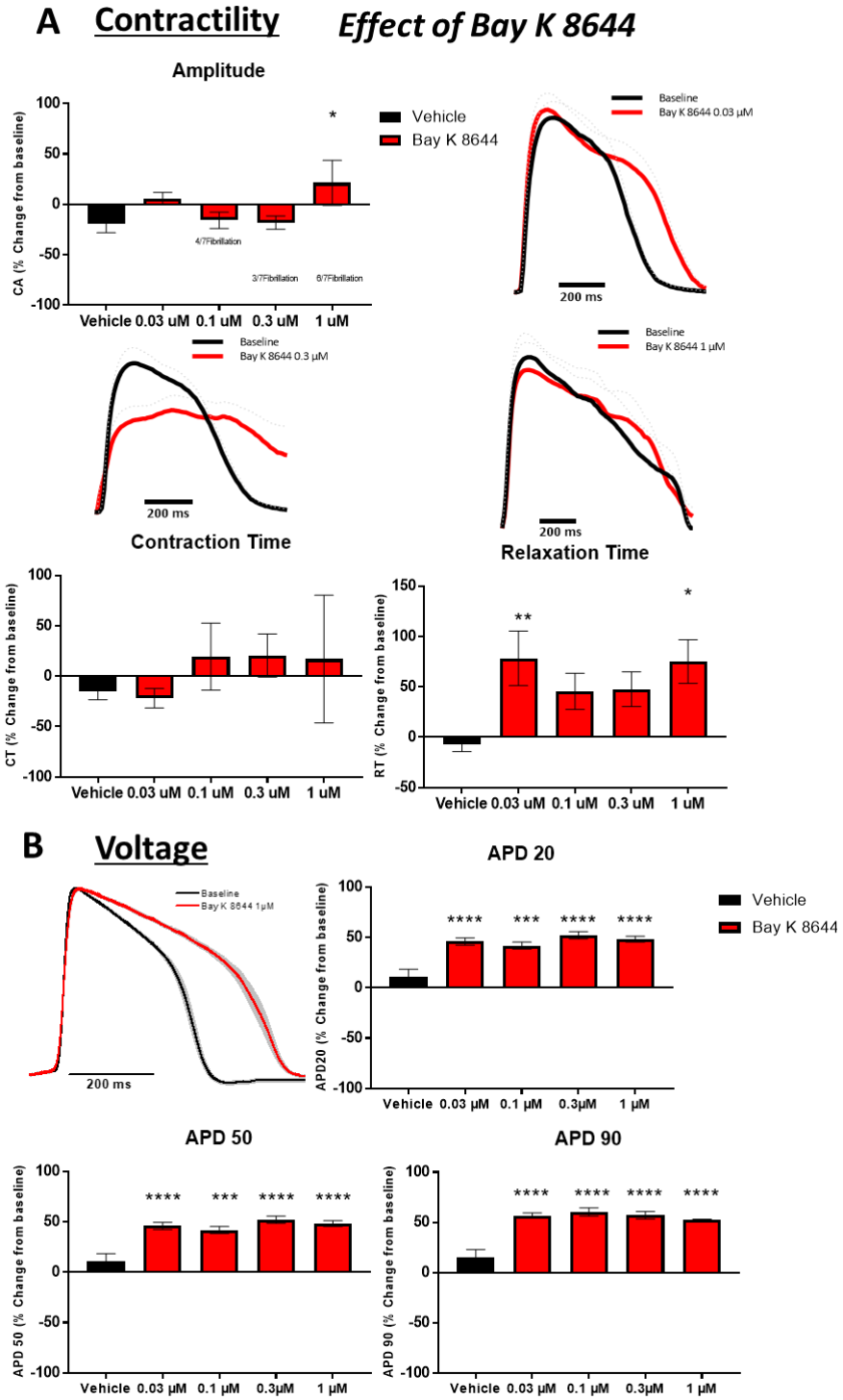


Figure 3.15: Contractility and voltage electrophysiological analysis of R-PAT-CMs treated with Bay K 8644.

Bay K 8644 induced contraction at the highest concentration and prolonged APD in R-PAT-CMs. **(A)** An increase in contraction amplitude was observed at the highest concentration, but contractility traces reflect a biphasic response. For contractility, data are mean ± SEM, n=7 **(B)** Delayed repolarisation in all APDs was observed. For voltage, data are mean ± SEM, n=6. Statistical analysis was carried out using one-way ANOVA with Dunnett's multiple comparison test compared to the vehicle. Significance tests were based on p-values as follows: * $p < 0.05$; ** $p < 0.01$; *** $p < 0.001$; **** $p < 0.0001$

3.4.5.4 EMD 57033 treatment

EMD 57033 is a compound that acts as a calcium sensitiser by increasing the myofilaments response to calcium (sensitisation) (Radke et al., 2014, Schipke and Korbmacher, 1996). It can restore systolic function in heart failure patients. EMD 57033 was shown to be able to enhance contractility and prolong relaxation in an isolated rabbit heart (Hgashiyama et al., 1995). Thus it is known to increase the force of contraction and is pronounced as a PI (Endoh, 2002).

This set of experiments for EMD 57033 were done in 2 independent plates for contraction and voltage assessment. The contractility effects of EMD 57033 on R-PAT-CMs at the lower dose showed no significant increase in CA; 0.3 µM (+14.1 ± 7.6%) and 1 µM (-3.7 ± 6.2%) **(Figure 3.16A)**. While at higher concentrations of 3 µM, although overlaid with traces of treatment and the baseline showed a decrease in amplitude, statistically there was no change relative to the vehicle, resulting in -40.64 ± 14.98% **(Figure 3.16A)**. At the highest concentration of 10 µM, no statistical changes in CA were observed, +6.7 ± 14.3% and this was reflected in the overlaid contractility traces respectively **(Figure 3.16A)**. No changes in CT across concentrations **(Figure 3.16A)** were observed while RT positive significant changes were observed for concentrations of 0.3 µM (+13.1 ± 5.8%), 1 µM (+230.4 ± 3.7%) and highest 10 µM (+41 ± 4.6%) **(Figure 3.16A)**.

For voltage, significant decreases were seen in APD20, APD50 and APD90 for concentrations of 0.1 µM and decrease APD20 and APD50 for 10 µM were observed **(Figure 3.16B).** APD20 were -8.5 ± 1.9% and -23.68 ± 3% respectively for 0.1 and 10 µM **(Figure 3.16B).** APD50 were -10 ± 3.3% and -14.1 ± 2.9% respectively for 0.1 and 10 µM **(Figure 3.16B).** While APD90 were -4.8 ± 3.1% for 0.1 µM **(Figure 3.16B).** The decrease in repolarisation is reflected in the voltage traces **(Figure 3.16B)**.

The contractility data for EMD 57033 was unexpected as it showed a decrease in trend and no change for CA while based on the voltage findings, the result was expected as a decrease in APD was observed.

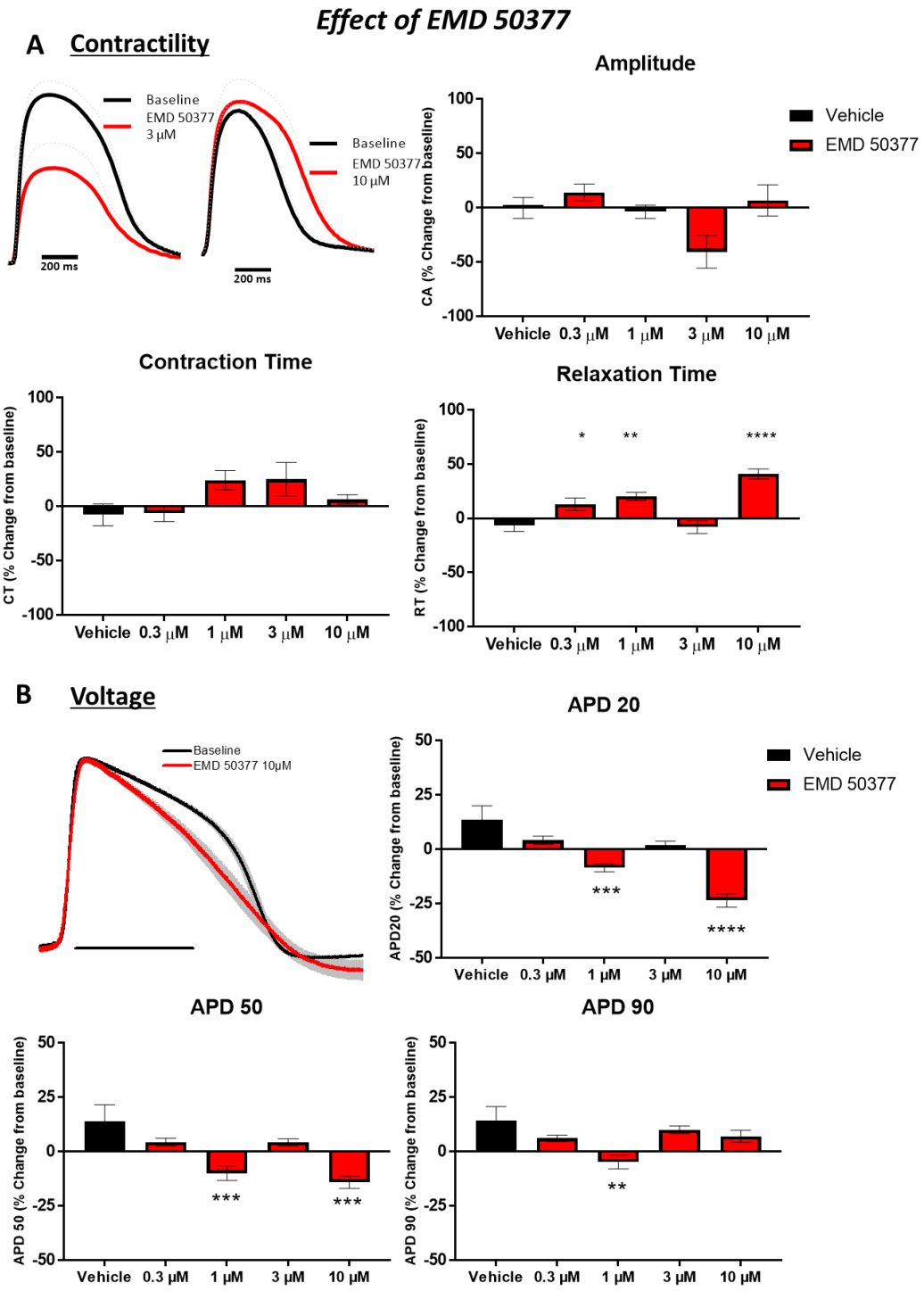


Figure 3.16: Contractility and voltage electrophysiological analysis of R-PAT-CMs treated with EMD 50377.
EMD 50377 showed no change in amplitude or potentially a NI; not as expected based on contractility. Correct prediction for voltage with a decrease in APD**.(A)** No changes in contraction amplitude were observed at all concentrations; contractility traces reflect reduction and no change in CA. For contractility, data are mean ± SEM, n=7 **(B)** Shorter repolarisation in all APDs was observed. For voltage, data are mean ± SEM, n=6. Statistical analysis was carried out using one-way ANOVA with Dunnett's multiple comparison test compared to the vehicle. Significance tests were based on p-values as follows: * $p < 0.05$; ** $p < 0.01$; *** $p < 0.001$; **** $p < 0.0001$

Negative inotropy

3.4.5.5 Nifedipine Treatment

Nifedipine is the LTCC blocker by decreasing the calcium influx, thus decreasing the cytosolic calcium concentration and therefore known as a negative inotrope. It has shown to produce a decrease in contractile force, and shorten APD in human papillary muscle strips and atrial trabeculae (Schwinger et al., 1990, Angus et al., 2000, Sarsero et al., 1998).

Contractility results showed no change in CA (-5.13 ± 5%), CT (-4.29 ± 4%), and RT (-0.3 ± 0.3%) for vehicle control **(Figure 3.17A)**. Meanwhile the nifedipine treatment showed a concentration-dependence for reduction in CA starting from 0.003 μM to 0.1 μM with the value of -20.5 ± 11.3% (0.003 μM), -29.9 ± 8% (0.01 μM), -54.6 ± 0.7% (0.03 μM) and -84.6 ± 1.3% (0.1 μM) **(Figure 3.17A)**. This was further supported by differences in traces between the baseline of the same condition before treatment (baseline; black) with the highest treatment concentration of (nifedipine 0.1 μM; red) **(Figure 3.17A)**. For CT in nifedipine treatments, no significant change was observed with 0.003 μM and 0.01 μM, while subsequently decreased at concentration 0.03 μM (-10.4 ± 3.4%) and 0.01 μM (-15.5 ± 11%)**(Figure 3.17 A)**. For RT , reduction was found in R-PAT-CMs with 0.003 μM (-30.7 ± 30.7%), a small change at 0.01 μM (-8.25 ± 31.7%) and 0.03 μM (-9.3 ± 10%), whilst an increase in RT at the maximum concentration of 0.1 μM (+33 ± 6%)**(Figure 3.17A)**.

For voltage electrophysiology assessment, no significant difference was found in any of the APDs of vehicle control relative to the baseline. Reduction in concentration-dependence was also observed, resulting in APD shortening **(Figure 3.17B)**. This resulted in APD20 (-15 ± 0.6%, -34.7 ± 5.7%, -40.5± 1.3%, -46.9± 0.1%), APD50 (-8.8 ± 1.3%, -18.5 ± 8.4%, -30± 2.5%, -42.5± 1.3%), APD90 (1.09 ± 8%, -9.2 ± 9.3%, -25.4± 3.4%, -40.2± 2.8%); respectively in 0.003, 0.01, 0.03, and 0.1 μM**(Figure 3.17B)**. It was further validated by voltage traces at the highest nifedipine concentration of 0.1 μM; the nifedipine treatment APD (red) relatively shortened (fast repolarisation) compared to the baseline (black) **(Figure 3.17B)**.

In summary, the results for nifedipine were correct and expected as NI.

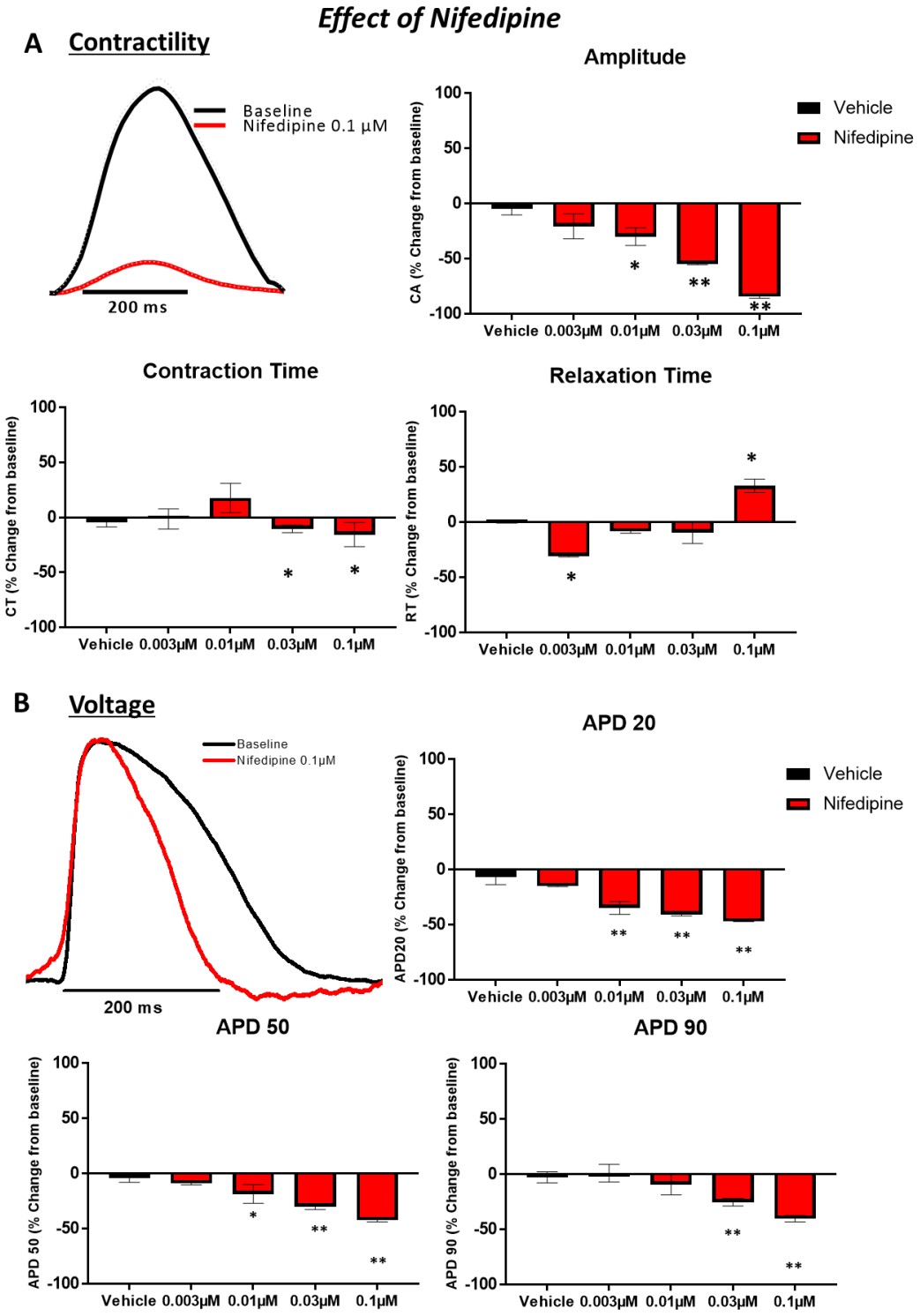


Figure 3.17: Contractility and voltage electrophysiological analysis of R-PAT-CMs treated with nifedipine.

Decreased in contraction and APD shortening **(A)** A concentration-dependence was observed causing a decrease in CA. CT and RT but RT significantly increase at 0.1 µM, which indicates a slower relaxation time. **(B)** Shortened repolarisation was observed in all APDs across all nifedipine concentrations with median = 0.03 µM. All data are mean ± SEM, n=6. Statistical analysis was carried out using one-way ANOVA with Dunnett's multiple comparison test compared to the vehicle. Significance tests were based on p-values as follows: * $p < 0.05$; ** $p < 0.01$; *** $p < 0.001$; **** $p < 0.0001$

3.4.5.6 Ryanodine treatment

Ryanodine is a known RyR receptor inhibitor. It acts by inhibiting the release of contractile calcium from intracellular stores and therefore decreases the cytosolic calcium concentration (Sutko and Willerson, 1980).

In ryanodine R-PAT-CMs assessment by CellOPTIQ, contractility results showed no significant change in CA across concentrations and this was reflected in contractility traces at the highest ryanodine 30 µM. However, there was a reduction trend of CA from concentration 1 µM (-6.5 ± 10.2%), 3 µM (-13.1 ± 12.6%) and 10 µM (-5.13 ± 8.4%)**(Figure 3.18A)**. At the highest concentration of 30 µM the trend increased CA (+6.99 ± 13.1%)**(Figure 3.18A)**. No significant change in CT and RT across varied ryanodine concentrations relative to the baseline **(Figure 3.18A)** were observed. The fluctuation response in CA across concentrations could be because of the biphasic response, as previously observed in rat papillary muscle (Sutko and Willerson, 1980).

For voltage electrophysiology assessment, no significant difference was observed in any APD of the vehicle control relative to the baseline. APD shortening was significant from concentration 3 µM to 30 µM **(Figure 3.18B)**. This resulted in APD20 (-20 ± 3.9%, -21.5 ± 1.4% and -22.1± 2.2%), APD50 (-14.8 ± 7.1%, -19.6 ± 5.7% and -21.3± 2.8), APD90 (-17.7 ± 1.9%, -26.4 ± 1.3% and -28.9± 4.0%); respectively for 3, 10, and 30 µM **(Figure 3.18B)**. It was further validated by voltage traces at the highest ryanodine concentration of 30 µM; the treatment APD (red) relatively shortened (fast repolarisation) compared to the baseline (black) **(Figure 3.18B)**.

In summary, the results for ryanodine were not as expected. The contractility reflects a biphasic response. However, the contractility traces exhibit it as a no effect drug while in voltage, the decrease in APD was not expected.

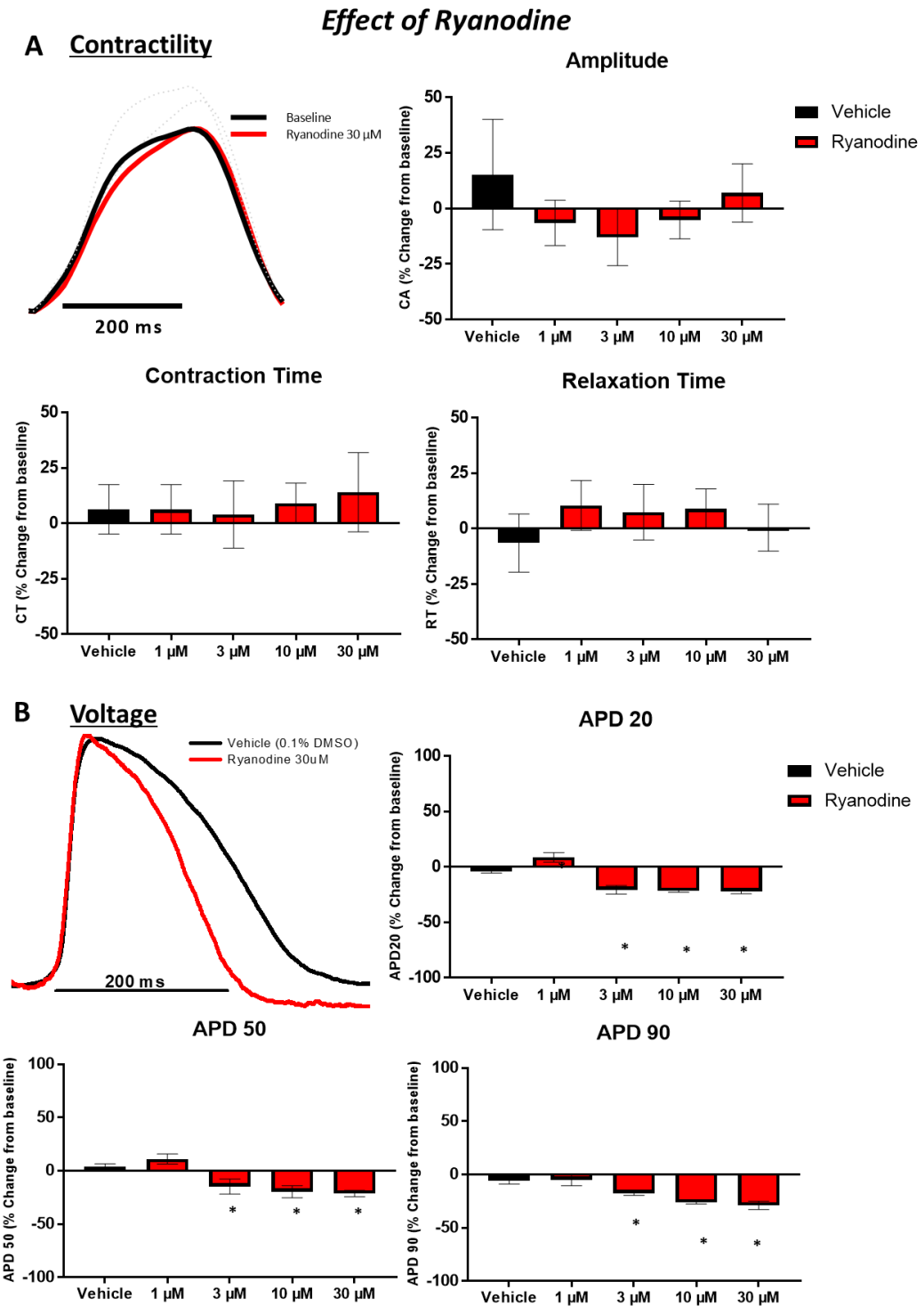


Figure 3.18: Contractility and voltage electrophysiological analysis of R-PAT-CMs treated with ryanodine.

No effect in contraction and decrease in APD **(A)** A biphasic effect in CA, No change in CT and RT **(B)** Shortened repolarisation was observed in all APDs across ryanodine at concentrations of 3, 10 and 30 µM. All data are mean ± SEM, n=6. Statistical analysis was carried out using one-way ANOVA with Dunnett's multiple comparison test compared to the vehicle. Significance tests were based on p-values as follows: * $p < 0.05$; ** $p < 0.01$; *** $p < 0.001$; **** $p < 0.0001$

3.4.5.7 Thapsigargin treatment

Thapsigargin is a non-competitive SERCA pump inhibitor, which disrupts calcium homeostasis by depleting calcium stores, thus causing cell death (Sehgal et al., 2017). It is expected to decrease in the force of contraction.

The thapsigargin assessment by CellOPTIQ, contractility results showed a significant reduction in CA at the highest concentration of 30 µM (-53.5 ± 11.8%)**(Figure 3.19A),** which was further validated with contractility traces as a reduction of CA. No significant changes in CT and RT**(Figure 3.19A)** were observed.

For voltage electrophysiology assessment, significant increases in APD were detected starting from 1 µM to 30 µM **(Figure 3.19B)**. This resulted in APD20 at 30 µM as +57.3 ± 5.9%. At APD50 (+26.6 ± 6.3%, +27.1 ± 4.5% and +70.5 ± 4.5) and APD90 (+32.9 ± 4.9%, +36.8 ± 2.2% and +73.8± 3.8%); respectively for 3, 10 and 30 µM**(Figure 3.19B)**. This was further validated by voltage traces at the highest thapsigargin concentration of 30 µM; the nifedipine treatment APD (red) showed relatively prolonged repolarisation (slower) compared to the baseline (black) **(Figure 3.19B)**.

In summary, the results for thapsigargin were correct and as expected as a NI

3.4.5.8 Tier 1 outcomes

The outcomes from Tier 1 as a standardised working practice are tabulated in **Table 3.1**

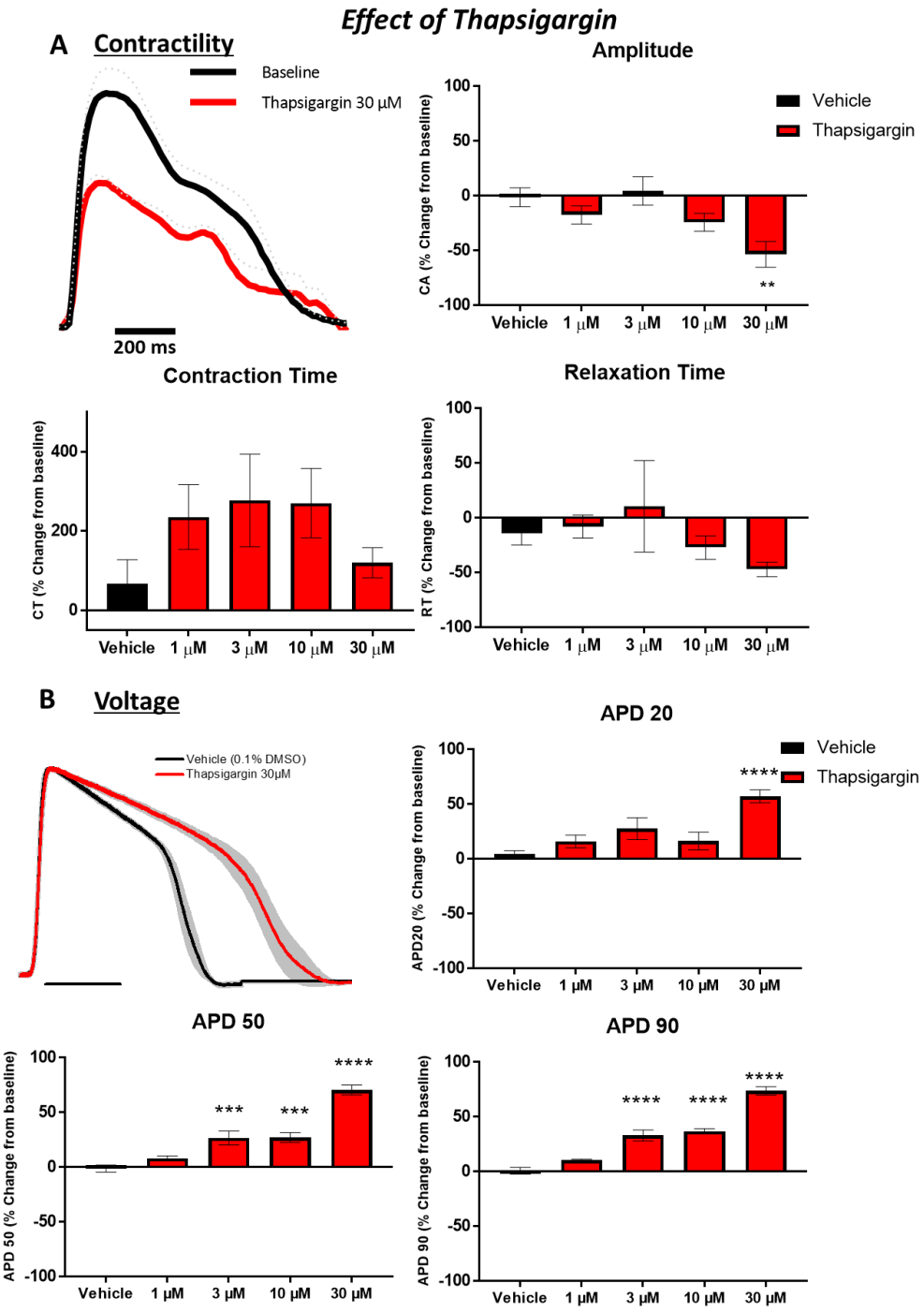


Figure 3.19: Contractility and voltage electrophysiological analysis of R-PAT-CMs treated with thapsigargin.
Thapsigargin reduced CA and prolonged repolarisation. **(A)** A decrease in contraction amplitude was observed at the highest concentration and further confirmed by contractility traces. Contractility data are mean ± SEM, n=7 **(B)** Delayed repolarisation in all APDs at highest thapsigargin concentration of 30 µM. For voltage, data are mean ± SEM, n=6. Statistical analysis was carried out using one-way ANOVA with Dunnett's multiple comparison test compared to the vehicle. Significance tests were based on p-values as follows: * $p < 0.05$; ** $p < 0.01$; *** $p < 0.001$; **** $p < 0.0001$

Drug	Main mechanism of action	Expected cardiac effects in vivo	Expected effect on contractility in isolated cardiomyocytes/heart muscles	Cellular mechanism of inotropic effect	Concentration range applied (μM)	FTPC (μM)	Refs	GSK Assignation	Tier 1 outcomes
Isoprenaline	β1- and β2-adrenoceptor agonist	PI, PC	PI, PC#, PCl, PL EC_{50} 0.01 μM	Increase in cAMP, Ca^{2+} influx, SR Ca^{2+} uptake and SR load	0.0003-0.1	0.0095	(Reyes et al., 1993)	Positive Inotropy (PI)	**PI**
Digoxin	Na^+/K^+ ATPase inhibitor	PI, arrhythmias	PI+ PL (< 1 μM, slowly developing, $t_{1/2}$ conc.-dependent) NI + diast. shortening (>1 μM)	Na^+/K^+ inhibition, Ca^{2+} increase via NCX	0.01-10	0.00075-0.0015	(Lullmann and Ravens, 1973)		**PI**
Bay K 8644	L-type Ca^{2+} channel agonist	PI (indirect NC because of RR increase)	PI, NL	Increase in Ca^{2+} influx	0.03-3	n.d.	(Aass et al., 1988)		**unexpected/biphasic NI**
EMD 57033	Calcium sensitizer, myosin activator	PI	PI, NL, EC_{50} ~5 μM, diastolic shortening at high conc.	Myofilament sensitization to Ca^{2+}	0.01-30	16 μM	(Hajjar et al., 1997), (de Zeeuw et al., 2000)		**NE**
Nifedipine	L-type Ca^{2+} channel blocker (dihydropyridine)	Small NI (direct) overridden by adrenergic activation, PC (indirect)	NI, IC_{50} 0.1 μM	Decreased Ca^{2+} influx	0.003-0.3	0.02	(Angus et al., 2000)	Negative Inotropy (NI)	**NI**
Ryanodine	Inhibitor of RyR2	n.d.	NI, NCl, species dependent biphasic, IC_{50} ~0.01 μM	Decreased SR Ca^{2+} release	1-30	n.d.	(Sutko and Willerson, 1980), (Fedorov et al., 2002)		**unexpected/biphasic PI**
Thapsigargin	Inhibitor of SR Ca^{2+} ATPase	n.d.	Heart muscle: NI ~50% at 500 μM, NL ~20% at 500 μM Isolated myocytes: ~90% NI at 0.1 μM	Decreased SR Ca^{2+} uptake and load	0.3-30	n.d.	(Kirby et al., 1992), (Baudet et al., 1993)		**NI**

Table 3.1: The details of Tier 1 'training set' drugs with known positive (PI) or negative inotropic (NI) effects, and the outcomes.
Compound selection within the CRACK-IT study. NE; no effect, FTPC;free therapeutic plasma concentration, PC;positive chronotropy, PCl; positive clinotropy, PL; positive lusitropy, Nc;negative chronotropic, NI;negative inotropy, NCl;negative clinotropy, NL;negative lusitropy, EC50; half-maximal effective concentration, IC50;half-maximal effective inhibitory concentration, GP; guineapig, hERG; human eag-related gene, NCX; Na+/Ca2+ exchanger,RyR2; ryanodine receptor 2, SR; sarcoplasmic reticulum.

3.5 Chapter Discussion

This chapter discusses the optimisation of the culture conditions for all three hiPSC-CMs and refinement of the configuration of 2D monolayer cells with CellOPTIQ platform by utilising Tier 1 drugs as unblinded training. In addition, the quality of large-scale differentiation of in-house R-PAT-CMs was evaluated with 80% cardiac purity and their recovery after thawing was moderate and similar to iCell^2, which means their recovery is similar to the commercial course.

The ventricular and atrial subtypes in all three hiPSC-CMs were also evaluated, together with the presence of ventricular gap junctions Connexin43. The Pluricyte exhibited high content of MLC2a+MLC2v together with CX43 and high RO index, which indicate that they are robust ventricular CMs. Both R-PAT-CMs and iCell^2 also demonstrated an RO index of more than 1.5, which indicates the presence of ventricular cells within them. All three hiPSC-CMs were able to be electronically paced and therefore are suitable for drug assessment in CellOPTIQ as the baseline of both contractility and voltage were successfully extracted. The varied baseline value among the three hiPSC-CMs was predicted as they all come from independent sources with independent differentiation, culture and cryopreservation protocols.

The prediction for R-PAT-CMs treated with isoprenaline was correct and parallelled with others finding. As such, both hESC-CMs and hiPSC-CMs tested by Zhao *et al.* (1017) showed increased in amplitude at 0.1, 1, and 10 µmol/L of isoprenaline (Zhao et al., 2017b); higher concentrations tested compared from Tier 1 unblinded dosage in R-PAT-CMs. Therefore as expected their increase in amplitude were significantly higher. Yokoo *et al.* (2009) was also observed increased in contraction amplitude in hiPSC-CMs, albeit in the MEA system with 10 minutes drugs incubation (Yokoo et al., 2009a).In term of APD changes, Zhang *et al.* (2009) observed shortening of APD at 1µmol/L in both hESC-CMs and hiPSCs (Zhang et al., 2009), similar to the finding in this chapter, wherein the shortening APD at 20%, 50% and 90% was observed in R-PAT-CMs treated with 0.03 µM isoprenaline.

The finding of R-PAT-CMs treated with digoxin in this chapter study was also parallel with other findings wherein increased in Ca^{2+}-wave amplitude with action potential shortening action potential was observed in hiPSC-CMs (iCells)(Guo et al., 2011). For nifedipine treatment, similar results were observed in the study conducted by Dempsey *et al*. (2016), wherein hiPSC-CMs treated with nifedipine, decreased in Ca^{2+}transient amplitude and shortening of APD at 50% and 90% repolarisation time was observed (Dempsey et al., 2016).

Incorrect prediction was also observed in this chapter study. For example, Bay K 8644 which supposed to be PI were predicted as biphasic (potentially NI). Nonetheless, the lack of significant increase effects in CA on R-PAT-CMs by Bay K might be considered common. Previously high variations of Bay K effects in hPSC-CMs have been reported between cell to cell and cell lines of different sources (Kang et al., 2012, Ji et al., 2014). This highlights the need for more than one cell line for future drug assessment.

Although APD shortening in R-PAT-CMs treated with EMD 57033 was expected and correctly observed in this chapter study, their contractility response showed no change for CA (while it supposed to be PI drugs). As EMD 57033 acts as calcium sensitiser by increasing the myofilament response to calcium, their response is dependant on myofibril organisation, thus more mature cardiomyocytes. As such, similarly, no change in twitch force was observed in neonatal cardiomyocytes treated with EMD 50733 due to less myofibril organisation (Rodriguez et al., 2013). This highlight the need for more mature CMs to test the impact of drug-induced changes.

Although some of the predictions regarding Tier 1 drugs were incorrect, the aim of establishing the CellOPTIQ as a drug screening platform towards evaluating contractility and voltage measurement is achievable. The algorithms for data analysis and platform setup were also able to correctly predict the correct mode of action (inotropy and electrophysiology) for some of Tier 1 drugs.

The training set has helped to establish the standard operating procedures (SOPs), subsequently used in the next stage of the study, the blinded evaluation of the ‘test set’ drugs of Tier 2 CRACK-IT. Along with the experiments, some

additional protocols were made to minimise electrolysis effects and sudden change and therefore, a 50% medium change performed during drug addition.

In addition, a standardised formula for analysis was set and known as the percentage of change in the drug-treated sample relative to untreated (vehicle) control using the formula ([drug/drug baseline]/[vehicle/vehicle baseline]*100-100. The baseline is the reading without (before) drug or vehicle treatment.

For contraction classification, the responses were sectioned into positive responses as the positive inotropy, which reflects an increase in contraction amplitude (CA), positive in clinotrophy, reflecting a decrease in contraction time (CT) and positive lusitrophy, reflecting a decrease in relaxation time (RT), while the negative responses are the opposite of the above statements **(Figure 3.20A).**

For voltage parameters, some modifications were made. Towards Tier 2, it was decided to include APD 30, APD 90 and Triangulation (APD90- APD30) as beneficial standardised parameters for voltage **(Figure 3.20B).**

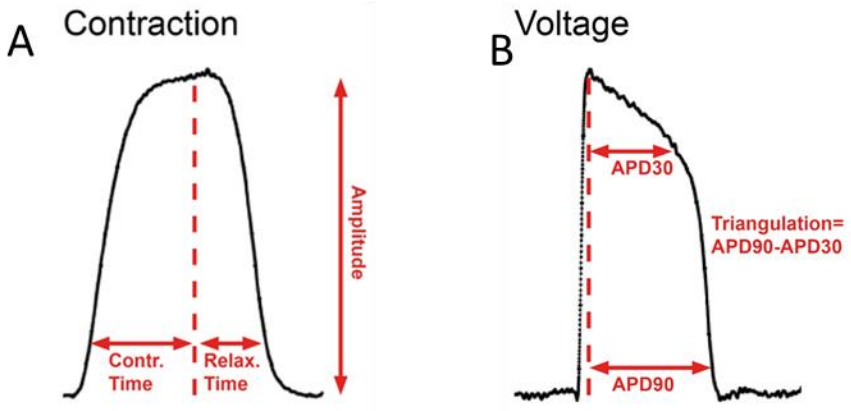


Figure 3.20: Schematic description of the parameters to be used to quantify drug effects in hiPSC-CMs.

Chapter 4 Blinded compound testing in hiPSC-CMs

4.1 Introduction

The previous chapter discussed the establishment and fine-tuning of the platform test system (CellOPTIQ) with a set of Tier 1 'training' drugs together with the development of hiPSC-CMs culture systems. This prework enabled the second phase of CRACK-IT, which was to conduct a blinded testing of Tier 2 drugs to generate and evaluate a physiologically relevant medium-throughput platform with different hiPSC-CMs to study the impact of drug-induced changes on cell function for safety assessment.

4.2 Tier 2 blinded test

As part of the CRACK-IT Initiative, this chapter focuses on the Tier 2 blinded testing. GSK was responsible for finalising the blinded test drugs and assigning them according to priority ranks. As such, up to 28 drugs were assigned by GSK. In Nottingham, hiPSC-CMs (iCell^2, Pluricyte and R-PAT-CMs) were tested as 2D monolayers on the CellOPTIQ. The blinded tests for the CellOPTIQ-hiPSC-CMs combination used the SOPs established in the previous phase, the Tier 1 training drug testing (**Table 4.1**) discussed in Chapter 3.

The Leiden team, led by Christine Mummery, used the TTM system with Pluricyte hiPSC-CMs, again as 2D monolayers. The Hamburg team, led by Thomas Eschenagen, used 3D EHTs in combination with R-PAT-hiPSC-CMs and their in-house ERC18 hiPSC-CM lines. The rationale for using different hiPSC-CMs derived from different hiPSC lines is explored in more detail in the discussion section of this chapter.

As a comparator, the Glasgow group, led by Godfrey Smith, ran parallel tests on the CellOPTIQ but using adult rabbit primary cardiomyocytes cultured as single cells in 2D.

Table 4.1: Established working Standard Operating Procedures (SOPs) for CellOPTIQ (CO) platforms.
In-house means the conditions or assays used for hiPSC-CMs derived from in-house hiPSC lines using in-house differentiation methods. Commercial means use of Pluricyte and/or iCell^2 hiPSC-CMs that were purchased from Ncardia and Cellular Dynamics International, respectively.

	Protocol	CellOPTIQ® (CO)
Starting conditions	Format	96-well plate
	Age	• Manufacturer instructions for commercial (5-8 days after thawing) • Differentiation time +10 day-old (R-PAT-CMs)
	Culture medium	• Manufacturer instructions for commercial • Standard culture medium (R-PAT-CMs)
	Quality control	• Cell purity >90% by a-actinin (R-PAT-CMs) • Spontaneous beat rate of ≤1.5 Hz • Response to 30 nM nifedipine
Experimental set-up	Medium	• 1.8 mM Ca DMEM Gibco#11966 + 10mM Galactose + 1mM NaPyr (serum/protein-free) • For R-PAT-CMs and iCell^2: 24h before assay changed media into SFM and assay conducted in 100%SFM • For Pluricyte: 24h before assay changed media into 50%Pluricyte+50% SFM medium and assay conducted in 100%SFM
	Cell loading	FluoVolt
	Recording: Baselines	Paced at 1.2-1.7 Hz; 10 sec/area
	Recording: Conc-response curves	Replicates: 5 wells/conc + time matched vehicle controls
		Solvent: max 0.1% DMSO
		Treatment duration: 30 mins
		Dosage: 5 concentrations in semi-logarithmic steps, single concentration/well
		Readings: Paced as follows: ≤1 Hz → 1.2 Hz; 1<x≤1.3 Hz → 1.5 Hz; 1.3<x≤1.5 Hz → 1.7 Hz; 20 ms, 8 volts; 10 sec/well
Follow-up	Analysis	Analysis is performed off line using CellOPTIQ software
	Recovery	n/a
	Repeat testing	No repeated use of cells

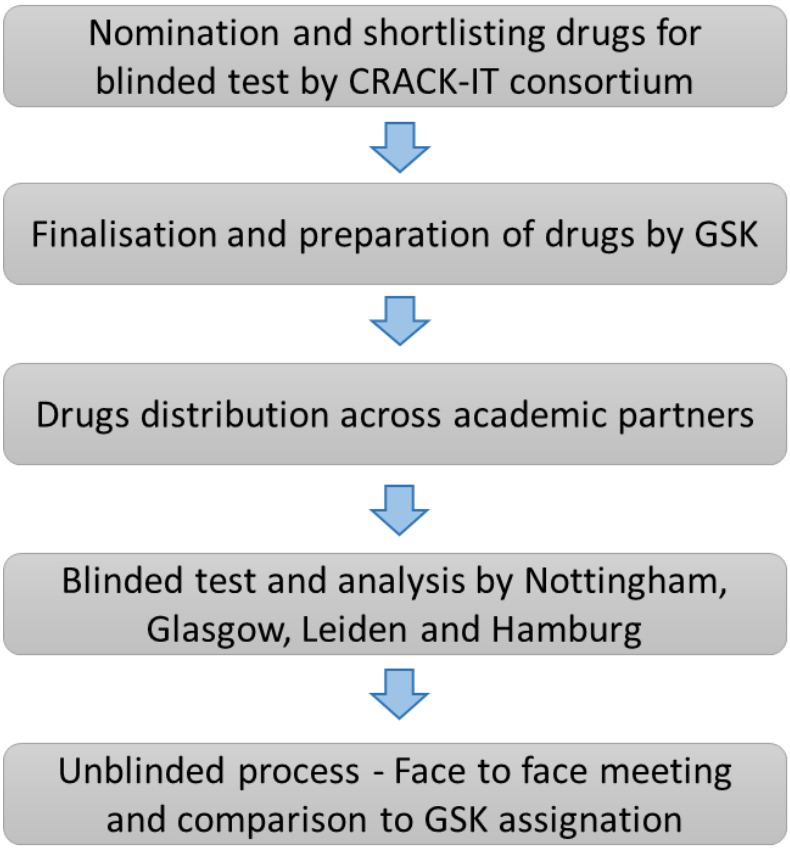


Figure 4.1: Tier 2 blinded test flow chart as part of the CRACK-IT consortium

4.2.1 Selection of drugs

The blinded drugs were nominated by the consortium based on their commercial availability, equal or balanced number between PI, NI and no effect (NE) in terms of contractility. This includes a wide range of contractility and toxicity-related modes of action, including ion channel modulation and cell membrane pumps ($I_{NaV1.5}$, I_{Kr}, I_{KATP}, I_{CaL}, I_f, NCX, Na+/K+-ATPase) or sarcoplasmic reticulum (RYR, SERCA), $ß_1$- and $ß_2$-adrenoceptors, Ca^{2+} sensitivity, signaling cascades (phosphodiesterase, adenylyl cyclase, cyclic AMP), energy production (ATP, mitochondrial stress), myofilament response and including less well known machinery (e.g. inhibition of tyrosine kinases). Also, the inotropic data are based on cardiomyocytes and/or data from heart function from more than one species, including human, *in-vitro*, *ex-vivo*, preclinical and clinical use. The data available are also based on free therapeutic plasma concentrations (FTPC). However, the finalised blinded drugs decision was made by GSK, as described in **Figure 4.1**.

4.2.2 Drug distribution and handling

GSK was responsible for the procurement, formulation, weighing, coding, and distribution of the blinded drugs across the testing laboratories in powder state at -20ºC. The drugs were contained in brown glass vials to avoid any deterioration or risk of light exposure (incase of light-sensitive compounds). The working stocks were prepared in testing laboratories according to the formula sheet prescribed by GSK and stored at -80ºC. As DMSO is known to be highly hygroscopic (absorb moisture), single-shots of DMSO were used to avoid falsification of the real concentration of the drugs. In order to prevent degradation and maintain their effectiveness, the drugs were used within two weeks with a maximum of two freeze-thaw cycles.

4.2.3 CellOPTIQ blinded experimental layout

Due to cost, availability and time, blinded drug testings for all hiPSC-CMs (iCell^2, Pluricyte and R-PAT) on the CellOPTIQ were restricted to the first ten priority drugs and the rest of the 27 drugs were done in R-PAT-CMs. For each drug, at least five repeats were used over a range of five different half-log concentrations, which were predetermined by GSK. To prevent toxicity, and ensure consistency between drugs and each point on the concentration range, every drug was prepared in a final concentration of DMSO of 0.1% v/v. In order to minimise electrolysis effects and sudden changes, a 50% medium change was performed during drug treatment. Electrical pacing was employed to deliver a uniform field for stimulation, well by well, with manual configuration of 8V, 2 ms duration according to adapted frequency (see Table 4.1 under the 'experimental set up' row).

4.2.4 Evaluation and analysis parameters

A standardised formula for analysis was agreed across partners and known as the percentage of change in the drug-treated sample relative to the untreated (vehicle) as control, using the formula: ((drug/drug baseline)/(vehicle/vehicle baseline)*100-100). The baseline is the reading without (before) drug or vehicle treatment.

The parameters for contractility were maintained as contraction amplitude (CA), relaxation time (RT) and contraction time (CT) **(Figure 4.2)**. These were further classified as 1) positive inotropy (increased in CA), 2) positive clinotrophy (decrease in CT) and 3) positive lusitrophy (decrease in RT) **(Figure 4.2)**. The negative responses were opposite to those listed above.

For uniformity across partners, the voltage parameters were agreed for action potential duration at 30% and 90% repolarisation (APD30 and APD90) **(Figure 4.2)**. Triangulation (APD90 – APD30) was calculated from voltage traces **(Figure 4.2)**. The outcomes are either altered electrophysiology (AE) or altered electrophysiology with arrhythmias (AE*)**(Figure 4.2)**.

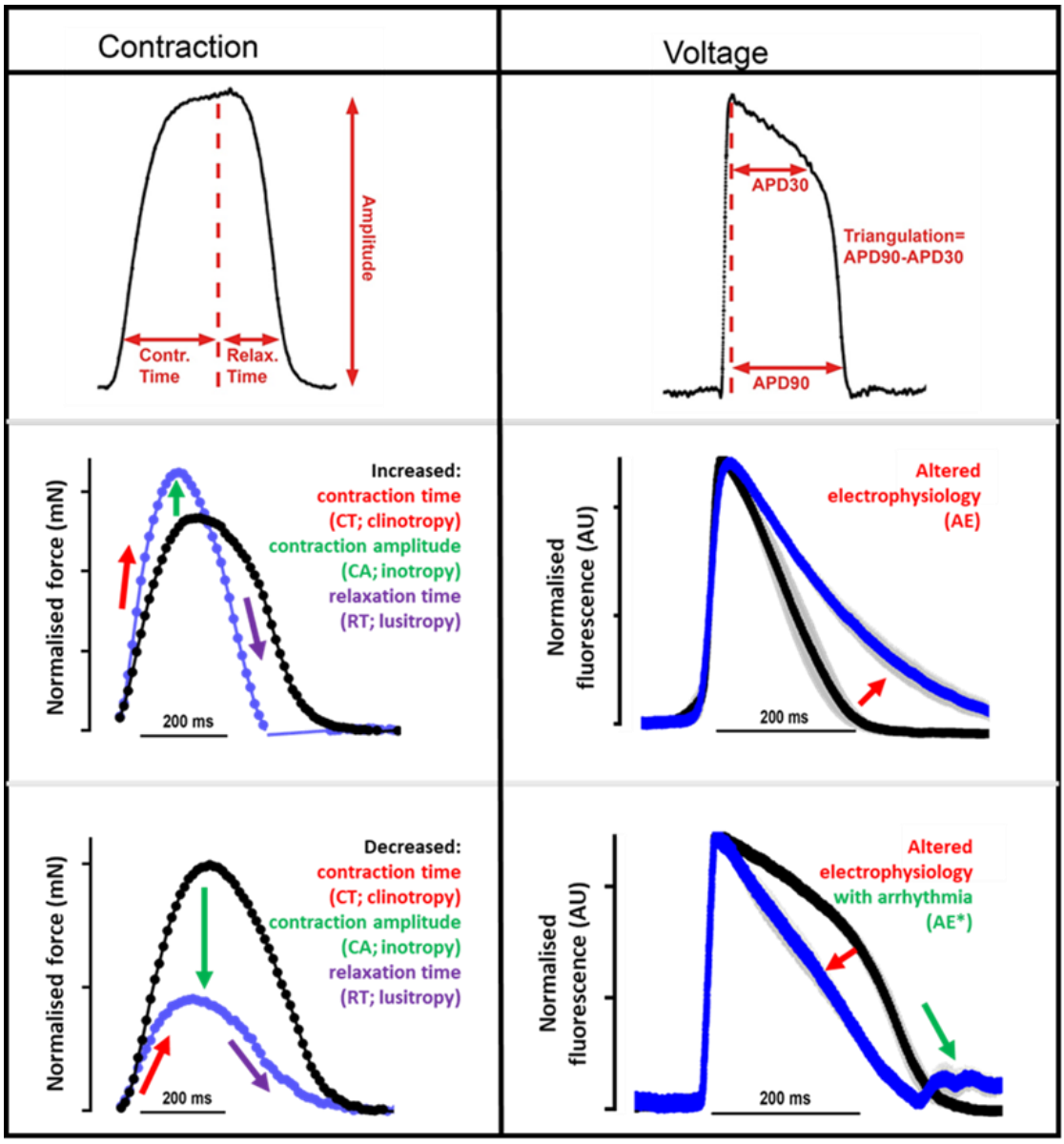


Figure 4.2: Schematic description for parameters used to quantify the drug effects and terminology used to evaluate the response in hiPSC-CMs.

Black traces are baseline readings, while the blue are traces after 30 minutes of drug treatment. The colours of arrow and text match the type of change.

4.2.5 The unblinding process

Blinded predictions were conducted during two days of face to face meetings between all CRACK-IT partners, with independent monitoring and observation by GSK and N3CRs. The investigators collectively assigned overall prediction individually to each blinded drug according to each platform: cell line combination as either positive (PI), negative (NI) or no effects (NE) for contractility. AE, AE* or no effect for voltage electrophysiology were used to support prediction for contractility. Due to the complexity of the data, some decisions were made based on the trends rather than the significant value, although these represented the minority of the predictions (3/47= 6.4%) for CellOPTIQ:hiPSC-CMs combination. At the end of the first day of face to face meetings, the predictions were finalised, and all documents then considered locked to avoid unconscious bias. GSK then unblinded the drugs to enable comparison with the drugs' known effects.

4.3 Chapter aims and objectives

The hiPSC-CMs hold promise for to study the impact of drug-induced changes for drug screening and safety assessment. This phase was part of the CRACK-IT consortium aimed to further test and validate the established cellOPTIQ system with blinded testing of up to 28 drugs provided by GSK on three different sets of hiPSC-CMs (iCell^2, Pluricyte and R-PAT-CMs). The contractility and voltage had to be sequentially measured after 30 minutes of treatment with blinded drugs. The outcome of the blinded tests had to be compared across GSK assignation in order to define their predictivity and sensitivity regarding drug safety. Also, the scope of this phase of the study was to determine how reliable the inotropic effects can be detected by CellOPTIQ platform. The following objectives had to be met to fulfil this aim:

5) Conduct contractility and voltage assays with the first top ten priority blinded drugs in all three sets of hiPSC-CMs (iCell^2, Pluricyte and R-PAT-CMs), while drugs ranking 11 onwards exclusively on R-PAT-CMs.

6) Predict whether the blinded drugs show positive, negative or no effect inotropes.

7) Compare the predictions with assignation from GSK after unblinding.

4.4 Results

In order to discuss the results, this result starts with a description of the drugs selected by GSK. As mentioned above, these were evaluated in a fully blinded fashion but for the purposes of this chapter, it helps the reader if the drugs are known. Accordingly, the drugs were a mixture of 8 PI, 9 NI and 11 NE (Table 4.2) and were placed randomly except for the first ten drugs which were indicated by GSK as top priority drugs. The additional information for each drug is further elaborated in Table 4.3, according to the grouping of PI, NI and NE.

Table 4.2: The rank, drugs coding number of blinded test drugs and drugs name with their assignation after unblinding by GSK. The dotted line consists of the 10 top priority drugs assigned by GSK. The PI indicates positive inotropy, NI indicates negative inotropy and NE indicate no effects drug.

Rank	Number	Drug name	GSK Assign
1	29	Epinephrine	PI
2	28	Forskolin	PI
3	05	Levosimendan	PI
4	26	Pimobendan	PI
5	19	Acetylsalicylic acid	NE
6	25	Atenolol	NE
7	17	Verapamil	NI
8	13	Doxorubicin	NI
9	22	Sunitinib	NI
10	20	Captopril	NE
11	01	Dobutamine	PI
12	03	Glibenclamide	NE
13	27	Milrinone	PI
14	07	Omecamtiv mecarbil	PI
15	02	Enalaprilat	NE
16	11	Citalopram	NI
17	24	Clonidine	NE
18	15	Itraconazole	NI
19	21	Sorafenib	NI
20	04	Ivabradine	NI
21	09	Terbutaline	PI
22	23	Flecainide	NI
23	06	Paracetamol	NE
24	08	Phentolamine	NI
25	16	Tolbutamide	NE
26	10	Pravastatin	NE
27	14	Sildenafil	NE
28	18	Zimelidine	NE

Table 4.3: Detailed information about Tier 2 blinded drugs within the CRACK-IT study.
Abbreviations: n.d, not defined; n.a, not applicable; PC, positive chronotropy; PI, positive inotropy; PCl, positive clinotropy; PL, positive lusitropy; NC, negative chronotropy; NI, negative inotropy; NCl, negative clinotropy; NL, negative lusitropy; inotropy is defined as change in peak force, clinotropy as change in time-to-peak force (generally from 20% above baseline to peak and "positive" being an abbreviation) and lusitropy as change in relaxation time (time from peak force generally to 80% relaxation and "positive" being an abbreviation); EC_{50}, half maximal effective concentration; IC_{50}, half maximal effective inhibitory concentration; GP, guinea pig; hERG, human eag-related gene; NCX, Na^+/Ca^{2+} exchanger; RR, blood pressure; RyR2, ryanodine receptor 2; SR, sarcoplasmic reticulum; * indicates lack of clarity in literature on inotropic effect; # in spontaneously contracting preparations.

Drug	PI, NI, NE	The main mechanism of action	Expected cardiac effects in vivo	Expected effect on contractility in isolated cardiomyocytes/heart muscles	Cellular mechanism of inotropic effect	Concentration range applied (μM)	FTPC (μM)	Refs
Epinephrine	PI	Non-selective α1-, β1- and β2-adrenoceptor agonist	PI, PC	PI, PC#, PCl, PL EC_{50} 0.1 μM	Increase in cAMP, Ca^{2+} influx, SR Ca^{2+} uptake and SR load	0.01 - 1	0.0002-0.050	(Molenaar et al., 2007) (Wortsman et al., 1984)
Forskolin	PI	Adenylyl cyclase stimulator	PI, PC	PI, PC#, PCl, PL EC_{50} 5-10 μM	Increase in cAMP, Ca^{2+} influx, SR Ca^{2+} uptake and SR load	0.1 - 10	0.012-0.024 (colforsin)	(Bristow et al., 1984, Kikura et al., 2004)
Levosimendan	PI	PDE3 inhibitor (IC_{50} 25 nM) Calcium sensitizer	PI, PC (more heart rate increase and RR	Small PI (~50%), PC#, PCl+PL (14%), EC_{50} ~0.1 μM	Increase in cAMP and myofilame	0.01 - 1	0.026-0.35	(Boknik et al., 1997, Hasenfuss et al., 1998, Mebazaa et al., 2007,

		K_{ATP} channel agonist	decrease than dobutamine)		nt sensitizatio n to Ca^{2+}			Papp et al., 2012, Orstavik et al., 2014a, Abi-Gerges et al., 2013, Puttonen et al., 2008)
Pimobendan	PI	Calcium sensitizer PDE inhibitor (partial)	PI, small PC	PI, small PC#, PL and NL at low/high conc., EC_{50} 34 µM	Increase in cAMP and myofilame nt sensitizatio n to Ca^{2+}	1 - 100	0.005-0.01	(Honerjager et al., 1984, Berger et al., 1985, Chu et al., 1995)
Dobutamine	PI	α1-, β1- and β2 adrenoceptor agonist	PI, PC, less HR-stimulation than epinephrine	PI, PC#, PCl, PL. EC_{50} 1-3 µM	Increase in cAMP, Ca^{2+} influx, SR Ca^{2+} uptake and SR load	0.1 - 10	0.07-1	(Ishihata et al., 1988, Brown et al., 1987, Mahoney et al., 2016)
Milrinone	PI	PDE3 inhibitor	PI, PC (more heart rate increase and RR decrease than dobutamine)	Small PI, PC#, PCl, PL (smaller than ISO) EC_{50} 60 µM	Increase in cAMP, Ca^{2+} influx, SR Ca^{2+} uptake and SR load	1-100	0.1-0.15	(Brown et al., 1986, Bailey et al., 1994)
Omecamtiv mecarbil	PI	Cardiac specific myosin activator	PI, prolonged ejection time, small decrease in heart rate	PI, NCl, NL, diastolic shortening (dog myocytes). EC_{50} 1 µM	Increased number of myosin heads binding to actin, no affection	0.01 - 1	0.05 - 0.42	(Cleland et al., 2011, Planelles-Herrero et al., 2017, Horvath et al., 2017, Teerlink et al., 2011, Liu et al., 2016)

					of Ca^{2+} transient			
Terbutaline	PI	β2-adrenoceptor agonist	Small PI and PC	PI, PC#, PCl, PL. EC_{50} 3 µM	Increase in cAMP, Ca^{2+} influx, SR Ca^{2+} uptake and SR load	0.1 - 10	1.3	(Schafers et al., 1994, Dyreborg et al., 2016)
Verapamil	NI	L-type Ca^{2+} channel blocker, hERG blocker	NI (direct) partially masked by adrenergic activation (indirect), NC or none, ND (direct)	NI, IC_{50} 0.1 µM	Decreased Ca^{2+} influx	0.01 - 1	0.05	(Angus et al., 2000), (Giacomini et al., 1984)
Doxorubicin	NI	Impairs Ca^{2+} transport mechanisms in sarcoplasmic reticulum	NI, time course of cardiotox dose-dependent	PI+NCl and reduced post-rest potentiation at 30 µM (GP), but strong NI at 1000 µM (GP, rat); rate-dependent	Complex, including increased mitochondrial ROS	0.1 - 10	1-2	(Temma et al., 1993, Hofling and Bolte, 1981, Matsushita et al., 2000, Danesi et al., 1999)
Sunitinib	NI	Multi-targeted TK inhibitor	NI, NC at high doses, chronic cardiotox	NI, IC_{50} 10 µM	Complex	0.1 - 10	0.003	(Mooney et al., 2015, Abi-Gerges et al., 2013, Bello et al., 2006)
Citalopram	NI	SSR inhibitor, hERG & L type Ca^{2+} channel inhibitor	None (at therapeutic doses), higher risk of TdP	NI at 30 µM (-57% in hEHT, -38% in human atria)	Decrease in Ca^{2+} influx	1 - 100	0.05	(Witchel et al., 2002, Mannhardt et al., 2017b, Rao, 2007)
Itraconazole	NI	Triazole antifungal, inhibitor of Na^{+} channels and	NI	NI (-30% at 0.3 µM; rabbit heart)	Decreased Na^{+} influx (?)	0.1 - 10	0.00086 (higher	(Head et al., 2015, Qu et al., 2013, Bellmann, 2007)

		mitochondrial voltage-dependent anion channel 1					in tissues)	
Sorafenib	NI	Multi-targeted kinase inhibitor	None or NI at high doses, delayed cardiotox	None (feline and canine CM, but cell death), NI (rat heart)	n.d.	0.1 - 10	0.03 (higher tissue levels)	(Henderson et al., 2013, Duran et al., 2014, Abi-Gerges et al., 2013, Kim et al., 2013)
Ivabradine*	NI	I_f inhibitor	NC (therapeutic)	None, NC at >10 µM (spontaneously beating preps), NIE (-13/-60% in guinea pig atria/PM, -38% human trabeculae at 100 µM); PI in mouse left atria and 30% of human trabeculae	Decrease in Ca^{2+} transient peak	0.1 - 10	0.01-0.1	(Perez et al., 1995, Boldt et al., 2010, Bois et al., 1996, Mesirca et al., 2014, Choi et al., 2016)
Flecainide	NI	Na^+ channel blocker, hERG blocker	NI	NI, IC_{50} 0.3 µM	Decreased Na^+ influx (?)	0.1 - 10	0.2-0.4	(Abi-Gerges et al., 2013, McQuinn et al., 1988)
Phentolamine	NI	Non-selective α adrenoceptor antagonist, Na^+ and Ca^{2+} channel blocker at high conc.	PC (indirect)	NI, IC_{50} ~20 µM	Decreased Na^+ and Ca^{2+} influx	1-100	2.25	(Sada, 1978, Rosen et al., 1971)
Zimelidine*	NI	SSR inhibitor	None (at ther. doses), QT and QRS widening at high doses	n.d.	n.d.	1 - 100	0.78	(Lindbom and Forsberg, 1981, Forsberg and Lindbom, 1983, Naranjo et al., 1984)
Acetylsalicylic acid	NE	Cyclooxygenase inhibitor	None	None	n.a.	1 - 100	0.3-2	(Abi-Gerges et al., 2013)

Atenolol	NE	β1>β2 adrenoceptor antagonist	NI, NC, ND	None (in absence of agonist) until 3000 µM (in contrast to e.g. propranolol)	n.a.	0.1 - 10	1	(Lemoine et al., 1988, Kaumann and Blinks, 1980)
Captopril	NE	ACE inhibitor	None	None	n.a.	1-100	1-2	(Abi-Gerges et al., 2013, Giudicelli et al., 1987)
Glibenclamide	NE	K_{ATP} channel antagonist	None or PI in ischemia	None; PI in ischemia or presence of K_{ATP} opener; NI in adrenalectomized dogs, NE in isolated dog heart trabeculae	n.a.	0.1 - 10	0.02-0.06	(Satoh et al., 1990, Murakami et al., 1992, Pogatsa and Dubecz, 1977, Rydberg et al., 1997)
Enalaprilat	NE	ACE inhibitor	None	None	n.a.	1 - 100	0.12	(Stage et al., 2017)
Clonidine	NE	α2-adrenoceptor agonist	NI, NC	None	n.a.	0.01 - 1	0.002-0.004	(Jarrott et al., 1979b, Kleiber et al., 2017)
Paracetamol	NE	Prostaglandin synthesis inhibitor	None	None	n.a.	10 - 1000	50	(Marks et al., 2012, Kamali et al., 1993, Brown et al., 1992)
Tolbutamide	NE *	K_{ATP} channel antagonist, weak adenylyl cyclase stimulator	None or PI (dogs, men)	None (canine CM) or small PI (rabbit atria, rat heart), EC_{50} ~30 µM	Increase in cAMP (?)	1 - 100	20-30	(Levey et al., 1971, Lasseter et al., 1972, Abi-Gerges et al., 2013, Whiting et al., 1981)
Pravastatin	NE	HMG CoA reductase inhibitor	None	None	n.a.	1 - 100	0.018	(Costantine et al., 2016)
Sildenafil	NE	PDE5 Inhibitor	None or PI+PC (indirect)	None	n.a.	0.3 - 30	0.02	(Sugiyama et al., 2001, Walker et al., 1999)

4.4.1 Blinded testing

By utilising the SOPs (see **Table 4.1)**, up to 27 drugs were assigned to be tested in Nottingham in the rank order that was predetermined by GSK (see **Table 4.3)**. The first ten drugs were defined as the main priority by GSK and therefore were tested accordingly across platforms and cell lines. In Nottingham, the first 10 priority drugs were tested in all three hiPSC-CMs (iCell^2, Pluricyte and R-PAT-CMs) in CellOPTIQ.

The drug stocks were made fresh on the day with 5 different final test concentrations within range, as illustrated in **Table 4.3,** together with vehicle concentration of 0.1% DMSO. The baseline recording was obtained before drug treatment; the CMs were then incubated with the respective drug solution for 30 minutes, followed by treatment recording.

In order to predict what is correct or incorrect to the very complex dataset, the trends or significant changes in the parameters measured were looked at. In addition, any cut off on how much change was considered meaningful (for example >15% change and statistical significance) were not applied. The drugs were normalised as the percentage of change from baseline and were compared to the vehicle control.

4.4.2 Blinded test on top 10 priority drugs with iCell^2, Pluricyte and R-PAT-CMs

The top 10 drugs were unblinded and were identified as PIs (epinephrine, forskolin, levosimendan, pimobendan), NIs (verapamil, sunitinib), NEs (acetylsalicylic acid, atenolol, captopril), as illustrated in the dotted box of Table 4.2.

The data for top 10 priority drugs were illustrated for each cell line respectively for both contractility and voltage and were predicted whether PI, NI or NE respectively as below.

4.4.2.1 Rank 1; Epinephrine treatment (PI)

For contractility readouts, the traces showed no significant difference or trends between CA, CT and RT for either Pluricyte or R-PAT CMs throughout all concentrations of 0.01, 0.03, 0.1, 0.3 and 1 μM **(Figure 4.3A)**, and as such, were both predicted as NE. For iCell^2, there were no changes in CA or RT. However for CT in iCell^2, there was a trend of decreased CT at 0.03 to 1 μM; CT (0.03 μM = -42.93 ± 3.92% , 0.1 μM = -37.92 ± 8.93% , 0.3 μM = -39.86 ± 2.97% and 1 μM = -27.74 ± 16.17%). Therefore the effects of epinephrine to iCell^2 were classified as positive clinotropy and hence, predicted as PI **(Figure 4.3)**.

For voltage readouts, there were no effects on electrophysiology for both iCell^2 and R-PAT-CMs. However, for Pluricyte there was altered electrophysiology based on a decrease of APD30 and increase triangulation only at the highest concentration of 1 μM epinephrine**(Figure 4.3B)**.

4.4.2.2 Rank 2; Forskolin treatment (PI)

For contractility readouts, the traces show no significant difference or trends between CA, CT and RT for either Pluricyte or R-PAT CMs, throughout all concentrations of 0.1, 0.3, 1, 3 and 10 μM forskolin **(Figure 4.4A)**, and as such, both were predicted as NE. For iCell^2, there were no changes in CT or RT. However, for CA in iCell^2, there was a trend and decrease in CA at 10 μM, -43.8 ± 5.4% **(Figure 4.4 dotted red line)**. Therefore the effects of forskolin to iCell^2 were classified as negative inotropy and hence predicted as NI **(Figure 4.4)**.

For voltage readouts, there was altered electrophysiology with arrhythmias for both iCell^2 and Pluricyte (Figure 4.4B). For iCell^2 there was a reduction in APD30 at concentration of 3 μM = -40.58 ± 8.47 % and 10 μM = -38.95 ± 7%; including reduction in APD90 at 3 μM = -27.36 ± 1.17%. The iCell^2 treatment with forskolin also caused cells to not follow the pace (arrhythmias) **(Figure 4.4B)**. For Pluricyte, there was a reduction in APD30 at a concentration of 0.1 μM = -34.88 ± 6.32%, 1 μM = -44.12 ± 8.59%, 3 μM = -32.64 ± 8.3% and 10 μM = -38.92 ± 6.67%. In addition, there was also a reduction in APD90 at all concentrations and altered triangulation at 3 μM = -28.94 ± 3.85% and 10 μM = -27.58 ± 5.22%, which caused altered electrophysiology with arrhythmias **(Figure 4.4B)**. For R-PAT-CMs, there

were no changes in any of the voltage parameters in regards to forskolin treatment **(Figure 4.4B)**.

4.4.2.3 Rank 3; Levosimendan treatment (PI)

For contractility readouts, the traces showed no significant difference or trends between CA, CT or RT for all three lines iCell^2, Pluricyte and R-PAT CMs throughout all concentrations of 0.01, 0.03, 0.1, 0.3 and 1 μM **(Figure 4.5A)** of levosimendan, and as such, all were predicted as NE **(Figure 4.5)**.

For voltage readouts, there were no effects on electrophysiology for either iCell^2 or Pluricyte. However, for R-PAT-CMs electrophysiology was altered based on an increase in repolarisation at APD30 and APD90 for concentration 0.1 μM (11.35 ± 2.76% and 10.41 ± 2.83%) and 1 μM (18.6 ± 2.54% and 14.4 ± 2.37%) of levosimendan respectively for APD30 and APD90. **(Figure 4.5B)**.

4.4.2.4 Rank 4; Pimobendan treatment (PI)

For contractility readouts, the traces showed no significant difference or trends between CA or RT for all three lines iCell^2, Pluricyte and R-PAT CMs throughout all concentrations of 1, 3, 10, 30 and 100 μM **(Figure 4.6A)** of pimobendan, and as such, were all predicted as NE **(Figure 4.6)**.

For voltage readouts, electrophysiology was altered with arrhythmias effects for all lines; iCell^2, Pluricyte and R-PAT-CMs. For iCell^2 effects were mixed in APD90 with shorter repolarisation for concentration 1 μM = -16.43 ± 4.91% and prolonged repolarisation for concentration 30 μM = 14.38 ± 2.16%, including ang increase in triangulation at concentration of 30 μM = 39.3 ± 6.52% and 100 μM = 29.46 ± 5.07% **(Figure 4.6B).** For Pluricyte, there was an increase in triangulation at concentration, 10 μM = 23.06 ± 7.48%, 30 μM = 28.86 ± 4.12% and 100 μM = 43.2 ± 8% **(Figure 4.6B).** For R-PAT-CMs, there was a trend of increased triangulation based on concentration-dependant**;** the cells were also recorded as not following the pace after drug treatment (arrhythmias) **(Figure 4.6B)**.

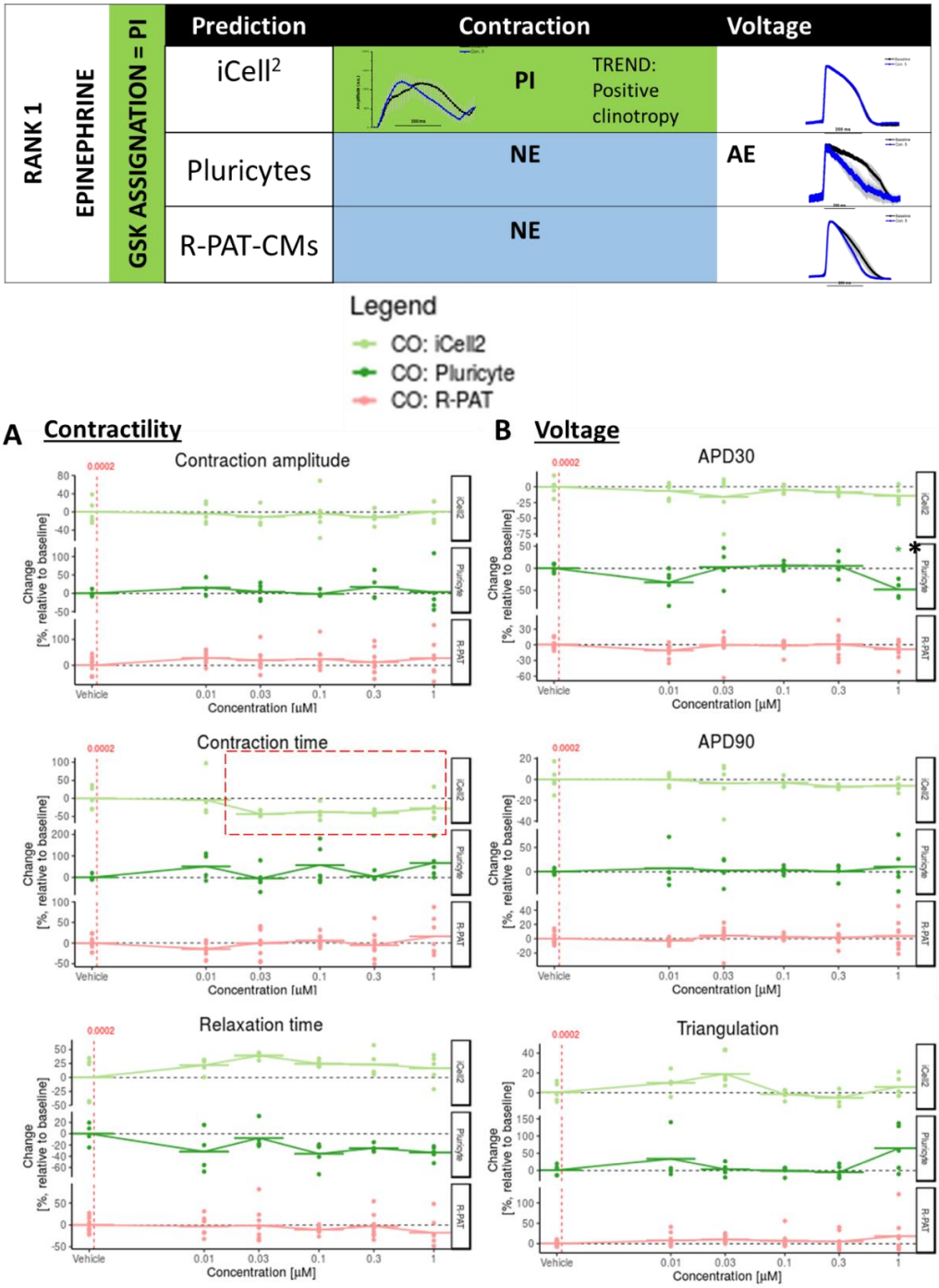


Figure 4.3 Contractility and voltage electrophysiological analysis of iCell², Pluricyte and R-PAT-CMs treated with epinephrine.

(A) For contractility, no effects in CA, CT and RT were observed in either Pluricyte or R-PAT-CMs. In iCell² no effects were seen in CA or RT; however, a decrease in trends for CT is highlighted in the red box. **(B)** For voltage, the electrophysiology was altered due to shortened repolarisation in APD30 and increase in triangulation at the highest epinephrine concentration of 1 µM for R-PAT-CMs. Red dotted line is free therapeutic plasma concentration (FTPC). All data are mean ± SEM; iCell², n=5; Pluricyte, n=5; and R-PAT-CMs, n=10. Statistical analysis was conducted using one-way ANOVA with Dunnett's multiple comparison test compared to the vehicle. Significance tests were based on p-values as follows: * $p < 0.05$; ** $p < 0.01$; *** $p < 0.001$; **** $p < 0.0001$.

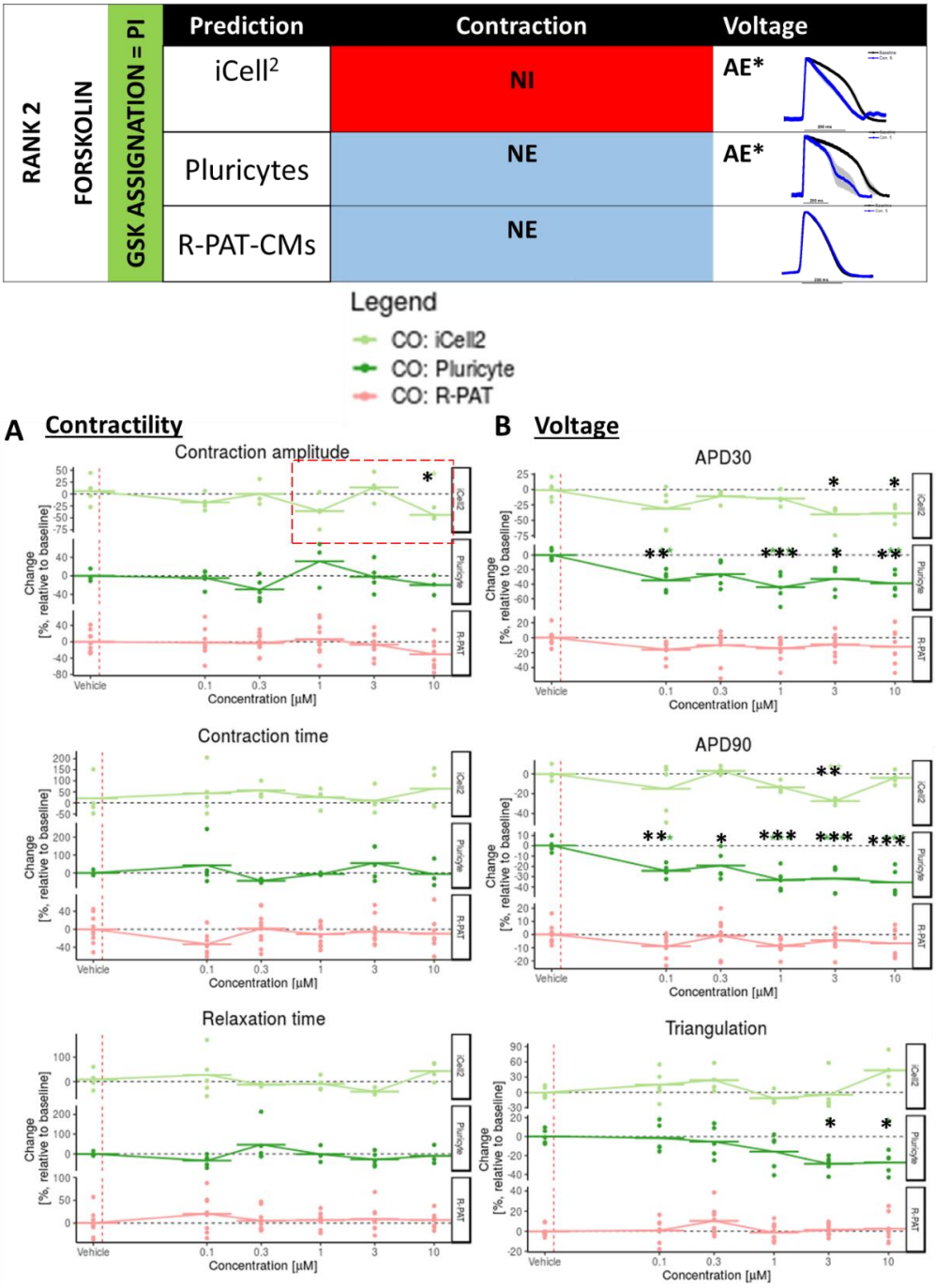


Figure 4.4: Contractility and voltage electrophysiological analysis of iCell², Pluricyte and R-PAT-CMs treated with forskolin.
(A)For contractility, no effects in CA, CT or RT were observed in either Pluricyte or R-PAT-CMs. In iCell² no effects in CT or RT were observed; however, a decrease in trends for CA are highlighted in the red box. **(B)**For voltage, electrophysiology was altered with arrhythmias due to shortened repolarisation in APD30 and APD90 for iCell²; electrophysiology with arrhythmias was altered due to shortened repolarisation in APD30, APD90 and triangulation for Pluricyte. Red dotted line is free therapeutic plasma concentration (FTPC). All data are mean ± SEM; iCell², n=5; Pluricyte, n=5; and R-PAT-CMs, n=10. Statistical analysis was conducted using one-way ANOVA with Dunnett's multiple comparison test compared to the vehicle. Significance tests were based on p-values as follows: * $p < 0.05$; ** $p < 0.01$; *** $p < 0.001$; **** $p < 0.0001$.

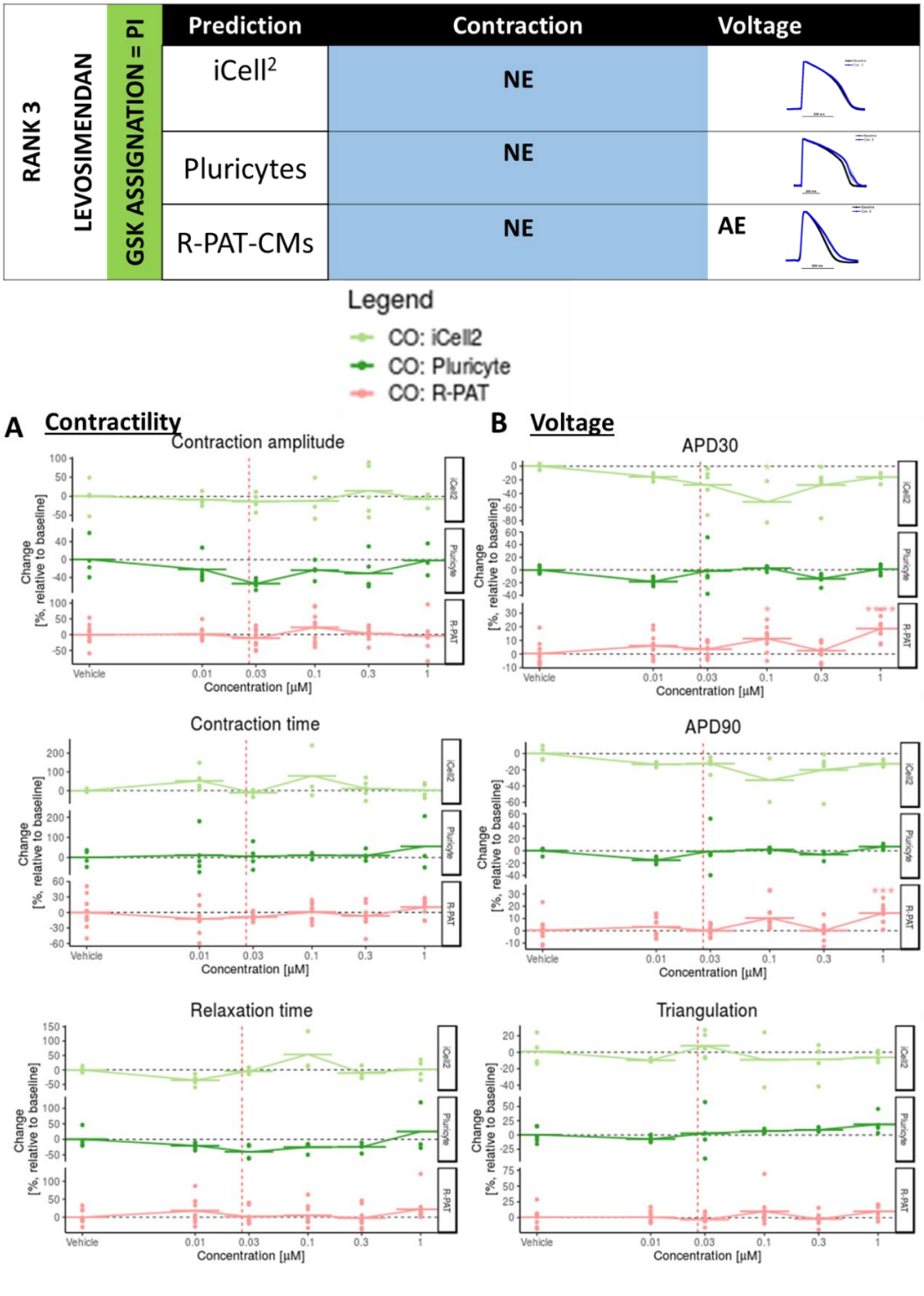


Figure 4.5: Contractility and voltage electrophysiological analysis of iCell², Pluricyte and R-PAT-CMs, treated with levosimendan

(A) For contractility, no effects in CA, CT and RT were observed in any iCell², Pluricyte and R-PAT-CMs. All lines were predicted as NE. **(B)** For voltage, altered electrophysiology was observed due to prolonged repolarisation in APD30 and APD90 for R-PAT-CMs. Red dotted line is free therapeutic plasma concentration (FTPC). All data are mean ± SEM; iCell², n=5; Pluricyte, n=5; and R-PAT-CMs, n=10. Statistical analysis was carried out using one-way ANOVA with Dunnett's multiple comparison test compared to the vehicle. Significance tests were based on p-values as follows: * $p < 0.05$; ** $p < 0.01$; *** $p < 0.001$; **** $p < 0.0001$.

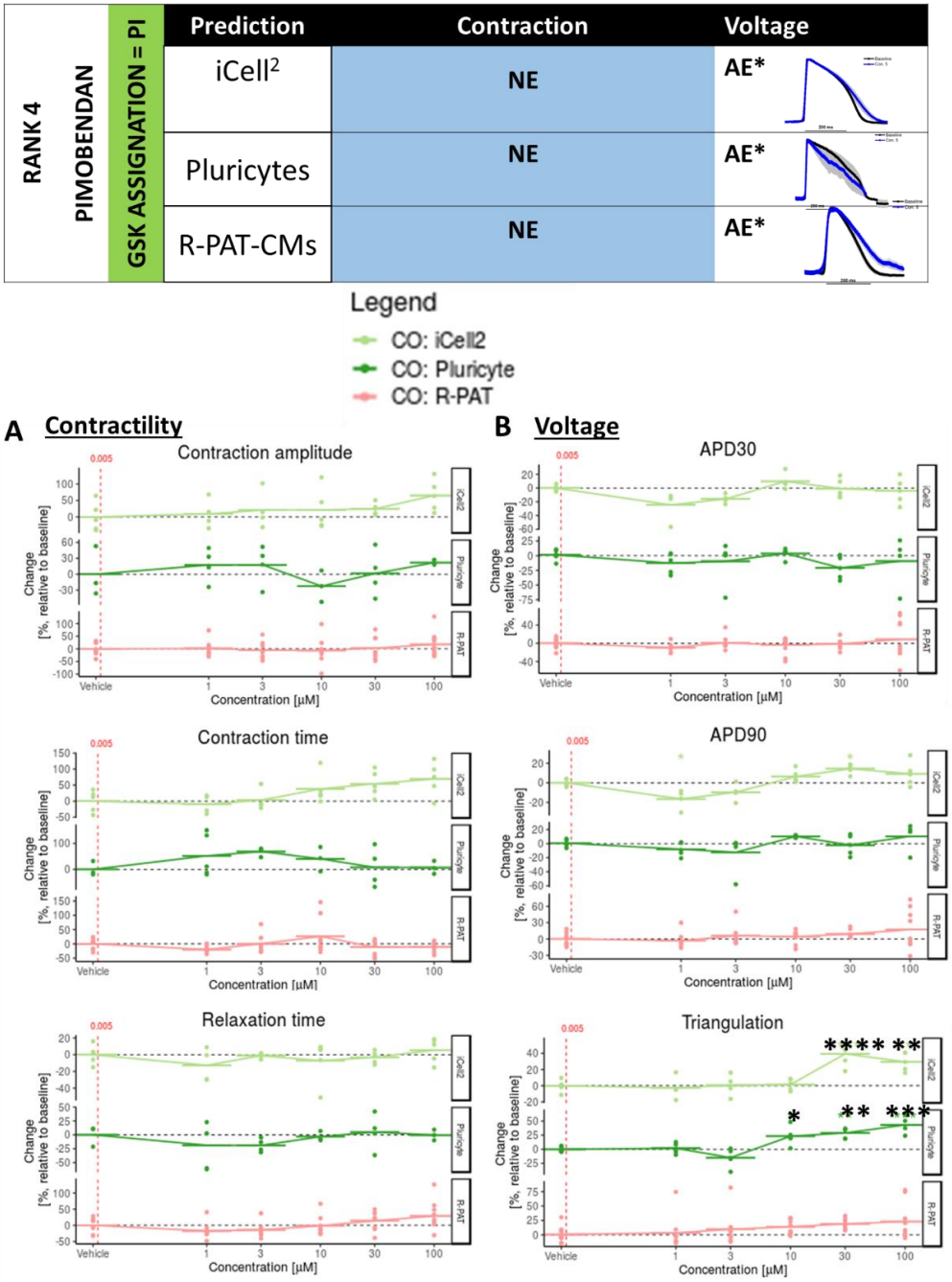


Figure 4.6: Contractility and voltage electrophysiological analysis of iCell², Pluricyte and R-PAT-CMs treated with pimobendan

(A) For contractility, no effects in CA, CT and RT were observed in any iCell², Pluricyte and R-PAT-CMs. All lines were predicted as NE. **(B)** For voltage, altered electrophysiology was observed with arrhythmias in all lines. Altered electrophysiology in iCell² due to an increase in trend of prolonged repolarisation in APD90 and increase in triangulation. Altered electrophysiology in Pluricyte due to increase in triangulation while for R-PAT-CMs there was increased in trends for triangulation. Red dotted line is free therapeutic plasma concentration (FTPC). All data are mean ± SEM; iCell², n=5; Pluricyte, n=5; and R-PAT-CMs, n=10. Statistical analysis was carried out using one-way ANOVA with Dunnett's multiple comparison test compared to the vehicle. Significance tests were based on p-values as follows: * $p < 0.05$; ** $p < 0.01$; *** $p < 0.001$; **** $p < 0.0001$.

4.4.2.5 Rank 5; Acetylsalicylic Acid (NE)

For contractility readouts, the traces showed no significant difference or trends between CA, CT and RT for any of the three lines iCell^2, Pluricyte and R-PAT CMs throughout all concentrations of 10, 30, 100, 300 and 1000 μM **(Figure 4.7A)** of acetylsalicylic acid, and as such were all predicted as NE **(Figure 4.7)**. Similarly, for voltage readouts, the traces showed no significant difference or trends in altered electrophysiology between APD30, APD90 and triangulation for either iCell^2 or Pluricyte. For R-PAT-CMs, although there was an increase in APD90 and triangulation at the highest concentration of 1000 μM, the voltage traces reflects that there was no altered electrophysiology **(Figure 4.7B)**.

4.4.2.6 Rank 6; Atenolol treatment (NE)

For contractility readouts, the traces showed no significant difference or trends between CA, CT and RT for both iCell^2 and Pluricyte throughout all concentration of 0.1, 0.3, 1, 3 and 10 μM **(Figure 4.8A)** of atenolol. As such, all three lines were predicted as NE **(Figure 4.8)**. For voltage readouts for iCell^2 and R-PAT-CMs, there were no trends of effect on electrophysiology **(Figure 4.8B**). For Pluricyte, there was altered electrophysiology; the trend decreased in APD30(-27.32 ± 9.74%) and APD90(-18.34 ± 6.23%) at the highest concentration of 10 μM atenolol. The Pluricyte was also unable to follow the pace at the highest concentration of atenolol, which is reflected in altered electrophysiology with arrhythmias **(Figure 4.8)**.

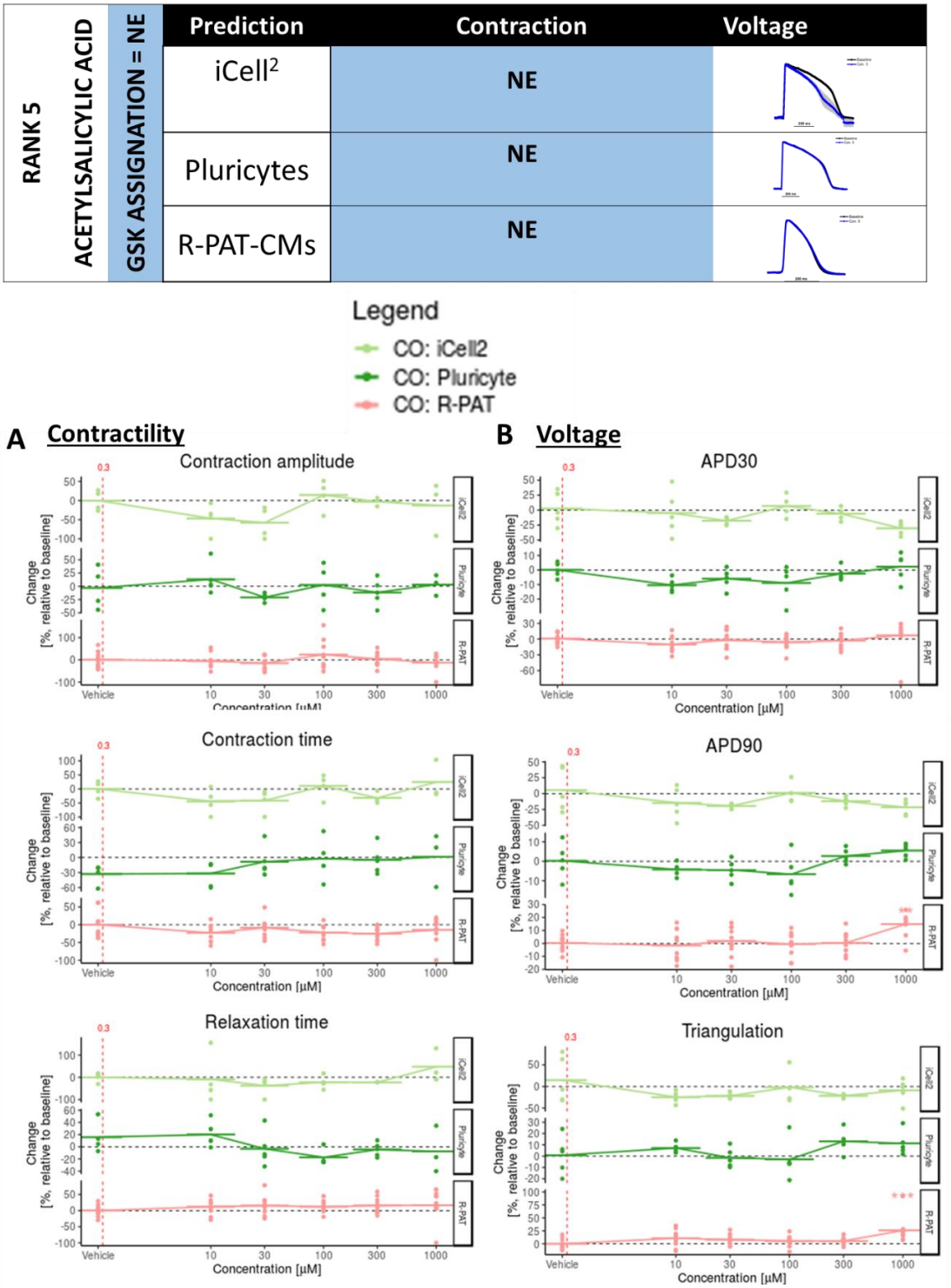


Figure 4.7: Contractility and voltage electrophysiological analysis of iCell², Pluricyte and R-PAT-CMs treated with acetylsalicylic acid.

(A) For contractility, no effects in CA, CT and RT were observed in any iCell², Pluricyte or R-PAT-CMs. All lines were predicted as NE. **(B)** For voltage, no altered electrophysiology was observed in any lines. Red dotted line is free therapeutic plasma concentration (FTPC). All data are mean ± SEM; iCell², n=5; Pluricyte, n=5; and R-PAT-CMs, n=10. Statistical analysis was carried out using one-way ANOVA with Dunnett's multiple comparison test compared to the vehicle. Significance tests were based on p-values as follows: * $p < 0.05$; ** $p < 0.01$; *** $p < 0.001$; **** $p < 0.0001$.

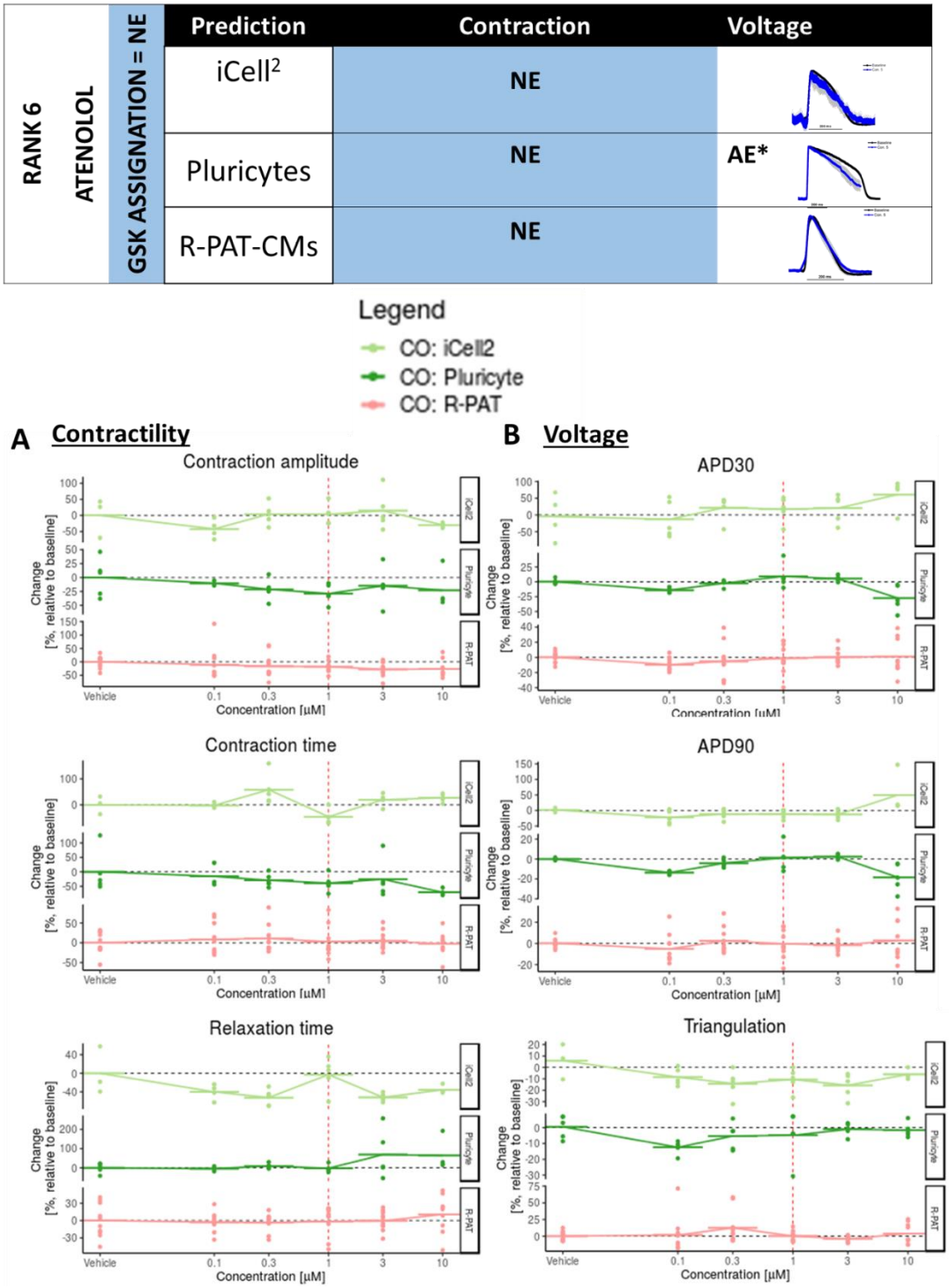


Figure 4.8: **Contractility and voltage electrophysiological analysis of iCell², Pluricyte and R-PAT-CMs treated with atenolol**

(A) For contractility, no trends for CA, CT and RT were observed in any iCell², Pluricyte and R-PAT-CMs. All lines were predicted as NE. **(B)** For voltage, altered electrophysiology with arrhythmias was observed at the highest atenolol concentration due to changes in APD30 and APD90 of Pluricyte. Red dotted line is free therapeutic plasma concentration (FTPC). All data are mean ± SEM; iCell², n=5; Pluricyte, n=5; and R-PAT-CMs, n=10. Statistical analysis was carried out using one-way ANOVA with Dunnett's multiple comparison test compared to the vehicle. Significance tests were based on p-values as follows: * $p < 0.05$; ** $p < 0.01$; *** $p < 0.001$; **** $p < 0.0001$

4.4.2.7 Rank 7; Verapamil treatment (NI)

For contractility readouts, for iCell^2, there was a change in trends for CA, CT and RT, with quiescent cells at the highest concentration of 1 μM; decreased in CA 0.3 μM = -39.6 ± 8.04% with significant quiescent cells at the highest concentration of 1 μM = -100 ± 0%, decreased trends for CT, and decreased trends for RT as the cells became quiescent at the highest concentration of 1 μM **(Figure 4.9A)**. For Pluricyte, there was a significant change in CA and RT with decreased trends for CT; decreased CA with quiescent cells at highest concentration of 1 μM = -100 ± 0%, decreased trend in CT with 0.3 μM = -41.48 ± 18.62%, and decreased trend in RT (0.3 μM = -59.18 ± 10.88%)**(Figure 4.9A)**. For R-PAT-CMs, there was a significant decrease in CA (1 μM = -90.15 ± 0.15%), significant decrease in CT at various concentrations (0.01 μM = -35.26 ± 5.64%, 0.3 μM = -36.58 ± 6.91% and 1 μM = -53.15 ± 2.15%), and significant decrease in trends for RT (0.3 μM = -25.46 ± 6.75% and 1 μM = -39.7 ± 6.8%)**(Figure 4.9A)**. As there was a decrease in CA, the effects of verapamil for all three cell lines were classified as NI **(Figure 4.4)**.

For voltage readouts, there was altered electrophysiology with arrhythmias (AE*) for all iCell^2, Pluricyte and R-PAT-CMs **(Figure 4.9B).** For iCell^2 there was a significant reduction in APD30, APD90 and triangulation at concentrations of 0.3 and 1 μM verapamil. The value of parameter for iCell^2 at APD30 (0.3 μM = -84.88 ± 9.36% and 1 μM = -87.56 ± 7.79%), APD90 (0.3 μM = -40.58 ± 8.47% and 1 μM = -40.58 ± 8.47%) and triangulation (0.3 μM = -40.58 ± 8.47% and 1 μM = -40.58 ± 8.47%)**(Figure 4.9B).** The iCell^2 treatment with verapamil was also recorded as not following the pace (slow) after 30 minutes of drug treatment and was fully quiescent at the highest concentration **(Figure 4.9).** Similarly for Pluricyte, there was a significant reduction with trends in reduction of APD30 (0.3 μM = -43.06 ± 5.05% and 1 μM = -83.82 ± 2.54%), APD90 (0.3 μM = -82.44 ± 10.81% and 1 μM = -84.94 ± 9.52%) and decreased triangulation (0.3 μM = -78.96 ± 12.97% and 1 μM = -81.74 ± 11.66%)**(Figure 4.9B).** The Pluricyte also did not follow the pace at concentration of 0.3 μM and became quiescent at 1 μM. For R-PAT-CMs, there was significant reduction with the following trends: decreased of APD30 (0.01 μM = -24.58 ± 2.98%, 0.3 μM = -42.77 ± 7.02% and 1 μM = -87.25 ± 5.6%), APD90 (0.01 μM = -20.34 ± 2.54%, 0.3 μM = -37.39 ± 7.49% and 1 μM = -

83.97 ± 8.18%) and decreased triangulation (0.01 µM = -15.23 ± 3.35%, 0.3 µM = -31.01 ± 8.5% and 1 µM = -78.52 ± 10.94%)**(Figure 4.9B).**

4.4.2.8 Rank 8; Doxorubicin treatment (NI)

For contractility readouts, the traces showed no significant difference or trends between CA, CT or RT for either iCell^2 and Pluricyte throughout all concentrations of 1, 3, 10, 30 and 100 µM **(Figure 4.10A)** of doxorubicin. For R-PAT-CMs, although there was a decrease in CA at the highest concentration due to cell death, it was not in trends, in addition, no trends for CT or RT were observed. As such, all three lines were predicted as NE **(Figure 4.10)**.

For voltage readouts, due to the nature of the doxorubicin drug (red colour) it caused the PMT in cellOPTIQ to overload and failed to capture the correct response from cells treated with 100 µM doxorubicin. Nonetheless, the voltage traces showed altered electrophysiology for all iCell^2, Pluricyte and R-PAT-CMs **(Figure 4.10)**. For iCell^{2,} there was a trend and a significant increase in APD90 and triangulation at a concentration of 30 and 100 µM doxorubicin. The percentage of change for iCell^2 at APD90 (30 µM = 16.93 ± 1.29% and 100 µM = 60.86 ± 10.23%) and triangulation (30 µM = 52.4 ± 12.93% and 100 µM = 261.2 ± 50.32%)**(Figure 4.10B)**. Similarly for Pluricyte there was a significant increase in trends in APD90 (100 µM = 99.42 ± 16.42%) and increased triangulation (100 µM = 226.6 ± 36.74%)**(Figure 4.10B).** For R-PAT-CMs electrophysiology was significantly disrupted for APD30, APD90, and triangulation at 100 µM due to cell death and quiescent **(Figure 4.10B).** The voltage traces of all three cell lines also reflected altered electrophysiology.

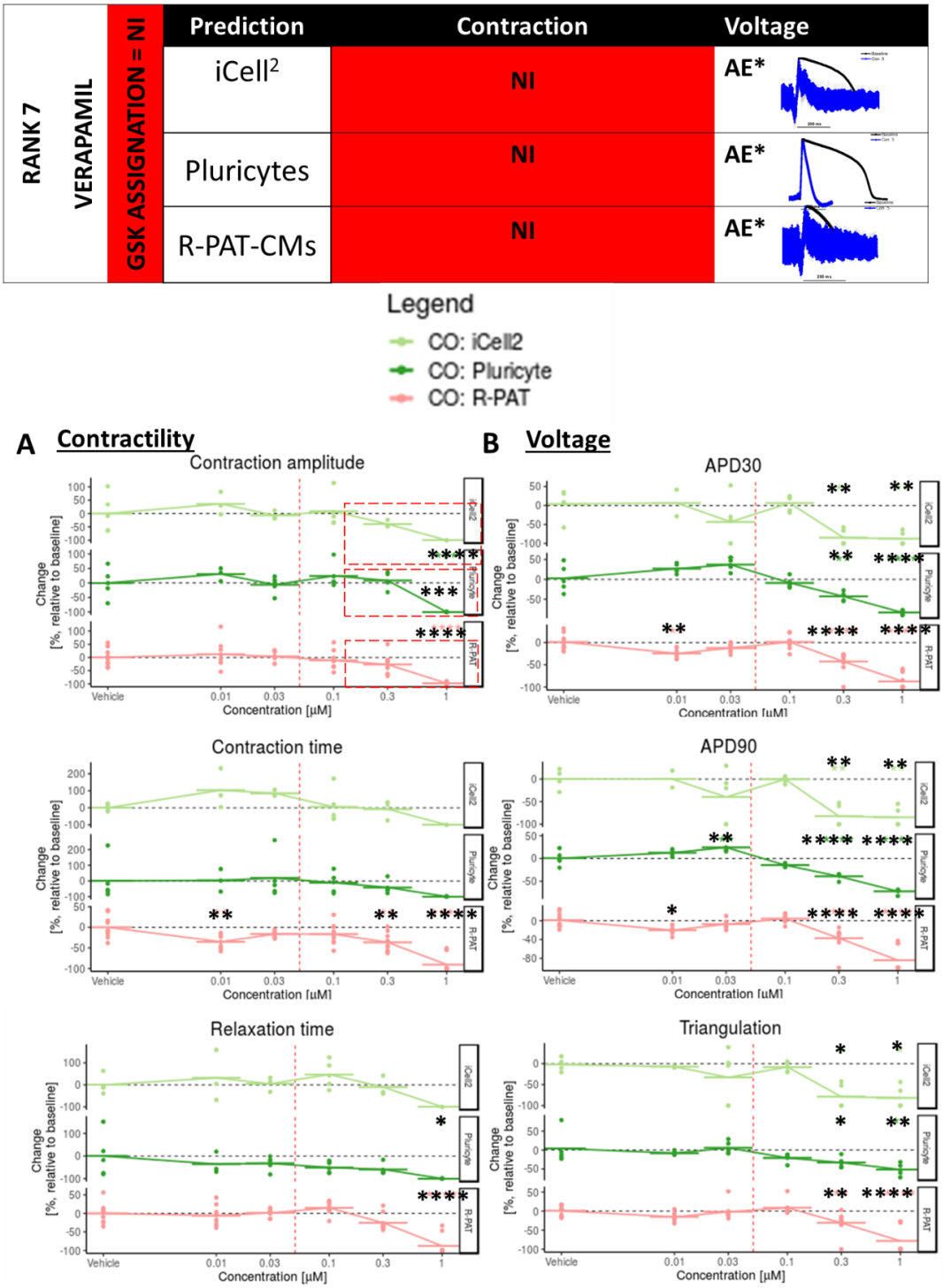


Figure 4.9: Contractility and voltage electrophysiological analysis of iCell², Pluricyte and R-PAT-CMs treated with verapamil

(A) For contractility, trends of reduction for CA, CT and RT were observed in all iCell², Pluricyte and R-PAT-CMs. All lines were predicted as NI. **(B)** For voltage, altered electrophysiology with arrhythmias observed due to changes in APD30, APD90 and triangulation. Red dotted line is free therapeutic plasma concentration (FTPC). All data are mean ± SEM; iCell², n=5; Pluricyte, n=5; and R-PAT-CMs, n=10. Statistical analysis was carried out using one-way ANOVA with Dunnett's multiple comparison test compared to the vehicle. Significance tests were based on p-values as follows: * $p < 0.05$; ** $p < 0.01$; *** $p < 0.001$; **** $p < 0.0001$

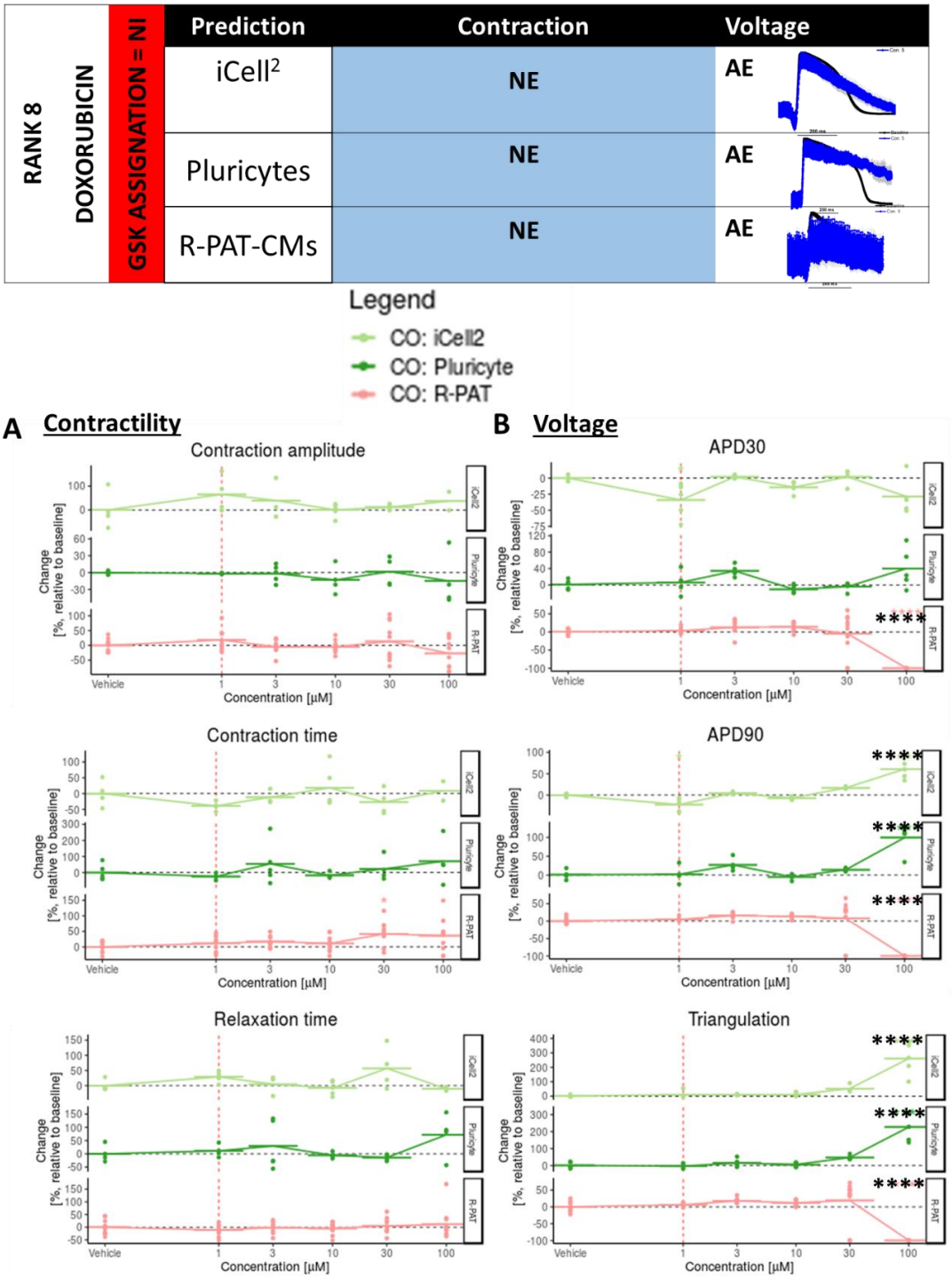


Figure 4.10: Contractility and voltage electrophysiological analysis of iCell², Pluricyte and R-PAT-CMs treated with doxorubicin

(A) For contractility, no trends for CA, CT and RT were observed in any iCell², Pluricyte and R-PAT-CMs. All lines were predicted as NE. **(B)** For voltage, altered electrophysiology was observed at the highest concentration due to changes in either APD30, APD90 and/or triangulation. Red dotted line is free therapeutic plasma concentration (FTPC). All data are mean ± SEM; iCell², n=5; Pluricyte, n=5; and R-PAT-CMs, n=10. Statistical analysis was carried out using one-way ANOVA with Dunnett's multiple comparison test compared to the vehicle. Significance tests were based on p-values as follows: * $p < 0.05$; ** $p < 0.01$; *** $p < 0.001$; **** $p < 0.0001$

4.4.2.9 Rank 9; Sunitinib treatment (NI)

For contractility readouts, the traces showed a decreased trend towards CA for iCell^2 at the highest concentration of 10 µM of sunitinib. Pluricyte showed a significant decrease towards CA and RT at the highest concentration of 10 µM of sunitinib. Therefore, both iCell^2 and Pluricyte with sunitinib were predicted as NI **(Figure 4.11A)**. The results showed no significant difference or trend between CA, CT or RT for R-PAT CMs throughout all concentrations of 0.1, 0.3, 1, 3 and 10 µM **(Figure 4.11A)**, and as such were predicted as NE.

For voltage readouts, electrophysiology was altered for iCell^2 electrophysiology was altered with arrhythmias for both Pluricyte and R-PAT-CMs **(Figure 4.11B)**. For iCell^2, there was prolonged repolarisation in APD90 at a concentration of 3 µM = 27.34 ± 8.26 % and 10 µM = 84.6 ± 4.47%, including altered triangulation at 3 µM =85.78 ± 10.45% and 10 µM =198.7 ± 21.81%**(Figure 4.11B)**. For Pluricyte, there was a reduction in APD30 at a concentration of 3 µM = -29.18 ± 5.54% and 10 µM = -70.2 ± 11.57%., altered triangulation at 3 µM =105.4 ± 9.21% and 10 µM =165.6 ± 43.37% which caused altered electrophysiology with arrhythmias due to cells not following pace **(Figure 4.11B)**. For R-PAT-CMs, there was an upward trend in APD90 and triangulation at 3 µM sunitinib and electrical disruption at 10 µM (**Figure 4.11B)**.

4.4.2.10 Rank 10; Captopril treatment (NE)

For contractility readouts, the traces showed no significant difference or trends between CA, CT or RT for any of the three lines iCell^2, Pluricyte and R-PAT CMs throughout all concentrations of 1, 3, 10, 30 and 100 µM **(Figure 4.12A)** of captopril, and as such all were predicted as NE **(Figure 4.12)**. Similarly, for voltage readouts, the traces showed no significant difference or trends in altered electrophysiology between APD30, APD90 or triangulation for any iCell^2, Pluricyte or R-PAT-CMs **(Figure 4.12B)**.

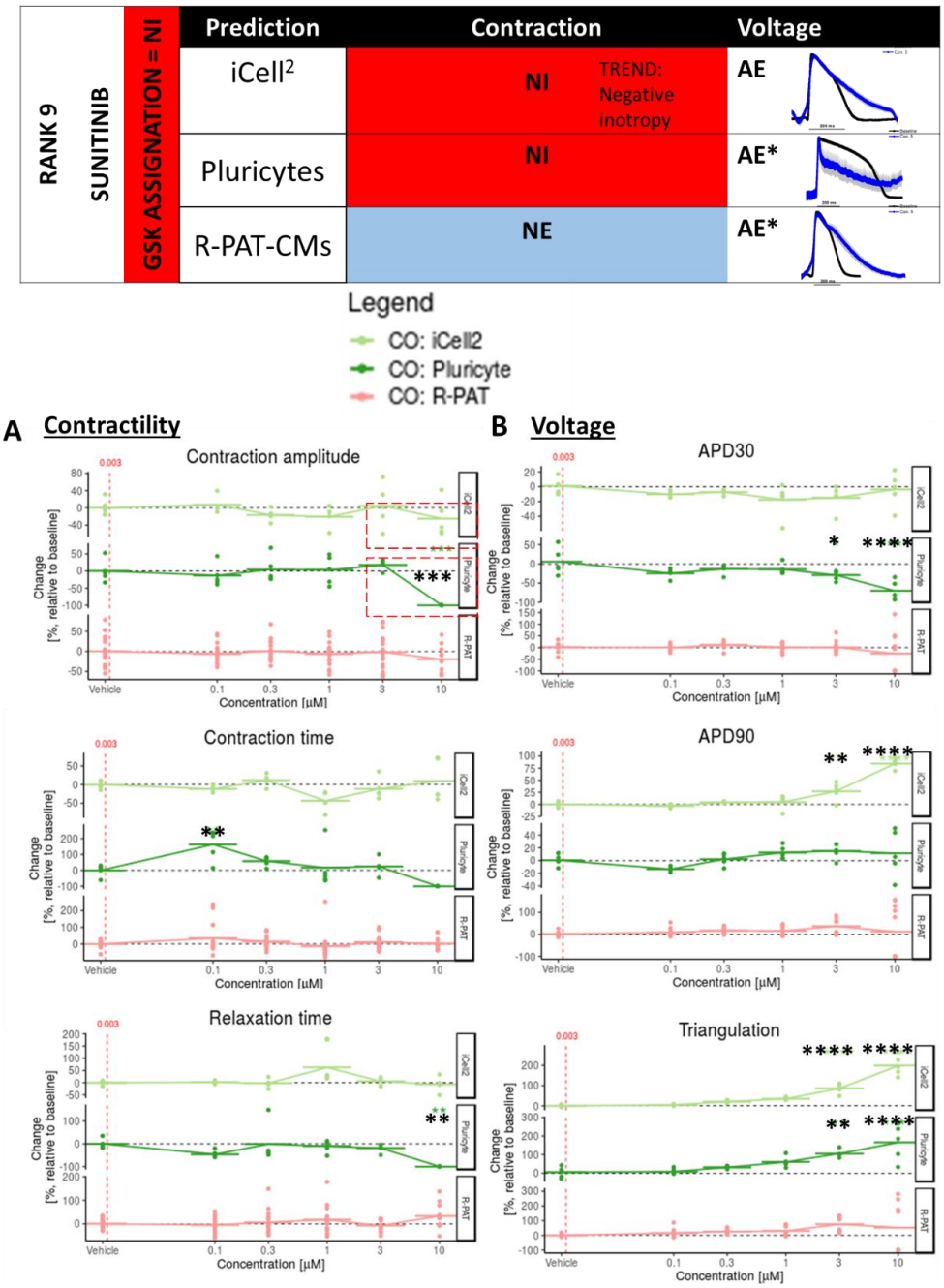


Figure 4.11: Contractility and voltage electrophysiological analysis of iCell², Pluricyte and R-PAT-CMs treated with sunitinib

(A) For contractility, trends of reduction for CA for iCell² significantly decreased in CA for Pluricyte and no changes were observed on R-PAT-CMs. The iCell2 and Pluricyte were predicted as NI, R-PAT-CMs as NE. **(B)** For voltage, altered electrophysiology was observed in iCell² due to increase in APD90 and triangulation. Altered electrophysiology with arrhythmias was observed due to changes in APD90 and triangulation for Pluricyte, as was altered electrophysiology with arrhythmias for R-PAT-CMs. Red dotted line is free therapeutic plasma concentration (FTPC). All data are mean ± SEM; iCell², n=5; Pluricyte, n=5; and R-PAT-CMs, n=10. Statistical analysis was carried out using one-way ANOVA with Dunnett's multiple comparison test compared to the vehicle. Significance tests were based on p-values as follows: * $p < 0.05$; ** $p < 0.01$; *** $p < 0.001$; **** $p < 0.0001$

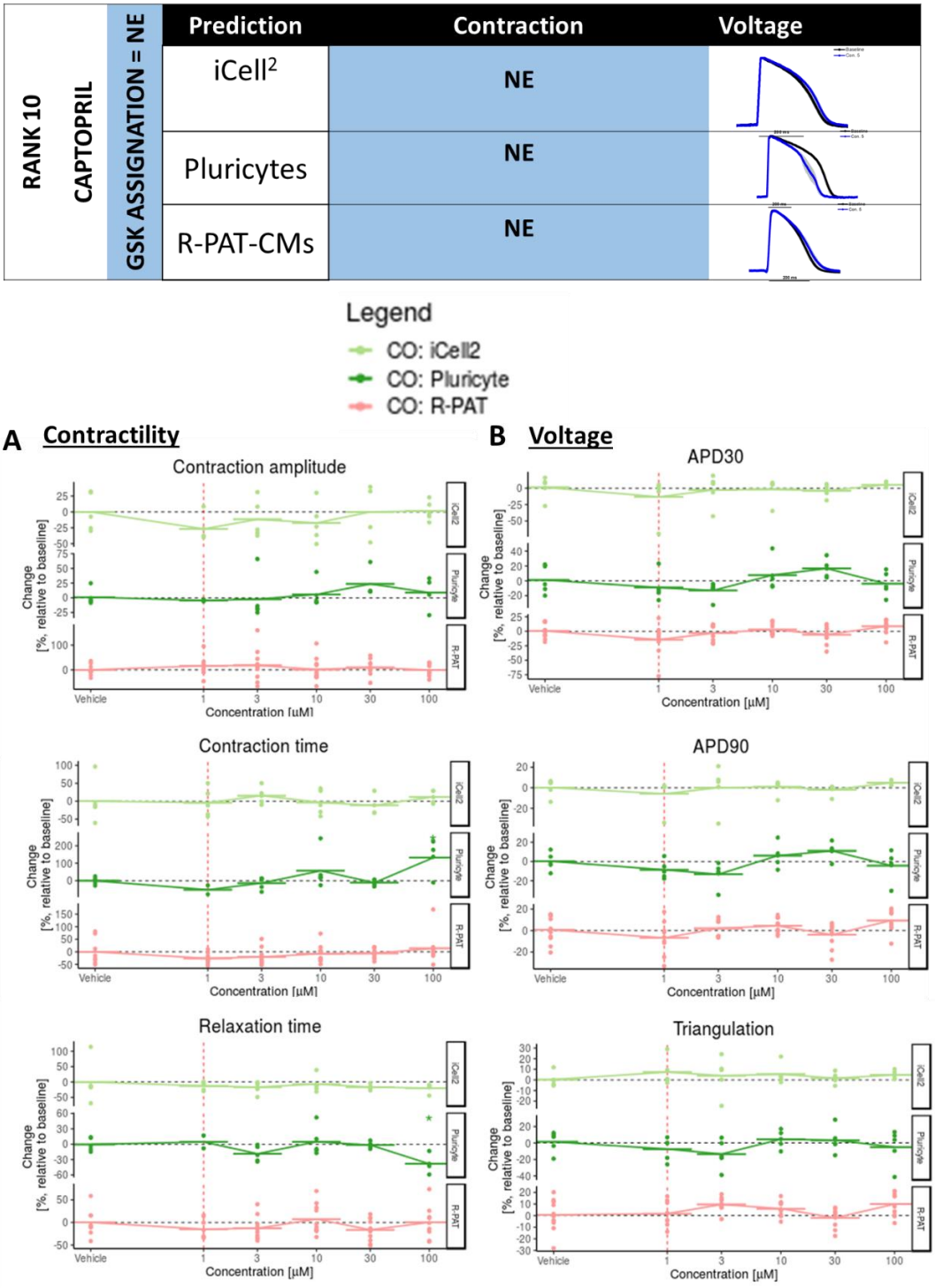


Figure 4.12: Contractility and voltage electrophysiological analysis of iCell², Pluricytes and R-PAT-CMs treated with captopril.

(A) For contractility, no effects in CA observed in either iCell², Pluricytes or R-PAT-CMs. All lines were predicted as NE. **(B)** For voltage, no altered electrophysiology was observed in any of the lines. Red dotted line is free therapeutic plasma concentration (FTPC). All data are mean ± SEM; iCell², n=5; Pluricytes, n=5; and R-PAT-CMs, n=10. Statistical analysis was carried out using one-way ANOVA with Dunnett's multiple comparison test compared to the vehicle. Significance tests were based on p-values as follows: * $p < 0.05$; ** $p < 0.01$; *** $p < 0.001$; **** $p < 0.0001$

4.4.3 Blinded test with drugs rank 11 onwards on R-PAT-CMs

The rest of the blinded drugs from rank 11 onwards were accordingly tested in R-PAT-CMs only due to the cost and the availability of the commercial lines. Similarly, like the top 10 priority drugs, drug responses were predicted according to the statistics and the trends when needed.

4.4.3.1 Rank 11; Dobutamine treatment (PI)

In contractility readouts of R-PAT treated with 0.1, 0.3, 1, 3 and 10 μM dobutamine, the measurements showed no significant difference between CA, CT or RT **(Figure 4.13A)**, and as such was predicted as NE **(Figure 4.13)**. For voltage readouts, there was altered electrophysiology with an increase in APD90 and triangulation **(Figure 4.13B)**.

4.4.3.2 Rank 12; Glibenclamide treatment (NE)

In contractility readouts of R-PAT treated with 0.1, 0.3, 1, 3 and 10 μM glibenclamide, the measurements showed no significant difference between CA, CT or RT **(Figure 4.14A)**, and as such was predicted as NE **(Figure 4.14)**. For voltage readouts, there was altered electrophysiology with an increase in APD90 and triangulation at 10 μM **(Figure 4.14B)**.

4.4.3.3 Rank 13; Milrinone treatment (PI)

In contractility readouts of R-PAT treated with 1, 3, 10, 30 and 100 μM milrinone, the measurements showed no significant difference between CA, CT and RT **(Figure 4.15A)**, and as such was predicted as NE **(Figure 4.15)**. For voltage readouts, there was no altered electrophysiology with no changes in APD30 or triangulation, although there was a decrease in APD30 at 1 μM **(Figure 4.15B)**.

4.4.3.4 Rank 14; Omecamtiv mecarbil treatment (PI)

In contractility readouts of R-PAT treated with 0.01, 0.03, 0.1, 0.3 and 1 μM omecamtiv mecarbil, the measurements showed an increased trend for CA with a significant increase at the highest 1 μM and a decreased trend in CT **(Figure 4.16A)**, and as such was predicted as NI **(Figure 4.16)**. For voltage readouts, there was no altered electrophysiology with no changes in APD30, APD90 or triangulation **(Figure 4.16B)**.

4.4.3.5 Rank 15; Enalaprilat treatment (NE)

In contractility readouts of R-PAT treated with 1, 3, 10, 30 and 100 μM enalaprilat, the measurements showed no significant difference between CA, CT and RT **(Figure 4.17A)**, and as such was predicted as NE **(Figure 4.17)**. For voltage readouts, there was an altered electrophysiology with a significant increase in APD90 and triangulation at the highest concentration of 100 μM **(Figure 4.17B)**.

4.4.3.6 Rank 16; Citalopram (NI)

In contractility readouts of R-PAT treated with 1, 3, 10, 30 and 100 μM citalopram, the measurements showed a significant decrease in CA, decrease in CT and decrease in RT **(Figure 4.18A)**, and as such was predicted as NI **(Figure 4.18)**. For voltage readouts, there was altered electrophysiology with arrhythmias since altered repolarisation which caused a significant decrease in APD30, APD90 and triangulation at 30 and 100 μM citalopram **(Figure 4.18B)**.

4.4.3.7 Rank 17; Clonidine (NE)

In contractility readouts of R-PAT treated with 0.01, 0.03, 0.1, 0.3 and 1 μM clonidine, the measurements showed no significant difference between CA, CT or RT **(Figure 4.19A)**, and as such was predicted as NE **(Figure 4.19)**. For voltage readouts, there was no change in APD30 or APD90 **(Figure 4.19B)**.

4.4.3.8 Rank 18; Itraconazole (NI)

In contractility readouts of R-PAT treated with 0.1, 0.3, 1, 3 and 10 μM itraconazole, the measurements showed a significant decrease in CA, decrease in CT and decrease in RT **(Figure 4.20A)**, and as such was predicted as NI **(Figure 4.20)**. For voltage readouts, there was altered electrophysiology with arrhythmias since altered repolarisation caused a significant decrease in APD30 at 10 μM itraconazole **(Figure 4.20B)**.

4.4.3.9 Rank 19; Sorafenib (NI)

In contractility readouts of R-PAT treated with 0.1, 0.3, 1, 3 and 10 μM sorafenib, the measurements showed a significant decrease in CA, decrease in CT and decrease in RT **(Figure 4.21A)**, and as such was predicted as NI **(Figure**

4.21). For voltage readouts, there was altered electrophysiology with arrhythmias due to altered repolarisation which caused a significant decrease in APD30, APD90 and triangulation at 3 and10 µM sorafenib **(Figure 4.21B).**

4.4.3.10 Rank 20; Ivabradine treatment (NI)

In contractility readouts of R-PAT treated with 0.1, 0.3, 1, 3 and 10 µM ivabradine, the measurements showed no significant differences between CA, CT or RT **(Figure 4.22A)**, and as such was predicted as NE **(Figure 4.22)**. For voltage readouts, there was altered electrophysiology with arrhythmias due to an increase in APD90 and triangulation at 1,3 and 10 µM ivabradine **(Figure 4.22B)**.

4.4.3.11 Rank 21; Terbutaline (PI)

In contractility readouts of R-PAT treated with 0.1, 0.3, 1, 3 and 10 µM terbutaline, the measurements showed no significant differences between CA, CT or RT **(Figure 4.23A)**, and as such was predicted as NE **(Figure 4.23)**. For voltage readouts, there was no altered electrophysiology with no changes in APD30, APD90 or triangulation **(Figure 4.23B)**.

4.4.3.12 Rank 22; Flecainide treatment (NI)

In contractility readouts of R-PAT treated with 0.1, 0.3, 1, 3 and 10 µM flecainide, the measurements showed no significant differences between CA, CT and RT **(Figure 4.24A)**, and as such was predicted as NE **(Figure 4.22)**. For voltage readouts, there was altered electrophysiology due to an increase in APD90 and triangulation at 1,3 and 10 µM **flecainide (Figure 4.24B)**.

4.4.3.13 Rank 23; Paracetamol treatment (NE)

In contractility readouts of R-PAT treated with 10, 30, 100, 300 and 1000 µM paracetamol, the measurements showed no significant differences between CA, CT or RT **(Figure 4.25A)**, and as such was predicted as NE **(Figure 4.25)**. For voltage readouts, there was altered electrophysiology due to an increase in APD30, APD90 and triangulation at 1000 µM paracetamol **(Figure 4.25B)**.

4.4.3.14 Rank 24; Phentolamine (NI)

In contractility readouts of R-PAT treated with 1, 3, 10, 30 and 100 μM phentolamine, the measurements showed a significant decrease in CA, decrease in CT and decrease in RT **(Figure 4.26A)**, and as such was predicted as NI **(Figure 4.26)**. For voltage readouts, there was altered electrophysiology with significant decreases in APD30 and APD90. Cells became quiescence at 30 and100 μM phentolamine **(Figure 4.26B)**.

4.4.3.15 Rank 25; Tolbutamide treatment (NE)

In contractility readouts of R-PAT treated with 1, 3, 10, 30 and 100 μM tolbutamide, the measurements showed no significant differences between CA, CT or RT **(Figure 4.27A)**, and as such was predicted as NE **(Figure 4.27)**. For voltage readouts, there was no altered electrophysiology with no significant changes in APD30, APD90 or triangulation **(Figure 4.27B)**.

4.4.3.16 Rank 26; Pravastatin treatment (NE)

In contractility readouts of R-PAT treated with 1, 3, 10, 30 and 100 μM pravastatin, the measurements showed no significant differences between CA, CT and RT **(Figure 4.28A)**, and as such was predicted as NE **(Figure 4.28)**. For voltage readouts, there was altered electrophysiology due to increases in APD30 and APD90 at 1, 10 and 30 μM pravastatin **(Figure 4.28B)**.

4.4.3.17 Rank 27; Sildenafil treatment (NE)

In contractility readouts of R-PAT treated with 0.1, 0.3, 1, 3 and 10 μM sildenafil, the measurements showed no significant differences between CA, CT or RT **(Figure 4.29A)**, and as such was predicted as NE **(Figure 4.29)**. For voltage readouts, there was altered electrophysiology due to increase in APD30, APD90 and triangulation **(Figure 4.29B)**.

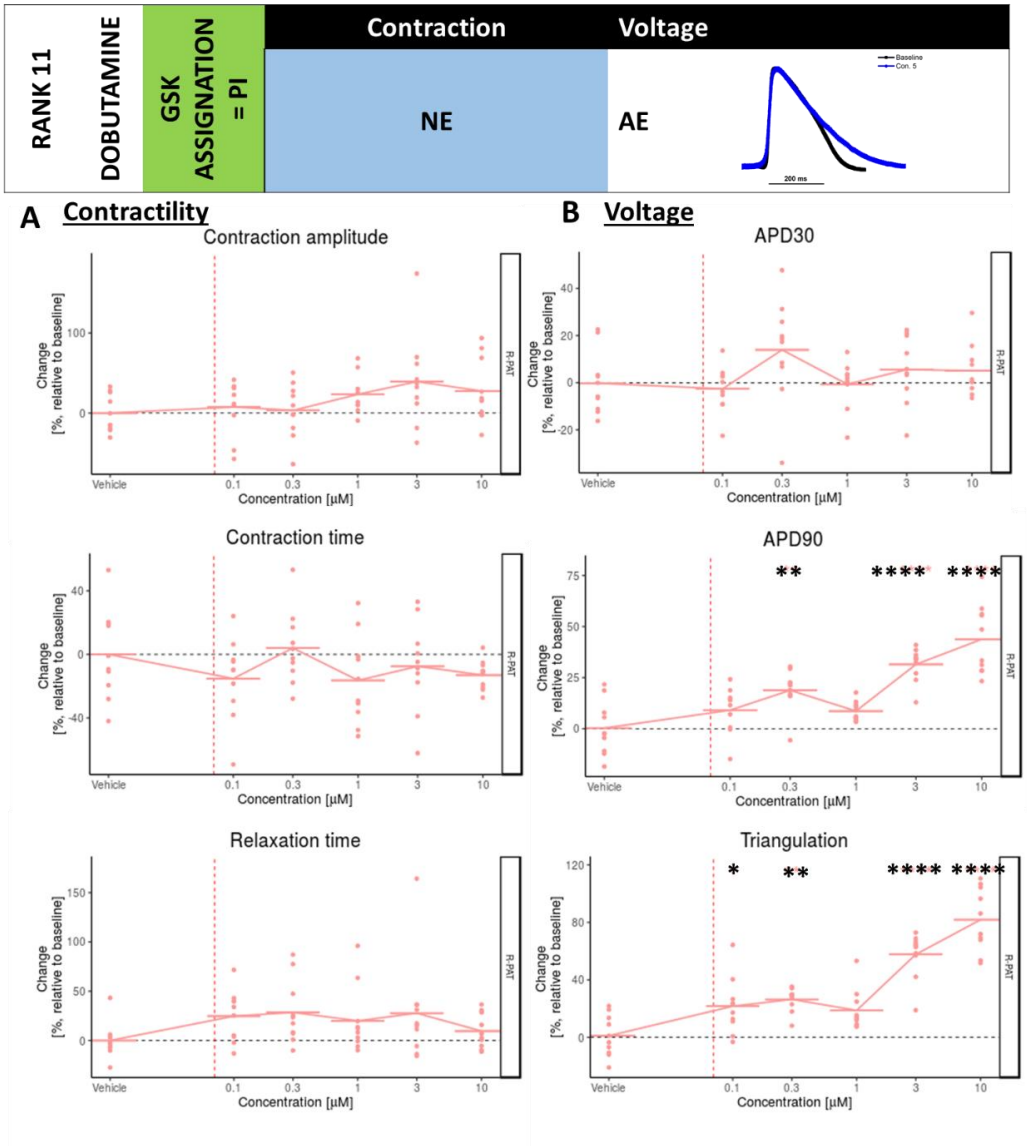


Figure 4.13: Contractility and voltage electrophysiological analysis of and R-PAT-CMs treated with dobutamine.

(A) For contractility, no effects in CA, CT or RT were detected, therefore, was predicted as NE. **(B)** For voltage, there was altered electrophysiology due to an increase in APD90 and triangulation. Red dotted line is free therapeutic plasma concentration (FTPC). All data are mean ± SEM; n=10. Statistical analysis was carried out using one-way ANOVA with Dunnett's multiple comparison test compared to the vehicle. Significance tests were based on p-values as follows: * $p < 0.05$; ** $p < 0.01$; *** $p < 0.001$; **** $p < 0.0001$

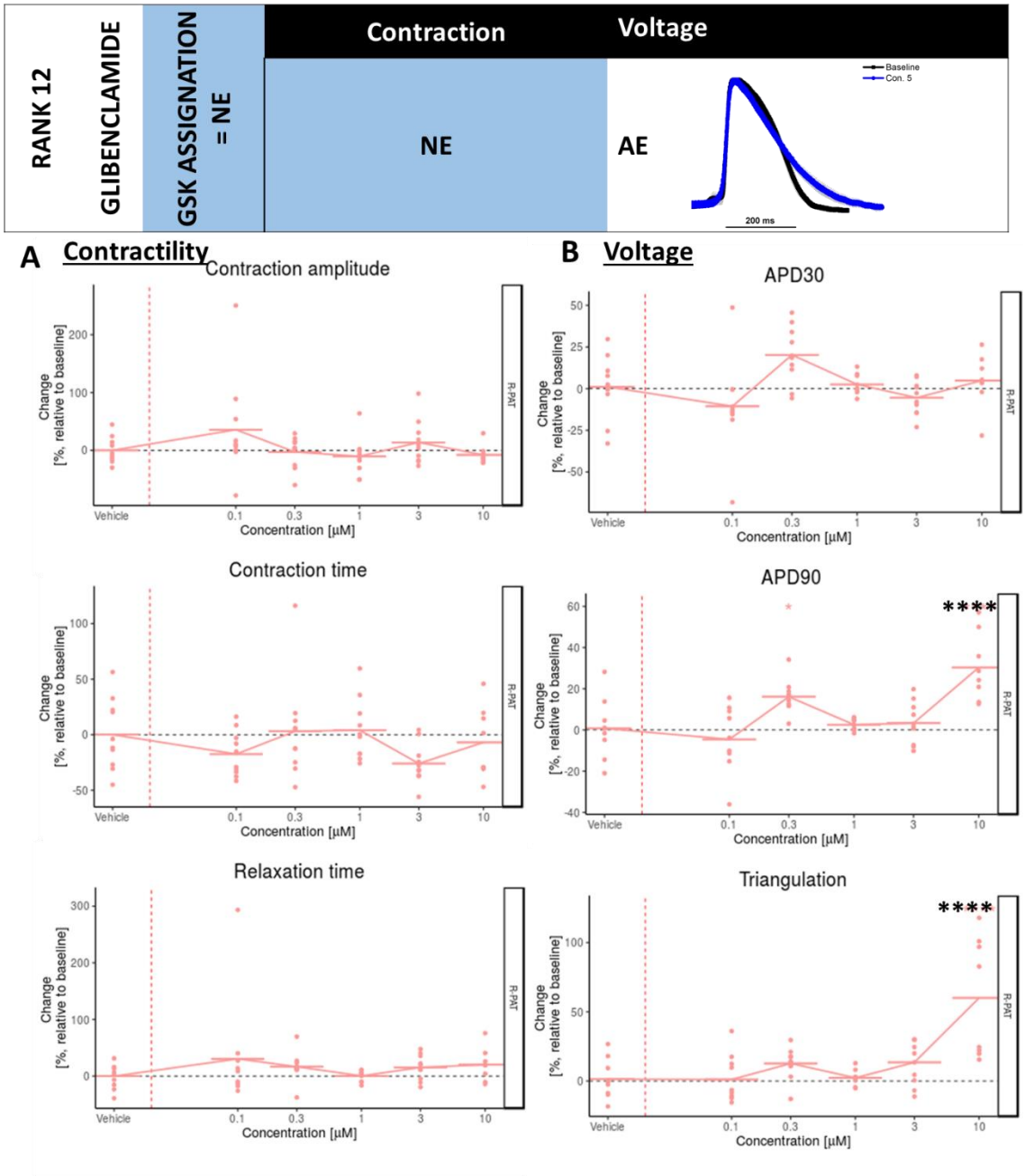


Figure 4.14: Contractility and voltage electrophysiological analysis of and R-PAT-CMs treated with glibenclamide.
(A) For contractility, no effects in CA, CT or RT were observed, therefore, was predicted as NE. **(B)** For voltage, electrophysiology was altered due to increase in APD90 and triangulation at the highest concentration. Red dotted line is free therapeutic plasma concentration (FTPC). All data are mean ± SEM; n=10. Statistical analysis was carried out using one-way ANOVA with Dunnett's multiple comparison test compared to the vehicle. Significance tests were based on p-values as follows: * $p < 0.05$; ** $p < 0.01$; *** $p < 0.001$; **** $p < 0.0001$

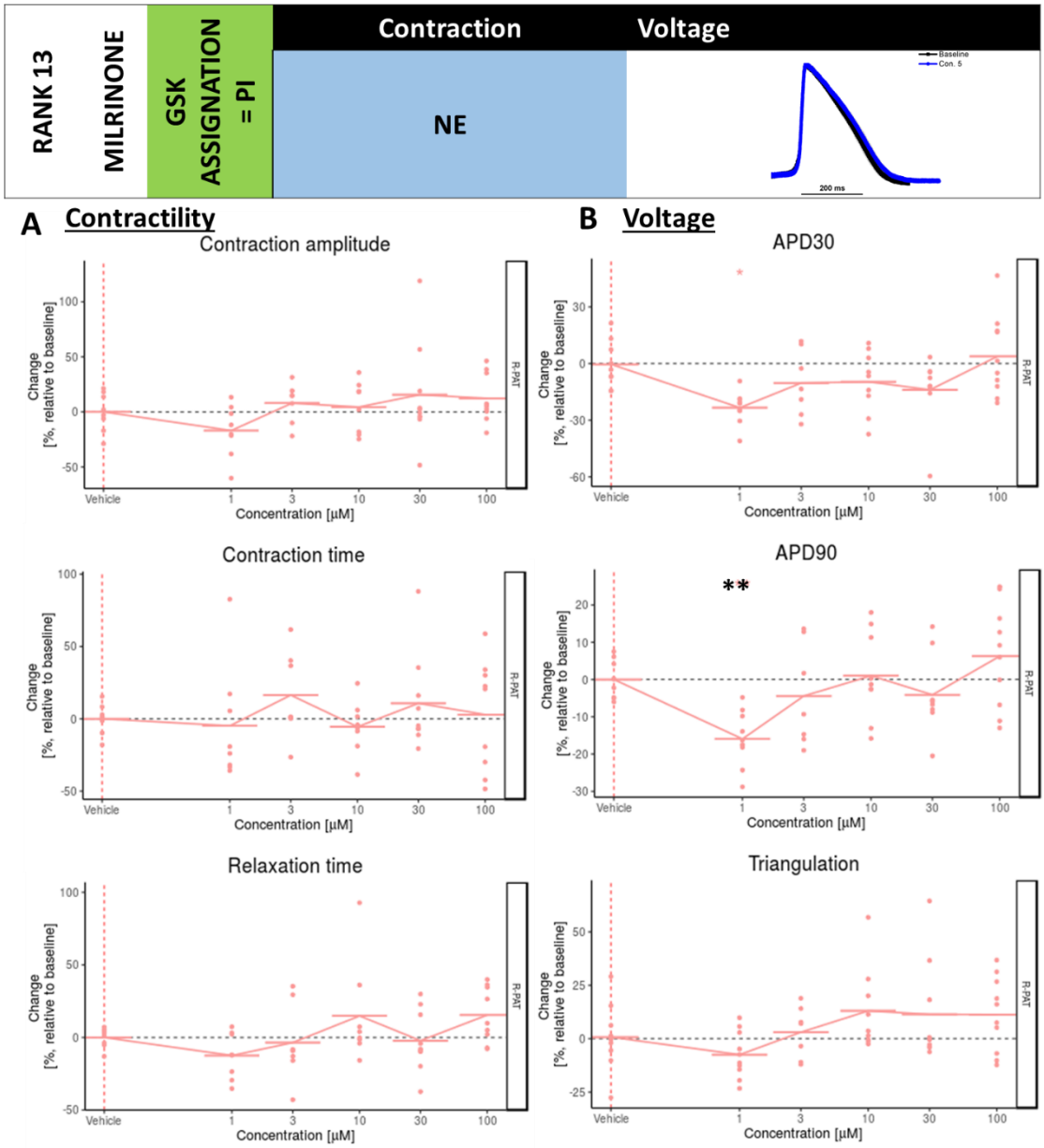


Figure 4.15: Contractility and voltage electrophysiological analysis of and R-PAT-CMs treated with milrinone.
(A) For contractility, no effects in CA, CT or RT were detected, therefore, was predicted as NE. **(B)** For voltage, overall there was no altered electrophysiology, although APD90 decreased at the smallest concentration; no significant change in APD30 and triangulation at the highest concentration was detected. Red dotted line is free therapeutic plasma concentration (FTPC). All data are mean ± SEM; n=10. Statistical analysis was carried out using one-way ANOVA with Dunnett's multiple comparison test compared to the vehicle. Significance tests were based on p-values as follows: * $p < 0.05$; ** $p < 0.01$; *** $p < 0.001$; **** $p < 0.0001$

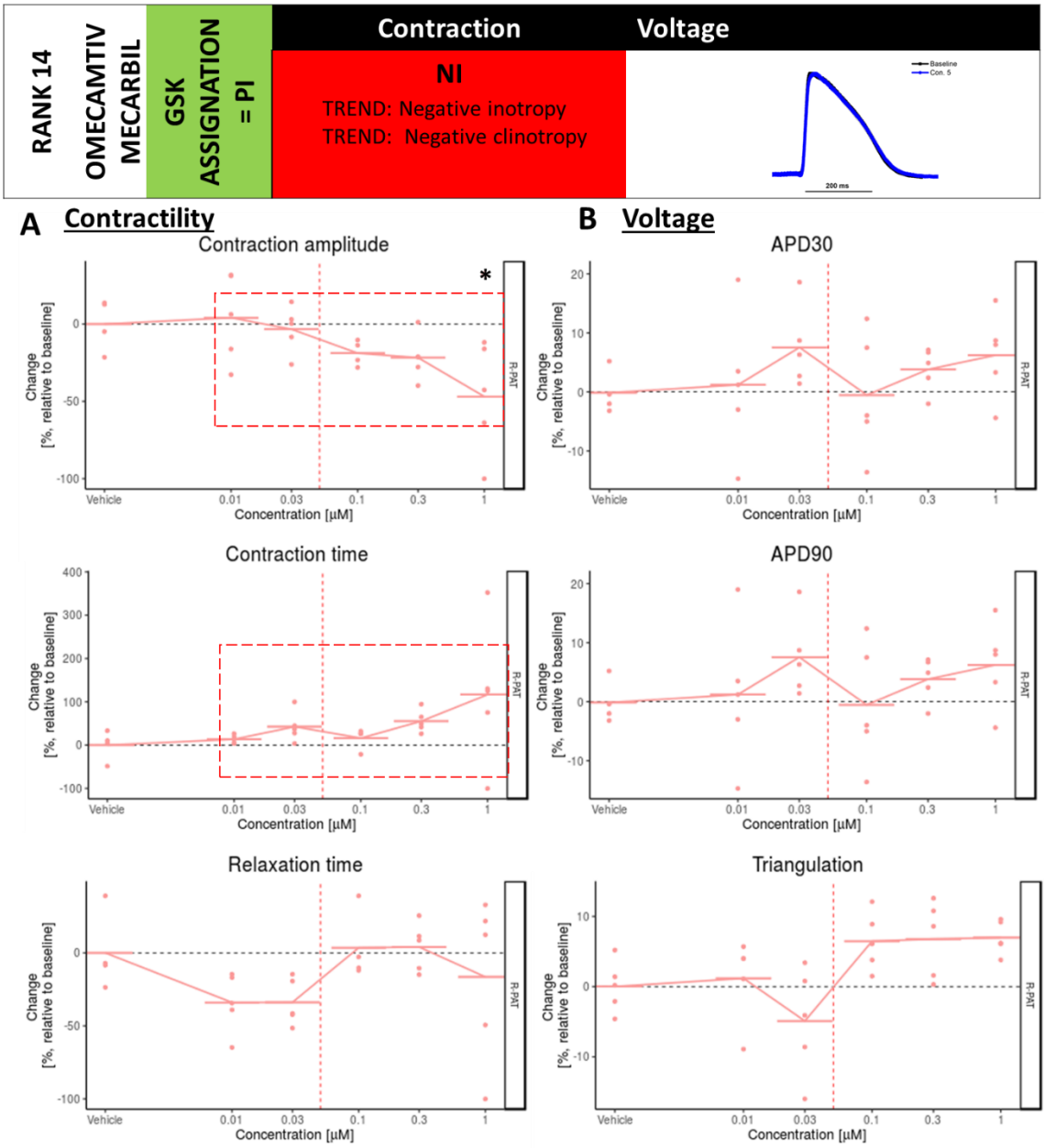


Figure 4.16: Contractility and voltage electrophysiological analysis of and R-PAT-CMs treated with omecamtiv mecarbil.
(A) For contractility, a trend decrease in CA was observed with a significant increase at the highest 1 µM and a trend increase in CT, therefore, NI was predicted **(B)** For voltage, there was no overall altered electrophysiology as no significant changes in APD30, APD90 or triangulation were observed. Red dotted line is free therapeutic plasma concentration (FTPC). All data are mean ± SEM; n=5. Statistical analysis was carried out using one-way ANOVA with Dunnett's multiple comparison test compared to the vehicle. Significance tests were based on p-values as follows: * $p < 0.05$; ** $p < 0.01$; *** $p < 0.001$; **** $p < 0.0001$

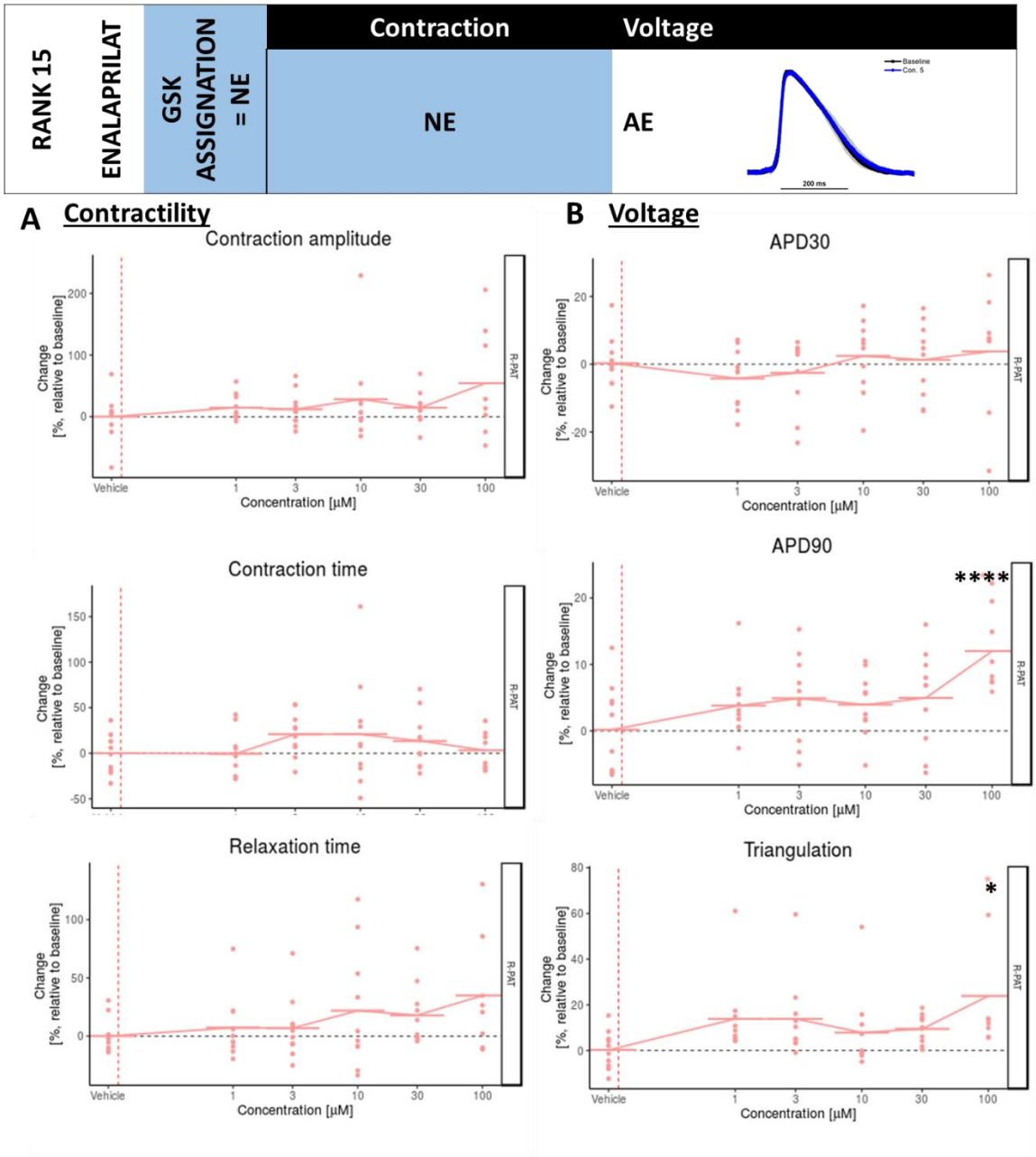


Figure 4.17: Contractility and voltage electrophysiological analysis of and R-PAT-CMs treated with enalaprilat.
(A) For contractility, no effects in CA, CT or RT were observed, therefore, was predicted as NE. **(B)** For voltage, there was altered electrophysiology by an increase in APD90 and triangulation at the highest concentration. Red dotted line is free therapeutic plasma concentration (FTPC). All data are mean ± SEM; n=10. Statistical analysis was carried out using one-way ANOVA with Dunnett's multiple comparison test compared to the vehicle. Significance tests were based on p-values as follows: * $p < 0.05$; ** $p < 0.01$; *** $p < 0.001$; **** $p < 0.0001$

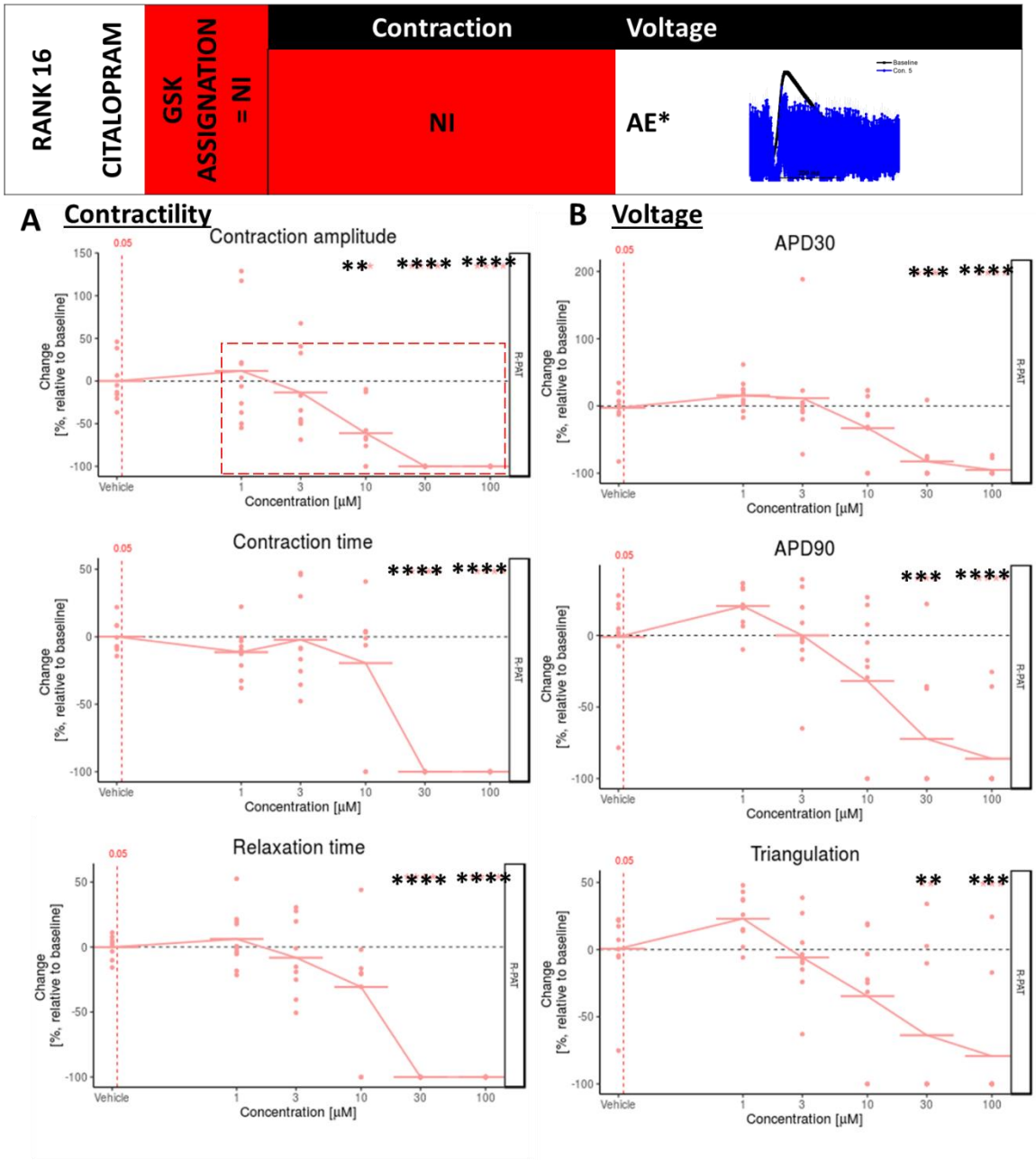


Figure 4.18: Contractility and voltage electrophysiological analysis of and R-PAT-CMs treated with citalopram.
(A) For contractility, a significant decreased in CA, significantly decreased in CT and significantly decreased in RT, therefore, was predicted as NI **(B)** For voltage, altered electrophysiology with arrhythmias by decreased in APD30, APD90 and triangulation. Red dotted line is free therapeutic plasma concentration (FTPC). All data are mean ± SEM; n=10. Statistical analysis was carried out using one-way ANOVA with Dunnett's multiple comparison test compared to the vehicle. Significance tests were based on p-values as follows: * $p < 0.05$; ** $p < 0.01$; *** $p < 0.001$; **** $p < 0.0001$

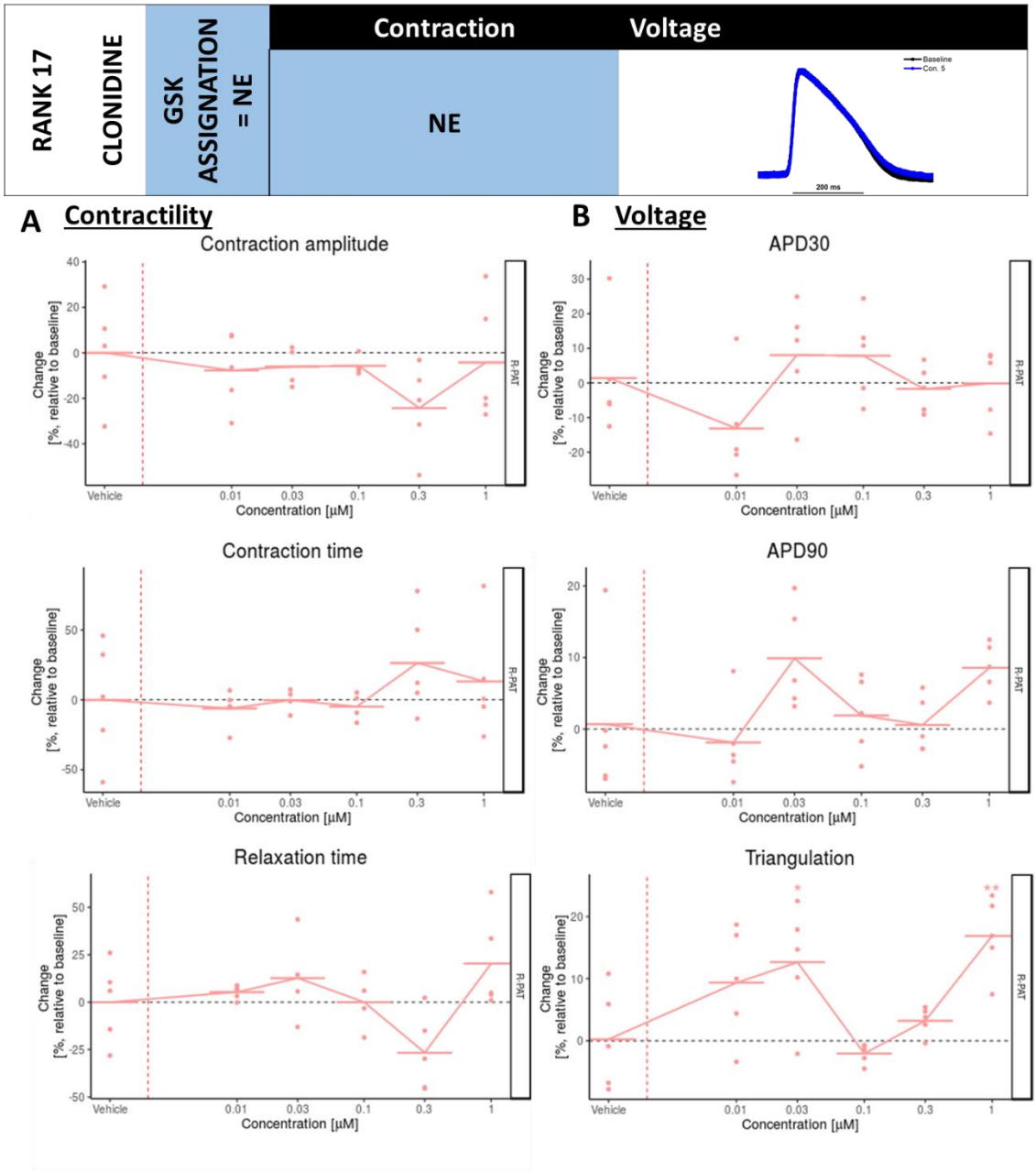


Figure 4.19: Contractility and voltage electrophysiological analysis of and R-PAT-CMs treated with clonidine.
(A) For contractility, no effects in CA, CT and RT, therefore, was predicted as NE. **(B)** For voltage, no changes in APD30 and APD90. Red dotted line is free therapeutic plasma concentration (FTPC). All data are mean ± SEM; n=5. Statistical analysis was carried out using one-way ANOVA with Dunnett's multiple comparison test compared to the vehicle. Significance tests were based on p-values as follows: * $p < 0.05$; ** $p < 0.01$; *** $p < 0.001$; **** $p < 0.0001$

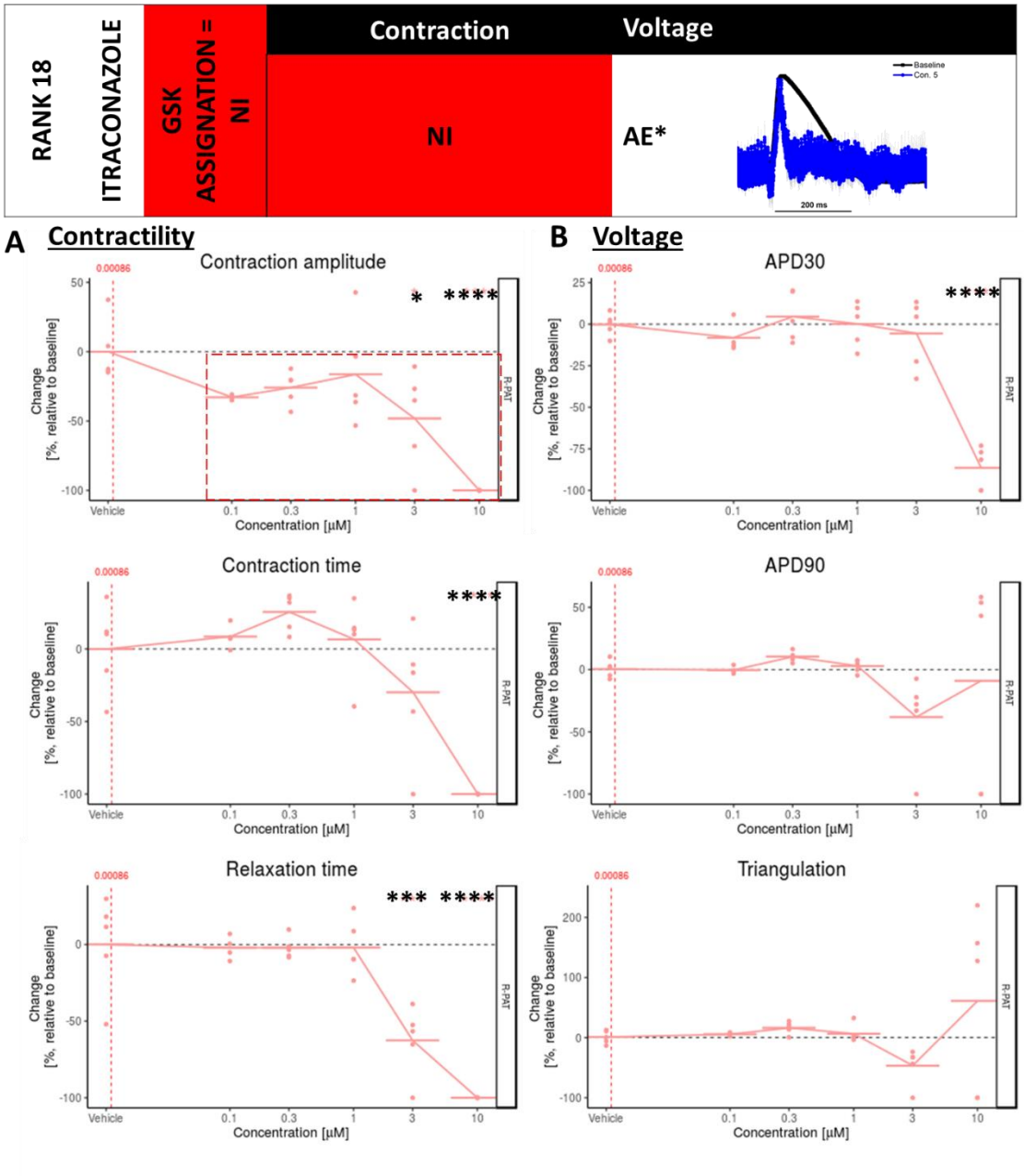


Figure 4.20: Contractility and voltage electrophysiological analysis of and R-PAT-CMs treated with itraconazole.
(A) For contractility, a significant decrease in CA was observed, as was a significant decrease in CT and significantly decreased in RT, therefore, was predicted as NI **(B)** For voltage, altered electrophysiology with arrhythmias decreased in APD30. Red dotted line is free therapeutic plasma concentration (FTPC). All data are mean ± SEM; n=5 Statistical analysis was carried out using one-way ANOVA with Dunnett's multiple comparison test compared to the vehicle. Significance tests were based on p-values as follows: * $p < 0.05$; ** $p < 0.01$; *** $p < 0.001$; **** $p < 0.0001$

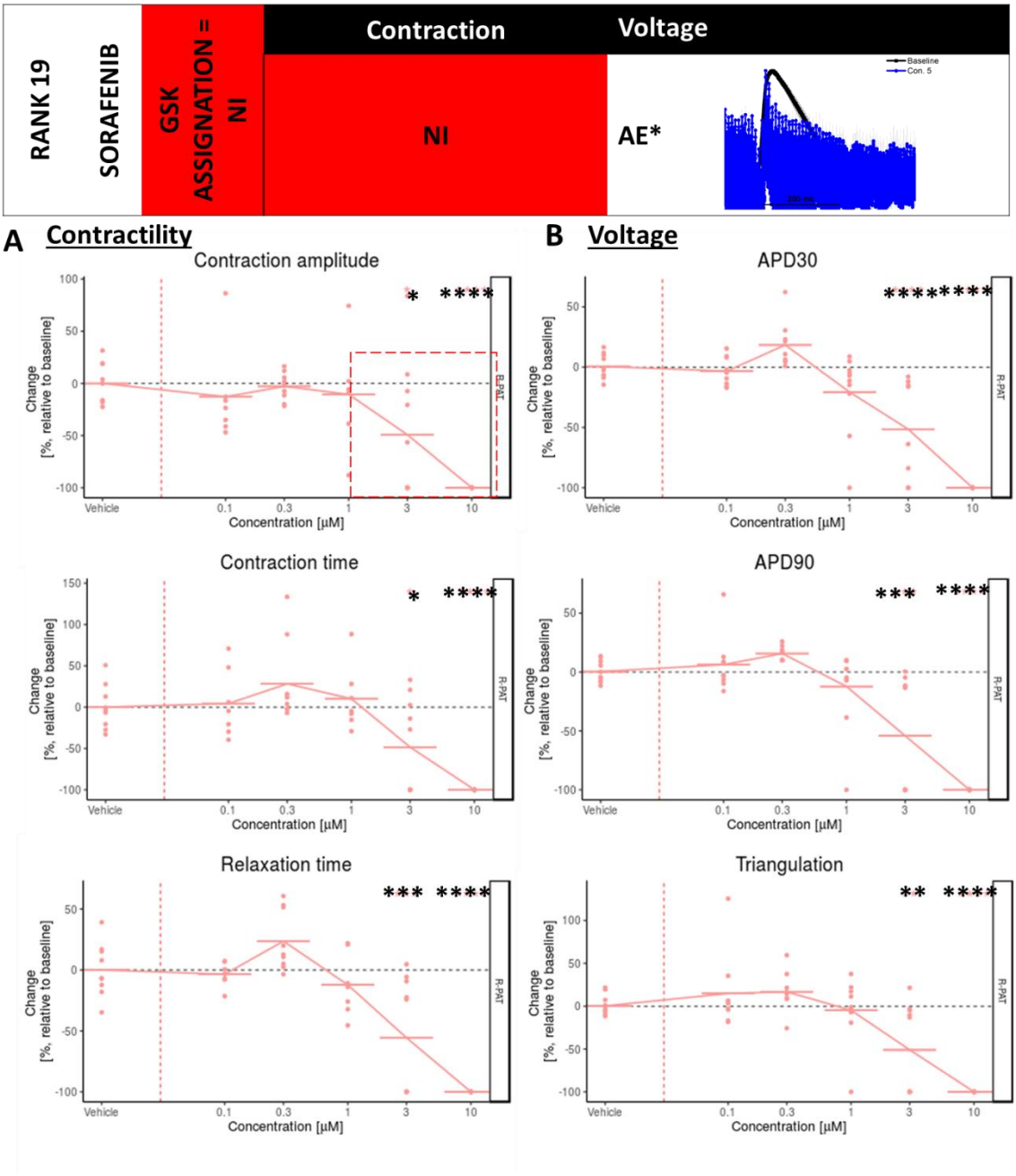


Figure 4.21: Contractility and voltage electrophysiological analysis of and R-PAT-CMs treated with sorafenib.
(A) For contractility, a significant decrease in CA was observed, as was a significant decrease in CT and a significant decrease in RT, therefore, was predicted as NI **(B)** For voltage, altered electrophysiology with arrhythmias decreased in APD30, APD90 and triangulation. Red dotted line is free therapeutic plasma concentration (FTPC). All data are mean ± SEM; n=10. Statistical analysis was carried out using one-way ANOVA with Dunnett's multiple comparison test compared to the vehicle. Significance tests were based on p-values as follows: * $p < 0.05$; ** $p < 0.01$; *** $p < 0.001$; **** $p < 0.0001$

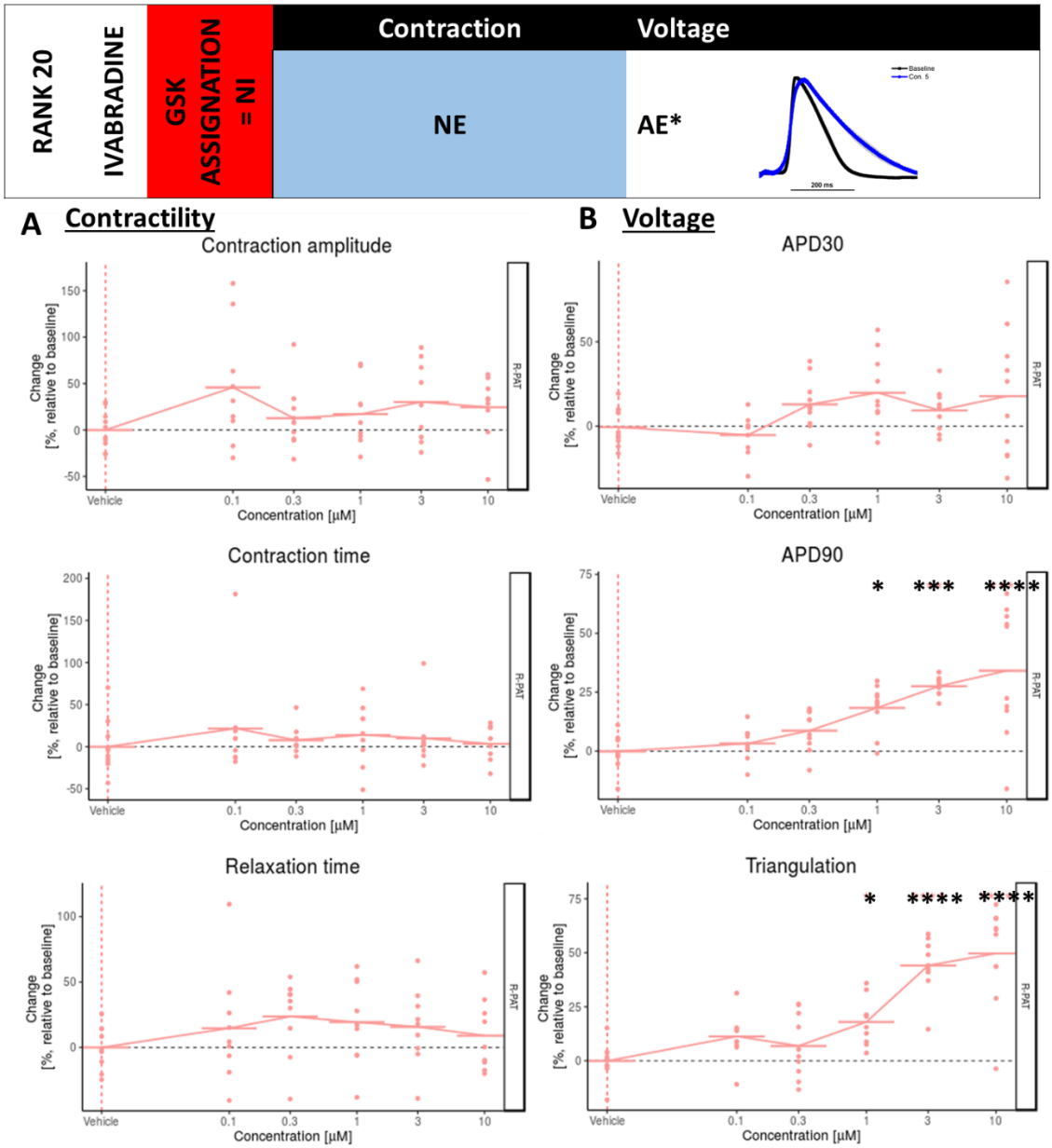


Figure 4.22: Contractility and voltage electrophysiological analysis of and R-PAT-CMs treated with ivabradine.
(A) For contractility, no effects in CA, CT and RT were observed, therefore, was predicted as NE. **(B)** For voltage, electrophysiology was altered with arrhythmias by an increase in APD90 and triangulation. Red dotted line is free therapeutic plasma concentration (FTPC). All data are mean ± SEM; n=10. Statistical analysis was carried out using one-way ANOVA with Dunnett's multiple comparison test compared to the vehicle. Significance tests were based on p-values as follows: * $p < 0.05$; ** $p < 0.01$; *** $p < 0.001$; **** $p < 0.0001$

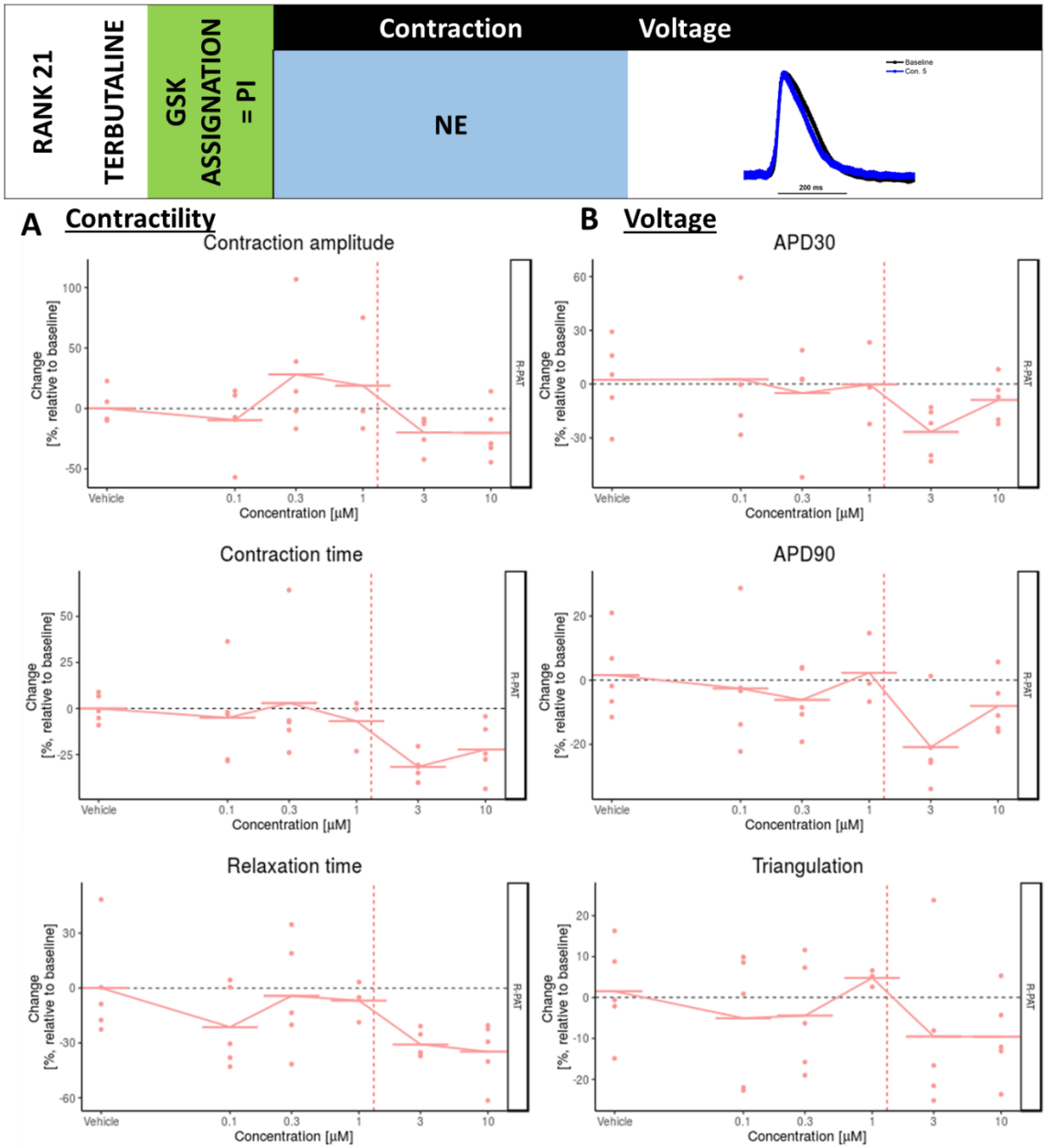


Figure 4.23: Contractility and voltage electrophysiological analysis of and R-PAT-CMs treated with terbutaline.
(A) For contractility, no effects in CA, CT and RT were observed, therefore, was predicted as NE. **(B)** For voltage, overall, there was no altered electrophysiology as there was no significant changes in APD30, APD90 or triangulation. Red dotted line is free therapeutic plasma concentration (FTPC). All data are mean ± SEM; n=5. Statistical analysis was carried out using one-way ANOVA with Dunnett's multiple comparison test compared to the vehicle. Significance tests were based on p-values as follows: * $p < 0.05$; ** $p < 0.01$; *** $p < 0.001$; **** $p < 0.0001$

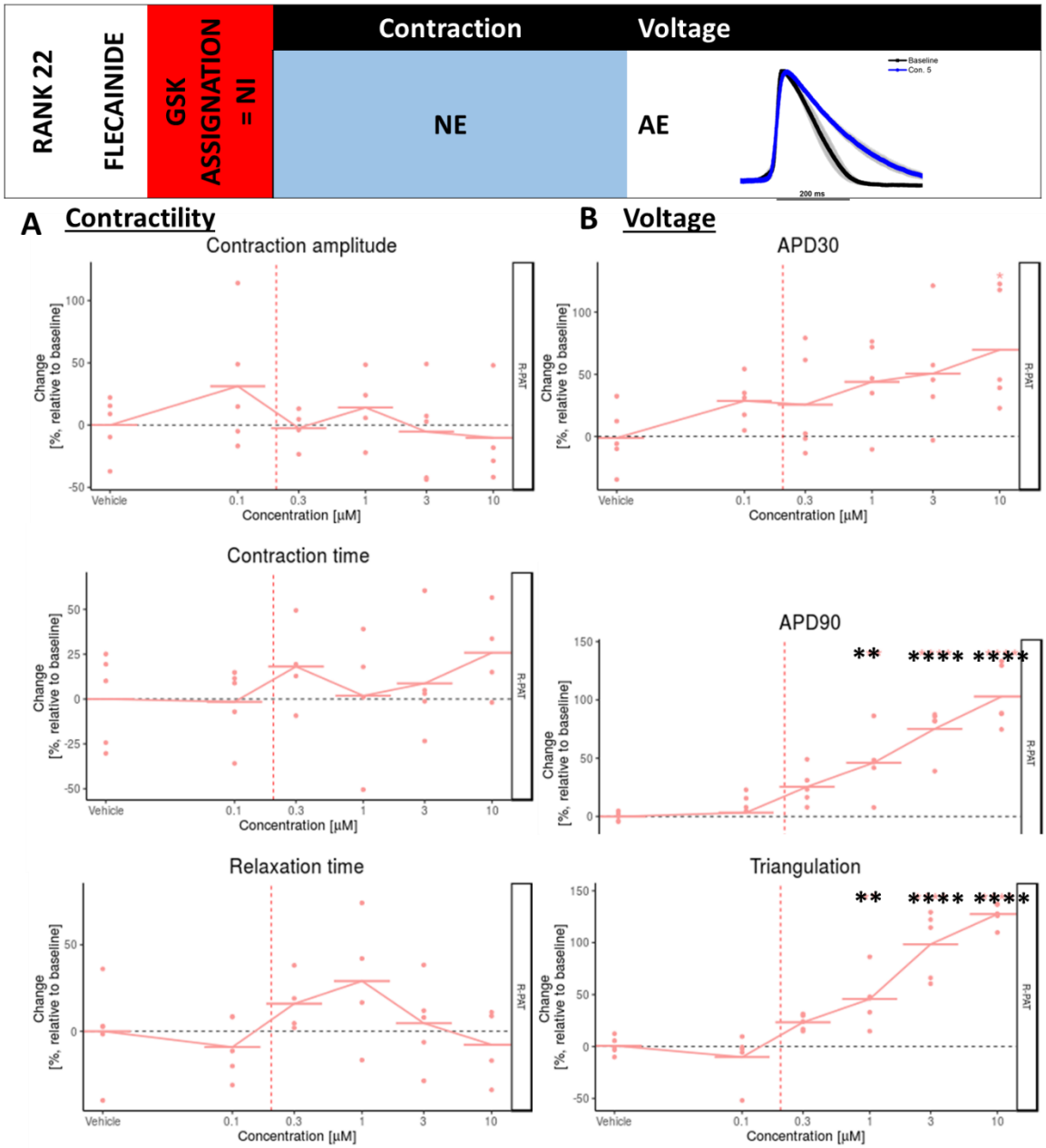


Figure 4.24: Contractility and voltage electrophysiological analysis of and R-PAT-CMs treated with flecainide.
(A) For contractility, no effects in CA, CT and RT were observed, therefore, was predicted as NE. **(B)** For voltage, electrophysiology was altered by an increase in APD90 and triangulation. Red dotted line is free therapeutic plasma concentration (FTPC). All data are mean ± SEM; n=5. Statistical analysis was carried out using one-way ANOVA with Dunnett's multiple comparison test compared to the vehicle. Significance tests were based on p-values as follows: * $p < 0.05$; ** $p < 0.01$; *** $p < 0.001$; **** $p < 0.0001$

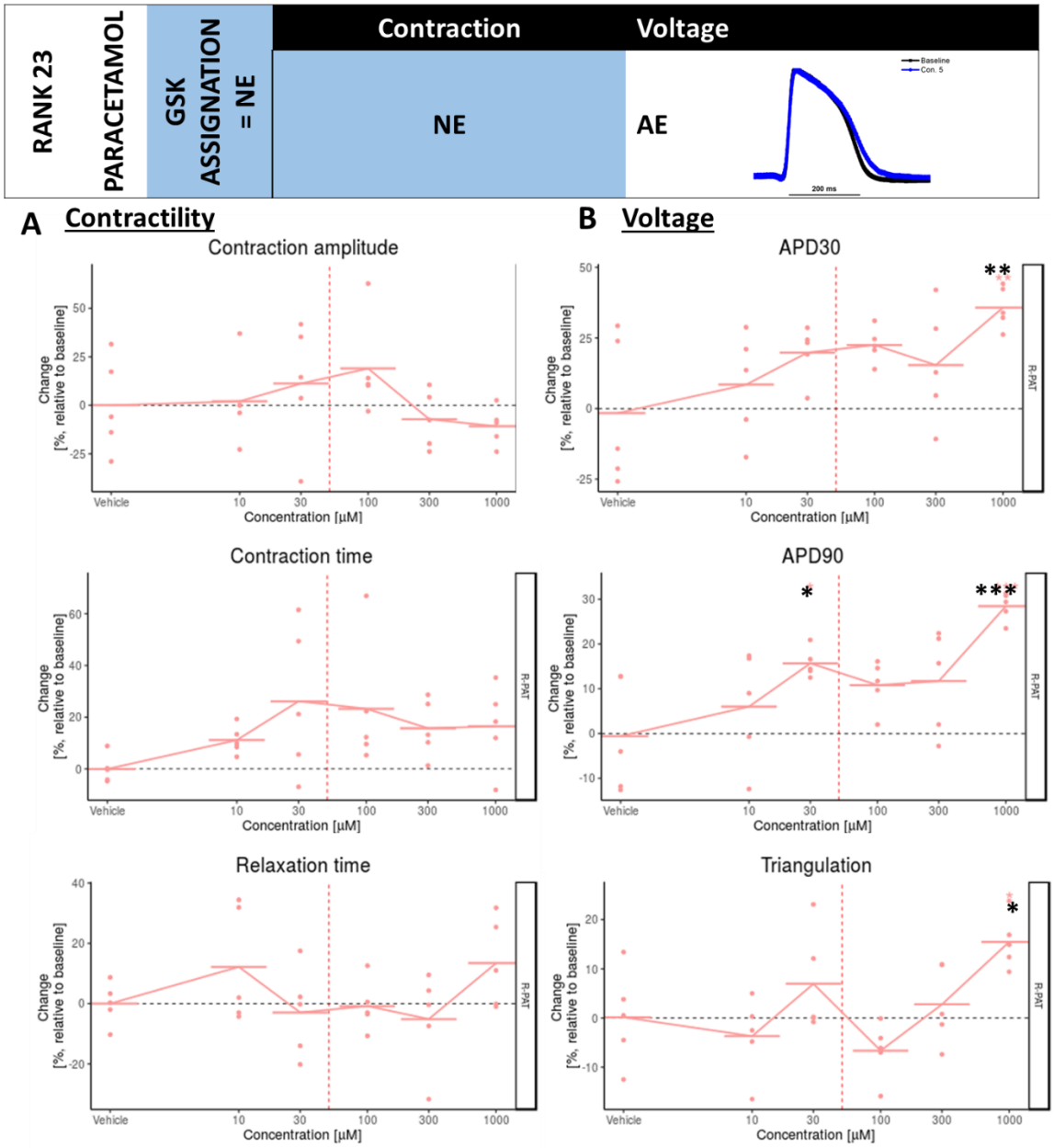


Figure 4.25: Contractility and voltage electrophysiological analysis of and R-PAT-CMs treated with paracetamol.
(A) For contractility, no effects were observed in CA, CT or RT, therefore, was predicted as NE. **(B)** For voltage, electrophysiology was altered with an increase in APD30, APD90 and triangulation. Red dotted line is free therapeutic plasma concentration (FTPC). All data are mean ± SEM; n=5. Statistical analysis was carried out using one-way ANOVA with Dunnett's multiple comparison test compared to the vehicle. Significance tests were based on p-values as follows: * $p < 0.05$; ** $p < 0.01$; *** $p < 0.001$; **** $p < 0.0001$

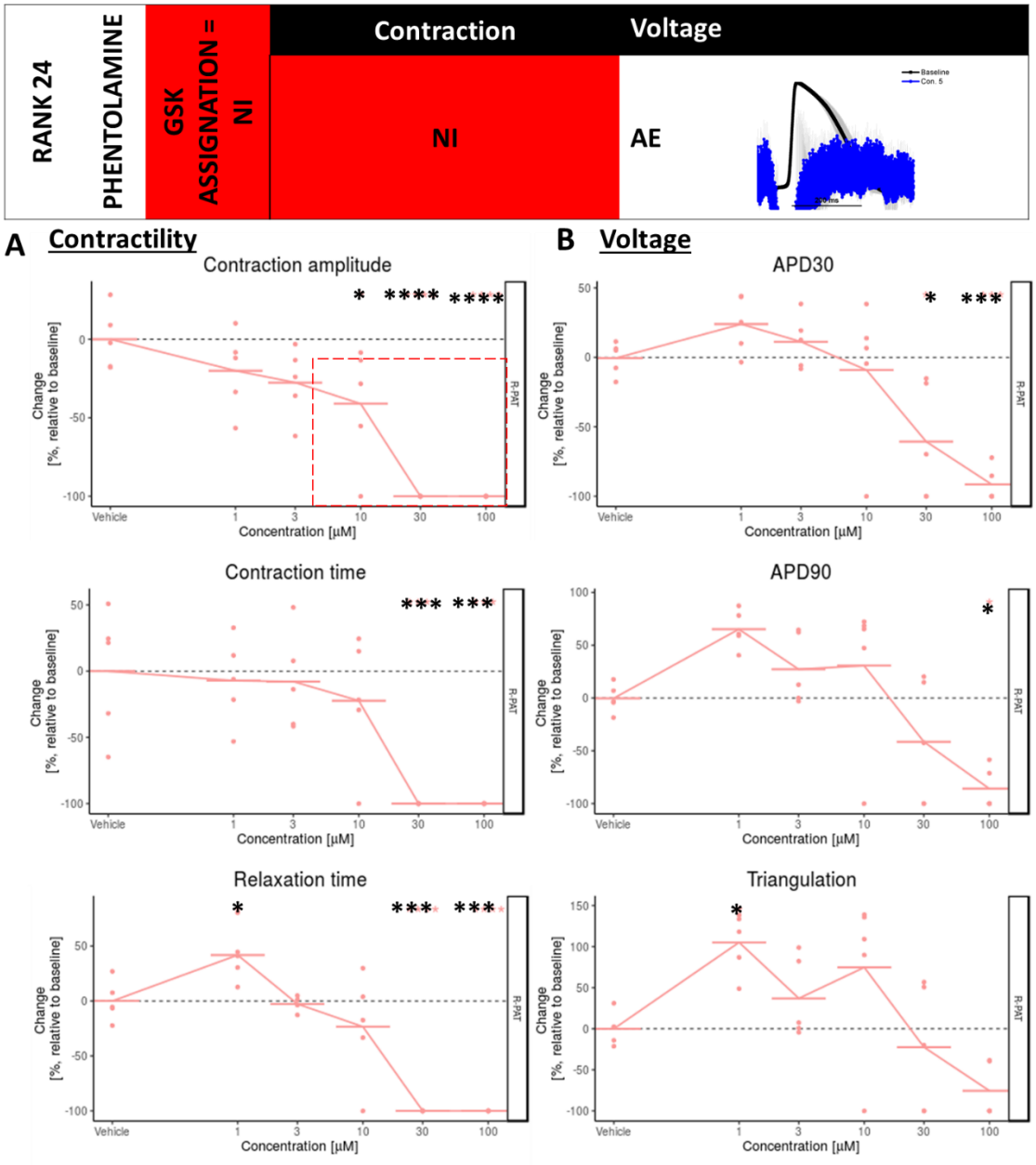


Figure 4.26: Contractility and electrophysiological voltage analysis of and R-PAT-CMs treated with phentolamine.
(A) For contractility, a significant decrease in CA was observed, as well as a significant decrease in CT and a significant decrease in RT, therefore, was predicted as NI **(B)** For voltage, altered electrophysiology was observed with a decrease in APD30 and APD90. Red dotted line is free therapeutic plasma concentration (FTPC). All data are mean ± SEM; n=5. Statistical analysis was carried out using one-way ANOVA with Dunnett's multiple comparison test compared to the vehicle. Significance tests were based on p-values as follows: * $p < 0.05$; ** $p < 0.01$; *** $p < 0.001$; **** $p < 0.0001$

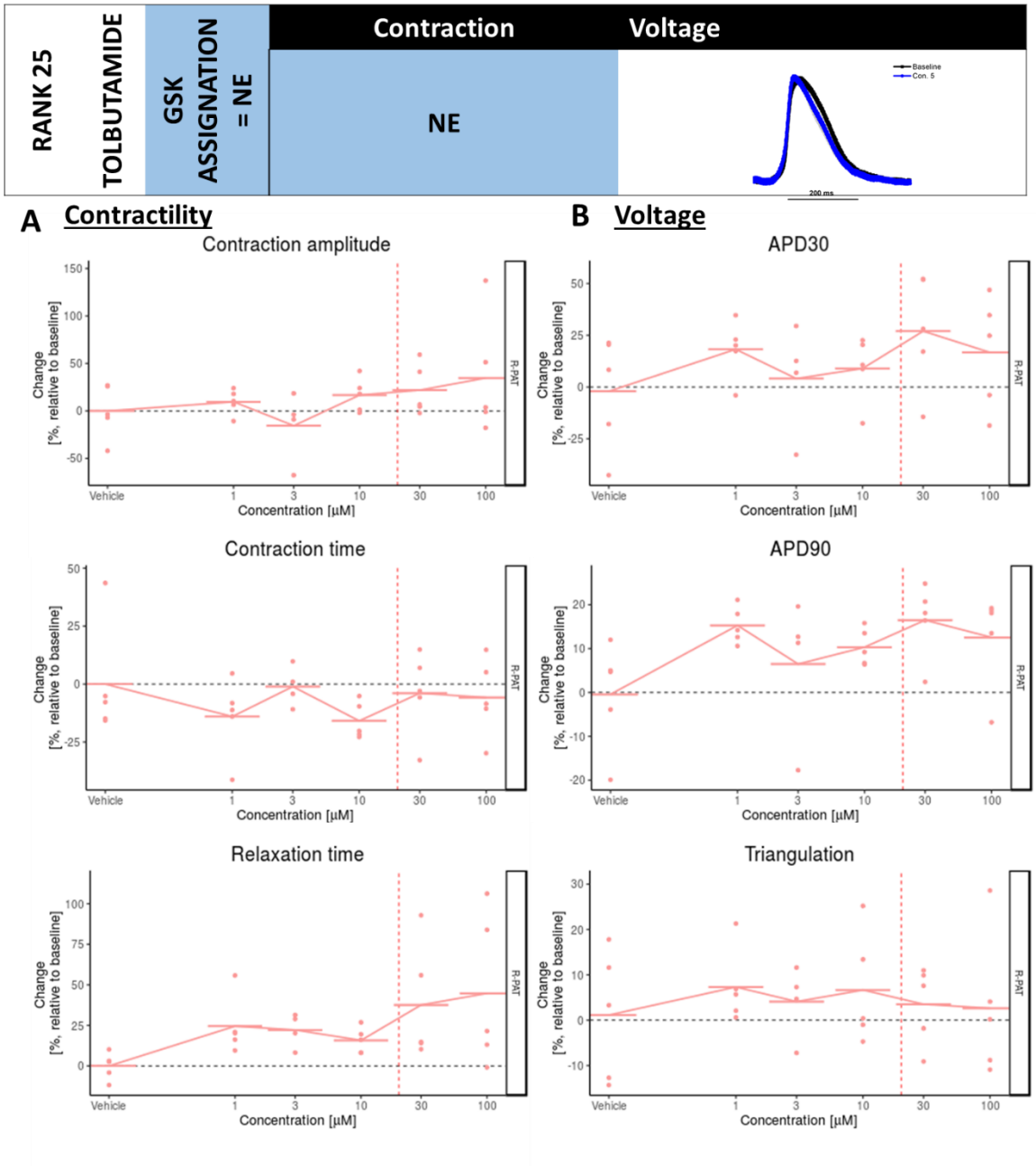


Figure 4.27: Contractility and voltage electrophysiological analysis of and R-PAT-CMs treated with tolbutamide.
(A) For contractility, no effects in CA, CT or RT were observed, therefore, was predicted as NE. **(B)** For voltage, overall no altered electrophysiology as no significant change in APD30, APD90 or triangulation. Red dotted line is free therapeutic plasma concentration (FTPC). All data are mean ± SEM; n=5. Statistical analysis was carried out using one-way ANOVA with Dunnett's multiple comparison test compared to the vehicle. Significance tests were based on p-values as follows: * $p < 0.05$; ** $p < 0.01$; *** $p < 0.001$; **** $p < 0.0001$

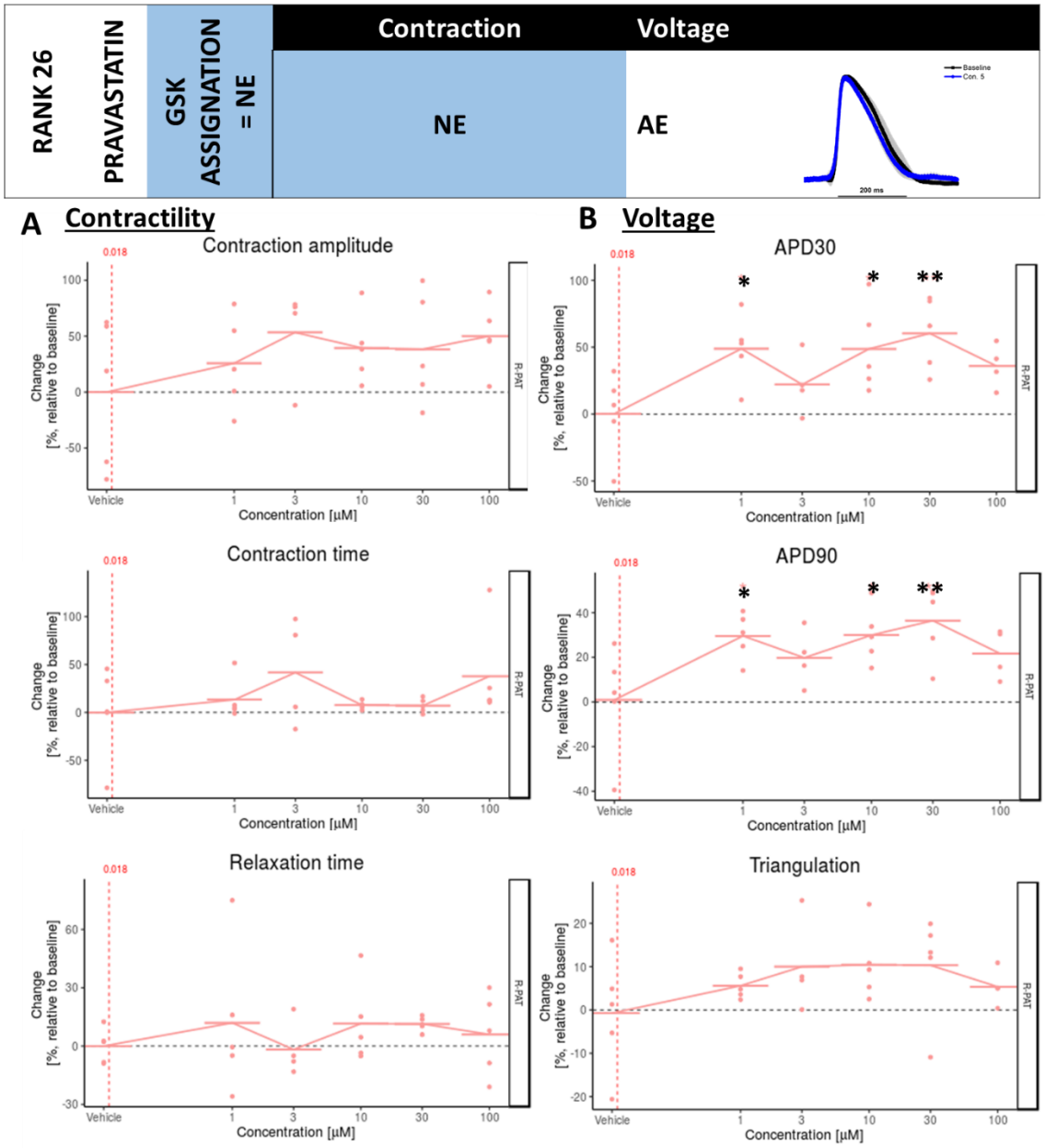


Figure 4.28: Contractility and voltage electrophysiological analysis of and R-PAT-CMs treated with pravastatin.
(A) For contractility, no effects in CA, CT or RT observed, therefore, was predicted as NE. **(B)** For voltage, there was altered electrophysiology with increase in APD30 and APD90 at concentrations of 1,10 and 30 µM pravastatin. Red dotted line is free therapeutic plasma concentration (FTPC). All data are mean ± SEM; n=5. Statistical analysis was carried out using one-way ANOVA with Dunnett's multiple comparison test compared to the vehicle. Significance tests were based on p-values as follows: * $p < 0.05$; ** $p < 0.01$; *** $p < 0.001$; **** $p < 0.0001$

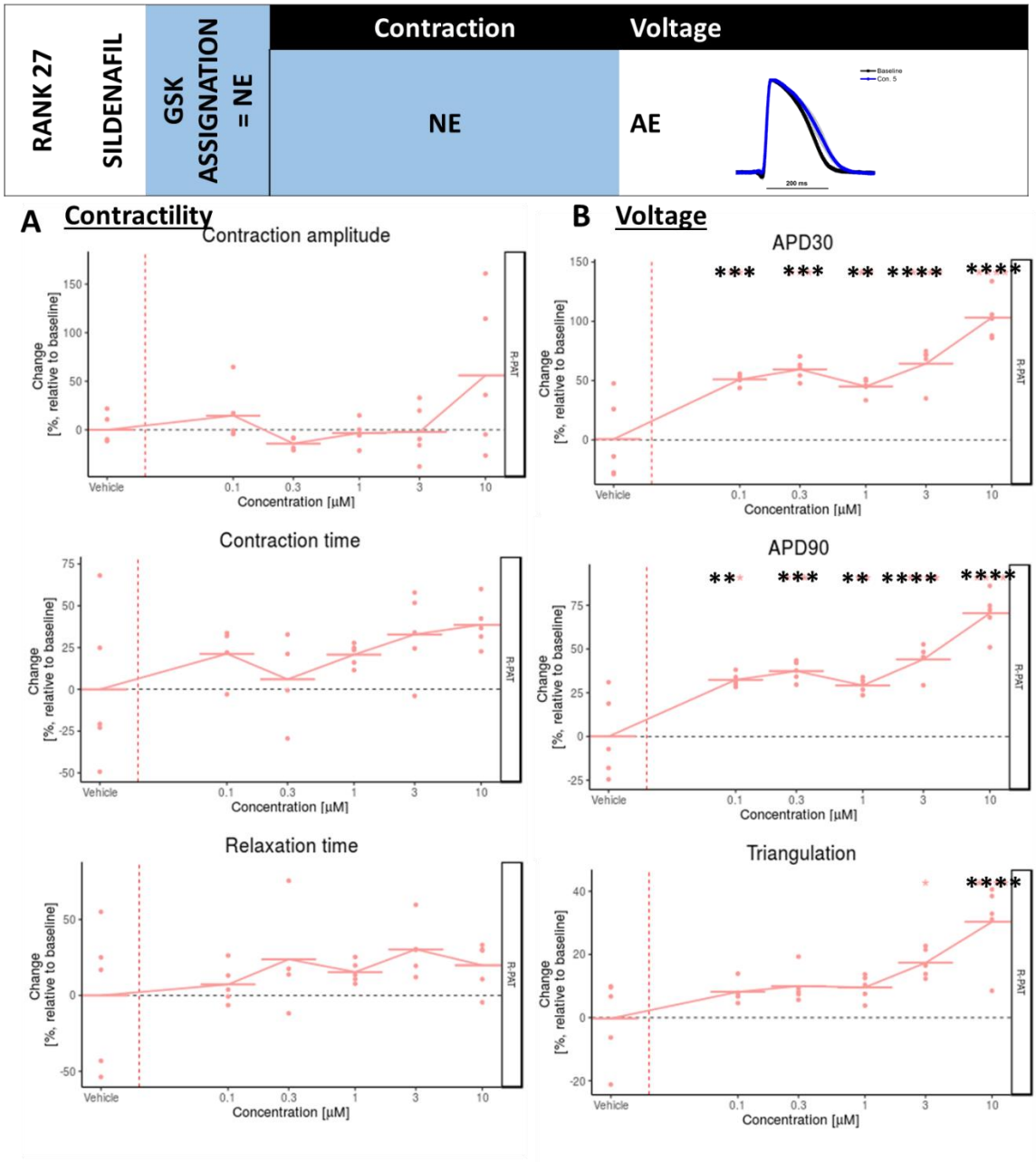


Figure 4.29: Contractility and voltage electrophysiological analysis of R-PAT-CMs treated with sildenafil.
(A) For contractility, no effects in CA, CT or RT were observed, therefore, was predicted as NE. **(B)** For voltage, electrophysiology was altered with an increase in APD30 and APD90 and triangulation. Red dotted line is free therapeutic plasma concentration (FTPC). All data are mean ± SEM; n=5. Statistical analysis was carried out using one-way ANOVA with Dunnett's multiple comparison test compared to the vehicle. Significance tests were based on p-values as follows: * $p < 0.05$; ** $p < 0.01$; *** $p < 0.001$; **** $p < 0.0001$

.

4.4.4 Blinded evaluation and assignment of Tier 2 drugs set across CRACK-IT partners

All the detailed data for contraction and voltage from all CRACK-IT partners are available via an interactive web tool, developed as part of CRACK-IT; https://bjvanmeer.shinyapps.io/crackit/. The data were grouped according to assignation given by GSK **(Table 4.4)**. Accordingly, the maximum response of each contractility and voltage parameters is tabulated in **Table 4.4,** irrespective of whether the prediction was correct or not.

Table 4.4: Effects of compounds on cardiomyocyte contractility *in vitro*.
Drugs were ranked by GSK to accommodate testing order, based on modes of action that were of interest. For each platform-cell combination, data listed represent the mean maximum measurable percentage changes relative to baseline for CA, CT and RT. The concentration at which this effect occurred is listed but when it was different for CA, CT and RT, information is superscripted. Green represents the assigned and predicted effect for the positive inotrope (PI). Red represents the assigned and predicted effect for the negative inotrope (NI). Blue represents the assigned and predicted effect for no effect inotrope (NE). Yellow represents the data for Nottingham CellOPTIQ that were conducted in this thesis chapter.T he Q is annotation for quiescent cells. Abbreviations: SSR inhibitor, selective serotonin reuptake inhibitor; ACE, angiotensin-converting enzyme; PDE, phosphodiesterase; FPTC, free plasma therapeutic concentration; PI, positive inotrope; NI, negative inotrope; NE, no effect. Analysis platforms were CO, CellOPTIQ; TTM, Triple Transient Measurement; EHT, engineered heart tissue. Cardiomyocyte types were rabbit adult cardiomyocytes (as a comparator) or hiPSC lines: P-Cyte, Pluricyte (Ncardia); iCell^2 (Cellular Dynamics International); R-PAT (University of Nottingham); ERC18 (University of Hamburg).

Compound	Rank	Mode of action	Platform	Cell	Measurement parameters			Test range µM	Conc µM	FPTC µM	GSK Assignatio	Blinded prediction
					CA	CT	RT					
Epinephrine	1	Non-selective α1-, β1- and β2-adrenoceptor agonist	CO	Rabbit	+196	-26	+6 $^{0.03\ \mu M}$	0.01-1	0.1	0.0002-0.05	PI	PI
			TTM	P-Cyte	+53 $^{0.03\ \mu M}$	-34 $^{1\ \mu M}$	-9		0.01			PI
			CO	P-Cyte	+18 $^{0.3\ \mu M}$	+67 $^{1\ \mu M}$	-36		0.1			NE
			CO	iCell2	-12 $^{0.3\ \mu M}$	-43	+39		0.03			PI
			CO	R-PAT	+27 $^{0.01\ \mu M}$	+16	-18		1			NE
			EHT	R-PAT	+22	-16 $^{1\ \mu M}$	-22 $^{0.3\ \mu M}$		0.1			PI
			EHT	ERC18	+8	-6 $^{1\ \mu M}$	-7		0.01			NE

Forskolin	2	Adenylyl cyclase stimulator	CO	Rabbit	-16	-34 $^{0.1\ \mu M}$	+45	0.1-10	3	0.012-0.024	PI	PI
			TTM	P-Cyte	+72 $^{10\ \mu M}$	-37 $^{3\ \mu M}$	-38		0.3			PI
			CO	P-Cyte	+31 $^{1\ \mu M}$	+55 $^{3\ \mu M}$	+47		0.3			NE
			CO	iCell2	-44	+64	+44		10			NI
			CO	R-PAT	-31 $^{10\ \mu M}$	-33	+20		0.1			NE
			EHT	R-PAT	+15 $^{10\ \mu M}$	-7	-22 $^{3\ \mu M}$		0.3			PI
			EHT	ERC18	+18 $^{3\ \mu M}$	-33	-23		10			PI
Levosimendan	3	Calcium sensitizer PDE3 inhibitor K_{ATP} channel agonist	CO	Rabbit	+16 $^{0.1\ \mu M}$	-33	-25	0.01-1	0.01	0.026-0.35	PI	NE
			TTM	P-Cyte	+42 $^{0.1\ \mu M}$	+11 $^{0.3\ \mu M}$	-12		0.03			NE
			CO	P-Cyte	-54	+54	-40		0.03			NE
			CO	iCell2	+14 $^{0.3\ \mu M}$	+80	+54		0.1			NE
			CO	R-PAT	+23 $^{0.1\ \mu M}$	-12	22 $^{1\ \mu M}$		0.01			NE
			EHT	R-PAT	+6	-7	-14 $^{0.3\ \mu M}$		0.01			NE
			EHT	ERC18	+13 $^{1\ \mu M}$	-9 $^{0.1\ \mu M}$	-4		0.01			NE
Pimobendan	4	Calcium sensitizer PDE3 inhibitor	CO	Rabbit	+132 $^{1\ \mu M}$	+72	+42	1-100	3	0.005-0.01	PI	NE
			TTM	P-Cyte	+55	-31 $^{10\ \mu M}$	+73		30			NE
			CO	P-Cyte	-23 $^{10\ \mu M}$	+69	-19		3			NE
			CO	iCell2	+65	+69	-13 $^{100\ \mu M}$		1			NE
			CO	R-PAT	+18	+26 $^{10\ \mu M}$	+29		100			NE
			EHT	R-PAT	+12	-3.5	+12 $^{100\ \mu M}$		1			NE
			EHT	ERC18	+13 $^{30\ \mu M}$	-13	+14 $^{100\ \mu M}$		3			PI
Dobutamine	11	α1-, β1- and β2-adrenoceptor agonist	CO	R-PAT	+39 $^{3\ \mu M}$	-16 $^{10\ \mu M}$	+29	0.1-10	0.3	0.07-1	PI	NE
			EHT	R-PAT	+44 $^{3\ \mu M}$	-25	-22		10			PI
			EHT	ERC18	+18 $^{3\ \mu M}$	-37 $^{10\ \mu M}$	+7		0.3			PI
Milrinone	13	PDE3 inhibitor	CO	R-PAT	-17	+16 $^{3\ \mu M}$	+15 $^{100\ \mu M}$	1-100	1	0.1-0.15	PI	NE
			EHT	R-PAT	+18	-11	-9		30			PI
			EHT	ERC18	+7	-18	-6 $^{30\ \mu M}$		100			PI
Omecamtiv mecarbil	14	Cardiac specific myosin activator	CO	R-PAT	-47	+117	-34 $^{0.01\ \mu M}$	0.01-1	1	0.05-4.2	PI	NI
			EHT	R-PAT	+53	+37	-26		0.3			PI
			EHT	ERC18	+22	+38	-6 $^{0.3\ \mu M}$		1			PI

Terbutaline	21	β2-adrenoceptor agonist	CO	R-PAT	+28	-32 $^{3\ \mu M}$	-35 $^{10\ \mu M}$	0.1-10	0.3	1.3	PI	NE
			EHT	R-PAT	+17	-24	-35 $^{0.3\ \mu M}$		3			PI
			EHT	ERC18	+29 $^{10\ \mu M}$	-30	-17		1			PI
Verapamil	7	L-type calcium channel blocker, hERG blocker	CO	Rabbit	-82 $^{0.03\ \mu M}$	+24	+61	0.01-1	0.1	0.05	NI	NI
			TTM	P-Cyte	-79	-68	-11		0.1			NI
			CO	P-Cyte	(5/5)Q	(5/5)Q	(5/5)Q		1			NI
			CO	iCell2	(4/5)Q	+103 $^{0.1\ \mu M}$	(4/5)Q		1			NI
			CO	R-PAT	-98	-91	-88		1			NI
			EHT	R-PAT	(5/5)Q $^{0.1\ \mu M}$	-7	-6		0.03			NI
			EHT	ERC18	(3/5)Q $^{0.3\ \mu M}$	-25 $^{0.1\ \mu M}$	-17		0.1			NI
Doxorubicin	8	Impairs Ca^{2+} transport mechanisms in sarcoplasmic reticulum	TTM	P-Cyte	-47	-46	+51	0.1-10	100	1-2	NI	NE
			CO	P-Cyte	-15	+70	+72		100			NE
			CO	iCell2	+65	-39	+57 $^{30\ \mu M}$		1			NE
			CO	R-PAT	-27 $^{100\ \mu M}$	+41 $^{30\ \mu M}$	-12		1			NE
Sunitinib	9	Multi-targeted TK inhibitor	CO	Rabbit	-78	+46	+300	0.1-10	10	0.003	NI	NI
			TTM	P-Cyte	+42	-23 $^{10\ \mu M}$	+28		0.1			NI
			CO	P-Cyte	(5/5)Q	+163 $^{0.1\ \mu M}$	(5/5)Q		10			NI
			CO	iCell2	-25 $^{10\ \mu M}$	-43	+62		1			NI
			CO	R-PAT	-20	+34 $^{0.1\ \mu M}$	+33		10			NE
			EHT	R-PAT	+11	+6	+4 $^{0.1\ \mu M}$		0.3			NE
			EHT	ERC18	-8	+6	-8		3			NE
Citalopram	16	SSR inhibitor, hERG & L-type calcium channel blocker	CO	R-PAT	(10/10)Q	(10/10)Q	(10/10)Q	1-100	30	0.05	NI	NI
			EHT	R-PAT	(4/4)Q $^{10\ \mu M}$	-6 $^{3\ \mu M}$	+5		1			NI
			EHT	ERC18	(5/5)Q $^{10\ \mu M}$	+2 $^{1\ \mu M}$	+7		3			NI

Itraconazole	18	Triazole antifungal, mechanism unclear	CO	R-PAT	(5/5)Q	(5/5)Q	(5/5)Q	0.1-10	10	0.00086	NI	NI
			EHT	R-PAT	-51	+14 $^{0.1\ \mu M}$	-33		3			NI
			EHT	ERC18	(5/5)Q $^{10\ \mu M}$	+11	-29 $^{3\ \mu M}$		1			NI
Sorafenib	19	Multi-targeted TK inhibitor	CO	R-PAT	(10/10)Q	(10/10)Q	(10/10)Q	0.1-10	10	0.03	NI	NI
			EHT	R-PAT	-50	+14	+6 $^{3\ \mu M}$		10			NI
			EHT	ERC18	-56	+6 $^{3\ \mu M}$	-24		10			NI
Ivabradine	20	I_f inhibitor	CO	R-PAT	+46	+22	+24 $^{0.3\ \mu M}$	0.1-10	0.1	0.01-0.1	NI	NE
			EHT	R-PAT	-16	-27	+3 $^{0.1\ \mu M}$		10			NI
			EHT	ERC18	-56	14	+45		10			NI
Flecainide	22	Sodium channel blocker, hERG blocker	CO	R-PAT	+31	+26 $^{10\ \mu M}$	+29 $^{1\ \mu M}$	0.1-10	0.1	0.2-0.4	NI	NE
			EHT	R-PAT	(6/6)Q $^{3\ \mu M}$	-16	-26 $^{1\ \mu M}$		0.3			NI
			EHT	ERC18	-74 $^{10\ \mu M}$	-21	+42		3			NI
Phentolamine	24	Non-selective α adrenoceptor antagonist	CO	R-PAT	(5/5)Q	(5/5)Q	(5/5)Q	1-100	30	2.25	NI	NI
			EHT	R-PAT	5/5)Q $^{10\ \mu M}$	-18	-28		3			NI
			EHT	ERC18	(5/5)Q	-30	+53		10			NI
Zimelidine	28	SSR inhibitor	EHT	R-PAT	18 $^{1\ \mu M}$	-15	-22	1-100	3	0.78	NI	NI
			EHT	ERC18	(5/5)Q $^{100\ \mu M}$	-25 $^{30\ \mu M}$	+43		3			NI
Acetylsalicylic acid	5	Cyclooxygenase inhibitor	CO	Rabbit	+26	-21	-13	10-1000	100	0.3-2	NE	NE
			TTM	P-Cyte	+34	-8 $^{1000\ \mu M}$	+24 $^{100\ \mu M}$		10			NE
			CO	P-Cyte	-21 $^{30\ \mu M}$	-35	+20		10			NE
			CO	iCell2	-58 $^{30\ \mu M}$	-44	+47 $^{1000\ \mu M}$		10			NE
			CO	R-PAT	+23	-26 $^{300\ \mu M}$	+17 $^{1000\ \mu M}$		100			NE
			EHT	R-PAT	-14	+8 $^{100\ \mu M}$	+15		1000			NE
			EHT	ERC18	+8 $^{300\ \mu M}$	-8	-15		1000			NE
Atenolol	6	β1>β2 adrenoceptor antagonist	CO	Rabbit	+16	-13	+968 $^{0.3\ \mu M}$	0.1-10	1	1	NE	NE

			TTM	P-Cyte	+54	+8	-19 $^{3\ \mu M}$		1			NE
			CO	P-Cyte	-29	-71 $^{10\ \mu M}$	+69 $^{3\ \mu M}$		1			NE
			CO	iCell2	-42 $^{0.1\ \mu M}$	+58	-52		0.3			NE
			CO	R-PAT	-28 $^{3\ \mu M}$	+11	+11 $^{10\ \mu M}$		0.3			NE
			EHT	R-PAT	-25	+7 $^{1\ \mu M}$	+14		10			NE
			EHT	ERC18	+3	-13	-9 $^{3\ \mu M}$		10			NE
Captopril	10	ACE inhibitor	CO	Rabbit	-91	+72	+212	1-100	100	1-2	NE	NI
			TTM	P-Cyte	+136	-5	-14 $^{10\ \mu M}$		1			NE
			CO	P-Cyte	+24 $^{30\ \mu M}$	+132	-38		100			NE
			CO	iCell2	-27	+15 $^{3\ \mu M}$	-20 $^{10\ \mu M}$		1			NE
			CO	R-PAT	+18 $^{3\ \mu M}$	-26	-16 $^{30\ \mu M}$		1			NE
			EHT	R-PAT	-18	-7 $^{100\ \mu M}$	-9 $^{10\ \mu M}$		3			NE
			EHT	ERC18	+7	-10	-6 $^{1\ \mu M}$		3			NE
Glibenclamide	12	K_{ATP} channel antagonist	CO	Rabbit	+66 $^{1\ \mu M}$	-27 $^{0.3\ \mu M}$	+61	0.1-10	0.1	0.02-0.06	NE	NE
			CO	R-PAT	+36	-26 $^{10\ \mu M}$	+31		0.1			NE
			EHT	R-PAT	+3	+6	-12		1			NE
			EHT	ERC18	+6	+10	-5 $^{3\ \mu M}$		10			NE
Enalaprilat	15	ACE inhibitor	CO	R-PAT	+54	+20 $^{10\ \mu M}$	+34	1-100	100	0.12	NE	NE
			EHT	R-PAT	+33	+5 $^{1\ \mu M}$	-14		30			PI
			EHT	ERC18	+2 $^{10\ \mu M}$	-3	-4		100			NE
Clonidine	17	α2-adrenoceptor agonist	CO	R-PAT	-24	+26	-27	0.01-1	0.3	0.002-0.004	NE	NE
			EHT	R-PAT	+10	+11 $^{0.1\ \mu M}$	-12		0.3			NE
			EHT	ERC18	+5 $^{0.3\ \mu M}$	+5	+4		0.1			NE
Paracetamol	23	Prostaglandin synthesis inhibitor	CO	R-PAT	+19 $^{100\ \mu M}$	+26	+13 $^{1000\ \mu M}$	10-1000	30	50	NE	NE
			EHT	R-PAT	-19	-20	-9 $^{100\ \mu M}$		1000			NE
			EHT	ERC18	+3 $^{100\ \mu M}$	-9	+10		1000			NE
Tolbutamide	25	K_{ATP} channel antagonist, Adenylyl cyclase stimulator	CO	R-PAT	+35	-16 $^{10\ \mu M}$	+45	1-100	100	20-30	NE	NE
			EHT	R-PAT	-12	+9	-8 $^{10\ \mu M}$		1			NE
			EHT	ERC18	+21	-3	-9		100			PI
Pravastatin	26	HMG CoA reductase inhibitor	CO	R-PAT	+53	+42	+12 $^{1\ \mu M}$	1-100	3	0.018	NE	NE

			EHT	R-PAT	-19	-15 [30 µM]	13 [100 µM]		3			NE
			EHT	ERC18	+19	+3 [30 µM]	-11 [100 µM]		10			PI
			CO	R-PAT	+56	+39	+30 [3 µM]		10			NE
Sildenafil	27	PDE5 inhibitor	EHT	R-PAT	-10	-16	+13 [3 µM]	0.3-30	10	0.02	NE	NE
			EHT	ERC18	+9	-4 [10 µM]	-6		1			NE

4.4.5 Predictivity scoring

4.4.5.1 Scoring for hiPSC-CMs in CellOPTIQ

Across the first ten priority drugs and all drugs evaluated, the CellOPTIQ platform correctly predicted 60% of the drugs for iCell^2, 50% of the drugs for Pluricyte and 40-56% of the drugs for R-PAT-CMs **(Table 4.5).** The percentages of correct prediction indicate that there was no difference regarding cell lines in improving prediction as the results were approximately similar within all three cell lines, iCell^2, Pluricyte and R-PAT-CMs.

In terms of predicting PI, NE and NI, the CellOPTIQ platform showed a high level of accuracy for NE drugs (100% correct) and to a lesser extent, NI drugs (56-60% correct)**(Table 4.5).** The PI prediction ranged from 0 to 25% across both categories of the top 10 drugs tested and all drugs assessed, hence representing the poorest prediction **(Table 4.5 yellow box).**

Table 4.5: Predictivity scoring for hiPSC-CMs in CellOPTIQ (CO) platform based on correct PI, NE and NI.

Platform: Cell	10 drugs in common			Correct prediction: Total	All drugs assessed			Correct prediction: Total
	PI	NE	NI		PI	NE	NI	
CO: iCell^2	1/4 (25%)	3/3 (100%)	2/3 (100%)	6/10 (60%)	1/4 (25%)	3/3 (100%)	2/3 (100%)	6/10 (60%)
CO: Pluricyte	0/4 (0%)	3/3 (100%)	2/3 (100%)	5/10 (50%)	0/4 (0%)	3/3 (100%)	2/3 (100%)	5/10 (50%)
CO: R-PAT	0/4 (0%)	3/3 (100%)	1/3 (50%)	4/10 (40%)	0/8 (0%)	10/10 (100%)	5/9 (56%)	15/27 (56%)
Total correct	1/12 (8%)	9/9 (100%)	5/9 (56%)		1/16 (6%)	16/16 (100%)	9/15 (60%)	

4.4.5.2 Scoring for hiPSC-CMs across all CRACK-IT platforms

Across all platforms, the poorest predictivity was for PI drugs, which ranged from 0-to 75%, with 42.5% mean correct across all platforms. This range was lower than NE (75-100 % correct; mean correct = 85%) and NI (56-100% correct, mean correct =76%) **(Table 4.6)**. The 3D EHT:hiPSC-CMs combination is more predictive of PI (75%) than CO:hiPSC-CMs (0-25%) **(Table 4.6)**. Overall the data implies that 3D EHT (81-85% correct) yielded more predictive contractility data than the cell motion sampled from a 2D culture (50-70% correct) **(Table 4.6)**.

Table 4.6: Predictivity scoring of data from all platform-cell combinations. The data extracted from CRACK-IT partners relating to all drugs evaluated based on correct PI, NE and NI predictivity

Platform: Cell	Config.	All drugs assessed			Correction prediction Total
		PI	NE	NI	
CO: iCell^2	2D	1/4 (25%)	3/3 (100%)	2/3 (67%)	6/10 (60%)
CO: Pluricyte	2D	0/4 (0%)	3/3 (100%)	2/3 (67%)	5/10 (50%)
CO: R-PAT	2D	0/8 (0%)	10/10 (100%)	5/9 (56%)	15/27 (56%)
TTM: Pluricyte	2D	2/4 (50%)	3/3 (100%)	2/3 (67%)	7/10 (70%)
CO: Rabbit	2D	2/4 (50%)	3/4 (75%)	2/2 (100%)	7/10 (70%)
EHT: R-PAT	3D	6/8 (75%)	9/10 (90%)	8/9 (89%)	23/27 (85%)
EHT: ERC	3D	6/8 (75%)	8/10 (80%)	8/9 (89%)	22/27 (81%)
Total correct		17/40 (42.5%)	39/46 (85%)	29/38 (76%)	

4.4.6 The platform: cell-combination sensitivity

The predictivity scoring allows us to examine the sensitivity of the CellOPTIQ:hiPSC-CM and other platforms. As such, where the platform-cell combinations correctly predicted the PI and NI drugs, the data were converted into a heat map to reflect the percentage of change for PI drugs **(Table 4.7)** and NI drugs **(Table 4.8)**. This was in the context of when a drug was predicted correctly, whether the concentration that elicited an effect in the hiPSC-CMs overlapped with the free therapeutic plasma concentration (FTPC). The heat map was created to see whether the CA, CT and RT are more informative to the correct prediction.

The only correctly predicted PI by CellOPTIQ is epinephrine with iCell^{2,} which was predicted according to trends rather than significant change. The heat map illustrated for epinephrine highlights that the highest percentage of change to the baseline was in CT and RT parameters and was detected within the FTPC range **(Table 4.7)**. However, for NI in CellOPTIQ, out of 6 drugs that were correctly predicted, 4 of them were detected within the FTPC range and at the higher concentration **(Table 4.8)**. Therefore it can be concluded that the sensitivity of the platform-cells combination for CellOPTIQ:hiPSC-CMs is rather low.

Table 4.7: Sensitivity of platform-cell combinations for predicting PIs.
Where positive inotropes were correctly predicted, data are presented as percentage changes relative to the baseline for any of the three contractility parameters (CA, contraction amplitude; CT, contraction time; RT, relaxation time). The bolded black text indicates where significance was reached using Dunnett's stats vs vehicle control and P<0.05. FPTC, Free plasma therapeutic concentration. NR, not recorded

				Concentration (μM)								
Drug	**Rank**	**CellLine**	**parameter**	**0.01**	**0.03**	**0.1**	**0.3**	**1**	**3**	**10**	**30**	**100**
Epinephrine	1		FTPC	0.0002 - 0.05 μM								
		CO: Rb	CA	30.07	65.04	**196.24**	NR	NR				
			CT	-5.19	-18.51	**-25.74**	NR	NR				
			RT	3.81	5.91	-1.28	NR	NR				
		EHT: R-PAT	CA	7.09	9.12	**21.56**	**20.03**	**19.01**				
			CT	**-8.25**	**-13.22**	**-5.5**	**-10.7**	**-15.73**				
			RT	**-13.66**	**-16.98**	**-21.16**	**-22.2**	**-12.31**				
		TTM:	CA	50.36	52.81	28.71	36.91	39.83				
			CT	-2.29	-11.44	-18.99	-31.56	**-33.84**				
			RT	-8.72	-5.98	-1.49	-2.16	-1.96				
		CO: iCell2	CA	-3.6	-10.7	-3.9	-11.66	0.88				
			CT	-4.16	-42.92	-37.92	-39.86	-27.74				
			RT	21.74	39.32	24.58	23.08	16.28				
Forskolin	2		FTPC	0.012 - 0.024 μM								
		CO: Rb	CA			-12.35	13.09	-4.22	-15.54	7.04		
			CT			-33.78	6.68	30.44	-5.28	8.26		
			RT			7.1	9.92	36.35	45.43	34.6		
		EHT: ERC	CA			-3.31	3.37	15.59	17.71	13.29		
			CT			**-23.21**	**-30.5**	**-32.53**	**-30.3**	**-32.7**		
			RT			**-11.15**	**-13**	**-18.03**	**-22.4**	**-23.2**		
		EHT: R-PAT	CA			5.07	3.93	9.63	-0.39	-15.07		
			CT			-2.05	**-7.33**	2.09	-0.56	-4.19		
			RT			-3.69	**-17.1**	**-20.9**	**-21.8**	**-19**		
		TTM:	CA			31.98	22.85	6.91	13.63	71.7		
			CT			-26.83	-26.78	**-31.31**	**-37.4**	**-35.1**		
			RT			11.15	-38.03	-37.12	-28.9	-33.23		
Pimobendan	4		FTPC	0.005 - 0.01 μM								
		EHT: ERC	CA					-3.26	-7.67	5.58	13.42	13.29
			CT					-9.17	**-12.5**	**-11.2**	-8.21	**-11.4**
			RT					-3.72	3.43	5	13.03	13.55
Dobutamine	11		FTPC			0.07 - 1 μM						
		EHT: ERC	CA			5.01	3.75	**17.2**	**18.07**	12.27		
			CT			-2.43	**-11.5**	**-26.23**	**-31.7**	**-37.2**		
			RT			1.97	7.23	-4.42	-6.38	1.23		
		EHT: R-PAT	CA			**17**	**28.48**	**37.5**	**43.62**	**31.95**		
			CT			**-9.74**	**-12.9**	**-11.53**	**-12.3**	**-25.2**		
			RT			**-20**	**-20.3**	**-18.29**	**-17.9**	**-21.6**		
Milrinone	13		FTPC			0.1 - 0.15 μM						
		EHT: ERC	CA					2.32	1.61	-0.59	7.51	7.64
			CT					**-7.84**	**-8.45**	**-12.9**	**-15.57**	**-17.6**
			RT					2.96	0.11	0.33	-6.06	-1.51
		EHT: R-PAT	CA					-1.98	-2.27	4.87	18.46	NR
			CT					0.4	-5.11	-1.59	-10.85	NR
			RT					-0.07	-2.91	-3.65	**-8.98**	NR
Omecamtiv mecarbil	14		FTPC			0.05 - 0.42 μM						
		EHT: ERC	CA	3.03	5.86	11.22	**20.63**	**21.75**				
			CT	0.66	0.04	3.8	18.9	37.51				
			RT	2.88	1.98	-1.06	-5.53	-1.94				
		EHT: R-PAT	CA	-12.48	0.75	17.48	**53.19**	NR				
			CT	-2.22	2.07	**19.04**	**36.85**	NR				
			RT	1.43	1.17	-9.2	**-25.8**	NR				
Terbutaline	21		FTPC					1.3 μM				
		EHT: ERC	CA			4.46	9.04	**16.84**	**23.59**	**29.18**		
			CT			**-22.01**	**-28.4**	**-29.62**	**-23.9**	**-22.3**		
			RT			-14.96	-16.51	-17.06	-16.25	-1.97		
		EHT: R-PAT	CA			7.94	1.9	14.3	**17.48**	NR		
			CT			**-14.82**	**-21.3**	**-16.82**	**-24.2**	NR		
			RT			**-24.73**	**-35.2**	**-30.03**	**-32.8**	NR		

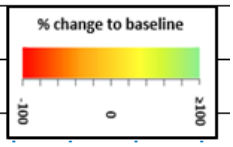
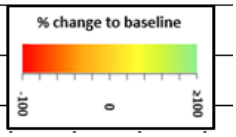


Table 4.8: Sensitivity of platform-cell combinations for predicting NIs.
Where negative inotropes were correctly predicted, data are presented as percentage changes relative to the baseline for any of the three contractility parameters (CA, contraction amplitude; CT, contraction time; RT, relaxation time).

				Concentration								
Drug	**Rank**	**CellLine**	**parameter**	**0.01**	**0.03**	**0.1**	**0.3**	**1**	**3**	**10**	**30**	**100**
Verapamil	7		FTPC		**0.05 µM**							
		CO: Rb	CA	**-54.95**	**-82.09**	**-80.27**	NR	NR				
			CT	-7.87	-7.92	24.26	NR	NR				
			RT	15.17	23.28	60.89	NR	NR				
		EHT: ERC	CA	-8.17	**-42.18**	**-89.19**	**-100**	**-100**				
			CT	-1.06	-9.48	-25.36	NR	NR				
			RT	-10.05	-17.26	-16.33	NR	NR				
		EHT: R-PAT	CA	5.93	-26.48	**-100**	**-100**	NR				
			CT	3.79	-7.32	NR	NR	NR				
			RT	4.07	-6.23	NR	NR	NR				
		TTM:	CA	-30.53	**-50.11**	**-78.76**	NR	NR				
			CT	-11.49	-31.01	-68.09	NR	NR				
			RT	-0.44	-8.95	-11.2	NR	NR				
		CO: iCell2	CA	36.23	-7.03	8.1	-39.6	-100				
			CT	103.13	84.97	4.58	-7.93	-100				
			RT	31.3	4.47	47.12	-10.27	-100				
		CO: Pluricyte	CA	30.6	-6	24.3	8.3	**-100**				
			CT	3.43	18.5	-11.54	-41.48	-100				
			RT	-35.77	-32.36	-50.72	-59.18	-100				
		CO: R-PAT	CA	12.04	3.47	-11.34	-26.84	**-98.03**				
			CT	-35.26	-16.5	-16.76	-36.58	-90.63				
			RT	-5.87	1.28	14.88	-25.46	-87.94				
Sunitinib	9		FTPC	**0.003 µM**								
		CO: Rb	CA	-	-	17.79	7.28	**-31.96**	**-57.64**	**-77.7**	-	-
			CT	-	-	4.17	-2.68	3.91	5.18	**45.93**	-	-
			RT	-	-	8.87	0.33	23.64	137.67	**300.4**	-	-
		TTM:	CA	-	-	42.31	27.58	15.24	-39.48	-20.73	-	-
			CT	-	-	9.95	13.19	-4.28	-17.53	-23.25	-	-
			RT	-	-	28.32	19.51	22.97	18.57	9.33	-	-
		CO: iCell2	CA	-	-	7.6	-16.86	-20.5	4.82	-24.76	-	-
			CT	-	-	-11.92	11.7	-43.4	-11.72	9.86	-	-
			RT	-	-	1.78	-2.26	**62.3**	5.38	-7.1	-	-
		CO: Pluricyte	CA	-	-	-13.02	4.46	3.08	17.57	**-100**	-	-
			CT	-	-	162.66	58.3	16.26	24.83	-100	-	-
			RT	-	-	-46.48	-1.14	-10.16	-19.22	-100	-	-
Citalopram	16		FTPC		**0.05 µM**							
		EHT: ERC	CA	-	-	-	-	-26.58	**-65.22**	**-100**	**-100**	**-100**
			CT	-	-	-	-	1.82	0.76	NR	NR	NR
			RT	-	-	-	-	5	7.72	NR	NR	NR
		EHT: R-PAT	CA	-	-	-	-	-1.52	**-30.72**	**-100**	NR	NR
			CT	-	-	-	-	6.49	-4.03	NR	NR	NR
			RT	-	-	-	-	4.96	-1.33	NR	NR	NR
		CO: R-PAT	CA	-	-	-	-	11.74	-13.54	**-61.3**	**-100**	**-100**
			CT	-	-	-	-	-11.44	-2.23	-19.46	-100	-100
			RT	-	-	-	-	6.18	-8.13	-30.71	-100	-100
Itraconazole	18		FTPC	**0.00086 µM**								
		EHT: ERC	CA	-	-	-9.9	-16.06	**-36.58**	**-51.18**	**-100**	-	-
			CT	-	-	6.88	6.19	**11.31**	8.49	NR	-	-
			RT	-	-	1.93	1.74	-10.18	-23.37	NR	-	-
		EHT: R-PAT	CA	-	-	5.93	-1.39	-15.86	**-51.14**	NR	-	-
			CT	-	-	**13.55**	4.63	4.61	12.2	NR	-	-
			RT	-	-	-2.65	-8.52	-19.46	-33.17	NR	-	-
		CO: R-PAT	CA	-	-	-32.83	-25.86	-16.36	**-48.12**	**-100**	-	-
			CT	-	-	8.5	25.46	6.66	-29.86	-100	-	-
			RT	-	-	-2.15	-2.14	-2.08	-62.62	-100	-	-
Sorafenib	19		FTPC		**0.03 µM**							
		EHT: ERC	CA	-	-	**-15.06**	**-16.8**	**-22.49**	**-37.56**	**-56.3**	-	-
			CT	-	-	-1.34	-2.42	3.62	6.27	4.68	-	-
			RT	-	-	3.4	2.78	-1.17	-14.39	-24.43	-	-
		EHT: R-PAT	CA	-	-	-1.68	-3.89	-11.75	-25.63	**-50.4**	-	-
			CT	-	-	3.22	1.8	8.7	6.42	**13.89**	-	-
			RT	-	-	0.22	1.31	-1.98	-6.48	1.55	-	-
		CO: R-PAT	CA	-	-	-12.8	-2.87	-10.56	**-49.21**	**-100**	-	-
			CT	-	-	4.36	28.21	10.03	-48.43	-100	-	-
			RT	-	-	-3.54	23.61	-12.26	-55.68	-100	-	-
Ivabradine	20		FTPC		**0.01 - 0.1 µM**							
		EHT: ERC	CA	-	-	-5.9	-7.34	-9.23	**-19.14**	**-55.6**	-	-
			CT	-	-	0.77	-0.27	-3.68	-8.35	-13.62	-	-
			RT	-	-	-1.61	-3.04	4.08	**27.35**	**45.3**	-	-
		EHT: R-PAT	CA	-	-	-6.21	-7.39	-2.05	8.83	-15.68	-	-
			CT	-	-	0.17	-7.87	-6.8	-13.46	-26.88	-	-
			RT	-	-	3.15	0.06	-1.13	-0.25	-2.34	-	-
Flecainide	22		FTPC			**0.2 - 0.4 µM**						
		EHT: ERC	CA	-	-	-8.14	-9.09	**-24.62**	**-38.05**	**-74.5**	-	-
			CT	-	-	3.26	-0.71	-4.9	-21.24	NR	-	-
			RT	-	-	0.83	1.07	**18.08**	**42.22**	NR	-	-
		EHT: R-PAT	CA	-	-	-5.47	**-20**	-6.8	**-100**	NR	-	-
			CT	-	-	-4.73	-15.53	-6.29	NR	NR	-	-
			RT	-	-	-5.29	-17.79	-25.78	NR	NR	-	-
Phentolamine	24		FTPC						**2.25 µM**			
		EHT: ERC	CA	-	-	-	-	-1.62	**-23.21**	**-89.9**	**-100**	**-100**
			CT	-	-	-	-	-8.02	-16.4	-30.49	NR	NR
			RT	-	-	-	-	**25.36**	**39.86**	**52.53**	NR	NR
		EHT: R-PAT	CA	-	-	-	-	-3.14	**-28.82**	NR	NR	NR
			CT	-	-	-	-	-4.82	-17.74	NR	NR	NR
			RT	-	-	-	-	-12.69	-27.78	NR	NR	NR
		CO: R-PAT	CA	-	-	-	-	-20.04	-27.6	**-41.1**	**-100**	**-100**
			CT	-	-	-	-	-7.2	-7.9	-22.32	-100	-100
			RT	-	-	-	-	**41.8**	-2.7	-23.44	-100	-100
Zimelidine	28		FTPC					**0.78 µM**				
		EHT: ERC	CA	-	-	-	-	5.12	-6.91	**-37.4**	**-95.23**	**-100**
			CT	-	-	-	-	-3.17	-8.58	-13.03	-24.92	NR
			RT	-	-	-	-	**23.76**	**42.78**	**42.59**	**27.92**	NR
		EHT: R-PAT	CA	-	-	-	-	18.37	-1.27	NR	NR	NR
			CT	-	-	-	-	-2.11	-15	NR	NR	NR
			RT	-	-	-	-	-7.02	-22.03	NR	NR	NR



4.4.7 Informative parameter

The sensitivity of the platform: cell-combination in the previous subchapter led to a further investigation as to which parameter was informative for the contractility inotropy prediction. When the prediction was correct, the parameters that reached significance at the lowest drug concentration were recorded (**Figure 4.30**). For PI drugs, the CT followed by RT were highly informative NI drugs; it was shown that CA was most informative (Figure 4.30A).

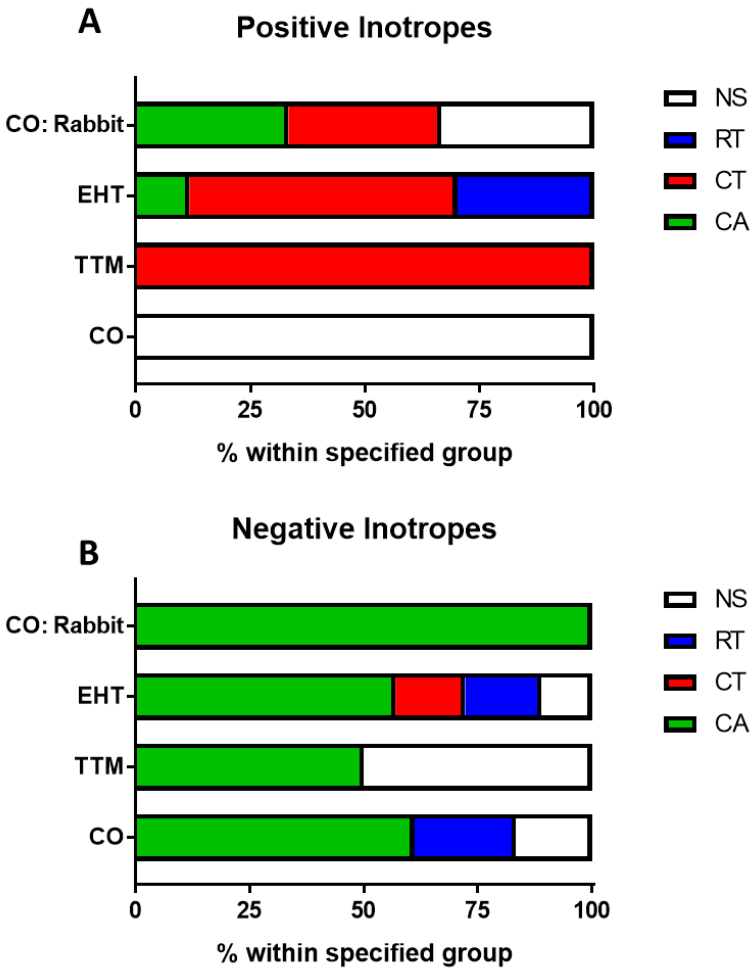


Figure 4.30: **Most informative contractility marker for inotropes prediction.** Parameters that led to the correct prediction of drug responses were assessed for **(A)** Positive inotropes and **(B)** Negative inotropes. Data show the breakdown by percentage for the parameters (CA, contraction amplitude; CT, contraction time; RT, relaxation time) that reached significance at the lowest concentration (Dunnett's stats vs vehicle control and $P<0.05$). White boxes (NS, not significant) indicate where predictions were made due to a trend rather than reaching significance, and/or by guidance from voltage and/or Ca^{2+} data.

4.5 Chapter discussion

4.5.1 The response and predictivity of different hiPSC-CMs lines

The data illustrate the utility of various hiPSC-CMs (iCell^2, Pluricyte and R-PAT-CMs) with the CellOPTIQ platform to study the impact of drug-induced changes on cell function by measuring changes in cardiac contractility upon drug administration for use in drug safety screening. Despite variable MLC-2a/MLC-2v ratio, different RO index and different baseline characterisation (data from Chapter 3), all hiPSC-CMs were able to respond to the blinded drugs in a similar manner with 60%, 50% and 40-56% **(Table 4.5)** correct predictivity for iCell^2, Pluricyte and R-PAT-CMs respectively.

The reasons for using different hiPSC-CMs derived from different hiPSC lines were because it becomes of interest to evaluate the effects of different hiPSC-CMs towards the drug. Cost is another crucial factor: each drug assessed typically required 1.6 million CMs (40 wells in 96-well plate), and 5 million (for 5 EHTs) hiPSC-CMs, corresponding to up t0 ~$3,000 per drug at current prices. For this reason, most of the assays in this study were carried out using 'in-house' hiPSC-CMs, which can be achieved at a cost of only ~$10 per million cells. Nevertheless, for both in-house and commercial hiPSC-CMs, batch to batch variation meant that the drug assays need to be repeated. This issue becomes more prominent when the larger tissue-engineered constructs are used.

4.5.2 Predictivity evaluation of CellOPTIQ:hiPSC-CMs combination

The results demonstrated in this chapter also highlight the poor predictivity and small effect size of change for PIs compared to the NIs in CellOPTIQ-hiPSC-CMs combination. The average size of change for CellOPTIQ(based on maximum effects regardless of the correct prediction or not based on data from **Table 4.4** for PI = CA (31.25 ± 3.79%), CT (48.06 ± 7.28%) and RT (30.88 ± 3.06%) (n= 16 set of experiments), compared to NI = CA (68.47 ± 9.404%), CT (75.47 ± 10.3%) and RT (71.8 ± 8.55%) (n= 16 set of experiments).The overall predictivity of CellOPTIQ for PI was 6-8%, and NI was 56-60% **(Table 4.5)**. While the NE were 100% correctly predicted **(Table 4.5).** These data reflect that hiPSC-CMs with CellOPTIQ platform is a suitable model to detect changes in drug effects based on contractility; however, the direction of change, especially for PI, is limited.

4.5.3 Positive inotropy limitations

Only epinephrine was correctly predicted as PI by iCell^2 in this stage by CellOPTIQ:hiPSC-CMs. All other PI drugs were wrongly predicted, mainly in the direction as NE **(Table4.4)**. Most of the PI drugs (7/8) provided appear to be related to a particular pharmacological class, which is the ß-adrenergic system/cAMP that mediates stimulation **(Table 4.3)**. The epinephrine, dobutamine, terbutaline are ß-adrenoreceptor agonist; the forskolin is an adenylyl cyclase stimulator while levosimendan, pimobendan and milrinone are PDE inhibitors. It could be hypothesised that this wrong inotropic prediction is due to the immature phenotype of hiPSC-CMs and suggests functional immaturity of the ß-adrenergic signalling cascade (Mummery et al., 2003, Scott et al., 2013, Mannhardt et al., 2017a). The immature hiPSC-CMs are lack in phospholamban, have reduced SERCA and minimal SR involvement, along with lacking T-tubules, which ultimately affects the contraction response (Pointon et al., 2017). In other words, drugs that should mediate effects via enhanced SR function or ß-adrenergic pathway have small effects on intracellular function and hence contraction.

On the other hand, the PI agents from ß-agonists do rapidly desensitise the ß-adrenergic receptor as a response mechanism to agonist exposure by a ß-arrestin endocytosis pathway(Jung et al., 2016). The desensitisation might attenuate the PI affects and could explain the lack of response in this chapter study. As such, a modification to increase the higher degree of hiPSC-CMs maturity and real-time monitoring of drugs effects in order to improve correct detection for PI might be beneficial, something that needs to be tackled in the future.

Interestingly, Butler (2015) suggested that using different pacing rates may improve the ability to detect inotropes (Butler et al., 2015). The stimulation of 0.5, 1, 1.5, and 2 Hz are equivalent to 30, 60, 90, and 120 beats/min. Therefore, it is essential to keep the culture beat rate low, in order to correctly detect inotropes.

To improve the predictivity of positive inotropy, it is better to further characterise their effects to both representative positive and negative inotropy drug controls, throughout the experiments for each run. The positive and

negative controls preferably should come from the correct prediction of Tier 1 drugs (Chapter 3) and come from the same stocks of Tier 1 drugs. Digoxin may not be a good positive control in these assay, because it was reported that digoxin therapeutic window is small, and at higher concentrations are toxic which lead to cease of beating (Mannhardt et al., 2017a). An alternative positive control may include isoprenaline, which frequently used but was reported to lead to small effects across hiPSC-CM models compared to human nonfailing heart tissue (Denning et al., 2016).

4.5.4 Negative inotropy limitations

The hiPSC-CMs-CellOPTIQ platform combination proved promising in predicting negative inotropes correctly under the short-term drug exposure in the majority of cases, except for doxorubicin and sunitinib **(Table 4.4)**. Those two drugs that wrongly predicted NIs do involve a structural toxic mode of action, especially in mitochondrial damage, which needs long term rather than the rapid onset of action (Clements et al., 2015, Gorini et al., 2018). This is further supported by Mannhardht and Van Meer(Mannhardt et al., 2017a, van Meer et al., 2019) who suggested that the lack of inotropic effect is very likely due to the short incubation of drugs. On the other hand, the short-term effects are as important as the long-term effects, especially in the scenario of lead optimisation stage of positive or negative inotropic drugs where the investigator often looks for the importance of short-term effects. Nonetheless, the retesting/refinement of these drugs under long-term onset are worth investigating in the next chapter.

4.5.5 Comparisons across other CRACK-IT platforms

The data presented also highlighted several deficiencies which include the challenge of detecting of PI drugs, particularly to the 2D platforms that include CO:hiPSC-CMs, CO: adult rabbit and TTM:hiPSC-CMs **(Table 4.5 and Table 4.6)**. This might occur because the discrimination changes in contractility from intermittent video measurement using motion algorithms on the 2D system was lower than the continuous measurement on 3D which is capable of measuring forces.

This poor prediction also highlights that the methods of measuring contractility in 2D versus 3D were more important than the cell types used. As such, for example, the testing of the same cells of Pluricyte on two platforms (TTM and CellOPTIQ) gave different accuracies (70% versus 50%). The same was true for R-PAT-CMs tested on EHT and CellOPTIQ platform (85% versus 56%) **(Table 4.6).** Even the prediction accuracies for adult rabbit myocytes was lower than 3D EHT.

The sensitivity of the platforms also varied between 2D and 3D systems. For example, as PI drugs are cardio-active drugs, it might be expected that the FTPC might align with the response from hiPSC-CMs. This was true for the EHT platform, where the responses were within or close to the FTPC. However, the sensitivity of 2D hiPSC-CMs culture and isolated rabbit cardiomyocytes was considerably lower. This is because, in contrast to 2D monolayers that evaluated hiPSC-CMs movement in unloaded conditions, the EHT platform measures forces of contraction under the influence of loaded conditions (Costa et al., 2013). The loaded condition facilitates maturation and the Frank-Starling mechanism for force generation are followed, which leads to high basal tone and cAMP signalling that are an important mode of actions for many PI drugs such as epinephrine, forskolin and milrinone (Huupponen, 1987, Uzun et al., 2016). Consistent with this, 'Biowire II' tissue-engineered constructs showed positive inotropy for milrinone, which also placed the hiPSC-CMs under the loaded condition to promote maturation(Zhao et al., 2019).

4.5.6 Drugs integrated mechanism of action and *in-vitro* predictivity

In the whole heart function, the integration with neurohormonal or haemodynamic feedback allows numerous parameters to be assessed, which includes Pmax, dP/dtmax (max rate of change if pressure) and left ventricular ejection fraction (Guth et al., 2015a). However, in *in-vitro* cardiomyocytes, this integration does not exist. As such, atenolol, a selective $ß_1$-adrenoceptor antagonist, requires intact sympathetic innervation and is a negative inotrope in the clinic but show no effects in hiPSC-CMs, consistent with a study in this chapter (Kaumann and Blinks, 1980, Lemoine et al., 1988). Another example is for clonidine, which works via presynaptic α-adrenoreceptors on sympathetic neurons, resulting in a reduced sympathetic drive and its effects on the heart function by reducing heart rate and force (Kleiber et al., 2017, Jarrott et al., 1979a). But these effects would not be detected in a 'cardiomyocytes only' model, thus resulting in NE predictivity. As such, in future, predictive screening that includes auxiliary cell types such as neural lineages to enable evaluation of drugs that work via the hormonal system, is highly beneficial.

4.5.7 Summary

As a summary, the combination of hiPSC-CMs with the CellOPTIQ optical platform has demonstrated to be a beneficial tool for assessing the early stage of drug screening based on contractility and basic electrophysiological investigation. It was also shown that hiPSC-CMs in 2D and 3D system could have considerable value in predictive safety pharmacology even in the current stage of development. However, more work is needed to refine the condition in order to improve the predictive direction.

Chapter 5 : Refinement to improve drug safety prediction

5.1 Introduction

The data presented after blind testing in the previous chapter (chapter 4) demonstrated two shortcomings, which include 1) the inability of the CellOPTIQ:hiPSC-CM combination to correctly detect the PIs and 2) the use of short treatment incubation times, hypothesised to contribute to failed prediction of some chronic toxicants such as doxorubicin and sunitinib. This chapter discusses how drug safety prediction might be enhanced by improving culture conditions and related tests.

5.1.1 Understanding the incorrect prediction of positive inotropes

In the previous chapter, it was speculated that a key factor in the poor prediction of PIs related to inadequate maturation, such as suboptimal myofilament organisation and electrophysiology handling. While improving hiPSC-CM maturity was beyond the scope and timeline of this thesis, different contributors to the incorrect predictions were considered.

One aspect was the reduction of signal-to-noise ratio in the test platform. This is due to the switching of a protein-containing medium (RPMI-B27) to serum-free/medium (SFM) without the protein, which increased the beat rate and beat rate variability within a plate and between plates. This creates a wide variance between the data, ultimately affecting its sensitivity by impacting on statistical comparisons between treatments **(Figure 5.1)**.

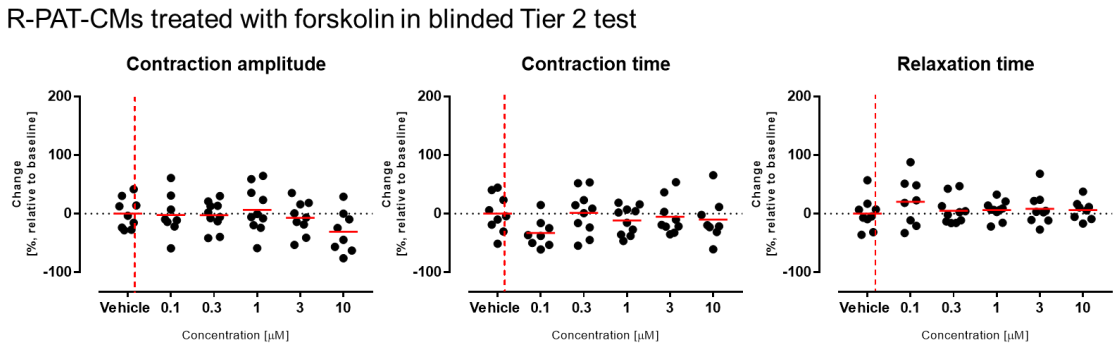


Figure 5.1: High variance between data masks drug effect and causes poor sensitivity of prediction.
An example of data from a previous blinded Tier 2 test: the distribution and wide variance between data have masked the drug effect. No significant change in CA, CT and RT observed. All data are mean ± SEM, n=8-10. Statistical analysis was carried out using one-way ANOVA with Dunnett's multiple comparison test vs vehicle control. The red dotted line represents the free therapeutic plasma concentration (FTPC).

The high beat rate was also suggested to mask the drugs inotrope effects. This is parallel with previous findings by Butler (2015), wherein native heart preparation with a lower beat rate was allied with the positive force-frequency relationship (FFR) up to 2 Hz and exhibited stronger inotropic effects of most PI drugs (Butler et al., 2015)**(Figure 5.2)**. However, the biggest challenge is how to allow cells to beat at less than 1 Hz, without affecting contractility.

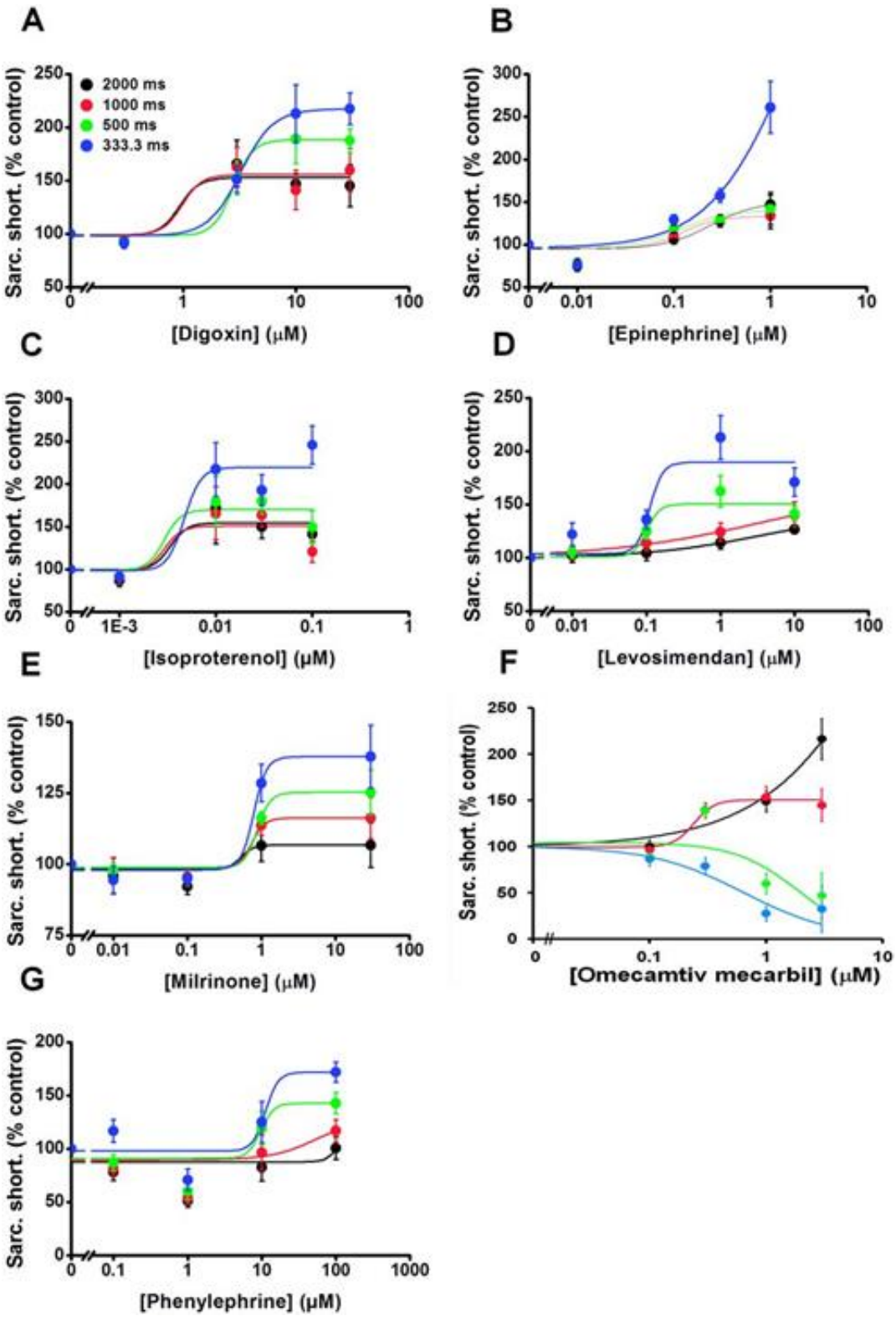


Figure 5.2: Cardiomyocytes paced at a different cycle length (333 ms lowest, highest 2000 ms) and their potency information generated from positive inotropes.
The difference in sarcomere shortening is higher in the low beat cardiomyocytes. Taken from (Butler et al., 2015).

5.1.2 Ivabradine as an agent to decrease spontaneous beating frequency

Ivabradine is a compound that reduces the heart rate via inhibition of the funny current (I_f), which is expressed in the pacemaker cells of the sinoatrial node (DiFrancesco, 2006). As ivabradine blocks the funny current channel, it reduces the pacemaker activity, allowing slower heart rate and more time for blood to flow to the myocardium. Its usage is vital in reducing heart rate without inducing clinically significant adverse effects, especially in the loss of contractility (Koruth et al., 2017, DiFrancesco, 2006). The mechanism of action of ivabradine is further illustrated in **Figure 5.3**.

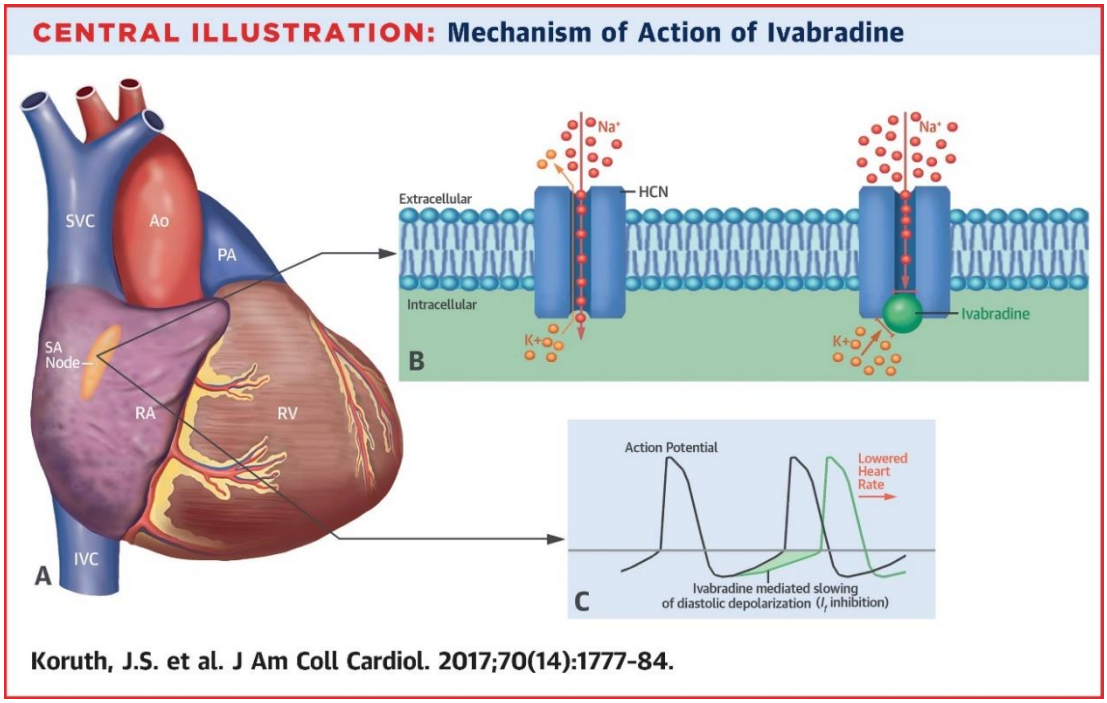


Figure 5.3: Mechanism of action for ivabradine
(A) The primary mechanism of action of ivabradine on cardiac tissue relies on the sinoatrial node (SA)which is positioned between the upper vena cava of the right atrium. **(B)** Ivabradine blocks the intracellular component of the hyperpolarisation-activated cyclic nucleotide (HCN) transmembrane channel protein which is responsible for transporting sodium (Na^+) and potassium (K^+) ions through the cell membrane, which results in inhibition of the funny current (I_f). **(C)** Through selectively inhibiting I_f, the slope of diastolic depolarisation decreases (shaded green area) and the length of diastole increases without altering the action potential resulting in slower heart rate. Adapted from (Koruth et al., 2017).

Previous findings by Mannhardt et al.,(Mannhardt et al., 2016) demonstrated that the usage of sub-µM ranges of ivabradine successfully decreased the spontaneous contraction in *in-vitro* hiPSC-CMs, albeit in EHTs (Mannhardt et al., 2016) **(Figure 5.4).** The optimum concentration to decrease the beat rate was 0.3 µM ivabradine with one hour incubation time **(Figure 5.4).** It was shown that by controlling the spontaneous contraction, there was an improvement in the physiological relevance of inotropic effects from tested drugs (Mannhardt et al., 2016). Hence it is hypothesised that by lowering the beat rate by using ivabradine, the prediction of positive inotropes could be improved.

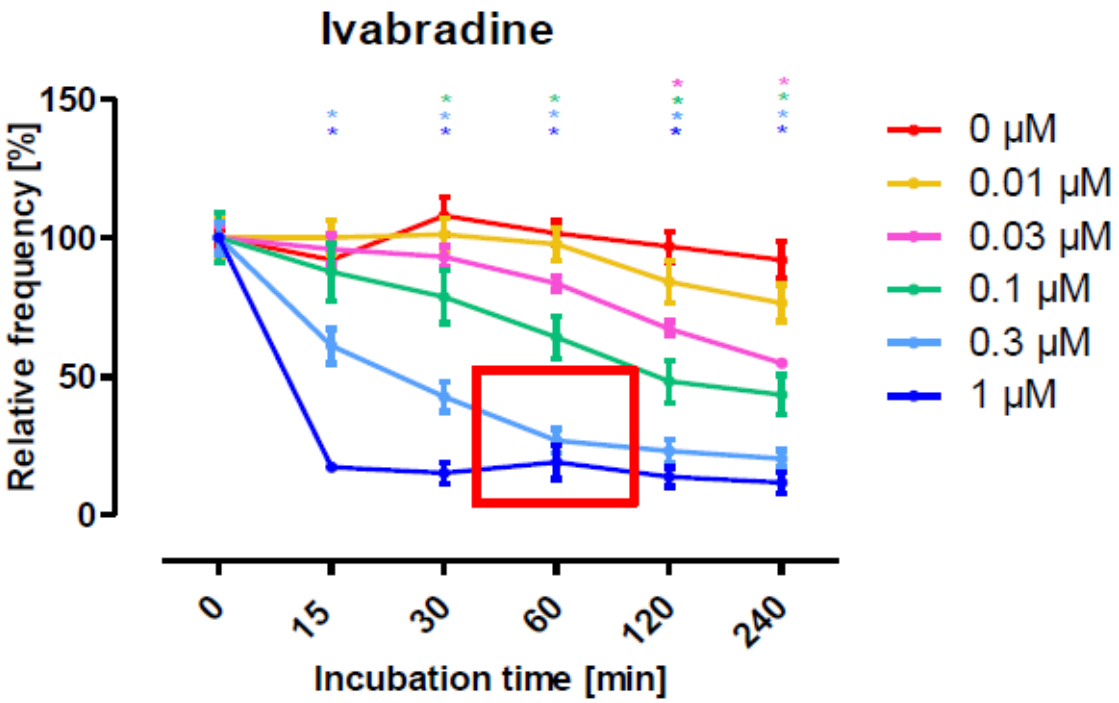


Figure 5.4: Ivabradine decreased the spontaneous beating frequency.
By using different concentrations of 0.01-1 µM ivabradine in a time-dependent manner, the spontaneous beating frequency decreased with complete inhibition at 1 µM. Data were taken from (Mannhardt et al., 2016).

5.1.3 Short- term and long-term incubation of the drugs

As discussed in chapter 4, some prediction for inotropes drugs was hypothesised to be due to short-term drug exposure (30 minutes). For drugs that induce a reduction in contractility or heart failure, chronic timelines of dosing may be needed before the impact on function is observed. Although concerns over the complexity of long-term effects of all 27 compounds tested in Tier 2 blinded study would be beyond the scope of this thesis, it would be beneficial to revalidate the failed NI drugs by retesting under chronic long-term exposure (≥24 hours).

However, it is a challenge to evaluate chronic studies in CellOPTIQ due to it not being an aseptic platform; hence cells are prone to infection by microbes. Therefore, some changes in SOPs were applied. In the short-term treatment: the baseline (before drug treatment) measurement and after drug treatment measurement was monitored from the same well at the same position. For the long-term treatment, the baseline reading before treatment was measured from the independent wells, not from the same well of drug treatment.

In addition, we were able to borrow a demo machine, the xCELLigence RTCA CardioECR (ACEA Biosciences), to carry our other longer-term exposure experiments to examine the impact of NIs on hiPSC-CM function.

5.1.4 RTCA CardioECR

The xCELLigence Real-Time Cell Analysis (RTCA) CardioECR System consists of four main components: 1) the 48-well electronic microtiter plate (E-Plate CardioECR 48), 2) RTCA CardioECR instrument, which accommodates cardio plate and is placed inside a 5% CO_2 37ºC tissue culture incubator, 3) RTCA CardioECR control unit, which operates the software and acquires data, and 4) RTCA Cardio analyser which connects the electronic signals between RTCA control unit and station (https://www.aceabio.com/products/rtca-cardioecr/)**(Figure 5.5)**. As the instrument is housed in a standard cell culture incubator, it allows a physiological and controlled environment during the whole

experimental time, especially in terms of the chronic effects of drugs. The instrument is capable of recording the impedance (surrogate measure of contraction) and field potential (integrated ion channel activity) simultaneously by using two different electrodes. Collectively, this offers a perspective of cardiomyocytes health, ion channel activity, contractility, enabling a more in-depth understanding of the mechanism underlying drug-induced liability for short (seconds) to long (days) time. It is claimed to be a high-throughput method for detecting functional and general *in-vitro* toxicity.

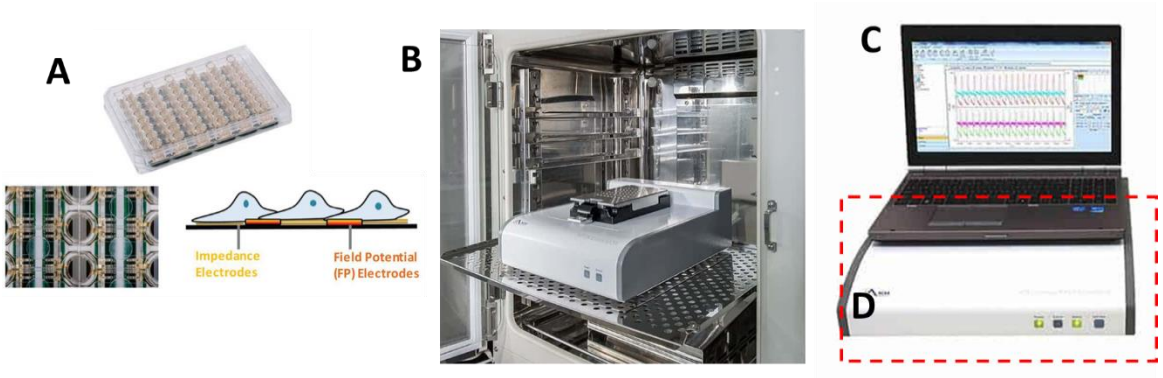


Figure 5.5: The components of xCELLigence Real-Time Cell Analysis (RTCA) CardioECR System.
(A) E-Plate CardioECR 48, a zoomed-in view of E-plate CardioECR 48 and graphic illustration of the interacting cells with impedance and field potential electrode**s, (B**) The RTCA CardioECR instrument which fits inside the CO_2 incubator **(C) The** RTCA CardioECR control unit which includes a computer and software and **(D) The** RTCA Cardio analyser.

5.2 Chapter aims and objectives

An accurate prediction in drug safety pharmacology is essential, especially during drug development, in order to prevent detrimental effects. A small improvement towards drug predictivity could have an enormous socioeconomic and 3Rs (replacement of animal use in experimentation) benefits. As such, predictivity refinement will facilitate the reuptake of hiPSC-CMs as a routine tool in safety pharmacology. In this chapter, the aim is to understand the incorrect assignment and discuss improvements made to the test platform by refining drugs predictivity. The following objectives had to be met to fulfil this aim:

8) Refine the culture conditions, with the aim of reducing the hiPSC-CM beat rate and improving the signal to noise ratio.

9) Conduct chronic exposure for up to ≥ 24 hours, with the aim of improving the predictivity of selected drugs.

10) Revalidate long-term exposure using RTCA CardioECR.

11) Compare the refinement results with the initial predictivity.

5.3 Results

5.3.1 Culture conditions refinement

Different culture conditions that may contribute to high beat rate and poor signal to noise were investigated, which include the state of hiPSC-CMs that had or had not undergone cryopreservation (termed here as 'cryo' vs 'fresh', respectively). In addition, different media compositions were investigated, as were possible ways to lower beat rate.

5.3.1.1 The beat rate in fresh vs cryo R-PAT-CMs

The beat rate between fresh and cryo R-PAT-CMs in the normal culture of RPMI-B27 was investigated. As such, no difference was found regarding the beat rate between both fresh (1.1 ± 0.07Hz) and cryo (1.1 ± 0.04Hz) R-PAT-CMs **(Figure 5.6).**

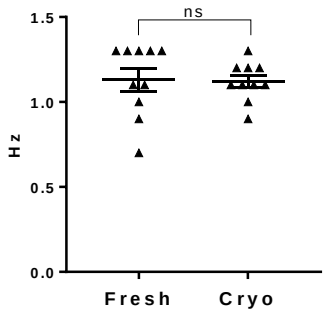


Figure 5.6: No difference in spontaneous beating rates between fresh and cryo R-PAT-CMs.
The spontaneous baseline recordings were evaluated in R-PAT-CMs monolayers cultured in RPMI-B27; no difference was observed between fresh and cryo CMs. Statistics: Mann Whitney, n=10.

5.3.1.2 Ivabradine lowered beat rate

In order to lower the spontaneous beat rate to be < 1 Hz, different concentrations of ivabradine were tested (0, 0.3, 1, 3, and 10 µM). The R-PAT-CMs were incubated for 3 hours with respective ivabradine concentrations, and their spontaneous beat rate after ivabradine treatment were measured. The CMs were paced based on adapted frequency guidelines to determine if cells could be correctly triggered. Ivabradine at the lowest 0.3 µM significantly decreased the spontaneous beat rate to 0.8 1± 0.04 Hz, comparable with other highest ivabradine concentrations of 1 µM(0.87 ± 0.05 Hz), 3 µM(0.84 ± 0.06 Hz) and 10 µM (0.74 ± 0.02 Hz) (**Figure5.7A**).

In terms of different effects of ivabradine concentration to contractility parameters, there were no significant effects on CA, CT or RT compared to the vehicle (0 µM (No) Iva) (**Figure5.7B, C, D**). In summary, the optimum ivabradine concentration to lower the beat rate was at 0.3 µM. This concentration could be prepared in a final concentration of DMSO of 0.003%; together with drug or vehicle control, the final concentration of DMSO is 0.103%, low enough for this solvent not to cause any adverse effects on hiPSC-CM function. The maximum concentration of DMSO that should be used for dilution purposes without causing any effect on osmolarity, pH, cell death or electrophysiological parameters in hiPSC-CMs was suggested at 0.3% (Hyun et al., 2017).

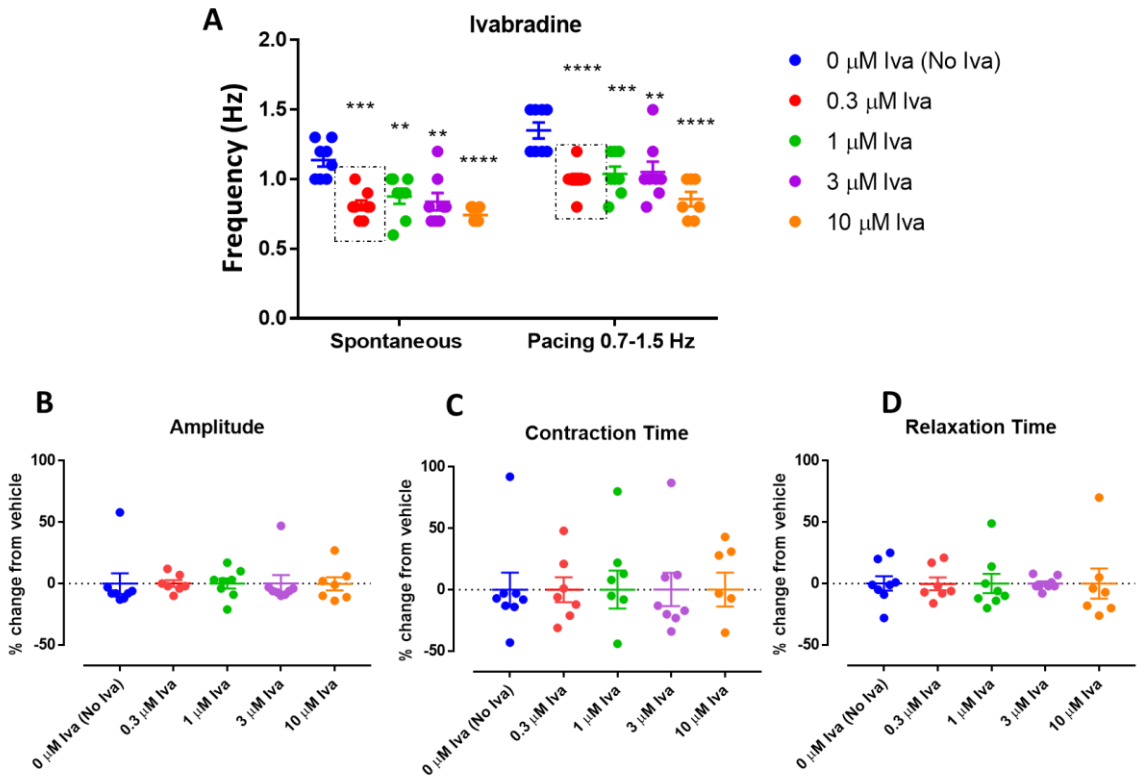


Figure 5.7: The ivabradine decrease spontaneous beating rates without changing contraction parameters.

By using CellOPTIQ platform, spontaneous baseline recordings were evaluated in R-PAT-CM monolayers treated with different concentrations of ivabradine, with 3 hours incubation **(A)** The spontaneous beating rate significantly decreased across a range of ivabradine concentrations. **(B)** No difference in contraction amplitude. **(C)** No difference in contraction time**(D)** No difference in relaxation time. All data are mean ± SEM, n=6-8. Statistical analysis was carried out using one-way ANOVA with Dunnett's multiple comparison test vs vehicle control (0 μM (N0) Iva). Significance tests were based on p-values as follows: * $p < 0.05$; ** $p < 0.01$; *** $p < 0.001$; **** $p < 0.0001$

5.3.1.3 Medium composition: Protein vs Protein-Free

In the blinded test, the assay was carried out in a serum/protein-free medium (SFM) to avoid protein-drug binding that may affect (blunt) the responses within the *in-vitro* system. However, it is hypothesised that the SFM medium composition in CellOPTIQ may have contributed to the poor signal to noise ratio, high spontaneous beat rate and hence low predictivity of PI drugs. To investigate this, experiments were conducted in RPMI-B27 (protein-containing) and SFM media (24-hour media changed prior to CellOPTIQ measurement). The spontaneous beat rates of each well of each condition were then measured, including CA, CT and RT. Switching from RPMI-B27 to SFM increased the beat rate from 0.7 Hz to ≥ 1.2 Hz, resulting in adaptive frequency pacing of 0.9 Hz for RPMI-B27 and ≥1.5 Hz pacing for SFM cultures **(Figure 5.8A**). Concurrently the variance spread of data for R-PAT-CMs in protein-containing RPMI-B27 versus protein-free SFM medium was reduced 12.1 vs 32.8, 14.5 vs 20.1 and 10.7 vs 26.9; respectively for CA, CT and RT. The variance was reduced in the protein-containing medium **(Figure 5.8B, C, D).** In summary, the inclusion of B27 supplement into RPMI medium as a source of protein has improved signal to noise ratio in the CellOPTIQ:hiPSC-CM combination compared to serum/protein-free conditions.

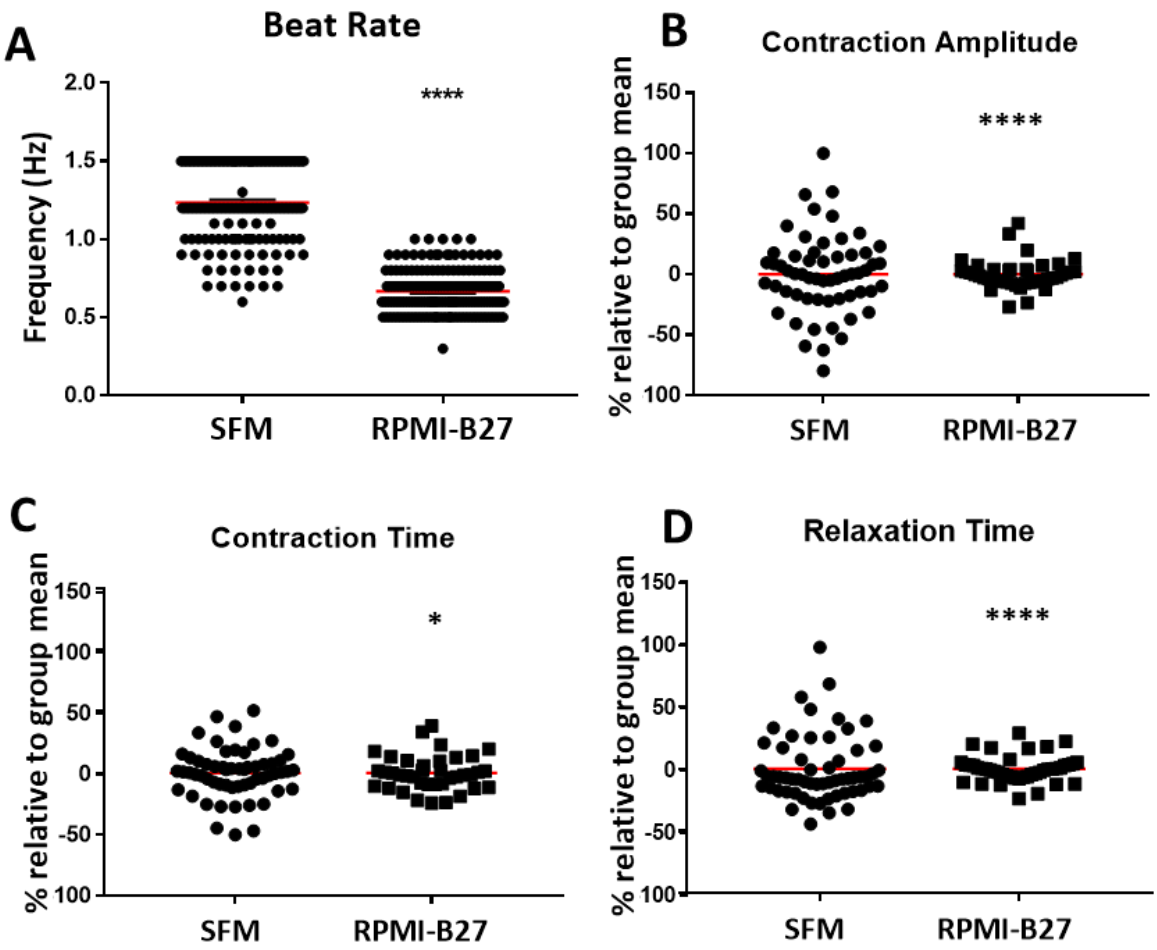


Figure 5.8: The protein-free medium (SFM) increases spontaneous beating rates and data distribution.
By using CellOPTIQ platform, spontaneous baseline recordings were evaluated in R-PAT-CMs monolayers cultured in protein-free medium (SFM) versus the protein-containing medium (RPMI-B27). **(A)** The spontaneous beating rate significantly increased in SFM (Statistical: Mann Whitney). **(B)** The variance of data distribution increased in SFM for CA parameter. **(C)** The variance of data distribution increased in SFM for CT parameter. **(D)** The variance of data distribution increased in SFM for RT parameter. Statistical analysis for variance distribution was carried out using F-test for the variance. Significance tests were based on p-values as follows: * $p < 0.05$; ** $p < 0.01$; *** $p < 0.001$; **** $p < 0.0001$.

5.3.1.4 Summary of culture condition refinement for R-PAT-CMs

Both ivabradine and protein-containing media were successful in reducing the beat rate. However, the protein-containing medium also tightened-up the data and increased the signal to noise ration, whilst not needing additional treatment with the pharmacological blockade of the I_f current. Therefore, the use of the protein-containing medium was selected as the method of choice in the refinement experiments. The SOP was changed to accommodate these improvements. As such, a refined SOP for CellOPTIQ: R-PAT-CMs combination to measure contractility was established **(Table 5.1)**(the modifications to the previous SOPs are highlighted in yellow);

Table 5.1: Refined contractility Standard Operating Procedures (SOPs) for R-PAT-CMs testing in CellOPTIQ.

	Protocol	CellOPTIQ® (CO)
Starting conditions	Format	96-well plate
	Age	• Differentiation time +10 day-old (R-PAT-CMs)
	Culture medium	• Standard culture medium (R-PAT-CMs)
	Quality control	• Cell purity >90% by a-actinin (R-PAT-CMs) • Spontaneous beat rate of ≤0.9 Hz, if more than ≥1 Hz: incubate with 0.3 µM Ivabradine for 3 hours • Response to 30 nM nifedipine
Experimental set-up	Medium	• 1.8 mM Ca DMEM Gibco#11966 + 10mM Galactose + 1mM NaPyr (serum/protein-free) • For R-PAT-CMs Voltage: 24h before assay changed media into SFM and assay conducted in 100%SFM • For R-PAT-CMs Contractility: Assay conducted in 100% RPMI-B27
	Cell loading	FluoVolt in independent well from contractility assay
	Recording: Baselines	Paced at 0.7-1 Hz; 10 sec/area
	Recording: Conc-response curves	Replicates: 5 wells/conc + time matched vehicle controls
		Solvent: max 0.1% DMSO
		Treatment duration: 30 mins
		Dosage: 5 concentrations in semi-logarithmic steps, single concentration/well
		Readings: Paced as follows: ≤0.5 Hz → 0.7 Hz; ≤0.7 Hz → 0.9 Hz; ≤0.9 Hz → 1.0 Hz
Follow-up	Analysis	Analysis is performed off line using CellOPTIQ software
	Recovery	n/a
	Repeat testing	No repeated use of cells

5.3.2 Retesting under the refined conditions

As the CellOPTIQ: R-PAT-CM combination proved poor predictive (0/8) for PI drugs in the previous blinded study, all 8 PI drugs were retested under refined conditions as described in the refined SOPs **(Table 5.1)**. The results are as follows in the next sections.

5.3.2.1 Refinement test: Epinephrine

Epinephrine did not change CA **(Figure 5.9)**. There was a significant decrease in CT (faster contraction) at a 1 µM (-39.2± 7.2%), and a significant decrease in RT (faster relaxation) at 0.3 µM (-32.03 ± 2.75%) and 1 µM (-37.78 ± 1.96%) **(Figure 5.9)**. In summary, the findings of R-PAT-CMs treated with epinephrine under refined conditions improved the accuracy of predictivity as PI due to decreased CT and decreased RT.

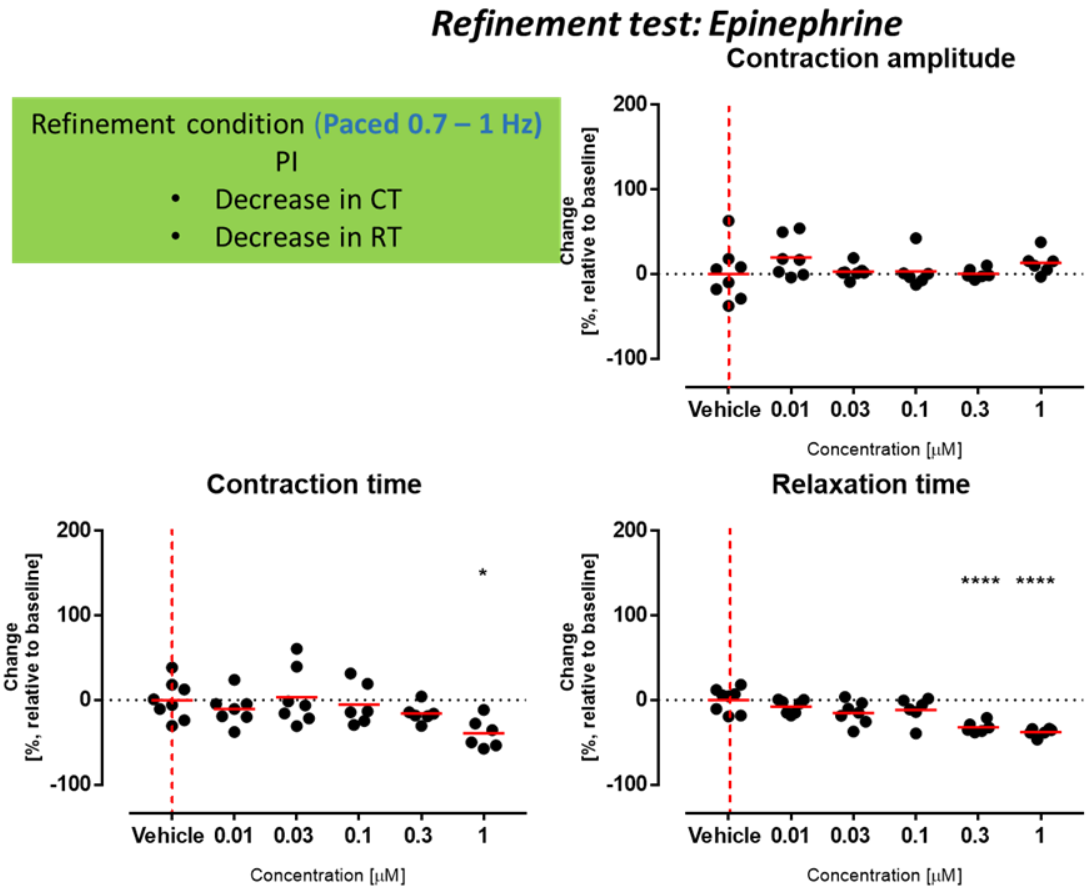


Figure 5.9: Epinephrine retesting in R-PAT-CMs under refined conditions. Significant decrease in CT and RT observed. All data are mean ± SEM, n=6-7. Statistical analysis was carried out using one-way ANOVA with Dunnett's multiple comparison test vs vehicle control. Significance tests were based on p-values as follows: * $p < 0.05$; ** $p < 0.01$; *** $p < 0.001$; **** $p < 0.0001$.The red dotted line is free therapeutic plasma concentration (FTPC).

5.3.2.2 Refinement test: Forskolin

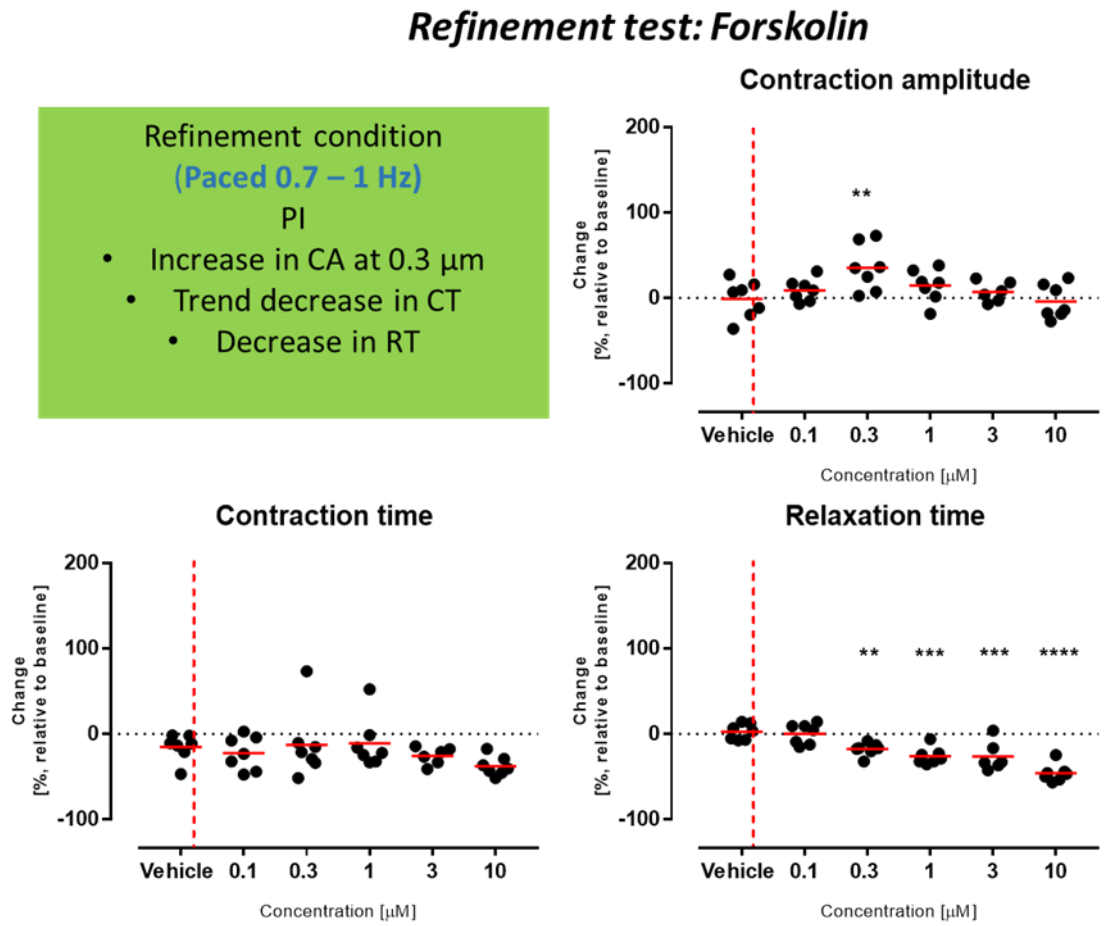


Figure 5.10: Forskolin retesting in R-PAT-CMs under refined conditions. Significant increase in CA, decrease in CT and decrease in RT observed. All data are mean ± SEM, n=6-7. Statistical analysis was carried out using one-way ANOVA with Dunnett's multiple comparison test vs vehicle control. Significance tests were based on p-values as follows: * $p < 0.05$; ** $p < 0.01$; *** $p < 0.001$; **** $p < 0.0001$.The red dotted line is free therapeutic plasma concentration (FTPC).

Forskolin did not have an obvious effect on CA, but did significantly increase this parameter at 0.3 µM=+35.4 ± 10.36% **(Figure 5.10)**. CT trended towards faster contraction (reduced CT) starting from 0.3 µM (-12.56 ± 15.23%), 1 µM (-10.99 ± 11.31%), 3 µM (-25.63 ± 4.09%) and 10 µM (-37.6 ± 4.30%). RT significantly decreased (faster relaxation) at 0.3 µM (-17.7 ± 2.77%), 1 µM (-25.9 ± 3.72%), 3 µM (-26.3 ± 6.98%) and 10 µM (-45.83 ± 3.91) **(Figure 5.10)**. In summary, the findings of R-PAT-CMs treated with forskolin under refined conditions improved accurate predictivity as PI due to increased CA, decreased CT and decreased RT.

5.3.2.3 Refinement test: Levosimendan

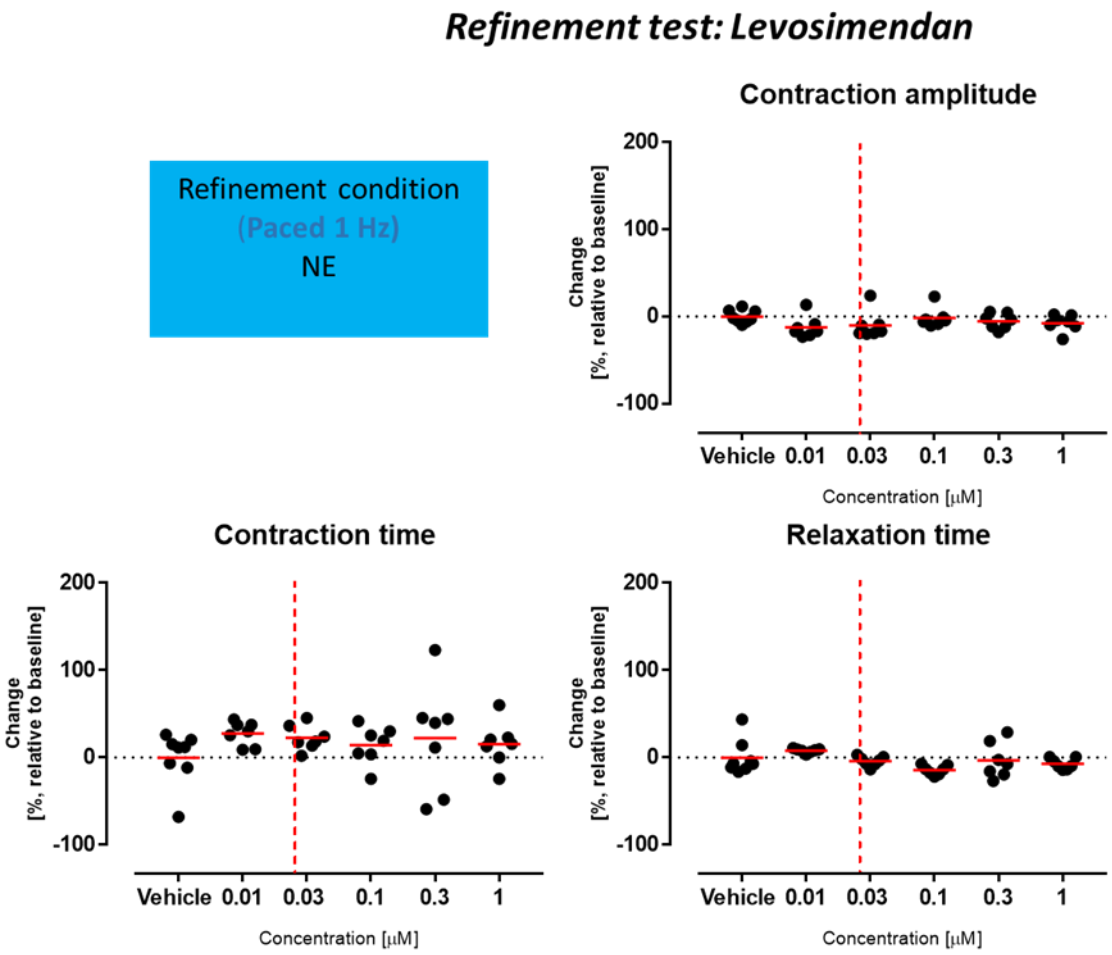


Figure 5.11: Levosimendan retesting in R-PAT-CMs under refined conditions. No significant change in CA, CT or RT observed. All data are mean ± SEM, n=6-7. Statistical analysis was carried out using one-way ANOVA with Dunnett's multiple comparison test vs vehicle control. Significance tests were based on p-values as follows: * $p < 0.05$; ** $p < 0.01$; *** $p < 0.001$; **** $p < 0.0001$.The red dotted line is free therapeutic plasma concentration (FTPC).

Levosimendan did not cause any significant change in CA, CT or RT at concentrations of 0.01, 0.03, 0.1, 0.3 and 1 μM **(Figure 5.11)**. In summary, R-PAT-CMs treated with levosimendan under refined conditions does not improve predictivity as it remains as NE.

5.3.2.4 Refinement test: Pimobendan

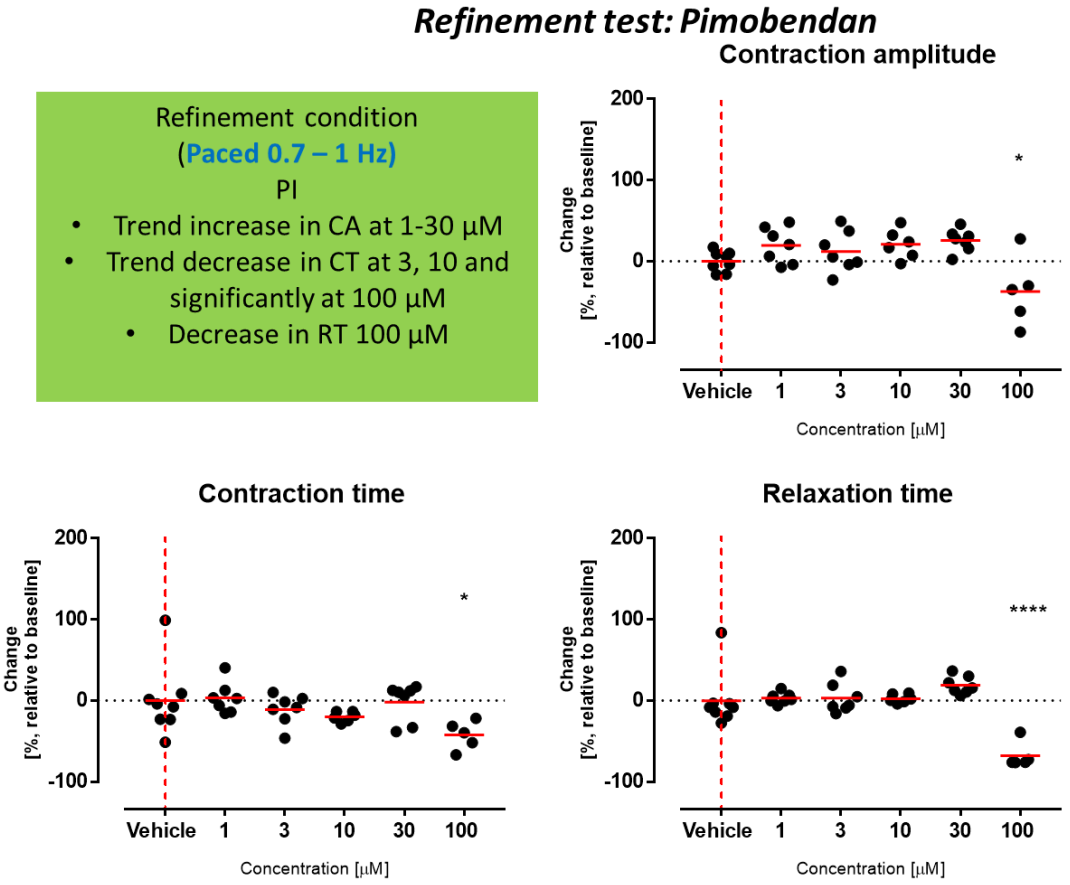


Figure 5.12: Pimobendan retesting in R-PAT-CMs under refined conditions. A trend increase in CA, decreased in CT and decreased in RT observed. All data are mean ± SEM, n=6-7. Statistical analysis was carried out using one-way ANOVA with Dunnett's multiple comparison test vs vehicle control. Significance tests were based on p-values as follows: * $p < 0.05$; ** $p < 0.01$; *** $p < 0.001$; **** $p < 0.0001$.The red dotted line is free therapeutic plasma concentration (FTPC).

Pimobendan does tend towards increased CA starting from concentration 1 to 30 µM, with decreased CA at the highest concentration of 100 µM **(Figure 5.12)**. A trend of decreased CT with significant change at 100 µM= -42.32 ± 7.87% was observed and decreased RT with significant change at 100 µM= -67.96 ± 7.25%. **(Figure 5.12)**. In summary, the findings of R-PAT-CMs treated with pimobendan under refined conditions does improve predictivity as PI due to increased CA (trend), decreased CT and decreased RT.

5.3.2.5 Refinement test: Dobutamine

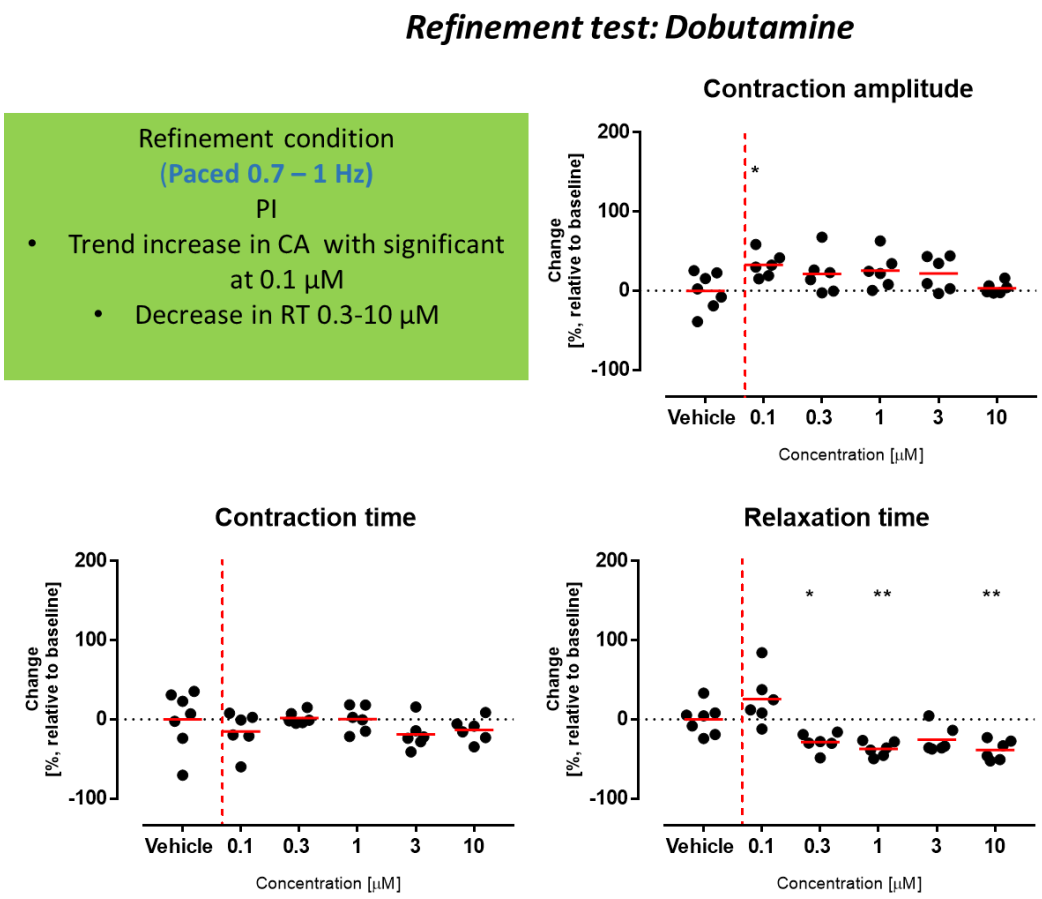


Figure 5.13: Dobutamine retesting in R-PAT-CMs under refined conditions.

Trends showing a significant increase in CA, and decrease in RT observed. All data are mean ± SEM, n=6-7. Statistical analysis was carried out using one-way ANOVA with Dunnett's multiple comparison test vs vehicle control. Significance tests were based on p-values as follows: * $p < 0.05$; ** $p < 0.01$; *** $p < 0.001$; **** $p < 0.0001$.The red dotted line is free therapeutic plasma concentration (FTPC).

Dobutamine did trend towards increased CA starting from a concentration of 0.1 to 3 µM, with significant value at 0.1µM= +32.75 ± 6.48% **(Figure 5.13)**. CT was unchanged, while RT significantly decreased at 0.3 µM= -28.6 ± 4.69%, 1 µM= -37.37 ± 3.77%, 10 µM= -38.78 ± 5.14% **(Figure 5.13)**. In summary, the findings of R-PAT-CMs treated with dobutamine under refined conditions does improve predictivity accuracy as PI due to increased CA (significant trend) and decreased RT.

5.3.2.6 Refinement test: Milrinone

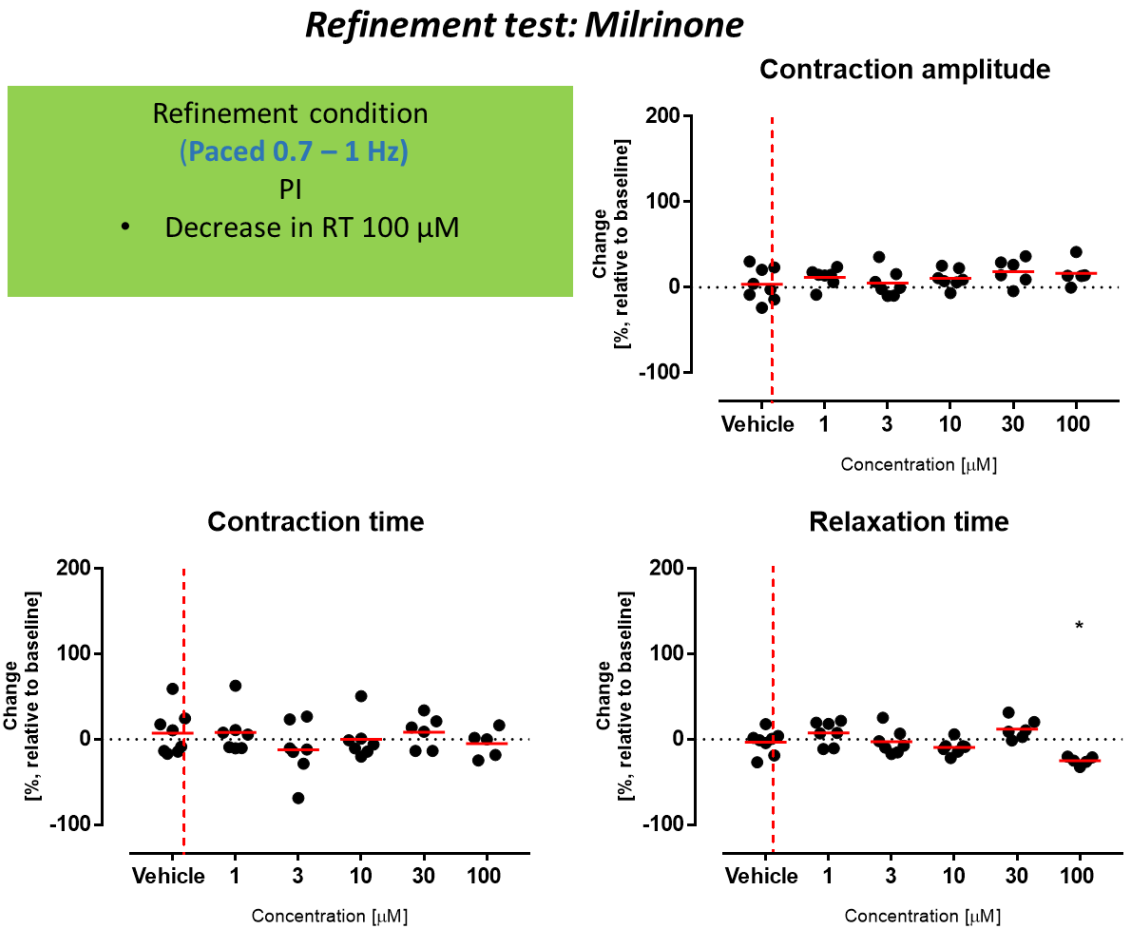


Figure 5.14: Milrinone retesting in R-PAT-CMs under refined conditions.

No changes in CA and CT, decrease in RT observed. All data are mean ± SEM, n=6-7. Statistical analysis was carried out using one-way ANOVA with Dunnett's multiple comparison test vs vehicle control. Significance tests were based on p-values as follows: * $p < 0.05$; ** $p < 0.01$; *** $p < 0.001$; **** $p < 0.0001$.The red dotted line is free therapeutic plasma concentration (FTPC).

Milrinone did not cause any significant changes or trends related to CA or CT. **(Figure 5.14)**, but there was a significant decrease for RT at 100 µM= -24.92 ± 2.17% **(Figure 5.14)**. In summary, the findings of R-PAT-CMs treated with milrinone under refined conditions did improve predictivity as PI due to decreased RT.

5.3.2.7 Refinement test: Omecamtiv Mecarbil

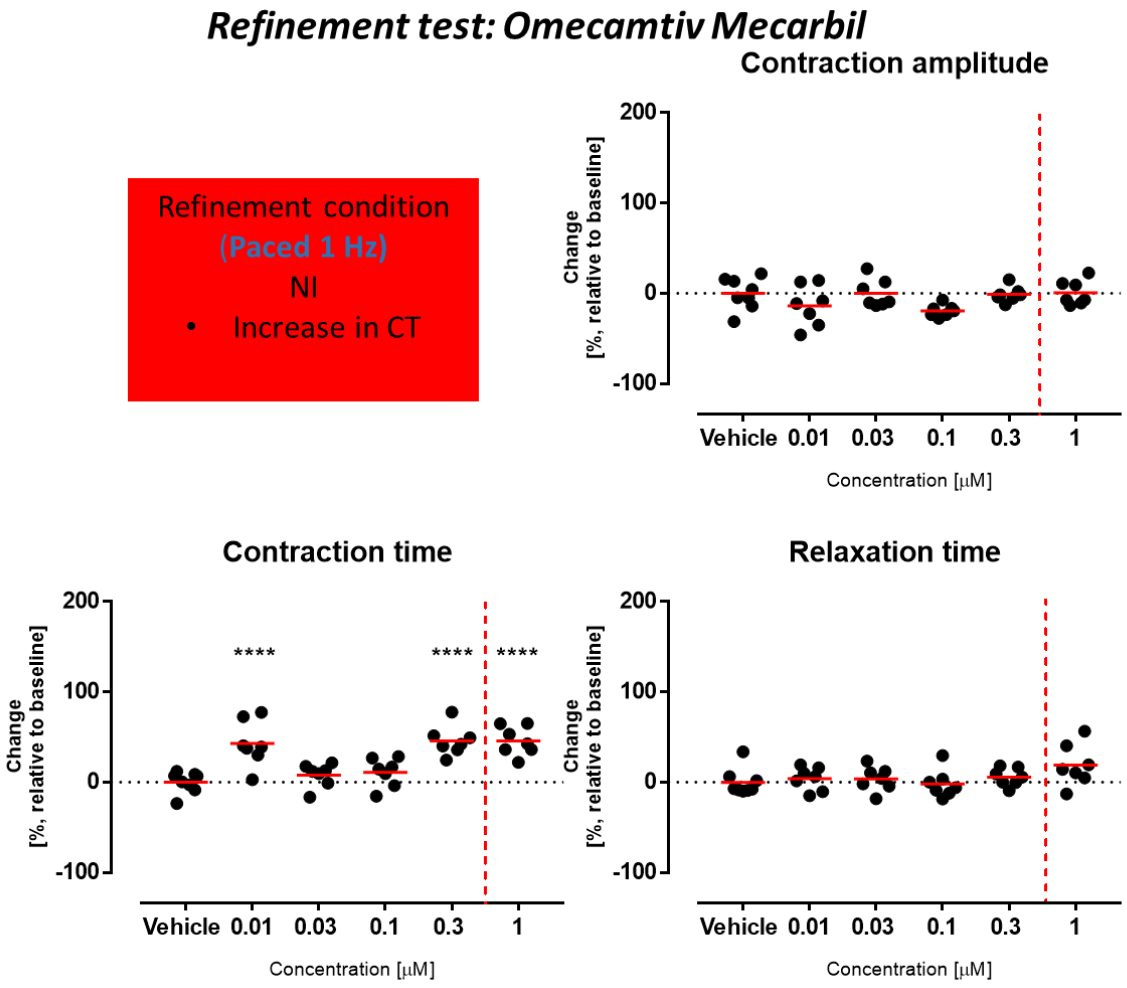


Figure 5.15: Omecamtiv mecarbil retesting in R-PAT-CMs under refined conditions.
No significant changes in CA or RT observed. A significant change with increase in trend for CT.All data are mean ± SEM, n=6-7. Statistical analysis was carried out using one-way ANOVA with Dunnett's multiple comparison test vs vehicle control. Significance tests were based on p-values as follows: * $p < 0.05$; ** $p < 0.01$; *** $p < 0.001$; **** $p < 0.0001$.The red dotted line is free therapeutic plasma concentration (FTPC).

Omecamtiv mecarbil did not cause any significant change in CA or RT at concentrations of 0.01, 0.03, 0.1, 0.3 and 1 µM. Significant changes were observed together with increased CT at concentrations of 0.01 µM=+42.84 ± 4.88%, 0.3 µM= +45.83 ± 6.26%, 1 µM= -45.76 ± 6.08% **(Figure 5.15)**. In summary, the findings of R-PAT-CMs treated with omecamtive mecarbil under refined conditions did not improve predictivity as it predicted NI.

5.3.2.8 Refinement test: Terbutaline

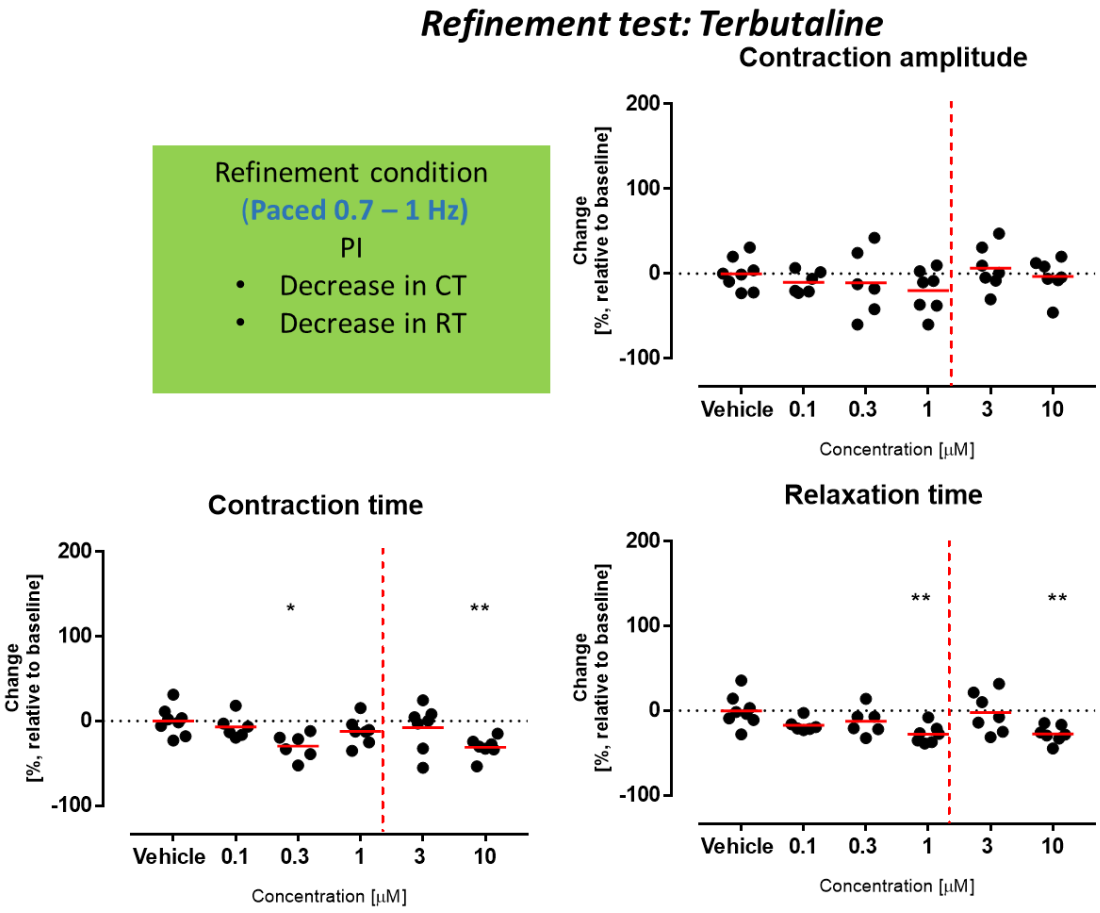


Figure 5.16: Terbutaline retesting in R-PAT-CMs under refined conditions. Significantly decreased in CT and RT observed. All data are mean ± SEM, n=6-7. Statistical analysis was carried out using one-way ANOVA with Dunnett's multiple comparison test vs vehicle control. Significance tests were based on p-values as follows: * $p < 0.05$; ** $p < 0.01$; *** $p < 0.001$; **** $p < 0.0001$.The red dotted line is free therapeutic plasma concentration (FTPC).

Terbutaline did not have any effects on CA **(Figure 5.16)**. There was a significant decrease in CT at concentrations of 0.3 µM= -29.53± 6.07%, and 10 µM -30.94 ± 4.46%. There was a significant decrease in RT at 1 µM= -27.7± 4.1%, and 10 µM= -27.4 ± 3.84%) **(Figure 5.16)**. In summary, the findings of R-PAT-CMs treated with terbutaline under refined conditions did improve accurate predictivity as PI due to decreased CT and decreased RT.

5.3.2.9 Retesting outcomes under refined conditions

The outcomes from PI drugs retesting under refined conditions are tabulated in Table 5.2. In these revised testing conditions, out of 8 PI drugs, 6/8 were correctly predicted as PIs as 6/8 showed reduced CT and/or RT **(Table 5.2),** consistent with previous indicators, wherein contraction and relaxation time were informative for positive inotropes. Also, it was proven that lowering beating frequencies associated well with increased predictivity for PI drugs. Thus, before the refinement 0% accuracy was obtained, while after refinement 75% accuracy was obtained for CellOPTIQ:R-PAT-CMs combination.

Table 5.2: The details R-PAT-CMs retesting of Tier 2 positive inotrope (PI) drugs: the outcomes under refined conditions.

Drug	The main mechanism of action	Cellular mechanism of inotropic effect	GSK assignation	T2 blinded outcome	Retest outcome
Epinephrine	Non-selective α1-, β1- and β2-adrenoceptor agonist	Increase in cAMP, Ca^{2+} influx, SR Ca^{2+} uptake and SR load	**PI**	**NE**	**PI Decreased CT Decreased RT**
Forskolin	Adenylyl cyclase stimulator	Increase in cAMP, Ca^{2+} influx, SR Ca^{2+} uptake and SR load		**NE**	**PI Increased CA; 0.3 µM Decreased CT Decreased RT**
Levosimendan	PDE3 inhibitor (IC_{50} 25 nM) Calcium sensitizer K_{ATP} channel agonist	Increase in cAMP and myofilament sensitization to Ca^{2+}		**NE**	**NE**
Pimobendan	Calcium sensitizer PDE inhibitor (partial)	Increase in cAMP and myofilament sensitization to Ca^{2+}		**NE**	**PI Increased CA (trend); 1-30 µM Decreased CT Decreased RT**
Dobutamine	α1-, β1- and β2 adrenoceptor agonist	Increase in cAMP, Ca^{2+} influx, SR Ca^{2+} uptake and SR load		**NE**	**PI Increased CA (trend); 0.1 µM Decreased RT**
Milrinone	PDE3 inhibitor	Increase in cAMP, Ca^{2+} influx, SR Ca^{2+} uptake and SR load		**NE**	**PI Decreased RT**
Omecamtiv mecarbil	Cardiac specific myosin activator	Increased number of myosin heads binding to actin		**NI**	**NI Increased CT**
Terbutaline	β2-adrenoceptor agonist	Increase in cAMP, Ca^{2+} influx, SR Ca^{2+} uptake and SR load		**NE**	**PI Decreased CT Decreased RT**
Total correct (Accuracy)				**0/8 (0%)**	**6/8 (75%)**

5.3.3 Long-term exposure of the drugs to improve NE outcomes

For NI drugs that were not correctly predicted based on contractility effects such as doxorubicin and sunitinib, their 30 minutes exposure to those drugs did alter the electrophysiological voltage. It was hypothesised that short 30 minute exposures to the NI drugs were not sufficient to cause changes in contractility, especially for action drugs with structural toxicant modes. As such it may be relevant to stimulate the CMs using a longer exposure time of ≥ 24 hours. The R-PAT-CMs were incubated for 24 hours in doxorubicin and sunitinib together with 24 hours vehicle (0.1% DMSO) control, and their contractility was assessed in CellOPTIQ. The analysis showed that the exposure to the highest concentration of doxorubicin **(Figure 5.17A)** and sunitinib **(Figure 5.17B)** for 24 hours led to a loss of contraction or cell death based on their CA (the most predictive marker for NI).

In summary, the short-term exposure to NI drugs perturbed the electrophysiology of hPSC-CMs, while the long-term exposure caused over toxicity and/or negative inotropy.

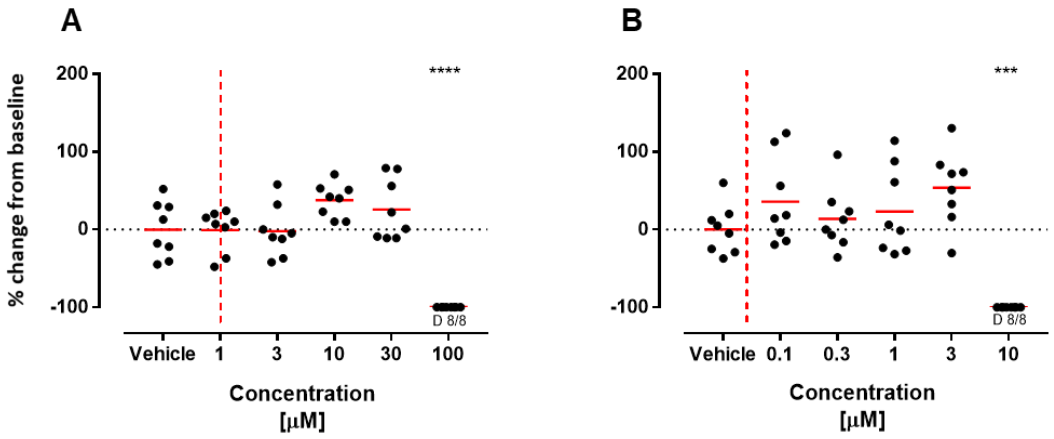


Figure 5.17: Prolonged exposure detects NIs in CellOPTIQ-R-PAT-CMs culture.
Contraction amplitude (CA) was measured in the CellOPTIQ platform-cell combination which exposed to various concentrations of **(A)** doxorubicin and **(B)** sunitinib for 24 hours, with the highest test concentration causing cell death. The red dotted line is free therapeutic plasma concentration (FTPC). CA is shown as normalized to time controls. Dunnett's stats vs vehicle control: *, P<0.05; **, P<0.01; ***, P<0.001; ****, P<0.0001.

5.3.4 RTCA CardioECR

In order to revalidate the long-term drug exposure, another platform was employed: the xCELLigence RTCA CardioECR (ACEA Biosciences) is capable of detecting real-time changes for a prolonged time. NI drugs (doxorubicin and sunitinib) and a PI drug (levosimendan) were selected as they were wrongly predicted in acute short-term treatment in CellOPTIQ, while a NE drug (acetylsalicylic acid) was selected as control. The drugs were applied at a high-concentration bolus, and their contractility was monitored 24 hours in RTCA CardioECR, with recording taken at 30 minutes, 2, 6, 12 and 24 hours after drug addition, according to the method described in subchapter 2.5. The measurements at each time points were taken under pacing condition of 0.7Hz, except for sunitinib which was carried out under spontaneous measurement as the machine was not able to pace the plate.

5.3.4.1 Doxorubicin (NI drug) long-term exposure by RTCA CardioECR

For readouts, the contractility traces at 0.7 Hz pacing show no alteration in contractility for vehicle control. However, for 100 µM doxorubicin, contractility reduced from 30 minutes to 6 hours and stopped beating at approximately 12 hours onwards **(Figure 5.18A),** which is also reflected in the beat rate recording **(Figure 5.18B)** The beat rates reduced at/after 12 and 24 hours of 100 µM doxorubicin addition; 12 hours = -77.17 ± 22.82% and 24 hours = -83.17 ± 16.84% **(Figure 5.18B).** The CA reduced after 6, 12 and 24 hours after drug addition with 6 hours = -57 ± 14.23%, 12 hours = -83.33 ± 16.67% and 24 hours = -91.5 ± 8.5% **(Figure 5.18C).** The CT was also reduced after 12 and 24 hours of drug addition, parallel with the beat rate as the cells stop beating; 12 hours = -92.5± 7.5% and 24 hours = -88.17 ± 11.83% **(Figure 5.18D)**. The RT increased (slower repolarisation) at 2 hours (+134.83 ± 30.93%) after drug addition **(Figure 5.18E)**.

In summary, the long-term exposure of 100 µM doxorubicin caused the cells to reduce in beat rate, CA and CT after 12 hours of drug treatment and increased in RT at 2 hours after treatment. As such, the R-PAT-CMs treated with doxorubicin were correctly predicted as NI after long-term exposure.

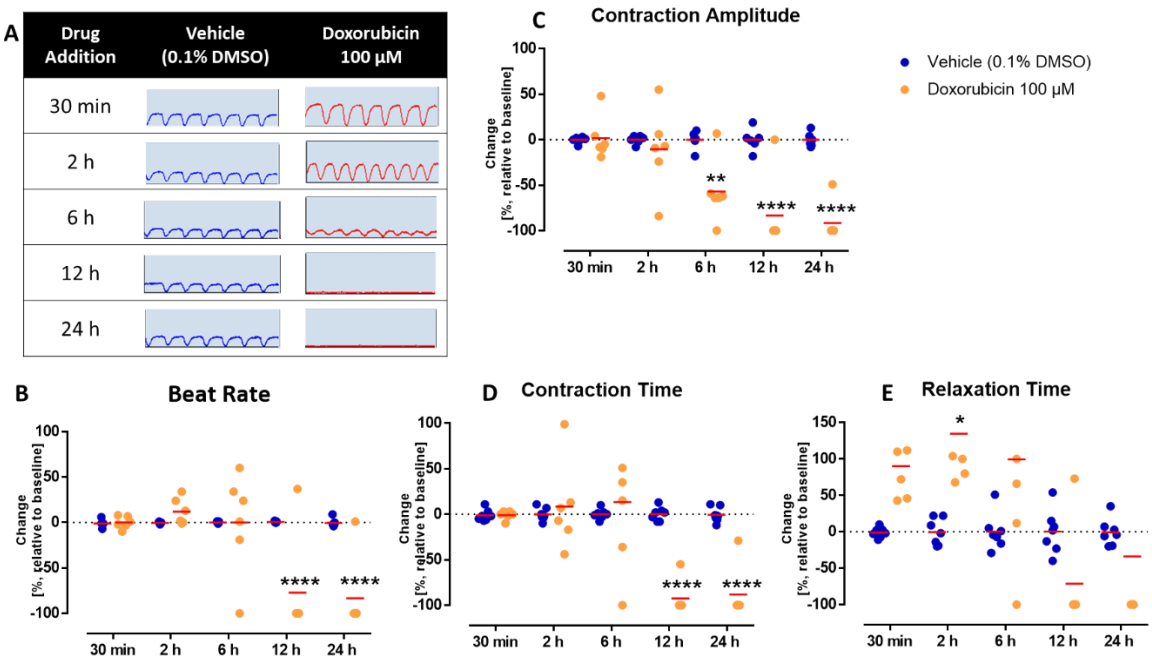


Figure 5.18: Contractility analysis of R-PAT-CMs treated with long-term exposure of the highest doxorubicin concentration (100 µM) in the RTCA CardioECR platform.
(A) Contractility traces **(B)** Beat rate **(C)** Contraction amplitude **(D)** Contraction time **(E)** Relaxation time . All data are mean ± SEM, n=6. Statistical analysis was carried out using two-way ANOVA with Sidak's multiple comparison test. Significance tests were based on p-values as follows: * $p < 0.05$; ** $p < 0.01$; *** $p < 0.001$; **** $p < 0.0001$.

5.3.4.2 Sunitinib (NI drug) long-term exposure by RTCA CardioECR

For readouts, the contractility traces under spontaneous contraction showed no alteration in contractility for vehicle control. However, at 10 μM sunitinib, the contractility reduced from 30 minutes to 2 hours and stopped beating at approximately 6 hours onwards **(Figure 5.19A),** which was also reflected in the beat rate recording **(Figure 5.19B)** The beat rates were reduced at 6, 12 and 24 hours after adding 10 μM sunitinib; 6 hours = -25 ± 48.29%, 12 hours = -100 ± 0% and 24 hours = -100 ± 0% **(Figure 5.19B).** The CA started to decline immediately after 30 minutes onwards; with 30 minutes = -55.67 ± 6.24%, 2 hours = -62.50 ± 5.09%, 6 hours = -97.33 ± 1.86%, 12 hours = -100 ± 0% and 24 hours = -100 ± 0% **(Figure 5.19C).** The CT also declined immediately 30 minutes after drug addition parallel with the heart rate and CA, as the cells were at a reduced beat; 30 minutes = -27.83 ± 3.87%, 2 hours = -48.50 ± 3.43%, 6 hours = -77.33 ± 14.99%, 12 hours = -100 ± 0% and 24 hours = -100 ± 0% **(Figure 5.19D)**. The RT was reduced after 12 hours as the cells stopped beating; 12 hours = -100 ± 0% and 24 hours = -100 ± 0% **(Figure 5.19E)**.

In summary, the long-term exposure of 10 μM sunitinib caused the cells to reduce in beat rate, CA and CT and/or RT after 30 minutes of drug treatment. As such the R-PAT-CMs treated with sunitinib correctly predicted as NI after long-term exposure.

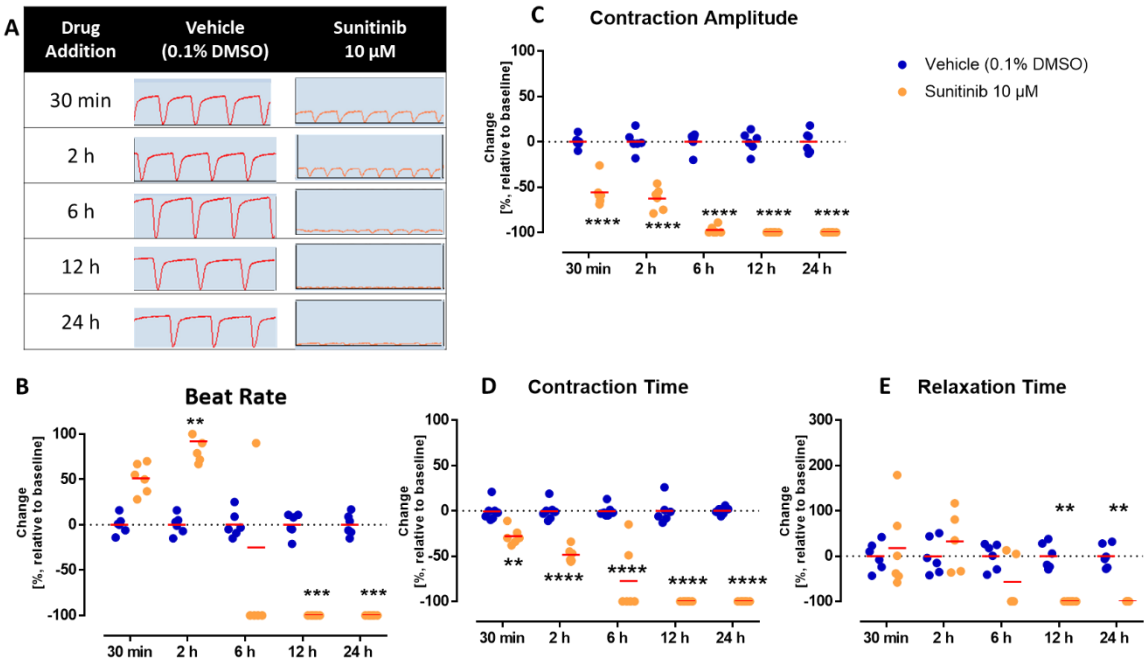


Figure 5.19: Contractility analysis of R-PAT-CMs treated with long-term exposure of highest doxorubicin concentration (100 µM) in RTCA CardioECR platform.

(A) Contractility traces (B) Beat rate **(C)** Contraction amplitude **(D)** Contraction time **(E)** Relaxation time . All data are mean ± SEM, n=6. Statistical analysis was carried out using two-way ANOVA with Sidak's multiple comparison test. Significance tests were based on p-values as follows: * $p < 0.05$; ** $p < 0.01$; *** $p < 0.001$; **** $p < 0.0001$

5.3.4.3 Levosimendan (PI drug) long-term exposure by RTCA CardioECR

Out of all PI drugs, levosimendan was selected for long-term exposure because testing under refined conditions failed to predict this drug correctly and it was assigned as NE (**Figure 5.11 and Table 5.2).** For readouts, the contractility traces at 0.7 Hz pacing showed no alteration in contractility for vehicle control **(Figure 5.20A)**. However, at 1 µM levosimendan, there was a trend towards increased beat rate from 6 to 24 hours, with significant increases at 24 hours (+19.4 ± 10.24%) after adding levosimendan **(Figure 5.20B).** Nonetheless, no changes in CA and CT were observed **(Figure 5.20C and D).** A trend towards increased RT was observed from 6 to 24 hours, with a significant change seen at 24 hours (+46.2 ± 19.58%) **(Figure 5.20E**). Since there were no changes in CA or CT but increases in RT, the levosimendan were classified as NE.

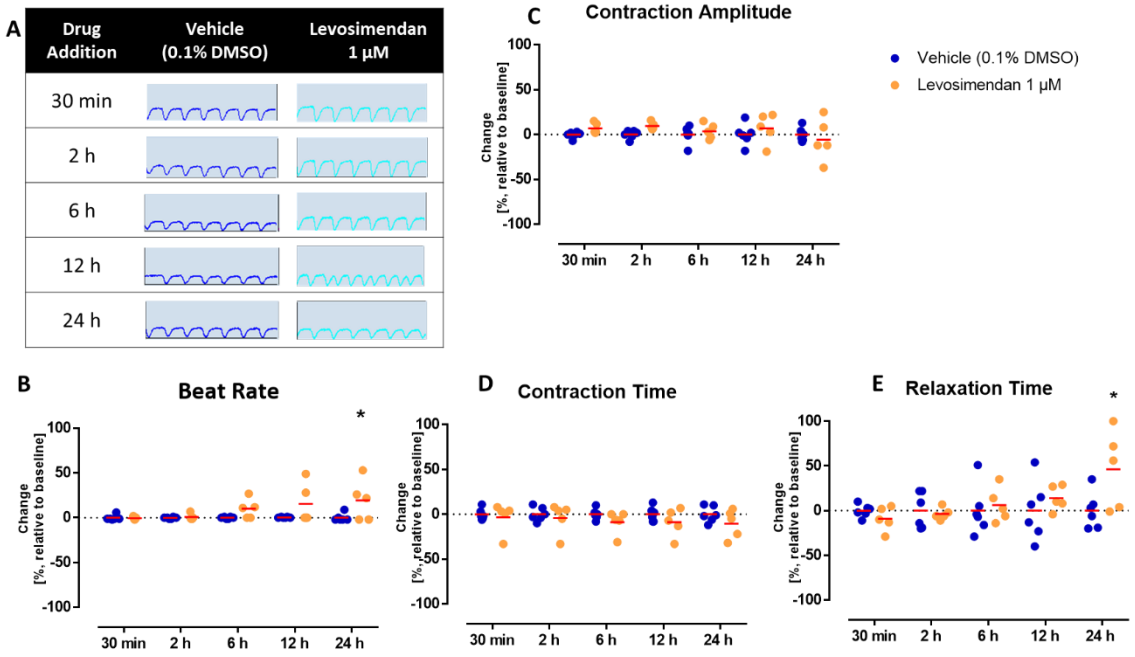


Figure 5.20: Contractility analysis of R-PAT-CMs treated with long-term exposure of highest levosimendan concentration (1 µM) in RTCA CardioECR platform.

(A) Contractility traces **(B)** Beat rate **(C)** Contraction amplitude **(D)** Contraction time (E) Relaxation time . All data are mean ± SEM, n=6. Statistical analysis was carried out using two-way ANOVA with Sidak's multiple comparison test . Significance tests were based on p-values as follows: * $p < 0.05$; ** $p < 0.01$; *** $p < 0.001$; **** $p < 0.0001$

5.3.4.4 Acetylsalicylic acid (NE drug) long-term exposure by RTCA CardioECR

For readouts, the contractility traces at 0.7 Hz pacing showed no alteration in contractility for vehicle control or 1000 µM acetylsalicylic acid at any time points, 30 minutes to 24 hours **(Figure 5.21A)**. No significant changes were observed from the beat rate **(Figure 5.20B)**, CA **(Figure 5.21C)**, CT **(Figure 5.21D)** or RT **(Figure 5.21E)**.

In summary, the long-term exposure of 1000 µM acetylsalicylic acid caused no significant changes in any of the contractility parameters at any time point and as such, R-PAT-CMs treated with acetylsalicylic acid correctly predicted as NE after long-term exposure.

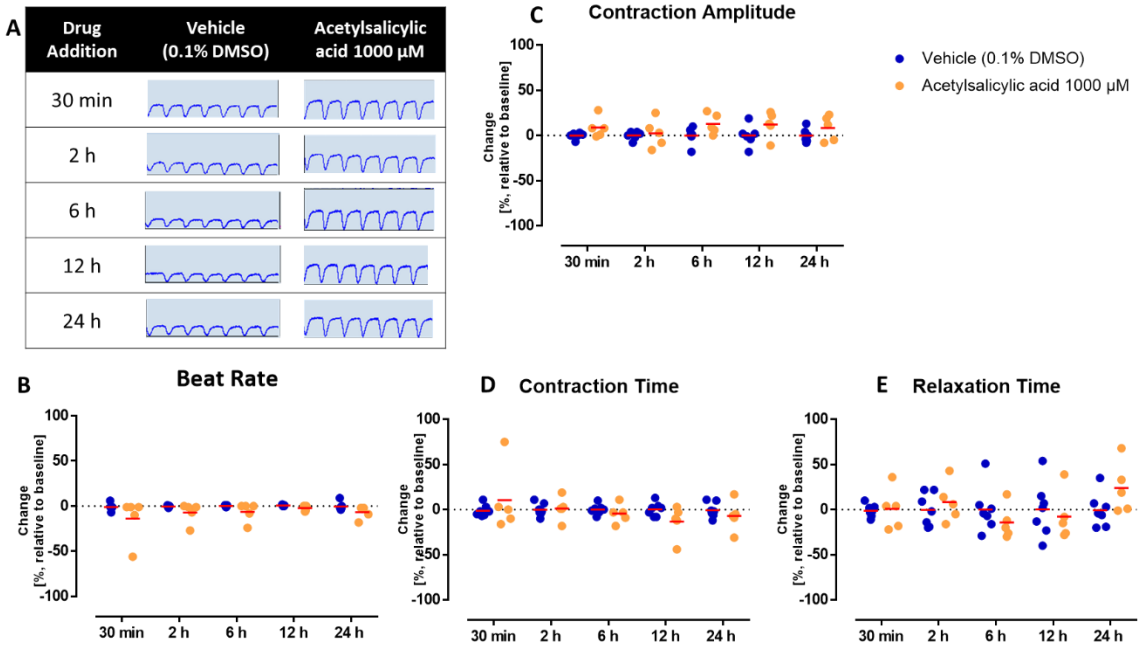


Figure 5.21: Contractility analysis of R-PAT-CMs treated with long-term exposure of highest acetylsalicylic acid concentration (1000 µM) on the RTCA CardioECR platform.
(A) Contractility traces **(B)** Beat rate **(C)** Contraction amplitude **(D)** Contraction time **(E)** Relaxation time **.** All data are mean ± SEM, n=5. Statistical analysis was carried out using two-way ANOVA with Sidak's multiple comparison test. Significance tests were based on p-values as follows: * $p < 0.05$; ** $p < 0.01$; *** $p < 0.001$; **** $p < 0.0001$.

5.3.4.5 Long-term exposure outcomes under the RTCA CardioECR platform

The outcomes from retesting under long-term drugs exposure in real-time RTCA CardiECR are tabulated in **Table 5.3**. In these revised conditions, out of 4 drugs, 3/4 were correctly predicted **(Table 5.3).** As such, assessing the function between short-term (30 minutes) to long-term (24 hours) exposure could improve prediction of the drugs. Thus, short-term exposure gave 25% accuracy, while long-term exposure gave 75% accuracy.

Table 5.3: The long-term exposure to drugs on the RTCA CardioECR platform and their respective outcomes.

Drug	The primary mechanism of action	Cellular mechanism of inotropic effect	GSK assignation	T2 blinded outcome	Retest outcome
Doxorubicin	Impairs Ca^{2+} transport mechanisms in sarcoplasmic reticulum	Complex, including increased mitochondrial ROS	**NI**	**NE**	**NI**
Sunitinib	Multi-targeted TK inhibitor	Complex	**NI**	**NE**	**NI**
Levosimendan	PDE3 inhibitor (IC_{50} 25 nM) Calcium sensitizer K_{ATP} channel agonist	Increase in cAMP and myofilament sensitization to Ca^{2+}	**PI**	**NE**	**NE**
Acetylsalicylic acid	Cyclooxygenase inhibitor	Not available⁺	**NE**	**NE**	**NE**
Total correct (Accuracy)				**1/4 (25%)**	**3/4 (75%)**

5.4 Chapter discussion

Like any other models, the CellOPTIQ platform does also have limitations. One of the limitations is the inability to test the effect of drugs at frequencies above 1 Hz to uncover frequency-dependent contractility risk of inotropes (Butler et al., 2015). The refinement discussed in this chapter aimed to improve prediction. Principally by comparing fresh and cryo CMs, there was no difference in regards to the beat rate between these two, the fresh and cryo CMs **(Figure 5.6)**. This demonstrates that the feasibility of cryo CMs for drug safety and discovery were not affected. Cryo CMs are preferable due to their scalability, ease of transportation within labs and ease of use, since the timing of cell differentiation does not need to be coordinated with drug testing experiments.

However, in the cryo, spontaneous beat rates were still above ≥1 Hz, which resulted in adapted the pacing frequency of ≥1.2Hz.To reduce the beat rates in order to improve predictability as suggested by Butler (Butler et al., 2015), the cryo cultures were further treated with different concentrations of ivabradine as suggested by Mannhardt (Mannhardt et al., 2016) for 3 hours. By using the different concentration of 0.3- 10 μM ivabradine, the spontaneous beating frequency was decreased to around 0.8 Hz **(Figure 5.7).** The finding is parallel with the previous finding in EHTs where spontaneous beating decreased, albeit with complete inhibition at 1 μM (Mannhardt et al., 2016).

Poor predictability was also hypothesised to be due to the poor signal-to-noise ratio on the CellOPTIQ platform in addition to the high beat rate (≥1.5Hz). By substituting the serum/protein-free medium with a protein-containing medium, the beat rate and the signal-to-noise issue were improved **(Figure 5.8).** The spontaneous beat rate should be <1 Hz, which can be achieved by modifying the culture medium or by using pharmacological blockage with ivabradine and/or selecting hPSC-CMs with slow intrinsic rates. The combination of ivabradine (required only if spontaneous beat ≥1Hz) and serum/protein-containing medium (RPMI-B27), new SOPs **(Table 5.1)** were designed and used for R-PAT-CMs retesting under refined conditions.

The refined system was further reassessed for PI drugs and 6/8 of PI drugs showed reduction in CT and/or RT **(Table 5.2)**, thus enhancing the accuracy and

prediction of PIs on CellOPTIQ: R-PAT from 0 to 75%. This indicates that the benefits of protein-containing media outweigh the concerns over drug binding and batch to batch variations of protein ingredients. Nevertheless, the FluoVolt interacts with proteins and reduces the signal-to-noise ratio, which makes the simultaneous recording of contraction and voltage problematic. However, this can be overcome by independent measurements of contraction and voltage (in different independent wells) or by measuring extracellular voltage.

The retesting was further conducted for failed to predict NI drugs. Acute 30 minute doxorubicin treatments caused changes in electrophysiology (refer to subchapter 4.4.7.8; Rank 8; Doxorubicin treatment (NI)) and gave a distinctive response compared to NE such as acetylsalicylic acid (refer to subchapter 4.4.7.5 Rank 5; Acetylsalicylic Acid (NE)). However, the acute 30-minutes exposure did not cause changes in inotropy for doxorubicin, which further suggests that it is essential to examine the appropriate concentration and/or drugs incubation time (van Meer et al., 2019, Jacob et al., 2016). By increasing exposure time from 24 hours to 7 days, doxorubicin and sunitinib were revealed as negative inotropes, which is consistent with an extended period in which the cardiotoxicity presents clinically and in previous studies using Tyrosine Kinase Inhibitors (TKI) (Jacob et al., 2016). In the retesting data across five concentrations of doxorubicin after 24 hours exposure in CellOPTIQ, at the both highest concentration of doxorubicin (100 µM) and sunitinib (10 µM), there were decreases in CT with cell death **(Figure 5.17)**. However, 24 hours exposure of less concentrated doxorubicin (10-30 µM) and sunitinib(0.1-3 µM) resulted in an increased trend of CA **(Figure 5.17)**. This is consistent with the study showing that the effects of doxorubicin are complex in that transient positive inotropy is followed by strong negative inotropy at higher concentrations (Kim et al., 1980, Vanboxtel et al., 1978, Wang and Korth, 1995).

To revalidate the long-term exposure of drugs under the highest concentration which caused the significant effects, the doxorubicin and sunitinib were further tested at their bolus concentration and monitored at 30 minutes, 2, 6, 12 and 24 hours after drug addition, using the real-time RTCA CardioECR platform. As such the CA was found to be significantly reduced after 6 hours and R-PAT-CMs stopped beating (cell death) after 12 hours of drug exposure **(Figure 5.18).** For

sunitinib, the CA immediately stopped after 30 minutes and cell death occurred after 6 hours of drug addition **(Figure 5.19).** The changes in cell-substrate adhesion in both doxorubicin and sunitinib in RTCA CardioECR has given the impression of increases in beat rate because the cells move more freely due to fewer anchor points with the substrate. Relative to the baseline, the heart rate increased initially but then decreased as time progressed.

Revalidation in RTCA CardioECR was also further conducted for levosimendan by retesting under the refined condition of an acute assay, it failed to detect changes in inotropy **(Figure 5.11)**. Therefore the drug exposure time was increased to up 24 hours to verify if the drug had chronic effects. However, under long-term exposure to bolus drug concentration, levosimendan failed to show any significant trend in inotropic effects based on CA but increased in RT after 24 hours of drug addition **(Figure 5.19). The** Levosimendan mechanism of actions involved combining action between a calcium sensitiser on myofilaments (binds to cardiac troponin), PDE3 inhibitor and opening of ATP dependent potassium K^+ channels, which results in multiple pharmacological effects of the compound (Orstavik et al., 2014b, Wallis et al., 2015, Yokoshiki et al., 1997). Nonetheless, the chronic long-term effects of drugs are much more complex as they involve the mechanism of desensitisation and other secondary pharmacological effects which might be cell- line dependent. Therefore, due to the complexity of drug-cell interaction, differential effects can occur depending on the concentration and time, and as such, categorising as PI, NI or NE were rather tricky**.** Unless categorising includes the combination of beat rate and amplitude to determine potency values of effects on hiPSC-CMs, as suggested by Scott et al. (2014), levosimendan could be categorised as PI as the beat rate increased after 24 hours exposure to 1 μM levosimendan(Scott et al., 2014) **(Figure 5.19).** Scott et al. (2014) also suggested that an increase in beat rate with little if any effect on amplitude may suggest the strongest connection with cellular signalling pathway rather than *in-vivo* classification (PI or NI). On the other hand, Scott et al. (2014) demonstrated that levosimendan was challenging to predict as PI in neonatal rat CMs and therefore classified as NE, in line with findings in this chapter.

Long-term exposure under RTCA CardioECR improved accuracy from 25% to 75% **(Table 5.3).** Therefore, to revise and improve prediction, it is worth repeating the experiments under new refined SOPs with long-term exposure of wrongly predicted drugs, at different time point measurements with a different concentration range. However, this could only be carried out in RTCA CardioECR as CellOPTIQ is labour intensive**.** In addition, the CardioECR system permeates a more mechanistic interpretation of acute and chronic exposure effects as it records the beat rate based on the cell index. However, the cost of a single-use RTCA CardioECR that consist of 48 well plates is about £300 per plate (2019 price lists), which is considerably more than for the CellOPTIQ platform, which uses a standard tissue culture plate. As suggested by Guth et al. (2019), the ideal platforms for early screening of preclinical drug development must be reasonably high throughput, cost-effective and provide mechanistic information of a given drug (Guth et al., 2019b).

As such, modifying the culture conditions and drug exposure time has allowed the accuracy of prediction using R-PAT-CMs to be increased to 75%, comparing favourably with what is currently possible in in-vivo animal models (Valentin et al., 2009). As a whole, the hPSC-CMs could be expected to be used in routine testing of whether the potential drugs have inotropic effects on CMs and in future tests and practice, both short-term and longer-term experiments should be carried out as supported by the data.

Chapter 6 : Genome-edited hESC (hPSCs) as Tools to Study the Functionality of ßeta$_2$-adrenergic Receptor Polymorphisms

6.1 Introduction

Many vertebrates' physiological and pathophysiological function are based on the G-protein coupled receptors (GPCRs) signal transduction. The GPCRs, also known as the seven-transmembrane (7TMRs) superfamily, contain seven membrane helices with an extracellular N terminal connected by three extracellular loops, three intracellular loops and an intracellular C terminal (Katritch et al., 2013). They consist of ~800 members of membrane receptors that activate heterotrimeric guanosine triphosphate (GTP) binding proteins (G proteins) following the binding of a ligand (Foord et al., 2005). The binding subsequently triggers responses; for example, in the brain process, vision, olfaction, immune and cardiovascular systems (Rosenbaum et al., 2009). GPCR targets are used to treat numerous conditions such as asthma, neurological disorders and cardiac malfunction, making them known as the largest clinically relevant family of target in the human genome, which represents 50% of the therapeutic drug target (Garland, 2013). Ligands directed to GPCRs represent nearly 30% of currently available clinical pharmaceutical agents, thus generating at least $180 billion of annual sales worldwide (Lundstrom, 2006, Santulli et al., 2013, Culhane et al., 2015, Hauser et al., 2018).

Increased understanding about the structure, molecular, genetic variations, and functional mechanism of GPCRs will not only benefit people with interest in cell signalling but also provide potential for new drug discoveries **(Figure 6.1)** (Insel et al., 2007) and ensure that both current and new drugs are safe and effective when reaching the consumer/patients. At the same time, due to natural genetic variation(s) in GPCRs, individual responses to the same medication might differ **(Figure 6.1)**. For instance, beta-blockers (ß-blockers), which are widely used in treating cardiovascular and non-cardiovascular disease, and also represent the 4th most frequently prescribed medicine on the market, is influenced by genetic variation within the beta-adrenergic receptors (ßARs)(Cresci et al., 2012, Nagele

and Liggett, 2011). Consequently, this leads to the need for pharmacogenomics studies that investigate how differences in the gene affect cell function and individual responses to drugs.

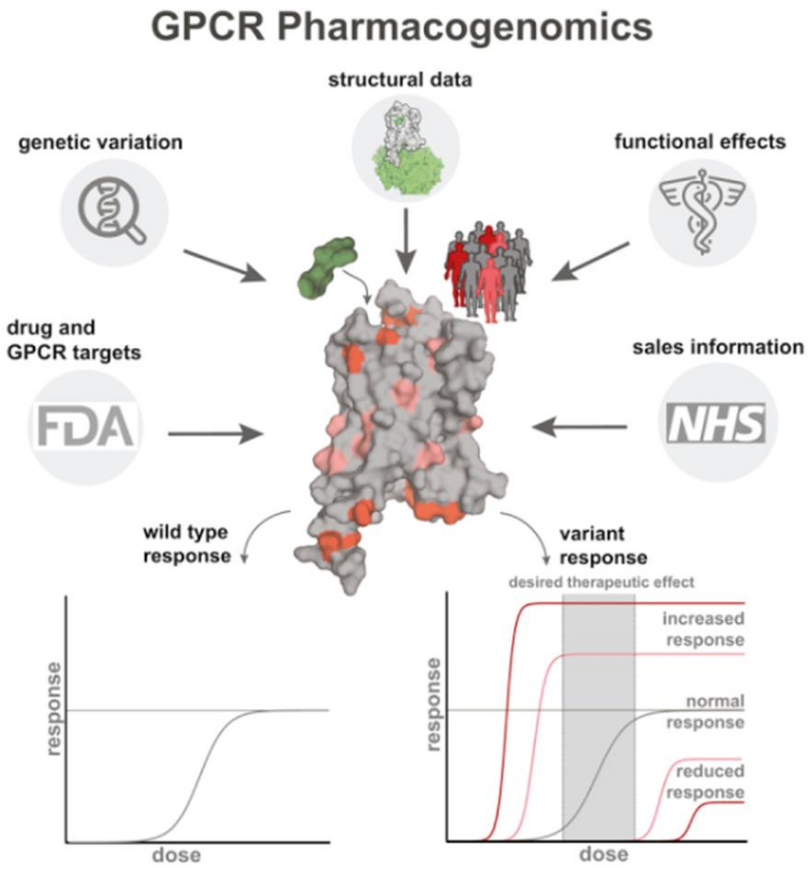


Figure 6.1: Schematic diagram of GPCR pharmacogenomics.
Genetic variation in GPCRs is one of the factors that contribute to the different variant responses. Picture obtained from (Hauser et al., 2018)

6.2 ßeta-adrenergic receptors (ßARs)

The ßARs are one of GPCRs grouping found on the human heart (de Lucia et al., 2018). The human ventricle heart has both beta1 ($ß_1$) and beta2 ($ß_2$) receptors, with predominantly about 80% of $ß_1$ subtype, while the other 20% is $ß_2$ (Bristow et al., 1986). Meanwhile, in the human atrium, the representation of $ß_1/ß_2$ ratio is 60%/40% (Brodde, 1991). Mechanically, the $ß_1$AR subtype appears to activate the Gs (stimulatory) solely, while $ß_2$AR behaviour is based on duet signalling that

includes both Gs (stimulatory) and Gi (inhibitory) (Salazar et al., 2007). Gs and Gi contribute to engagement and disengagement of the ßAR as the metabolic demand changes. In the heart, both $ß_1$AR and $ß_2$AR that are activated by ligand/catecholamines such as epinephrine and norepinephrine, are coupled via Gs, which in turn stimulate adenylyl cyclase (AC) and catalysing leads to the increased formation of the intracellular amount of cyclic 3',5'- adenosine monophosphate (cAMP) — thus activating the Gs-AC-cAMP cascade (Xiao, 2001). The elevated cAMP contributes to distinct downstream signalling, where $ß_1$ leads to cardiac contractility, while $ß_2$ contributes to the relaxation of smooth muscle on cardiac blood vessels and bronchial passages (Lohse et al., 2003).

6.2.1 ß-blockers

Therapeutically, ß-blockers are prescribed to antagonise the effects of ßARs stimuli by reducing systolic blood pressure, heart rate and cardiac contractility (Dezsi and Veronika, 2017). They are often prescribed for patients who have heart failure and myocardial infarction to slow down the heart rate and reduce infarction size by lessening oxygen demand (Noble and Roffi, 2017). Nonetheless, the long term usage of ß-blockers leads to the upregulation of ßARs and their removal in some individuals, leading to a fourfold increase in myocardial infarction (Psaty et al., 1990).

6.2.2 ß-agonists

Conversely, ß-agonists are commonly used to treat asthma and chronic obstructive pulmonary disease (COPD) by exerting the opposite physiological effect to ß-blockers (Salpeter et al., 2004). As such, the activation of ßARs induces changes in myocardial metabolism, heart rate, systolic and diastolic function. Although their activation is essential for the regulation of circulatory homeostasis, their chronic stimulation has detrimental consequences (de Lucia et al., 2018). Therefore, ß-agonist treatment is associated with increased risk of adverse cardiovascular outcomes such as cardiac ischemia, heart failure and cardiomyopathy (Sears, 2002).

6.2.3 Inconsistency in therapeutic response

Although treatments that target βARs are possible, the patient's response to both β-blockers and β-agonists are variable. Commonly, some individuals respond well, while others fail to respond to drug treatment. Also, some patients survive more than ten years, while others survive less than a year after being given the same medication (Pereira et al., 2010). These create challenges in regulating the standard treatment and subsequently, make it very difficult to tell how the condition will progress on an individual basis.

For years it has been known that differences in the magnitude of physiological responses, expression and function of GPCRs (including βARs), display distinct interindividual variation within the human population (Small et al., 2003). These differential interindividual responses may exist due to many factors such as the severity of the disease, comorbidities, treatment compliances, combination of drug-drug interactions, age and environmental factors (Hauser et al., 2018). Indeed, it has been estimated that 70% of the inconsistency in therapeutic response and safety to drugs is due to genetic variability (Cho, 2010).

Genetic variation includes gene polymorphism (single nucleotide polymorphism; SNP) or associated haplotypes. Polymorphism is a term that defines a variation in the DNA sequence that occurs with an allele frequency of >1% in the population (Karki et al., 2015, Ahles and Engelhardt, 2014). A polymorphism is different from a mutation. Mutations are rare variants which are necessary and sufficient for the disease. While polymorphisms may not affect, or have effects that are clinically silent but can be described with physiological testing and can act to modify diseases or ultimately, can alter the response to therapy (Small et al., 2003).

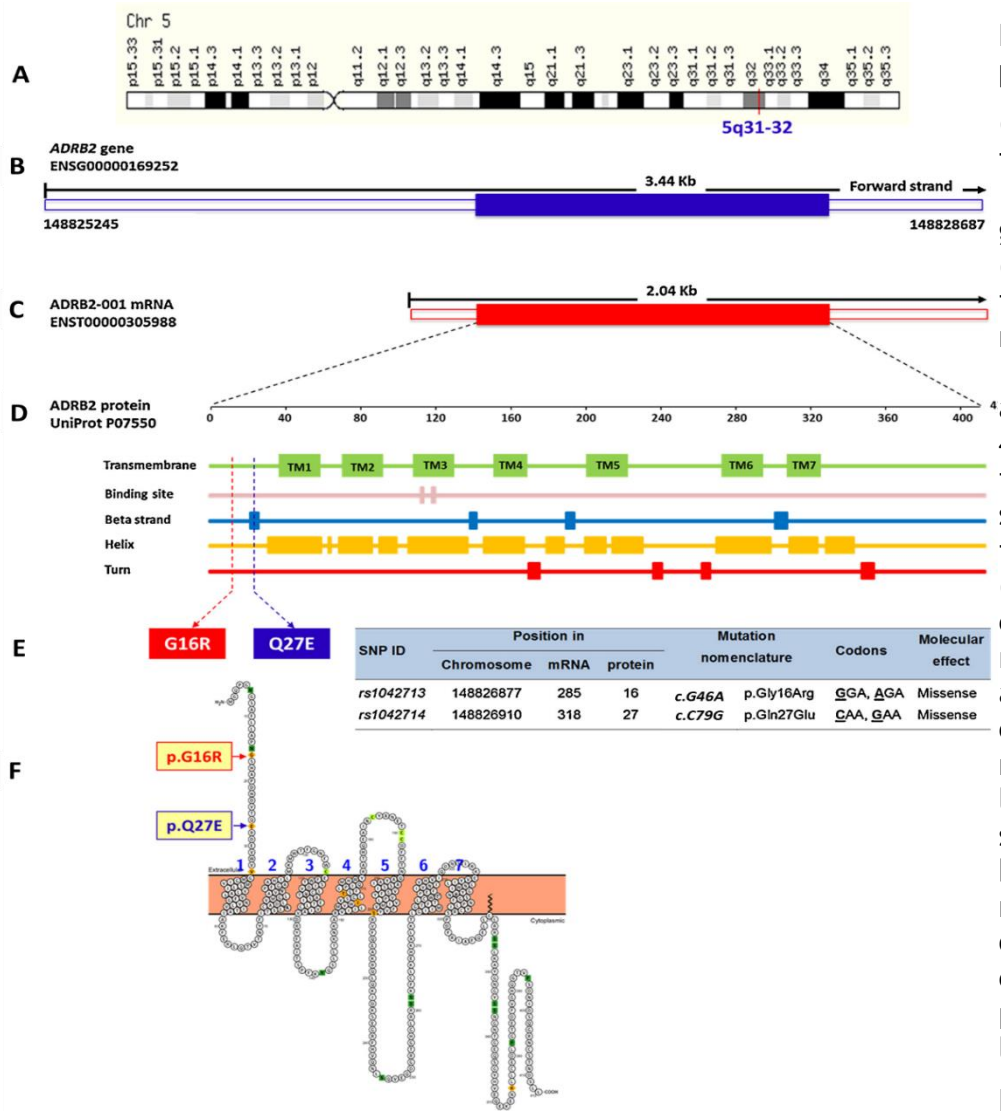
Since there are many reports on individual differences in regards to β_2-agonists which include a reduction in response or drug tolerance (tachyphylaxis), albeit in asthma, (Liggett, 2000), the human β_2AR gene polymorphism in cardiac settings, particularly polymorphisms at codons 16 and 27, are worth investigating further (Israel et al., 2000).

6.3 Beta$_2$-adrenergic receptor (β_2AR) and their polymorphisms

The *ADRB2* gene comprises 3,443 base pairs which encode the 413 amino acids of human β_2AR and are located on chromosome 5 (5q31-32) **(Figure 6.2A)**(https://www.ncbi.nlm.nih.gov/gene/154, 2019). Several functional SNPs have been identified in β_2AR (Reihsaus et al., 1993, Hawkins et al., 2006). These include two codon polymorphisms located extracellularly in the N terminal domain at amino acid position 16 (rs1042713) and 27 (rs1042714), which cause polymorphic changes at bases 46 (*c.G46A*) and 79 (*c.C79G*) **(Figure 6.2E)**(Ahles and Engelhardt, 2014). This results in amino acid changes at position 16 of Glycine to Arginine (Gly16Arg; termed G16R from here onwards), and position 27 of Glutamine to Glutamic acid (Gln27Glu; Q27E) **(Figure 6.2F)** **(**https://www.ncbi.nlm.nih.gov/snp/).

The allele frequency of Arg16 is 49% for African-American, 46% for Caucasians and 59% for Asians. Meanwhile, the allele frequency of Glu27 is, 20% for African-American, 35% for Caucasian and 7% for Asian (Small et al., 2003, Taylor and Bristow, 2004). Uniquely, β_2AR polymorphisms exist in linkage disequilibrium (they occur preferentially together). According to the study by Hall *et al.*(2000) there is notable linkage disequilibrium between codons 16 and 27; the obvious example is individual homozygous for Glu27Glu, almost always present in pairing with Glycine in codon 16 (Gly16Gly)(Hall et al., 2000), so the end product is Gly16Glu27, which from now on is known as GE **(Table 6.1)**. On the other hand, individuals who are homozygous in Gln27Gln can pair with both Gly16Gly and Arg16Arg from codon 16, with the end product Gly16Gln27 and Arg16Gln27, known as GQ and RQ respectively. The Arg16Glu27 (RE) variant is extremely rare, and can only be found in less than 1% in the population (Pereira et al., 2010). When linkage disequilibrium occurs, the polymorphism might be associated with a particular disease or drug response, even though it is not contributing to the particular phenotype by itself, unless in tandem with the responsible polymorphism (Garland and Biaggioni, 2001).

Therefore it has been suggested that these β_2AR polymorphisms could be accountable for the variable response to cardiovascular disease, which will be explored further in the next subchapter.



SNP ID	Position in Chromosome	mRNA	protein	Mutation nomenclature		Codons	Molecular effect
rs1042713	148826877	285	16	*c.G46A*	p.Gly16Arg	GGA, AGA	Missense
rs1042714	148826910	318	27	*c.C79G*	p.Gln27Glu	CAA, GAA	Missense

Figure 6.2: **The β_2AR gene (OMIM=109690) with polymorphism at codon position 16 and 27.**

(A) The gene encoding β_2AR is located on chromosome 5q31-32 from position 148825245 to 148828687 in human (https://www.ncbi.nlm.nih.gov/gene/154, 2019). **(B)** The gene is 3443 bp long, intronless and contains single coding exon. **(C)** The gene includes 5' and 3' untranslated region (UTR) together with a single transcript on the forward strand of 2042 nucleotides, which within the protein-coding region spans of 1242 nucleotides. **(D)** The nucleotides, which encode the 413 amino acid peptide, comes with a molecular weight of 46.5kDa(Johnson, 2006). The green region indicates the transmembrane spanning domain; the pink region is the binding site for either agonist or antagonist (position 113 and 118), blue is beta-strand region, orange is alpha-helix while turns in red. **(E)** The two sites of studied polymorphisms are both located extracellularly in the amino (N) terminal domain. The SNP with reference no rs1042713 is located at codon 16; G16R represent amino acid substitution from glycine to arginine (Gly16Arg) caused by a substitution change of guanine to adenine (G>A) at nucleotide 46. While, The SNP with reference no rs1042714 is located at codon 27; Q27E represents the amino acid substitution from glutamine to glutamic acid (Gln27Glu) caused by a substitution change of cytosine to guanine (C>G) at nucleotide 79. **(F)** Schematic topology of human β_2AR, consists of an extracellular N terminal, 2 intracellular and 3 extracellular loops with an intracellular C terminal. The primary amino acid sequence of β_2 is shown in the circle; single-letter amino acid nomenclature is used.

Picture adapted from (Hussein et al., 2017)

Table 6.1: Summary of *ADRB2* polymorphisms at position 16 and 27. G(allele)=GGA(codon)/Gly/Glycine(amino acid); R = AGA/Arg/Arginine; Q=CAA/Gln/Glutamine; E= GAA/Glu/Glutamic Acid

	Codon	Amino Acid	Codon	Amino Acid	Variants (Allele)
Codon position	16		27		
Reference SNP cluster ID	RS1042713		RS1042714		
	GGA	Glycine (Gly16)	GAA	Glutamic acid (Glu27)	GE
	GGA	Glycine (Gly16)	CAA	Glutamine (Gln27)	GQ
	AGA	Arginine (Arg16)	GAA	Glutamic acid (Glu27)	RE
	AGA	Arginine (Arg16)	CAA	Glutamine (Gln27)	RQ

6.3.1 ß$_2$AR polymorphisms in relation to cardiovascular diseases

The ß$_2$AR is vital in cardiovascular (CV) health and for CV illness therapy. For instance, the level of cardiac adrenergic from increased ßAR signalling is used as a prognostic evaluation for chronic heart failure (Taylor and Bristow, 2004). In terms of the relationship between ß$_2$AR polymorphisms and cardiovascular disease, a study in 5000 elderly patients revealed that Glu27 lowers the risk of developing coronary events compared to Gln27, therefore suggesting a protective association with Glu27 (Heckbert et al., 2003).

In contrast, a study in idiopathic dilated cardiomyopathy found that Arg16 and Gln27 lower the risk of heart failure while Gly16 and Glu27 increase the risk of developing heart failure (Forleo et al., 2004). Interestingly, despite many suggestions regarding ß$_2$AR polymorphism and cardiovascular disease, a case-control study conducted in heart failure patients revealed that ß$_2$AR gene polymorphisms (Arg16Gly, Gln27Glu) have no association with increased risk of heart failure (Covolo et al., 2004). However, the case-control was rather small, which needs to be considered when interpreting the data.

To conclude, while ß$_2$AR at position 16 and 27 polymorphisms do appear to be involved in cardiovascular disease and might alter the response, the data are contradictory as to the role of each variant.

6.3.2 SSeta$_2$-adrenergic receptor (ß$_2$AR) signal transduction

Before discussing further the effect of ß$_2$AR polymorphisms on the response to treatment, an understanding of these receptor's signalling is needed. As previously mentioned, the common classical pathway for ß$_2$ is via Gs activation (stimulation of adenylyl cyclase; AC) and Gi activation (inhibition of AC) **(Figure 6.3).**

6.3.2.1 Gs protein binding via adenylyl cyclase cascade

Upon catecholamines binding, the receptor undergoes a conformational change, which involves the exchange of GTP for GDP on α subunit and hence causing the dissociation of the Gßγ monomer (Jastrzebska, 2013). Activation on Gs encourages stimulation of AC, which results in increased cAMP levels (Robison and Sutherland, 1971). This cAMP subsequently activates protein kinase A (PKA), which leads to the phosphorylation of target proteins involved in cardiac excitation-contraction (EC) coupling as described in **Figure 6.3**. The phosphorylates L-type calcium channels (LTCC), sarcoplasmic reticulum (SR), phospholamban (PLB), ryanodine receptor (RyR), troponin 1 and calcium regulatory proteins ultimately increase the force of the contraction and heart rate (Dorn, 2010) **(Figure 6.3)**.

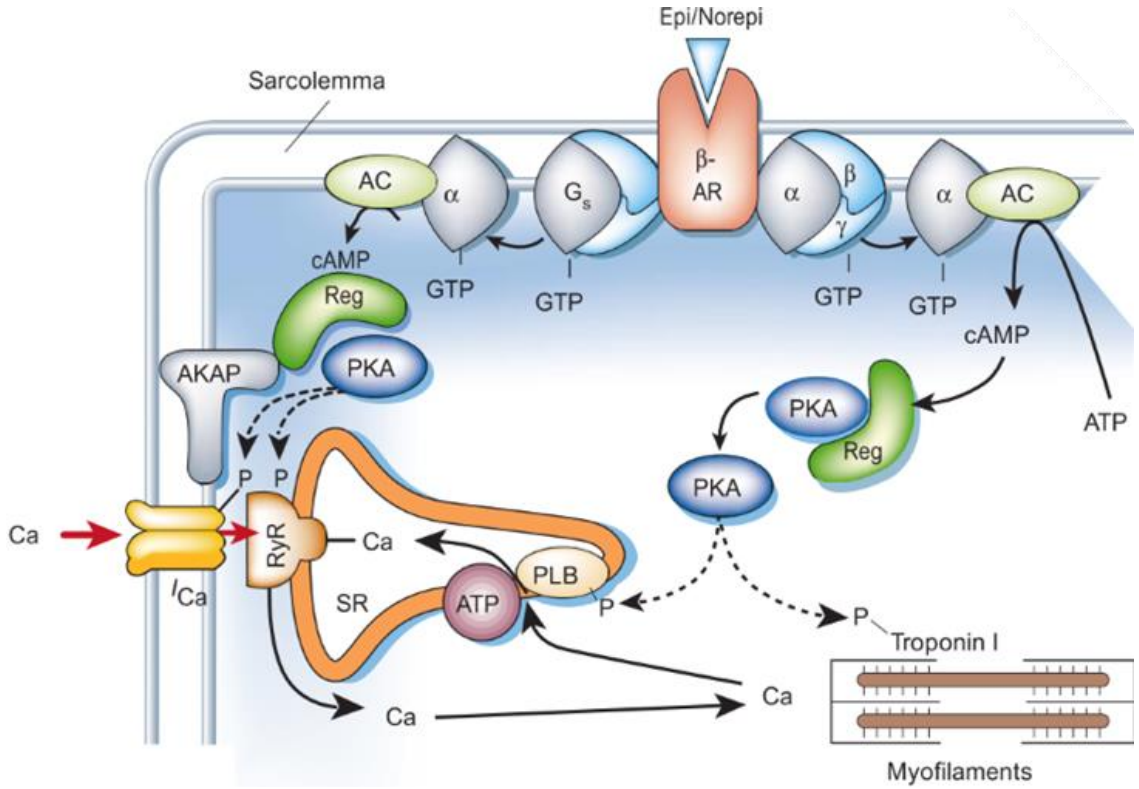


Figure 6.3: Schematic diagram ß-adrenergic receptor (βAR) via adenylyl cyclase signalling cascade.
The βAR stimulation by catecholamines epinephrine/norepinephrine (Epi/Norepi) induces coupling via Gs, which results in the α subunit binding to guanine triphosphate (GTP). The binding subsequently activates the adenylyl cyclase (AC) that elevate the generation of the second messenger cyclic adenosine monophosphate (cAMP) from adenosine triphosphate (ATP). The cAMP binds to the regulatory unit (Reg) on protein kinase A (PKA) and activates them. PKA then allow phosphorylation of different cell proteins such as on sarcoplasmic reticulum (SR) and voltage-gated channels (Ica), which promote an increase in the intracellular concentration of calcium (Ca). Calcium then binds to troponin 1 and promotes an increase in sarcomere contractility. PLB, Phospholamban; RyR, ryanodine; AKAP, A-kinase anchoring protein. Picture obtained from (Bers, 2002)

6.3.2.2 ßeta-arrestin mediated pathway

Other than the activation of downstream effectors by receptor-G protein binding, $ß_2$AR is also capable of activating a G-protein-independent pathway such as the ßeta-arrestin (ß-arrestin) mediated pathway **(Figure 6.4)**. The binding of ß-arrestin to the receptor leads to the uncoupling of the receptor from G-protein by phosphorylation, which is regulated by GPCR kinases (GRKs). ß-arrestin inhibits further G protein signalling by blocking GPCR-G protein interaction, thus promoting receptor desensitisation **(Figure 6.4)** (for recycling or lysosomal degradation). (Leftowitz and Shenoy, 2005).

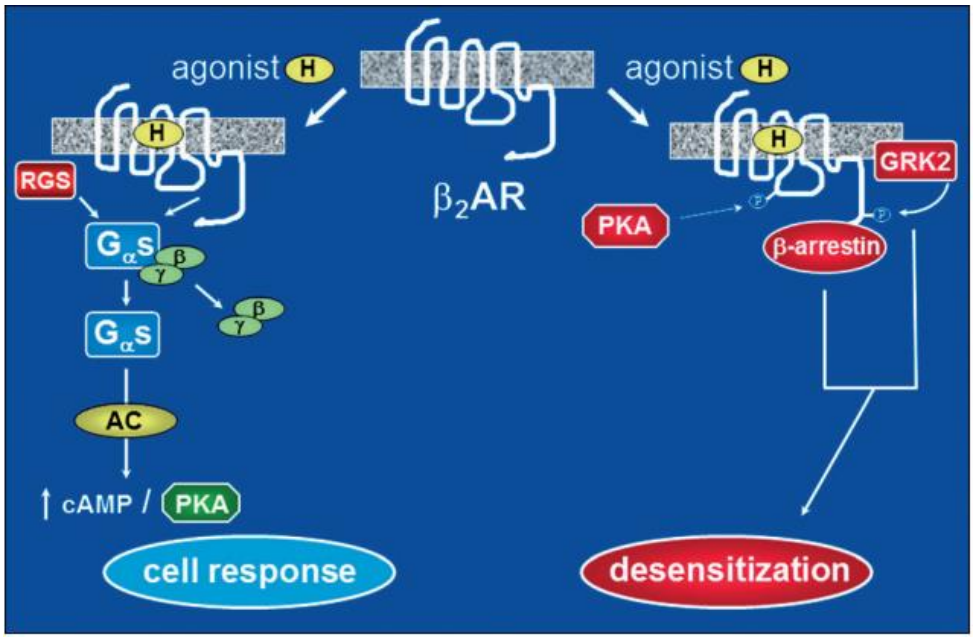


Figure 6.4: ßeta2-adrenergic signalling regulation.
By (1) Gs protein binding via adenylyl cyclase and by (2) ß-arrestin mediated pathway. Picture obtained from (Lefkowitz, 2013)

6.3.3 Desensitisation

Continuous receptor activation via Gs can lead to pathophysiological changes that eventually contribute to the sign and symptoms of failure (Najafi et al., 2016). For instance, the continuous activation of $ß_2$AR by agonist exposure results in desensitisation and downregulation of ßAR. To clarify, desensitisation is the situation where the receptor is exposed to the agonist and results in revoking of cellular response limit (Green et al., 1994, Turki et al., 1995).

The short-term (acute) agonist-promoted desensitisation is initiated within seconds to minutes (Lefkowitz et al., 1990). In this situation, both G protein kinase 2 (GRK2) and protein kinase A (PKA) play a role in the process of phosphorylation, which results in receptor uncoupling and internalisation to reduce the number of active receptors in the cell membrane, which is later subjected to receptor de-phosphorylation and recycled back to the plasma membrane (Rajagopal and Shenoy, 2017) **(Figure 6.5)**. It is also known as 'recycling'. In long-term (chronic) agonist-promoted desensitisation, prolonged or repeated ßAR activation over hours to days leads to loss of receptor density at the plasma membrane by lysosomal degradation – this is known as downregulation (Koryakina et al., 2012) **(Figure 6.5)**.

In general, at the physiological level, desensitisation is activated to both inhibit downstream signalling and cause loss of responsiveness. Therefore, in the clinical setting, desensitisation may limit the utility of administered therapeutic agonists on repeat prescription. These phenomena have been extensively investigated for $ß_2$AR and speculated to be related to polymorphisms positions 16 and 27. A summary by (Kitsios and Zintzaras, 2007) shows the results of the association between the different polymorphisms and the risk of ischemic heart failure and found conflicting data for downregulation and desensitisation for $ß_2$AR amino acid position 16, as summarised in **Table 6.2**.

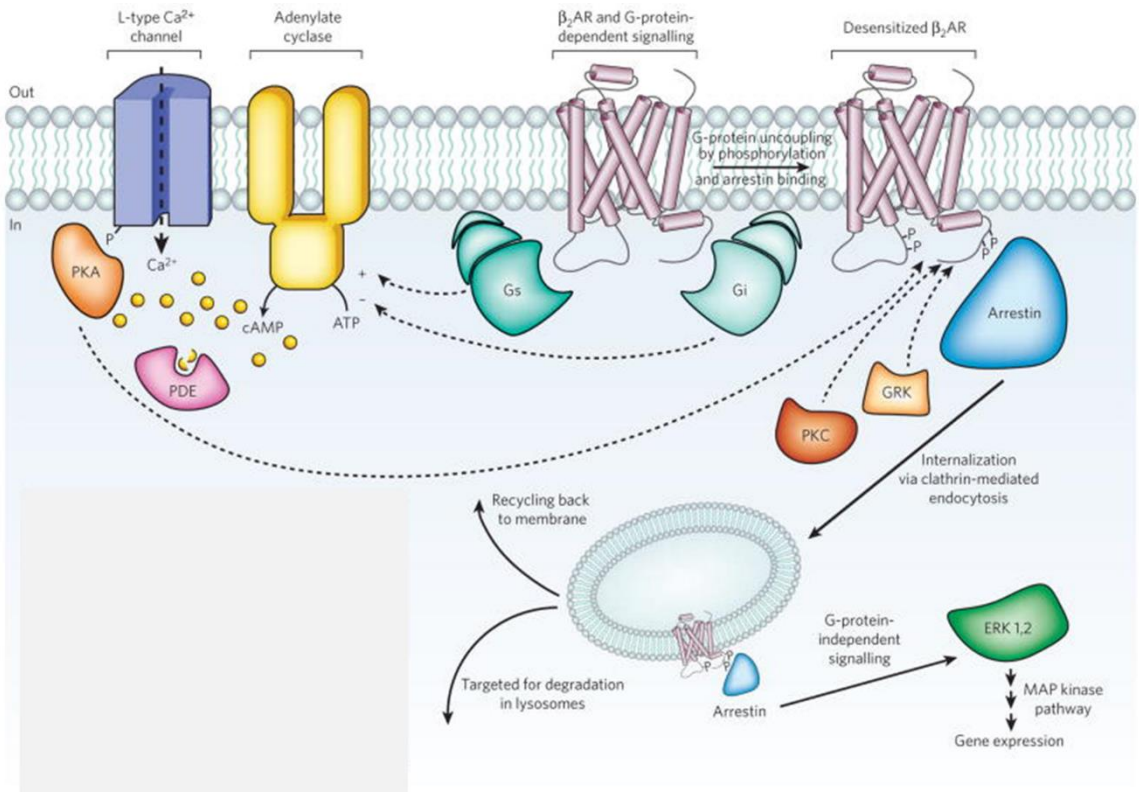


Figure 6.5: β_2AR desensitisation pathways.
Desensitisation starts with phosphorylation of βARs via PKA (activated by Gαs), protein kinase C (PKC) (activated by Gβγ) and GRK (Najafi et al., 2016). The phosphorylated C-terminal of βARs allows the binding of β-arrestin. The β-arrestin induces uncoupling of G-proteins and prevents further activation of Gαs. It also activates βARs internalisation via clathrin-mediated endocytosis. Once in the endosome, the receptor's fate will be determined. The function of βARs can be restored and recycle back to the plasma membrane. While under the sustained presence of β-agonist, the βARs remain internalised and will be subjected to downregulation by lysosomal degradation. Picture adapted from (Rosenbaum et al., 2009)

Table 6.2: The *ADRB2* gene polymorphisms characteristics and their functional implications to ischemic heart failure.
Adapted from (Kitsios and Zintzaras, 2007). Reference SNP (Rs) cluster-ID available at the following website: https://www.ncbi.nlm.nih.gov/snp/

Reference SNP cluster -ID	Base change	Amino acid change	Functional effect (reference)
Rs1042713	Exon1: A46G	Arg16Gly	Controversial data regarding downregulation, desensitisation (Green et al., 1994, Dishy et al., 2001)
Rs1042714	Exon1: C79G	Gln27Glu	Resistance to down-regulation (Liggett, 1997)

6.4 Models to study positions 16 and 27 polymorphisms

Although $ß_2$AR is a well-studied receptor, especially in positions 16 and 27, the role of the different polymorphisms is still poorly understood, as previous studies were carried out for example on transgenic animal models, $ß_2$AR overexpression, genetic association studies and airway cell/lung models.

Even though animal models have made a significant contribution to understanding the basic polymorphism concerning cardiovascular disease, their interspecies dissimilarity at the genetic and physiological level has limited the ability to translate the findings into human treatment (Brandao et al., 2017).

6.5 $ß_2$AR Isogenic Lines

Since Arg16Gly and Glu27Gln exist in linkage disequilibrium as discussed in subchapter 6.3, a large population would need to be studied to determine the importance of $ß_2$AR polymorphism in patients (Johnson, 2006). However, this is not possible as some polymorphisms are low in the population, such as Arg16Glu27 (RE). The value of human-induced pluripotent stem cells can be undermined because of high genetic variability between individuals, which may cause more significant phenotypic differences than the associated polymorphisms. Therefore, to overcome this, there is a need to study polymorphisms using isogenic lines.

The isogenic lines, which were created using precise gene targeting technology like CRISPR/Cas9, are capable of differing in the polymorphism of interest, while the overarching genetic backgrounds are unchanged, which makes them useful for inter-comparison of the influence of polymorphisms. Thus, this eliminates the irrelevant 'noise' from an estimated ~11 million single nucleotide polymorphisms (SNPs), 2.8 million short indels, and ~500,000 block substitutions that exist between individuals (Shen et al., 2013). It also permits multiple variants to be created simultaneously, e.g., at both positions 16 and 27, in a controlled manner, thus making four variants combination of Arg16Gly and Glu27Gln possible: (Gly16Glu27) GE, (Gly16Gln27) GQ, (Arg16Glu27) RE and (Arg16Gln27) RQ.

6.6 Human pluripotent stem cell-derived cardiomyocytes (hPSC-CMs)

Human PSCs have shown promise as an *in-vitro* platform to understand the variety of human disease, as they are capable of prolonged cell division into any somatic cell type, including cardiomyocytes. This is in contrast to primary cardiac human cells sources that are limited and difficult to manipulate in culture as they indeed have a limited lifetime. Correspondingly, hPSC-CMs recapitulate many cellular, molecular and functional aspects of the human heart in normal and pathological physiology conditions, including their response to cardioactive drugs, which makes them an ideal candidate to study the aforementioned polymorphisms and facilitates insight into disease mechanisms (Giacomelli et al., 2017). Also, the high scalability of hPSC to CMs makes them a suitable candidate for high throughput functionality assays.

6.7 Chapter rationale and objectives

Patient response to drugs could be influenced by polymorphisms within the β_2AR, particularly at amino acid positions 16 and 27, which are also associated with cardiovascular disorders including asthma and heart failure. The majority of the data available so far are based on the results of genetic association studies or models other than humans, which often leads to conflicting mechanistic explanations. For example, different groups have reported different polymorphisms that are involved in the agonist-promoted downregulation of receptors.

This chapter aims to explore how hESC (hPSCs) can be genome-edited by using CRISPR/Cas9 technology to create homozygous polymorphic isogenic variants that differ in β_2AR amino acid combinations at positions 16 and 27, resulting in (Gly16Glu27) GE, (Gly16Gln27) GQ, (Arg16Glu27) RE and (Arg16Gln27) RQ variants. By using these variants, their ability to maintain pluripotency and ability to differentiate into cardiomyocytes will be comprehended. The aim was to understand the impact and functional difference of *ADRB2* gene for β_2AR polymorphism at positions 16 and 27 in the edited hESC-CMs. To fulfil these aims, the following objectives were addressed as described in **Figure 6.6**.

1. Generate β_2AR homozygous GE, GQ, RE and RQ polymorphic isogenic variants by using CRISPR/Cas9 system within the HUES7 hESC (hPSC) genome.

2. Characterise the engineered β_2AR variants for pluripotency and cardiac differentiation capabilities.

3. Development of functional assays to quantify the β_2AR functional differences in acute desensitisation (recycling) and/or chronic desensitisation (downregulation) by measuring cyclic adenosine monophosphates (cAMP) production in response to β_2 induction (GloSensor cAMP assay)

6.8 Results

In this chapter, the functional differences of polymorphisms at amino acid positions 16 and 27 of β_2AR in the context of hESC-derived cardiomyocytes is presented.

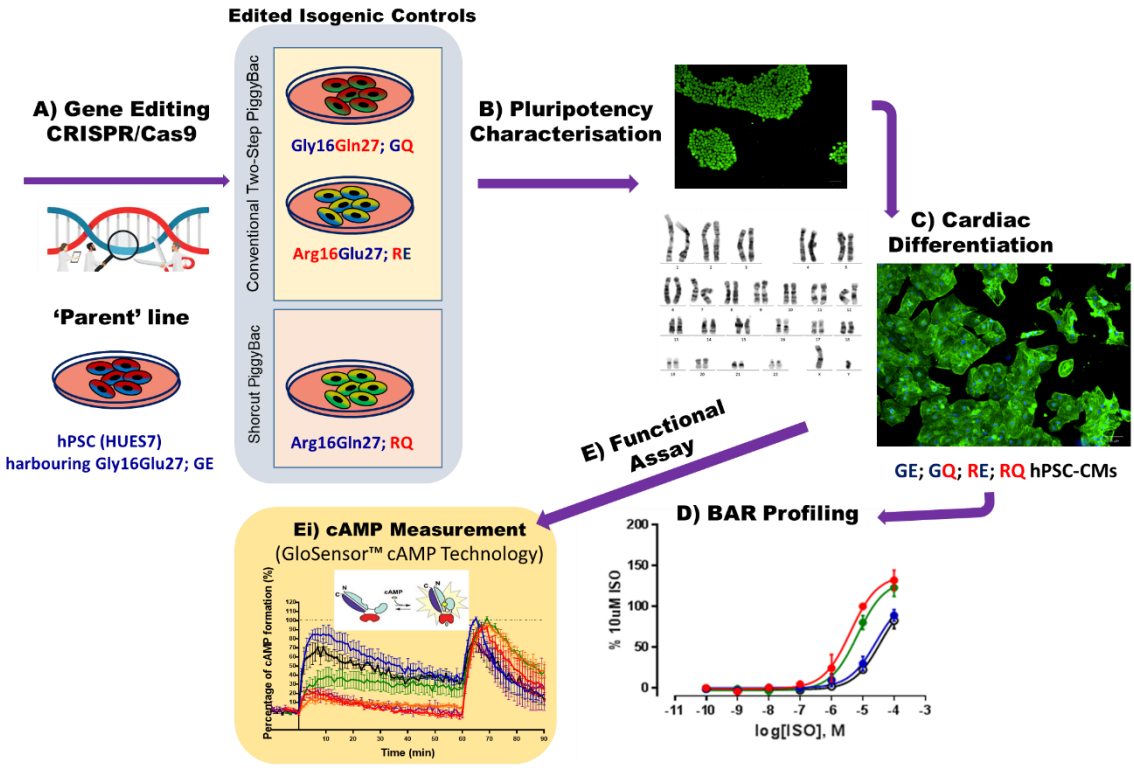


Figure 6.6: **Overview of the works.**

(A) Four sets of isogenic variants harbouring β_2 polymorphism at positions 16 and 27 were introduced into the 'parent' line, the HUES7, using CRISPR/Cas9. **(B)** The gene-edited isogenic hESC variants were characterised to validate their pluripotency capabilities. **(C)** The gene-edited hESC variants were differentiated to generate isogenic sets of hESC-cardiomyocytes. **(D)** The βAR's profile for the isogenic hESC-CMs was determined. **(E)** Phenotyping from the functional assay was determined in terms of cyclic AMP measurement.

6.8.1 Generation of β_2AR isogenic variants

To enable the study of β_2AR polymorphisms at positions 16 and 27 without the influence of any other genetic background, CRISPR/Cas9 genetic engineering was used to establish an allelic panel of isogenic hESCs by inserting an appropriate modification and selection (footprint) cassette. However, the footprint needed to be removed after targeting as the residual could alter or eliminate the neighbouring gene expression and might disrupt cell signalling (Kondrashov et al., 2018). Nevertheless, by creating a selection cassette free

(footprint-free) in isogenic β_2AR variants ensured that all cells within the panel contained the same genetic background and the difference in molecular or functional measurement could be directly attributed to Arg16Gly and Glu27Gln variations in the human cellular context.

6.8.1.1 The general editing strategy

In order to achieve this, β_2AR hESC variants generated by Dr Alexander Kondrashov from HUES7 (Harvard University Embryonic Stem Cell-Line 7) hESC line were utilised (Cowan et al., 2004). The variants harbouring position 16 amino acid (codon): G (GGA) and position 27 amino acid (codon): E (GAA); GE variant with appropriate substitution bases were 'edited' using CRISPR/Cas9 **(Table 6.3).**

The *ADRB2* locus general editing strategy was performed by using specific gRNAs, together with Cas9 and a donor targeting vector **(Figure 6.7).** The two guide RNAs were designed: to target amino acid position 16 (gRNAB5); to covert Glycine (G) to Arginine (R) (nucleotide position 46 G->A) and 27 (gRNAA1); to convert Glutamic Acid (E) to Glutamine (Q) (nucleotide position 79 G->C) by introducing nonsynonymous change in peptide in order to create specific isogenic polymorphisms from the hESC (HUES7; GE) **(Table 6.3 and Figure 6.8).** The component of the targeting vector included Puro-ΔTK (puromycin-N-acetyltransferase- thymidine kinase) as a positive-negative drug selection cassette in the targeting vector and *PiggyBac* recombination sites for footprint-free editing (Kondrashov et al., 2018) **(Figure 6.7)**.

Table 6.3: **Summary of *ADRB2* gene editing.**

The table represents the CRISPR/Cas9 gene-editing methods, the modification of single bases in the codon (highlight in red colour) at positions 16 and 27 and subsequently, the end product of isogenic variants. G(allele)=GGA(codon)/Gly/Glycine(amino acid); R = AGA/Arg/Arginine; E= GAA/Glu/Glutamic Acid; Q=CAA/Gln/Glutamine. The Red represents a subsequent change from the 'parent' line

Position 16 (RS1042713) (codon)	Position 27 (RS1042714) (codon)	Variants (amino acid)
GGA	**G**AA	**GE** (Gly16Glu27)
GGA	**C**AA	**GQ**(Gly16Gln27)
AGA	**G**AA	**RE**(Arg16Glu27)
AGA	**C**AA	**RQ**(Arg16Gln27)

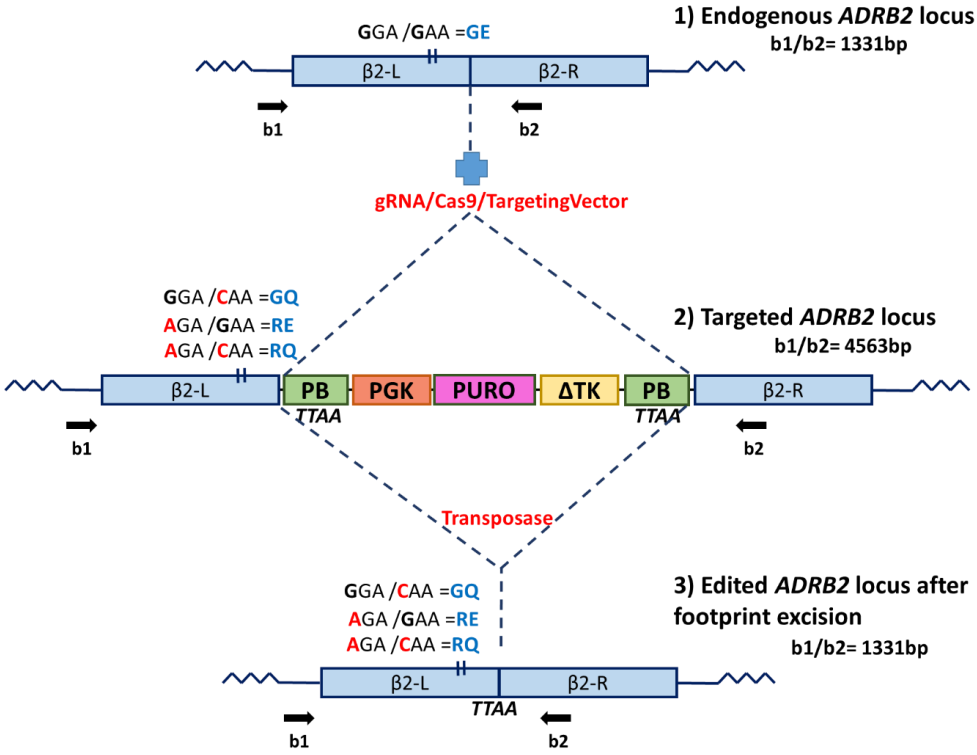


Figure 6.7: **The general CRISPR/Cas9-*PiggyBac* editing strategy for SNPs position 16 and 27 of HUES7 hESCs *ADRB2* locus.**
(1)*ADRB2* locus structure before targeting. (2)*ADRB2* recombined locus after insertion with PiggyBac positive-negative selection cassette and (3)*ADRB2* locus structure after cassette excision.
The black highlight (**G**GA/**G**AA=**GE**) and **red** substitution indicate the polymorphic change location induced for base 46(position 16) and 79(position27). B2-L is left while B2-R is right arm homology. The b1 and b2 are primer sites together with PCR product size. PB,*PiggyBac;* PGK,phosphoglycerate kinase promoter; PURO,puromycin-N-acetyltransferase; TK, thymidine kinase. Picture adapted from (Kondrashov et al., 2018)

6.8.1.2 The footprint (scarless) strategy

In order to remove the insertion cassette footprint, a TTAA site was needed. Interestingly, in isogenic lines generation, the TTAA excision site, which is vital for *PiggyBac* recombination and to enable the transposon to excise the selection cassette, was 748 bases away from the target sites, which surpasses the distance recommended for editing. The ideal distance between TTAA side and base to edit should not be more than 50 bp (Jarazo et al., 2019).

Therefore, the TTAA sites were manually created near the targeted editing sites by introducing a single nucleotide substitution change at nucleotide position 124 C->T and position 126 C->A of the *ADRB2* locus **(Figure 6.8).** The TTAA changes were synonymous (changes occur only in nucleotide sequence but not the amino acid sequence of the targeted protein) and crucially, maintained the native Leu41-Ile42 peptide sequence (Kondrashov et al., 2018).

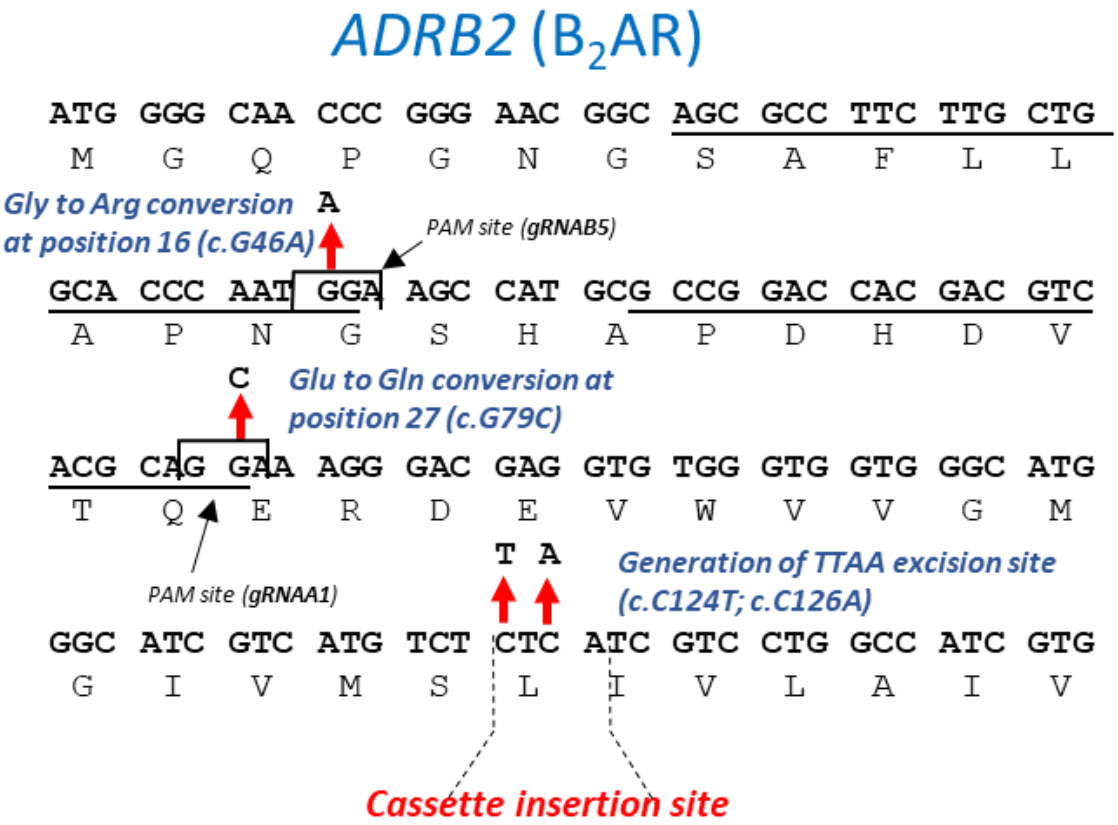


Figure 6.8: The targeting strategy introduced changes at nucleotide position 46 and 79 (nonsynonymous in peptide) and 124 and 126 (synonymous in peptide) as indicated.
The details of nucleotide and translated single-letter amino acid for 5' region of *ADRB2* locus. Location of the gRNA is *underlined*, PAM site *boxed* and TTAA *PiggyBac* cassette insertion site. PAM, Protospacer adjacent motif

6.8.2 Genotyping confirmation of genome-edited ß$_2$AR isogenic variants

To analyse the successful variants obtained from genome editing modification, a PCR-based screening of targeted variants was run. A pair of primers was designed to amplify the editing region **(Figure 6.9A)**. The location of the primers for genotyping has been illustrated in **Figure 6.9A** and details of the forward and reverse (b1 and b2) primers are tabulated in **Figure 6.9B**. If the final variants still contain the selection cassette, the size of the PCR product would be 4563bp, thus no band would appear in a gel with a 100bp ladder, while if the selection cassette in edited variants is successfully removed, the size of the PCR product would be 1331bp.

The results from PCR indicate that final variants for all four sets of ß$_2$AR isogenic were successful **(Figure 6.9C)**.To strengthen the results, amplicons obtained from each variant were sent for DNA sequencing. Predictably, the DNA sequencing chromatogram data from 'parent' line hues7; **GE** confirmed that the nucleotide at position 46 was indeed **G**GA and position 79 was **G**AA. The edited **GQ** variant confirmed nucleotide position 46(**G**GA)and position 79(**C**AA), the **RQ** variant confirmed nucleotide at position 46 (**A**GA) and position 79(**G**AA), and finally, the **RE** variant confirmed nucleotide at position 46(**A**GA) and position 79(**C**AA) **(Figure 6.9D)**.

The sequencing results also showed that all edited variants were a successful intact sequence at the PB integration site (**TTAA**), with changes on nucleotide at position 124(**T**) and position 126(**A**) **(Figure 6.9D).**

These editing experiments resulted in isogenic models that consisted of a suite of four ß$_2$AR homozygous variants GE, GQ, RE, RQ in intronless *ADRB2* gene at chromosome 5, to study ß$_2$AR polymorphism in hESC-CMs.

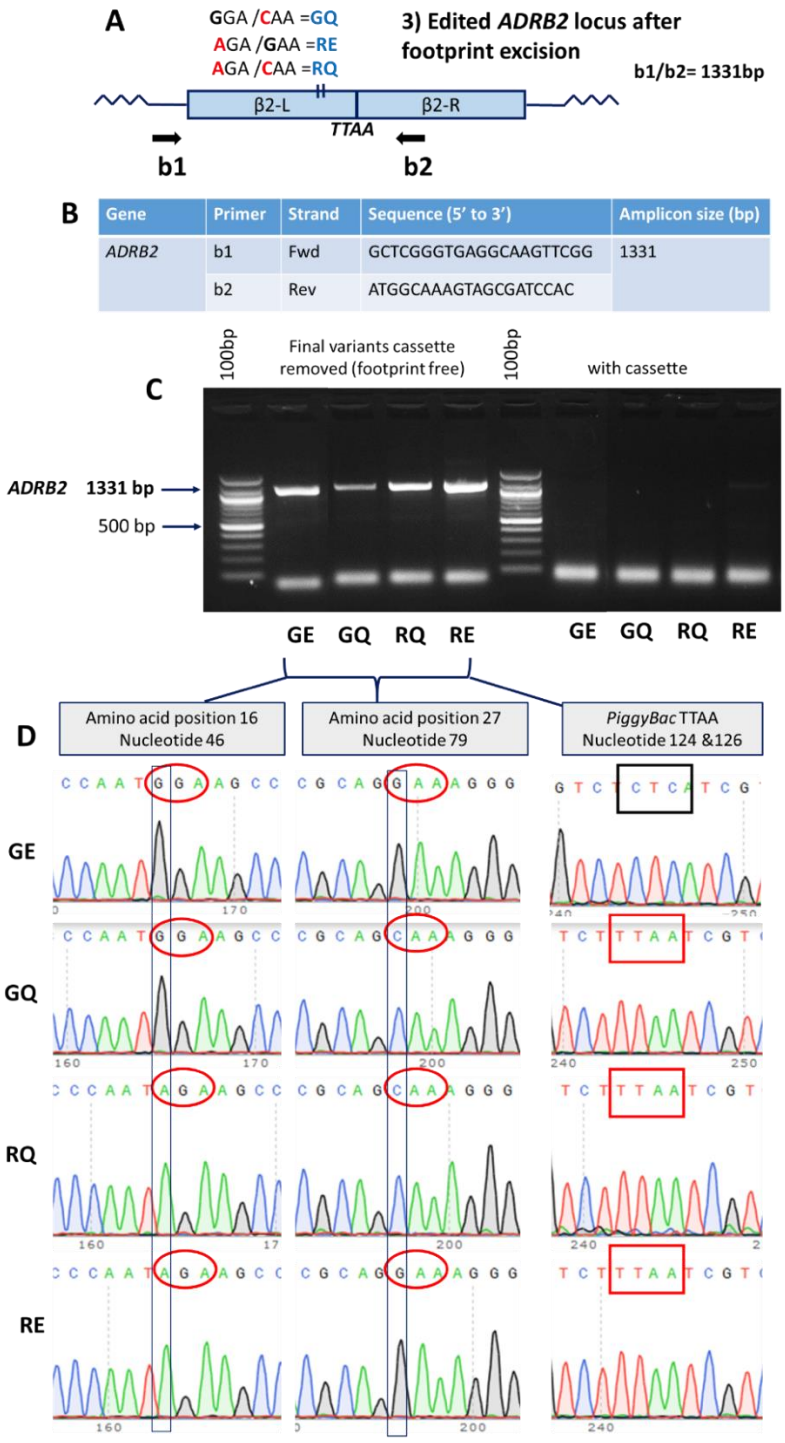


Figure 6.9: **Genotyping confirmation of engineered ß$_2$AR isogenic variants derived from a conventional two-step Footprint free and Shortcut approach.** **(A)** Location of genotyping primer b1/b2. **(B)** Primers used to amplify the DNA sequence spanning the *ADRB2* polymorphism. **(C)** Gel analysis of PCR products amplified using primer b1/b2 showed a 1331 bp band from isolated edited ß$_2$AR variants before and after transposase-mediated cassette removal. **(D)** DNA sequencing results of the final clones. The chromatograms represent different polymorphism GE, GQ, RQ and RE. The modified nucleotide at nucleic acid positions 46 and 79 indicate the successful modification. The TTAA sequence was observed as expected at the transposon excision site.

6.8.3 Pluripotency characterisation of successful modified clones

To make sure the edited β_2AR isogenic variants maintained their pluripotency after genome editing, a set of assays were performed. This included a growth curve, immunostaining of pluripotent transcription factors (OCT4, SOX2 and NANOG) and karyotyping analysis after prolonged serial culture**.**

As shown in **Figure 6.11A**, continuous monitoring of cell morphology from bright-field microscopy revealed the cells maintained their undifferentiated state with a high ratio of nucleus to cytoplasm, prominent nucleoli and a compact colony structure in confluent culture - as indicative for embryonic stem cell characteristic (Cowan et al., 2004). The cells exhibited a population doubling time of 21.9± 1.8 hours, 20.6± 1.2 hours, 25± 2.9 hours and 23± 2.3 hours, respectively for GE, GQ, RE and RQ (Mean±SEM) **(Figure 6.10B).**

The karyotyping validated a normal 46 XY karyotype between passage p35 to p45 in all lines (GE, GQ, RE, RQ) **(Figure 6.10C)**. These cells were also maintained at lowest passages after editing, which were p10-p25 and up to 10 passage after thawing to minimise mutation frequency.

The immunostaining of nuclear pluripotent transcription factors (OCT4, SOX2 and NANOG) showed positive stain for all GE, GQ, RE and RQ hESCs **(Figure 6.10D)**. As a conclusion, the genome editing and stem cell culture condition employed for β_2AR isogenic variants were shown to maintain cells in their undifferentiated state, which is necessary for the derivation of other cells, including cardiomyocytes.

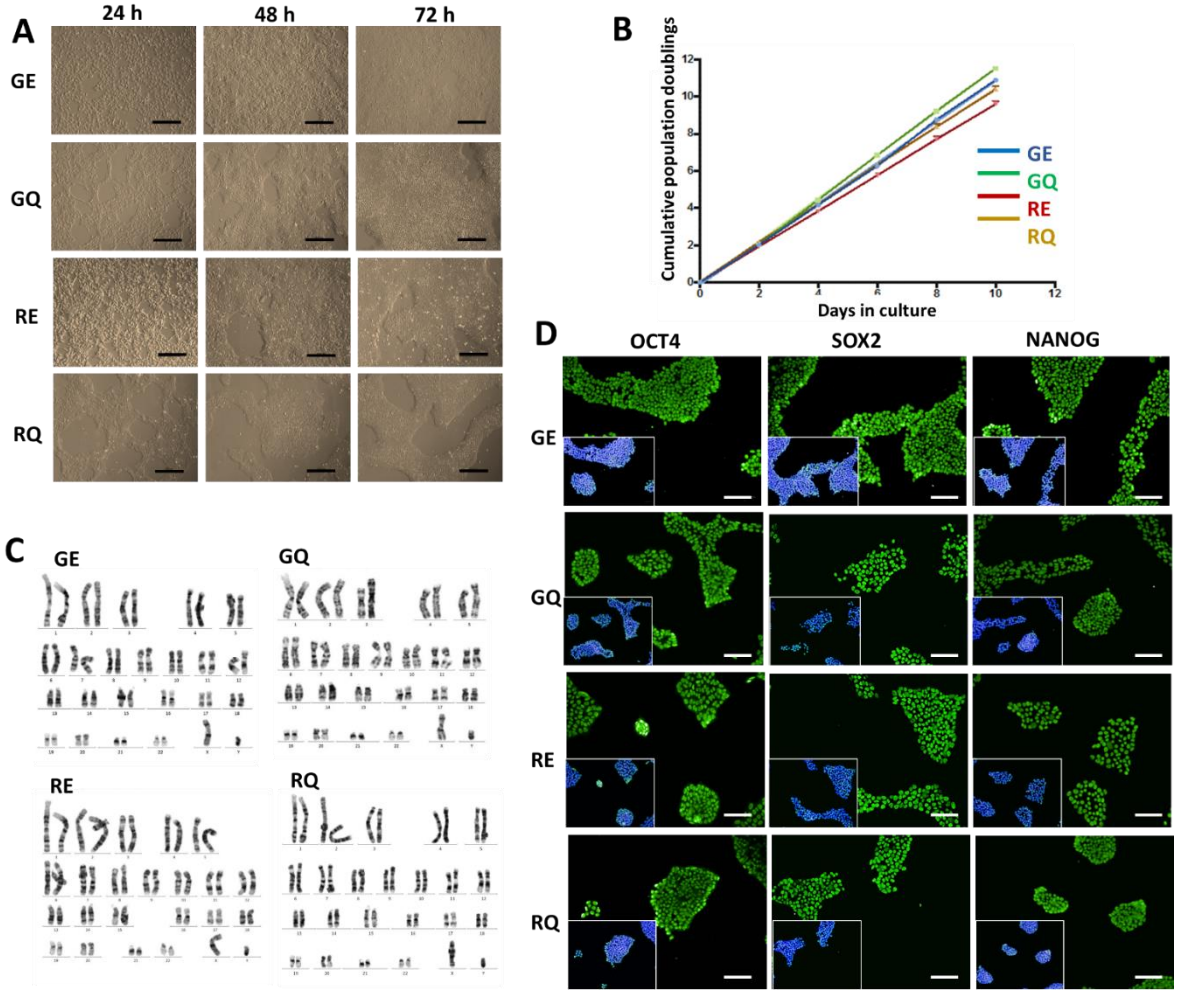


Figure 6.10: **Cell culture, karyotyping and phenotype assessment of β_2AR isogenic variants (GE, GQ, RE and RQ)**

(A) Brightfield images of HUES7; GE(p35), GQ(p43), RE(p45), RQ(p35) grown on Matrigel coated flask with E8 medium at 24 h, 48 h and 72 h following a routine split (1.0-1.2 million cells per T25 flask as initial seeding density) (Scale bars represent 100 µm).

(B) Representative growth curve for GE, GQ, RE and RQ variants demonstrating a population doublings time of 21.9±1.8 (GE), 20.6±1.2 (GQ), 25±2.9 (RE) and 23±2.3 (RQ) (Mean±SEM) (GE and GQ n=3, RE and RQ n=2).

(C) Representative karyogram of GE, GQ, RE and RQ variants of metaphase spread, revealing normal 46XY karyotype between p35 to 45.

(D) Immunofluorescence images demonstrating the positive expression of OCT4, SOX2 and NANOG in GE, GQ, RE and RQ hESCs,protein expression was captured with FITC channel, while the overlay represents DAPI (nuclear staining) (Scale bars represent 100 µm).

6.8.4 Generation and cardiac differentiation efficiency of β_2AR isogenic variants

Since the aim was to assess the functional difference of β_2AR isogenic variants in cardiovascular settings, it was essential to be able to successfully differentiate them into cardiomyocytes. The monolayer cardiac differentiation, as described in Chapter 2 (Materials and Methods), was adapted to differentiate these cell lines into cardiac subtypes. The RQ variant notably had a 'noodle-like' structure compared to a 'cheese-like structure' after preconditioning (StemPro34, Matrigel, BMP4) **(Figure 6.11A).** All variants were successfully differentiated into cardiomyocytes and formed beating monolayer around day ten onwards **(Figure 6.11A).**

For functional analysis, it is important that only a high purity cardiomyocyte with reduced non-cardiomyocyte cells (potentially fibroblasts) is used as an actual representation of a cardiac function. The presence of cardiac-specific proteins was determined by dissociating the beating monolayer cardiomyocytes and staining them with the α-actinin antibody. As shown in **Figure 6.11B**, the representatives of GE, GQ, RE and RQ showed the presence of cardiac myofilament with a similar organisation: α-actinin appeared as longitudinal striation throughout the cells.

Cardiac purity was subsequently quantitated. The analysis demonstrated that high purity cardiomyocytes from all β_2AR isogenic variants were able to be generated from the Nottingham in-house cardiac differentiation protocol: 88.4 ±1.9%, 98.65 ±0.2%, 89.17 ±2.4% and 99.2 ±0.1% respectively for GE, GQ, RE and RQ (Mean±SEM)**(Figure 6.11C)**. For the functional analysis in this study, only a high purity cardiomyocyte (>80%) was used.

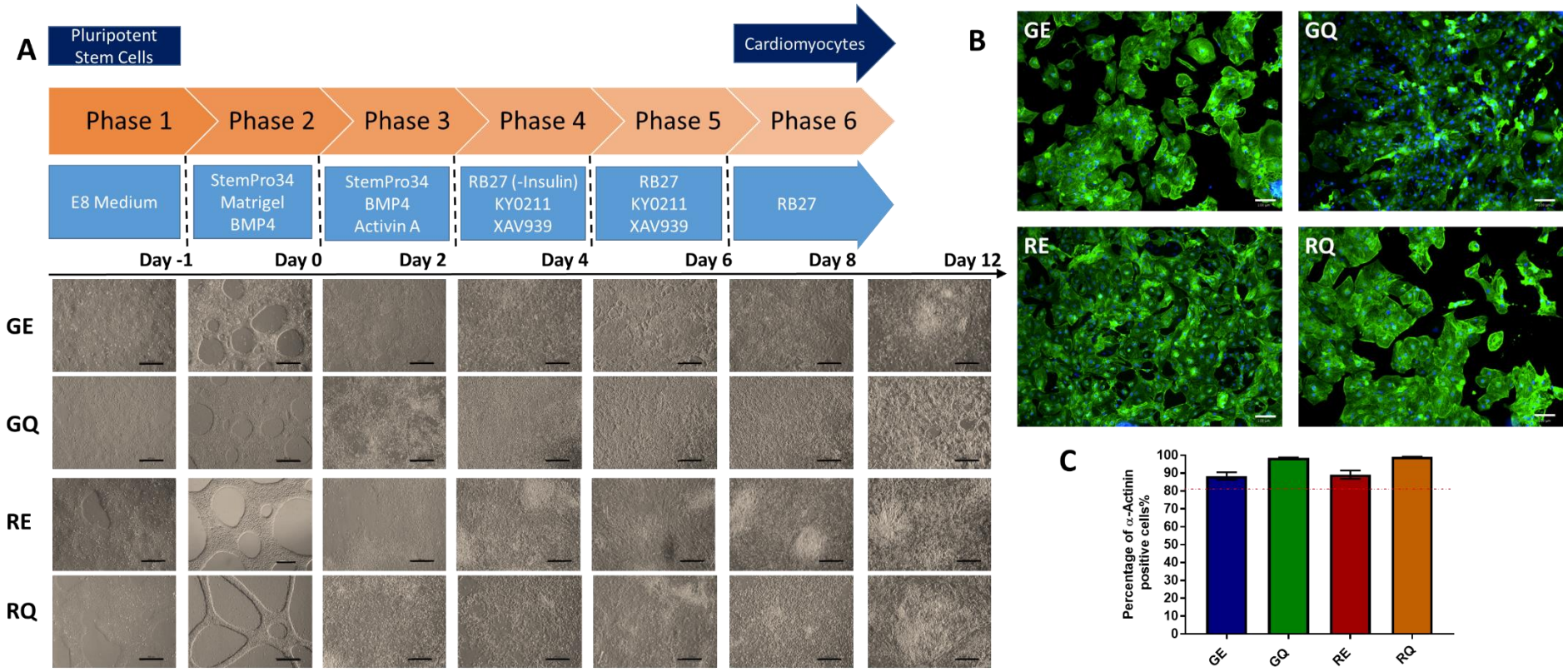


Figure 6.11: Generation and cardiac differentiation efficiency of β_2AR isogenic variants
(A) Summary of Nottingham in-house cardiac differentiation protocol and representative differentiation images from GE, GQ, RE and RQ (Scale bars represent 100 µm). **(B)** Immunostaining of GE, GQ, RE and RQ derived cardiomyocytes (CMs) by marker α-actinin (green) and costained with nuclear DNA stain DAPI (blue) highlighting a characteristic of cardiac muscle striations. (Scale bars represent 100 µm). **(C)** Cardiomyocytes purity quantification by detecting α-actinin positive cells using Operetta high content imaging Mean±SEM (n=3 Biological repeat, n=9(GE); 8(GQ); 6(RE) and 8(RQ) Technical replicates) (Scale bars represent 100 µm).

6.8.5 Gene expression profiles of beta-adrenergic systems

As previously mentioned, the differentiation of hPSC-CMs was accompanied by the specific regulation of βAR signalling related proteins (Wu et al., 2015). To investigate the expression profiling of genes related to BAR during maturation (differentiation), RNA was extracted from β_2AR isogenic hESC-CMs on days 0, 20, 30, 40 and 66 of differentiation. The qRT-PCR was performed for the *ADRB1* (β_1 receptor) and *ADRB2* (β_2 receptor) genes by Nguyen Vo.

The results showed that both *ADRB1* and *ADRB2* gene expression increases with time following differentiation. These genes upregulated after day 20 of differentiation and both genes stabilised at least after day 30 differentiation **(Figure 6.12)**. In RQ, the minimal β_2AR expression was present on day 20 but increased dramatically by day 30. This indicates that the beta-adrenergic gene expression in our β_2AR isogenic hESC-CMs steadied at or after day 30 of differentiation. This observation suggests that in order to obtain precise data, only hESC-CMs aged more than 30 days post-differentiation should be utilised for any functional investigation related to adrenergic signalling.

These data indicate that transcripts for *ADRB1* and *ADRB2* were present in the β_2AR isogenic hESC-CMs. The next step was to evaluate if these transcripts led to the functional production of receptors which could be modulated by pharmacology.

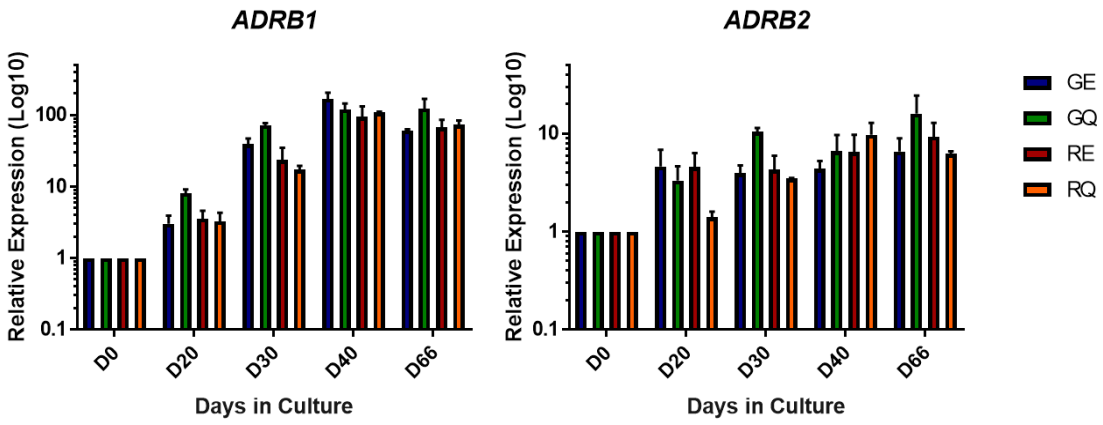


Figure 6.12: ßeta-adrenergic gene expression profile of $ß_2$AR isogenic hESC-CMs.
Realtime-PCR verification of the expression levels of *ADRB1* and *ADRB2* gene of $ß_2$AR isogenic hESC-CMs at day 0, 20, 30, 40 and 66 posts cardiac differentiation. Error bar= SEM, (n=2 Biological repeat).

6.8.6 Beta-adrenergic function by the cAMP accumulation

In 2017, it was mentioned that $ß_2$AR was mostly absent in myocytes and detected in only 5% of myocytes (Myagmar et al., 2017). However, the findings were from mice, which can be difficult to extrapolate to humans. While it is known that $ß_1$AR:$ß_2$AR ratio in the adult heart is 4:1 (Garland and Biaggioni, 2001), the hPSC-CMs produced in this study share many similarities with human fetal cardiomyocytes (Sayed et al., 2016a). Therefore, it is essential to define which components of the beta-adrenergic pharmacology expressed are functional (are all the parts present?) in the $ß_2$AR isogenic hESC-CMs variants.

To investigate the proportion of $ß_1$AR and $ß_2$AR contribution (response), the availability of highly selective ß subtype blockers has allowed a better evaluation of the role of each ßAR subtype (Monopoli et al., 1993). An antagonist study was conducted where different components were modulated (i.e. no blockade, or $ß_1$AR, $ß_2$AR or dual $ß_1$AR+$ß_2$AR blockade). For this, the following reagents were used: CGP 20712A (CGP, a $ß_1$AR blocker) and ICI 118551 (ICI, a $ß_2$AR blocker) either singly or in combination.

To determine whether the $ß_1$AR and $ß_2$AR are functional, agonist-induced cAMP production was assayed at the signal transduction level in cultured $ß_2$AR isogenic hESC-CMs variants. As a stimulus, isoprenaline (ISO) was used, and as a readout,

cAMP was measured. The ISO was chosen as ßARs catecholamine because $ß_2$AR has the highest affinity towards ISO, which is more efficient when coupled to Gs, followed by epinephrine and norepinephrine (Weitl and Seifert, 2008, Shoichet and Kobilka, 2012). The cAMP was chosen because it is a secondary product from the activity of cellular adenylyl cyclase activation by ISO stimulation (Abraham et al., 2004). One of the approaches is through indirect measurement of cAMP accumulation over the incorporation of tritiated adenine (^{3}H-adenine prelabelling approach) (Hill et al., 2010).

Cells were seeded in 48-well plates. maintained till at least day 30 of cardiac differentiation, and the experiment was conducted with the help of project collaborator Dr Joelle Goulding from the Cell Signalling Research Group, University of Nottingham. The cAMP production was determined using a modification of the [^{3}H]adenine prelabelling technique (Donaldson et al., 1988). On the day of the experiment, the medium was removed and the isogenic $ß_2$AR hESC-CMs of GE, GQ, RE and RQ were incubated with 2µCi.mL^{-1} [^{3}H]adenine in serum-free medium DMEM (SFM) for 2 hours at 37°C and 5% CO_2 to pre-label the adenine nucleotide pool (Hill et al., 2010). Cells were then washed with SFM and the medium replaced with SFM containing or not containing the antagonists CGP (100 nM) and ICI (100 nM) separately or in combination for 15 minutes, 37°C. The 100 nM CGP 20712A was chosen as it was previously shown as the lowest concentration before reaching saturation to occupy $ß_1$AR (Dunigan et al., 2000) while 100 nM ICI 118551 was chosen as it was starting concentration that indicates interaction at $ß_2$AR (Monopoli et al., 1993), hence the blockade.

The cells were then incubated with agonist ISO with increased single concentrations (100 pM to 100 µM) to each well, with 1 mM 3-isobutyl-1-methylxanthine (IBMX) for 5 hours. IBMX is the phosphodiesterase IV inhibitor which prevents cAMP breakdown, therefore, the cAMP measured was the absolute cAMP produced, hence this was termed the 'accumulation' assay. The reaction was terminated, and cells were lysed with 50ul concentrated hydrochloric acid (HCl), followed by the addition of 100ul [^{14}C]-cAMP standard into each well to enabled intracellular cAMP to come in contact with anti-cAMP antibody (Hill et al., 2010). Assay plates were frozen and stored at -20°C to be run at a later time point. Plates were thawed and accumulated and [^{3}H]-cAMP

was separated from other ^{3}H-nucleotides (tritium-labelled adenine derivatives) (Hill et al., 2010) using sequential Dowex and alumina column chromatography, as described by (Donaldson et al., 1988).

The incorporation of tritiated adenine was measured and normalised to following 10 µM ISO alone within a given experiment. The 10 µM ISO was chosen for normalisation as the curve was saturated beyond this concentration. Based on the results, stimulation of all cultured isogenic hESC-CMs variants with Isoprenaline alone in the absence of ICI or CGP blockers led to a steep increase in cAMP accumulation from 100 nM ISO to the maximum 100 µM ISO. This confirmed that all genome-edited β_2AR variants were functional. A similar profile was observed in all isogenic variants treated with ISO with pre-incubated CGP (β_1AR blocker). The EC_{50} (log (ISO), M) and E_{max} (% 10 µM ISO) values of ISO concentration curves for ISO alone and ISO pre-incubated CGP were near to each other **(Table 6.4).** The ISO alone and ISO+CGP exhibited the highest potency with an EC_{50} (Mean ISO alone ± SEM ISO alone; Mean ISO+CGP ± SEM ISO+CGP) of GE (-5.83 ± 0.18; -5.9 ± 0.29), GQ (-6.06 ± 0.09; -5.66 ± 0.12), RE (-6.07 ± 0.08; -5.94 ± 0.11) and RQ (-5.39 ± 0.13; -5.17 ± 0.10) **(Table 6.4)**. These indicated that the cAMP generation was mediated by β_2AR subtypes, whereas cAMP profile for the treatment of ISO with pre-incubated ICI (β_2AR blocker) was similar to the ISO plus CGP+ICI (β_1AR+β_2AR blockers), where both had lower cAMP accumulation based on EC_{50} (log (ISO), M) and E_{max} (% 10 µM ISO) values **(Table 6.4)**. These indicated that the β_1AR subtype was almost not present in all isogenic hESC-CMs variants **(Figure 6.13A and Figure 6.13 B)**.

To conclude, the β_2AR subtype expression via functional G-protein coupling and downstream function of adenylyl cyclase was high and significantly more abundant in all isogenic hESC-CMs variants (GE, GQ, RE and RQ) than the β_1AR subtype.

Table 6.4: The EC_{50} and E_{max} values of ISO concentration curves in the presence of ß-antagonists (ICI, CGP, ICI+CGP) in $ß_2AR$ isogenic hPSC-CMs variants; GE, GQ, RE and RQ. GE (n=6), GQ (n=7), RQ (n=5) and RE (n=5).Data represent mean and ± SEM.

		EC_{50} (log (ISO),M)				E_{max} (% 10 µM ISO)			
		GE	**GQ**	**RE**	**RQ**	**GE**	**GQ**	**RE**	**RQ**
Isoprenaline alone ($ß_1AR + ß_2AR$ response)	**Mean** ±SEM	**-5.83** ± 0.18	**-6.06** ± 0.09	**-6.07** ± 0.08	**-5.39** ± 0.13	**126.8** ± 10.35	**104** ± 3.76	**107.4** ± 3.63	**138.2** ± 8.48
+ ICI 118551 ($ß_1AR$ response)	**Mean** ± SEM	**-4.71** ± 0.22	**-5.01** ± 0.15	**-4.70** ± 0.12	**-4.58** ± 0.16	**108.7** ± 16.31	**83.22** ± 6.39	**79.37** ± 6.13	**112.2** ± 12.19
+ CGP 20712A ($ß_2AR$ response)	**Mean** ± SEM	**-5.9** ± 0.29	**-5.66** ± 0.12	**-5.94** ± 0.11	**-5.17** ± 0.10	**136.7** ± 16.33	**113.9** ± 5.81	**112.5** ± 5.40	**132.2** ± 7.51
+ ICI 118551 + CGP 20712A (No $ß_1AR$ + No $ß_2AR$ response)	**Mean** ± SEM	**-4.72** ± 0.27	**-4.67** ± 0.14	**-4.54** ± 0.11	**-4.43** ± 0.16	**119.2** ± 21.88	**90.32** ± 8.29	**91.2** ± 7.11	**113.4** ± 14.34

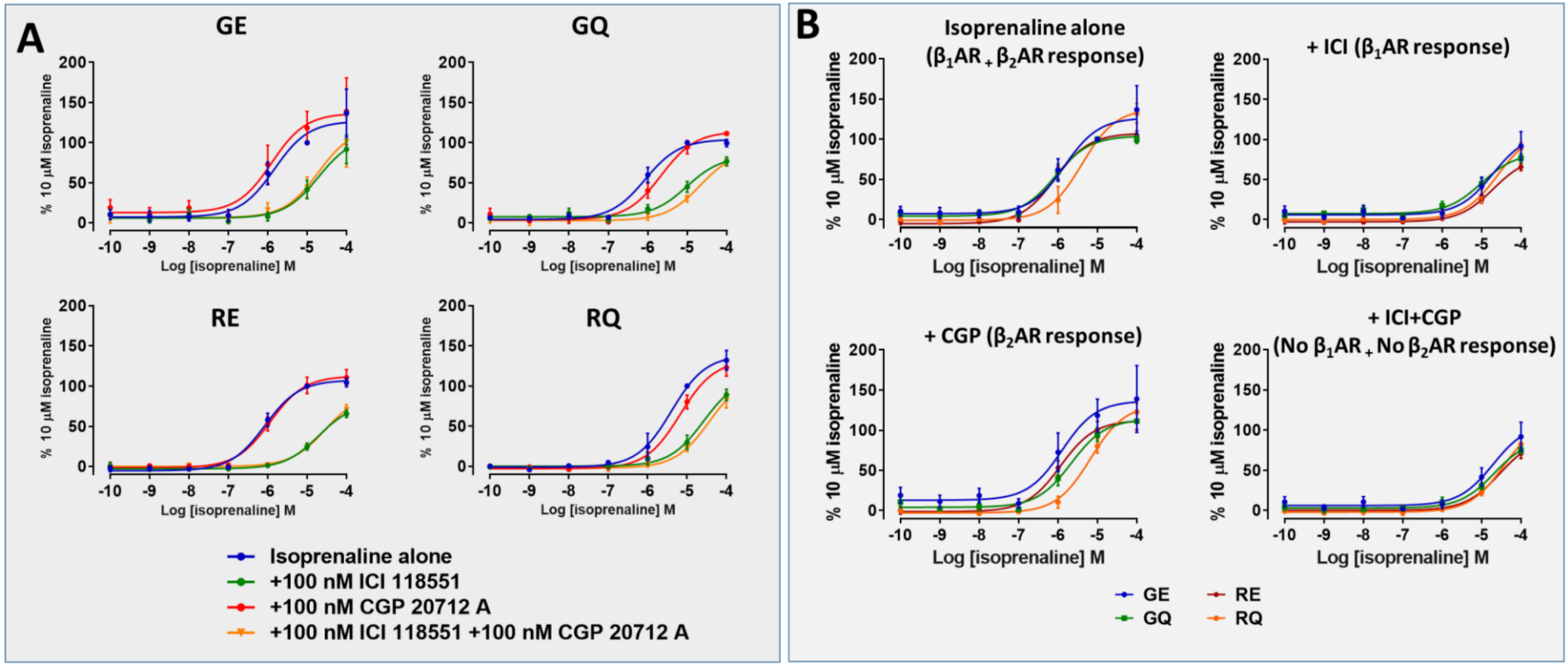


Figure 6.13: Accumulation of cAMP as measured through the incorporation of tritiated adenine.

Concentration-response curve normalised to relative signal from 10 µM ISO (%) against logarithmic values of ISO concentration on β_2AR isogenic hESC-CMs day 30 post-differentiation. **(A)** GE, GQ, RE and RQ. **(B)** Incubation with 100 nM CGP 20712 A (CGP, β_1AR blocker)) reflects β_2AR response which similar to ISO only (β_1AR+β_2AR response) shifted to the left in all variant. Incubation with 100 nM ICI 118,551 (ICI, β_2AR blocker)) reflects β_1AR response that similar to ICI+CGP (No β_1AR+ No β_2AR response) reflects the low presence of functional β_1AR in the systems. GE (n=6), GQ (n=7), RQ (n=5) and RE (n=5).

6.9 Functional assay to investigate the difference in the polymorphisms of ß$_2$AR isogenic hESC-CMs variants

The principle function ß$_2$AR is to transmit information from the extracellular environment to the cell interior by interacting with G-proteins, which later participates in various aspects of regulation. As a mechanism of homeostasis, the cellular response to ß-agonists is usually rapidly attenuated by desensitisation, which consists of few-cycle of that includes receptor uncoupling from G-protein, receptor endocytosis, recycling of internalised receptor (resensitisation) and downregulation (Bohm et al., 1997, Baker, 2010). This regulatory mechanism that governs the ability of ß$_2$AR to respond to an agonist might be influenced by the ß$_2$AR polymorphisms positions 16 and 27.

A variety of strategies need to be used to probe these functionality differences in ß$_2$AR polymorphisms. However, some of them have limitations. For example, in our isogenic models, the traditional radioligand-binding assay is not possible as the expression of ß$_2$AR is low. On the other hand, microscopy detection is not feasible as the ß$_2$AR antibody has insufficient specificity and is unstable in detergent (Ahles and Engelhardt, 2014).

While conventional cAMP accumulation assay, as described in subchapter 6.8.6 involved sample disruption (by cell lysis) of thousand cells for cAMP evaluation, and therefore provide only a single time point measurement which relatively low throughput, time-consuming, limit the kinetics measurement over time and costly (Paramonov et al., 2015, Hill et al., 2010). As a lysis process involve; thus, the inability to provide precise information on cAMP.

Due to this reason, a suitable assay to investigate the difference in ß$_2$AR polymorphisms was further explored, and this is described in the next section.

6.9.1 GloSensor™ cAMP measurement assay

One of the assays to quantitate the difference in β_2AR polymorphism is by performing a functional assay that measures the proximal β_2AR signalling by-product. The GloSensor™ cAMP Technology (Promega) is a functional GPCR assay based on proximal measurement of GPCR second messenger (cAMP), hence was selected to be used in this study.

There are two types of the cAMP plasmids for GloSensor™ cAMP Technology, which are pGloSensor™-22F cAMP and pGloSensor™-20F cAMP (Binkowski et al., 2011). The pGloSensor™-20F cAMP was prefered as it performed well at 37°C, while the 22F cAMP luminescence is challenging to detect at a physiological temperature, which is essential for living cardiomyocytes.

The technology utilises genetically modified firefly *Photinus pyralis* luciferase into a reversible cAMP biosensor to monitor the real-time activation of Gs/Gi GPCR, by quantifying intracellular changes in cAMP concentration inside the live non-lytic cells **(Figure 6.14A)**. This permuted luciferase is fused with cAMP binding domain B from protein kinase A, regulatory subunit type IIß (RIIßB) **(Figure 6.14B).** Once the cAMP binds to the domain, it leads to enzymatically conformational alteration changes in the biosensor and thus emits light **(Figure 6.14C)** (Binkowski et al., 2011, Fan et al., 2008).

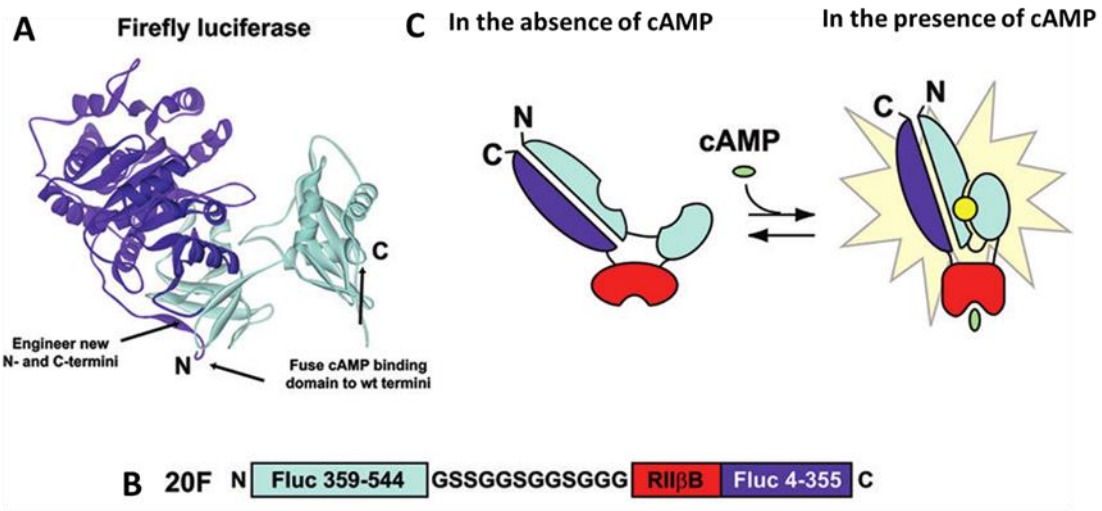


Figure 6.14: **Description of GloSensor™ cAMP Technology. The cAMP assay based on luminescence intensity.**
(A) Genetically modified firefly luciferase was fused with cAMP-binding domain into the unique N and C termini **(B)** pGloSensor™-20F cAMP vector plasmid construct **(C)** The cAMP bind to the binding domain, causing a conformational change and escalate the luminescence from the luciferase activity.

6.9.1.1 The rationale principle behind GloSensor™

The magnitude of $ß_2$AR polymorphisms could be directly measured by measuring the kinetics signal produce from the second messenger, cAMP. The Gs-ßARs activation stimulates the adenylyl cyclase (AC), which leads to an increase at the intracellular cAMP level, while Gi- ßARs activation inhibits AC, which leads to a decrease in cAMP levels **(Figure 6.15)**. Once cAMP binds to the GloSensor™, it causes a conformational change. The conformational change causes the luciferin, which acts as substrates, to breakdown into oxyluciferin and eventually leads to a substantial increase in luminescence production with the emission of light at 550-570 nM, according to following reaction (Kumar et al., 2017, Hill et al., 2010) **(Figure 6.15)**.

Therefore the scale of luminescence produced is directly proportional to the amount of cAMP present and indirectly reflects the induction of ßARs activity (Zhang and Xie, 2012). The hypothesis is that any of functional

$ß_2$AR polymorphisms difference in desensitisation and downregulation is feasible by detecting luminesce output from cAMP and eventually, current receptor levels.

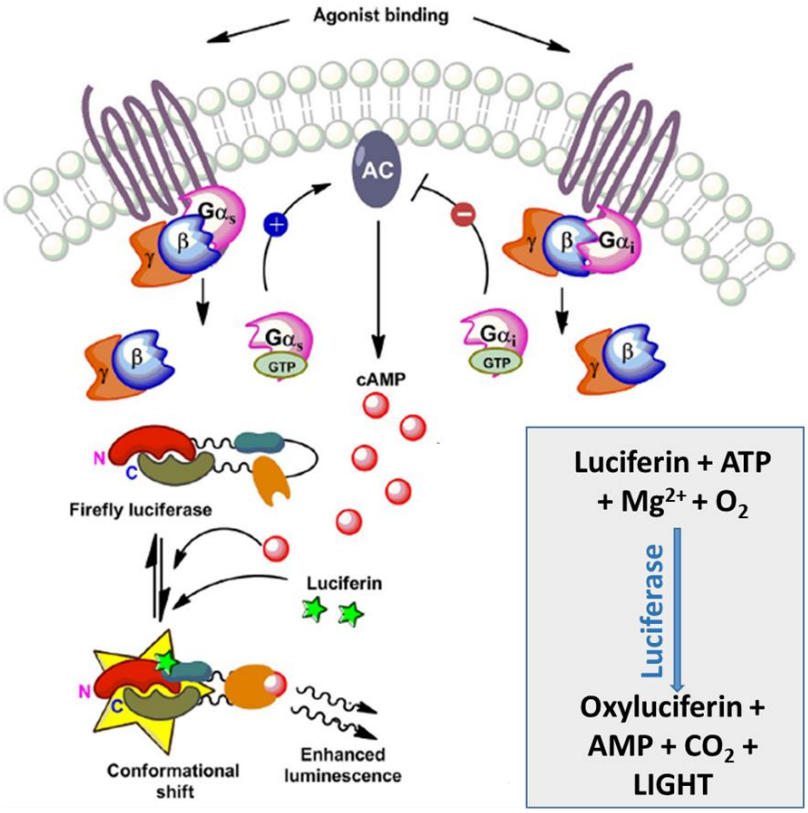


Figure 6.15: **Representation of GloSensor™ cAMP reporter assay to quantify ßARs activity**

ßARs activation is stimulated by agonist binding. Once activated, it leads to dissociation of Gα from Gßγ subunit. The Gαs subunit stimulates the adenylyl cyclase (AC) to produce a second messenger, cAMP. Fluctuations in intracellular cAMP can be measured by the luminescence produced. Once cAMP is bound to GloSensor™ reporter binding domain, it will undergo a conformational change that causes luciferase to oxidise its substrate luciferin into oxyluciferin and light output (luminescence). Picture obtained from Kumar et al.(2017).

6.9.2 Optimisation of cultures condition for high-efficiency hESC-CMs transfection

The assay described above relies on moderate transfection rates but this can be difficult to achieve in sensitive cells such as hESC-CMs. In order to confirm that β_2AR isogenic hESC-CMs are capable of being transfected and can express an optimum expression of the desired biosensor (GloSensor™) for functional assay, transfection optimisation was performed. Transfection efficiency until at least day 32 GE hESC-CMs, was optimised using Lipofectamine 3000 reagent.

The transient expression of pmaxGFP™ Vector plasmid was used as a control to assess the efficiency of 48 hours post-transfection, in a 96 well plate format seeded with 40,000 cells/well. Two DNA plasmids concentrations of 100 ng and 500 ng per well were used as recommended by the manufacturer (Promega) with a different combination of 'Transfection reagent: DNA ratio'; 0:1, 1:1, 1.5:1, 3:1 and 4:1, as suggested by the manufacturer **(Figure 6.16A)**. At 24 hours after transfection, cells were changed into normal RPMI-B27 medium and allowed to grow up to 72 hours. By using Operetta high content image analysis, transfection efficiency was calculated as the percentage area of cells that were GFP positive.

A transfection reagent, DNA ratio of 1.5:1, was found to have the most significant area of GFP positive cells in both DNA plasmid concentrations 100 ng (51.25%± 0.79%) and 500 ng (40.74%± 1.94%)**(Figure 6.16B)**. The higher 500 ng DNA plasmid and the higher amount of transfection reagents, however, resulted in toxicity and subsequently cell death.

Considering the number of transfected cells and cell death, 1.5:1 ratio with 100 ng DNA was the best condition **(Figure 6.16B)**. The GFP expressions from 24 to 72 hours (day of the assay) were monitored and validated**(Figure 6.16C)**.

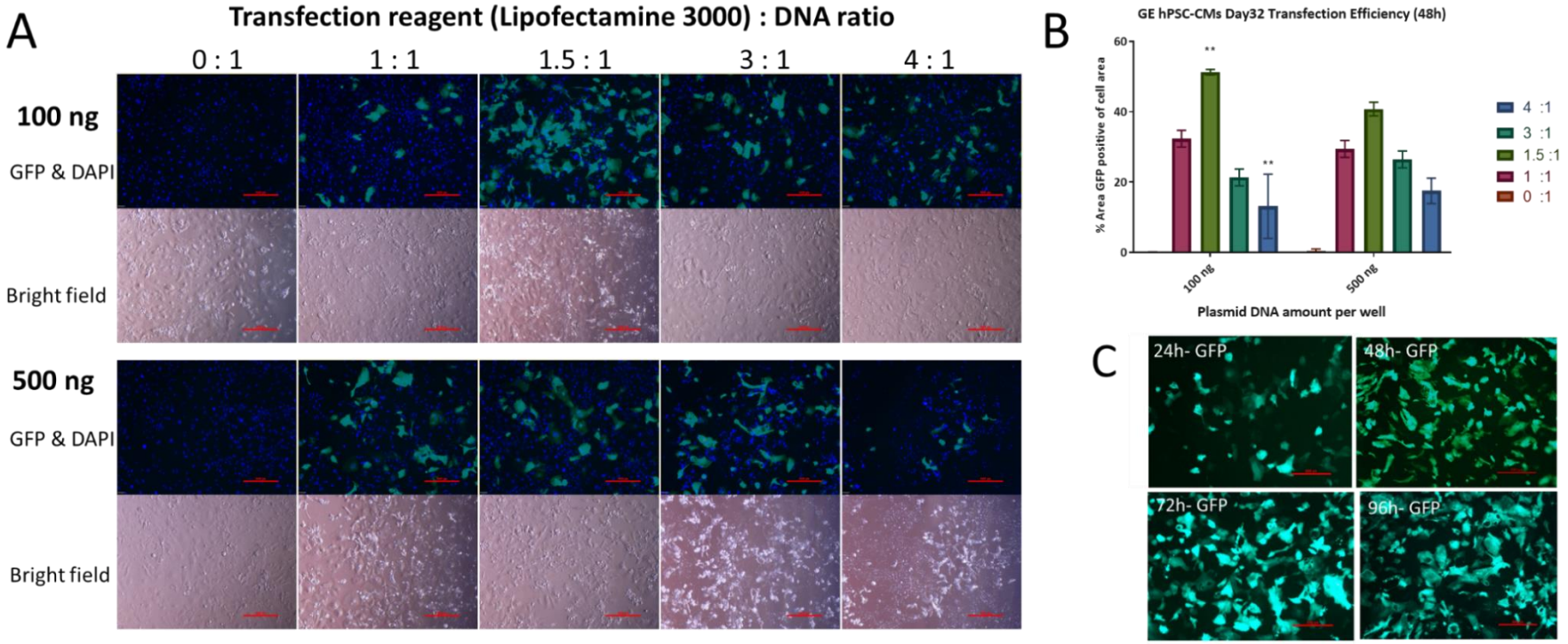


Figure 6.16: **Efficiency of Lipofectamine 3000 mediated transfection of GE hESC-CMs**
(A) Qualitative live imaging of transfected GE hESC-CMs at different pmaxGFPTM vector plasmid DNA concentration (100 ng & 500ng/ per well) and different transfection reagent: DNA plasmid ratios of fixed 40.000 cells/well density. Magnification = 10x. Scale bars = 100 µm. **(B)** Comparison of quantitative transfection efficiency across four different transfection reagent: DNA ratio and two DNA plasmid concentrations. Transfection efficiency percentage calculated as the area of cells that are GFP positive compared to untransfected control (0 DNA ratio) using Operretta™ Live Imaging system and Columbus for image analysis. Data presented as mean ± SEM (n=2 Biological repeat with n=3 technical repeat). One way ANOVA with Dunnett's multiple comparison test relative to 1:1,** $p < 0.01$ **(C)** Live imaging of actual optimum condition 1.5:1 of transfection reagent: DNA ratio using 100ng pmaxGFPTM vector per well (96 well) observed at 24, 48,72 to 96-hours post-transfection

6.9.3 Measurement of real-time intracellular cAMP production in response to Isoprenaline treatment by GloSensor™ cAMP Technology

As the scale of luminescence produce is directly proportional to the amount of cAMP present and indirectly reflects the induction of ßARs activity, the systems were tested for validation. The hypothesis is that with GloSensor™ cAMP Technology, fluctuation of BARs activity could be observed; for example, the induction of ßARs by agonist and receptor desensitisation over time.

6.9.3.1 The general response of $ß_2$AR isogenic hESC-CMs using GloSensor™-20F cAMP Assay

The underlying protocol of these assays involved the transfection of cells with GloSensor™ 20F plasmid. After 72 hours, attached cells were pre-equilibrated with 2% GloSensor™ cAMP reagent (luciferin) for 2 hours, the dispensation of appropriate compound (for example ß-agonist ISO) and finally, luminescence measurement by a plate reader **(Figure 6.17)**.

Representatively, the results from absolute measurements indicated during baseline conditions (without ISO), show that the mean cAMP amounted to 1000 relative light units (RLU) while the addition of 1 µM ISO, an agonist for both $ß_1$AR and $ß_2$AR a significant maximum cAMP signal of 650-850 fold (7500-9500 relative light unit (RLU)) from the baseline, was produced within 5 minutes of ISO induction (**Figure 6.18A**). After 50 minutes of achieving the maximum of ISO induction, the signal level returned to nearly half of the unstimulated state, even though under the continued presence of the agonist (**Figure 6.18A&C**). These situations observed (signal declined over time) reflect the desensitisation of receptors; as ßARs was phosphorylated, it reduced the amount of cAMP by time, a clear example of homeostasis (Lefkowitz, 2013).

Paramanov has suggested that the GloSensor™ assay is dependent on the substrate for luciferase and may affect the signal readout as the concentration and availability of substrate might be depleted and hence affect the signal generation (Paramonov et al., 2015). However, after the addition of 10 µM FSK, the signal increased up to 850 fold (9500 RLU) in the luminescent signal within 3 minutes of FSK induction (**Figure 6.18A**). This indicates that the reduced signal

was not due to depletion of the substrate (luciferin) but instead was caused by the reduction of the active pool of receptors. Nonetheless, the suggestion was taken into account, and therefore, in subsequent experiments, the medium was refreshed with new substrate before the assay.

The assay might have limitations as it needs the necessity of expression, meaning transfection, which might cause poor efficacy of construct delivery and therefore, have direct effects on the variability of sensor expression level, both well to well and run to run. Therefore, to eliminate variability, the kinetics signal reading was normalised to mean of maximum forskolin for each well (as a positive control, that maximises total cAMP) respectively after subtracting the baseline (**Figure 6.18B**) and quantitated as a percentage of cAMP formation (%) in each well (**Figure 6.18C**). The following formula was used (**Figure 6.18B&C**) for baseline correction and normalisation, and the graph after normalisation to maximum FSK was illustrated (**Figure 6.18C**).

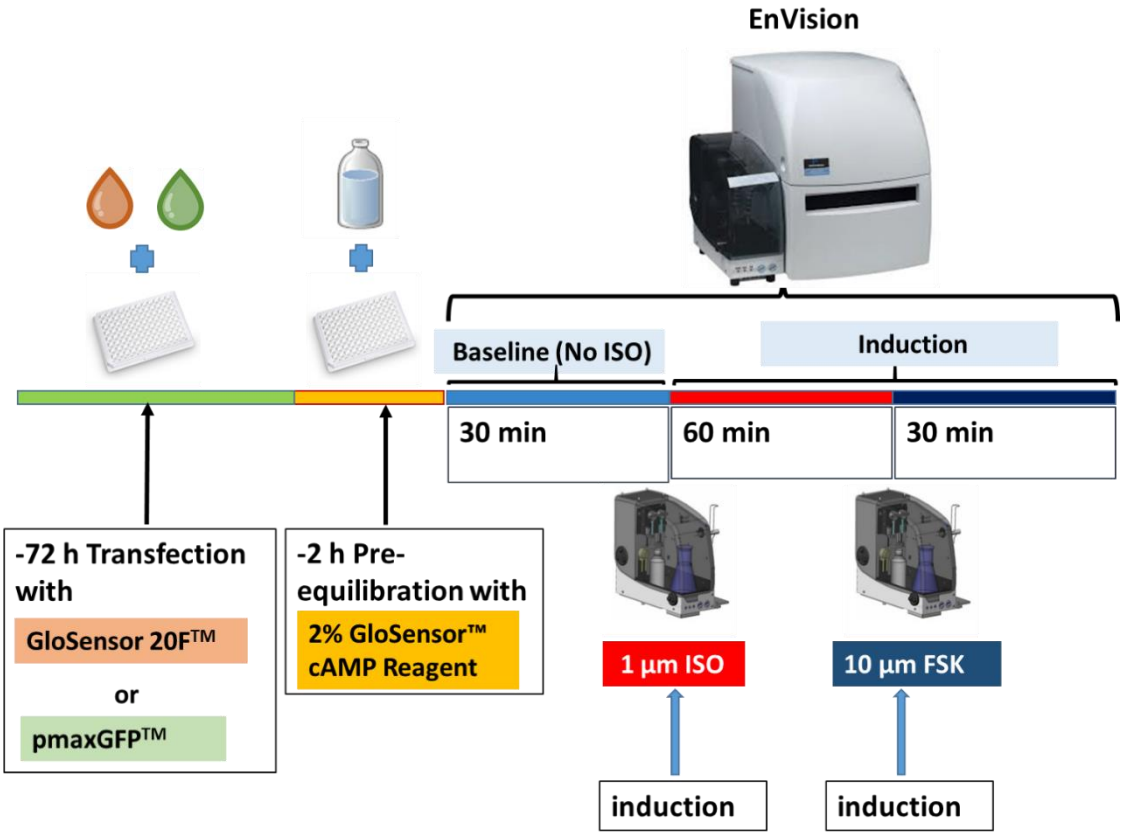


Figure 6.17: **An overview of the GloSensor™-20F cAMP Assay.**

Cells were transfected with 100 ng GloSensor™ 20F plasmid, followed by 2 hours incubation with 2% GloSensor™ cAMP reagent (72 h post-transfection), challenged with tested compound (ISO and FSK) and luminescence was measured by EnVision™ Plate Reader. ISO; Isoprenaline = *ADRB2* agonist, FSK; forskolin = cell-permeable activator of adenylyl cyclase

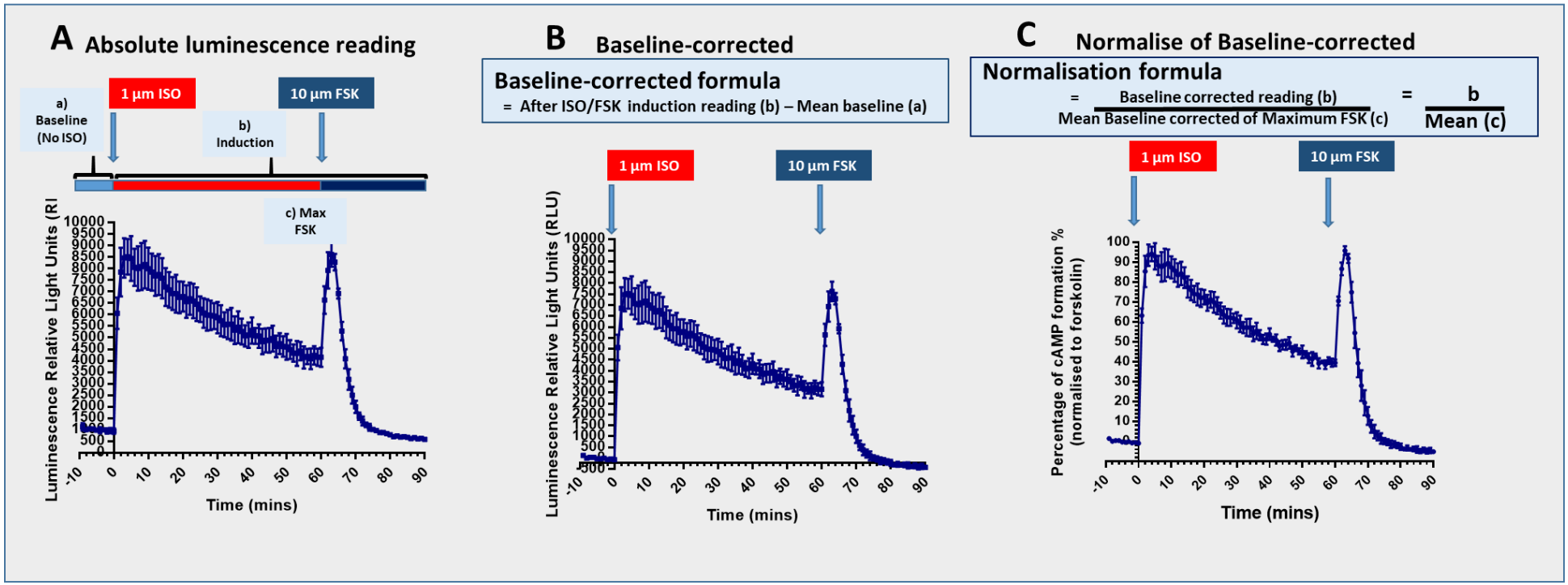


Figure 6.18: **Kinetic response of the GloSensor™-20F cAMP Assay.**

Isogenic β_2AR hESC-CMs expressing pGloSensor™-20F cAMP plasmid were treated sequentially with Isoprenaline 1 µM (ISO) and forskolin 10 µM (FSK). The nonlytic, live cells were used to monitor real-time cAMP levels. **(A)** Kinetic graph with absolute luminescence cAMP measurement expressed as relative light units (RLU). (B) Baseline-corrected graph **(C)** Normalise of Baseline-corrected kinetic graph as a percentage of cAMP formation (%) normalised to maximum FSK. Data are mean ± SEM, n=3

6.9.3.2 Investigation on the β_1AR and β_2AR kinetic profile of β_2AR isogenic variants in response to isoprenaline

The kinetic and desensitisation profiles could be different between β_2AR isogenic variants, GE, GQ, RE and RQ. As in subchapter 6.8.6 (Beta-adrenergic function by the cAMP accumulation), the pharmacological kinetic profiles of βARs in response to ISO and antagonists (ICI and CGP) were recapitulated by using the real-time cAMP assay. The general protocol for Glosensor™ was modified by integrating preincubation with (-)-antagonists (ICI and CGP) with 2% GloSensor™ cAMP reagent for 2 hours to determine the difference in response between β_1AR and β_2AR in isogenic hESC-CM variants. To prevent substrate depletion, the glosensor reagent was refreshed after 2 hours incubation with 2% cAMP reagents together with (-)-antagonists (ICI and CGP), just before the luminescence reading. The cells were then treated with 1 µM ISO and 10 µM FSK to stimulate AC, which produced cAMP, as illustrated in **Figure 6.19**.

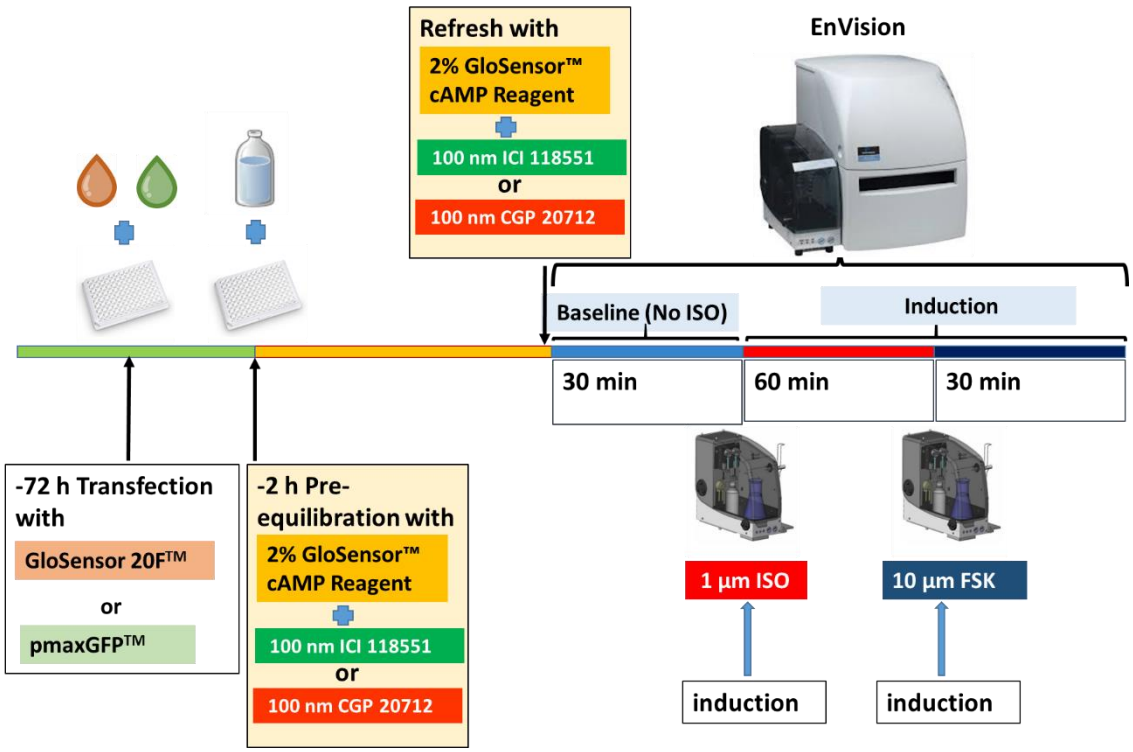


Figure 6.19: **GloSensor™-20F cAMP assay to determine β_1AR and β_2AR kinetics profile in β_2AR isogenic hESC-CMs.**

The procedure was modified by preincubation with (-)-antagonist 100 nM ICI 118,551 (ICI, β_2AR blocker)) which reflects β_1AR response and 100 nM CGP 20712 A (CGP, β_1AR blocker)) which reflects β_2AR response. The 2% GloSensor™ reagent was refreshed before the luminescence reading to prevent substrate depletion.

The maximum cAMP signals produced from both of β_1AR+ β_2AR (no antagonist) were 70.8±9.2%, 75.6±17%, 96.5±5.2% and 78±9.8%, respectively for GE, GQ, RE and RQ (Mean±SEM) **(Figure 6.20B),** while the maximum cAMP signal produced from β_2AR only (CGP) was 85.1±9.9%, 81.7±10.7%, 95.2±5.2% and 69.7±7%, respectively for GE, GQ, RE and RQ **(Figure 6.20B)**. On the other hand, the maximum cAMP signals produced from β_1AR only (ICI) were 38.4±10.4%, 42.6±6.7%, 49.5±6.3% and 25.2±2.8%, respectively for GE, GQ, RE and RQ, almost half of the response produced by β_2AR **(Figure 6.20B)**. Consistent with the previous findings (see Figure 6.13), the pharmacological analysis of real-time Glosensor™ response to ISO with antagonists revealed that responses in all GE, GQ, RE and RQ hESC-CMs were primarily mediated by β_2AR, while the β_1AR response was lower in all **(Figure 6.20A&B)**.

The subsequent experiments in this study were focused on β_2AR (i.e. with the β_1AR blocker, CGP, only) because of its potential to provide more conclusive information on the dynamics of B2AR. This suits our primary objective which was to investigate the effect of β_2AR variants on cardiomyocyte function

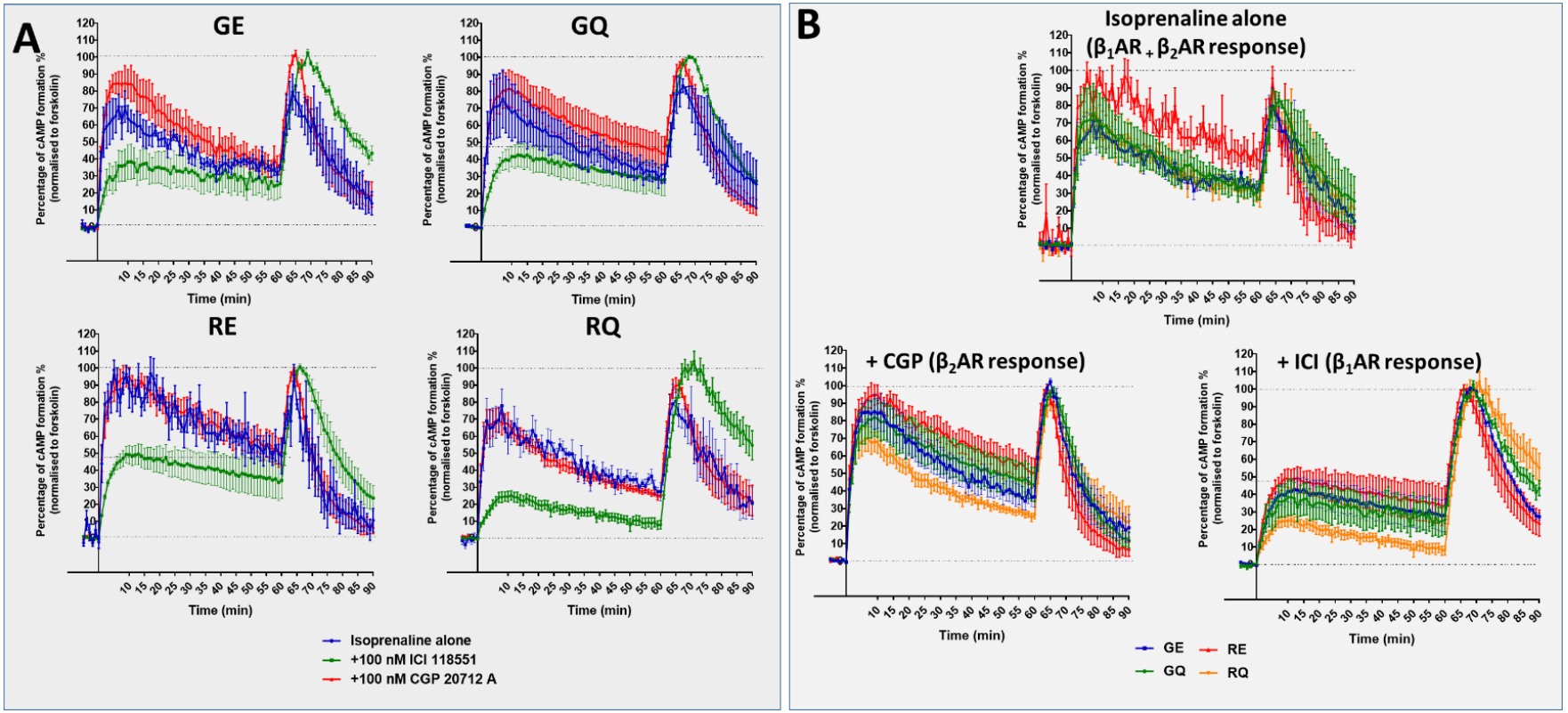


Figure 6.20: **Real-time cAMP Glosensor™ luminescence kinetic profile for ß$_2$AR isogenic hESC-CMs treated with the antagonist and stimulated with ß-agonist (ISO)**

(A) GE, GQ, RE and RQ. **(B)** Incubation with (-)-antagonist 100 nM CGP 20712 A (CGP, ß$_1$AR blocker) reflects ß$_2$AR response which similar to ISO only (ß$_1$AR+ß$_2$AR response). Incubation with 100 nM ICI 118,551 (ICI, ß$_2$AR blocker) reflects ß$_1$AR response that is approximately half of ß$_2$AR response, validated the low presence of functional ß$_1$AR in the systems. (n=2-3 biological repeats, each with n=3 technical repeats). Data are mean ± SEM expressed as the percentage of cAMP formation

6.9.4 ß$_2$AR functional differences; desensitisation in acute and chronic phases

As previously discussed, agonist exposure could cause ß$_2$AR to be uncoupled, internalised and recycled back to the plasma membrane via recycling/resensitisation (Hanyaloglu et al., 2005) and some channelled to the lysosome for degradation/ downregulation (Moore et al., 1999). This mechanism contributes to the heart-related reduction in ßARs response to the agonist. The hypothesis is that there are differences in recycling and downregulation of the ß$_2$AR isogenic variants due to reported contradictory responses. To determine the difference in receptor desensitisation on ß$_2$AR isogenic hESC-CMs in the short-term (acute), within minutes and long-term (chronic) over hours, the cells were pretreated with an agonist to stimulate uncoupling/recycling and downregulation respectively **(Figure 6.21).** The respective cAMP response was then monitored consequently by 'rechallenge' the system by using the agonist, thereby contributing to determine the maximal response difference through their intrinsic activity. In this way, it was hoped to evaluate the possible different response in ß$_2$AR polymorphism.

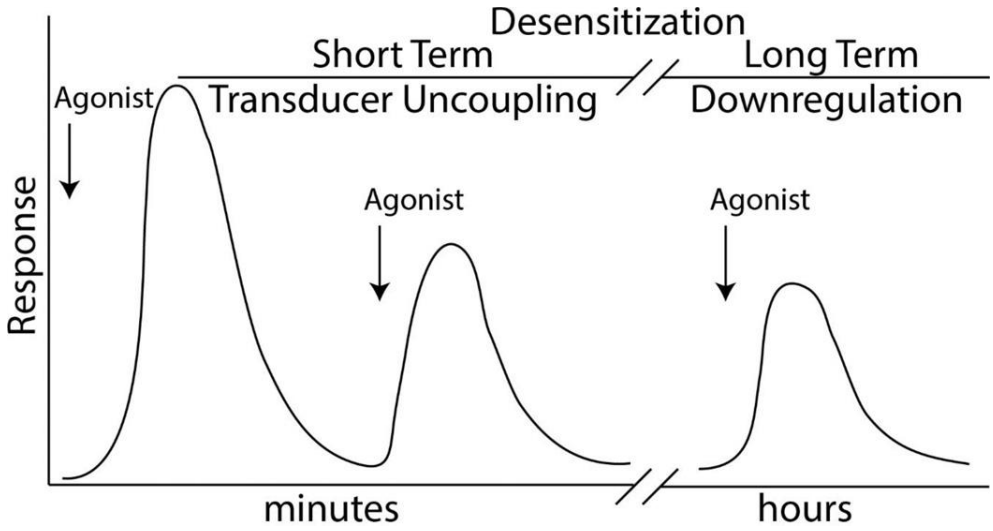


Figure 6.21: Acute and chronic phases of desensitisation.
Acute desensitisation involved repeated and short term stimulation with an agonist over the time frame of minutes to hours, which might decrease the response while chronic desensitisation involved long term prolonged stimulation with an agonist over a period of hours to days, which may have resulted in decreased receptor expression. Picture adapted from (Rajagopal and Shenoy, 2017)

6.9.5 Acute short-term desensitisation

To evaluate the receptor desensitisation over acute agonist treatment, the general protocol for Glosensor™ (see subchapter 6.9.3) was modified by integrating pretreatment of the agonist 1 µM ISO with antagonists (100 µM CGP) with 2% GloSensor™ cAMP reagent for 2 hours. At the start of pretreatment, a final concentration of 1 µM ISO was added into respective wells at 2 hours and 30 minutes time points to stimulate desensitisation (this time points were selected based on the previous study by (Oostendorp et al., 2005)). As a negative control, cells with 2 hours 2% GloSensor™ cAMP reagent+CGP pretreatment with no ISO (untreated) were used. From now on each condition will be known as No 1 µM ISO, 30 minutes 1 µM ISO and 2 hours 1 µM ISO.

After pretreatment of 2 hours and 30 minutes with (-)-1µM ISO, in order to understand the differences in recycling/resensitisation, cells were washed thoroughly twice with fresh wash medium (RPMI-B27) without ISO for a total duration of 10 minutes at 37ºC to remove ß-agonist ISO, followed with refreshment of 2% Glosensor™ cAMP reagent+CGP without ISO. Luminescence was measured by the EnVision Plate Reader in a temperature-controlled chamber at 37ºC. The basal baseline signal was measured for 10 minutes. ISO was added to the wells at 1 µM final concentration to 'rechallenge' the system and luminescence was measured for 30 minutes. Later, a final 10 µM FSK was added into the wells to stimulate the total cAMP and luminescence was read for another 15 minutes. The signal was measured by subtracting the baseline and normalizing it to the maximum Forskolin of each well. Three to five separate experiments, each done in at least duplicate, were quantitated and analysed using Microsoft Excel and GraphPad Prism. The outline of this procedure is illustrated in **Figure 6.22.**

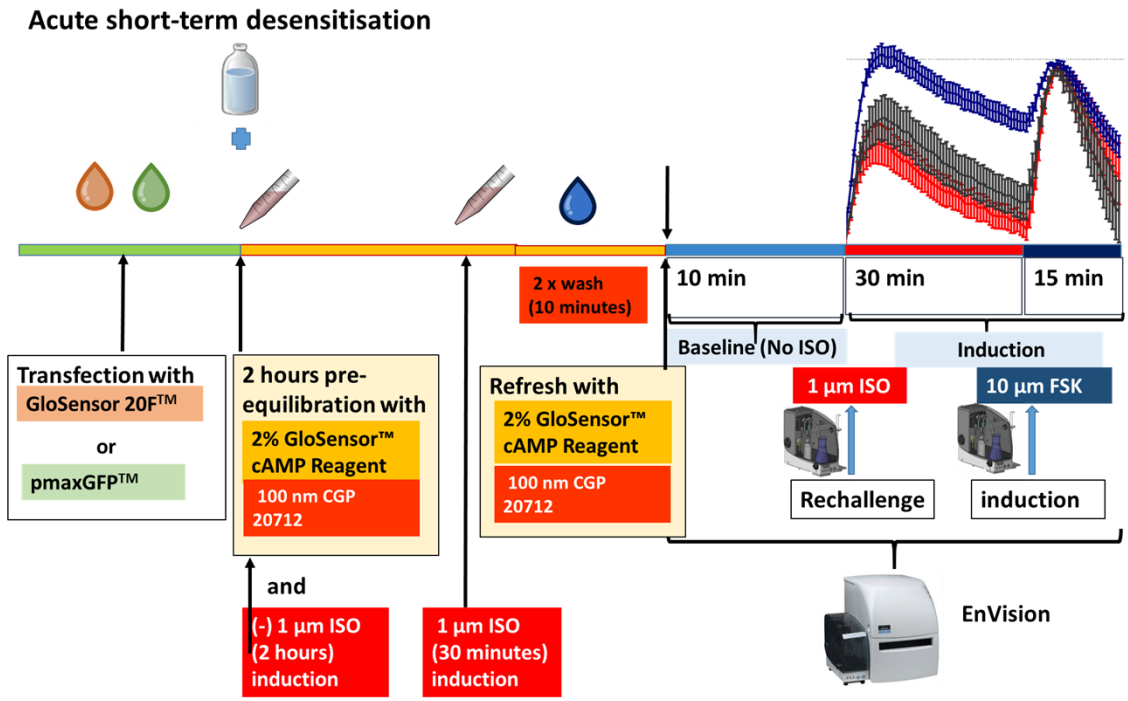


Figure 6.22: Layout for acute short-term desensitisation (2 hours and 30 minutes ISO pretreatment) followed by ISO acute rechallenge and FSK induction.

As speculated in Figure 6.21, the β_2AR response (from cAMP kinetics measurement) in general confirms the hypothesis, where the β_2AR responses of pretreatment (30 minutes and 2 hours ISO) after being rechallenged with 1 µM ISO reduced accordingly due to acute desensitisation, as demonstrated in **Table 6.5** and **Figure 6.23 .**

Table 6.5: The average percentage of maximum cAMP response

after rechallenging with 1 μM, ISO normalised to the maximum FSK response in β_2AR isogenic hESC-CMs variants GE, GQ, RE and RQ. GE (n=7), GQ (n=14), RQ (n=9) and RE (n=10).Data represents mean and ± SEM.

+ CGP 20712A (β_2AR response)		1 μM ISO pretreatment time		
		No ISO	30 mins	2 hours
GE (n=7)	Maximum cAMP response, % (mean±SEM)	114.2 ± 2.4	62.1 ± 1.6	47.7 ± 1.5
	Time to (max cAMP) after rechallenge, minutes	7	8	6
GQ (n=14)	Maximum cAMP response, % (mean±SEM)	109.6.2 ± 2.4	53.6 ± 3.5	32.8 ± 1.3
	Time to (max cAMP) after rechallenge, minutes	6	7	5.5
RE (n=9)	Maximum cAMP response, % (mean±SEM)	101.3 ± 3	67.3 ± 6.7	53.9 ± 5.8
	Time to (max cAMP) after rechallenge, minutes	6.5	7	6
RQ (n=10)	Maximum cAMP response, % (mean±SEM)	87.4 ± 2.3	56.9 ± 3.3	40.1 ± 1.6
	Time to (max cAMP) after rechallenge, minutes	7	7.5	5

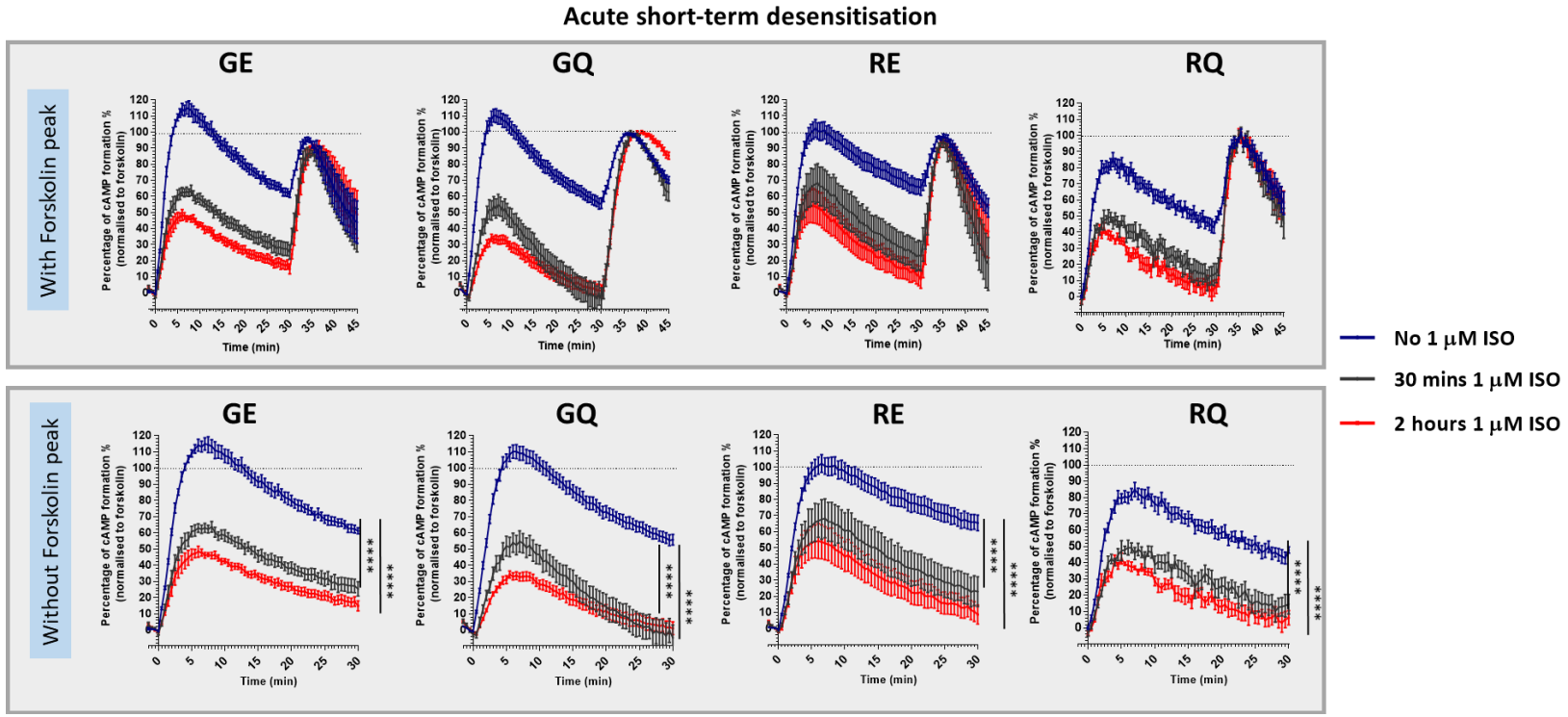
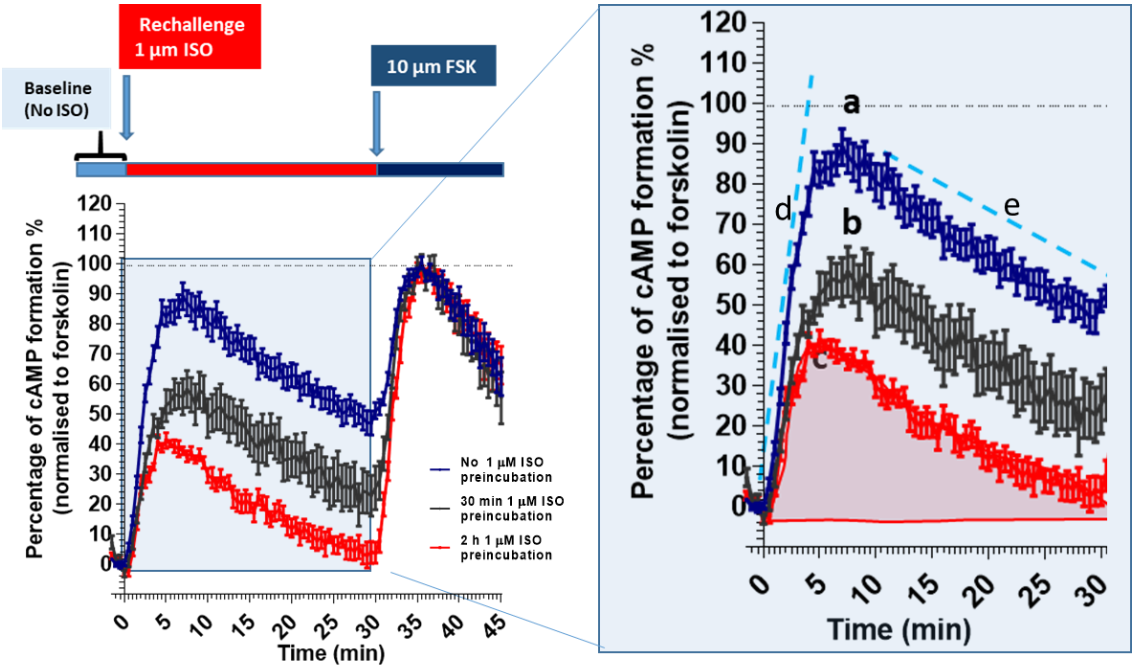


Figure 6.23: The effects of short-term ISO exposure ISO (30 minutes and 2 hours) over ß$_2$AR isogenic hESC-CMs variants;

GE, GQ, RE and RQ to stimulate acute desensitisation. All treatment was performed in conjunction with 100 nM CGP and rechallenged with 1 µM ISO to induce cAMP response. ISO was added in the culture at 0 minutes while FSK added at 30-minutes. The real-time changes in cAMP kinetics over ISO rechallenged was monitored for 30 minutes. Data were obtained in GE (n=7), GQ (n=14), RQ (n=9) and RE (n=10). Graph with mean and SEM.

To validate the difference in β_2AR response between the isogenic hESC-CMs over acute short term desensitisation, the following parameters as described in **Figure 6.24** were quantitated:



Measured metrics

1) cAMP response based on

i) Maximum cAMP peak= average peak a, b, c

ii) Total cAMP = Area under the curve

2) **Percentage of cAMP change** relative to No ISO pretreatment

i) 30 mins = (b/mean a)x 100

ii) 2 hours = (c/ mean a)x 100

3) **Percentage of β_2AR desensitisation (uncoupling)** = 100- percentage of cAMP change

4) **Rate of receptor activation** = cAMP up (d)

5) **Rate of receptor uncoupling** = cAMP down (e)

Figure 6.24: Measured metrics to quantitate the difference in β_2AR response between isogenic hESC-CMs over acute short-term desensitisation.

6.9.5.1 The cAMP response on ISO induced acute short term desensitisation

The cAMP response to rechallenged ISO were measured using two comparable methods: 1) by measuring the maximum cAMP peak as the highest receptor activity and 2) by measuring the area under each curve as the total cAMP produced. Relatively, both methods revealed similar trends. Statistically, a significant desensitisation of ISO induced cAMP was observed at both 30 minutes and 2 hours pretreatment condition compared to No ISO pretreatment in all variants GE, GQ, RE and RQ **(Figure 6.23 and Figure 6.25A)**. The pre-incubation with 1 μM ISO for 30 minutes and 2 hours does reduce the β_2AR response based on cAMP formation, which might be due to the receptor uncoupling and internalising from the plasma membrane**.**

The cAMP response based on maximum peaks and area under the curves in untreated/No ISO pretreatment revealed that RQ response was statistically the lowest compared to GE and GQ (based on maximum cAMP response; maximum peak) **(Figure 6.25A)**, while based on the total cAMP (area under the curve), the RQ was lowest compared to all GE, GQ and RE variants **(Figure 6.25B)**. This could indicate that the RQ has a lower initial β_2AR density.

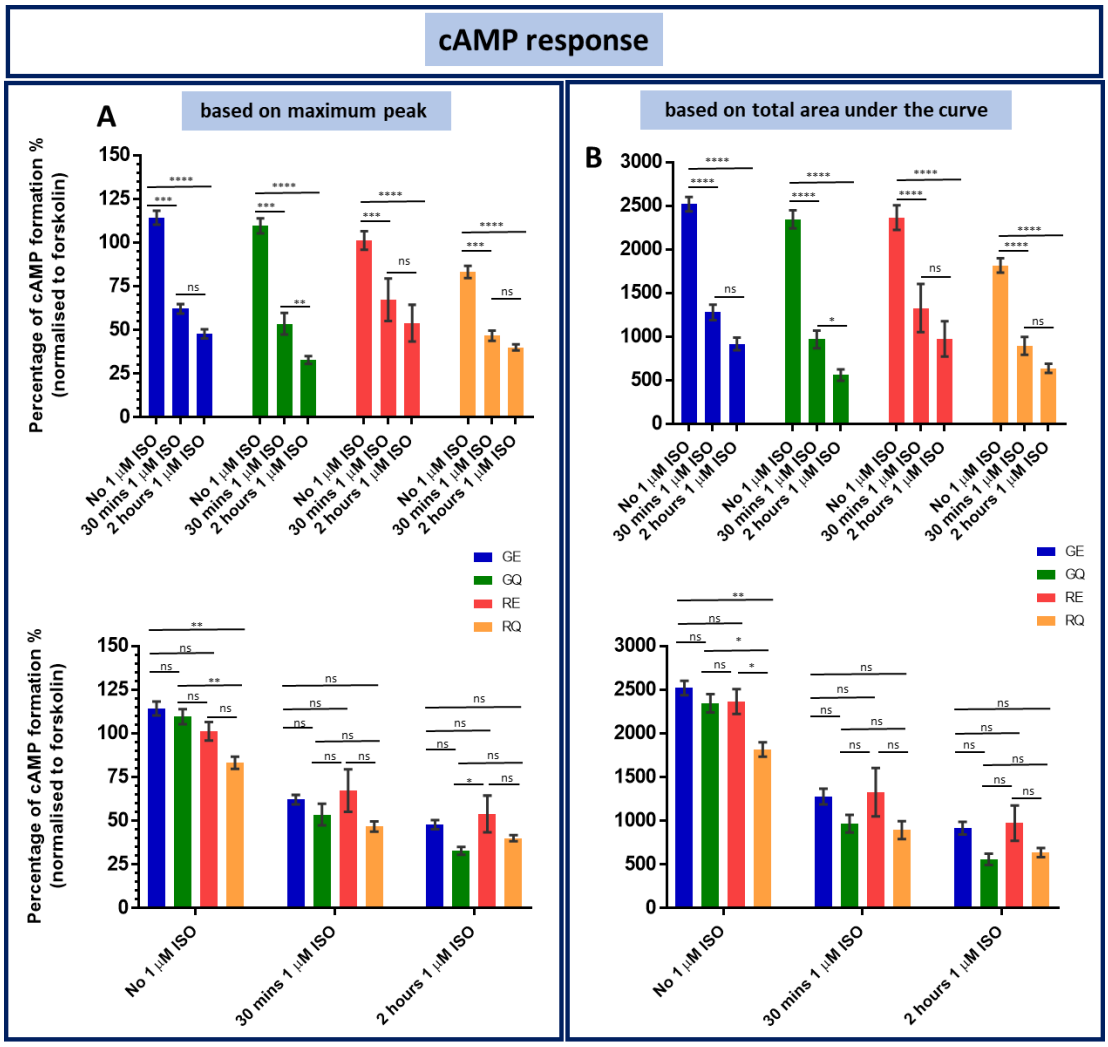


Figure 6.25: cAMP response on ISO induced acute short term desensitisation after being untreated, 30 minutes and 2 hours of 1 µM ISO pretreatment.

(A) Effects of untreated,30 minutes and 2 hours of 1 µM ISO pretreatment on cAMP response based on the maximum peak value (maximum cAMP response) on isogenic β_2AR hESC-CMs variant. **(B)** Effects of untreated,30 minutes and 2 hours of 1 µM ISO pretreatment on cAMP response based on the total area under the curve (total cAMP) on isogenic β_2AR hESC-CMs variant. Pretreatment conditions (up) were compared and variants (bottom) were compared. Data were obtained in GE (n=7), GQ (n=14), RQ (n=9) and RE (n=10). Graph with mean and SEM. Statistics are based on two-way ANOVA with Tukey's multiple comparisons test. Significance tests were based on p-values as follows: * $p < 0.05$; ** $p < 0.01$; *** $p < 0.001$; **** $p < 0.0001$ ns= not significant

6.9.5.2 Percentage of cAMP change

To quantitate the different responses within β_2AR isogenic hESC-CMs variants concerning positions 16 and 27 polymorphism and the percentage of cAMP change relative to No ISO pretreatment were measured. As expected, cAMP change on agonist-induced desensitisation after 2 hours pretreatment was lower than after 30 minutes compared to No ISO in all variants **(Figure 6.26 upper)**. However, only GQ was statistically different between 30 minutes and 2 hours (48.9±3.2% vs. 30±1.2%; $p < 0.03$ based on maximum peak and 41.3±4.4% vs. 23.8±2.8%; $p < 0.03$ based on total cAMP/area under the curve)**(Figure 6.26 upper)**. This indicates that GQ is more prone to desensitisation. In contrast, GE, GQ and RE were not statistically different between 30 minutes and 2 hours pretreatment, which could mean their β_2AR recycles/resensitises faster upon exposure to the agonist.

6.9.5.3 Percentage of β_2AR desensitisation

A similar trend was observed in percentages of β_2AR desensitisation (uncoupling). Significant ISO-induced desensitisation was observed for every β_2AR variants both 30 minutes and 2 hours of ISO pretreatment **(Figure 6.27 upper)**. However, between variants, there was no significant change in the mean of desensitisation of each line after 30 minutes of ISO pretreatment **(Figure 6.27 bottom)**. In contrast, after 2 hours of pretreatment, the mean percentage of ISO-induced desensitisation in GQ (70.1±1.2% and 58.7±4.3%) was significantly higher than RE (46.7±35.8% and 43.9±11.6% ; $p< 0.03$) **(Figure 6.27 bottom).** This indicates that GQ has the highest desensitisation upon 2 hours pretreatment and slower recycling, while GE, RE and RQ recover quickly from desensitisation between 30 minutes and 2 hours pretreatment.

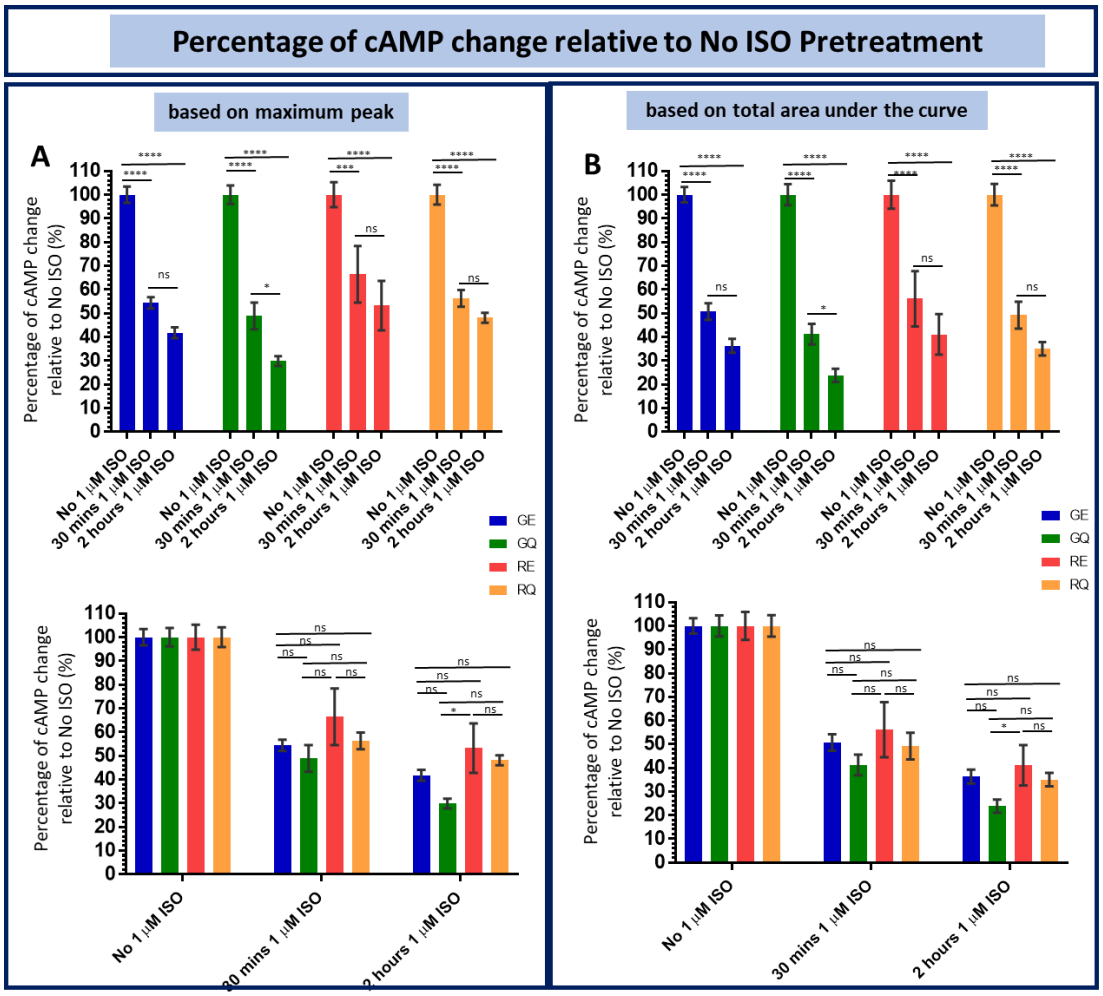


Figure 6.26: Percentage of cAMP change relative to No ISO pretreatment with 30 minutes and 2 hours of 1 µM ISO pretreatment.

(A) Percentage of cAMP change based on the maximum peak value (maximum cAMP response) on the isogenic ß$_2$AR hESC-CMs variant. **(B)** Percentage of cAMP change based on the total area under the curve (total cAMP) on the isogenic ß2AR hPSC-CMs variant. Differences between pretreatment conditions (up) and between variants (bottom) were compared. Data were obtained in GE (n=7), GQ (n=14), RQ (n=9) and RE (n=10). Graph with mean and SEM. Statistics are based on two-way ANOVA with Tukey's multiple comparisons test. Significance tests were based on p-values as follows: * $p < 0.05$; ** $p < 0.01$; *** $p < 0.001$; **** $p < 0.0001$ ns= not significant

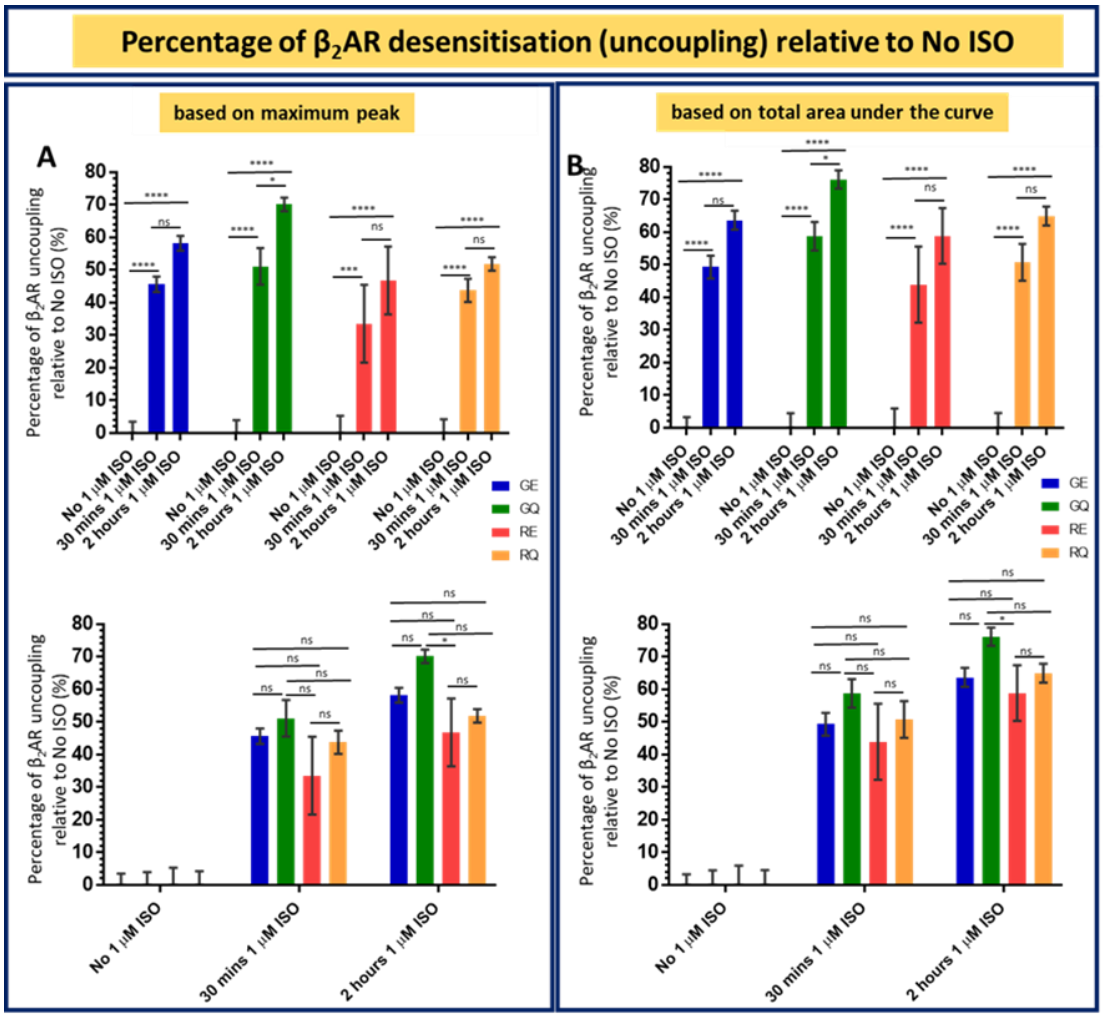


Figure 6.27: Percentage of ß2AR desensitisation (uncoupling) relative to No ISO pretreatment in 30 minutes and 2 hours of 1 μM ISO pretreatment.

(A)Based on the maximum peak value (maximum cAMP response) on isogenic ß2AR hESC-CMs variant. (B)Based on the total area under the curve (total cAMP) on isogenic ß2AR hESC-CMs variant. Differences between pretreatment conditions (up) and differences between variants (bottom) were compared. Data were obtained in GE (n=7), GQ (n=14), RQ (n=9) and RE (n=10). Graph with mean and SEM. Statistics are based on two-way ANOVA with Tukey's multiple comparisons test. Significance tests were based on p-values as follows: * $p < 0.05$; ** $p < 0.01$; *** $p < 0.001$; **** $p < 0.0001$ ns= not significant.

6.9.5.4 Rate of receptor activation

To evaluate the starting 'active' receptors upon ISO pretreatment, the rate of receptor activation based on up linear regression were quantitated. It was observed that the active $ß_2$AR pool was high in both Gly16, the GE and GQ at basal condition (No ISO pretreatment) (**Figure 6.28A)**. Both GE and GQ have a significant rate of activation between 30 minutes and 2 hours, while no significant difference in the rate of activation between 30 minutes and 2 hours of RE and RQ (**Figure 6.28B)**. This means the Gly16 desensitises more while Arg16 is resistant to desensitisation and recycles faster.

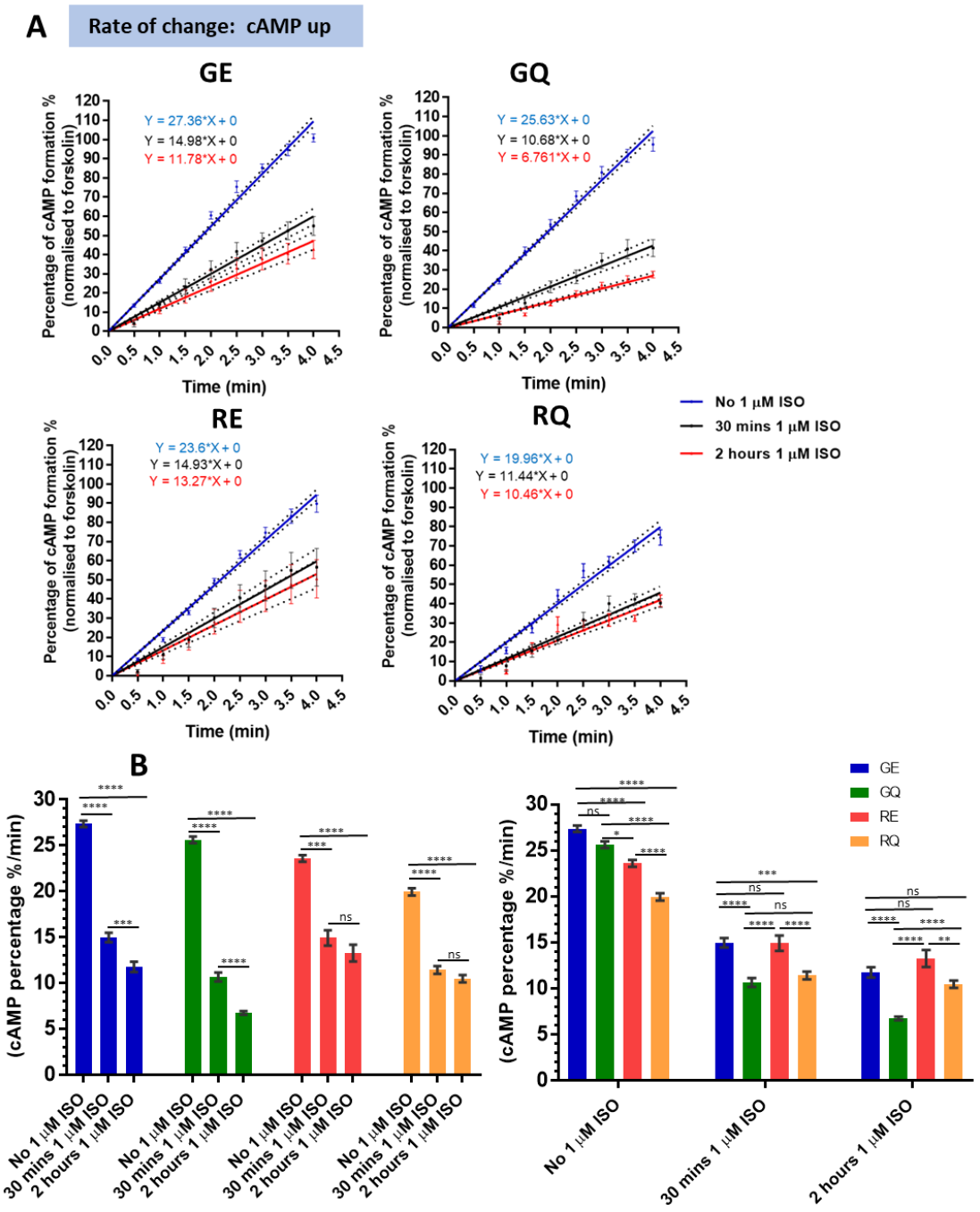


Figure 6.28: Rate of receptor activation based on linear regression of cAMP up.

(A) The linear regression graph with the slope equation. **(B)** The differences in rate of receptor activation between pretreatment conditions (right) and between variants (left). Data were obtained in GE (n=7), GQ (n=14), RQ (n=9) and RE (n=10). **Graph with mean and SEM**. Statistics are based on two-way ANOVA with Tukey's multiple comparisons test. Significance tests were based on p-values as follows: * $p < 0.05$; ** $p < 0.01$; *** $p < 0.001$; **** $p < 0.0001$ ns= not significant.

6.9.5.5 Rate of receptor uncoupling

To evaluate the receptor uncoupling after the acute-induced desensitisation, the linear regression of cAMP down was quantitated. It was observed that the GQ uncoupled the highest at 30 minutes ISO pretreatment condition (-2.6±0.13%/min vs -1.6±0.06%/min; $p<0.0001$ (GE), vs -1.98±0.19%/min; $p<0.0001$ (RE) and vs -1.6±0.06/min; $p < 0.0001$(RQ)) **(Figure 6.29A and B).** This again confirms that GQ is prone to desensitisation. RE has the lowest uncoupling at the basal (No ISO pretreatment), and the highest receptor uncoupling at 2 hours pretreatment, which indicates that RE is resistant to desensitisation and has faster receptor recycling **(Figure 6.29B)**

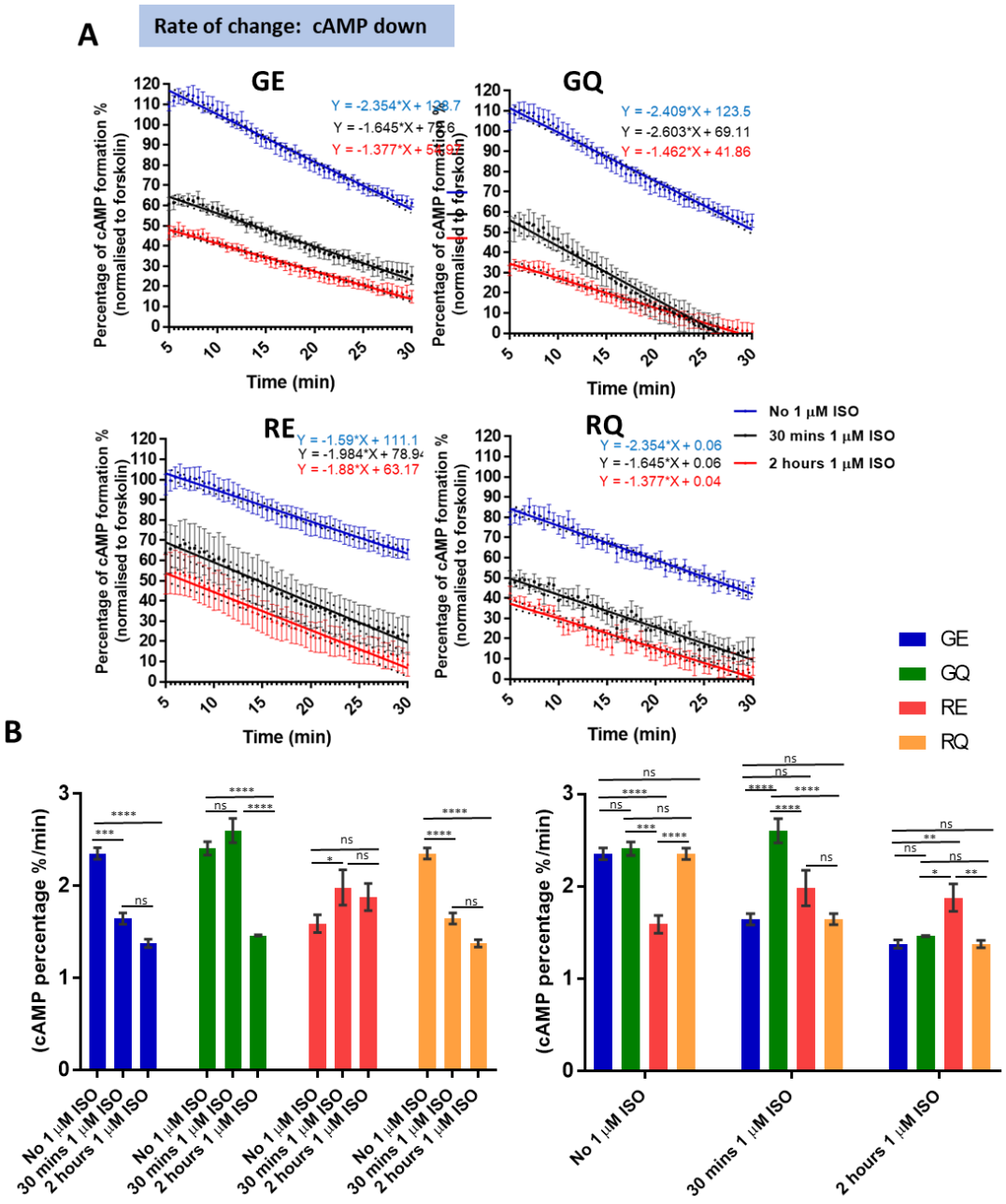


Figure 6.29: Rate of receptor uncoupling based on linear regression of cAMP down.

(A) The linear regression graph with the slope equation. **(B)** The differences in the rate of receptor uncoupling between pretreatment conditions (right) and between variants (left). Data were obtained in GE (n=7), GQ (n=14), RQ (n=9) and RE (n=10). Graph with mean and SEM. Statistics are based on two-way ANOVA with Tukey's multiple comparisons test. Significance tests were based on p-values as follows: * $p < 0.05$; ** $p < 0.01$; *** $p < 0.001$; **** $p < 0.0001$ ns= not significant.

6.9.6 Chronic long-term desensitisation

It was suggested that cells could become total 'desensitised' or 'tolerant' over further stimulation of agonist due to receptor downregulation. We further speculated that the downregulation depends on both concentrations of agonist and the time of exposure (Barisione et al., 2010). By using the same GloSensor™ principle, the extent to which differences in agonist-induced downregulation for β_2AR isogenic hESC-CM variants were determined. To assess this, hESC-CMs were either untreated or chronically pretreated for 24 hours(longer exposure time) with 10 µM ISO (higher concentration) to stimulate receptor downregulation. The cAMP produced was then measured in response to acute ISO re-challenged. The experiment is illustrated in **Figure 6.30**.

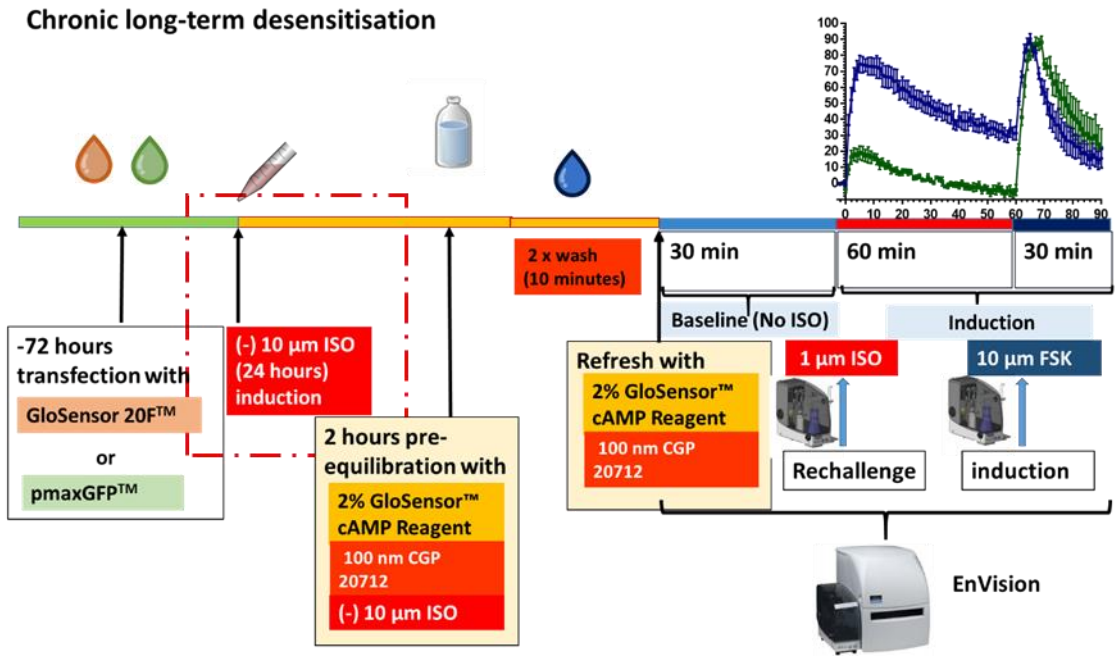


Figure 6.30: Layout for chronic long-term desensitisation (24 hours 10 µM ISO pretreatment) followed by ISO acute rechallenge and FSK induction.

As speculated, exposure to 24 hours of 10 μM ISO resulted in β_2AR downregulation in all variants **(Figure 6.31),** although the GQ variant seems to have undergone the highest downregulation (with lowest percentage of cAMP change) (10.7±1.3% (GQ) vs 24.8±3.2% (GE), vs 20.1±2.8% (RE) and vs 18.13±1.7% (RQ)) based on maximum peak **(Figure 6.32A)** and (8.7±1.9% (GQ) vs 15.7±2.9% (GE), vs 15.6±1.9% (RE) and vs 14.3±2.5% (RQ)) on the area under the curve **(Figure 6.32B)** respectively. The differences were not significant.

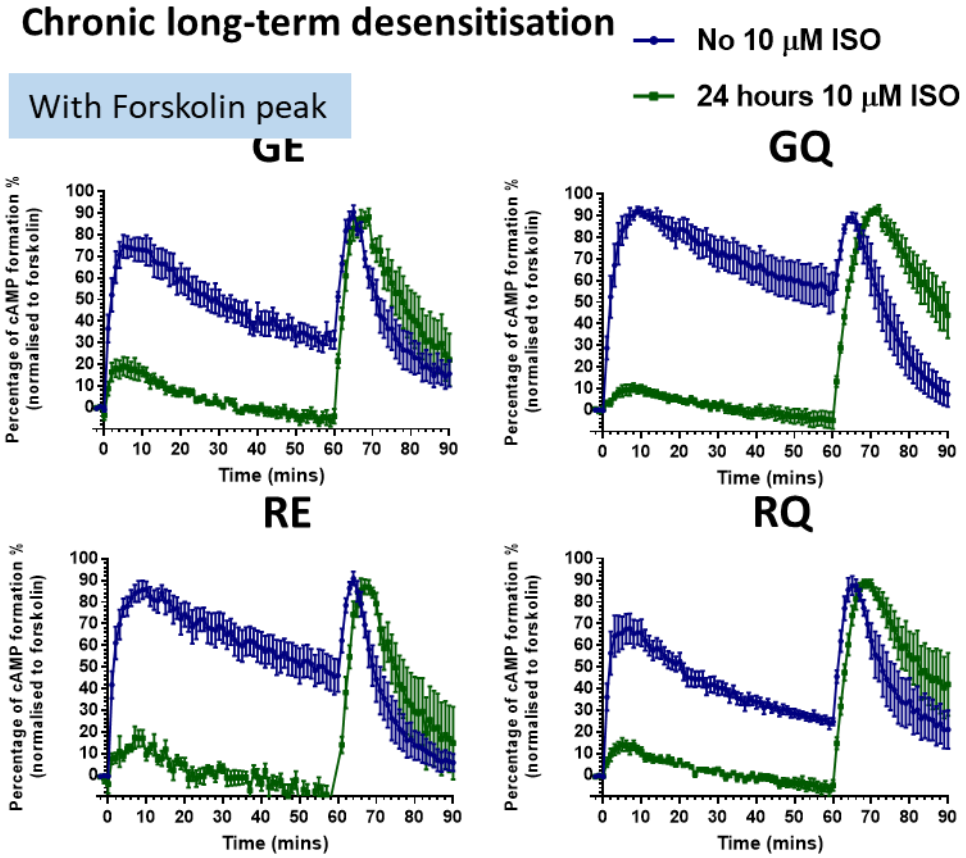


Figure 6.31: The effects of long-term ISO exposure ISO (24 hours 10 μM ISO) over β2AR isogenic hESC-CMs variants

GE, GQ, RE and RQ to stimulate chronic desensitisation. All treatment was carried out in conjunction with 100 nM CGP and rechallenged with 1 μM ISO at 0 minute to induce cAMP response,while FSK was added at 60-minutes. The real-time changes in cAMP kinetics over ISO rechallenged was monitored for 60 minutes. Data were obtained in GE (n=9), GQ (n=9), RQ (n=9) and RE (n=9). Graph with mean and SEM.

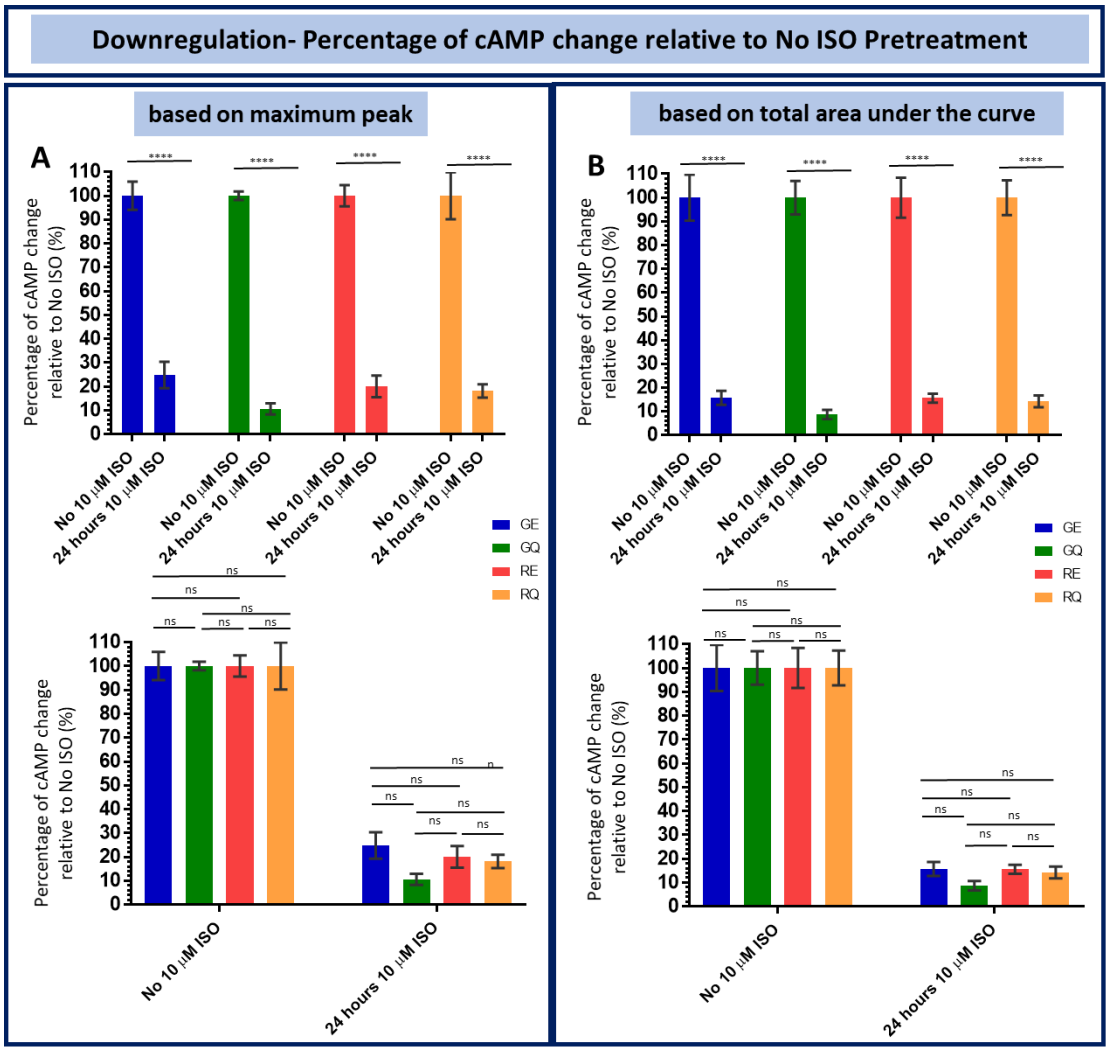


Figure 6.32: Percentage of cAMP change relative to No ISO pretreatment in 24 hours of 10 µM ISO pretreatment.

(A) Percentage of cAMP change based on the maximum peak value (maximum cAMP response) on isogenic β_2AR hESC-CMs variant. **(B)** Percentage of cAMP change based on the total area under the curve (total cAMP) on isogenic β_2AR hESC-CMs variant. Comparison of differences between pretreatment conditions (up) and comparison of differences between variants (bottom). Data were obtained in GE (n=9), GQ (n=9), RQ (n=9) and RE (n=9). Graph with mean and SEM. Statistics generated by two-way ANOVA, Tukey's multiple comparisons test. Significance tests were based on p-values as follows: * $p < 0.05$; ** $p < 0.01$; *** $p < 0.001$; **** $p < 0.0001$ ns= not significant.

6.10 Chapter discussion and conclusion

This chapter discusses the impact of gene-induced changes in cell function by studying β_2AR polymorphism at amino acid positions 16 and 27. One of the findings of this phase of the research is that the hESC (hPSC) is capable of harbouring genome-edited isogenic β_2AR polymorphisms position 16 and 27. The possible variants combination resulted in four β_2AR variants (GE, GQ, RE and RQ).

This is the first time that demonstrated the chosen β_2AR variants were created by using hESC-CMs. The original research by Green 1994, studied all four possible variants in recombinant cells (Green et al., 1994), including the rarely found variants of RE (McGraw et al., 1998). The majority of data on β_2AR subtypes are based on transgenic overexpression models that were created to increase readouts. Whether these overexpression models represent an accurate model of β subtypes at the physiological level is questionable as it may cause unphysiological responses compared to the native expression levels. Contrast data has been shown between several β_2AR overexpression models.

For example, a study by Rengo *et al.* (2012) shows that overexpressed β_2AR improved cardiac contractility and increased in angiogenesis, while other models have shown cardiac dysfunction, interstitial fibrosis and higher mortality (Du et al., 2000, Nguyen et al., 2015, Rengo et al., 2012). These data further support a previous study by (Dorn et al., 1999) which concluded that a high level of β_2AR (300 fold overexpression) caused abnormal cardiac effects. Therefore it was suggested that only a low, moderate level of β_2AR is beneficial to study β_2AR polymorphisms (de Lucia et al., 2018). As such the β_2AR variants by gene-induced changes created in this chapter via CRISPR/Cas9 suits the previous drawback.

Correspondingly, hPSC-CMs recapitulate many cellular, molecular and functional aspect of the human heart at normal and pathological physiology condition including their response to cardioactive drugs, which make them an ideal candidate to study the mentioned polymorphisms and facilitate insight into disease mechanism (Giacomelli et al., 2017). Also, the high scalability of hPSC to CMs make them a suitable candidate for medium-high throughput functionality assay.

The genome-edited ß$_2$AR variants (demonstrated normal pluripotency, retained stable karyotype and successfully differentiated at high efficiency into beating hESC-CMs (hPSC-CMs). The variants were also able to translate their differences in the functional response of receptor upon agonist stimulation via cAMP assay.

Previously it was reported that SNPs in positions 16 and 27 could influence receptor response to long term agonist (downregulation) but do not affect receptor-ligands binding or coupling to Gs/ adenylyl cyclase (Insel et al., 2007). An experiment conducted on a Chinese hamster ovarian fibroblast by mutating nucleic acids 46 (adenine to guanine) and 79 (cytosine to guanine) or both, generated constructs encoded for amino acids residue position 16 (Gly16Arg/G16R), 27(Gln27Glu/ Q27E) or both combination (Gly16Arg + Gln27Glu /G16R + Q27E).

It was suggested that all mutated receptor displayed standard agonist binding and coupling to Gs, but that their polymorphism could affect their susceptibility to agonist-induced downregulation (Green et al., 1994). Another study conducted in primary cultured bronchial smooth muscle cells (Hall, 1996) revealed that Gly16 is prone to downregulation after exposure to ß$_2$-agonist while Glu27 appears to be resistant to an agonist-induced downregulation in an experiment. Meanwhile, double mutant Gly16Glu27(GE) undergoes more significant downregulation whereas Arg16Glu27(RE) was utterly resistant to receptor downregulation (Green et al., 1994).

The suggestion was further validated by a retrospective study which was conducted in asthma patients where Arg16 variants showed less response to short or long-acting ß$_2$-agonists than patients with Gly16, which suggests that Gly16 may be susceptible to receptor desensitisation (Israel et al., 2004).

These data are, however, contrary to a case study conducted by Dishy et al., (2001) according to the measurement of vascular response in dorsal hands. Unlike the study by Green et al. (1994), they concluded that, instead of being prone to downregulation, Gly16 is, in fact, resistant to agonist-mediated receptor desensitisation.

To date, none of the studies has examined the association of β_2AR polymorphisms within the same genetic background to rule out the possible role of *ADRB2* variants in clinical outcome and therapeutic response in cardiac setting. The study in this chapter focuses on adding new knowledge relating to *ADRB2* gene function and β_2-AR polymorphism in the isogenic hESC(hPSC)-derived cardiomyocytes at position 16 and 27. As such, based on the cAMP response upon ISO stimulation, the RQ was revealed to produce the lowest cAMP, and hence this could indicate that the RQ has lower initial β_2AR density **(Figure 6.25)**.

The cAMP analysis uncovered that in acute (short-term) agonist exposure, the GQ has the highest desensitisation. In contrast GE, RQ and RE were not statistically different between 30 minutes and 2 hours pretreatment, which could mean their β_2AR recycled/resensitised faster upon exposure to the agonist **(Figure 6.27)**. A different way of quantification has validated that Gly16 prone to desensitisation, while Arg16 resistant to desensitisation with RE has a faster receptor recycling **(Figure 6.28 and Figure 6.29)**. Meanwhile, in chronic long-term agonist exposure, although there is no significant difference with regards to downregulation across all four β_2AR variants, GQ has a trend as the most downregulated **(Figure 6.32)**.

Nevertheless, the molecular function of these polymorphism on cell-function is still not well understood. However, the possible mechanism of enhanced desensitisation and recycling are yet to be discovered for example by monitoring their trafficking with compartment markers colocalisation. The comparative analysis of these compartment markers might provide information on the dynamics of recycling of different polymorphisms.

Another suggestion is to introduce the same polymorphism into patient-specific induced pluripotent stem cells (iPSCs), generating two genetically distinct isogenic β_2AR and control lines. The usage of iPSCs would address the ethical limitations of hESCs too. This must also involve the characterisation of molecular details and its regulation across varieties of drugs. These gene-induced changes models will hopefully provide the basis for the differences in clinical response among patients and could make possible direct tailoring for drug prescription,

hence personalised healthcare, to maximize efficacy and safety while reducing side effects.

Chapter 7 General Discussion

This thesis aimed to investigate the potential of utilising human pluripotent stem cell-derived cardiomyocytes (hPSC-CM) to assess the impact of drug and gene-induced changes on cell function in order to address cardiac safety and efficacy issues. The hPSC-CMs, which consists of hiPSC-CMs (utilised for drug-induced changes chapters) and hESC-CMs (utilised for gene-induced changes chapter), is the most humanised platform available that can help to accelerate the drug development process and individualised treatment towards personalised therapy, into the market in a reliable and cost-effective manner.

The hPSC-CMs exhibit most characteristics of functional human cardiomyocytes (albeit their immaturity), can be cultured *in-vitro* for an extended period and are potentially scalable for large scale production, which make them appropriate for the purposes of this thesis study. They recapitulate many cellular, molecular and functional aspects of the human heart in normal and pathological conditions, including their response to cardioactive drugs that make them the ideal candidate to study drug safety prediction and for mentioned polymorphism, to facilitate insight into drug and disease mechanisms (Giacomelli et al., 2017).

The studies reported in this thesis have demonstrated the value of hiPSC-CMs in drug testing by not only by investigating the voltage electrophysiology and/or cardiac arrhythmia but also and primarily, by focusing on contractility, which was the primary unaddressed area of interest to one of the CRACK-IT partners, GSK. This thesis is distinct as relatively few studies have used hiPSC-CMs contractility in predicting safety assessment. As a whole, similar multi-platform and multi-blinded comparisons are extremely important to make advances in the field, towards implementing hiPSC-CMs in preclinical drug development. Without the head to head comparison that was carried out, pharmacy companies would be reluctant to adopt the technology as it is beyond their scope and expertise.

Meanwhile, the feasibility and utility of genome editing tools in hPSC-CMs (in this thesis, by utilising hESC-CMs) is critical to expanding the field of human

disease modelling, with regards to understand gene function. To removed genetic variation between hPSC-CMs, isogenic sibling cell lines were generated by altering only a few nucleotides to establish a genetically defined condition for more precise comparative analysis when modelling diseases. As such, four isogenic lines of β_2AR (GE, GQ, RE and RQ) were created. These isogenic cell lines can be used not only to understand certain consequences of polymorphisms (positions 16 and 27) but also can be used to perform medium-throughput genetic and pharmacological screens to understand the underlying pathological mechanism which, in future, might help to develop therapeutic agents to prevent, treat or improve efficacy of treatment of such polymorphisms or diseases.

7.1 Fulfilment of thesis objectives

There were four main thesis objectives outlined in **section 1.13** which have been addressed throughout this thesis:

7.1.1 Objective 1: Establish the CellOPTIQ drug screening system by sequentially analysing contractility and voltage output by validating 'training' sets of drug compounds and developing the culture systems.

The culture systems for hiPSC-CMs for the drug-induced changes chapter were successfully established, specifically for the in-house large scale production of R-PAT-CMs. Despite some initial setbacks, such as different baseline measurements and atrial/ventricular phenotypes between hiPSC-CMs, all hiPSC-CMs baseline were able to be quantitated on the CellOPTIQ platform. The difference in their phenotyping might result in different cardiac differentiation protocols, days of differentiation, methods of cryopreservation, especially for commercial lines by which their recipes are proprietary to the company. The training set of 7 drugs was used in R-PAT-CMs to unify the methods for testing, analysing and presentation. This helped to establish the standard operating procedures (SOPs), which were used for the subsequent blinded evaluation of Tier 2 test set drugs.

7.1.2 Objective 2: Blinded compound testing in hiPSC-CMs

By using SOPs established in objective 1, up to 28 blinded drugs were tested in rank order that was predefined by GSK. The differentiation of the in-house hiPSC-CMs (R-PAT-CMs) was sufficient to test all available drugs on CellOPTIQ, while testing was restricted to the top 10 first priority drugs in commercial hiPSC-CMs (Pluricytes and iCell^2) due to cost, availability and timelines. The accuracy of the CellOPTIQ:hiPSC-CMs combination ranged from 40-60%, with the poorest predictivity being for PI, which ranged from 0- 25%, while NE and NI were predicted most accurately (up to 100%). Comparing across CRACK-IT partners platforms, the EHT:hiPSC-CMs combination appeared to be more predictive than CellOPTIQ:hiPSC-CMs and the data implied that continuous measurement from a 3D preparation yielded more predictive contractility data

than cell motion sampled from a 2D culture. The EHT also seems to be the most sensitive platform compared to others. In terms of the most predictive contractility markers, the CT followed by RT is highly informative for PI drugs, and CA clearly provided informative parameters for NI drugs.

7.1.3 Objective 3: To refine and improve the CellOPTIQ and culture system after 'unblinding', if needed.

Based on the blinded Tier 2 test, the evaluation of the results showed that PI drugs were least well predicted by hiPSC-CMs. Incorrect predictions were also observed for NI drugs. It was hypothesised that high beat rate (≥1 to 1.5 Hz) of hiPSC-CMs might cause the cells to 'max out' and hence not respond correctly to the stimuli. Under the refined conditions, the beat rate was reduced and the signal to noise ratio was improved by 1) using the protein-containing medium (RPMI-B27) to replace serum-free media (SFM), 2) Ivabradine pretreatment. For NI drugs, accuracy was improved under refinement test condition of chronic long-term drugs exposure. The refinement of the culture system successfully improved accuracy on drugs predictability, leading to accuracy of up to 75% for the CellOPTIQ:hiPSC-CMs combination.

7.1.4 Objective 4: To investigate the ß$_2$-adrenergic receptor polymorphism via gene-induced changes to cell function by utilising genome-editing hPSC-CMs

The findings in this chapter are preliminary and provide the proof of the concept that the gene-induced changes. variants' specific expression and their phenotype regulation can potentially provide an association of genetic information and in-depth phenotype of human 'disease' and their pharmacogenomics studies.

The HUES7-hESC-CMs was successfully genome-edited to create four ß$_2$AR isogenic lines (GE, GQ, RE and RQ) to study positions 16 and 27 polymorphism. The isogenic lines were not only able to retain their pluripotency but also able to pinpoint a cell type in which the 'disease' manifests. As such, the isogenic

lines were able to differentiate effectively into cardiac cells (cardiomyocytes) to identify molecular or cellular phenotypic readouts of the 'disease' state. Accordingly, the pharmacological test revealed that the β_2AR isogenic lines were abundant with β_2 while almost non-existent in β_1. This contradicts previous findings by Bristow (1986), which observed proportions of β_1 (77%) and β_2 (23%) in the isolated cardiac tissue of non-failing human ventricular.

Meanwhile, in a failing heart ventricle, the proportion of β_1:β_2 ration was markedly different; 60:38 (Bristow et al., 1986). It was suggested that the increase in β_2AR subtype in progressive heart failure is to inhibit apoptosis events and increase the inotropy (Panebra et al., 2010). Thus the potential of the different β_2AR variants to affect the heart failure progression or influence the efficacy of β-blockers is worth further investigation, using the variants proposed in this thesis.

The downregulation conducted in this thesis during chronic agonist exposure does represent the major mechanism of tachyphylaxis. To date, no association studies have used the full β_2AR variants with β-agonist or β-blockers in heart failure (Panebra et al., 2010). Given the phenotypes of β_2AR variants were successfully created in this research, it is appropriate to carry out further such studies. Such an approach hopefully could improve the predictiveness of β_2AR variations with the relevant clinical phenotypes and solve the discrepancies between studies. In addition, β_1AR does not undergo any genome-editing modification; therefore, the difference of each polymorphism is exclusive to the β_2AR, and hence their functional differences might be able to be quantitated.

7.2 Limitation of the study

7.2.1 Drug-induced changes chapters

Immaturity

The hiPSC-CMs have been widely reported to have characteristics that are similar to fetal cardiomyocytes rather than adult human cardiomyocytes (Robertson et al., 2013, Sayed et al., 2016b, Veerman et al., 2015). These immature characteristics represent a challenge for drug testing and cardiotoxicity. Therefore, although the data correctly predicted some drugs, it is essential to note that these hiPSC-CMs still lack some important structural elements that reflect mature phenotypes. In this regard, the EHT was more accurate in predicting as it is more mature. Therefore, improving the maturation of hPSC-CMs would improve predictive accuracy. Some progress has been made in terms of improving the maturation of hiPSC-CMs, including using defined synthetic substrate (Patel et al., 2015) and development of the first generation of maturation medium (Ribeiro et al., 2015); however, their integration into CRACK-IT could not be accomplished in the time frame of the research conducted for this thesis.

Interpreting results

Conversely, some care needs to be taken when interpreting the results from hiPSC-CMs as there are substantial differences between hiPSC-CMs and adult CMs: hPSC-CMs are on average smaller, lack T-tubule and have a lower contractile force. The subcellular differences need to be further understood in order to translate the findings in hPSC-CMs to adult myocytes and subsequently, the mechanisms involved. Although these findings are encouraging, it is not always straightforward to translate hiPSC-CM -related parameters of CA, CT, RT and chronotropy (beat rate) to clinically relevant data.

Excessive pacing

Among the inconvenient challenges is to tackle the spontaneous activity that varies in hiPSC-CMs during the assay and influence that underlying the action

potential duration. Therefore, it was essential to correct the action potential for the known effects using graphite electrodes, which were placed in the thermostated atmosphere to stimulate them according to their adaptive frequency. Under pacing conditions, the beat rate was the same before and after drug treatment, unless the drugs caused the changes. The hiPSC-CMs were stimulated using a short pulse (10 ms) and used voltage as low as possible (8V) while still activating the cells. However compared to the other 2D monolayer platform of TTM, the CellOPTIQ had lower accuracy, although the same kind of hiPSC-CMs were used (Pluricytes). Unlike TTM which could be stimulated simultaneously for all 3 parameters (contractility, voltage and calcium) for only twice (baseline and after treatment) (van Meer et al., 2019), CellOPTIQ involved at least 4 pacings on the same well (baseline contraction, treatment contraction, baseline voltage and treatment voltage), which might increase the susceptibility of response during subsequent measurement.

7.2.2 Gene-induced changes chapters

hESC-CMs disease model

These $ß_2$AR isogenic variants were created from hESC-CMs, which are less desirable when compared to hiPSC-CMs due to ethical issues. In addition, occasionally, the HUES7 hESC cell lines were a bit sensitive and difficult to differentiate. Therefore if time had not been an issue, it would have been best to genome edit the variants from the hiPSC line rather than the hESC line.

Potential clonal variation

In $ß_2$AR isogenic variants, due to the different clonal selections and genome editing, some variables might alter the epigenome variants (Ojala et al., 2012). In this thesis, only one clonal for each variant was selected. The best way is to select more than one clone of each variant and compare their response towards agonist exposure (acute and chronic), to validate if the same profile is reproducible.

7.3 Implications of this investigation

7.3.1 3Rs (Replacement, reduction and refinement)

Cardiotoxicity is the leading cause of compound loss. Accordingly, from GSK's own data, it is suggested that direct damage to the myocardium and electrical system account for 30% and 22% respectively for cardiovascular liability. This inflates the cost of drug development. If drug attrition could be reduced or eliminated, the cost of new drug development would be reduced by 75%. The use of hPSC-CMs would also potentially reduce the number of animals needed for preclinical testing. In this regard, this research has enhanced the availability of using hPSC-CMs as a tool.

7.3.2 In-vitro clinical trials

This success of monitoring drug-induced changes would allow hPSC-CM derivates to be used for in-vitro clinical trials. A selection panel of different hiPSC-CMs with different genome-edited isogenic lines could provide resources that reflect the patient populations more accurately than current clinical trials, where numbers of participants are low and the inclusion of individuals who have comorbidities is rare, including the rare 'disease' phenotypes which are not widely available during human clinical trials recruitment (de Korte et al., 2019).

7.3.3 Commercialisation

The success of the testing platform hiPSC-CMs and isogenic variants of 'disease' model could be sold, licensed or offered as a service to a broad range of end-users who would benefit from the 3Rs, drug development pipeline and personalised medicine.

7.4 Final remarks and future work

Several future experiments could be conducted to strengthen the findings of this thesis and further its aims. These are discussed below.

7.4.1 Drug-induced changes chapters

1. Another platform could be employed and all the blinded drugs retested under short and long term exposure, for example, by using RTCA Cardio ECR. In CardioECR, 1) there is less plate manipulation involved (pacing electrodes are in-built so less manual intervention is needed), 2) dyes are not needed to measure electrophysiology (prevents dye toxicity and prevents binding to the protein in the medium), 3) continuous monitoring for baseline, acute and chronic reading can be provided (unfeasible in CellOPTIQ which are labour-intensive), 4) data analysis is simplified 5) continuous pacing to improve hiPSC-CMs maturation is possible.

2. Some mode of action could be included which is not represented on the drug panel, such as the SERCA activator CDN1163 (Kang et al., 2016, Dahl, 2017), or the myosin inhibitor blebbistatin (Kovacs et al., 2004).

3. Maturity could be improved by integrating different cell types into a 2D configuration, which includes cardiomyocytes, fibroblast, endothelial cells, smooth muscle cells subtypes, to mimic the actual heart and hopefully, improve prediction (Mummery, 2018).

4. Additional parameters could be included to enhance the prediction such as beat rate, cell viability and structural changes upon exposure to drugs, to unveil more mechanistic effects.

7.4.2 Gene-induced changes chapter

1. A different panel of drugs to the isogenic variants could be used to evaluate the response of each $ß_2$AR variant in order to translate them into more 'personalised' therapy.

2. Genome editing of $ß_2$AR could be carried out into other sources of hiPSC-CMs, especially from healthy and 'diseased' patients, to revalidate the findings.

3. The molecular and possible mechanisms of enhanced desensitisation, recycling and downregulation are yet to be discovered. Therefore, their trafficking monitoring might provide information about these dynamic systems in regards to their polymorphisms.

References

2017. Abstracts from the 34th Annual Meeting, European Section of the International Society for Heart Research, July 24–27, 2017, Hamburg, Germany. *Journal of Molecular and Cellular Cardiology,* 109, 1-62.

AASEN, T. & IZPISUA BELMONTE, J. C. 2010. Isolation and cultivation of human keratinocytes from skin or plucked hair for the generation of induced pluripotent stem cells. *Nature Protocols,* 5, 371-382.

AASS, H., SKOMEDAL, T. & OSNES, J. B. 1988. Increase of cyclic AMP in subcellular fractions of rat heart muscle after beta-adrenergic stimulation: prenalterol and isoprenaline caused different distribution of bound cyclic AMP. *J Mol Cell Cardiol,* 20, 847-60.

ABI-GERGES, N., POINTON, A., PULLEN, G. F., MORTON, M. J., OLDMAN, K. L., ARMSTRONG, D., VALENTIN, J. P. & POLLARD, C. E. 2013. Preservation of cardiomyocytes from the adult heart. *J Mol Cell Cardiol,* 64, 108-19.

ABRAHAM, G., KNEUER, C., EHRHARDT, C., HONSCHA, W. & UNGEMACH, F. R. 2004. Expression of functional ß2-adrenergic receptors in the lung epithelial cell lines 16HBE14o−, Calu-3 and A549. *Biochimica et Biophysica Acta (BBA) - Molecular Cell Research,* 1691, 169-179.

AHLES, A. & ENGELHARDT, S. 2014. Polymorphic Variants of Adrenoceptors: Pharmacology, Physiology, and Role in Diseases. *Pharmacological Reviews,* 66, 598-637.

ALDRED, E. M., BUCK, C. & VALL, K. 2009. Chapter 24 - Glycosides. *In:* ALDRED, E. M., BUCK, C. & VALL, K. (eds.) *Pharmacology*. Edinburgh: Churchill Livingstone.

ANGUS, J. A., SARSERO, D., FUJIWARA, T., MOLENAAR, P. & XI, Q. 2000. Quantitative analysis of vascular to cardiac selectivity of L- and T-type voltage-operated calcium channel antagonists in human tissues. *Clin Exp Pharmacol Physiol,* 27, 1019-21.

ANTZELEVITCH, C., BELARDINELLI, L., ZYGMUNT, A. C., BURASHNIKOV, A., DI DIEGO, J. M., FISH, J. M., CORDEIRO, J. M. & THOMAS, G. 2004. Electrophysiological effects of ranolazine, a novel antianginal agent with antiarrhythmic properties. *Circulation,* 110, 904-10.

ARROWSMITH, J. & MILLER, P. 2013. Trial watch: phase II and phase III attrition rates 2011-2012. *Nat Rev Drug Discov*. England.

AVIOR, Y., SAGI, I. & BENVENISTY, N. 2016. Pluripotent stem cells in disease modelling and drug discovery. *Nature Reviews Molecular Cell Biology,* 17, 170-182.

BAILEY, J. M., LEVY, J. H., KIKURA, M., SZLAM, F. & HUG, C. C., JR. 1994. Pharmacokinetics of intravenous milrinone in patients undergoing cardiac surgery. *Anesthesiology,* 81, 616-22.

BAKER, J. G. 2010. The selectivity of beta-adrenoceptor agonists at human beta(1)-, beta(2)- and beta(3)-adrenoceptors. *British Journal of Pharmacology,* 160, 1048-1061.

BASSETT, A. R. 2017. Editing the genome of hiPSC with CRISPR/Cas9: disease models. *Mammalian genome : official journal of the International Mammalian Genome Society,* 28, 348-364.

BATALOV, I. & FEINBERG, A. W. 2015. Differentiation of Cardiomyocytes from Human Pluripotent Stem Cells Using Monolayer Culture. *Biomarker Insights,* 10, 71-76.

BAUDET, S., SHAOULIAN, R. & BERS, D. M. 1993. Effects of thapsigargin and cyclopiazonic acid on twitch force and sarcoplasmic reticulum Ca2+ content of rabbit ventricular muscle. *Circ Res,* 73, 813-9.

BEDUT, S., SEMINATORE-NOLE, C., LAMAMY, V., CAIGNARD, S., BOUTIN, J. A., NOSJEAN, O., STEPHAN, J. P. & COGE, F. 2016. High-throughput drug profiling with voltage-and calcium-sensitive fluorescent probes in human iPSC-derived cardiomyocytes. *American Journal of Physiology-Heart and Circulatory Physiology,* 311, H44-H53.

BELLMANN, R. 2007. Clinical pharmacokinetics of systemically administered antimycotics. *Curr Clin Pharmacol,* 2, 37-58.

BELLO, C. L., SHERMAN, L., ZHOU, J., VERKH, L., SMERAGLIA, J., MOUNT, J. & KLAMERUS, K. J. 2006. Effect of food on the pharmacokinetics of sunitinib malate (SU11248), a multi-targeted receptor tyrosine kinase inhibitor: results from a phase I study in healthy subjects. *Anticancer Drugs,* 17, 353-8.

BERGER, C., MEYER, W., SCHOLZ, H. & STARBATTY, J. 1985. Effects of the benzimidazole derivatives pimobendan and 2-(4-hydroxy-phenyl)-5-(5-methyl-3-oxo-4,5-dihydro-2H-6- pyridazinyl) benzimidazole . HCl on phosphodiesterase activity and force of contraction in guinea-pig hearts. *Arzneimittelforschung,* 35, 1668-73.

BERS, D. M. 2002. Cardiac excitation-contraction coupling. *Nature,* 415, 198-205.

BINKOWSKI, B. F., BUTLER, B. L., STECHA, P. F., EGGERS, C. T., OTTO, P., ZIMMERMAN, K., VIDUGIRIS, G., WOOD, M. G., ENCELL, L. P., FAN, F. & WOOD, K. V. 2011. A Luminescent Biosensor with Increased Dynamic Range for Intracellular cAMP. *Acs Chemical Biology,* 6, 1193-1197.

BIRD, S. D., DOEVENDANS, P. A., VAN ROOIJEN, M. A., BRUTEL DE LA RIVIERE, A., HASSINK, R. J., PASSIER, R. & MUMMERY, C. L. 2003. The human adult cardiomyocyte phenotype. *Cardiovasc Res,* 58, 423-34.

BLINOVA, K., DANG, Q., MILLARD, D., SMITH, G., PIERSON, J., GUO, L., BROCK, M., LU, H. R., KRAUSHAAR, U., ZENG, H., SHI, H., ZHANG, X., SAWADA, K., OSADA, T., KANDA, Y., SEKINO, Y., PANG, L., FEASTER, T. K., KETTENHOFEN, R., STOCKBRIDGE, N., STRAUSS, D. G. & GINTANT, G. 2018. International Multisite Study of Human-Induced Pluripotent Stem Cell-Derived Cardiomyocytes for Drug Proarrhythmic Potential Assessment. *Cell Reports,* 24, 3582-3592.

BOHM, S. K., GRADY, E. F. & BUNNETT, N. W. 1997. Regulatory mechanisms that modulate signalling by G-protein-coupled receptors. *Biochemical Journal,* 322, 1-18.

BOIS, P., BESCOND, J., RENAUDON, B. & LENFANT, J. 1996. Mode of action of bradycardic agent, S 16257, on ionic currents of rabbit sinoatrial node cells. *Br J Pharmacol,* 118, 1051-7.

BOKNIK, P., NEUMANN, J., KASPAREIT, G., SCHMITZ, W., SCHOLZ, H., VAHLENSIECK, U. & ZIMMERMANN, N. 1997. Mechanisms of the contractile effects of levosimendan in the mammalian heart. *J Pharmacol Exp Ther,* 280, 277-83.

BOLDT, A., GERGS, U., PONICKE, K., SIMM, A., SILBER, R. E. & NEUMANN, J. 2010. Inotropic effects of ivabradine in the mammalian heart. *Pharmacology,* 86**,** 249-58.

BOVARD, D., SANDOZ, A., LUETTICH, K., FRENTZEL, S., ISKANDAR, A., MARESCOTTI, D., TRIVEDI, K., GUEDJ, E., DUTERTRE, Q., PEITSCH, M. C. & HOENG, J. 2018. A lung/liver-on-a-chip platform for acute and chronic toxicity studies. *Lab on a Chip,* 18**,** 3814-3829.

BRANDAO, K. O., TABEL, V. A., ATSMA, D. E., MUMMERY, C. L. & DAVIS, R. P. 2017. Human pluripotent stem cell models of cardiac disease: from mechanisms to therapies. *Disease Models & Mechanisms,* 10**,** 1039-1059.

BRANDÃO, K. O., TABEL, V. A., ATSMA, D. E., MUMMERY, C. L. & DAVIS, R. P. 2017. Human pluripotent stem cell models of cardiac disease: from mechanisms to therapies. *Disease Models & Mechanisms,* 10**,** 1039.

BRISTOW, M. R., GINSBURG, R., STROSBERG, A., MONTGOMERY, W. & MINOBE, W. 1984. Pharmacology and inotropic potential of forskolin in the human heart. *J Clin Invest,* 74**,** 212-23.

BRISTOW, M. R., GINSBURG, R., UMANS, V., FOWLER, M., MINOBE, W., RASMUSSEN, R., ZERA, P., MENLOVE, R., SHAH, P., JAMIESON, S. & STINSON, E. B. 1986. BETA-1-ADRENERGIC-RECEPTOR AND BETA-2-ADRENERGIC-RECEPTOR SUBPOPULATIONS IN NONFAILING AND FAILING HUMAN VENTRICULAR MYOCARDIUM - COUPLING OF BOTH RECEPTOR SUBTYPES TO MUSCLE-CONTRACTION AND SELECTIVE BETA-1-RECEPTOR DOWN-REGULATION IN HEART-FAILURE. *Circulation Research,* 59**,** 297-309.

BRODDE, O. E. 1991. BETA-1-ADRENOCEPTORS AND BETA-2-ADRENOCEPTORS IN THE HUMAN HEART - PROPERTIES, FUNCTION, AND ALTERATIONS IN CHRONIC HEART-FAILURE. *Pharmacological Reviews,* 43**,** 203-242.

BROWN, L., NABAUER, M. & ERDMANN, E. 1986. The positive inotropic response to milrinone in isolated human and guinea pig myocardium. *Naunyn Schmiedebergs Arch Pharmacol,* 334**,** 196-201.

BROWN, L., NABAUER, M. & ERDMANN, E. 1987. Dobutamine: positive inotropy by nonselective adrenoceptor agonism in isolated guinea pig and human myocardium. *Naunyn Schmiedebergs Arch Pharmacol,* 335**,** 385-90.

BROWN, R. D., WILSON, J. T., KEARNS, G. L., EICHLER, V. F., JOHNSON, V. A. & BERTRAND, K. M. 1992. Single-dose pharmacokinetics of ibuprofen and acetaminophen in febrile children. *J Clin Pharmacol,* 32**,** 231-41.

BRUYNEEL, A. A. N., MCKEITHAN, W. L., FEYEN, D. A. M. & MERCOLA, M. 2018. Will iPSC-cardiomyocytes revolutionize the discovery of drugs for heart disease? *Current Opinion in Pharmacology,* 42**,** 55-61.

BURRIDGE, P. W., LI, Y. F., MATSA, E., WU, H., ONG, S.-G., SHARMA, A., HOLMSTROM, A., CHANG, A. C., CORONADO, M. J., EBERT, A. D., KNOWLES, J. W., TELLI, M. L., WITTELES, R. M., BLAU, H. M., BERNSTEIN, D., ALTMAN, R. B. & WU, J. C. 2016. Human induced pluripotent stem cell-derived cardiomyocytes recapitulate the predilection of breast cancer patients to doxorubicin-induced cardiotoxicity. *Nature Medicine,* 22**,** 547-556.

BURRIDGE, P. W., MATSA, E., SHUKLA, P., LIN, Z. C., CHURKO, J. M., EBERT, A. D., LAN, F., DIECKE, S., HUBER, B., MORDWINKIN, N. M., PLEWS, J. R., ABILEZ, O. J., CUI, B., GOLD, J. D. & WU, J. C. 2014. Chemically defined generation of human cardiomyocytes. *Nat Methods,* 11**,** 855-60.

BURRIDGE, P. W., THOMPSON, S., MILLROD, M. A., WEINBERG, S., YUAN, X., PETERS, A., MAHAIRAKI, V., KOLIATSOS, V. E., TUNG, L. & ZAMBIDIS, E. T. 2011. A universal system for highly efficient cardiac differentiation of human induced pluripotent stem cells that eliminates interline variability. *PLoS One,* 6**,** e18293.

BUTLER, L., CROS, C., OLDMAN, K. L., HARMER, A. R., POINTON, A., POLLARD, C. E. & ABI-GERGES, N. 2015. Enhanced characterization of contractility in cardiomyocytes during early drug safety assessment. *Toxicol Sci,* 145**,** 396-406.

CAO, N., LIANG, H., HUANG, J., WANG, J., CHEN, Y., CHEN, Z. & YANG, H.-T. 2013. Highly efficient induction and long-term maintenance of multipotent cardiovascular progenitors from human pluripotent stem cells under defined conditions. *Cell research,* 23**,** 1119-1132.

CARCAMO-ORIVE, I., HOFFMAN, G. E., CUNDIFF, P., BECKMANN, N. D., D'SOUZA, S. L., KNOWLES, J. W., PATEL, A., PAPATSENKO, D., ABBASI, F., REAVEN, G. M., WHALEN, S., LEE, P., SHAHBAZI, M., HENRION, M. Y. R., ZHU, K., WANG, S., ROUSSOS, P., SCHADT, E. E., PANDEY, G., CHANG, R., QUERTERMOUS, T. & LEMISCHKA, I. 2017. Analysis of Transcriptional Variability in a Large Human iPSC Library Reveals Genetic and Non-genetic Determinants of Heterogeneity. *Cell Stem Cell,* 20**,** 518-532.e9.

CARSON, D., HNILOVA, M., YANG, X., NEMETH, C. L., TSUI, J. H., SMITH, A. S., JIAO, A., REGNIER, M., MURRY, C. E., TAMERLER, C. & KIM, D. H. 2016. Nanotopography-Induced Structural Anisotropy and Sarcomere Development in Human Cardiomyocytes Derived from Induced Pluripotent Stem Cells. *ACS Appl Mater Interfaces,* 8**,** 21923-32.

CASINI, S., VERKERK, A. O. & REMME, C. A. 2017. Human iPSC-Derived Cardiomyocytes for Investigation of Disease Mechanisms and Therapeutic Strategies in Inherited Arrhythmia Syndromes: Strengths and Limitations. *Cardiovascular Drugs and Therapy,* 31**,** 325-344.

CHANG, W. T., YU, D., LAI, Y. C., LIN, K. Y. & LIAU, I. 2013. Characterization of the Mechanodynamic Response of Cardiomyocytes with Atomic Force Microscopy. *Analytical Chemistry,* 85**,** 1395-1400.

CHEN, J., KUBALAK, S. W., MINAMISAWA, S., PRICE, R. L., BECKER, K. D., HICKEY, R., ROSS, J., JR. & CHIEN, K. R. 1998. Selective requirement of myosin light chain 2v in embryonic heart function. *J Biol Chem,* 273**,** 1252-6.

CHEN, K.-Y. & KNOEPFLER, P. S. 2016. To CRISPR and beyond: the evolution of genome editing in stem cells. *Regenerative medicine,* 11**,** 801-816.

CHO, S. H. 2010. Pharmacogenomic Approaches to Asthma Treatment. *Allergy Asthma & Immunology Research,* 2**,** 177-182.

CHOI, H. Y., BAE, K. S., CHO, S. H., GHIM, J. L., CHOE, S., JUNG, J. A. & LIM, H. S. 2016. Population plasma and urine pharmacokinetics of ivabradine and its active metabolite S18982 in healthy Korean volunteers. *J Clin Pharmacol,* 56**,** 439-49.

CHRISTIDI, E., HUANG, H. M. & BRUNHAM, L. R. 2018. CRISPR/Cas9-mediated genome editing in human stem cell-derived cardiomyocytes: Applications for cardiovascular disease modelling and cardiotoxicity screening. *Drug discovery today. Technologies,* 28**,** 13-21.

CHU, K. M., SHIEH, S. M. & HU, O. Y. 1995. Pharmacokinetics and pharmacodynamics of enantiomers of pimobendan in patients with dilated cardiomyopathy and

congestive heart failure after single and repeated oral dosing. *Clin Pharmacol Ther,* 57**,** 610-21.

CHUN, Y. W., DURBIN, M. D. & HONG, C. C. 2018. Genome Editing and Induced Pluripotent Stem Cell Technologies for Personalized Study of Cardiovascular Diseases. *Curr Cardiol Rep,* 20**,** 38.

CHURKO, J. M., BURRIDGE, P. W. & WU, J. C. 2013. Generation of human iPSCs from human peripheral blood mononuclear cells using non-integrative Sendai virus in chemically defined conditions. *Methods Mol Biol,* 1036**,** 81-8.

CHUVA DE SOUSA LOPES, S. M., HASSINK, R. J., FEIJEN, A., VAN ROOIJEN, M. A., DOEVENDANS, P. A., TERTOOLEN, L., BRUTEL DE LA RIVIÈRE, A. & MUMMERY, C. L. 2006. Patterning the heart, a template for human cardiomyocyte development. *Developmental Dynamics,* 235**,** 1994-2002.

CLELAND, J. G., TEERLINK, J. R., SENIOR, R., NIFONTOV, E. M., MC MURRAY, J. J., LANG, C. C., TSYRLIN, V. A., GREENBERG, B. H., MAYET, J., FRANCIS, D. P., SHABURISHVILI, T., MONAGHAN, M., SALTZBERG, M., NEYSES, L., WASSERMAN, S. M., LEE, J. H., SAIKALI, K. G., CLARKE, C. P., GOLDMAN, J. H., WOLFF, A. A. & MALIK, F. I. 2011. The effects of the cardiac myosin activator, omecamtiv mecarbil, on cardiac function in systolic heart failure: a double-blind, placebo-controlled, crossover, dose-ranging phase 2 trial. *Lancet,* 378**,** 676-83.

CLEMENTS, M., MILLAR, V., WILLIAMS, A. S. & KALINKA, S. 2015. Bridging Functional and Structural Cardiotoxicity Assays Using Human Embryonic Stem Cell-Derived Cardiomyocytes for a More Comprehensive Risk Assessment. *Toxicological Sciences,* 148**,** 241-260.

COCKERILL, S. L. & MITCHESON, J. S. 2006. Direct Block of Human Ether-a-go-go-Related Gene Potassium Channels by Caffeine. *Journal of Pharmacology and Experimental Therapeutics,* 316**,** 860.

COHEN, M. A., ITSYKSON, P. & REUBINOFF, B. E. 2007. Neural differentiation of human ES cells. *Curr Protoc Cell Biol,* Chapter 23**,** Unit 23.7.

COLATSKY, T., FERMINI, B., GINTANT, G., PIERSON, J. B., SAGER, P., SEKINO, Y., STRAUSS, D. G. & STOCKBRIDGE, N. 2016. The Comprehensive in Vitro Proarrhythmia Assay (CiPA) initiative Update on progress. *Journal of Pharmacological and Toxicological Methods,* 81**,** 15-20.

COSTA, V. M., CARVALHO, F., DUARTE, J. A., BASTOS, M. D. L. & REMIAO, F. 2013. The Heart As a Target for Xenobiotic Toxicity: The Cardiac Susceptibility to Oxidative Stress. *Chemical Research in Toxicology,* 26**,** 1285-1311.

COSTANTINE, M. M., CLEARY, K., HEBERT, M. F., AHMED, M. S., BROWN, L. M., REN, Z., EASTERLING, T. R., HAAS, D. M., HANELINE, L. S., CARITIS, S. N., VENKATARAMANAN, R., WEST, H., D'ALTON, M., HANKINS, G., EUNICE KENNEDY SHRIVER NATIONAL INSTITUTE OF CHILD, H. & HUMAN DEVELOPMENT OBSTETRIC-FETAL PHARMACOLOGY RESEARCH UNITS, N. 2016. Safety and pharmacokinetics of pravastatin used for the prevention of preeclampsia in high-risk pregnant women: a pilot randomized controlled trial. *Am J Obstet Gynecol,* 214**,** 720 e1-720 e17.

COVOLO, L., GELATTI, U., METRA, M., NODARI, S., PICCICHE, A., PEZZALI, N., ZANI, C., ALBERTI, A., DONATO, F., NARDI, G. & CAS, L. D. 2004. Role of beta 1- and beta 2-adrenoceptor polymorphisms in heart failure: a case-control study. *European Heart Journal,* 25**,** 1534-1541.

COWAN, C. A., KLIMANSKAYA, I., MCMAHON, J., ATIENZA, J., WITMYER, J., ZUCKER, J. P., WANG, S. P., MORTON, C. C., MCMAHON, A. P., POWERS, D. & MELTON, D. A. 2004. Derivation of embryonic stem-cell lines from human blastocysts. *New England Journal of Medicine,* 350, 1353-1356.

CRESCI, S., DORN, G. W., JONES, P. G., BEITELSHEES, A. L., LI, A. Y., LENZINI, P. A., PROVINCE, M. A., SPERTUS, J. A. & LANFEAR, D. E. 2012. Adrenergic-Pathway Gene Variants Influence Beta-Blocker-Related Outcomes After Acute Coronary Syndrome in a Race-Specific Manner. *Journal of the American College of Cardiology,* 60, 898-907.

CULHANE, K. J., LIU, Y., CAI, Y. & YAN, E. C. Y. 2015. Transmembrane signal transduction by peptide hormones via family B G protein-coupled receptors. *Frontiers in Pharmacology,* 6.

DAHL, R. 2017. A new target for Parkinson's disease: Small molecule SERCA activator CDN1163 ameliorates dyskinesia in 6-OHDA-lesioned rats. *Bioorganic & Medicinal Chemistry,* 25, 53-57.

DANESI, R., CONTE, P. F. & DEL TACCA, M. 1999. Pharmacokinetic optimisation of treatment schedules for anthracyclines and paclitaxel in patients with cancer. *Clin Pharmacokinet,* 37, 195-211.

DASGUPTA, A. 2012. Chapter 11 - Challenges in Therapeutic Drug Monitoring of Digoxin and Other Anti-Arrhythmic Drugs. *In:* DASGUPTA, A. (ed.) *Therapeutic Drug Monitoring*. Boston: Academic Press.

DAVIS, J. P. & TIKUNOVA, S. B. 2007. Ca2+ exchange with troponin C and cardiac muscle dynamics. *Cardiovascular Research,* 77, 619-626.

DE KORTE, T., KATILI, P. A., MOHD YUSOF, N. A. N., VAN MEER, B. J., SALEEM, U., BURTON, F. L., SMITH, G. L., CLEMENTS, P., MUMMERY, C. L., ESCHENHAGEN, T., HANSEN, A. & DENNING, C. 2019. Unlocking Personalized Biomedicine and Drug Discovery with Human Induced Pluripotent Stem Cell–Derived Cardiomyocytes: Fit for Purpose or Forever Elusive? *Annual Review of Pharmacology and Toxicology*.

DE LUCIA, C., EGUCHI, A. & KOCH, W. J. 2018. New Insights in Cardiac beta-Adrenergic Signaling During Heart Failure and Aging. *Frontiers in Pharmacology,* 9.

DE ZEEUW, S., TRINES, S. A., KRAMS, R., DUNCKER, D. J. & VERDOUW, P. D. 2000. In vivo evidence that EMD 57033 restores myocardial responsiveness to intracoronary Ca(2+) in stunned myocardium. *Eur J Pharmacol,* 403, 99-109.

DEMPSEY, G. T., CHAUDHARY, K. W., ATWATER, N., NGUYEN, C., BROWN, B. S., MCNEISH, J. D., COHEN, A. E. & KRALJ, J. M. 2016. Cardiotoxicity screening with simultaneous optogenetic pacing, voltage imaging and calcium imaging. *J Pharmacol Toxicol Methods,* 81, 240-50.

DENNING, C., BORGDORFF, V., CRUTCHLEY, J., FIRTH, K. S. A., GEORGE, V., KALRA, S., KONDRASHOV, A., HOANG, M. D., MOSQUEIRA, D., PATEL, A., PRODANOV, L., RAJAMOHAN, D., SKARNES, W. C., SMITH, J. G. W. & YOUNG, L. E. 2016. Cardiomyocytes from human pluripotent stem cells: From laboratory curiosity to industrial biomedical platform. *Biochimica Et Biophysica Acta-Molecular Cell Research,* 1863, 1728-1748.

DEZSI, C. A. & VERONIKA, S. 2017. The Real Role of beta-Blockers in Daily Cardiovascular Therapy. *American Journal of Cardiovascular Drugs,* 17, 361-373.

DIFRANCESCO, D. 2006. Funny channels in the control of cardiac rhythm and mode of action of selective blockers. *Pharmacol Res,* 53, 399-406.

DIMASI, J. A., GRABOWSKI, H. G. & HANSEN, R. W. 2016. Innovation in the pharmaceutical industry: New estimates of R&D costs. *Journal of Health Economics,* 47, 20-33.

DIMASI, J. A., HANSEN, R. W. & GRABOWSKI, H. G. 2003. The price of innovation: new estimates of drug development costs. *J Health Econ,* 22, 151-85.

DISHY, V., SOFOWORA, G. G., XIE, H. G., KIM, R. B., BYRNE, D. W., STEIN, C. M. & WOOD, A. J. J. 2001. The effect of common polymorphisms of the beta(2)-adrenergic receptor on agonist-mediated vascular desensitization. *New England Journal of Medicine,* 345, 1030-1035.

DIXON, J. A. & SPINALE, F. G. 2009. Large Animal Models of Heart Failure A Critical Link in the Translation of Basic Science to Clinical Practice. *Circulation-Heart Failure,* 2, 262-271.

DOHERTY, K. R., TALBERT, D. R., TRUSK, P. B., MORAN, D. M., SHELL, S. A. & BACUS, S. 2015. Structural and functional screening in human induced-pluripotent stem cell-derived cardiomyocytes accurately identifies cardiotoxicity of multiple drug types. *Toxicology and Applied Pharmacology,* 285, 51-60.

DONALDSON, J., BROWN, A. M. & HILL, S. J. 1988. INFLUENCE OF ROLIPRAM ON THE CYCLIC 3',5'-ADENOSINE-MONOPHOSPHATE RESPONSE TO HISTAMINE AND ADENOSINE IN SLICES OF GUINEA-PIG CEREBRAL-CORTEX. *Biochemical Pharmacology,* 37, 715-723.

DORN, G. W., II 2010. Adrenergic Signaling Polymorphisms and Their Impact on Cardiovascular Disease. *Physiological Reviews,* 90, 1013-1062.

DORN, G. W., TEPE, N. M., LORENZ, J. N., KOCH, W. J. & LIGGETT, S. B. 1999. Low- and high-level transgenic expression of beta(2)-adrenergic receptors differentially affect cardiac hypertrophy and function in G alpha q-overexpressing mice. *Proceedings of the National Academy of Sciences of the United States of America,* 96, 6400-6405.

DU, X. J., GAO, X. M., WANG, B. H., JENNINGS, G. L., WOODCOCK, E. A. & DART, A. M. 2000. Age-dependent cardiomyopathy and heart failure phenotype in mice overexpressing beta(2)-adrenergic receptors in the heart. *Cardiovascular Research,* 48, 448-454.

DUNCAN, G., FIRTH, K., GEORGE, V., HOANG, M. D., STANIFORTH, A., SMITH, G. & DENNING, C. 2017. Drug-Mediated Shortening of Action Potentials in LQTS2 Human Induced Pluripotent Stem Cell-Derived Cardiomyocytes. *Stem Cells and Development,* 26, 1695-1705.

DUNIGAN, C. D., CURRAN, P. K. & FISHMAN, P. H. 2000. Detection of beta-adrenergic receptors by radioligand binding. *Methods in Molecular Biology; Adrenergic Receptor Protocols,* 126, 329-343.

DURAN, J. M., MAKAREWICH, C. A., TRAPPANESE, D., GROSS, P., HUSAIN, S., DUNN, J., LAL, H., SHARP, T. E., STAROSTA, T., VAGNOZZI, R. J., BERRETTA, R. M., BARBE, M., YU, D., GAO, E., KUBO, H., FORCE, T. & HOUSER, S. R. 2014. Sorafenib cardiotoxicity increases mortality after myocardial infarction. *Circ Res,* 114, 1700-1712.

DYREBORG, A., KROGH, N., BACKER, V., RZEPPA, S., HEMMERSBACH, P. & HOSTRUP, M. 2016. Pharmacokinetics of Oral and Inhaled Terbutaline after Exercise in Trained Men. *Front Pharmacol,* 7, 150.

EGASHIRA, T., YUASA, S. & FUKUDA, K. 2011. Induced Pluripotent Stem Cells in Cardiovascular Medicine. *Stem Cells International*, 7.

EGUIZABAL, C., ARAN, B., CHUVA DE SOUSA LOPES, S. M., GEENS, M., HEINDRYCKX, B., PANULA, S., POPOVIC, M., VASSENA, R. & VEIGA, A. 2019. Two decades of embryonic stem cells: a historical overview. *Hum Reprod Open,* 2019, hoy024.

EISNER, D. 2014. Calcium in the heart: from physiology to disease. *Experimental Physiology,* 99, 1273-1282.

EISNER, D. A., CALDWELL, J. L., KISTAMAS, K. & TRAFFORD, A. W. 2017. Calcium and Excitation-Contraction Coupling in the Heart. *Circ Res,* 121, 181-195.

ENDOH, M. 2002. Mechanisms of action of novel cardiotonic agents. *J Cardiovasc Pharmacol,* 40, 323-38.

EVANS, M. J. & KAUFMAN, M. H. 1981. Establishment in culture of pluripotential cells from mouse embryos. *Nature,* 292, 154-156.

FAN, F., BINKOWSKI, B. F., BUTLER, B. L., STECHA, P. F., LEWILS, M. K. & WOOD, K. V. 2008. Novel genetically encoded biosensors using firefly luciferase. *Acs Chemical Biology,* 3, 346-351.

FEDOROV, V. V., SHARIFOV, O. F., PIATAKOVA, O. P., BELOSHAPKO, G. G., IUSHMANOVA, A. V. & ROZENSHTRAUKH, L. V. 2002. [Effects of ryanodine receptors block on spontaneous initiation of atrial fibrillation in the intact canine heart]. *Kardiologiia,* 42, 59-71.

FERMINI, B., HANCOX, J. C., ABI-GERGES, N., BRIDGLAND-TAYLOR, M., CHAUDHARY, K. W., COLATSKY, T., CORRELL, K., CRUMB, W., DAMIANO, B., ERDEMLI, G., GINTANT, G., IMREDY, J., KOERNER, J., KRAMER, J., LEVESQUE, P., LI, Z., LINDQVIST, A., OBEJERO-PAZ, C. A., RAMPE, D., SAWADA, K., STRAUSS, D. G. & VANDENBERG, J. I. 2016. A New Perspective in the Field of Cardiac Safety Testing through the Comprehensive In Vitro Proarrhythmia Assay Paradigm. *Journal of Biomolecular Screening,* 21, 1-11.

FOORD, S. M., BONNER, T. I., NEUBIG, R. R., ROSSER, E. M., PIN, J. P., DAVENPORT, A. P., SPEDDING, M. & HARMAR, A. J. 2005. International Union of Pharmacology. XLVI. G protein-coupled receptor list. *Pharmacological Reviews,* 57, 279-288.

FORLEO, C., RESTA, N., SORRENTINO, S., GUIDA, P., MANGHISI, A., DE LUCA, V., ROMITO, R., IACOVIELLO, M., DE TOMMASI, E., TROISI, F., RIZZON, B., GUANTI, G., RIZZON, P. & PITZALIS, M. V. 2004. Association of beta-adrenergic receptor polymorphisms and progression to heart failure in patients with idiopathic dilated cardiomyopathy. *American Journal of Medicine,* 117, 451-458.

FORSBERG, T. & LINDBOM, L. O. 1983. Cardiovascular effects of zimelidine and tricyclic antidepressants in conscious rats. *Acta Pharmacol Toxicol (Copenh),* 53, 223-9.

FRIEDRICHS, G. S., PATMORE, L. & BASS, A. 2005. Non-clinical evaluation of ventricular repolarization (ICH S7B): Results of an interim survey of international pharmaceutical companies. *Journal of Pharmacological and Toxicological Methods,* 52, 6-11.

FROTSCHER, R., KOCH, J. P. & STAAT, M. 2015. Computational Investigation of Drug Action on Human-Induced Stem Cell-Derived Cardiomyocytes. *Journal of Biomechanical Engineering-Transactions of the Asme,* 137, 7.

FUJITA, J., TOHYAMA, S., KISHINO, Y., OKADA, M. & MORITA, Y. 2019. Concise Review: Genetic and Epigenetic Regulation of Cardiac Differentiation from Human Pluripotent Stem Cells. *Stem Cells,* 37**,** 992-1002.

GARLAND, E. M. & BIAGGIONI, I. 2001. Genetic polymorphisms of adrenergic receptors. *Clinical Autonomic Research,* 11**,** 67-78.

GARLAND, S. L. 2013. Are GPCRs Still a Source of New Targets? *Journal of Biomolecular Screening,* 18**,** 947-966.

GHICULESCU, R. A. 2008. Therapeutic drug monitoring: Which drugs, why, when and how to do it. *Australian Prescriber,* 31**,** 42-44.

GIACOMELLI, E., MUMMERY, C. L. & BELLIN, M. 2017. Human heart disease: lessons from human pluripotent stem cell-derived cardiomyocytes. *Cellular and Molecular Life Sciences,* 74**,** 3711-3739.

GIACOMINI, K. M., MASSOUD, N., WONG, F. M. & GIACOMINI, J. C. 1984. Decreased binding of verapamil to plasma proteins in patients with liver disease. *J Cardiovasc Pharmacol,* 6**,** 924-8.

GINTANT, G. 2011. An evaluation of hERG current assay performance: Translating preclinical safety studies to clinical QT prolongation. *Pharmacology & Therapeutics,* 129**,** 109-119.

GIUDICELLI, J. F., RICHER, C. & MATTEI, A. 1987. Pharmacokinetics and biological effects of captopril and hydrochlorothiazide after acute and chronic administration either alone or in combination in hypertensive patients. *Br J Clin Pharmacol,* 23 Suppl 1**,** 51S-63S.

GOLAN, D. E. & TASHJIAN, A. H. 2012. *Principles of pharmacology : the pathophysiologic basis of drug therapy,* Philadelphia, Wolters Kluwer Health/Lippincott Williams & Wilkins.

GONZALEZ, F., BOUE, S. & IZPISUA BELMONTE, J. C. 2011. Methods for making induced pluripotent stem cells: reprogramming a la carte. *Nat Rev Genet,* 12**,** 231-42.

GONZÁLEZ, F., BOUÉ, S. & BELMONTE, J. C. I. 2011. Methods for making induced pluripotent stem cells: reprogramming à la carte. *Nature Reviews Genetics,* 12**,** 231-242.

GORDON, S. G. & KITTLESON, M. D. 2008. Chapter 17 - Drugs used in the management of heart disease and cardiac arrhythmias. *In:* MADDISON, J. E., PAGE, S. W. & CHURCH, D. B. (eds.) *Small Animal Clinical Pharmacology (Second Edition)*. Edinburgh: W.B. Saunders.

GORINI, S., DE ANGELIS, A., BERRINO, L., MALARA, N., ROSANO, G. & FERRARO, E. 2018. Chemotherapeutic Drugs and Mitochondrial Dysfunction: Focus on Doxorubicin, Trastuzumab, and Sunitinib. *Oxid Med Cell Longev,* 2018**,** 7582730.

GRANT AUGUSTUS, O. 2009. Cardiac Ion Channels. *Circulation: Arrhythmia and Electrophysiology,* 2**,** 185-194.

GREEN, S. A., TURKI, J., INNIS, M. & LIGGETT, S. B. 1994. AMINO-TERMINAL POLYMORPHISMS OF THE HUMAN BETA(2)-ADRENERGIC RECEPTOR IMPART DISTINCT AGONIST-PROMOTED REGULATORY PROPERTIES. *Biochemistry,* 33**,** 9414-9419.

GREENBERG, M. J., DAILY, N. J., WANG, A., CONWAY, M. K. & WAKATSUKI, T. 2018. Genetic and Tissue Engineering Approaches to Modeling the Mechanics of

Human Heart Failure for Drug Discovery. *Frontiers in Cardiovascular Medicine,* 5, 120.

GROSBERG, A., KUO, P. L., GUO, C. L., GEISSE, N. A., BRAY, M. A., ADAMS, W. J., SHEEHY, S. P. & PARKER, K. K. 2011. Self-Organization of Muscle Cell Structure and Function. *Plos Computational Biology,* 7.

GULICK, J., HEWETT, T. E., KLEVITSKY, R., BUCK, S. H., MOSS, R. L. & ROBBINS, J. 1997. Transgenic remodeling of the regulatory myosin light chains in the mammalian heart. *Circ Res,* 80, 655-64.

GUO, L., QIAN, J. Y., ABRAMS, R., TANG, H. M., WEISER, T., SANDERS, M. J. & KOLAJA, K. L. 2011. The electrophysiological effects of cardiac glycosides in human iPSC-derived cardiomyocytes and in guinea pig isolated hearts. *Cell Physiol Biochem,* 27, 453-62.

GUTH, B. D., CHIANG, A. Y., DOYLE, J., ENGWALL, M. J., GUILLON, J.-M., HOFFMANN, P., KOERNER, J., MITTELSTADT, S., OTTINGER, S., PIERSON, J. B., PUGSLEY, M. K., ROSSMAN, E. I., WALISSER, J. & SARAZAN, D. 2015a. The evaluation of drug-induced changes in cardiac inotropy in dogs: Results from a HESI-sponsored consortium. *Journal of Pharmacological and Toxicological Methods,* 75, 70-90.

GUTH, B. D., CHIANG, A. Y., DOYLE, J., ENGWALL, M. J., GUILLON, J. M., HOFFMANN, P., KOERNER, J., MITTELSTADT, S., OTTINGER, S., PIERSON, J. B., PUGSLEY, M. K., ROSSMAN, E. I., WALISSER, J. & SARAZAN, R. D. 2015b. The evaluation of drug-induced changes in cardiac inotropy in dogs: Results from a HESI-sponsored consortium. *J Pharmacol Toxicol Methods,* 75, 70-90.

GUTH, B. D., ENGWALL, M., ELDRIDGE, S., FOLEY, C. M., GUO, L., GINTANT, G., KOERNER, J., PARISH, S. T., PIERSON, J. B., RIBEIRO, A. J. S., ZABKA, T., CHAUDHARY, K. W., KANDA, Y. & BERRIDGE, B. 2019a. Considerations for an In Vitro, Cell-Based Testing Platform for Detection of Adverse Drug-Induced Inotropic Effects in Early Drug Development. Part 1: General Considerations for Development of Novel Testing Platforms. *Frontiers in Pharmacology,* 10, 12.

GUTH, B. D., ENGWALL, M., ELDRIDGE, S., FOLEY, C. M., GUO, L., GINTANT, G., KOERNER, J., PARISH, S. T., PIERSON, J. B., RIBEIRO, A. J. S., ZABKA, T., CHAUDHARY, K. W., KANDA, Y. & BERRIDGE, B. 2019b. Considerations for an In Vitro, Cell-Based Testing Platform for Detection of Adverse Drug-Induced Inotropic Effects in Early Drug Development. Part 1: General Considerations for Development of Novel Testing Platforms. *Frontiers in pharmacology,* 10, 884-884.

GWATHMEY, J. K., TSAIOUN, K. & HAJJAR, R. J. 2009. Cardionomics: a new integrative approach for screening cardiotoxicity of drug candidates. *Expert Opinion on Drug Metabolism & Toxicology,* 5, 647-660.

HAJJAR, R. J., DISALVO, T. G., SCHMIDT, U., THAIYANANTHAN, G., SEMIGRAN, M. J., DEC, G. W. & GWATHMEY, J. K. 1997. Clinical correlates of the myocardial force-frequency relationship in patients with end-stage heart failure. *J Heart Lung Transplant,* 16, 1157-67.

HALL, I. 1996. B2-Adrenoreceptor polymorphism : are they clinically important? *Thorax,* 51, 351-353.

HALL, I. P., WHEATLEY, A. P. & DEWAR, J. C. 2000. Genetic polymorphisms of adrenergic receptors. *Adrenergic Receptor Protocols,* 136, 117-126.

HANSEN, A., EDER, A., BONSTRUP, M., FLATO, M., MEWE, M., SCHAAF, S., AKSEHIRLIOGLU, B., SCHWOERER, A. P., UEBELER, J. & ESCHENHAGEN, T. 2010. Development of a drug screening platform based on engineered heart tissue. *Circ Res,* 107**,** 35-44.

HANYALOGLU, A. C., MCCULLAGH, E. & VON ZASTROW, M. 2005. Essential role of Hrs in a recycling mechanism mediating functional resensitization of cell signaling. *Embo j,* 24**,** 2265-83.

HASENFUSS, G., PIESKE, B., CASTELL, M., KRETSCHMANN, B., MAIER, L. S. & JUST, H. 1998. Influence of the novel inotropic agent levosimendan on isometric tension and calcium cycling in failing human myocardium. *Circulation,* 98**,** 2141-7.

HAUSER, A. S., CHAVALI, S., MASUHO, I., JAHN, L. J., MARTEMYANOV, K. A., GLORIAM, D. E. & BABU, M. M. 2018. Pharmacogenomics of GPCR Drug Targets. *Cell,* 172**,** 41-+.

HAWKINS, G. A., TANTISIRA, K., MEYERS, D. A., AMPLEFORD, E. J., MOORE, W. C., KLANDERMAN, B., LIGGETT, S. B., PETERS, S. P., WEISS, S. T. & BLEECKER, E. R. 2006. Sequence, haplotype, and association analysis of ADR beta 2 in a multiethnic asthma case-control study. *American Journal of Respiratory and Critical Care Medicine,* 174**,** 1101-1109.

HAZELTINE, L., SIMMONS, C., SALICK, M., LIAN, X., BADUR, M., HAN, W., DELGADO, S., WAKATSUKI, T., CRONE, W., PRUITT, B. & PALECEK, S. 2012. Effects of Substrate Mechanics on Contractility of Cardiomyocytes Generated from Human Pluripotent Stem Cells. *International journal of cell biology,* 2012**,** 508294.

HEAD, S. A., SHI, W., ZHAO, L., GORSHKOV, K., PASUNOOTI, K., CHEN, Y., DENG, Z., LI, R. J., SHIM, J. S., TAN, W., HARTUNG, T., ZHANG, J., ZHAO, Y., COLOMBINI, M. & LIU, J. O. 2015. Antifungal drug itraconazole targets VDAC1 to modulate the AMPK/mTOR signaling axis in endothelial cells. *Proc Natl Acad Sci U S A,* 112**,** E7276-85.

HECKBERT, S. R., HINDORFF, L. A., EDWARDS, K. L., PSATY, B. M., LUMLEY, T., SISCOVICK, D. S., TANG, Z. H., DURDA, J. P., KRONMAL, R. A. & TRACY, R. P. 2003. beta(2)-adrenergic receptor polymorphisms and risk of incident cardiovascular events in the elderly. *Circulation,* 107**,** 2021-2024.

HENDERSON, K. A., BORDERS, R. B., ROSS, J. B., HUWAR, T. B., TRAVIS, C. O., WOOD, B. J., MA, Z. X. J., HONG, S. P., VINCI, T. M. & ROCHE, B. M. 2013. Effects of tyrosine kinase inhibitors on rat isolated heart function and protein biomarkers indicative of toxicity. *Journal of Pharmacological and Toxicological Methods,* 68**,** 150-159.

HERRON TODD, J., LEE, P. & JALIFE, J. 2012. Optical Imaging of Voltage and Calcium in Cardiac Cells & Tissues. *Circulation Research,* 110**,** 609-623.

HGASHIYAMA, A., WATKINS, M. W., CHEN, Z. & LEWINTER, M. M. 1995. Effects of EMD 57033 on contraction and relaxation in isolated rabbit hearts. *Circulation,* 92**,** 3094-104.

HILL, S. J., WILLIAMS, C. & MAY, L. T. 2010. Insights into GPCR pharmacology from the measurement of changes in intracellular cyclic AMP; advantages and pitfalls of differing methodologies. *British Journal of Pharmacology,* 161**,** 1266-1275.

HOCKEMEYER, D. & JAENISCH, R. 2016. Induced Pluripotent Stem Cells Meet Genome Editing. *Cell Stem Cell,* 18**,** 573-586.

HOFLING, B. & BOLTE, H. D. 1981. Acute negative inotropic effect of adriamycin (doxorubicin). *Naunyn Schmiedebergs Arch Pharmacol,* 317, 252-6.

HONDEGHEM, L. M. & SNYDERS, D. J. 1990. Class III antiarrhythmic agents have a lot of potential but a long way to go. Reduced effectiveness and dangers of reverse use dependence. *Circulation,* 81, 686-90.

HONERJAGER, P., HEISS, A., SCHAFER-KORTING, M., SCHONSTEINER, G. & REITER, M. 1984. UD-CG 115--a cardiotonic pyridazinone which elevates cyclic AMP and prolongs the action potential in guinea-pig papillary muscle. *Naunyn Schmiedebergs Arch Pharmacol,* 325, 259-69.

HORTIGON-VINAGRE, M. P., ZAMORA, V., BURTON, F. L., BUTLER, P. & SMITH, G. L. 2018. Measurements of voltage, intracellular Ca2+ and contraction from spontaneous iPSC-derived cardiomyocytes using CellOPTIQ (R) platform reveals complex effects from drugs that parallel in vivo cardiac effects. *Journal of Pharmacological and Toxicological Methods,* 93, 119-120.

HORVATH, B., SZENTANDRASSY, N., VERESS, R., ALMASSY, J., MAGYAR, J., BANYASZ, T., TOTH, A., PAPP, Z. & NANASI, P. P. 2017. Frequency-dependent effects of omecamtiv mecarbil on cell shortening of isolated canine ventricular cardiomyocytes. *Naunyn Schmiedebergs Arch Pharmacol,* 390, 1239-1246.

HTTPS://WWW.NCBI.NLM.NIH.GOV/GENE/154 2019. ADRB2 adrenoceptor beta 2 [H*omo sapiens* (human)]. *In:* NATIONAL CENTER FOR BIOTECHNOLOGY INFORMATION, U. S. N. L. O. M. (ed.) 16-Jul-2019 ed.

HUANGFU, D., MAEHR, R., GUO, W., EIJKELENBOOM, A., SNITOW, M., CHEN, A. E. & MELTON, D. A. 2008. Induction of pluripotent stem cells by defined factors is greatly improved by small-molecule compounds. *Nature Biotechnology,* 26, 795-797.

HUMMA, L. M. & TERRA, S. G. 2002. Pharmacogenetics and cardiovascular disease: impact on drug response and applications to disease management. *Am J Health Syst Pharm,* 59, 1241-52.

HUSSEIN, M. H., SOBHY, K. E., SABRY, I. M., EL SERAFI, A. T. & TORAIH, E. A. 2017. Beta(2)-adrenergic receptor gene haplotypes and bronchodilator response in Egyptian patients with chronic obstructive pulmonary disease. *Advances in Medical Sciences,* 62, 193-201.

HUUPPONEN, R. 1987. Adverse Cardiovascular Effects of Sulfonylurea Drugs Clinical-Significance. *Medical Toxicology and Adverse Drug Experience,* 2, 190-209.

HYUN, S. W., KIM, B. R., HYUN, S. A. & SEO, J. W. 2017. The assessment of electrophysiological activity in human-induced pluripotent stem cell-derived cardiomyocytes exposed to dimethyl sulfoxide and ethanol by manual patch clamp and multi-electrode array system. *J Pharmacol Toxicol Methods,* 87, 93-98.

ICH 2005. The Non-Clinical Evaluation of the Potential for Delayed Ventricular Repolarization (QT Interval Prolongation) by Human Pharmaceutical. ICH Harmonised Tripartite Guideline.

ICHE14 2005. International Conference on Harmonization (ICH) of technical requirements for registration of pharmaceuticals for human use, E14 Clinical Evaluation of QT/QTc Interval Prolongation and Proarrhythmic Potential for Non-Antiarrhythmic Drugs. *In:* GUIDELINE, I. H. T. (ed.). London, UK.

INSEL, P. A., TANG, C. M., HAHNTOW, I. & MICHEL, M. C. 2007. Impact of GPCRs in clinical medicine: Monogenic diseases, genetic variants and drug targets. *Biochimica Et Biophysica Acta-Biomembranes,* 1768**,** 994-1005.

ISHIHATA, A., KUSHIDA, H. & ENDOH, M. 1988. Enantiomers of dobutamine increase the force of contraction via beta adrenoceptors, but antagonize competitively the positive inotropic effect mediated by alpha-1 adrenoceptors in the rabbit ventricular myocardium. *J Pharmacol Exp Ther,* 246**,** 1080-7.

ISRAEL, E., CHINCHILLI, V. M., FORD, J. G., BOUSHEY, H. A., CHERNIACK, R., CRAIG, T. J., DEYKIN, A., FAGAN, J. K., FAHY, J. V., FISH, J., KRAFT, M., KUNSELMAN, S. J., LAZARUS, S. C., LEMANSKE, R. F., LIGGETT, S. B., MARTIN, R. J., MITRA, N., PETERS, S. P., SILVERMAN, E., SORKNESS, C., SZEFLER, S. J., WECHSLER, M. E., WEISS, S. T., DRAZEN, J. M. & NATL HEART LUNG BLOOD INST, A. 2004. Use of regularly scheduled albuterol treatment in asthma: genotype-stratified, randomised, placebo-controlled cross-over trial. *Lancet,* 364**,** 1505-1512.

ISRAEL, E., DRAZEN, J. M., LIGGETT, S. B., BOUSHEY, H. A., CHERNIACK, R. M., CHINCHILLI, V. M., COOPER, D. M., FAHY, J. V., FISH, J. E., FORD, J. G., KRAFT, M., KUNSELMAN, S., LAZARUS, S. C., LEMANSKE, R. F., MARTIN, R. J., MCLEAN, D. E., PETERS, S. P., SILVERMAN, E. K., SORKNESS, C. A., SZEFLER, S. J., WEISS, S. T., YANDAVA, C. N. & NATL HEART LUNG BLOOD, I. 2000. The effect of polymorphisms of the beta(2)-adrenergic receptor on the response to regular use of albuterol in asthma. *American Journal of Respiratory and Critical Care Medicine,* 162**,** 75-80.

JACOB, F., YONIS, A. Y., CUELLO, F., LUTHER, P., SCHULZE, T., EDER, A., STREICHERT, T., MANNHARDT, I., HIRT, M. N., SCHAAF, S., STENZIG, J., FORCE, T., ESCHENHAGEN, T. & HANSEN, A. 2016. Analysis of Tyrosine Kinase Inhibitor-Mediated Decline in Contractile Force in Rat Engineered Heart Tissue. *Plos One,* 11.

JANSSEN, P. M. L., BIESIADECKI, B. J., ZIOLO, M. T. & DAVIS, J. P. 2016. The Need for Speed: Mice, Men, and Myocardial Kinetic Reserve. *Circulation research,* 119**,** 418-421.

JARAZO, J., QING, X. & SCHWAMBORN, J. C. 2019. Guidelines for Fluorescent Guided Biallelic HDR Targeting Selection With PiggyBac System Removal for Gene Editing. *Frontiers in Genetics,* 10.

JARROTT, B., LOUIS, W. J. & SUMMERS, R. J. 1979a. Characteristics of Clonidine-H-3 Binding to an Alpha-Adrenoceptor in Membranes from Guinea-Pig Kidney. *British Journal of Pharmacology,* 65**,** 663-670.

JARROTT, B., LOUIS, W. J. & SUMMERS, R. J. 1979b. The characteristics of [3H]-clonidine binding to an alpha-adrenoceptor in membranes from guinea-pig kidney. *Br J Pharmacol,* 65**,** 663-70.

JASTRZEBSKA, B. 2013. GPCR: G protein complexes-the fundamental signaling assembly. *Amino Acids,* 45**,** 1303-1314.

JI, J., KANG, J. & RAMPE, D. 2014. L-type Ca2+ channel responses to bay k 8644 in stem cell-derived cardiomyocytes are unusually dependent on holding potential and charge carrier. *Assay and drug development technologies,* 12**,** 352-360.

JOHNSON, M. 2006. Molecular mechanisms of beta(2)-adrenergic receptor function, response, and regulation. *Journal of Allergy and Clinical Immunology,* 117**,** 18-24.

JUNG, G., FAJARDO, G., RIBEIRO, A. J. S., KOOIKER, K. B., CORONADO, M., ZHAO, M. M., HU, D. Q., REDDY, S., KODO, K., SRIRAM, K., INSEL, P. A., WU, J. C., PRUITT, B. L. & BERNSTEIN, D. 2016. Time-dependent evolution of functional vs. remodeling signaling in induced pluripotent stem cell-derived cardiomyocytes and induced maturation with biomechanical stimulation. *Faseb Journal,* 30**,** 1464-1479.

KALLUR, T., BLOMBERG, P., STENFELT, S., TRYGGVASON, K. & HOVATTA, O. 2017. Quality Assurance in Stem Cell Banking: Emphasis on Embryonic and Induced Pluripotent Stem Cell Banking.

KAMALI, F., THOMAS, S. H. & FERNER, R. E. 1993. Paracetamol elimination in patients with non-insulin dependent diabetes mellitus. *Br J Clin Pharmacol,* 35**,** 58-61.

KANDA, Y., YAMAZAKI, D., OSADA, T., YOSHINAGA, T. & SAWADA, K. 2018. Development of torsadogenic risk assessment using human induced pluripotent stem cell-derived cardiomyocytes: Japan iPS Cardiac Safety Assessment (JiCSA) update. *J Pharmacol Sci,* 138**,** 233-239.

KANE, C. & TERRACCIANO, C. M. N. 2017. Concise Review: Criteria for Chamber-Specific Categorization of Human Cardiac Myocytes Derived from Pluripotent Stem Cells. *Stem cells (Dayton, Ohio),* 35**,** 1881-1897.

KANG, J., CHEN, X. L., JI, J., LEI, Q. & RAMPE, D. 2012. Ca(2)(+) channel activators reveal differential L-type Ca(2)(+) channel pharmacology between native and stem cell-derived cardiomyocytes. *J Pharmacol Exp Ther,* 341**,** 510-7.

KANG, S., DAHL, R., HSIEH, W., SHIN, A., ZSEBO, K. M., BUETTNER, C., HAJJAR, R. J. & LEBECHE, D. 2016. Small Molecular Allosteric Activator of the Sarco/Endoplasmic Reticulum Ca2+-ATPase (SERCA) Attenuates Diabetes and Metabolic Disorders. *Journal of Biological Chemistry,* 291**,** 5185-5198.

KARAKIKES, I., AMEEN, M., TERMGLINCHAN, V. & WU, J. C. 2015. Human Induced Pluripotent Stem Cell-Derived Cardiomyocytes Insights Into Molecular, Cellular, and Functional Phenotypes. *Circulation Research,* 117**,** 80-88.

KARKI, R., PANDYA, D., ELSTON, R. C. & FERLINI, C. 2015. Defining "mutation" and "polymorphism" in the era of personal genomics. *Bmc Medical Genomics,* 8.

KATRITCH, V., CHEREZOV, V. & STEVENS, R. C. 2013. Structure-Function of the G Protein-Coupled Receptor Superfamily. *Annual Review of Pharmacology and Toxicology, Vol 53, 2013,* 53**,** 531-556.

KAUMANN, A. J. & BLINKS, J. R. 1980. Stimulant and depressant effects of beta-adrenoceptor blocking agents on isolated heart muscle. A positive inotropic effect not mediated through andrenoceptors. *Naunyn Schmiedebergs Arch Pharmacol,* 311**,** 205-18.

KEHAT, I., KENYAGIN-KARSENTI, D., SNIR, M., SEGEV, H., AMIT, M., GEPSTEIN, A., LIVNE, E., BINAH, O., ITSKOVITZ-ELDOR, J. & GEPSTEIN, L. 2001. Human embryonic stem cells can differentiate into myocytes with structural and functional properties of cardiomyocytes. *The Journal of clinical investigation,* 108**,** 407-414.

KIKURA, M., TAKADA, T. & SATO, S. 2004. Age- and sex-specific incidence, risk, and latency period of a perioperative acute thromboembolism syndrome (PATS). *Thromb Haemost,* 91, 725-32.

KILLEEN, M. J. 2012. *Cardiac drug therapy: a bench to bedside approach*, World Scientific Publishing Co.

KIM, A., DOMBI, E., TEPAS, K., FOX, E., MARTIN, S., WOLTERS, P., BALIS, F. M., JAYAPRAKASH, N., TURKBEY, B., MURADYAN, N., CHOYKE, P. L., REDDY, A., KORF, B. & WIDEMANN, B. C. 2013. Phase I trial and pharmacokinetic study of sorafenib in children with neurofibromatosis type I and plexiform neurofibromas. *Pediatr Blood Cancer,* 60, 396-401.

KIM, C. 2015. iPSC technology-Powerful hand for disease modeling and therapeutic screen. *Bmb Reports,* 48, 256-265.

KIM, D. H., AKERA, T. & BRODY, T. M. 1980. Inotropic Actions of Doxorubicin in Isolated Guinea-Pig Atria - Evidence for Lack of Involvement of Na+,K+-Adenosine Triphosphatase. *Journal of Pharmacology and Experimental Therapeutics,* 214, 368-374.

KIRBY, M. S., SAGARA, Y., GAA, S., INESI, G., LEDERER, W. J. & ROGERS, T. B. 1992. Thapsigargin inhibits contraction and Ca2+ transient in cardiac cells by specific inhibition of the sarcoplasmic reticulum Ca2+ pump. *J Biol Chem,* 267, 12545-51.

KITSIOS, G. & ZINTZARAS, E. 2007. Genetic variation associated with ischemic heart failure: A HuGE review and meta-analysis. *American Journal of Epidemiology,* 166, 619-633.

KLEIBER, N., MATHOT, R. A. A., AHSMAN, M. J., WILDSCHUT, E. D., TIBBOEL, D. & DE WILDT, S. N. 2017. Population pharmacokinetics of intravenous clonidine for sedation during paediatric extracorporeal membrane oxygenation and continuous venovenous hemofiltration. *Br J Clin Pharmacol,* 83, 1227-1239.

KOCI, B., LUERMAN, G., DUENBOSTELL, A., KETTENHOFEN, R., BOHLEN, H., COYLE, L., KNIGHT, B., KU, W. R., VOLBERG, W., WOSKA, J. R. & BROWN, M. P. 2017. An impedance-based approach using human iPSC-derived cardiomyocytes significantly improves in vitro prediction of in vivo cardiotox liabilities. *Toxicology and Applied Pharmacology,* 329, 121-127.

KONDRASHOV, A., HOANG, M. D., SMITH, J. G. W., BHAGWAN, J. R., DUNCAN, G., MOSQUEIRA, D., MUNOZ, M. B., VO, N. T. N. & DENNING, C. 2018. Simplified Footprint-Free Cas9/CRISPR Editing of Cardiac-Associated Genes in Human Pluripotent Stem Cells. *Stem Cells and Development,* 27, 391-404.

KORUTH, J. S., LALA, A., PINNEY, S., REDDY, V. Y. & DUKKIPATI, S. R. 2017. The Clinical Use of Ivabradine. *Journal of the American College of Cardiology,* 70, 1777-1784.

KORYAKINA, Y., JONES, S. M., CORNETT, L. E., SEELY, K., BRENTS, L., PRATHER, P. L., KOFMAN, A. & KURTEN, R. C. 2012. Effects of the β-agonist, isoprenaline, on the down-regulation, functional responsiveness and trafficking of β2-adrenergic receptors with N-terminal polymorphisms. *Cell biology international,* 36, 1171-1183.

KOVACS, M., TOTH, J., HETENYI, C., MALNASI-CSIZMADIA, A. & SELLERS, J. R. 2004. Mechanism of blebbistatin inhibition of myosin II. *Journal of Biological Chemistry,* 279, 35557-35563.

KRAMER, J., OBEJERO-PAZ, C. A., MYATT, G., KURYSHEV, Y. A., BRUENING-WRIGHT, A., VERDUCCI, J. S. & BROWN, A. M. 2013. MICE Models: Superior to the HERG Model in Predicting Torsade de Pointes. *Scientific Reports,* 3.

KRATZ, J. M., GRIENKE, U., SCHEEL, O., MANN, S. A. & ROLLINGER, J. M. 2017. Natural products modulating the hERG channel: heartaches and hope. *Natural product reports,* 34, 957-980.

KUMAR, B. A., KUMARI, P., SONA, C. & YADAV, P. N. 2017. GloSensor assay for discovery of GPCR-selective ligands. *In:* SHUKLA, A. K. (ed.) *G Protein-Coupled Receptors, 2nd Edition, Pt A*. San Diego: Elsevier Academic Press Inc.

KUO, I. Y. & EHRLICH, B. E. 2015. Signaling in muscle contraction. *Cold Spring Harbor perspectives in biology,* 7, a006023-a006023.

KWANG SEO, H. & VAN BREEMEN, C. 1985. Effects of the Ca agonist bay K8644 on 45Ca influx and net Ca uptake into rabbit aortic smooth muscle. *European Journal of Pharmacology,* 116, 299-305.

LAFLAMME, M. A. & MURRY, C. E. 2011. Heart regeneration. *Nature,* 473, 326-35.

LAMORE, S. D., KAMENDI, H. W., SCOTT, C. W., DRAGAN, Y. P. & PETERS, M. F. 2013. Cellular Impedance Assays for Predictive Preclinical Drug Screening of Kinase Inhibitor Cardiovascular Toxicity. *Toxicological Sciences,* 135, 402-413.

LASSETER, K. C., LEVEY, G. S., PALMER, R. F. & MCCARTHY, J. S. 1972. The effect of sulfonylurea drugs on rabbit myocardial contractility, canine purkinje fiber automaticity, and adenyl cyclase activity from rabbit and human hearts. *J Clin Invest,* 51, 2429-34.

LAURILA, E., AHOLA, A., HYTTINEN, J. & AALTO-SETÄLÄ, K. 2016. Methods for in vitro functional analysis of iPSC derived cardiomyocytes — Special focus on analyzing the mechanical beating behavior. *Biochimica et Biophysica Acta (BBA) - Molecular Cell Research,* 1863, 1864-1872.

LEFKOWITZ, R. J. 2013. A Brief History of G-Protein Coupled Receptors (Nobel Lecture). *Angewandte Chemie-International Edition,* 52, 6366-6378.

LEFKOWITZ, R. J., HAUSDORFF, W. P. & CARON, M. G. 1990. ROLE OF PHOSPHORYLATION IN DESENSITIZATION OF THE BETA-ADRENOCEPTOR. *Trends in Pharmacological Sciences,* 11, 190-194.

LEFTOWITZ, R. J. & SHENOY, S. K. 2005. Transduction of receptor signals by beta-arrestins. *Science,* 308, 512-517.

LEITOLIS, A., ROBERT, A. W., PEREIRA, I. T., CORREA, A. & STIMAMIGLIO, M. A. 2019. Cardiomyogenesis Modeling Using Pluripotent Stem Cells: The Role of Microenvironmental Signaling. *Frontiers in Cell and Developmental Biology,* 7, 164.

LEMME, M., ULMER, B. M., LEMOINE, M. D., ZECH, A. T. L., FLENNER, F., RAVENS, U., REICHENSPURNER, H., ROL-GARCIA, M., SMITH, G., HANSEN, A., CHRIST, T. & ESCHENHAGEN, T. 2018. Atrial-like Engineered Heart Tissue: An In Vitro Model of the Human Atrium. *Stem Cell Reports,* 11, 1378-1390.

LEMOINE, H., SCHONELL, H. & KAUMANN, A. J. 1988. Contribution of beta 1- and beta 2-adrenoceptors of human atrium and ventricle to the effects of noradrenaline and adrenaline as assessed with (-)-atenolol. *Br J Pharmacol,* 95, 55-66.

LEMOINE, M. D., KRAUSE, T., KOIVUMAEKI, J. T., PRONDZYNSKI, M., SCHULZE, M. L., GIRDAUSKAS, E., WILLEMS, S., HANSEN, A., ESCHENHAGEN, T. & CHRIST, T. 2018. Human Induced Pluripotent Stem Cell-Derived Engineered Heart Tissue as a Sensitive Test System for QT Prolongation and Arrhythmic Triggers. *Circulation-Arrhythmia and Electrophysiology,* 11.

LESTER, R. M., PAGLIALUNGA, S. & JOHNSON, I. A. 2019. QT Assessment in Early Drug Development: The Long and the Short of It. *Int J Mol Sci,* 20.

LEVEY, G. S., PALMER, R. F., LASSETER, K. C. & MCCARTHY, J. 1971. Effect of tolbutamide on adenyl cyclase in rabbit and human heart and contractility of isolated rabbit atria. *J Clin Endocrinol Metab,* 33**,** 371-4.

LEVI, A. J., BOYETT, M. R. & LEE, C. O. 1994. THE CELLULAR ACTIONS OF DIGITALIS GLYCOSIDES ON THE HEART. *Progress in Biophysics & Molecular Biology,* 62**,** 1-54.

LI, R. A., KEUNG, W., CASHMAN, T. J., BACKERIS, P. C., JOHNSON, B. V., BARDOT, E. S., WONG, A. O. T., CHAN, P. K. W., CHAN, C. W. Y. & COSTA, K. D. 2018. Bioengineering an electro-mechanically functional miniature ventricular heart chamber from human pluripotent stem cells. *Biomaterials,* 163**,** 116-127.

LIAN, X., HSIAO, C., WILSON, G., ZHU, K., HAZELTINE, L. B., AZARIN, S. M., RAVAL, K. K., ZHANG, J., KAMP, T. J. & PALECEK, S. P. 2012. Robust cardiomyocyte differentiation from human pluripotent stem cells via temporal modulation of canonical Wnt signaling. *Proceedings of the National Academy of Sciences,* 109**,** E1848.

LIANG, P., LAN, F., LEE, A. S., GONG, T., SANCHEZ-FREIRE, V., WANG, Y., DIECKE, S., SALLAM, K., KNOWLES, J. W., WANG, P. J., NGUYEN, P. K., BERS, D. M., ROBBINS, R. C. & WU, J. C. 2013. Drug screening using a library of human induced pluripotent stem cell-derived cardiomyocytes reveals disease-specific patterns of cardiotoxicity. *Circulation,* 127**,** 1677-91.

LIGGETT, S. B. 1997. Polymorphisms of the beta(2)-adrenergic receptor and asthma. *American Journal of Respiratory and Critical Care Medicine,* 156**,** S156-S162.

LIGGETT, S. B. 2000. The pharmacogenetics of ß₂-adrenergic receptors: Relevance to asthma. *Journal of Allergy and Clinical Immunology,* 105**,** S487-S492.

LINDBOM, L. O. & FORSBERG, T. 1981. Cardiovascular effects of zimelidine and other antidepressant in conscious rats. *Acta Psychiatr Scand Suppl,* 290**,** 380-4.

LIU, L. C., DORHOUT, B., VAN DER MEER, P., TEERLINK, J. R. & VOORS, A. A. 2016. Omecamtiv mecarbil: a new cardiac myosin activator for the treatment of heart failure. *Expert Opin Investig Drugs,* 25**,** 117-27.

LOHSE, M. J., ENGELHARDT, S. & ESCHENHAGEN, T. 2003. What is the role of beta-adrenergic signaling in heart failure? *Circulation Research,* 93**,** 896-906.

LOUCH, W. E., SHEEHAN, K. A. & WOLSKA, B. M. 2011. Methods in cardiomyocyte isolation, culture, and gene transfer. *J Mol Cell Cardiol,* 51**,** 288-98.

LULLMANN, H. & RAVENS, U. 1973. The time courses of the changes in contractile force and in transmembfane potentials induced by cardiac glycosides in guinea-pig papillary muscle. *Br J Pharmacol,* 49**,** 377-90.

LUNDSTROM, K. 2006. Latest development in drug discovery on G protein-coupled receptors. *Current Protein & Peptide Science,* 7**,** 465-470.

MA, J., GUO, L., FIENE, S. J., ANSON, B. D., THOMSON, J. A., KAMP, T. J., KOLAJA, K. L., SWANSON, B. J. & JANUARY, C. T. 2011. High purity human-induced pluripotent stem cell-derived cardiomyocytes: electrophysiological properties of action potentials and ionic currents. *American Journal of Physiology-Heart and Circulatory Physiology,* 301, H2006-H2017.

MA, Q. & LU, A. Y. H. 2011. Pharmacogenetics, Pharmacogenomics, and Individualized Medicine. *Pharmacological Reviews,* 63, 437.

MAACK, C., ESCHENHAGEN, T., HAMDANI, N., HEINZEL, F. R., LYON, A. R., MANSTEIN, D. J., METZGER, J., PAPP, Z., TOCCHETTI, C. G., YILMAZ, M. B., ANKER, S. D., BALLIGAND, J. L., BAUERSACHS, J., BRUTSAERT, D., CARRIER, L., CHLOPICKI, S., CLELAND, J. G., DE BOER, R. A., DIETL, A., FISCHMEISTER, R., HARJOLA, V. P., HEYMANS, S., HILFIKER-KLEINER, D., HOLZMEISTER, J., DE KEULENAER, G., LIMONGELLI, G., LINKE, W. A., LUND, L. H., MASIP, J., METRA, M., MUELLER, C., PIESKE, B., PONIKOWSKI, P., RISTIC, A., RUSCHITZKA, F., SEFEROVIC, P. M., SKOURI, H., ZIMMERMANN, W. H. & MEBAZAA, A. 2018. Treatments targeting inotropy. *Eur Heart J.*

MACDONALD, J. S. & ROBERTSON, R. T. 2009. Toxicity Testing in the 21st Century: A View from the Pharmaceutical Industry. *Toxicological Sciences,* 110, 40-46.

MACLENNAN, D. H. & KRANIAS, E. G. 2003. Phospholamban: a crucial regulator of cardiac contractility. *Nature Reviews Molecular Cell Biology,* 4, 566-577.

MAEHR, R., CHEN, S., SNITOW, M., LUDWIG, T., YAGASAKI, L., GOLAND, R., LEIBEL, R. L. & MELTON, D. A. 2009. Generation of pluripotent stem cells from patients with type 1 diabetes. *Proceedings of the National Academy of Sciences of the United States of America,* 106, 15768-15773.

MAGDY, T., SCHULDT, A. J. T., WU, J. C., BERNSTEIN, D. & BURRIDGE, P. W. 2018. Human Induced Pluripotent Stem Cell (hiPSC)-Derived Cells to Assess Drug Cardiotoxicity: Opportunities and Problems. *Annu Rev Pharmacol Toxicol,* 58, 83-103.

MAHONEY, L., SHAH, G., CROOK, D., ROJAS-ANAYA, H. & RABE, H. 2016. A Literature Review of the Pharmacokinetics and Pharmacodynamics of Dobutamine in Neonates. *Pediatr Cardiol,* 37, 14-23.

MALI, P., YANG, L., ESVELT, K. M., AACH, J., GUELL, M., DICARLO, J. E., NORVILLE, J. E. & CHURCH, G. M. 2013. RNA-guided human genome engineering via Cas9. *Science (New York, N.Y.),* 339, 823-826.

MANNHARDT, I., BRECKWOLDT, K., LETUFFE-BRENIERE, D., SCHAAF, S., SCHULZ, H., NEUBER, C., BENZIN, A., WERNER, T., EDER, A., SCHULZE, T., KLAMPE, B., CHRIST, T., HIRT, M. N., HUEBNER, N., MORETTI, A., ESCHENHAGEN, T. & HANSEN, A. 2016. Human Engineered Heart Tissue: Analysis of Contractile Force. *Stem Cell Reports,* 7, 29-42.

MANNHARDT, I., EDER, A., DUMOTIER, B., PRONDZYNSKI, M., KRAEMER, E., TRAEBERT, M., SOEHREN, K.-D., FLENNER, F., STATHOPOULOU, K., LEMOINE, M. D., CARRIER, L., CHRIST, T., ESCHENHAGEN, T. & HANSEN, A. 2017a. Blinded Contractility Analysis in hiPSC-Cardiomyocytes in Engineered Heart Tissue Format: Comparison With Human Atrial Trabeculae. *Toxicological Sciences,* 158, 164-175.

MANNHARDT, I., EDER, A., DUMOTIER, B., PRONDZYNSKI, M., KRAMER, E., TRAEBERT, M., SOHREN, K. D., FLENNER, F., STATHOPOULOU, K., LEMOINE, M. D., CARRIER, L., CHRIST, T., ESCHENHAGEN, T. & HANSEN, A. 2017b.

Blinded Contractility Analysis in hiPSC-Cardiomyocytes in Engineered Heart Tissue Format: Comparison With Human Atrial Trabeculae. *Toxicol Sci,* 158**,** 164-175.

MANSOR, M. A. & AHMAD, M. R. 2015. Single Cell Electrical Characterization Techniques. *Int J Mol Sci,* 16**,** 12686-712.

MARKS, L., BORLAND, S., PHILP, K., EWART, L., LAINEE, P., SKINNER, M., KIRK, S. & VALENTIN, J. P. 2012. The role of the anaesthetised guinea-pig in the preclinical cardiac safety evaluation of drug candidate compounds. *Toxicol Appl Pharmacol,* 263**,** 171-83.

MARTIN, G. R. 1981. Isolation of a pluripotent cell line from early mouse embryos cultured in medium conditioned by teratocarcinoma stem cells. *Proc Natl Acad Sci U S A,* 78**,** 7634-8.

MARTINS-MARQUES, T., CATARINO, S., MARQUES, C., PEREIRA, P. & GIRAO, H. 2015. To beat or not to beat: degradation of Cx43 imposes the heart rhythm. *Biochem Soc Trans,* 43**,** 476-81.

MATSUSHITA, T., OKAMATO, M., TOYAMA, J., KODAMA, I., ITO, S., FUKUTOMI, T., SUZUKI, S. & ITOH, M. 2000. Adriamycin causes dual inotropic effects through complex modulation of myocardial Ca2+ handling. *Jpn Circ J,* 64**,** 65-71.

MCGLYNN, K. P., LACHAUD, Q., BURTON, F. L. & SMITH, G. L. 2018. Measurements of action potentials, intracellular Ca2+ and contraction in stimulated isolated adult cardiomyocytes using CellOPTIQ® platform for lead development screening. *Journal of Pharmacological and Toxicological Methods,* 93**,** 119.

MCGRAW, D. W., FORBES, S. L., KRAMER, L. A. & LIGGETT, S. B. 1998. Polymorphisms of the 5 ' leader cistron of the human beta(2)-adrenergic receptor regulate receptor expression. *Journal of Clinical Investigation,* 102**,** 1927-1932.

MCQUINN, R. L., PENTIKAINEN, P. J., CHANG, S. F. & CONARD, G. J. 1988. Pharmacokinetics of flecainide in patients with cirrhosis of the liver. *Clin Pharmacol Ther,* 44**,** 566-72.

MEBAZAA, A., NIEMINEN, M. S., PACKER, M., COHEN-SOLAL, A., KLEBER, F. X., POCOCK, S. J., THAKKAR, R., PADLEY, R. J., PODER, P., KIVIKKO, M. & INVESTIGATORS, S. 2007. Levosimendan vs dobutamine for patients with acute decompensated heart failure: the SURVIVE Randomized Trial. *JAMA,* 297**,** 1883-91.

MERCOLA, M., COLAS, A. & WILLEMS, E. 2013. Induced pluripotent stem cells in cardiovascular drug discovery. *Circ Res,* 112**,** 534-48.

MESEGUER-RIPOLLES, J., KHETANI, S. R., BLANCO, J. G., IREDALE, M. & HAY, D. C. 2017. Pluripotent Stem Cell-Derived Human Tissue: Platforms to Evaluate Drug Metabolism and Safety. *The AAPS Journal,* 20**,** 20.

MESIRCA, P., ALIG, J., TORRENTE, A. G., MULLER, J. C., MARGER, L., ROLLIN, A., MARQUILLY, C., VINCENT, A., DUBEL, S., BIDAUD, I., FERNANDEZ, A., SENIUK, A., ENGELAND, B., SINGH, J., MIQUEROL, L., EHMKE, H., ESCHENHAGEN, T., NARGEOT, J., WICKMAN, K., ISBRANDT, D. & MANGONI, M. E. 2014. Cardiac arrhythmia induced by genetic silencing of 'funny' (f) channels is rescued by GIRK4 inactivation. *Nat Commun,* 5**,** 4664.

MIKA, D., BOBIN, P., POMERANCE, M., LECHENE, P., WESTENBROEK, R. E., CATTERALL, W. A., VANDECASTEELE, G., LEROY, J. & FISCHMEISTER, R. 2013. Differential regulation of cardiac excitation-contraction coupling by cAMP phosphodiesterase subtypes. *Cardiovasc Res,* 100**,** 336-46.

MILANI-NEJAD, N. & JANSSEN, P. M. L. 2014. Small and large animal models in cardiac contraction research: advantages and disadvantages. *Pharmacology & therapeutics,* 141**,** 235-249.

MOLENAAR, P., SAVARIMUTHU, S. M., SARSERO, D., CHEN, L., SEMMLER, A. B., CARLE, A., YANG, I., BARTEL, S., VETTER, D., BEYERDORFER, I., KRAUSE, E. G. & KAUMANN, A. J. 2007. (-)-Adrenaline elicits positive inotropic, lusitropic, and biochemical effects through beta2 -adrenoceptors in human atrial myocardium from nonfailing and failing hearts, consistent with Gs coupling but not with Gi coupling. *Naunyn Schmiedebergs Arch Pharmacol,* 375**,** 11-28.

MONOPOLI, A., CONTI, A., FORLANI, A. & ONGINI, E. 1993. ß1 and ß2 Adrenoceptors are Involved in Mediating Vasodilation in the Human Coronary Artery. *Pharmacological Research,* 27**,** 273-280.

MOON, S.-H., BAE, D., JUNG, T.-H., CHUNG, E.-B., JEONG, Y.-H., PARK, S.-J. & CHUNG, H.-M. 2017. From Bench to Market: Preparing Human Pluripotent Stem Cells Derived Cardiomyocytes for Various Applications. *International journal of stem cells,* 10**,** 1-11.

MOONEY, L., SKINNER, M., COKER, S. J. & CURRIE, S. 2015. Effects of acute and chronic sunitinib treatment on cardiac function and calcium/calmodulin-dependent protein kinase II. *Br J Pharmacol,* 172**,** 4342-54.

MOORE, R. H., TUFFAHA, A., MILLMAN, E. E., DAI, W., HALL, H. S., DICKEY, B. F. & KNOLL, B. J. 1999. Agonist-induced sorting of human beta2-adrenergic receptors to lysosomes during downregulation. *Journal of Cell Science,* 112**,** 329.

MORETTI, A., BELLIN, M., WELLING, A., JUNG, C. B., LAM, J. T., BOTT-FLUGEL, L., DORN, T., GOEDEL, A., HOHNKE, C., HOFMANN, F., SEYFARTH, M., SINNECKER, D., SCHOMIG, A. & LAUGWITZ, K. L. 2010. Patient-Specific Induced Pluripotent Stem-Cell Models for Long-QT Syndrome. *New England Journal of Medicine,* 363**,** 1397-1409.

MOSQUEIRA, D., MANNHARDT, I., BHAGWAN, J. R., LIS-SLIMAK, K., KATILI, P., SCOTT, E., HASSAN, M., PRONDZYNSKI, M., HARMER, S. C., TINKER, A., SMITH, J. G. W., CARRIER, L., WILLIAMS, P. M., GAFFNEY, D., ESCHENHAGEN, T., HANSEN, A. & DENNING, C. 2018. CRISPR/Cas9 editing in human pluripotent stemcell-cardiomyocytes highlights arrhythmias, hypocontractility, and energy depletion as potential therapeutic targets for hypertrophic cardiomyopathy. *European Heart Journal,* 39**,** 3879-+.

MUMMERY, C., WARD-VAN OOSTWAARD, D., DOEVENDANS, P., SPIJKER, R., VAN DEN BRINK, S., HASSINK, R., VAN DER HEYDEN, M., OPTHOF, T., PERA, M., DE LA RIVIERE, A. B., PASSIER, R. & TERTOOLEN, L. 2003. Differentiation of human embryonic stem cells to cardiomyocytes: role of coculture with visceral endoderm-like cells. *Circulation,* 107**,** 2733-40.

MUMMERY, C. L. 2018. Perspectives on the Use of Human Induced Pluripotent Stem Cell-Derived Cardiomyocytes in Biomedical Research. *Stem Cell Reports,* 11**,** 1306-1311.

MURAKAMI, M., FURUKAWA, Y., KARASAWA, Y., REN, L. M., TAKAYAMA, S. & CHIBA, S. 1992. Inhibition by glibenclamide of negative chronotropic and inotropic responses to pinacidil, acetylcholine, and adenosine in the isolated dog heart. *J Cardiovasc Pharmacol,* 19**,** 618-24.

MURATA, M., TOHYAMA, S. & FUKUDA, K. 2010. Impacts of recent advances in cardiovascular regenerative medicine on clinical therapies and drug discovery. *Pharmacology & Therapeutics,* 126**,** 109-118.

MUSUNURU, K. 2013. Genome editing of human pluripotent stem cells to generate human cellular disease models. *Disease Models & Mechanisms,* 6**,** 896.

MYAGMAR, B. E., FLYNN, J. M., COWLEY, P. M., SWIGART, P. M., MONTGOMERY, M. D., THAI, K., NAIR, D., GUPTA, R., DENG, D. X., HOSODA, C., MELOV, S., BAKER, A. J. & SIMPSON, P. C. 2017. Adrenergic Receptors in Individual Ventricular Myocytes The Beta-1 and Alpha-1B Are in All Cells, the Alpha-1A Is in a Subpopulation, and the Beta-2 and Beta-3 Are Mostly Absent. *Circulation Research,* 120**,** 1103-+.

NAGELE, P. & LIGGETT, S. B. 2011. Genetic Variation, beta-blockers, and Perioperative Myocardial Infarction. *Anesthesiology,* 115**,** 1316-1327.

NAJAFI, A., SEQUEIRA, V., KUSTER, D. W. D. & VAN DER VELDEN, J. 2016. beta-adrenergic receptor signalling and its functional consequences in the diseased heart. *European Journal of Clinical Investigation,* 46**,** 362-374.

NAKAGAWA, M., KOYANAGI, M., TANABE, K., TAKAHASHI, K., ICHISAKA, T., AOI, T., OKITA, K., MOCHIDUKI, Y., TAKIZAWA, N. & YAMANAKA, S. 2008. Generation of induced pluripotent stem cells without Myc from mouse and human fibroblasts. *Nature Biotechnology,* 26**,** 101-106.

NARANJO, C. A., SELLERS, E. M., KAPLAN, H. L., HAMILTON, C. & KHOUW, V. 1984. Acute kinetic and dynamic interactions of zimelidine with ethanol. *Clin Pharmacol Ther,* 36**,** 654-60.

NARSINH, K. H., PLEWS, J. & WU, J. C. 2011. Comparison of human induced pluripotent and embryonic stem cells: fraternal or identical twins? *Molecular therapy : the journal of the American Society of Gene Therapy,* 19**,** 635-638.

NERBONNE, J. M., NICHOLS, C. G., SCHWARZ, T. L. & ESCANDE, D. 2001. Genetic manipulation of cardiac K(+) channel function in mice: what have we learned, and where do we go from here? *Circ Res,* 89**,** 944-56.

NGUYEN, M. N., KIRIAZIS, H., RUGGIERO, D., GAO, X. M., SU, Y. D., JIAN, A., HAN, L. P., MCMULLEN, J. R. & DU, X. J. 2015. Spontaneous ventricular tachyarrhythmias in beta(2)-adrenoceptor transgenic mice in relation to cardiac interstitial fibrosis. *American Journal of Physiology-Heart and Circulatory Physiology,* 309**,** H946-H957.

NOBLE, S. & ROFFI, M. 2017. Routine beta-blocker administration following acute myocardial infarction: why still an unsolved issue? *Journal of Thoracic Disease,* 9**,** 4191-4194.

OJALA, M., RAJALA, K., PEKKANEN-MATTILA, M., MIETTINEN, M., HUHTALA, H. & AALTO-SETALA, K. 2012. Culture Conditions Affect Cardiac Differentiation Potential of Human Pluripotent Stem Cells. *Plos One,* 7.

OKITA, K., YAMAKAWA, T., MATSUMURA, Y., SATO, Y., AMANO, N., WATANABE, A., GOSHIMA, N. & YAMANAKA, S. 2013. An Efficient Nonviral Method to

Generate Integration-Free Human-Induced Pluripotent Stem Cells from Cord Blood and Peripheral Blood Cells. *Stem Cells,* 31, 458-466.

ONAKPOYA, I. J., HENEGHAN, C. J. & ARONSON, J. K. 2016. Post-marketing withdrawal of 462 medicinal products because of adverse drug reactions: a systematic review of the world literature. *Bmc Medicine,* 14.

OOSTENDORP, J., POSTMA, D. S., VOLDERS, H., JONGEPIER, H., KAUFFMAN, H. F., BOEZEN, H. M., MEYERS, D. A., BLEECKER, E. R., NELEMANS, S. A., ZAAGSMA, J. & MEURS, H. 2005. Differential desensitization of homozygous haplotypes of the beta(2)-adrenergic receptor in lymphocytes. *American Journal of Respiratory and Critical Care Medicine,* 172, 322-328.

ORSTAVIK, O., ATA, S. H., RIISE, J., DAHL, C. P., ANDERSEN, G. O., LEVY, F. O., SKOMEDAL, T., OSNES, J. B. & QVIGSTAD, E. 2014a. Inhibition of phosphodiesterase-3 by levosimendan is sufficient to account for its inotropic effect in failing human heart. *Br J Pharmacol,* 171, 5169-81.

ORSTAVIK, O., ATA, S. H., RIISE, J., DAHL, C. P., ANDERSEN, G. O., LEVY, F. O., SKOMEDAL, T., OSNES, J. B. & QVIGSTAD, E. 2014b. Inhibition of phosphodiesterase-3 by levosimendan is sufficient to account for its inotropic effect in failing human heart. *British Journal of Pharmacology,* 171, 5169-5181.

PANEBRA, A., WANG, W. C., MALONE, M. M., PITTER, D. R. G., WEISS, S. T., HAWKINS, G. A. & LIGGETT, S. B. 2010. Common ADRB2 Haplotypes Derived from 26 Polymorphic Sites Direct beta(2)-Adrenergic Receptor Expression and Regulation Phenotypes. *Plos One,* 5.

PAPP, Z., EDES, I., FRUHWALD, S., DE HERT, S. G., SALMENPERA, M., LEPPIKANGAS, H., MEBAZAA, A., LANDONI, G., GROSSINI, E., CAIMMI, P., MORELLI, A., GUARRACINO, F., SCHWINGER, R. H., MEYER, S., ALGOTSSON, L., WIKSTROM, B. G., JORGENSEN, K., FILIPPATOS, G., PARISSIS, J. T., GONZALEZ, M. J., PARKHOMENKO, A., YILMAZ, M. B., KIVIKKO, M., POLLESELLO, P. & FOLLATH, F. 2012. Levosimendan: molecular mechanisms and clinical implications: consensus of experts on the mechanisms of action of levosimendan. *Int J Cardiol,* 159, 82-7.

PARAMONOV, V. M., MAMAEVA, V., SAHLGREN, C. & RIVERO-MULLER, A. 2015. Genetically-encoded tools for cAMP probing and modulation in living systems. *Frontiers in Pharmacology,* 6, 21.

PASQUALINI, F. S., SHEEHY, S. P., AGARWAL, A., ARATYN-SCHAUS, Y. & PARKER, K. K. 2015. Structural Phenotyping of Stem Cell-Derived Cardiomyocytes. *Stem Cell Reports,* 4, 340-347.

PATEL, A. K., CELIZ, A. D., RAJAMOHAN, D., ANDERSON, D. G., LANGER, R., DAVIES, M. C., ALEXANDER, M. R. & DENNING, C. 2015. A defined synthetic substrate for serum-free culture of human stem cell derived cardiomyocytes with improved functional maturity identified using combinatorial materials microarrays. *Biomaterials,* 61, 257-65.

PEREIRA, S. B., GAVA, I. A., GIRO, C. & MESQUITA, E. T. 2010. Adrenergic Receptor Polymorphisms in Heart Failure: what Can Genetics Explain? *Arquivos Brasileiros De Cardiologia,* 94, 841-849.

PEREZ, O., GAY, P., FRANQUEZA, L., CARRON, R., VALENZUELA, C., DELPON, E. & TAMARGO, J. 1995. Effects of the two enantiomers, S-16257-2 and S-16260-2, of a new bradycardic agent on guinea-pig isolated cardiac preparations. *Br J Pharmacol,* 115, 787-94.

PINNELL, J., TURNER, S. & HOWELL, S. 2007. Cardiac muscle physiology. *Continuing Education in Anaesthesia Critical Care & Pain,* 7**,** 85-88.

PLANELLES-HERRERO, V. J., HARTMAN, J. J., ROBERT-PAGANIN, J., MALIK, F. I. & HOUDUSSE, A. 2017. Mechanistic and structural basis for activation of cardiac myosin force production by omecamtiv mecarbil. *Nat Commun,* 8**,** 190.

PLOTNIKOV, S. V., SABASS, B., SCHWARZ, U. S. & WATERMAN, C. M. 2014. High-resolution traction force microscopy. *Methods in cell biology,* 123**,** 367-394.

POGATSA, G. & DUBECZ, E. 1977. The direct effect of hypoglycaemic sulphonylureas on myocardial contractile force and arterial blood pressure. *Diabetologia,* 13**,** 515-9.

POINTON, A., ABI-GERGES, N., CROSS, M. J. & SIDAWAY, J. E. 2013. Phenotypic Profiling of Structural Cardiotoxins In Vitro Reveals Dependency on Multiple Mechanisms of Toxicity. *Toxicological Sciences,* 132**,** 317-326.

POINTON, A., PILLING, J., DORVAL, T., WANG, Y., ARCHER, C. & POLLARD, C. 2017. High-Throughput Imaging of Cardiac Microtissues for the Assessment of Cardiac Contraction during Drug. *Toxicological Sciences,* 155**,** 444-457.

PRADHAPAN, P., KUUSELA, J., VIIK, J., AALTO-SETALA, K. & HYTTINEN, J. 2013. Cardiomyocyte MEA data analysis (CardioMDA)--a novel field potential data analysis software for pluripotent stem cell derived cardiomyocytes. *PLoS One,* 8**,** e73637.

PSATY, B. M., KOEPSELL, T. D., WAGNER, E. H., LOGERFO, J. P. & INUI, T. S. 1990. THE RELATIVE RISK OF INCIDENT CORONARY HEART-DISEASE ASSOCIATED WITH RECENTLY STOPPING THE USE OF BETA-BLOCKERS. *Jama-Journal of the American Medical Association,* 263**,** 1653-1657.

PUTTONEN, J., KANTELE, S., RUCK, A., RAMELA, M., HAKKINEN, S., KIVIKKO, M. & PENTIKAINEN, P. J. 2008. Pharmacokinetics of intravenous levosimendan and its metabolites in subjects with hepatic impairment. *Journal of Clinical Pharmacology,* 48**,** 445-454.

QU, Y., FANG, M., GAO, B., AMOUZADEH, H. R., LI, N., NARAYANAN, P., ACTON, P., LAWRENCE, J. & VARGAS, H. M. 2013. Itraconazole decreases left ventricular contractility in isolated rabbit heart: mechanism of action. *Toxicol Appl Pharmacol,* 268**,** 113-22.

RADKE, M. B., TAFT, M. H., STAPEL, B., HILFIKER-KLEINER, D., PRELLER, M. & MANSTEIN, D. J. 2014. Small molecule-mediated refolding and activation of myosin motor function. *Elife,* 3**,** e01603.

RAJAGOPAL, S. & SHENOY, S. K. 2017. GPCR desensitization: Acute and prolonged phases. *Cellular Signalling,* 41**,** 9-16.

RAJAMOHAN, D., MATSA, E., KALRA, S., CRUTCHLEY, J., PATEL, A., GEORGE, V. & DENNING, C. 2013. Current status of drug screening and disease modelling in human pluripotent stem cells. *Bioessays,* 35**,** 281-298.

RAO, C., PRODROMAKIS, T., KOLKER, L., CHAUDHRY, U. A., TRANTIDOU, T., SRIDHAR, A., WEEKES, C., CAMELLITI, P., HARDING, S. E., DARZI, A., YACOUB, M. H., ATHANASIOU, T. & TERRACCIANO, C. M. 2013. The effect of microgrooved culture substrates on calcium cycling of cardiac myocytes derived from human induced pluripotent stem cells. *Biomaterials,* 34**,** 2399-411.

RAO, N. 2007. The clinical pharmacokinetics of escitalopram. *Clin Pharmacokinet,* 46, 281-90.

REIHSAUS, E., INNIS, M., MACINTYRE, N. & LIGGETT, S. B. 1993. MUTATIONS IN THE GENE ENCODING FOR THE BETA-2-ADRENERGIC RECEPTOR IN NORMAL AND ASTHMATIC SUBJECTS. *American Journal of Respiratory Cell and Molecular Biology,* 8, 334-339.

RENGO, G., ZINCARELLI, C., FEMMINELLA, G. D., LICCARDO, D., PAGANO, G., DE LUCIA, C., ALTOBELLI, G. G., CIMINI, V., RUGGIERO, D., PERRONE-FILARDI, P., GAO, E., FERRARA, N., LYMPEROPOULOS, A., KOCH, W. J. & LEOSCO, D. 2012. Myocardial beta(2)-adrenoceptor gene delivery promotes coordinated cardiac adaptive remodelling and angiogenesis in heart failure. *British Journal of Pharmacology,* 166, 2348-2361.

REUBINOFF, B. E., PERA, M. F., FONG, C. Y., TROUNSON, A. & BONGSO, A. 2000. Embryonic stem cell lines from human blastocysts: somatic differentiation in vitro. *Nat Biotechnol,* 18, 399-404.

REYES, G., SCHWARTZ, P. H., NEWTH, C. J. & ELDADAH, M. K. 1993. The pharmacokinetics of isoproterenol in critically ill pediatric patients. *J Clin Pharmacol,* 33, 29-34.

RIBEIRO, A. J. S., GUTH, B. D., ENGWALL, M., ELDRIDGE, S., FOLEY, C. M., GUO, L., GINTANT, G., KOERNER, J., PARISH, S. T., PIERSON, J. B., BROCK, M., CHAUDHARY, K. W., KANDA, Y. & BERRIDGE, B. 2019. Considerations for an In Vitro, Cell-Based Testing Platform for Detection of Drug-Induced Inotropic Effects in Early Drug Development. Part 2: Designing and Fabricating Microsystems for Assaying Cardiac Contractility With Physiological Relevance Using Human iPSC-Cardiomyocytes. *Frontiers in Pharmacology,* 10, 19.

RIBEIRO, A. J. S., SCHWAB, O., MANDEGAR, M. A., ANG, Y. S., CONKLIN, B. R., SRIVASTAVA, D. & PRUITT, B. L. 2017. Multi-Imaging Method to Assay the Contractile Mechanical Output of Micropatterned Human iPSC-Derived Cardiac Myocytes. *Circ Res,* 120, 1572-1583.

RIBEIRO, M. C., TERTOOLEN, L. G., GUADIX, J. A., BELLIN, M., KOSMIDIS, G., D'ANIELLO, C., MONSHOUWER-KLOOTS, J., GOUMANS, M. J., WANG, Y. L., FEINBERG, A. W., MUMMERY, C. L. & PASSIER, R. 2015. Functional maturation of human pluripotent stem cell derived cardiomyocytes in vitro--correlation between contraction force and electrophysiology. *Biomaterials,* 51, 138-150.

RIBEIRO-RODRIGUES, T. M., MARTINS-MARQUES, T., MOREL, S., KWAK, B. R. & GIRAO, H. 2017. Role of connexin 43 in different forms of intercellular communication - gap junctions, extracellular vesicles and tunnelling nanotubes. *J Cell Sci,* 130, 3619-3630.

RICHARDSON, C. D., RAY, G. J., DEWITT, M. A., CURIE, G. L. & CORN, J. E. 2016. Enhancing homology-directed genome editing by catalytically active and inactive CRISPR-Cas9 using asymmetric donor DNA. *Nature Biotechnology,* 34, 339.

ROBERTSON, C., TRAN, D. D. & GEORGE, S. C. 2013. Concise review: maturation phases of human pluripotent stem cell-derived cardiomyocytes. *Stem Cells,* 31, 829-37.

ROBISON, G. A. & SUTHERLAND, E. W. 1971. CYCLIC AMP AND FUNCTION OF EUKARYOTIC CELLS - INTRODUCTION. *Annals of the New York Academy of Sciences,* 185, 5-+.

RODEN, D. M. 2008. Cellular basis of drug-induced torsades de pointes. *Br J Pharmacol,* 154**,** 1502-7.

RODRIGUEZ, A. G., RODRIGUEZ, M. L., HAN, S. J., SNIADECKI, N. J. & REGNIER, M. 2013. Enhanced contractility with 2-deoxy-ATP and EMD 57033 is correlated with reduced myofibril structure and twitch power in neonatal cardiomyocytes. *Integr Biol (Camb),* 5**,** 1366-73.

RONALDSON-BOUCHARD, K., YEAGER, K., TELES, D., CHEN, T., MA, S., SONG, L., MORIKAWA, K., WOBMA, H., VASCIAVEO, A., RUIZ, E., YAZAWA, M. & VUNJAK-NOVAKOVIC, G. 2019. Engineering of human cardiac muscle electromechanically matured to an adult-like phenotype. *Nature Protocols.*

ROSEN, M. R., GELBAND, H. & HOFFMAN, B. F. 1971. Effects of phentolamine on electrophysiologic properties of isolated canine purkinje fibers. *J Pharmacol Exp Ther,* 179**,** 586-93.

ROSENBAUM, D. M., RASMUSSEN, S. G. F. & KOBILKA, B. K. 2009. The structure and function of G-protein-coupled receptors. *Nature,* 459**,** 356-363.

ROWNTREE, R. K. & MCNEISH, J. D. 2010. Induced pluripotent stem cells: opportunities as research and development tools in 21st century drug discovery. *Regen Med,* 5**,** 557-68.

ROY, M., DUMAINE, R. & BROWN, A. M. 1996. HERG, a primary human ventricular target of the nonsedating antihistamine terfenadine. *Circulation,* 94**,** 817-23.

RYDBERG, T., JONSSON, A., KARLSSON, M. O. & MELANDER, A. 1997. Concentration-effect relations of glibenclamide and its active metabolites in man: modelling of pharmacokinetics and pharmacodynamics. *Br J Clin Pharmacol,* 43**,** 373-81.

SADA, H. 1978. Effect of phentolamine, alprenolol and prenylamine on maximum rate of rise of action potential in guinea-pig papillary muscles. *Naunyn Schmiedebergs Arch Pharmacol,* 304**,** 191-201.

SAGER, P. T., GINTANT, G., TURNER, J. R., PETTIT, S. & STOCKBRIDGE, N. 2014. Rechanneling the cardiac proarrhythmia safety paradigm: A meeting report from the Cardiac Safety Research Consortium. *American Heart Journal,* 167**,** 292-300.

SALA, L., VAN MEER, B. J., TERTOOLEN, L. G. J., BAKKERS, J., BELLIN, M., DAVIS, R. P., DENNING, C., DIEBEN, M. A. E., ESCHENHAGEN, T., GIACOMELLI, E., GRANDELA, C., HANSEN, A., HOLMAN, E. R., JONGBLOED, M. R. M., KAMEL, S. M., KOOPMAN, C. D., LACHAUD, Q., MANNHARDT, I., MOL, M. P. H., MOSQUEIRA, D., ORLOVA, V. V., PASSIER, R., RIBEIRO, M. C., SALEEM, U., SMITH, G. L., BURTON, F. L. & MUMMERY, C. L. 2018. MUSCLEMOTION: A Versatile Open Software Tool to Quantify Cardiomyocyte and Cardiac Muscle Contraction In Vitro and In Vivo. *Circulation Research,* 122**,** e5-e16.

SALAZAR, N. C., CHEN, J. & ROCKMAN, H. A. 2007. Cardiac GPCRs: GPCR signaling in healthy and failing hearts. *Biochimica Et Biophysica Acta-Biomembranes,* 1768**,** 1006-1018.

SALPETER, S. R., ORMISTON, T. M. & SALPETER, E. E. 2004. Cardiovascular effects of beta-agonists in patients with asthma and COPD - A meta-analysis. *Chest,* 125**,** 2309-+.

SANTULLI, G., TRIMARCO, B. & IACCARINO, G. 2013. G-protein-coupled receptor kinase 2 and hypertension: molecular insights and pathophysiological

mechanisms. *High blood pressure & cardiovascular prevention : the official journal of the Italian Society of Hypertension,* 20, 5-12.

SARSERO, D., FUJIWARA, T., MOLENAAR, P. & ANGUS, J. A. 1998. Human vascular to cardiac tissue selectivity of L- and T-type calcium channel antagonists. *Br J Pharmacol,* 125, 109-19.

SASAKI, K., ICHIKAWA, H., TAKEI, S., NO, H. S., TOMOTSUNE, D., KANO, Y., YOKOYAMA, T., SIRASAWA, S., MOGI, A., YOSHIE, S., SASAKI, S., YAMADA, S., MATSUMOTO, K., MIZUGUCHI, M., YUE, F. & TANAKA, Y. 2009. Hepatocyte differentiation from human ES cells using the simple embryoid body formation method and the staged-additional cocktail. *ScientificWorldJournal,* 9, 884-90.

SATOH, E., YANAGISAWA, T. & TAIRA, N. 1990. Specific antagonism by glibenclamide of negative inotropic effects of potassium channel openers in canine atrial muscle. *Jpn J Pharmacol,* 54, 133-41.

SAYED, N., LIU, C. & WU, J. 2016a. Translation of Human-Induced Pluripotent Stem Cells. *Journal of the American College of Cardiology,* 67, 2161-2176.

SAYED, N., LIU, C. & WU, J. C. 2016b. Translation of Human-Induced Pluripotent Stem Cells From Clinical Trial in a Dish to Precision Medicine. *Journal of the American College of Cardiology,* 67, 2161-2176.

SCHAFERS, R. F., ADLER, S., DAUL, A., ZEITLER, G., VOGELSANG, M., ZERKOWSKI, H. R. & BRODDE, O. E. 1994. Positive inotropic effects of the beta 2-adrenoceptor agonist terbutaline in the human heart: effects of long-term beta 1-adrenoceptor antagonist treatment. *J Am Coll Cardiol,* 23, 1224-33.

SCHIPKE, J. D. & KORBMACHER, B. 1996. EMD 57033: A Novel Ca2+ Sensitizing Agent. *Cardiovascular Drug Reviews,* 14, 334-350.

SCHMITTO, J. D., MOKASHI, S. A. & CHEN, F. Y. 2010. Letter by Schmitto et al Regarding Article "Large Animal Models of Heart Failure: A Critical Link in the Translation of Basic Science to Clinical Practice". *Circulation-Heart Failure,* 3, E3-E3.

SCHRAMM, M., THOMAS, G., TOWART, R. & FRANCKOWIAK, G. 1983. Novel dihydropyridines with positive inotropic action through activation of Ca2+ channels. *Nature,* 303, 535-7.

SCHULDINER, M., YANUKA, O., ITSKOVITZ-ELDOR, J., MELTON, D. A. & BENVENISTY, N. 2000. Effects of eight growth factors on the differentiation of cells derived from human embryonic stem cells. *Proc Natl Acad Sci U S A,* 97, 11307-12.

SCHWINGER, R. H., BOHM, M. & ERDMANN, E. 1990. Negative inotropic properties of isradipine, nifedipine, diltiazem, and verapamil in diseased human myocardial tissue. *J Cardiovasc Pharmacol,* 15, 892-9.

SCOTT, C. W., PETERS, M. F. & DRAGAN, Y. P. 2013. Human induced pluripotent stem cells and their use in drug discovery for toxicity testing. *Toxicology Letters,* 219, 49-58.

SCOTT, C. W., ZHANG, X., ABI-GERGES, N., LAMORE, S. D., ABASSI, Y. A. & PETERS, M. F. 2014. An Impedance-Based Cellular Assay Using Human iPSC-Derived Cardiomyocytes to Quantify Modulators of Cardiac Contractility. *Toxicological Sciences,* 142, 331-338.

SEARS, M. R. 2002. Adverse effects of ß-agonists. *Journal of Allergy and Clinical Immunology,* 110, S322-S328.

SEHGAL, P., SZALAI, P., OLESEN, C., PRAETORIUS, H. A., NISSEN, P., CHRISTENSEN, S. B., ENGEDAL, N. & MOLLER, J. V. 2017. Inhibition of the sarco/endoplasmic reticulum (ER) Ca(2+)-ATPase by thapsigargin analogs induces cell death via ER Ca(2+) depletion and the unfolded protein response. *J Biol Chem,* 292**,** 19656-19673.

SHARMA, A., MCKEITHAN, W. L., SERRANO, R., KITANI, T., BURRIDGE, P. W., DEL ALAMO, J. C., MERCOLA, M. & WU, J. C. 2018. Use of human induced pluripotent stem cell-derived cardiomyocytes to assess drug cardiotoxicity. *Nature Protocols,* 13**,** 3018-3041.

SHEN, H., LI, J., ZHANG, J. G., XU, C., JIANG, Y., WU, Z. K., ZHAO, F. P., LIAO, L., CHEN, J., LIN, Y., TIAN, Q., PAPASIAN, C. J. & DENG, H. W. 2013. Comprehensive Characterization of Human Genome Variation by High Coverage Whole-Genome Sequencing of Forty Four Caucasians. *Plos One,* 8.

SHOICHET, B. K. & KOBILKA, B. K. 2012. Structure-based drug screening for G-protein-coupled receptors. *Trends Pharmacol Sci,* 33**,** 268-72.

SIBBALD, B. 2004. Rofecoxib (Vioxx) voluntarily withdrawn from market. *CMAJ : Canadian Medical Association journal = journal de l'Association medicale canadienne,* 171**,** 1027-1028.

SMALL, K. M., MCGRAW, D. W. & LIGGETT, S. B. 2003. Pharmacology and physiology of human adrenergic receptor polymorphisms. *Annual Review of Pharmacology and Toxicology,* 43**,** 381-411.

SMITH, J. G. W., OWEN, T., BHAGWAN, J. R., MOSQUEIRA, D., SCOTT, E., MANNHARDT, I., PATEL, A., BARRIALES-VILLA, R., MONSERRAT, L., HANSEN, A., ESCHENHAGEN, T., HARDING, S. E., MARSTON, S. & DENNING, C. 2018. Isogenic Pairs of hiPSC-CMs with Hypertrophic Cardiomyopathy/LVNC-Associated ACTCI E99K Mutation Unveil Differential Functional Deficits. *Stem Cell Reports,* 11**,** 1226-1243.

SMYTH, J. W. & SHAW, R. M. 2012. The gap junction life cycle. *Heart rhythm,* 9**,** 151-153.

SOLDNER, F., HOCKEMEYER, D., BEARD, C., GAO, Q., BELL, G. W., COOK, E. G., HARGUS, G., BLAK, A., COOPER, O., MITALIPOVA, M., ISACSON, O. & JAENISCH, R. 2009. Parkinson's Disease Patient-Derived Induced Pluripotent Stem Cells Free of Viral Reprogramming Factors. *Cell,* 136**,** 964-977.

SOTTILE, V., THOMSON, A. & MCWHIR, J. 2003. In vitro osteogenic differentiation of human ES cells. *Cloning Stem Cells,* 5**,** 149-55.

STADTFELD, M., NAGAYA, M., UTIKAL, J., WEIR, G. & HOCHEDLINGER, K. 2008. Induced pluripotent stem cells generated without viral integration. *Science,* 322**,** 945-9.

STAGE, C., JURGENS, G., GUSKI, L. S., THOMSEN, R., BJERRE, D., FERRERO-MILIANI, L., LYAUK, Y. K., RASMUSSEN, H. B., DALHOFF, K. & CONSORTIUM, I. 2017. The Pharmacokinetics of Enalapril in Relation to CES1 Genotype in Healthy Danish Volunteers. *Basic Clin Pharmacol Toxicol,* 121**,** 487-492.

STINGL, J. C., WELKER, S., HARTMANN, G., DAMANN, V. & GERZER, R. 2015. Where Failure Is Not an Option –Personalized Medicine in Astronauts. *PLOS ONE,* 10**,** e0140764.

SUGIYAMA, A., SATOH, Y., SHIINA, H., TAKAHARA, A., YONEYAMA, M. & HASHIMOTO, K. 2001. Cardiac electrophysiologic and hemodynamic effects of sildenafil, a PDE5 inhibitor, in anesthetized dogs. *J Cardiovasc Pharmacol,* 38**,** 940-6.

SUN, C. & KONTARIDIS, M. I. 2018. Physiology of Cardiac Development: From Genetics to Signaling to Therapeutic Strategies. *Current opinion in physiology,* 1, 123-139.

SUTKO, J. L. & WILLERSON, J. T. 1980. Ryanodine alteration of the contractile state of rat ventricular myocardium. Comparison with dog, cat, and rabbit ventricular tissues. *Circ Res,* 46, 332-43.

TAKAHASHI, K., TANABE, K., OHNUKI, M., NARITA, M., ICHISAKA, T., TOMODA, K. & YAMANAKA, S. 2007. Induction of pluripotent stem cells from adult human fibroblasts by defined factors. *Cell,* 131, 861-72.

TAKAHASHI, K. & YAMANAKA, S. 2006. Induction of pluripotent stem cells from mouse embryonic and adult fibroblast cultures by defined factors. *Cell,* 126, 663-76.

TAKAHASHI, K. & YAMANAKA, S. 2016. A decade of transcription factor-mediated reprogramming to pluripotency. *Nat Rev Mol Cell Biol,* 17, 183-93.

TAYLOR, A. E., ZAMORA, V., HORTIGON-VINAGRE, M. P., ALLAN, A., BURTON, F. L., ANSON, B. D., CRAIG, M. A. & SMITH, G. L. 2016. Electrophysiological characterization of iCell2 hiPSC derived cardiomyocytes: The new generation of CDI hiPSC-CMs. *Journal of Pharmacological and Toxicological Methods,* 81, 388.

TAYLOR, M. R. G. & BRISTOW, M. R. 2004. The emerging pharmacogenomics of the beta-adrenergic receptors. *Congestive heart failure (Greenwich, Conn.),* 10, 281-8.

TEERLINK, J. R., CLARKE, C. P., SAIKALI, K. G., LEE, J. H., CHEN, M. M., ESCANDON, R. D., ELLIOTT, L., BEE, R., HABIBZADEH, M. R., GOLDMAN, J. H., SCHILLER, N. B., MALIK, F. I. & WOLFF, A. A. 2011. Dose-dependent augmentation of cardiac systolic function with the selective cardiac myosin activator, omecamtiv mecarbil: a first-in-man study. *Lancet,* 378, 667-75.

TEMMA, K., AKERA, T., CHUGUN, A., KONDO, H., HAGANE, K. & HIRANO, S. 1993. Comparison of cardiac actions of doxorubicin, pirarubicin and aclarubicin in isolated guinea-pig heart. *Eur J Pharmacol,* 234, 173-81.

THOMSON, J. A., ITSKOVITZ-ELDOR, J., SHAPIRO, S. S., WAKNITZ, M. A., SWIERGIEL, J. J., MARSHALL, V. S. & JONES, J. M. 1998. Embryonic stem cell lines derived from human blastocysts. *Science,* 282, 1145-1147.

THOMSON, J. A., KALISHMAN, J., GOLOS, T. G., DURNING, M., HARRIS, C. P., BECKER, R. A. & HEARN, J. P. 1995. Isolation of a primate embryonic stem cell line. *Proc Natl Acad Sci U S A,* 92, 7844-8.

TURKI, J., PAK, J., GREEN, S. A., MARTIN, R. J. & LIGGETT, S. B. 1995. GENETIC POLYMORPHISMS OF THE BETA(2)-ADRENERGIC RECEPTOR IN NOCTURNAL AND NONNOCTURNAL ASTHMA - EVIDENCE THAT GLY16 CORRELATES WITH THE NOCTURNAL PHENOTYPE. *Journal of Clinical Investigation,* 95, 1635-1641.

TURNER, J. R. 2019. The International Council for Harmonisation and a Case Study in Regulatory Science. *Therapeutic Innovation & Regulatory Science,* 53, 561-563.

URNOV, F. D., MILLER, J. C., LEE, Y.-L., BEAUSEJOUR, C. M., ROCK, J. M., AUGUSTUS, S., JAMIESON, A. C., PORTEUS, M. H., GREGORY, P. D. & HOLMES, M. C. 2005. Highly efficient endogenous human gene correction using designed zinc-finger nucleases. *Nature,* 435, 646-651.

UZUN, A. U., MANNHARDT, I., BRECKWOLDT, K., HORVATH, A., JOHANNSEN, S. S., HANSEN, A., ESCHENHAGEN, T. & CHRIST, T. 2016. Ca2+-Currents in Human Induced Pluripotent Stem Cell-Derived Cardiomyocytes Effects of Two Different Culture Conditions. *Frontiers in Pharmacology,* 7.

VALENTIN, J.-P., BIALECKI, R., EWART, L., HAMMOND, T., LEISHMANN, D., LINDGREN, S., MARTINEZ, V., POLLARD, C., REDFERN, W. & WALLIS, R. 2009. A framework to assess the translation of safety pharmacology data to humans. *Journal of Pharmacological and Toxicological Methods,* 60**,** 152-158.

VAN KEMPEN, M. J. A., VELDE, I. T., WESSELS, A., OOSTHOEK, P. W., GROS, D., JONGSMA, H. J., MOORMAN, A. F. M. & LAMERS, W. H. 1995. Differential connexin distribution accommodates cardiac function in different species. *Microscopy Research and Technique,* 31**,** 420-436.

VAN MEER, B. J., KROTENBERG, A., SALA, L., DAVIS, R. P., ESCHENHAGEN, T., DENNING, C., TERTOOLEN, L. G. J. & MUMMERY, C. L. 2019. Simultaneous measurement of excitation-contraction coupling parameters identifies mechanisms underlying contractile responses of hiPSC-derived cardiomyocytes. *Nature Communications,* 10**,** 4325.

VAN OPSTAL, J. M., SCHOENMAKERS, M., VERDUYN, S. C., DE GROOT, S. H., LEUNISSEN, J. D., VAN DER HULST, F. F., MOLENSCHOT, M. M., WELLENS, H. J. & VOS, M. A. 2001. Chronic amiodarone evokes no torsade de pointes arrhythmias despite QT lengthening in an animal model of acquired long-QT syndrome. *Circulation,* 104**,** 2722-7.

VANBOXTEL, C. J., OLSON, R. D., BOERTH, R. C. & OATES, J. A. 1978. Doxorubicin - Inotropic Effects and Inhibitory Action on Ouabain. *Journal of Pharmacology and Experimental Therapeutics,* 207**,** 277-283.

VEERMAN, C. C., KOSMIDIS, G., MUMMERY, C. L., CASINI, S., VERKERK, A. O. & BELLIN, M. 2015. Immaturity of Human Stem-Cell-Derived Cardiomyocytes in Culture: Fatal Flaw or Soluble Problem? *Stem Cells and Development,* 24**,** 1035-1052.

WALKER, D. K., ACKLAND, M. J., JAMES, G. C., MUIRHEAD, G. J., RANCE, D. J., WASTALL, P. & WRIGHT, P. A. 1999. Pharmacokinetics and metabolism of sildenafil in mouse, rat, rabbit, dog and man. *Xenobiotica,* 29**,** 297-310.

WALLIS, R., GHARANEI, M. & MADDOCK, H. 2015. Predictivity of in vitro non-clinical cardiac contractility assays for inotropic effects in humans - A literature search. *Journal of Pharmacological and Toxicological Methods,* 75**,** 62-69.

WALLIS, R. M. 2010. Integrated risk assessment and predictive value to humans of non-clinical repolarization assays. *Br J Pharmacol,* 159**,** 115-21.

WANG, Y. X. & KORTH, M. 1995. Effects of Doxorubicin on Excitation-Contraction Coupling in Guinea-Pig Ventricular Myocardium. *Circulation Research,* 76**,** 645-653.

WARREN, L., MANOS, P. D., AHFELDT, T., LOH, Y. H., LI, H., LAU, F., EBINA, W., MANDAL, P. K., SMITH, Z. D., MEISSNER, A., DALEY, G. Q., BRACK, A. S., COLLINS, J. J., COWAN, C., SCHLAEGER, T. M. & ROSSI, D. J. 2010. Highly efficient reprogramming to pluripotency and directed differentiation of human cells with synthetic modified mRNA. *Cell Stem Cell,* 7**,** 618-30.

WEITL, N. & SEIFERT, R. 2008. Distinct Interactions of Human beta(1)- and beta(2)-Adrenoceptors with Isoproterenol, Epinephrine, Norepinephrine, and

Dopamine. *Journal of Pharmacology and Experimental Therapeutics,* 327, 760-769.

WHITING, B., WILLIAMS, R. L., LORENZI, M., VARADY, J. C. & ROBINS, D. S. 1981. Effect of naproxen on glucose metabolism and tolbutamide kinetics and dynamics in maturity onset diabetics. *Br J Clin Pharmacol,* 11, 295-302.

WILSBACHER, L. D. & COUGHLIN, S. R. 2015. Analysis of cardiomyocyte development using immunofluorescence in embryonic mouse heart. *Journal of visualized experiments : JoVE*, 52644.

WITCHEL, H. J., PABBATHI, V. K., HOFMANN, G., PAUL, A. A. & HANCOX, J. C. 2002. Inhibitory actions of the selective serotonin re-uptake inhibitor citalopram on HERG and ventricular L-type calcium currents. *FEBS Lett,* 512, 59-66.

WOLTJEN, K., MICHAEL, I. P., MOHSENI, P., DESAI, R., MILEIKOVSKY, M., HAMALAINEN, R., COWLING, R., WANG, W., LIU, P. T., GERTSENSTEIN, M., KAJI, K., SUNG, H. K. & NAGY, A. 2009. piggyBac transposition reprograms fibroblasts to induced pluripotent stem cells. *Nature,* 458, 766-U106.

WORTSMAN, J., FRANK, S. & CRYER, P. E. 1984. Adrenomedullary response to maximal stress in humans. *Am J Med,* 77, 779-84.

WU, H., LEE, J., VINCENT, L. G., WANG, Q., GU, M., LAN, F., CHURKO, J. M., SALLAM, K. I., MATSA, E., SHARMA, A., GOLD, J. D., ENGLER, A. J., XIANG, Y. K., BERS, D. M. & WU, J. C. 2015. Epigenetic Regulation of Phosphodiesterases 2A and 3A Underlies Compromised beta-Adrenergic Signaling in an iPSC Model of Dilated Cardiomyopathy. *Cell Stem Cell,* 17, 89-100.

XI, B. A., WANG, T. X., LI, N., OUYANG, W., ZHANG, W., WU, J. Y., XU, X., WANG, X. B. & ABASSI, Y. A. 2011. Functional Cardiotoxicity Profiling and Screening Using the xCELLigence RTCA Cardio System. *Jala,* 16, 415-421.

XIAO, R. P. 2001. Beta-adrenergic signaling in the heart: dual coupling of the beta2-adrenergic receptor to G(s) and G(i) proteins. *Science's STKE : signal transduction knowledge environment,* 2001, re15-re15.

YAMAMOTO, W., ASAKURA, K., ANDO, H., TANIGUCHI, T., OJIMA, A., UDA, T., OSADA, T., HAYASHI, S., KASAI, C., MIYAMOTO, N., TASHIBU, H., YOSHINAGA, T., YAMAZAKI, D., SUGIYAMA, A., KANDA, Y., SAWADA, K. & SEKINO, Y. 2016. Electrophysiological Characteristics of Human iPSC-Derived Cardiomyocytes for the Assessment of Drug-Induced Proarrhythmic Potential. *Plos One,* 11.

YOKOO, N., BABA, S., KAICHI, S., NIWA, A., MIMA, T., DOI, H., YAMANAKA, S., NAKAHATA, T. & HEIKE, T. 2009a. The effects of cardioactive drugs on cardiomyocytes derived from human induced pluripotent stem cells. *Biochem Biophys Res Commun,* 387, 482-8.

YOKOO, N., BABA, S., KAICHI, S., NIWA, A., MIMA, T., DOI, H., YAMANAKA, S., NAKAHATA, T. & HEIKE, T. 2009b. The effects of cardioactive drugs on cardiomyocytes derived from human induced pluripotent stem cells. *Biochemical and Biophysical Research Communications,* 387, 482-488.

YOKOSHIKI, H., KATSUBE, Y., SUNAGAWA, M. & SPERELAKIS, N. 1997. Levosimendan, a novel Ca2+ sensitizer, activates the glibenclamide-sensitive K+ channel in rat arterial myocytes. *Eur J Pharmacol,* 333, 249-59.

YU, J., HU, K., SMUGA-OTTO, K., TIAN, S., STEWART, R., SLUKVIN, II & THOMSON, J. A. 2009. Human induced pluripotent stem cells free of vector and transgene sequences. *Science,* 324**,** 797-801.

YU, J., VODYANIK, M. A., SMUGA-OTTO, K., ANTOSIEWICZ-BOURGET, J., FRANE, J. L., TIAN, S., NIE, J., JONSDOTTIR, G. A., RUOTTI, V., STEWART, R., SLUKVIN, II & THOMSON, J. A. 2007. Induced pluripotent stem cell lines derived from human somatic cells. *Science,* 318**,** 1917-20.

ZHANG, J., WILSON, G. F., SOERENS, A. G., KOONCE, C. H., YU, J., PALECEK, S. P., THOMSON, J. A. & KAMP, T. J. 2009. Functional cardiomyocytes derived from human induced pluripotent stem cells. *Circ Res,* 104**,** e30-41.

ZHANG, R. & XIE, X. 2012. Tools for GPCR drug discovery. *Acta Pharmacologica Sinica,* 33**,** 372-384.

ZHAO, M. T., CHEN, H. D., LIU, Q., SHAO, N. Y., SAYED, N., WO, H. T., ZHANG, J. Z., ONG, S. G., LIU, C., KIM, Y., YANG, H. X., CHOUR, T., MA, H., GUTIERREZ, N. M., KARAKIKES, I., MITALIPOV, S., SNYDER, M. P. & WU, J. C. 2017a. Molecular and functional resemblance of differentiated cells derived from isogenic human iPSCs and SCNT-derived ESCs. *Proceedings of the National Academy of Sciences of the United States of America,* 114**,** E11111-E11120.

ZHAO, Q., WANG, X., WANG, S., SONG, Z., WANG, J. & MA, J. 2017b. Cardiotoxicity evaluation using human embryonic stem cells and induced pluripotent stem cell-derived cardiomyocytes. *Stem cell research & therapy,* 8**,** 54-54.

ZHAO, Y., RAFATIAN, N., FERIC, N. T., COX, B. J., ASCHAR-SOBBI, R., WANG, E. Y., AGGARWAL, P., ZHANG, B., CONANT, G., RONALDSON-BOUCHARD, K., PAHNKE, A., PROTZE, S., LEE, J. H., DAVENPORT HUYER, L., JEKIC, D., WICKELER, A., NAGUIB, H. E., KELLER, G. M., VUNJAK-NOVAKOVIC, G., BROECKEL, U., BACKX, P. H. & RADISIC, M. 2019. A Platform for Generation of Chamber-Specific Cardiac Tissues and Disease Modeling. *Cell*.

ZHOU, H., WU, S., JOO, J. Y., ZHU, S., HAN, D. W., LIN, T., TRAUGER, S., BIEN, G., YAO, S., ZHU, Y., SIUZDAK, G., SCHOLER, H. R., DUAN, L. & DING, S. 2009. Generation of induced pluripotent stem cells using recombinant proteins. *Cell Stem Cell,* 4**,** 381-4.

ZHOU, T., BENDA, C., DUNZINGER, S., HUANG, Y., HO, J. C., YANG, J., WANG, Y., ZHANG, Y., ZHUANG, Q., LI, Y., BAO, X., TSE, H.-F., GRILLARI, J., GRILLARI-VOGLAUER, R., PEI, D. & ESTEBAN, M. A. 2012. Generation of human induced pluripotent stem cells from urine samples. *Nature Protocols,* 7**,** 2080-2089.

ZHU, H., LENSCH, M. W., CAHAN, P. & DALEY, G. Q. 2011. Investigating monogenic and complex diseases with pluripotent stem cells. *Nature Reviews Genetics,* 12**,** 266-275.